

Lecture Notes in Civil Engineering

Pala Gireesh Kumar
Kolluru V. L. Subramaniam
S. Moses Santhakumar
Neelima Satyam D. *Editors*

Recent Advances in Civil Engineering

Proceedings of the 2nd International
Conference on Sustainable Construction
Technologies and Advancements in Civil
Engineering (ScTACE 2021)

 Springer

Lecture Notes in Civil Engineering

Volume 233

Series Editors

Marco di Prisco, Politecnico di Milano, Milano, Italy

Sheng-Hong Chen, School of Water Resources and Hydropower Engineering,
Wuhan University, Wuhan, China

Ioannis Vayas, Institute of Steel Structures, National Technical University of
Athens, Athens, Greece

Sanjay Kumar Shukla, School of Engineering, Edith Cowan University, Joondalup,
WA, Australia

Anuj Sharma, Iowa State University, Ames, IA, USA

Nagesh Kumar, Department of Civil Engineering, Indian Institute of Science
Bangalore, Bengaluru, Karnataka, India

Chien Ming Wang, School of Civil Engineering, The University of Queensland,
Brisbane, QLD, Australia

Lecture Notes in Civil Engineering (LNCE) publishes the latest developments in Civil Engineering - quickly, informally and in top quality. Though original research reported in proceedings and post-proceedings represents the core of LNCE, edited volumes of exceptionally high quality and interest may also be considered for publication. Volumes published in LNCE embrace all aspects and subfields of, as well as new challenges in, Civil Engineering. Topics in the series include:

- Construction and Structural Mechanics
- Building Materials
- Concrete, Steel and Timber Structures
- Geotechnical Engineering
- Earthquake Engineering
- Coastal Engineering
- Ocean and Offshore Engineering; Ships and Floating Structures
- Hydraulics, Hydrology and Water Resources Engineering
- Environmental Engineering and Sustainability
- Structural Health and Monitoring
- Surveying and Geographical Information Systems
- Indoor Environments
- Transportation and Traffic
- Risk Analysis
- Safety and Security

To submit a proposal or request further information, please contact the appropriate Springer Editor:

- Pierpaolo Riva at pierpaolo.riva@springer.com (Europe and Americas);
- Swati Meherishi at swati.meherishi@springer.com (Asia - except China, and Australia, New Zealand);
- Wayne Hu at wayne.hu@springer.com (China).

All books in the series now indexed by Scopus and EI Compendex database!

More information about this series at <https://link.springer.com/bookseries/15087>

Pala Gireesh Kumar · Kolluru V. L. Subramaniam ·
S. Moses Santhakumar · Neelima Satyam D.
Editors

Recent Advances in Civil Engineering

Proceedings of the 2nd International
Conference on Sustainable Construction
Technologies and Advancements in Civil
Engineering (ScTACE 2021)

Editors

Pala Gireesh Kumar
Department of Civil Engineering
Shri Vishnu Engineering College for
Women
Bhimavaram, Andhra Pradesh, India

Kolluru V. L. Subramaniam
Department of Civil Engineering
Indian Institute of Technology Hyderabad
Kandi
Kandi, Telangana, India

S. Moses Santhakumar
Department of Civil Engineering
National Institute of Technology
Tiruchirappalli
Tiruchirappalli, Tamil Nadu, India

Neelima Satyam D.
Department of Civil Engineering
Indian Institute of Technology Indore
Indore, Madhya Pradesh, India

ISSN 2366-2557

ISSN 2366-2565 (electronic)

Lecture Notes in Civil Engineering

ISBN 978-981-19-0188-1

ISBN 978-981-19-0189-8 (eBook)

<https://doi.org/10.1007/978-981-19-0189-8>

© The Editor(s) (if applicable) and The Author(s), under exclusive license to Springer Nature Singapore Pte Ltd. 2022

This work is subject to copyright. All rights are solely and exclusively licensed by the Publisher, whether the whole or part of the material is concerned, specifically the rights of translation, reprinting, reuse of illustrations, recitation, broadcasting, reproduction on microfilms or in any other physical way, and transmission or information storage and retrieval, electronic adaptation, computer software, or by similar or dissimilar methodology now known or hereafter developed.

The use of general descriptive names, registered names, trademarks, service marks, etc. in this publication does not imply, even in the absence of a specific statement, that such names are exempt from the relevant protective laws and regulations and therefore free for general use.

The publisher, the authors and the editors are safe to assume that the advice and information in this book are believed to be true and accurate at the date of publication. Neither the publisher nor the authors or the editors give a warranty, expressed or implied, with respect to the material contained herein or for any errors or omissions that may have been made. The publisher remains neutral with regard to jurisdictional claims in published maps and institutional affiliations.

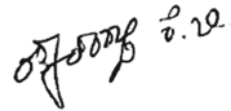
This Springer imprint is published by the registered company Springer Nature Singapore Pte Ltd.

The registered company address is: 152 Beach Road, #21-01/04 Gateway East, Singapore 189721, Singapore

*In the memory of **Late Dr. Bhupathiraju Vissam Raju**, Founder Chairman of Sri Vishnu Educational Society, and **Late Smt. Bhupathiraju Seethamma**, “Recent Advances in Civil Engineering: Proceedings of the 2nd International Conference on Sustainable Construction Technologies and Advancements in Civil Engineering (ScTACE 2021)” is dedicated in their honor for their commendable contributions, endowments, benefactions, and service to society.*

Foreword

Civil engineering is an embrace of copious disciplines with diversified strands of research opportunities. Invigorating the zest and zeal to explore the expanse of civil engineering is an engrossing quest, one such fascinating endeavor of civil engineering cognates to “Recent Advances in Civil Engineering: Proceedings of the 2nd International Conference on Sustainable Construction Technologies and Advancements in Civil Engineering (ScTACE 2021).” With sustainability as a principal firm, the proceedings of ScTACE 2021 encompassed the innovational analysis, investigations, and research works targeting new-flanged trends of civil engineering disciplines. It has dazzled my spirit and enthusiasm for supplemental learning and proposals of novel techniques. The intensity of sustainable approaches with avant-garde technology is a culmination where the readers discover it to be credible with all the advanced and futuristic gatherings at one locus. Pointing to the necessity of sustainable strategies, the authors have intensified the concepts with facts and records obtained from tests and trials. The factual tone of methods of ScTACE 2021 Proceedings has dented me with a remarkable outreach for an acquaintance in recent inclinations. And I take utmost gusto in proposing a word of the work proffered through the proceedings and believe it is worth spending time in exploring the concepts embodied in it.



Er. K. B. Rathnakara Reddy
Managing Director
Infra Support Engineering Consultants Pvt. Ltd.
Bengaluru, India

Preface

Research has always set a gateway for new theories and proposals. These hold ascendancy and escalation of knowledge. In the accord to appraise the society on sustainability relating to the value-added research in terms of the latest technologies, the 2nd International Conference on Sustainable Construction Technologies and Advancements in Civil Engineering, ScTACE 2021, convened on October 14–16, 2021, has devised to formulate as Recent Advances in Civil Engineering: Proceedings of ScTACE 2021. Elevating the aspect of research as the peak core of any field, ScTACE 2021 is tasked up with exposing new studies and innovative research works to the competitive world outside through the proceedings. Besides the honorable commendation to the innovations and studies, ScTACE 2021 toiled the feature of exchanging knowledge. As education is focal and highly fascinated with the revamping of new trends, technologies, and advancements in civil engineering, this proceedings of ScTACE 2021 intensified socializing of research works and studies carried by rendering a notable lecture series put together to summon strength in technical aspects of civil engineering. Holding on to the intent, ScTACE 2021 contrived and comprehended lecture series with the goal of sharing knowledge by emphasizing eminence to all the fields concerning civil engineering such as structures, transportation, geotechnical, environmental, remote sensing, water resources, hydraulics, with interdisciplinary studies and research proposals. With the comprehended research works embodied collectively, ScTACE 2021 featured sustainability as a supreme motive behind all the aspects as it holds the future of a nation. To ignite the prosperity of civil engineering by correlating it to sustainability, “Recent Advances in Civil Engineering: Proceedings of the 2nd International Conference on Sustainable Construction Technologies and Advancements in Civil Engineering (ScTACE 2021)” tasks up the act of propounding the power of sustainability that

can heal, rule, and dwell the world into a better and sophisticated place of livelihood with advancements in both, nature and technology sustainably.

Bhimavaram, India
Kandi, India
Tiruchirappalli, India
Indore, India

Pala Gireesh Kumar
Kolluru V. L. Subramaniam
S. Moses Santhakumar
Neelima Satyam D.

Acknowledgements

With the collective efforts of honorable and dearly beloved and their praiseworthy contribution, ScTACE 2021 has witnessed the charm of success. In this regard, I express my sincere thankfulness and appreciation to the co-editors of “Recent Advances in Civil Engineering: Proceedings of the 2nd International Conference on Sustainable Construction Technologies and Advancements in Civil Engineering (ScTACE 2021),” Prof. Kolluru V. L. Subramaniam, IIT Hyderabad; Prof. S. Moses Santhakumar, NIT Trichy; and Dr. Neelima Satyam D., IIT Indore, for being the most radiant aid to the proceedings.

Also, I extend my thankfulness to the General Chair of ScTACE 2021, Prof. Shen-En Chen, from the University of North Carolina; General Co-Chair, Dr. Narasimha Murthy, Transportation & Traffic Engineering Consultant, USA; Scientific Committee Chair, Prof. D. Nagesh Kumar from IISc Bangalore; and Program Committee Co-Chair, Mr. Mahdi Feizbahr from Iran; for being such an honor to ScTACE 2021. Furthermore, I like to acknowledge the continuous efforts of the CRC Committee for their honest and ethical reviews. Likewise, I proffer my thankfulness to Sri K. V. Vishnu Raju Garu, Chairman, SVES; Sri Ravichandran Rajagopal Garu, Vice-Chairman, SVES; Sri K. Aditya Vissam Garu, Secretary, SVES; Dr. G. Srinivasa Rao, Principal, SVECW; Dr. P. Srinivasa Raju, Vice Principal, SVECW; and the entire management of Sri Vishnu Educational Society and SVECW for providing the needed support and encouragement. Also, sincere thankfulness and warm wishes to all the authors who bestowed valuable time and work with ScTACE 2021.

Ultimately, I extend my heartfelt gratitude to value the support rendered by every individual who aided in the successful completion of “Recent Advances in Civil Engineering: Proceedings of the 2nd International Conference on Sustainable Construction Technologies and Advancements in Civil Engineering (ScTACE 2021).”



Dr. Pala Gireesh Kumar
Conference Chair and Chief Editor—ScTACE 2021
Head and Associate Professor—CE, SVECW (A)

Contents

Self-compacting Concrete Using Tobacco Waste Ash	1
K. Ashwin Thammaiah, P. Manu Prasad, C. N. Nishchel, Ravi S. Ballavur, and Y. M. Rohith	
Shear Strengthening of RC Beams by NSM Technique Using GFRP Strips for Sustainable and Resilient Infrastructure	15
T. Rashmi, Y. Kusuma, V. Nikitha Anand, and N. C. Balaji	
3D Concrete Printing Technology Current Progress and Future Perspective: A State-of-the-Art Review	27
C. Venkata Siva Rama Prasad	
A BIM-Based Approach of Electrical Network Analysis and Applications Using GIS Tools	41
V Tejaswini, P. Kesava Rao, E. N. Dhanamjaya Rao, R. Nagaraja, S. K. Sinha, and K. S. Rajan	
Generation of LOD-2 3D Building Models from High-resolution Stereo Satellite Data Using Remote Sensing and Photogrammetry	53
Venkumahanti Tejaswini, Pyla Kesava Rao, E. N. Dhanamjaya Rao, Ravoori Nagaraja, S. K. Sinha, and K. S. Rajan	
Experimental Investigations on Flexural Behaviour of Steel Fibres Reinforced Quaternary Blended Self-compacting Concrete Slabs Using Mineral Admixtures	65
G. Sree Lakshmi Devi, C. Venkata Siva Rama Prasad, and P. Srinivasa Rao	
Influence of Mineral Admixtures and M-Sand on Fresh and Hardened Properties of Self-Compacting Concrete	77
S. Bhavanishankar, N. Jayaramappa, C. V. Sai Nagendra, and C. Venkata Siva Rama Prasad	

Experimental Investigation on Compressive Strength and Permeability of Pervious Concrete Pavement (PCP) with Alternative Mixes	91
Pala Gireesh Kumar, Abhirami Priyanka Pathivada, and Velugoti Sasi Jyothshima Himaja	
Evaluation of Functional Effectiveness of Speed Humps in Accordance to IRC Specifications	105
Satya Ranjan Samal, Malaya Mohanty, Pala Gireesh Kumar, and S. Moses Santhakumar	
An Endeavor for Accomplishing GFRG Panel as a Load-Bearing Member in Civil Engineering	115
V. Johnpaul, N. Balasundaram, K. Ramadevi, M. Jemimah Carmichael, and S. Solai Mathi	
Comparative Study of Regular and Irregular Buildings Using Framed Tube Structure and Viscous Dampers	123
Abdul Rahman Khan and G. Sathya Prakash	
The Application of Statistics and Fuzzy Logic in Predicting Slope Stability	137
Arunav Chakraborty and Anasuya Goswami	
Utilization of Red Mud as Sustainable Material: A State of Art Review	149
Akhilesh Buxi Pattanaik and Lasyamayee Garanayak	
Usage of Polyacrylic Acid in Cold Mix Applications: A Review	161
Vikram Patel, Jayesh Juremalani, and S. Shankar	
Self-healing Concrete Based on Bacteria for Sustainable Infrastructure: A State-of-the-Art Review	171
Chiranjeevi Rahul Rollakanti and Kota Srinivasu	
Digital Concrete for Sustainable Construction Industry: A State-of-the-Art Review	183
Chiranjeevi Rahul Rollakanti, C. Venkata Siva Rama Prasad, and Adams Joe	
Identification and Ranking of Construction Productivity Factors in Construction Projects in Wilayah A’Seeb	197
Salim Abdullah Salim Al Sinaidi and Kiran Kumar Poloju	
Performance of Pervious Concrete as a Sustainable Alternative toward Green Infrastructure Using Marginal Aggregates	209
Barnali Debnath and Partha Pratim Sarkar	
A Study on Urban Heat Island Using Geospatial Techniques	221
N. Haripavan, Nisha Radhakrishnan, and D. Kannamma	

A Comprehensive Study on Vehicular Pollution and Predictive Simulation—A Review 231
 Pala Gireesh Kumar, Abhirami Priyanka Pathivada, and Musini Tejaswi

Intelligent Traffic Control System for Smart Transportation—A Way Forward 241
 Pala Gireesh Kumar, Gudimetla Likhitha, Inapagolla Teja Sahithi, Bandi Lavanya Reddy, and Poliseti Sunyuha

Performance Evaluation of Potassium Based Additives for Black Cotton Soil Stabilization 251
 N. Mallikarjuna and K. S. R. Prasad

Possible Utilization of Expansive Soil Incorporated with Bagasse Ash and Bagasse Fibre 263
 J. Harisha Deepthi and S. Satish

Improving the Geotechnical Properties of Silty Sands by Using GGBS and Coir Fibre 277
 G. Hima Bindu and V. Mallikarjuna

Mode Choice Model Development for the Effect of Road Transport Service on Air Travel Demand—A Case Study from Jumla to Nepalgunj, Nepal 289
 Vidya Rajesh, Yagendra Dharala, Prabesh Adhikari, and Sathees Kumar

Analyzing the Demand and Pattern of Electric-Rickshaw Trips: En Route to Sustainable Travel Option 303
 Sandeep Singh and S. Moses Santhakumar

Compressive Strength of Quaternary Blended Self-Compacting Concrete Made with Supplementary Cementitious Materials Through Regression Analysis 317
 G. Sree Lakshmi Devi, C. Venkata Siva Rama Prasad, and P. Srinivasa Rao

Analysis and Comparison of RCC and Steel–Concrete Composite High Rise Buildings 331
 Mahmoud Magdi Eldeib and Kiran Kumar Poloju

A Study on Deformation Characteristics of Splice Connection in Steel Structures 341
 V. Ramana Kollipara, T. D. Gunneswara Rao, and P. Sridhar

A Comparative Study on Strength Characteristics of Fiber Reinforced Geoactivator Activated Geopolymer Concrete 353
 S. Jagandas, G. Mallikarjuna Rao, and M. Venu

Stone Crushers: A Technical Review on Significant Part of Construction Industry 365
 Shubhangi Gurway and Padmanabh Gadge

3D Concrete Printing in Construction Industry—A State of the Art 385
 Harika Sesetti, Muthina Venu Lalithya, and Pala Gireesh Kumar

Effect of Steel–Polyester Fiber Combination on the Fresh and Mechanical Properties of Concrete 397
 S. Sathish, C. Chella Gifta, and K. Sharmila Devi

Modal Analysis of Bridges with New Concretes: Replacing the Regular Construction Material Under the Action of Seismic Load 411
 Nilanjan Tarafder, Endow Mazumder, and L. V. M. Prasad

Effect of Speed Calming Measures on Vehicular Speed for Rural Roads 431
 Kuldeep, Akshata Badiger, M. R. Archana, and V. Anjaneyappa

Engineering Properties of Concrete Containing Hazardous Drywalls Waste and GGBS 443
 T. Raghavendra, H. P. Vageesh, M. Lokeshwari, S. Sunil, and L. Durga Prashanth

Mechanical Properties of an Industrial Waste Concrete with Self-compacting Geopolymerization 457
 Endow Mazumder, Nilanjan Tarafder, and L. V. M. Prasad

Workers Safety at Indian Construction Sites—A Survey 467
 M. V. Krishna Rao, G. Tarun, and V. Hari Leela

Sediment Transport Modelling in Stream Flow by HEC-RAS Model—A State-of-the-Art 481
 Bahnisikha Das and T. Senthil Vadivel

Application of Waste Tyre Rubber Crumbs in Strengthening of Bituminous Roads 493
 Santanu Haldar, T. Senthil Vadivel, and Sukanta Das

Effect of Fly Ash Inclusion on Fresh and Hardened Properties of Concrete: A Review 505
 Subhadip Pramanik, Shashwati Soumya Pradhan, and Umesh Mishra

Flexural Performance of Steel Fibre Reinforced Ternary Concrete Slabs 517
 V. B. Reddy Suda

Influential Factors and Facilities of Pedestrian Crossings in Heterogeneous Traffic Conditions at Unsignalized Intersections—A Comprehensive Review 527
Pala Gireesh Kumar and Abhirami Priyanka Pathivada

Study on Characteristics of Geopolymer Concrete 539
Ward Nasser Al Banna and Kiran Kumar Poloju

A Machine Learning Perspective for Remote Sensing 553
Nagendra Panini Challa, Parupally Sridhar, and J. S. Shyam Mohan

A Review on Structural Stabilization and Strengthening Through Retrofitting 561
Pala Gireesh Kumar and Sahitya Yeegalapati

Performance Analysis of Jute Fiber Reinforced Concrete Composite ... 577
Bidhan Ghosh and T. Senthil Vadivel

Numerical Investigation on the Flexural Behaviour of CFRP Strengthened Steel Pipes 589
A. Cyril Thomas, Mubashir Qayoom, S. Manoranjith, K. Madhan Kumar, and N. Praveen Kumar

Traffic Crowd Assessment and Placing of Traffic Signal at Unsignalized Intersection—A State of Art 601
Pala Gireesh Kumar, Satya Ranjan Samal, and Abhirami Priyanka Pathivada

Stabilization of Marine Clay Using Palm Bunch Ash 613
Bernard Oruabena, Okoh Elechi, Ebiteisintei Nelson, Okiridu Ugochukwu, and George Deinbofa

About the Editors

Dr. Pala Gireesh Kumar Head and Associate Professor of Department of Civil Engineering, Shri Vishnu Engineering College for Women (Autonomous), Bhimavaram, has obtained his B.E. (Civil Engineering) from Sri Venkateswara University College of Engineering Tirupati, India; Masters in Transportation Engineering and Management from National Institute of Technology Tiruchirappalli (NITT), India and Ph.D. in Civil Engineering from National Institute of Technology Tiruchirappalli (NITT), India. He was honored with a National Award from the Government of Tamil Nadu for the best project during the year 2014, Best Paper Award received for the Paper presented in International Conference (FEAST 2018), NIT Trichy, and also won the International Best Researcher Award of the year 2020 in the area of Terramechanics and Nano Materials in Pavements from Idamas Learning Center, Malaysia and World Research Council (WRC). He holds the position as a National Advisory Committee member of the International Conference on “Advancements and Innovations in Civil Engineering” (IC-AICE-2021). Dr. Pala was induced as the Editorial board member of *Journal of Review in Science and Engineering* and also a reviewer of the Transportation Research Board (TRB), *International Journal of Engineering Sciences Advanced Computing & Bio-Technology* (IJESACBT), *Global Journal of Research in Engineering*, USA, *Silicon Journal* and two more journals. Besides all, Dr. Pala is the Ambassador of PROCEDIA, the Conference Managing System, representing India. He has blazoned 18 publications at International Conferences, 15 plus at National Conferences, 30 plus Publications in well reputed international and national journals, and a monograph titled *Speed Detection and Management—An ITS Application*, with Lambert Publishers, UK and authored two book chapters as well. Dr. Pala successfully organized two editions of Conference Series on Sustainable Construction Technologies and Advancements in Civil Engineering and was the mastermind behind the milestone success. Dr. Pala’s area of interest relates to Terramechanics and Nano Materials in Pavements, Traffic Safety, Pedestrian and Driver Behaviour Analysis, Self Healing Pavements, Pavement Evaluation, and Management, and Traffic Simulation.

Prof. Kolluru V. L. Subramaniam Professor of Department of Civil Engineering, Indian Institute of Technology Hyderabad, has obtained his B.E. (Civil Engineering) from Indian Institute of Technology Delhi, India; M.S. from University of Toledo, Toledo, USA and Ph.D. from Northwestern University, Evanston, USA. He was awarded Teaching Excellence Award in IIT Hyderabad (2011 and 2016), Outstanding Young Researcher Award & Catell Research Fellow award in 2006, Early Career Award from National Science Foundation of USA in 2003, ASCE Faculty Award from City College of New York in 2003, ACI—James Instrument Award in 1999 for research in Nondestructive Testing of Concrete and Walter P. Murphy Fellowship from Northwestern University (1995–1996). Prof. Subramaniam fashioned the position of Editorial Board Member of *Cement and Concrete Composites* (Elsevier), Associate Editor of *Journal of Materials in Civil Engineering* (ASCE) from 2004–2010. 2018–current, Associate Editor of *Journal of Bridge Engineering* (ASCE) in 2009 and a Guest Editor of *International Journal for Computational Methods in Engineering Science and Mechanics* in 2014. He has 45 publications at International and National Conferences, 90 plus Publications in well reputed international and national journals and authored two book chapters as well. Professor Subramaniam's areas of interest are behavior of concrete and masonry structures; alkali-activated binders and geopolymers; rheology control and 3D printing; fiber-reinforced concrete; sensor development for concrete structures and infrastructure monitoring; low-cost housing solutions with prefabricated elements; and repair systems and strengthening of concrete.

Prof. S. Moses Santhakumar Professor of Department of Civil Engineering, National Institute of Technology, Tiruchirappalli, has obtained his B.E. (Civil Engineering), Masters (Transportation Engineering) and Ph.D. (Transportation Engineering) from Indian Institute of Technology, Madras. He holds lifetime membership in Indian Roads Congress, ISTE, Institute of Urban Transport, and also a member of Highway Research Board & Institution of Engineers. Professor Moses has 10 publications in International and 19 publications in National journals. He has about 47 articles published in National Conferences and 14 in International Conferences. Professor Moses is known for his expertise in consultancy works and has successfully completed 13 consultancy activities. In addition, he has a major advancement in the field of sponsored research activities that included Indo-German Project on Transportation System Management for Indian Cities, DOD Project on Sea Trial of Wave Energy Device at the Ocean Engineering Centre, MHRD Project on Strengthening of the Transportation Engineering Laboratory, Election Commission Project on Computerization of Electoral Process, AICTE Project on Multimedia Tools for Teaching of Civil Engineering, MHRD Project on GIS-GPS Based Monitoring of Public Transport Vehicles, DRD Project on On-line Monitoring of Rural Development Schemes (ongoing), NRRDA Responsibility of Scrutiny of PMGSY Project Proposals (ongoing), NRRDA Project on Traffic Volume Studies on PMGSY Roads (ongoing), NRRDA Project on Rural Road Pavement Performance Study (ongoing) and, Coir Board Project on Coir Geotextiles for Rural Roads

(ongoing). Professor Moses research interests comprehends CAD in Transportation Engineering, Transportation Planning, Computer Simulation and GIS.

Dr. Neelima Satyam D. Head and Associate Professor of Department of Civil Engineering, Indian Institute of Technology Indore, has obtained her B.E. (Civil Engineering) from Sri Venkateswara University, Tirupati, India; Masters (Geotechnical Engineering) and Ph.D. (Civil Engineering) from Indian Institute of Technology Delhi. Dr. Neelima was honoured with numerous awards embracing CIDC Vishwakarma Academician Award 2021 from Construction Industry Development Council, Overseas famous scientist project from Ministry of Science and Technology, Guangdong, China (2020–2021), JSPS Research Fellow Award from University of Tokyo (2012–2013), Career Award for Young Teachers (CAYT) from AICTE in 2012, Young Engineers Award from The Institution of Engineers (India) in 2011, Young Scientist Research Award, BRNS from Department of Atomic Energy in 2011, Young Woman Engineer award from INWES-International Network of Women Engineers and Scientists in 2012 and Best technical paper award from IGC (IIT Madras, Chennai) for the Innovations in field exploration and In situ testing in 2006. In addition to the honours and achievements, Dr. Neelima holds membership in American Concrete Institute, Institution of Engineers (India), American Society of Civil Engineering, Earthquake Engineering Research Institute, International Geosynthetics Society (India), International Society for Rock Mechanics and Rock Engineering (India), International Society for Soil Mechanics and Geotechnical Engineering, and Engineering Council of India. She is also a life member of Association of Consulting Civil Engineers (India), Indian Science Congress Association, Indian Society for Technical Education, Indian Concrete Institute, Indian Society of Engineering Geology, Indian Society of Earthquake Technology, European Geosciences Union (EGU), and Indian Geotechnical society. She has published 39 articles in international and national journals and seven articles in conference proceedings. Dr. Neelima's area of research interest includes geotechnical earthquake engineering, dynamic soil structure interaction analysis, liquefaction hazard and mitigation, environmental geotechnics, landslide research and rock mechanics and underground structures.

Self-compacting Concrete Using Tobacco Waste Ash



K. Ashwin Thammaiah, P. Manu Prasad, C. N. Nishchel, Ravi S. Ballavur, and Y. M. Rohith

Abstract The present experimental investigation is an effort to understand characteristics of Tobacco Waste Ash and to examine fresh and hardened state characteristics of self-compacting concrete manufactured using Tobacco Waste Ash as a partial replacement for cement. Tobacco Waste Ash is an industrial by-product that is considered as a waste but has the potential to be utilized as partial replacement for cement thereby reducing cement demand and contributing towards sustainability. Energy Dispersive X-ray Analysis is performed to have a knowledge of elemental composition of tobacco waste ash along with cement and fly ash. Nan Su's method of mix design is followed to proportion self-compacting concrete. Optimum replacement percentage corresponding to maximum compressive strength is determined by partially replacing cement with tobacco waste ash at 10, 12, 14, 16, 20, 25 and 30%. Fresh state properties are assessed by Slump flow test, L-box test, V-funnel test and U-box test and later hardened concrete properties are determined. The results indicated an improvement in fresh state properties like cohesiveness and segregation resistance and also had positive effect on hardened properties like compressive, flexural tensile and split tensile strength when cement is replaced at optimum replacement percentage.

Keywords Self-compacting concrete · Tobacco waste ash · Supplementary cementitious materials · Optimum replacement percentage

K. Ashwin Thammaiah (✉) · P. Manu Prasad · C. N. Nishchel · R. S. Ballavur · Y. M. Rohith
Department of Civil Engineering, Rashtreeya Vidyalaya College of Engineering, Bengaluru,
Karnataka 560059, India
e-mail: ashwinthammaiahk@rvce.edu.in

P. Manu Prasad
e-mail: manuprasadp.cv17@rvce.edu.in

C. N. Nishchel
e-mail: nishchelcn.cv17@rvce.edu.in

R. S. Ballavur
e-mail: ravisballavur.cv17@rvce.edu.in

Y. M. Rohith
e-mail: rohithym.cv17@rvce.edu.in

1 Introduction

In early 1980s the construction sector began to emerge as a prominent sector in the society, and subsequently, the need for quality concrete grew rapidly. But, the issue of concrete structures long term durability had become a significant problem in the construction industry together with the reduction in availability of skilled workers. As an attempt to overcome this problem, Okamura proposed a type of High-Performance Concrete known as self-compacting concrete in the year 1986 in Japan with the first prototype being developed in 1988 [1, 2]. SCC was the greatest discovery in Concrete Technology which overcame the drawbacks of ordinary concrete like ability to fill and pass along with segregation resistance. SCC is a type of concrete that can easily flow into sections that are narrow and heavily reinforced by the virtue of its own weight without the need for any kind of external or internal mechanical vibration. To achieve these rheological properties, it is necessary to have high percentage of fines like cement in the mix, but this being uneconomical it is also undesirable considering its effect on concrete and environment [3].

The annual production of cement worldwide in 2020 was 4.1 billion tonnes and by 2050 this is further estimated to increase upto 5.8 billion tonnes. India is the second-largest producer of cement worldwide with an annual production of 329 million tonnes whereas in terms of consumption India stands at 327 million tonnes in the 2020 and is expected that by 2025 it may rise to 550 million tonnes. A new way to satisfy this spiking demand for cement is to increase the use of SCMs, pozzolans or fines in production of concrete and at the same time, there is need to unlock new SCMs. Reduced carbon footprint of SCMs results in lesser impact on environment than OPC [4]. Partial replacement of cement with SCMs is an economical way to produce durable concrete [5]. The rising pressure for sustainable waste management and resource efficiency is a pressing issue. Another solution to this is the use of industrial and agro by-products which are generally considered as waste as they reduce cement demand and contribute to sustainability. Greener and sustainable SCC with enhanced properties could be achieved by using agro and industrial by-products [6]. In addition to increased compressive strength, they have reduced materials cost and carbon dioxide emissions which encourages the use of agro-waste ash [7]. Tobacco waste ash is one such material that has the required properties to be used in concrete.

TWA is a by-product from tobacco processing unit obtained by incineration of processing waste which primarily contains ashes of dried tobacco stems and midribs of tobacco leaves. As TWA has lower specific gravity than cement, it increases the paste content per unit volume of concrete and also the unit weight of mortars made with this waste ash is lesser than that of plain cement mortars [4, 8]. The studies have found that it leads to an increase in compressive, flexural tensile and split tensile strength values of the specimens increases by adding 10–12.5% of TWA [5, 9]. Till date a very few researches have been conducted on utilization of tobacco waste ash and its application in concrete.

2 Materials

A good knowledge of various materials and the selection of most suitable material is the first essential step in production of any type of concrete. By proper choice of materials that meet our requirements, we can achieve the desired properties upto a certain limit through conventional concrete. So, materials selection becomes a vital part of production of concrete.

2.1 Cement

53 Grade Ordinary Portland Cement (OPC) that conforms to IS: 12269-2013 was utilized in the mix and tests were performed in accordance to IS: 4031 (Part V)–1988. The cement used had a specific gravity of 3.048 and had an initial setting time of 185 min and a final setting time of 315 min.

2.2 Fly Ash

The adverse effects of high cement content in concrete and also on environment can be reduced utilization of alternate materials like this. Class F fly ash is utilized in the mix and it is found to have a specific gravity of 1.97.

2.3 Tobacco Waste Ash

TWA is relatively a new material and most of its characteristics are still unexplored. So initially the materials' specific gravity was tested using kerosene to prevent any reaction that might take place between them during testing. Specific gravity of TWA was 2.42 which is lesser than that of cement but is more than that of fly ash.

2.4 Fine Aggregate

The fine aggregate used in mix is manufactured sand. They are inert in nature and act as filler and give bulk to the concrete. They are prepared by crushing the hard stones such as granite, trap, basalt, etc. The properties are listed in Table 1 and were tested as per the standard procedure coated in IS 2386:1983. The fineness modulus of fine aggregates was determined to be 2.699 and as per IS specifications they corresponded to Zone-II.

Table 1 Fine and coarse aggregate properties

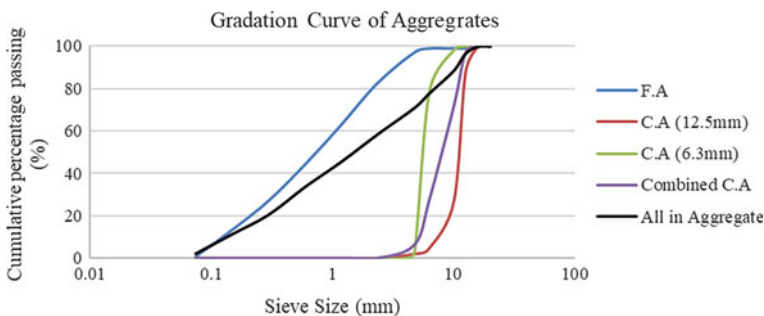
Sl. No.	Properties	Result	
		Fine aggregate	Coarse aggregate
1	Specific gravity	2.692	2.602
2	Water absorption (%)	3.92	0.799
3	Bulk density of loose aggregate (kg/m ³)	1674	1415
4	Bulk density of compacted aggregate (kg/m ³)	1858	1505

2.5 Coarse Aggregate

In SCC the coarse aggregate size is usually restricted to maximum of 20 mm. In structures with congested reinforcement, 10 mm size aggregate suits the best. However, when the reinforcement spacing is high 20 mm size aggregates can be used whenever. Well graded cubical or rounded aggregate best suits the requirement of SCC. In the present study, 12.5 mm and 6.3 mm nominal size granite stone aggregates are used. The properties were tested as per IS 2386:1983 and are specified below in Table 1 along with fine aggregate properties.

2.6 Sieve Analysis

Sieve analysis was done for fine aggregates, coarse aggregates of 12.5 mm and downsize, coarse aggregates of 6.3 mm and downsize, combined coarse aggregate in which the 12.5 mm and 6.3 mm aggregates were taken in the proportion of 60:40, respectively by weight and then combined coarse and fine aggregates in the proportion of 43:57, respectively by volume. The gradation curve of all aggregate proportions used is presented in Fig. 1.

**Fig. 1** Gradation curve of aggregates

2.7 Superplasticizer

In our present study Master Glenium SKY 8233 was the superplasticizer used, which conforms to the specifications of IS:9103–1999 and its specific gravity is 1.08. It is a polycarboxylic ether based new generation superplasticizer. The dosage of superplasticizer was determined by performing Marsh cone test and was found to be 0.3%.

3 Methodology

The following sections explain the methodology adopted for design of SCC using TWA, sample preparation and testing procedures.

3.1 Energy Dispersive X-ray Analysis

To understand the elemental composition of TWA, EDAX test was performed on it. Along with TWA, EDAX test was also conducted on cement and fly ash as it would serve as a reference in analysing the characteristics of TWA. Energy Dispersive X-Ray Analysis works on the principle that X-ray is a type of high energy electromagnetic radiation when incident on an atom of the material, core electrons gets ejected. The electron removed from the atom creates a vacant space in the stable system which can be occupied by another electron of higher energy and this is accompanied by release of energy which is unique to each element of periodic table. Using this principle, it is possible to identify various elements present in a material along with the proportion in which each individual element exists. The EDAX spectrum of all the three materials can be seen in Figs. 2, 3 and 4. The quantitative results of EDAX tests present the weight percentage and atomic percentages of various elements present in a sample and are presented in Table 2. From quantitative results, it can be inferred that cement has highest percentage of elemental calcium which makes it hydraulic in nature. TWA also has good amount of elemental calcium but is slightly lower in comparison to cement. This calcium can help in improving the properties of concrete

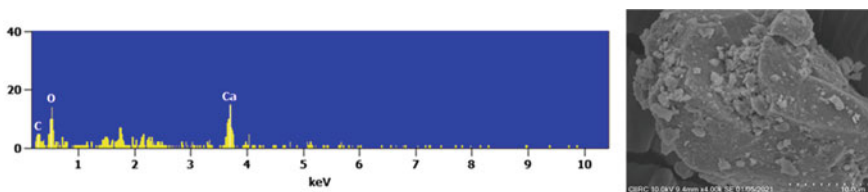


Fig. 2 EDAX spectrum and SEM image of cement

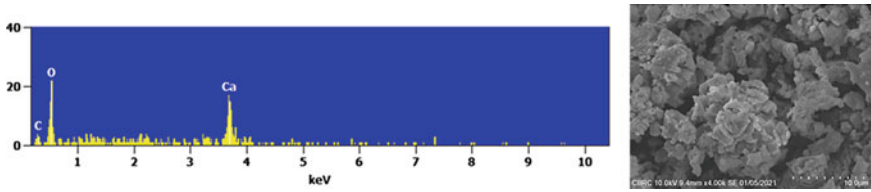


Fig. 3 EDAX spectrum and SEM image of TWA

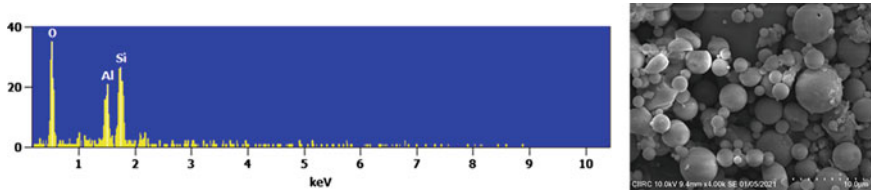


Fig. 4 EDAX spectrum and SEM image of fly ash

Table 2 Quantitative results of EDAX test on cement

Elements	Weight %	Atom %	Weight %	Atom %	Weight %	Atom %
	Cement		TWA		Fly Ash	
C K	2.13	5.16	1.12	2.56	–	–
Ca K	76.24	55.43	69.48	47.31	–	–
O K	21.63	39.40	29.39	50.13	29.22	41.69
Al K	–	–	–	–	23.32	19.74
Si K	–	–	–	–	47.46	38.57
Total	100.00	100.00	100.00	100.00	100.00	100.00

when cement is partially replaced with TWA. Further, it is understood from the spectrum that the amount of silicon and aluminium is less in cement and negligible in TWA. This implies that TWA may only be slightly pozzolanic in nature due to low silicon and aluminium elemental percentages. It is not mentioned in the quantitative results as its percentage is relatively in comparison to quantity of other elements. However, in fly ash, the elemental composition of silicon and aluminium is high which makes it evident that it is pozzolanic in nature while the amount of elemental calcium is very less so it is not mentioned in quantitative results. Along with these results, SEM images of cement, TWA and fly ash were captured. Figures 2, 3 and 4, respectively show the images of particles of these materials at a magnification of 10 microns. From these figures, it can be seen that TWA and fly ash particle sizes are lesser than cement at same magnification level. This implies that they are finer than cement and can fill up the voids in them making concrete more impermeable

and durable. Also, it can be seen that the fly ash particle shape is spherical and this enhances rheology of fresh concrete by ball bearing effect.

3.2 Determination of W/C Ratio

Trial mixes were prepared with different w/c ratios ranging between 0.35 and 0.45 which is said to be an ideal range and water content is not allowed to exceed 210 L/m³ as per EFNARC guidelines [6, 10]. Based on the slump flow, cohesiveness of the mixes and visible bleeding if any, a w/c ratio of 0.40 was selected for design of SCC.

3.3 Determination of Optimum Replacement Percentage

Literature review suggests that for most of the materials the graph of mineral admixture replacement of cement versus its compressive strength follows as optimal curve. The compressive strength reaches a maximum value at certain point of replacement than the rest and value corresponding to that strength is known as optimum replacement percentage. Initially, eight different mortars including control mix were prepared by replacing OPC with TWA by 10, 12, 14, 16, 20, 25 and 30%. 70.6 mm size mortar cubes were cast at first. After curing it for 14 days, compressive strength test was done. Then using these results, concrete cubes of 100 mm size were cast using three different replacement percentages which had higher mortar compressive strength than the rest. Finally, among these three one was selected as optimum replacement percentage which yielded the highest compressive strength of concrete.

3.4 Mix Proportioning

The materials characteristics were tested first, then using these results a trial mix was designed to determine the w/c ratio. Final mix was designed using the selected w/c ratio and correspondingly proportion of various materials was calculated. For proportioning of SCC, Nan Su's method of mix design was adopted. The value of Nan Su's coefficient was taken as 10, a packing factor of 1.06 and ratio of fine to total aggregates by volume is considered as 0.57 and it ranges between 0.50 and 0.57 in Nan Su's method [2]. The mix proportions of control SCC mix and SCC with optimum TWA is presented in Table 3.

Table 3 Mix proportions

Mix	Water (kg/m ³)	Cement (kg/m ³)	Fly ash (kg/m ³)	TWA (kg/m ³)	Fine Agg. (kg/m ³)	Coarse Agg. (kg/m ³)	Superplasticizer dosage (%)
Control Mix	199.13	432.5	65.34	–	1011.43	645.18	0.3
SCC TWA	199.13	380.6	65.34	51.9	1011.43	645.18	0.3

3.5 Tests on Fresh Concrete

Fresh state properties of SCC were tested as per the standard specifications provided in EFNARC guidelines. After the concrete was mixed it was immediately used for testing as delaying it causes a change in fresh state characteristics. Slump flow test, L-Box, V-Funnel, U-Box and segregation resistance test was conducted on fresh mix.

3.6 Casting of Concrete Specimens

After quickly assessing the fresh state characteristics, the same concrete sample was used for casting cubes, beams and cylinders. Moulds were previously prepared and the inner surfaces were oiled so that concrete does not adhere to the surface. Cubes of 100 mm size, cylinders of 200 mm height and 100 mm diameter and beams of size 100 mm × 100 mm × 500 mm were cast. Concrete was left to harden for a day as superplasticizer was used, later demoulded and immersion curing was done to test the hardened properties of SCC.

3.7 Tests on Hardened Concrete

Hardened state characteristics is also a significant part of SCC as a concrete with good fresh state properties but uncertain hardened properties would not have much significance. So, it is essential for SCC to have required hardened properties along with good fresh characteristics. The compressive, flexural tensile and split tensile strength of hardened concrete was tested as per standard guidelines.

4 Results and Discussion

The optimum replacement percentage and test results of fresh and hardened concrete are discussed in the upcoming sections.

4.1 Optimum Replacement Percentage

Mortar cubes of 70.6 mm size were cast with various replacement percentages and compression test was conducted on these mortar cubes at an age of 14 days and variation in compressive strength is shown in Fig. 5.

The graph shows that average mortar compressive strength is highest for the replacement percentage of OPC with TWA in the range of 10–14%. Beyond 14% the compressive strength starts to reduce gradually at a study rate and decreases at a higher rate when replacement is increased beyond 25% upto 30%. At 25% replacement, the compressive strength is almost same as that of the control mix mortar. But it is difficult to conclude the optimum value from the graph as there does not exist a single. So further three concrete mixes containing 10%, 12% and 14% TWA were prepared along with control mix and 100 mm size cubes were cast whose compressive strength was tested after curing for 7 and 28 days. The comparison of 7 days and 28 days compressive strength is presented in Fig. 6.

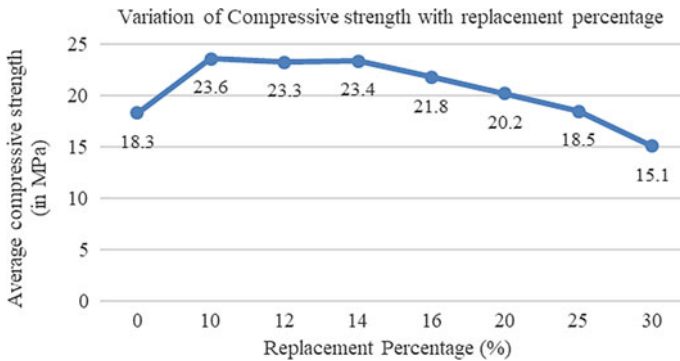
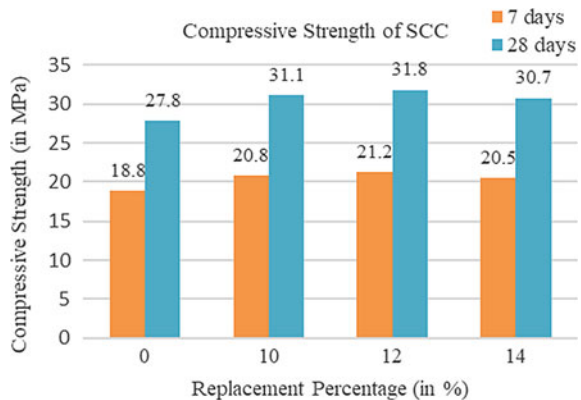


Fig. 5 Variation of compressive strength of mortar cube with replacement percentage

Fig. 6 Comparison of compressive strength of SCC at various replacement percentages



The results show that compressive strength of concrete is maximum at a replacement level of 12% compared to the rest. This implies that optimum replacement percentage of OPC with TWA is 12% by weight. In upcoming sections, SCC containing 12% TWA as replacement for OPC will be denoted as SCC TWA.

4.2 Fresh Concrete Properties

Various tests conducted on fresh state SCC is presented in Fig. 7 and their outcomes are listed in Table 4. Slump flow of SCC containing TWA was less than that of control mix. But even though there is a reduction in slump flow, by visible observation we were able to identify that SCC containing TWA was more cohesive, resistant to segregation and also has good viscosity. The results of T_{500} was parallel to slump flow and as SCC TWA had higher cohesiveness and viscosity it takes more time to reach the 500 mm spread circle in comparison to control mix but both the results were found to be within the specified range.

The time taken by concrete to empty V-Funnel was higher for SCC TWA. Small flow time does not alone mean good filling ability, but as V-Funnel flow time also gives an indication of plastic viscosity to a certain extent, it can be inferred that SCC TWA has higher viscosity than the control mix. Further flow time after 5 min was



Fig. 7 Tests on fresh concrete: slump flow, V-Funnel, L-Box and U-Box test, respectively

Table 4 Fresh state properties of SCC

Test method	Control mix	SCC TWA	EFNARC recommendations
Slump flow (in mm)	690	640	550–850
T_{500} (in s)	3.2	4.6	>2
V-Funnel (in s)	8.3	10.7	6–12
V-Funnel $T_{5 \text{ min}}$ (in s)	10.4	11.9	Increase upto 3 s in V-funnel flow time
L-box (H_2/H_1)	0.89	0.84	0.8–1.0
U-box ($H_2 - H_1$)	22	26	0–30
Sieve segregation resistance (in %)	16.3	12.4	0–20

also tested. This gives an indication of segregation of concrete. As the control mix was less cohesive and viscous, the increase in flow time was higher after 5 min due to slight segregation compared to SCC TWA which had only slight increase in flow time which indicates that it is less prone to segregation.

The ratio of heights of concrete flow is higher for control mix, still slight segregation of aggregates was observed behind the rebars. However, the mix was uniform over the total length of flow in case of SCC TWA and despite lower height ratio, it had good passing ability. The results were found to be within the range specified by EFNARC.

The difference between the results of U-Box test of SCC TWA and control mix is not very high. In control mix, upward flow of concrete is due to lower viscosity of control mix while SCC TWA flows uniformly upward in the adjacent section as a cohesive mix maintaining homogeneity.

The sieve segregation test results were found to lie within the range specified by EFNARC guidelines. The results indicated that SCC TWA has higher segregation resistance and visible observations helped to identify that the water retention ability of SCC TWA was improved in comparison to control mix.

4.3 Hardened Concrete Properties

Curing of casted cubes, beams and cylinders was done by immersing in water so that the concrete gets required moisture and temperature to develop strength. Due to the prevailing pandemic situation, it was unable to test the hardened concrete after 7 and 28 days of curing but were rather tested at an age of 60 days and results are listed in Table 5.

Based on these results it is noticed that 60 days average concrete compressive strength with optimum replacement percentage of TWA is about +13.59% higher than the control mix which does not contain any amount of TWA. The chemical characterization results have shown that TWA contains good amount of elemental calcium and also its particles are fine than that of cement. So, the increase in strength of concrete containing TWA can be presumed to be result of filler effect and nucleation by TWA.

Cylinders of height 200 mm and diameter 100 mm were used for split tensile test at 60 days age. From the results, it is noticed that there is an increment in split tensile strength of about +5.1% in SCC containing 12% TWA in comparison with control mix.

Table 5 Hardened state properties of SCC

Mix type	Compressive strength (MPa)	Split tensile strength (MPa)	Flexural strength (MPa)
Control Mix	33.1	2.94	1.78
SCC TWA	37.6	3.09	1.84

Beams of length 500 mm, width 100 mm and depth 100 mm was tested at the age of 60 days to obtain the flexural tensile strength of SCC by application of two-point loading. An increase in only about +3.3% was noticed in the flexural strength of SCC containing 12% TWA in comparison with control mix.

5 Conclusions

From the key findings of this experimental investigation we were able to draw the following conclusions:

- Nan Su's method of mix design is a simple tool to proportion SCC mixes. Based on our results we were able to identify that this method yields low paste volumes which affect the target strength of SCC. It is balanced using TWA as partial replacement for OPC that has lower specific gravity than cement, which increases the amount of powder content per cubic meter of concrete
- TWA enhances the rheological properties of SCC in fresh state by improving the cohesiveness, segregation resistance, water retention ability and passing ability due to its increased fineness and lower specific gravity than cement
- The strength of SCC at early ages is lower than the target strength due to the utilization of fly ash but later increases beyond the age of 28 days. The designed target strength of SCC is achieved at an age of 60 days
- The increase in compressive strength of SCC by TWA in addition to that of OPC is attributed to its filler effect and nucleation in SCC
- At 12% replacement of OPC with TWA the compressive strength of cubes increases by +13.59%, split tensile strength of cylinder specimen increases by +5.1% and flexural tensile strength of beams is found to increase by +3.3% in comparison to the control mix with no TWA
- TWA can be effectively utilized in SCC as a partial replacement for OPC to enhance its rheological and mechanical properties provided it is replaced at optimum percentage.

References

1. Okamura H, Ouchi M (2003) Self compacting concrete. *J Adv Concr Technol* 1(1):5–15
2. Su N, Hsu KC, Chai HW (2001) A simple mix design method for self-compacting concrete. *Cem Concr Res* 31(12):1799–1807. [https://doi.org/10.1016/S0008-8846\(01\)00566-X](https://doi.org/10.1016/S0008-8846(01)00566-X)
3. Gesoğlu M, Güneyisi E, Kocabağ ME, Bayram V, Mermerdaş K (2012) Fresh and hardened characteristics of self compacting concretes made with combined use of marble powder, limestone filler, and fly ash. *Constr Build Mater* 37:160–170. <https://doi.org/10.1016/j.conbuildmat.2012.07.092>
4. Juenger M, Provis JL, Elsen J (2012) Supplementary cementitious materials for concrete: characterization needs. *Mater Res Soc Online Proc Library* 1488:8–22

5. Su N, Miao B (2003) A new method for the mix design of medium strength flowing concrete with low cement content. *Cement Concr Compos* 31(2):215–222
6. Kumar KR, Shyamala G, Awoyera PO et al (2020) Cleaner production of self-compacting concrete with selected industrial rejects-an overview. *SILICON*. <https://doi.org/10.1007/s12633-020-00636-6>
7. Moreno P, Fragozo R, Vesga S et al (2018) Tobacco waste ash: a promising supplementary cementitious material. *Int J Energy Environ Eng* 9(4):499–504
8. Celikten S, Canbaz M (2017) A study on the usage of tobacco waste ash as a mineral admixture in concrete technology. In: Paper presented at the international conference on engineering technologies, Konya, Turkey, pp 545–548
9. Kumar N, Vivekananthan V, Chithra P (2019) Study the effects of tobacco waste ash and waste glass powder as a partial replacement of cement on strength characteristics of concrete. *Int J Multidisciplinary Res Trans* 1(1):1–8
10. The Self-Compacting Concrete European Project Group (2005) The European guidelines for self-compacting concrete may, 1-63 May 2005

Shear Strengthening of RC Beams by NSM Technique Using GFRP Strips for Sustainable and Resilient Infrastructure



T. Rashmi, Y. Kusuma, V. Nikitha Anand, and N. C. Balaji

Abstract Infrastructure must be resilient to changing environments while utilising limited resources in a sustainable manner. Existing structural components need to be strengthened due to increase in the load demand on the building, changes in the use of the structure, design and construction faults, environmental factors, resulting in a longer service life. This paper describes the NSM-FRP is utilised to improve the shear performance of reinforced beams. Studying the behaviour of control beam (CB) with the shear enhanced beam. In this work RC beams were divided into control beam, strengthened beams with NSM-FRP at an angle of 60° and 75° in different spacings. Load bearing capacity, deflection at mid-span and quarter-span, cracking pattern, and various types of failure were among the test findings.

Keywords Shear strengthening · NSM-FRP · NSM orientation

1 Introduction

Enhancing of reinforced beams are frequently required owing to a variety of causes, including a load demand on the building, alterations in the structure's use, design and construction faults. The beam should be strengthened for flexure as well as shear in regaining beam load capacity while retaining flexibility. RC beams can be improved using a variety of techniques, including jacketing and externally bonded reinforcement (EBR). More recently, an alternative use of EBR method, to improve the beam's shear strength, near surface mounted (NSM) FRP bars and strips are used. The NSM method entails cutting grooves on both sides of the beam, and the GFRP is inserted at the intervals within the filling element used particularly epoxy. NSM technique is most effective method opted for enhancing the performance of deteriorated RC segment, due to resistance to corrosion and simplicity in construction. De Lorenziset al. [1] NSM reinforcement has the benefits of being more resistant to debonding, being easier to anchor into adjacent structural members, it's notably beneficial for fortifying slab and beam negative moment zones. Rashmi et al. [2]

T. Rashmi (✉) · Y. Kusuma · V. Nikitha Anand · N. C. Balaji
Department of Civil Engineering, The National Institute of Engineering, Mysuru, India

Shear strengthening is much effective when the NSM method was used. The ultimate load of RC beams reinforced with NSM outperformed that of the CB. When compared to 90° direction, the reinforced beams with 45° angled GFRP have a higher shear bearing capability. Andrea Rizzo et al. [3] the beam enhanced with externally bonded U-wrapped composite increased its shear capacity by around 16%, while the beams reinforced with NSM increased their shear capacity by 22–44%. Sabol et al. [4] the NSM technique is clearly an efficient means of shear strengthening structural members, results of experimental study, quantitative simulation and research methods. Parvin et al. [5] NSM-FRP strengthening may achieve greater stresses than EBR, increase the efficiency use of the FRP component and improved RC beam bending and shear capabilities along with flexibility.

2 Details and Experimental Program on the Specimens

The size of the beam considered for this analysis is 150 mm × 150 mm × 700 mm. The beams were made to be under-reinforced. 2 bars of $\Phi = 10$ mm were placed in the tension zone, and 2 bars of $\Phi = 8$ mm were placed on compression zone. Shear reinforcement was provided by 2LVS of $\Phi = 8$ mm at 100 mm spacing. Beams enhanced with GFRP strips, and 2 beams have been chosen as reference beams and designated as control beams in group A. Group B beams have NSM orientation 60° and varying with groove spacing's 8 and 50 mm. Group C beams have NSM orientation 75° and varying with groove spacing's 100 and 60 mm. Table 1 depicts the designation of shear strengthened beam. The groove's minimum depth must be equivalent to the total of the strip width plus 3 mm, and the groove's minimum width must be equivalent to the total of the strip thickness plus 3 mm, epoxy thickness is

Table 1 Details of the reinforced concrete beam testing programme

Group	Beam designation	Cases of beams	Groove angle	Number of strips	Spacing of GFRP (mm)
A	CB	Control beam			
B	B4S60	Enhanced beams	60	GFRP strip = 2 × 4 (2 × 12 mm ²)	80
	B6S60		60	GFRP strip = 2 × 6 (2 × 12 mm ²)	50
C	B4S75		75	GFRP strip = 2 × 4 (2 × 12 mm ²)	100
	B6S75		75	GFRP strip = 2 × 6 (2 × 12 mm ²)	60

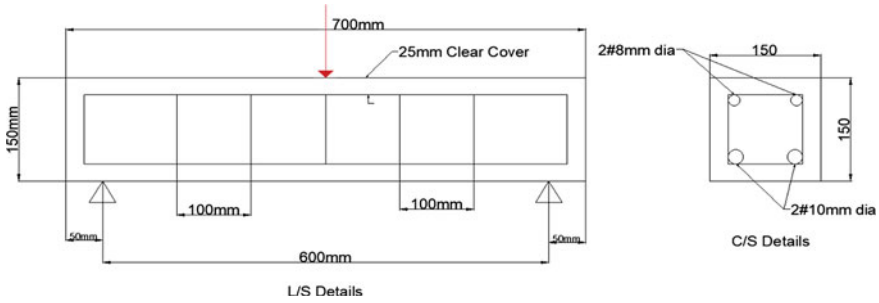


Fig. 1 RC beam sectional details

1 mm to 2 mm. 18 mm and 7 mm have been chosen as the groove depth and width, respectively. RC beam detailing can be seen in Fig. 1.

3 Procedure for NSM Strengthening

NSM technique is followed by the following steps in the experimental study: (a) Saw cutting machines are used to cut grooves. (b) Cutting of GFRP. (c) Epoxy resin and hardener were combined correctly in a 1:9 ratio. (d) Grooves must be free from the fine particles and dust before filling of epoxy hence grooves are cleaned using wire brush. (e) Epoxy resin was used to fill the grooves to slightly more than one-fourth depth. (f) GFRP strips were pushed into the grooves. (g) Excess adhesive should be removed and the surface should be levelled. (h) After that, the beams were painted white to study the crack patterns.

4 Test Setup

The test equipment comprises of a UTM with a load carrying capacity of 100Ton, which is used to evaluate the shear resistance capacity of beams. Figure 2 represents a bending test with a total span of 600 mm that was done using single-point loads under simply supported conditions. The related mid-span deflection, quarter span deflection, crack pattern, mode of failure, first crack load, ultimate capacity, and deformation measurement at reference locations were observed and investigated for each increment in load. Figure 2 represents two 0.01 mm deflection gauges set at mid-span and quarter span to measure deflection at regular intervals, and they are located at soffit of the beam. The strain reference points that are placed on the side face along each neutral axis of the beam at a gauge length of 200 mm that was used to measure linear deformation using a demountable mechanical strain gauge with a least count of 0.002 mm.

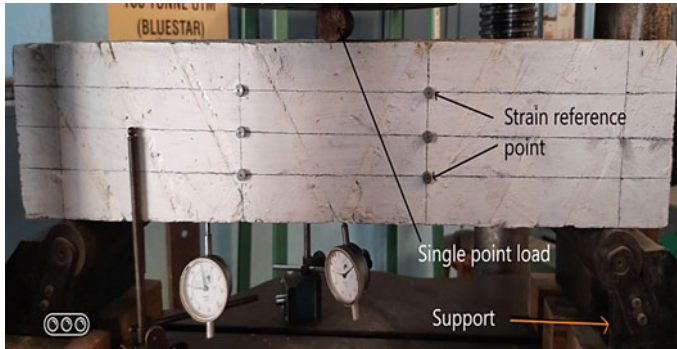


Fig. 2 Experimental test set-up

5 Results and Discussions

5.1 Behaviour of Load Deflection and Crack Pattern

Single-point loading was applied to determine the shear capacity of CB, B4S60, B6S60, B4S75 and B6S75 beam specimens. Table 2 shows the mid-span deflections, first crack load, ultimate load for test specimens. Figure 3 depicts the crack pattern of all the tested specimens. The outcomes of the enhanced beams are analysed to a CB result.

5.2 Control Beam (CB)

Initial crack formed at even a load of 25 kN, and since the load starts to rise, more vertical cracks appeared. Figure 3 shows the crack pattern. Whenever the load increases to 60 kN, the cracks started to expand, and the dial gauges were removed. At 75 kN, the mid-span and quarter span deflections were 2.95 mm and 2.2 mm, respectively, with a corresponding strain of 1.2×10^{-3} . Due to the combined impact of flexure and shear, the beam failed at a load of 75 kN.

5.3 B4S60 Strengthened Beam

At a load of 50 kN, a hairline crack began to propagate in the beam B4S60, and these cracks propagated from the bottom mid-span to the top fibre, resulting in a shear crack. Figure 3 depicts the crack pattern of beam B4S60. Due to the combined impact of shear and flexure, as the load was raised beyond 85 kN, a diagonal shear crack

Table 2 Experimental outcomes of tested specimens

Beam designation	Initial crack load (kN)	Service load (kN)	Ultimate load (kN)	Ultimate shear (kN)	Ultimate deflection (mm)		Ultimate tensile strain (10^{-3})	Increase in service load (%)	Increase in ultimate shear capacity (%)
					Mid-span	Quarter span			
CB	25	70	75	37.5	2.95	2.2	1.2	-	-
B4S60	50	98.2	130	65	3.6	2.25	1.7	40.3	73.33
B6S60	50	80	120	60	3.9	3.4	1.72	14.3	60
B4S75	40	80	110	55	4	2.9	1.2	14.3	40
B6S75	35	78	100	50	3.5	2.4	0.98	11.4	33.33

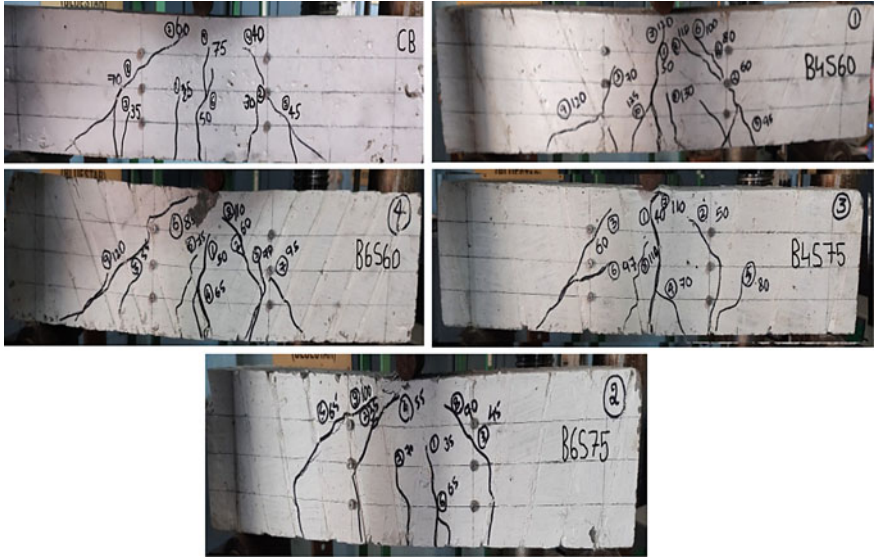


Fig. 3 Crack pattern for tested beams

developed and propagated from the support to the top mid-span. Beyond 105 kN, the crack began to widen, and the deflection gauge was removed. Under a concentrated load of 130 kN, mainly as a result of flexure and shear. Table 2 indicates the tabulated outcomes of an experiment. As indicated in Fig. 4 at a load of 15kN, the CB beam begins to deflect, while the strengthened beam B4S60 begins to deflect at a load of 30 kN. As a consequence, the enhanced beam can withstand double the load of the CB. The ultimate load deflection capacity is 3.6 mm, that was 22.1% higher from the CB. The beam B4S60 which is strengthened for shear increases the load at

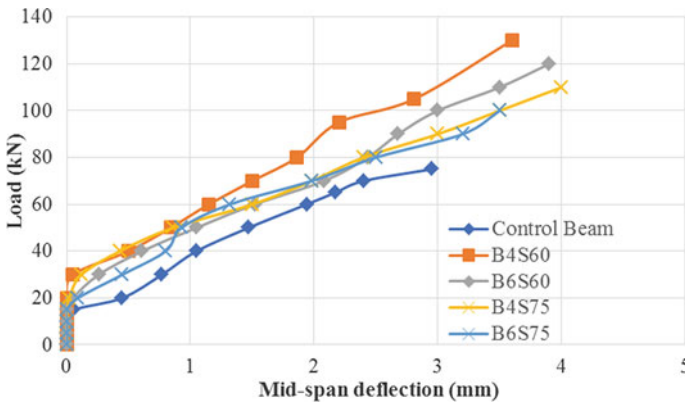


Fig. 4 Mid-span load–deflection

3.6 mm deflection and ultimate shear capacity by 40.3% and 73.3% when compared to control beam.

5.4 *B6S60 Strengthened Beam*

At a load of 50 kN, a hairline crack began to propagate in the beam B6S60, and these cracks propagated from the bottom mid-span to the top fibre, resulting in a shear crack. Figure 3 depicts the crack pattern of beam B6S60. Due to the combined impact of shear and flexure, as the load was raised beyond 75 kN, a diagonal shear crack developed and propagated from the support to the top mid-span. Beyond 95 kN, the crack began to widen, and the deflection gauge was removed. Under a concentrated load of 120 kN, mainly as a result of flexure and shear, Table 2 indicates the tabulated outcomes of an experiment. As indicated in Fig. 4 at a load of 15 kN, the CB beam begins to deflect, while the strengthened beam B6S60 begins to deflect at a load of 20 kN. As a consequence, the enhanced beam can withstand 1.3 times more load of the CB beam. The maximum load deflection capacity was 3.9 mm, which is 32.2% higher than the CB beam. The beam B6S60 which is strengthened for shear increases the load at 3.9 mm deflection and ultimate shear capacity by 14.3 and 60% when compared to control beam.

5.5 *B4S75 Strengthened Beam*

At a load of 40 kN, a hairline crack began to propagate in the beam B4S75, and these cracks propagated from the bottom mid-span to the top fibre, resulting in a shear crack. Figure 3 depicts the crack pattern of beam B4S75. Due to the combined impact of shear and flexure, as the load was raised beyond 65 kN, a diagonal shear crack developed and propagated towards the GFRP strips. Beyond 85 kN, the crack began to widen, and the deflection gauge was removed. Under a concentrated load of 110 kN, mainly as a result of flexure and shear. Table 2 indicates the tabulated outcomes of an experiment. As indicated in Fig. 4 at a load of 15 kN, the CB beam begins to deflect, while the strengthened beam B4S75 begins to deflect at a load of 20 kN. As a consequence, the enhanced beam can withstand 1.3 times more load of the CB beam. The maximum load deflection capacity was 4 mm, which is 35.6% higher than the CB beam. The beam B4S75 which is strengthened for shear increases the load at 4 mm deflection and ultimate shear capacity by 14.3 and 46.7% when compared to control beam.

5.6 B6S75 Strengthened Beam

At a load of 35 kN, a hairline crack began to propagate in the beam B6S75, and these cracks propagated from the bottom mid-span to the top fibre, resulting in a shear crack. Figure 3 depicts the crack pattern of beam B6S75. Due to the combined impact of shear and flexure, as the load was raised beyond 60 kN, a diagonal shear crack developed and propagated towards the GFRP strips. Beyond 75 kN, the crack began to widen, and the deflection gauge was removed. Under a concentrated load of 100 kN, mainly as a result of flexure and shear, Table 2 indicates the tabulated outcomes of an experiment. As indicated in Fig. 4 at a load of 15 kN, the CB beam begins to deflect, while the strengthened beam B6S75 begins to deflect at a load of 20 kN. As a consequence, the enhanced beam can withstand 1.3 times more load of the CB beam. The maximum load deflection capacity is 3.5 mm, that was 18.6% higher from the CB. The beam B6S75 which is strengthened for shear increases the load at 3.5 mm deflection and ultimate shear capacity by 11.4% and 33.3% when compared to control beam (Figs. 5 and 6).

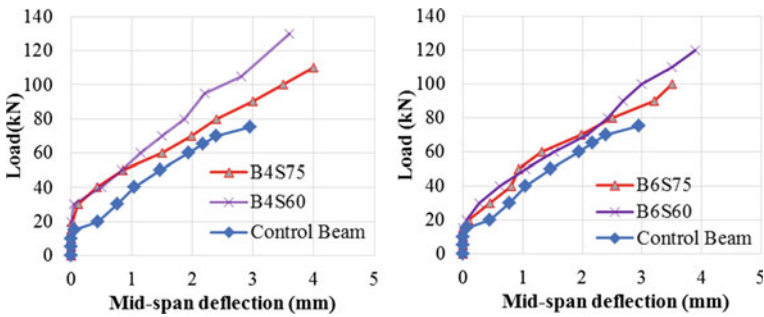


Fig. 5 Load–deflection of NSM orientation

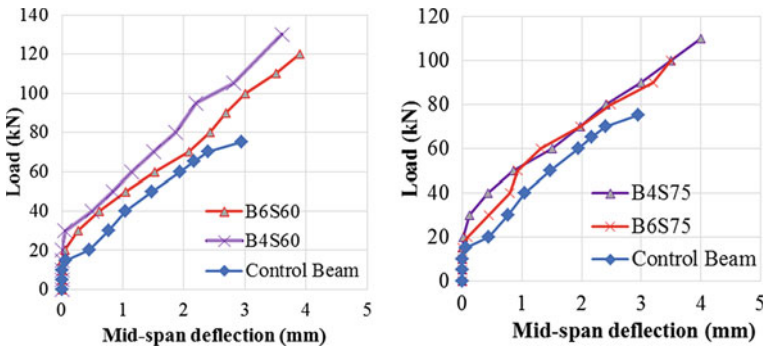


Fig. 6 Load–deflection at various spacing's of NSM

Table 3 Compares the effects of NSM orientation on enhanced beams

Designated Beams	B4S60	B4S75	B6S60	B6S75
NSM orientation (degree)	60°	75°	60°	75°
Initial Crack Load (kN)	50	40	50	35
Ratio	1.25		1.43	
Load bearing capacity (%)	73.33	46.7	60	33.33
Initial deflection (kN)	30	20	25	20
Ratio	1.5		1.25	
Service Load (kN)	98.2	80	80	78
Over 60° NSM orientation increase in service load (%)	40.3		14.3	

6 Effects of NSM Orientation

The beams are shear strengthened with NSM orientation of 60° and 75° with respect to beam axis. The experimental results of strengthened beams B4S60 and B4S75 are compared, the load carrying capability increased by 73.3% and 46.7%, respectively, when the inclination of NSM was changed between 60° and 75°. Table 3 compares the effects of inclination of NSM on enhanced beams. For beams B6S60 and B6S75 shows the load carrying capability increased by 60% and 33.33%, respectively. In comparison to beams strengthened with 75° NSM orientation, 60° angled GFRP increased shear bearing capacity. The 60° angled strips outperformed the 75° angled GFRP.

7 Effect of GFRP Strip Spacing on Strengthened Beams

As seen on above Table 4, reducing the beam spacing from 80 to 50 mm improved

Table 4 Compares the effect of GFRP strip spacing on strengthened beams

Designated Beams	B4S60	B6S60	B4S75	B6S75
GFRP strips, NSM orientation	4-60°	6-60°	4-75°	6-75°
GFRP spacing (mm)	80	50	100	60
Initial Crack Load (kN)	50	50	40	35
Ratio	1		1.14	
Load bearing capacity (%)	73.33	60	46.7	33.33
Initial deflection (kN)	30	25	20	20
Ratio	1.2		1	
Service Load (kN)	98.2	80	80	78
Increase in service load over 80 and 100 mm spacing (%)	22.75		2.6	

Table 5 The effect of GFRP-enhanced beams

RC beams	Shear force, V_r (kN)	$V_c + V_s$ (kN)	Effect of GFRP, V_{frp} (kN)
CB	45	45	–
B4S60	78	45	33
B6S60	72	45	27
B4S75	66	45	21
B6S75	60	45	15

load bearing capacity by 73.33% and 60%, accordingly. The load at initial crack in beam B4S60 and B6S60 was 50kN, as shown in Table 4. NSM strips with 80 mm spacing carry a higher load than those with 50 mm spacing. As indicated in Table 4, reducing the beam spacing from 100 to 60 mm improved load bearing capacity by 46.7 and 33.3%, accordingly, for beams B6S60 and B6S75. The load at initial crack in beam B4S75 and B6S75 was 40kN and 35kN, correspondingly, while the initial crack load for 100 mm spacing beam B4S75 was 1.14 times slower than for B6S75.

8 The Effect of GFRP—Enhanced Beams

The shear bearing capacity of the reinforced beam was determined using ACI 440 [6].

$V_r = 0.6 \times$ maximum force. The effects of GFRP to the enhanced beam are seen in Table 5

$$V_r = V_c + V_s + V_{frp} \quad (1)$$

where, V_c = concrete contribution, V_s = steel rebars contribution and V_{frp} = FRP strips contribution.

9 Stress–Strain Behaviour of Tested Beams

The shear stresses for RC beams were calculated using the incremental load equation; the limiting maximum shear stress as per IS specification with reference to grade M30 is 3.5 N/mm², so the evaluated shear stress at a specific load (25 kN) was 3.33 N/mm², and the corresponding strains were marked, which were then compared to strengthened beams. Figure 7 indicates a shear stress strain curve for B4S60, as well as a similar graph are obtained for all tested specimens. Table 6 displays the stress–strain values of all the beams that were tested.

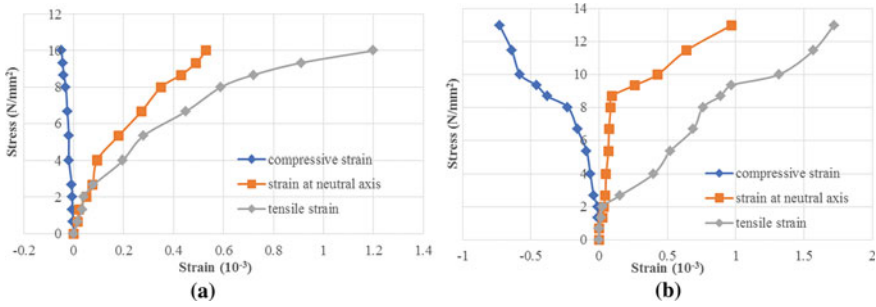


Fig. 7 Shear stress versus shear strain for **a** CB, **b** B4S60

Table 6 Stress strain values of all tested specimens

Beam designations	Nominal shear stress as per IS 456	Shear stress $\tau = \text{Fay/Ib}$	Compression strain (10^{-3})	Strain at Neutral Axis (10^{-3})	Tensile strain (10^{-3})
CB	0.690	3.330	-0.012	0.045	0.13
B4S60	0.690	3.330	-0.05	0.05	0.25
B6S60	0.690	3.330	-0.033	0.054	0.12
B4S75	0.690	3.330	-0.06	0.043	0.06
B6S75	0.690	3.330	-0.06	0.045	0.07

10 Conclusion

An experiment using GFRP strips and the NSM method to strengthen RC beams in shear. The aim of this experiment was to show the effects of the orientation and spacing of the GFRP strips. The final conclusion may be taken from the experiment’s study results:

- Shear strengthening was more effective when the NSM technique was used. The shear capacity of reinforced beam with NSM outperformed that of the CB.
- In the case of strengthened beams, various properties such as load at initial crack, ultimate shear capacity, deflection, and stress–strain relationship are enhanced.
- The deflection of all enhanced specimens was less than the CB for a given load. In comparison to 75° NSM oriented beams, B4S60 and B6S60 beams showed better deflection control.
- When compared to 75° NSM orientation, the strengthened beams with 60° inclined GFRP strips have a higher shear carrying capacity.
- As the NSM orientation was changed from 60° to 75°, shear capacity increased by 73.33% and 46.7%, respectively, when compared to the CB.
- When compared to the control beam, B4S60 showed a 73.33% increase in shear capacity.

- In comparison to 75° GFRP strips, 60° inclined strips were more effective in strengthening beams. This is mostly owing to the fact that the direction of 60° angle GFRP is perpendicular to the inclination of crack failures due to shear, limiting shear crack development due to stress and therefore delaying shear crack propagation.
- By changing the beam spacing of GFRP strips in 60° and 75° NSM orientations increases load bearing capacity, service load, deflection and prevent cracks.
- By changing the spacing of GFRP strips on a strengthened beam with a 60° NSM orientation, the service load is increased 1.3 times and the shear capacity is increased by 22.2%. As a consequence, the B4S60 beam's shear capacity was enhanced.
- The reinforced beam offers the advantage of strain than the CB. Strain resistance is a characteristic of GFRP strips. 60° NSM orientation demonstrated superior strain resistance than 75° NSM orientation.

References

1. De Lorenzis L, Teng JG (2006) Near-surface mounted FRP reinforcement: an emerging technique for strengthening structures. *Compos B Eng* 38(2):119–143
2. Rashmi M, Nikitha Anand V, Balaji NC (2020) Shear strengthening of RC beams using near surface mounted technique with glass fiber reinforced polymer. In: AIP conference proceedings 2327, 020012
3. Rizzo A, De Lorenzis L (2009) Behavior and capacity of RC beams strengthened in shear with NSM FRP reinforcement. *Constr Build Mat* 23:1555–1567
4. Sabola P, Priganc S (2013) Shear strengthening of concrete members using NSM method. Department of Concrete and Masonry Structures, Institute of Structural Engineering, Faculty of Civil Engineering, Technical University of Kosice
5. Parvin A, Shah TS (2016) Fiber reinforced polymer strengthening of structures by near-surface mounting method. The University of Toledo, Toledo, OH 43606, USA
6. ACI Committee 440 (2002) Guide for the design and construction of externally bonded FRP systems for strengthening concrete structures

3D Concrete Printing Technology Current Progress and Future Perspective: A State-of-the-Art Review



C. Venkata Siva Rama Prasad

Abstract 3D printing is a transformative window of opportunity to have a tremendous economic and societal influence over the next years. The technique, originally contained in the production of tiny objects, developed shape in the 1980s and moves into large-scale building application using concrete and additional cement and binding materials. This article offers state-of-the-art 3D concrete printing achievements in the field of equipment, materials and computer modeling. There will be several demonstration projects and potential and difficulties related to 3D concrete printing will be explored. Formulation of ink using local and local products is and will continue to be a serious difficulty. Further developments in large-scale 3D printers will continue. The review should be fascinating both to experienced engineers and beginners in 3D printing, even those focusing mostly on transition through current study to implementation of 3D printing in construction. This content covers evolution of 3D printing concrete with regard to its functionality, mechanical features and the construction plan, in attempt to implement 3D printed concrete reachable thoroughly. Furthermore, the applications of 3D printed concrete and its development have also been highlighted.

Keywords 3D concrete · Digital concrete · 3D concrete printing technology · Construction techniques · 3D concrete buildings · Additive manufacturing

1 Introduction

The first 3D printer, created in 1984, has become one of the fastest developing technologies in the recent decades. It was highly complex in the beginning and, furthermore, costly machinery. Since decades, 3D printing began to be widespread in all sorts of areas of business and printers were often utilized. Much has been accomplished in the medical, automobile and aerospace industries. Open source solutions make the development of new products, as well as creative 3D printing applications,

C. Venkata Siva Rama Prasad (✉)
Department of Civil Engineering, St. Peter's Engineering College (Autonomous),
Maisammaguda, Dhulapally, Medchal (Dist), Hyderabad, Telangana 500100, India

available to everybody in many areas. The aim for many firms in various industries all over the world was to improve the printing material and 3D technology. Real change in the building business began in 2014, when the first home was printed and a new building technology chapter began. There has been significant talk, in particular in recent years, about the lack of innovation in the construction business [1]. The productivity of the construction industry has remained constant, or even decreased, as compared to other sectors (for example manufacturing and agriculture) which have witnessed a notable rise in productivity in the last two decades. A recent thorough McKinsey research identified many major initiatives to solve this productivity gap, including the integration of digital technologies, novel materials and enhanced automation. Many new developments that have transformed others have slowly been adopted by the construction industry. Newer trends have suggested that digitalization, new materials and technology and sophisticated automation are progressing in the sector [2]. For example, the relatively quick use of BIMs, particularly in East Asian locations like Singapore, has proven the prospective to transform the whole building sector in the form of digital technology. This highlighted the potential of RILEM which was held in Zürich, Switzerland in September 2018 and which has led to new innovations in digital manufacturing techniques like 3D printing with concrete and additional additive manufacturing procedures.

With 40% of the industry participants, the construction industry has taken note, and it would seem that most observers, as well as many other academic and industrial conferences on this issue, concur on the inevitability of the digitization progress. In this document we reiterate the reasoning behind digital concrete manufacture, and subsequently highlight the latest developments in the field of digital concrete manufacture, which are rapidly developing, as regards (1) material and processing, (2) structure and performance and (3) applications that lead to research. In future, automation of labor in the construction sector looks more probable; given the technical development 3D printing is indeed a noteworthy advancement in today's society and additive production process [3]. Some people feel that the adoption of this skill may lead the way for lower construction costs and timeframes, and permit building at further distant sites and further flexible designs and not just in advance, but also to the revolutionization of the building industry. It also offers some unique sustainable advantages that are not typically present in building. Because of the continuous development of automated 3D printing technologies in order to achieve more efficiency than existing techniques of building, the latest study suggests that construction materials and workforce needs may be significantly cut. Additional production is a technique of producing 3D things by generating additional layers of computer control-guided materials. The first 3D printer produced in 1984 was tried in the early 1980s [4]. To now, 3D construction demonstration projects include the manufacture of structural apparatus, houses etc. As an illustration, a research group from UK has developed 3D modeling that consent to mathematically complicated structures in a computer controlled manner. They were meant to immediately pour concrete without further formworks on the building site. Researchers used robotic weapons to print concrete constructions in various curved forms during testing performed by Loughborough University. In China, research teams use 3D-printed concrete structural

parts to experiment with the building of a whole structure. On a further thriving note, 3D printing technology has evolved to the point where rebar inserted 3D concrete may be printed before the printing process, enabling the reinforcement of 3D printed Beton just as normal reinforcing techniques would enable. Over the last two decades, NASA has supported a number of studies aimed at creating new 3D printing processes that can be used to create structures utilizing alien materials. The development of helpful technology for building off-earth shelters for humans, equipment and the like on the Moon or Mars habitat is predicted to result in this type of work [5]. There are many 3D printing processes, including extrusion, pulver bonding and additive soldering that may be utilized at the building scale. Contour Crafting has been particularly popular among scientific and technical groups, as it permits quick prototyping, manufacture of complicated geometries, multi-material combinations and customization of products. Contour Crafting is a manufacturing method based on extrusion additives, which may be done by several means from gathering materials to stages of heating, prices & technical preparedness, it additionally permits accumulated thick strata of a smooth surface to be finished by putting down wet concrete into a pin and a side sharp bobble [6]. A single storey home constructed in one day with 10,134\$ is an example where Contour Crafting was used (US dollars). The foundation and the walls of this project were printed using the Contour Crafting method, which was continued after the prints of the major buildings, after completion, doors would be fixed. Many engineers foresee a promising future in building for 3D printing, and other industry specialists feel that these technologies can ignite a new manufacturing revolt [7]. Overall, the possible benefits of 3D concrete printing include quicker building, reduced working expenses, higher complexity and precision, increased function integration and less waste-producing utilization of recycled resources. This study highlights contemporary advances in 3D concrete printing research and development, including applications in alien environments [8].

2 3D Concrete Printing Latest Technology and Its Materials

The introduction of additives to synthetic resins, which reasoned the polymerization practice to instigate after the resins were bleached, was the initial step in budding the technique. Stereo lithography is a technology that can craft items with remarkably high exactness and multifaceted geometry, which is why it is utilized in a multiplicity of disciplines such as medicine, the car and aviation industries, and even art and design [9]. Selective laser sintering (SLS) has become a piece of digital in which a light ray is used to merge powder particles collectively to create an object. The materials utilized in SLS technique are typically strong and flexible. Nylon or polystyrene are the most common. Modeling of fused deposition FDM is a technology developed by S. Scott Crump in 1988. Ductile materials are extruded through a double headed nozzle as they solidify throughout the cooling process. The cross-section layers



Fig. 1 Apis Cor house contour crafting [12]

produced from the digital replica supporting the printer are used to deposit both modeling and supporting materials. Resistive heaters in the nozzle keep the filament at the proper melting point, allowing it to flow freely through the nozzle and build the layers [10]. After generating one layer, a platform is lowered and the next layer is constructed, much like in other technologies. This procedure is repeated until the entire object has been finished. Materials commonly utilized in FDM expertise are known as filaments and employed as rolls of thermoplastic products in printers, such as ABS, or PLA, a thermoplastic of a completely different kind. It is biodegradable and better for the planet than ABS. Fused deposition modeling has been in the last two decades the world's most trendy and commonly used 3D printing process. Due to its different qualities and applications, wide-ranging materials were created during the last decades that enable the appearance of wood in the prints [11] (Fig. 1).

In the late 1980s Contour Crafting was initially established, depicted. Adapting the latest technology and advancing 3D printing method (e.g. application of computer-guided grid structure) allows for even quicker, more efficient construction of structures or structural components. Its unique layered production approach also enables constructing components with a rather smooth surface finish. The extruder may be obtained with the application of side sharpening troubles that can be set for the different layer and slope of the surfaces by coerced extruded flow in either horizontal or vertical direction. The outlet comprises of multiple winding systems, one on both sides and one inside a wall. Non-orthogonal surfaces can be produced by bending the dust. Contour Crafting is also able to use aggregates along with fiber enhancements such as additives [13].

D-shaped prints, often used in printing building models, utilize powder deposition, selectively hardened to compact with the desired thickness by applying a binder and fine aggregate layers. A fully built D-formed printing device comprises of about 300 rough shells, which are mounted on an aluminum box. The printer moves across the printed area and deposits binding ingredients during the construction process. Select sections from a loose precipitate deposit are excavated once finished. Ground materials require to be combined with powdered metal oxide beforehand to act in response with the fluid binder applied [14] (Figs. 2 and 3).

Fig. 2 Contour crafting 3D printer [12]



Fig. 3 D-shape 3D printed structure [12]



3 3D PRINTING Construction on MARS

There has been a dramatic increase in human populations on Earth, currently reaching 7.5 billion by 2018, with an estimate of 10 billion by 2056. As human populations increase rapidly and natural resources become apparently depleted, scientists and researchers explore the potential to settle adjacent planets. NASA has financed several research programs over recent decades to create revolutionary 3D printing technology that might potentially be used to construct “off-earth” homes such as Mars habitats. Three major aspects, among others, are addressed while building a shelter or construction on Mars: materials, strength and build ability [15]. First of all, the ideal approach to create a construction on Mars would be to employ local materials because building materials from the Earth would significantly amplify the payload of the rocket. Sulfur concrete can be the best choice for house structures or structural components on Mars. Sulfur concrete is called a “rich-sweetened” planet. Sulfur concrete requires no water but comprises of aggregates and elemental sulfur,

it is also crucial that a structure should be created for its longevity since humans will require high-quality structures for living and working after it reaches the red planet. Computer simulation using finite element modeling can be used, in conjunction with physical testing, for investigating mechanical reactions of structures with varied factors, including ecological loads, that'll be essentially diverse according to planet. Ultimately 3D printing technologies can improve the construction process on Mars, with very limited support for life. While the use of sulfur in concrete is scarcely a novel design as the use of elementary sulfur as a bonding agent has occurred in ancient times, Leonard and Johnson first suggested sulfur concrete as building material for extraterrestrial missions. The ability in extraterrestrial applications of employing sulfur concrete would be one of the key advantages: it could achieve full strength without water over a very short time period. The viability of employing molten sulfur as construction material in lunar structures has been examined in a study carried out by Omar [16]. The fundamental concept of this work was to use indigenous materials more logically than economically in extraterrestrial construction. Sulfur concrete blends with varying sulfur-to-soil ratios conducted series compressive and tensile strength testing to examine minimum sulfur needed for an optimal force. Some of the mixtures have been added to examine the impact of metal and glass fibers on sulfur concrete. An end outcome of this, investigation shows a max 33.8 MPa (4.9 ksi), for sulfur contents of 35% by weight, was the compressive strength of sulfur cement while 45.5 MPa, for a further 2% by weight, was added to the same sulfur concrete (6.6 ksi) [16] (Fig. 4).

Producing Martian concrete through 3D Contour Crafting seems immense budding to building applications in space of a protective protection for astronauts and device covering sheets, taking advantage of indigenously available resources at the Martian market (e.g. sulfur, basalt, etc.). Experimentation on a simple level, the 3D Contour Crafting Auger extruder is used for make Martian cement, include 60% of the Martian regolith stimulant (& 30% elementary sulfur powder). Yuan [40] used the mini-scale augur extruder and novel, complete extrusion extruder to create Martian cement. In the mini-scale method, a revolving auger was added to the



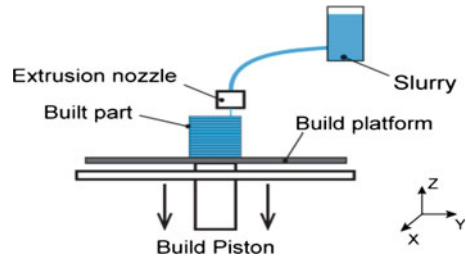
Fig. 4 Construction on Mars using 3D printer [12]

mixture by a funnel to the extrusion tube while heating and maintaining electrical heating elements in the extrusion tube at 140–150 °C (284–302 °F). The researchers mounted a piezo transducer on egg and lateral vibrating piezo on the nozzle outlet to robotically eliminate the bridging consequence and to avoid severe friction in the extrusion process [17]. In order to fully heat the whole mixing and extruder chamber to a specified temperature, a novel blender/extruder combo mechanism has been introduced for complete Contour Crafting. The extruder utilized in the experiment featured a larger container for the treatment of huge quantities of sulfur concrete. The material was pushed down through a mixing mechanism in the top parts as opposed to the mini-scales auger extruder, and the principal extrusion force was delivered by a unique extruder at the end of the tubular [18]. Moreover, the friction of the nozzles walls was much higher than those of the pre-heated or air mix when compared to the mini-scale experiment, because it was totally molten before the nozzle came into contact. To rapidly lower the demand of the releasing ingredient, an aluminum extension end was attached to the pin's exit [19].

4 3D Printing in Concrete Applications in Construction Industry

As NASA's standards on in-situ application of resource application (ISRU) of Mars structural buildings appear to satisfy, the potential for NAS' Mars missions may be large for sulfur concrete built from Martian soil. Recently Wan has undertaken research to create the optimum "martian concrete" mixing ratio, including sulfur element and the JSC Mars-1A Martian simulator rich in metal oxides. Resources of JSC Mars-1A Mixed Sulfur produced by heating of even more than 120 °C (248 °F) were evaluated by researchers in this study. On the basis of compression and tensile tests carried out to assess the strength development, the strength of Martian concrete looked to be double the force of sulfur concrete mixed with regular soil. Analytical analysis also showed the effect of the distribution of the particle size on the ultimate strength of the combination. The finding shows that the optimal mix ratio for Martian concrete and the highest strength was above 50 MPa with a maximum overall size of 1 mm and a 50 percent Martian soil simulator (7.3 ksi). Producing Martian hormigon using 3D-contour production would be quite capable of using local resources on the Martian market, for example, producing a refuge for astronauts and protective hangers for equipment (e.g. sulfur, basalt, etc.). The mini-scale Contour Crafting Auger extruder was used for the small-scale experiment for the construction of Martian cement, consists 60% of Martian regolith (JSC Mar 1, A) & 30% of mostly sulfur powder. Even in case of process of making Martian cement, Yuan used a mini-scale augur extruder and unique, full extruder. A rotating auger was inserted into the combination with a drum on a mini-scale approach, while the extrusion chamber was heater and maintained electrical heating elements at 140–150 °C (284–302 °F) in the extrication chamber. In order to reduce the bridging

Fig. 5 Schematic of extrusion-based technique [21]



effect automatically by a horizontal vibration piezo and to avoid intense friction in the extrusion progression, the researchers attached a piezo transducer on the egg. A new blender/extruder combination mechanism was introduced to complete Contour Crafting in order to fully heat the entire blending and extruder chamber to a set temperature. The extruder used to process enormous amounts of sulfur concrete that was equipped with a large container [20].

5 Latest 3D Concrete Printing Technologies in the World

In recent times, various 3DCP methods to apply AM in concrete building have been created. Such solutions are primarily focused on different approaches, specifically, extruder & powder-based technologies. These methodologies are discussed in the following sub-sections. The resemblance and variation between the various 3DCP technologies and merits and cons have been emphasized.

5.1 Extrusion-Based Method

The extruded method is similar to the fused deposit modeling (FDM) method within this cemented material is extruded from a nozzle attached to the portal grid, or 6-axis robot arm in order to build a building step by step. This approach has been intended for construction purposes in the field, construction works includes intricate geometry and huge budding to contribute significantly to the construction sector. Figure 1 illustrates a drawing of powder-based approach (Fig. 5).

5.2 Contour Crafting Method

University of Southern California, USA, has created Contour Crafting (CC) technology. This equipment uses the extrusion technique to extrude a vertical concrete

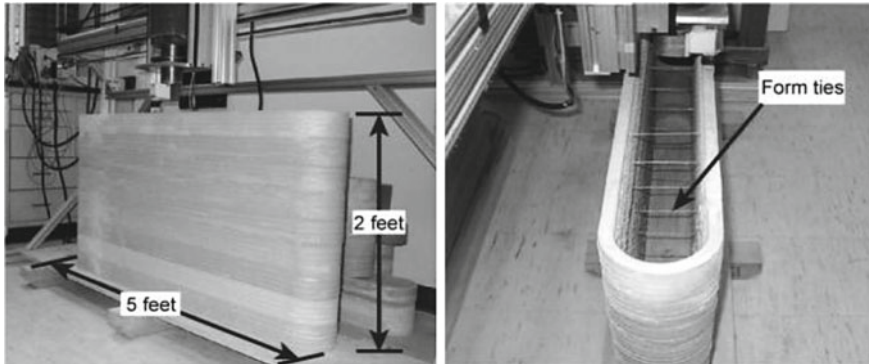


Fig. 6 A CC machine-fabricated concrete wall block with custom-made reinforcing ties manually placed within layers [12]

shaping by two layers of cement mix. Manually custom constructed ties of reinforcement are placed (horizontally and vertically every 30 and 13 cm), while the device extrudes the layers constantly. Smoothly extruded surfaces are connected to the print head. After finishing the extruded shape, the concrete is next sprayed manually to 13 cm high and after a hour, the very first batch is sprayed, with such a second batch and the lateral pressure of the concrete can be controlled by allowing a one-hour batch to partially heal and solidify. The CC machine creates a concrete wall form (Fig. 6).

5.3 Concrete Printing Method

A team of Loughborough University in the UK has been developed for concrete printing technology. The technology likewise utilizes a technology based on extrusion and is related to CC technology to a certain extent. The 3D printing method nevertheless been created keeps 3D mobility and has reduced deposition resolution, allowing for more flexibility of inside and outer geometry. Furthermore, the material used for concrete printing is fiber-reinforced, high performance finely aggregated concrete with greater material qualities than those achieved using CC technique [22]. A full scale bench produced with concrete printing is shown in below figure. The bench had a length of 2 m and a max width 0.9 mts and ht 0.8 m. The bank consists of 12 vectors which minimizes weight and could be used for additional construction services as an acoustic structure, thermal isolation and/or path. The bank also shows a strengthening technique in which properly selected void shape leads for post-reinforcement positioning (Fig. 7).



Fig. 7 Concrete printing created a full-scale bench with usable voids and post-tensioned reinforcing [21]

5.4 Concrete On-Site 3D Printing

The use of novel and sophisticated machines, the small mineral aggregates (fine aggregate mortar instead of concrete), and the small sizes of printed items Contour Crafting and Concrete Printing equipments show numerous technological benefits and are subject to certain inherent limitations (i.e. specifically, the 3D printer's length must be greater than the size of the element to be generated). To get over these restrictions, the TU Dresden, German, is now developing the new approach to 3DCP on-site construction technology called CONPrint3D, which aims to direct 3DCP to building sites. High geometric freedom, utilization of commonly used building tools and low dependence on professional labor constitute the key benefits of CONPrint3D technology. CONPrint3D focuses not only on developing improved construction processes that are time, work and efficient on resources but also on making the new process cost-effective while increasing the acceptability of existing industry professionals. This is achieved through as far as feasible the use of existing construction and fabrication processes and the adaptation of the new process to building restrictions. One key feature is the adaptation of concrete pump autonomously and accurately provides material to particular positions utilizing a specialized printer head attached to the boom.

5.5 3DCP Using Ultra-High Performance Concrete in Large Scale Construction Industry

In France, a research team was able to offer a novel method with UHPC on awareness due to constraints observed in listed CC and concrete printing methods. The method



Fig. 8 Multifunctional wall element [21]

employed to deposition UHPC layer via an extrusion printed head installed on a 6-axis robotic arm uses the extrusion-based technique. Major advantages of the proposed technology is (1) that 3D printed georamas not relying on temporary aids can be produced, (2) that 3D printing can be fully utilized by using the tangential continuity method of slicing, leading to mechanically sound structural designs.

The technology being proposed produced the “multifunctional wall element” (Fig. 5) consisting an absorbent shape that may be either filled with UHPC components and insulated material such as thermal insulation material. Few portions have been deliberately left empty to accommodate pipes or electrical cables. The wall element manufacture with a weight of $1360 \text{ mm} = 1500 \text{ mm}/170 \text{ mm}$, took around 12 h (for 139 layers), with a weight of 450 kg (Fig. 8).

6 Conclusions

- Additional building component manufacturing is moderately novel but may provide an innovative technique to build architectural and structural components. 3D printing technology offers a great budding for solving several problems in the construction sector, e.g., time consumption, wasteful building approaches etc.
- While 3D printing technology is at an early level, lots of academics suppose it will open new doors to generating new trends that will make building more cost-effective, sustainable, eco-friendly and speedier.
- Worldwide research is undertaken to improve efficiency, bonding & application of 3D printed concrete structures. Furthermore, attempts are being made to produce 3D printed concrete standards/specifications in order to commence and proceed toward codal provisions of the 3D printing concrete construction.
- Use of minerals & contour manufacturing in more ways shows promise, other essential problems, such as building in a low atmosphere and low severity, have yet to be studied.

- Although these challenges still need to be overcome, ongoing research can provide a solution to extraterrestrial shelters on planetary surfaces for human professionals and robotics technology (e.g., radiation from an electromagnetic space etc.). Furthermore, new options for space exploration and the design of space missions are projected to remain.

References

1. Lim S, Buswell RA, Le TT, Austin SA, Gibb AG, Thorpe T (2012) Developments in construction-scale additive manufacturing processes. *Autom Constr* 21:262–268
2. Mechtcherine V, Grafe J, Nerella VN, Spaniol E, Hertel M, Füssel U (2018) 3D-printed steel reinforcement for digital concrete construction—manufacture, mechanical properties and bond behaviour. *Constr Build Mater* 179:125–137
3. Khoshnevis B, Hwang D, Yao KT, Yeh Z (2006) Mega-scale fabrication by contour crafting. *Int J Ind Syst Eng* 1(3):301–320
4. Zhang J, Khoshnevis B (2013) Optimal machine operation planning for construction by contour crafting. *Autom Constr* 29:50–67
5. Mechtcherine V, Nerella VN, Ogura H, Grafe J, Spaniol E, Hertel M, Füssel U (2018) Alternative reinforcements for digital concrete construction. In: RILEM international conference on concrete and digital fabrication. Springer, Cham, pp 167–175
6. Khoshnevis B, Kwon H, Bukkapatnam S (2001) Automated construction using contour crafting. In: 2001 international solid freeform fabrication symposium
7. Nerella VN, Ogura H, Mechtcherine V (2018) Incorporating reinforcement into digital concrete construction. In: Proceedings of IASS annual symposia, vol 2018, no 7. International Association for Shell and Spatial Structures (IASS), pp 1–8
8. Gaget L (2018) Concrete 3D printer: the new challenge of the construction business. In: 3D printers, materials, and technologies
9. Khoshnevis B (2004) Automated construction by contour crafting—related robotics and information technologies. *Autom Constr* 13(1):5–19
10. Hossain M, Zhumabekova A, Paul SC, Kim JR (2020) A review of 3D printing in construction and its impact on the labor market. *Sustainability* 12(20):8492
11. Khoshnevis B, Bukkapatnam S, Kwon H, Saito J (2001) Experimental investigation of contour crafting using ceramics materials. *Rapid Prototyping J*
12. Lee Y-S, Kim S, Hischke G (2018) 3D printing in concrete materials and its applications. *Int J Civil Struct Eng Res* 6:187–195
13. Bester F, van den Heever M, Kruger J, van Zijl G (2020) Reinforcing digitally fabricated concrete: a systems approach review. In: Additive manufacturing, 101737
14. Khajavi SH, Tetik M, Mohite A, Peltokorpi A, Li M, Weng Y, Holmström J (2021) Additive manufacturing in the construction industry: the comparative competitiveness of 3D concrete printing. *Appl Sci* 11(9):3865
15. Buswell RA, Soar RC, Gibb AG, Thorpe A (2007) Freeform construction: mega-scale rapid manufacturing for construction. *Autom Constr* 16(2):224–231
16. Nematollahi B, Xia M, Sanjayan J (2017) Current progress of 3D concrete printing technologies. In: ISARC. Proceedings of the international symposium on automation and robotics in construction, vol 34. IAARC Publications
17. Pegna J (1997) Exploratory investigation of solid freeform construction. *Autom Constr* 5(5):427–437
18. Leonard RS, Johnson SW (1988) Sulfur-based construction materials for lunar construction. In: Engineering, construction, and operations in space. ASCE, pp 1295–1307

19. Ford S, Despeisse M (2016) Additive manufacturing and sustainability: an exploratory study of the advantages and challenges. *J Clean Prod* 137:1573–1587
20. Marchment T, Sanjayan JG, Nematollahi B, Xia M (2019). Interlayer strength of 3D printed concrete: influencing factors and method of enhancing. In: *3D concrete printing technology*. Butterworth-Heinemann, pp 241–264
21. Nematollahi B, Xia M, Sanjayan J (2017) Current progress of 3D concrete printing technologies. In: *34th international symposium on automation and robotics in construction (ISARC 2017)*
22. Al-Qutaifi S, Nazari A, Bagheri A (2018) Mechanical properties of layered geopolymer structures applicable in concrete 3D-printing. *Constr Build Mater* 176:690–699

A BIM-Based Approach of Electrical Network Analysis and Applications Using GIS Tools



V Tejaswini, P. Kesava Rao, E. N. Dhanamjaya Rao, R. Nagaraja, S. K. Sinha, and K. S. Rajan

Abstract Building Information Modeling is a sophisticated technology possessing intellectual tools that help planners and architects to design sustainable buildings and carryout performance analysis based on various aspects. Apart from the existing building elements, a network connecting each building component is of vital importance in order to generate organized plans. Building Information Modeling when embedded with Geographic Information System delivers versatile applications in the world of both Geo Spatial field of studies as well as Architecture, Engineering and Construction Industry. The current research is one such attempt to understand the power of Geographic Information System tools in building models especially in solving complicated network connections. Designing the electrical network and planning the circuitry information in such a way so as to avoid faulty or poor connections in between the inter circuit elements is successfully achieved with the help of

V. Tejaswini (✉)

International Institute of Information Technology (IIIT), Hyderabad, National Institute of Rural Development and Panchayat Raj (NIRDPR), Hyderabad, India
e-mail: tejaswini.v@research.iiit.ac.in

P. Kesava Rao

Centre for Geo Informatics Application in Rural Development (CGARD), National Institute of Rural Development and Panchayat Raj, Hyderabad, India
e-mail: kesava.nird@gov.in

E. N. Dhanamjaya Rao

Department of Geology, Andhra University, Visakhapatnam, Andhra Pradesh, India

R. Nagaraja

Department of Science and Technology, International Institute of Information Technology (IIIT), Hyderabad, India

S. K. Sinha

National Institute for Geo-Informatics Science and Technology (NIGST), Survey of India, Uppal, Hyderabad, India
e-mail: sk.sinha soi@gov.in

K. S. Rajan

Lab for Spatial Informatics, International Institute of Information Technology (IIIT), Gachibowli, Hyderabad, India
e-mail: rajan@iiit.ac.in

this integration. Initially, building model is generated to the high level of detail and electrical fixtures are organized with in a power distribution system using Revit Architecture. The virtual network wiring made in Building model is physically connected using three dimensional Polyline features in Geographic Information System platform and the created Network of electrical elements is utilized for Geometric Network Analysis.

Keywords Building Information Modelling · Geographic Information System · Electrical Network Design · Geometrical Network Analysis

1 Introduction

Building Information Modeling is a single window solution type of technology for multidisciplinary conceptual analysis. There exists an added advantage of combining two or more such standalone technologies such as BIM merged with GIS environment. BIM provides a higher degree of constructability and productivity which aids numerous societal, technical and economic planners [1]. BIM accounts for many applications in the field of AEC Industry with the help of inbuilt Mechanical Electrical and Plumbing MEP tools in Revit Architecture software. BIM particularly in the field of electrical analysis results in Renewable energy potential assessment, coordination and circuit validation [2]. Interoperability is a stage that plays a crucial role in the parameter modeling applications of BIM. The actual and potential value of interoperability is statistically measured based on the type of interaction and depth of impact [3]. The existing research in the field of electrical network analysis of BIM is limited to choose the best software for the use case [4]. A study was implemented with major objectives that provide insight into the future applications of BIM in electrical construction industry based on the survey and validation [5]. BIM has the advantage of facility management and prior simulation to assess and analyze the building design at each stage of construction with the help of automated tools and reliable user interface. Building models with such state of art tools upon integration with powerful GIS tools provide micro level analysis of Geo Spatial data which is the demandable and interesting phase for managers and planners. BIM benefits rich semantic information along with geometric models throughout the building life cycle whereas GIS benefits for geo visualization, decision-making and management of geospatial data [6]. GeoBIM integration generates a strong support for design and planning well organized building models embedded with data interoperability capabilities that would result in various urban and smart city planning projects [7, 8]. A parametric model created in Revit is integrated with 3D GIS using FME by Safe Soft that allows for ease of data interoperability between the two models [9]. BIM-based Electrical System Design ESD in GIS-based smart power system planning provides modeling and design of lighting and power circuitry, connectivity checking and balanced energy model systems [10]. The current study develops a

sustainable construction of building electrical network model and carries out analysis on functionality using the advantages provided by the combined BIM and GIS technologies.

2 BIM for Electrical Network Design (END)

A sustainable building construction can be achieved with the help of advanced BIM tools. Such type of intelligent tools is profoundly incorporated in Autodesk Revit Architecture software. Revit provides an access to the Mechanical Electrical and Plumbing MEP Template wizard for planning and implementing the building design useful for multiple applications related to real-time scenarios. The current study uses Autodesk Revit Architecture software for the construction of Level of Detail LOD4 building model. A group of electrical components are conceptually interconnected for estimation, coordination and manipulation of circuitry information to build electrical system design. The design of electrical network in the two floors of the building model is distributed and the entire work flow of electrical network is shown in Fig. 1.

Initially the detailed building model with inbuilt attribute information is created in Revit software and the thus generated LOD 4 building model is linked to the electrical template. The current building model contains two floors (ground floor and first floor). Each electrical component incorporated into the building model follows a particular hierarchy. The first step for the design contains selection of floors and ceiling to fix the electrical components. The second step involves placing the electrical receptacles that accounts for dedicated and well established path for planning the power circuit. They provide a place in a wiring system where current is taken to run electrical devices based on voltage levels for example 120/240 or 180/220 V electrical receptacles. The current building model uses load capacity of 180 V Amperes and outlet capacity of

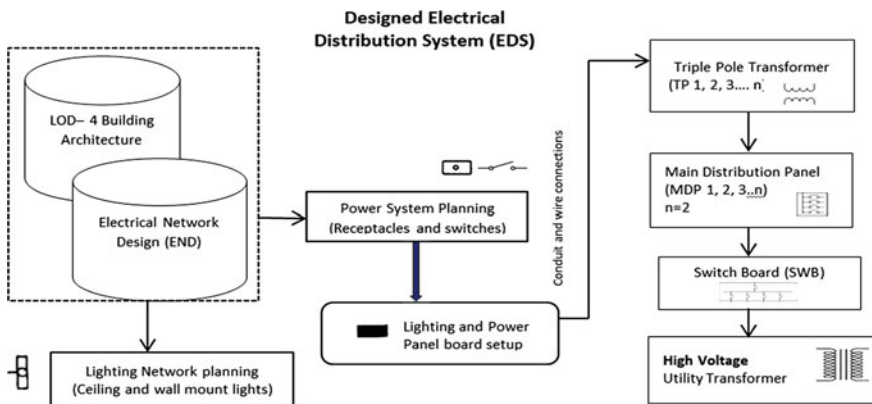


Fig. 1 Electrical network design (END) of building model in revit software

220 V (apparent voltage). Receptacles become electrical outlets when the electrical appliances are connected [11]. Required number of receptacles have been placed at different positions in each room where there is a necessity based on the occupancy.

2.1 Panel Board Connections

According to National Electrical Code (NEC), a panel board is a single or group of units equipped with or without switches for the control of light or power circuits installed against a wall or partition supports [12]. The receptacles, lighting and power appliances connected to the panel board are based on the capacity and rating of the circuit. For instance, the receptacles connected in the building model have the capacity of 180/220 V. Therefore, the panel settings are modified as 240/480 V (a higher capacity for avoiding overload current) and are sequentially connected. Revit Architecture software has the capacity of denying the circuit connection if any overload or harmonic currents are detected and provides the panel properties such as type of panel, electrical loads, estimated demand, mains and apparent load for each phase and electrical datasets [13]. Sixteen panel boards of capacity 240/480 V are placed in four wings of the building in both the floors each wing containing four panel boards.

2.2 Wiring Connections

Revit provides an intelligent network of power connections through automatic and manual wiring systems. The software has the inbuilt technology of calculating the wiring size and the way they are displayed in the project template [14]. The wiring connections between receptacles and panel boards in the building model are shown in Fig. 2.

2.3 Creation of Lighting Fixtures

The electrical circuits also include lighting and power plans. The basic step that must be performed to plan for the lighting is to create a ceiling plan. The lighting fixtures belong to the ceiling hosted families. Therefore, lighting plan is provided based on the floor plan. While placing lighting fixtures on the ceiling, the placement is made along the face to adjust the linear and vertical models. In the current model, Recessed Fluorescent lights and Ceiling light 120 V linear box fixtures have been used.

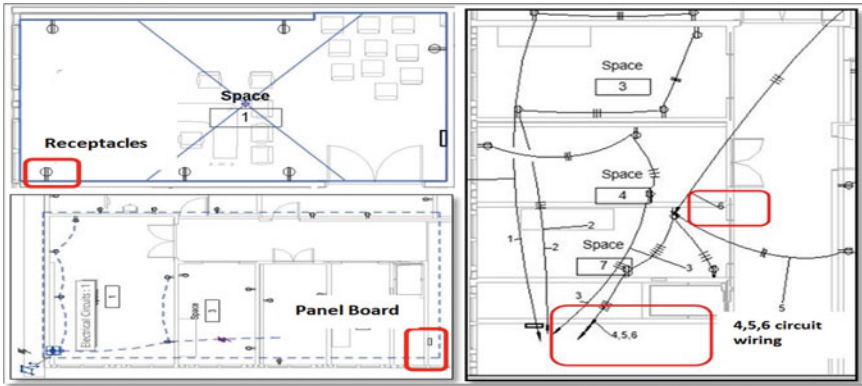


Fig. 2 Wiring and connections between receptacles and panel board

2.4 Creation of Switching Circuits

Single pole switch is the most common light switches in a home or office. Switches in any electrical network burn till null currents are achieved and it permits energy dissipation with the inclusion of resistances [15]. While inserting switches in the current model, number of switches is created in each floor plan similar to the power circuits. The thus created lighting and switching fixtures are cascaded hierarchically to the corresponding panels distributed all over the wings and upon selection of a particular fixture; its electrical circuit gets highlighted both in the project template as well as in the system browser. The switching circuitry is illustrated in Fig. 3.

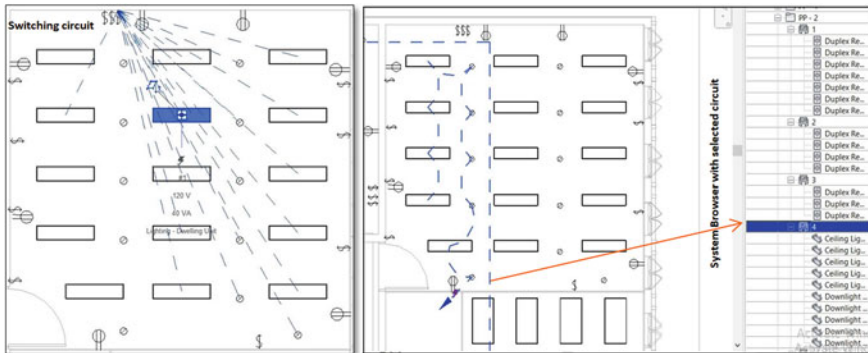


Fig. 3 Selection of switches and circuit connections viewed in system browser

2.5 Creation of Power Distribution System

The electrical distribution system contains three major portions namely creation, distribution and transmission of each distribution system that accounts for major losses and utmost care should be taken for efficient power delivery [16]. In the building model, Static VAR Compensator Transformer (T-SVC) with 480-208Y120-NEMA type 2 Revit transformer family is used as high voltage utility transformer. The power is stepped down to 480/277 V using the above transformer and this high rated transformer is connected to Switch Board (SWB) 480/277 V 3 phase SWB. Switch board is a single large panel assembly device which divides the current into minor currents and provides protection by distributing power to Main Distribution Panels MDP [17]. The SWB is internally connected to MDP with 480 V rating. The connections are made in such a way that each floor contains at least one MDP. It is observed that MDP has the ratings of 480/277 V whereas the panel boards have the ratings of 208/120 V. Therefore, a step down triple pole transformer is used (TP) at each floor to reduce 480/277 V to 208/120 V. The flow of the current in power distribution system is clearly illustrated in the Fig. 4.

3 Geo BIM Analysis of Electrical System Design

An attempt is performed by integrating the electrical network model created in Revit Architecture software using the previous procedure with 3D Geographic Information System (GIS) environment. There are two types of performing the integration between BIM and GIS models in the study. One way is to directly import the Revit model into GIS environment and the other way is to export the Revit model into

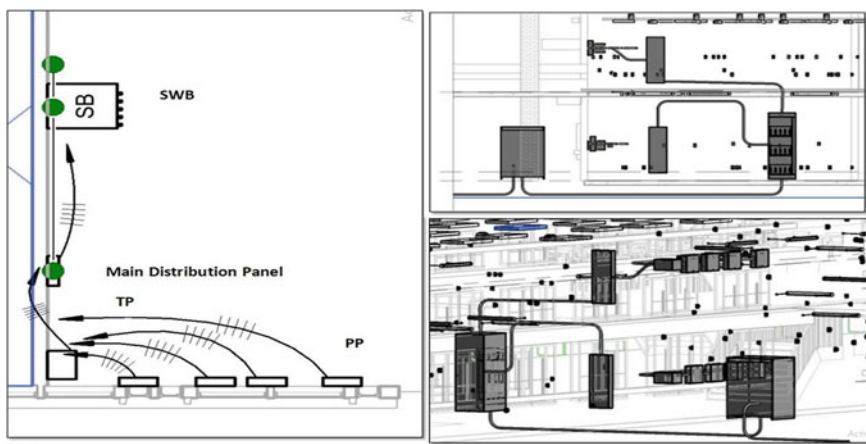


Fig. 4 Electrical distribution system in the building model

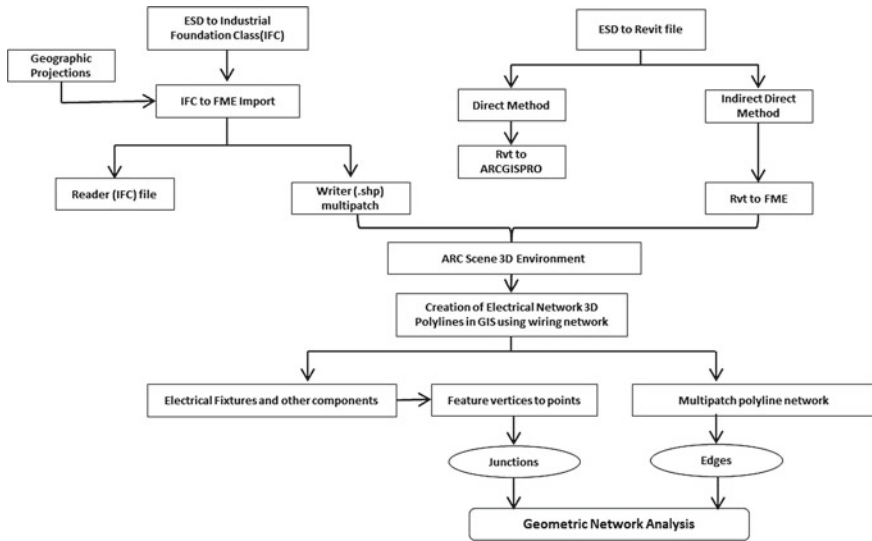


Fig. 5 Work flow of integrating BIM electrical network to GIS platform

Industrial Foundation Class IFC, convert IFC to Multipatch shape files reflecting all the attribute information and finally to carry out the Geometric network analysis in GIS. The methodology in Fig. 5 explains the process of translation that solves the interoperability issues and the network analysis of electrical system is analyzed.

The created electrical network when converted to shape file, it is observed that each feature class is renamed different from the output obtained through Revit Software. Table 1 and Fig. 6 below infer the difference between the modified features attributes during transformation from Industrial Foundation Class (.ifc) file to multipatch shape file (.shp) and from Revit file (.rvt) to multipatch shape file (.shp) converted through FME Work Bench viewed in Arc GIS Environment.

It is observed that in both the above cases, the wiring network from Revit software is transformed into GIS environment virtually which cannot be represented in existing real feature. Therefore, one intermediate step need to be performed which includes creation of 3D Polyline shape file connecting the Revit circuitry in the GIS environment.

4 Geometric Network Analysis (GNA)

Integration of GIS and engineering analysis involves extraction of data models, control of information, data updation, network tracing and validation for maintaining high quality datasets in utility corporate system [18]. GIS has the advantage of providing geographic location of electrical components and mapping of

Table 1 Difference between modified features from IFC and revit to shape files

Multipatch feature class	Revit name
<i>.IFC to .shp Conversion</i>	
Space surface	Rooms
Covering surface	Compound ceiling
Flow terminal surface	Lighting fixtures (ceiling lights and surface fixtures)
Flow segment	Conduits without fittings
Flow fitting surface	Conduit elbow
Building element proxy	SWB, Transformer, Receptacles ad switches
<i>.RVT to .shp Conversion</i>	
Architectural ceiling	Ceiling and its hosted lighting fixtures
Electrical equipment	Distribution boards (SWB, Panels, MDP Transformers)
Electrical lighting fixtures	Ceiling and surface lights related to Revit electrical and lighting systems
Electrical fixtures	Duplex receptacles

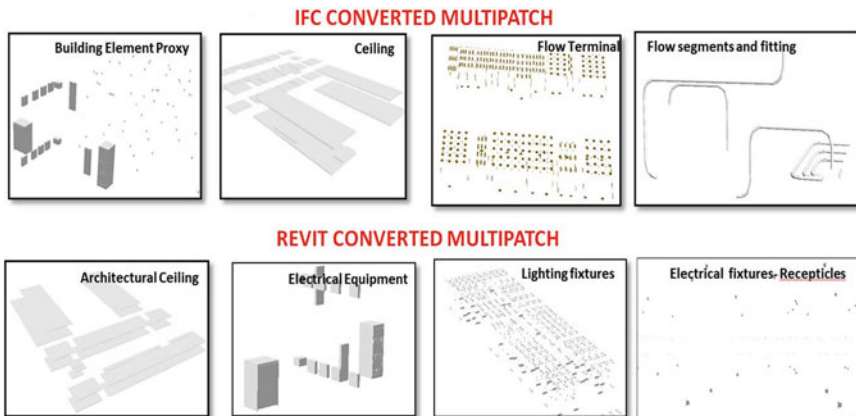


Fig. 6 Few examples of Ifc converted and revit converted multipatch shape files in GIS

complete electrical systems that include layers of information, asset management thereby giving large scope of analysis for utility managers and other decision-makers [19]. One of the major applications provided by geometric network tools of GIS is the detection of electrical short circuit by finding the loops with in the network elements and it also contributes upstream and downstream tracing to find out the common shared elements facing faulty connections [20]. In the current study, Geometric Network Analysis of ArcGIS tools are utilized to find out tracing of electrical components, identification of loops for short circuit information, disconnected network elements and flow direction analysis. Each building electrical component

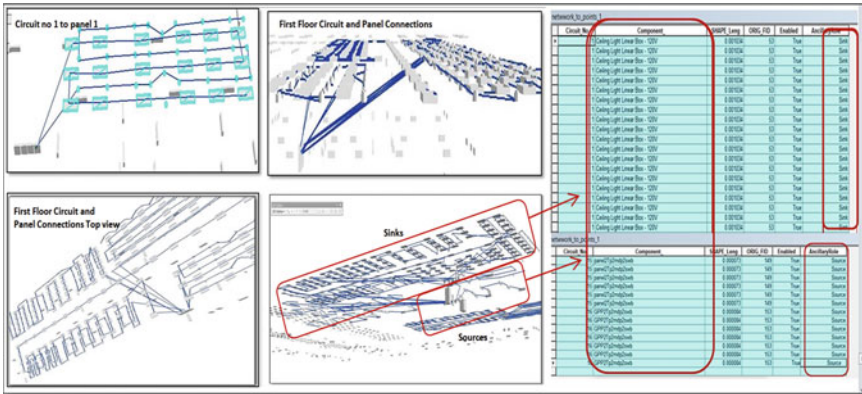


Fig. 7 3D polyline electrical wiring features created in ARCGIS

acts as a junction and the created polylines wiring network acts as edges which connect along the junctions.

For generating Geometric Network in GIS platform, initially new geo database is created containing electrical network (edges) and network to point features (junctions) as feature classes where junctions act as sources or sinks. The attribute table indicates that all the electrical components in BIM are represented as sinks and the electrical equipment which supply the current such as panels, transformers and switches act as sources. The classification of the electrical fixtures that acts as sources and sinks are illustrated in the Fig. 7.

4.1 Detection of Short Circuits in ESD

The Trace Network tool in Geometric Network Analysis of ARCGIS solves the particular network analysis issues by performing spatial search using input flags or barrier. The flags help for trace travel beginning node [21]. There exists many trace tasks such as Finding Common Ancestors, Find Connected, Find Disconnected, Loop Identification, Upstream and Downstream Tracing [22].

4.2 Detection of Disconnected Network in ESD

Utility network analysis tool in ARCGIS helps to find the connected and disconnected network that helps to save the energy of power systems. By using the tools Find Connected and Find Disconnected, the analysis on the particular network is examined for internal connections and distribution. Figure 8 indicates the detected electrical

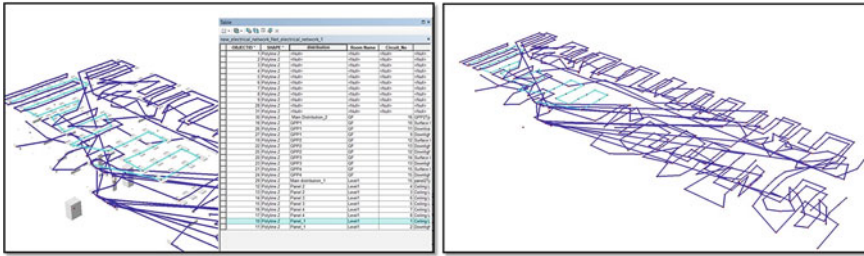


Fig. 8 Detection of short circuit or faulty circuit in electrical network

circuit highlighting the connectivity that is prone to short circuiting through formation of loops and disconnected network in the distribution model.

4.3 Estimation of Flow Direction in ESD

By adding flags along the network junctions, the origin of flow direction is set. Trace upstream and trace downstream tools are run by finding common ancestors using barriers at the junctions and edges along sources and sinks. The network of connected and disconnected features and their flow direction are determined in the Fig. 9.

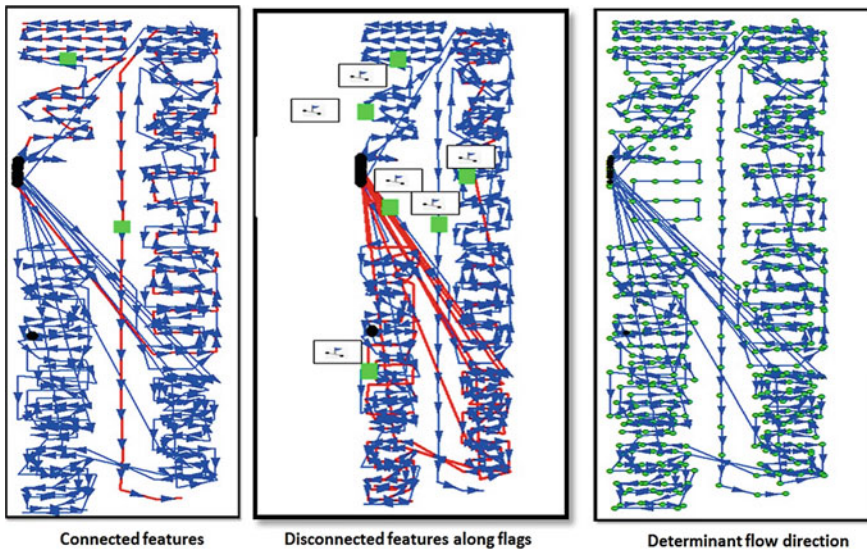


Fig. 9 Estimation of flow direction of current shown with connectivity issues

5 Conclusions

GIS and BIM, the integration of two most powerful technologies have proven to be a robust solution provider to the problems associated with electrical engineering. This study provides a great insight into the concepts of Electrical System Design and its distribution in Revit Architecture software and later an attempt was made to integrate this generated building information-based electrical system design to 3D geographic information system. The current approach helped to solve the issues of interoperability associated with electrical database design and attribution in the electrical network. Geometric and utility network analysis tools and techniques of GIS are used for examining and verifying the circuit information and are validated against the laws of Electrical Engineering network theory. Electrical components and their distribution constitute the important infrastructure which is essential to every house or any other type of building business/commercial/educational and hence their generation, transmission and distribution can be planned with scheduled and virtual circuit information that create a strong foundation by maintaining the network standards using GIS technology and mapping.

Acknowledgements We are thankful to the Department of Science and Technology (DST), Government of India who has been funding the project and supporting us with requisite inputs. The authors are also thankful to NIGST, Survey of India for providing an opportunity to explore the resources and undergo training essential for the research, International Institute of Information Technology, Hyderabad (IIITH) and CGARD, National Institute of Rural Development (NIRDPR) for standing as important advisory for the further developments and improvements in the project.

References

1. Eastman C, Teicholz P, Sacks R, Liston K (2011) BIM handbook: a guide to building information modeling for owners, managers, designers, engineers and contractors, 2nd edn. Wiley, New Jersey, pp 351–389
2. Farooq J, Sharma P, Kumar S (2017) Applications of building information modeling in electrical system design. *J Eng Sci Technol* 10(6):119–128
3. Grillo A, Jardim Goncalves R (2010) Value proposition on interoperability of BIM and collaborative working environments. *J Autom Constr* 19(5):522–553
4. Simonian L, Korman T (2011) Building information modeling for electrical contractors: current practice and recommendations. In: Architectural engineering conference, March 2011, Oakland, California, pp 456–463. [https://doi.org/10.1061/41168\(399\)53](https://doi.org/10.1061/41168(399)53)
5. Hanna A, Asce F, Boodai M et al (2013) State of practice of building information modelling in mechanical and electrical construction industries. *J Constr Eng Manag* 139(10):1–8. [https://doi.org/10.1061/\(ASCE\)CO.1943-7862.0000747](https://doi.org/10.1061/(ASCE)CO.1943-7862.0000747)
6. Berry JK (1996) GIS evolution and future trends. Beyond Mapping III compilation of beyond mapping columns appearing in geo world magazine, BASIS Press, Quincy, USA <http://www.innovativegis.com/basis/MapAnalysis>
7. Ma Z, Ren Y (2017) Integrated application of BIM and GIS: an overview. *Proc Eng* 196:1072–1079. <https://doi.org/10.1016/j.proeng.2017.08.064>

8. Fosu R, Suprabhas K, Rathore Z, Cory C (2015) Integration of building information modelling (BIM) and geographic information systems (GIS)—a literature review and future needs. In: Proceedings of 32nd CIB W78 conference, Eindhoven, the Netherlands, 27–29 October 2015
9. Vacca G, Quaquero E, Pili D, Brandolini M (2018) Integrated BIM and GIS data to support the management of large building stocks. *Int Arch Photogramm Remote Sens Spat Inf Sci* 42:647–653. <https://doi.org/10.5194/isprs-archives-XLII-4-647-2018>
10. Farooq J, Sharma P, Kumar S (2017) Applications of building information modeling in electrical system design. *J Eng Sci Technol Rev* 10(6):119–128. <https://doi.org/10.25103/jestr.106.16>
11. Rutherford C (2018) Building maintenance and construction: tools and maintenance tasks. In: Communicology, building maintenance, and OER. Training Press Books, Hawaii. <http://pressbooks.oer.hawaii.edu>
12. East Coast Power Systems (2012) National Electric Code (NEC) Article 408, New Jersey. <https://www.ecpowersystems.com/resources/panelboards>
13. Autodesk Help (2021) Revit products support: about panel properties. Retrieved from <https://knowledge.autodesk.com/support/revit-products/learn-explore/caas/CloudHelp/cloudhelp/2021/ENU/Revit-MEPEng/files/GUID-62144CB0-8C7F-461B-82E3-BF242CBC5D92-htm.html>
14. Autodesk Help (2021) Revit products support: about wiring types. <https://knowledge.autodesk.com/support/revit-products/learn-explore/caas/CloudHelp/cloudhelp/2021/ENU/Revit-MEPEng/files/GUID-7E332D00-2B13-4E8D-AFEF-7D4BB7E0E2C2-htm.html>
15. Greenwood AN, Stokes AD (1991) Electric power switches. *IEEE Trans Plasma Sci* 19(6):1132–1142
16. Pillay A, Sharma K, Karthikeyan SP, Rangarajan SS (2014) Analysis on power distribution system in India-Patna city—a case study. In: International conference on computation of power, energy, information and communication, 16–17 April 2014, pp 304–309. <https://doi.org/10.1109/ICCPEIC.2014.6915381>
17. United States Department of Labour (2007) Occupational safety and health administration: electrical standard final rule, vol 72, pp 7135–7221. <https://www.osha.gov/laws-regs/federalregister>. Accessed 14 Feb 2007
18. Smith PH (2005) Electrical distribution modeling: an integration of engineering analysis and geographic information systems. Dissertation, Virginia Polytechnic Institute and State University. <http://hdl.handle.net/10919/36158>
19. Mathankumar S, Loganathan P (2015) GIS based electrical system planning and network analysis. *World Eng Appl Sci J* 6(4):215–225
20. Environmental Systems Research Institute ESRI (2016) Geometric networks: ArcGIS for desktop help. <https://desktop.arcgis.com/en/arcmap/10.3/manage-data/geometric-networks/what-are-geometric-networks-.htm>
21. Environmental Systems Research Institute ESRI (2016) Trace geometric network: ArcGIS for desktop help. <https://desktop.arcgis.com/en/arcmap/10.3/tools/data-management-toolbox/trace-geometric-network.htm>
22. Environmental Systems Research Institute ESRI (2021) Utility network trace types-ArcGIS Pro Documentation. <https://pro.arcgis.com/en/pro-app/latest/help/data/utility-network/utility-network-trace-types.htm>

Generation of LOD-2 3D Building Models from High-resolution Stereo Satellite Data Using Remote Sensing and Photogrammetry



Venkumahanti Tejaswini, Pyla Kesava Rao, E. N. Dhanamjaya Rao, Ravoori Nagaraja, S. K. Sinha, and K. S. Rajan

Abstract Building products designed at each level of detail provide single window solutions for Smart City applications. In view of this, the current study uses the tools and techniques to generate second level of detailed buildings that include building shape and height parameters. The extrusion from 2D has been performed altogether in multiple platforms and 3D data handling software. The basic inputs considered for extracting the polygon shapefiles are obtained from high-resolution stereo pair satellite images acquired using Cartosat-I imagery. Eight ground control points are collected using high precision Differential Global Positioning System having millimeters of accuracy. The image adjustments and Digital Surface Model are generated by using the process and concepts of Photogrammetry such as block creation using Rational Polynomial Coefficient text files, internal geometry set up

V. Tejaswini (✉)

International Institute of Information Technology (IIIT), Hyderabad, National Institute of Rural Development and Panchayat Raj (NIRDPR), Hyderabad, India
e-mail: tejaswini.v@research.iiit.ac.in

P. Kesava Rao

Centre for Geo Informatics Application in Rural Development (CGARD), National Institute of Rural Development and Panchayat Raj, Hyderabad, India
e-mail: kesava.nird@gov.in

E. N. Dhanamjaya Rao

Department of Geology, Andhra University, Visakhapatnam, Andhra Pradesh, India

R. Nagaraja

Department of Science and Technology, International Institute of Information Technology (IIIT), Hyderabad, India
e-mail: nagaraja.ravoori@iiit.ac.in

S. K. Sinha

National Institute for Geo-Informatics Science and Technology (NIGST), Survey of India, Uppal, Hyderabad, India
e-mail: sk.sinha soi@gov.in

K. S. Rajan

Lab for Spatial Informatics (LSI), International Institute of Information Technology (IIIT), Gachibowli, Hyderabad, India
e-mail: rajan@iiit.ac.in

such as interior and exterior orientation, Tie point generation and control point adjustments, and Automated Terrain Extraction. The thus obtained terrain model is overlaid on ortho photograph and the building heights are extracted and compared by using spatial profile graph as well as stereoscopic visualization methods. The height-derived attribute tables are attached to corresponding building footprints and are visualized in different GIS platforms.

Keywords Photogrammetry · Remote sensing · Buildings · Digital surface models · City engine · FME

1 Introduction

Advanced tools and techniques utilized in Remote Sensing and Photogrammetry add an intuitive essence to the diversified applications. The current analysis considers one of such use cases which imparts great knowledge to the decision-makers and planners about integrated approach of Geo-Spatial technology with respect to the 3D building models. High-Resolution Stereo Pair Satellite Imagery, an alternative to Drone or Aerial imagery operated for the extraction of buildings in 3D environment solves major data-related complications such as inaccessibility, excessive cost, and unavailability of datasets [1]. The current study is an attempt to extrude 3D building heights from 2D footprints using Digital Surface Models obtained from stereo pair remote sensing data and techniques of Photogrammetry processing. The elemental key for 3D GIS includes the representation of its terrain in the form of Digital Elevation Model which is divided into two types Digital Terrain Model DTM and Digital Surface Model DSM. DTM constitutes the bare ground whereas DSM indicates the surface models associated with height of the features such as buildings and trees [2, 3]. The stereo data is processed in Photogrammetric software to create ortho imagery which is a computer-generated digital data that eliminates the distortions caused by the terrain elevation and tilt of the camera [4]. The orthoimages are geometrically rectified with respect to the world geodetic coordinates since these images are obtained as an outcome of GCP assigned triangulation products, DSM and ortho imagery are intuitively overlaid for the reconstruction of 3D buildings using CAD model matching against the image [5], data and mode driven reconstruction [6] using genetic algorithm [7]. The satellite data acts as a source of light for building modeling when it is almost impossible to measure through aerial datasets [8]. Spatial profile analysis was performed by computing the difference DSM between high-resolution imagery of CARTOSAT-I and aerial photograph resulting in the estimation of accuracy assessment and Root Mean Square Error RMSE [9]. In the current approach, surveying is carried out in the study area for assigning ground control points. GCP accuracy is improved with the help of differential GPS [10]. DGPS contains a receiver that involves a reference base communicating with GNSS satellites with respect to geographic coordinates. The created global measurement error is corrected using Real-Time Kinematic RTK method [11]. Static mode of data acquisition is more

accurate in terms of positions [12]. The generated DSM is thus linked with the actual terrain profile with surface relief and design of 3D buildings is abstracted and visualized in different geo-spatial platforms such as ESRI City Engine, Q GIS, ARC GIS PRO, FME workbench, and ARC Scene.

2 Materials and Methods

The complete methodology involved in the current analysis begins at the stage of surveying in the field of study includes Pre- and Post-processing, usage of Remote Sensing data products, Photogrammetric data processing, and 3D building modeling in different softwares. The surveyed data output is processed further and the control points are assigned as shown in Fig. 1.

2.1 DGPS Surveying

The Differential Global Positioning System DGPS surveying equipment used in the study shown in Fig. 2 include a base station Trimble R 10 GNSS receiver that contains GNSS antenna and internal radio receiver providing nearly 440 satellite tracking channels [13] with horizontal and vertical accuracy of several mm to cm in static mode of GNSS survey [14]. A power receiver R4 Rover is connected to the base station to establish error-free or corrected data by receiving signals from satellite base station that calculates grade [15].

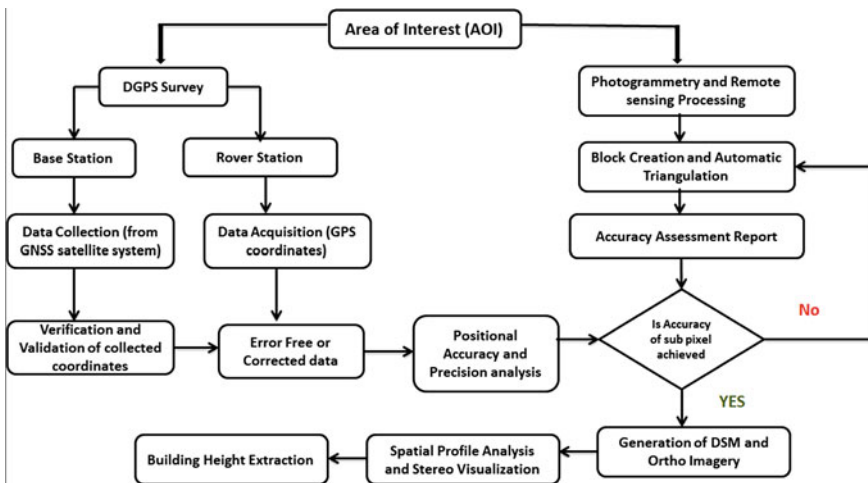


Fig. 1 Processing of stereo data and building height extraction



Fig. 2 DGPS survey equipment used in the field

2.2 Remote Sensing Data Products

Cartosat-1 stereo pair satellite images of band A and band F are used for the preparation of above-added outputs in the analysis. Cartosat-1, first Indian Remote Sensing Satellite providing stereo images with a resolution of 2.5 m [16] contains two high-resolution PAN cameras that record and acquire stereo images [17]. The stereo pair datasets provide multidisciplinary applications especially related to the extraction of building height parameters using DSM [18] Delineation of natural features and terrain DEM for various use cases in environment [19] disaster management and mitigation measures [20] and 3D city modeling [21]. The photogrammetric approach for extruding the building heights contributes to good quality products in 3D modeling. The acquired ortho kit Geo TIFF product contains WGS 84 Ellipsoid as datum and is attached with RPC text file that represents the imaging geometry [22].

2.3 Photogrammetric Data Processing

Leica Photogrammetric Suite LPS is a powerful photogrammetric package that provides digital photogrammetry processing and smooth workflow of deriving Stereo Geo-Spatial products [23]. The 3D visualization in the present study is achieved with photogrammetric equipment such as 3D Stealth Mouse and Liquid Crystal Shutter Glasses (LCS).

2.3.1 Block Creation and Control Generation

Creation of block is the initial phase of processing a stereo pair data in LPS software. A block comprises position and datum information and their geometric relationships. In the initial model set up, Cartosat RPC text file is used for geometric model category,

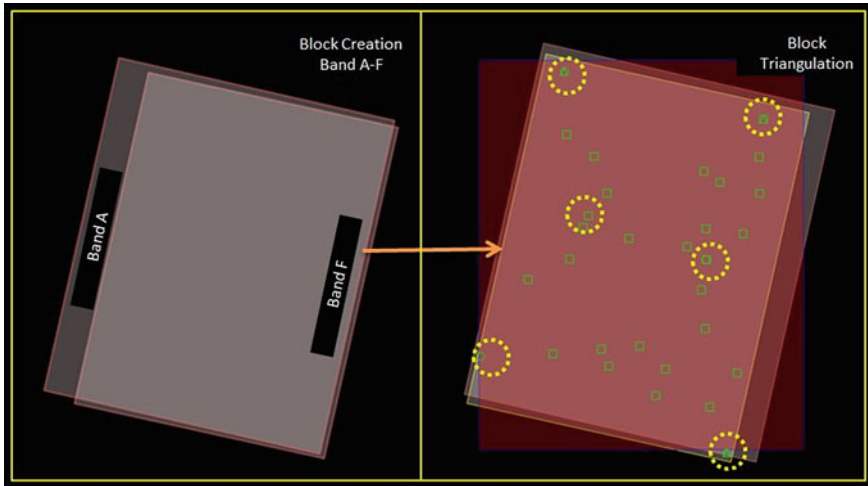


Fig. 3 Block creation and bundle block adjustment

and the vertical elevation information is chosen as World Geodetic System (WGS) 84 and the horizontal datum as Universal Transverse Mercator (UTM).

2.3.2 Block Triangulation and Automatic Tie Point Generation

The Tie point generation for image matching plays a very important role in the Photogrammetric framework that involves complexity of workflow especially when the data is inaccurate [24]. The Block Triangulation method establishes mathematical relationship between the images and the ground truth data [25]. After generating Automatic Tie Points, Triangulation is performed and bundle block adjustment is carried out by increased accuracy and reduced RMSE. The output of bundle block adjustment is shown in Fig. 3 and classic point measurements are illustrated in the PAN image in Fig. 4.

2.3.3 Generation of DSM and Ortho Image

The Triangulated Stereo images with Control Points and Tie Points have resulted in an acceptable RMSE error of 0.0862 pixels including Ground X, Y, Z errors as 0.095, 0.021, 0.003, and image X, Y as 0.127 and 0.02, respectively. Cartosat-1 stereo imagery correlated with Ground Control Points has been extensively operated in many studies deriving the high-quality DEM products and a comparison has also been performed between ASTERDEM, Topographic contour maps, SRTM DEM which concludes that Cartosat derived DEM products accounts for more accuracy [26]. Digital Elevation Model DEM in LPS is obtained using Automatic Terrain

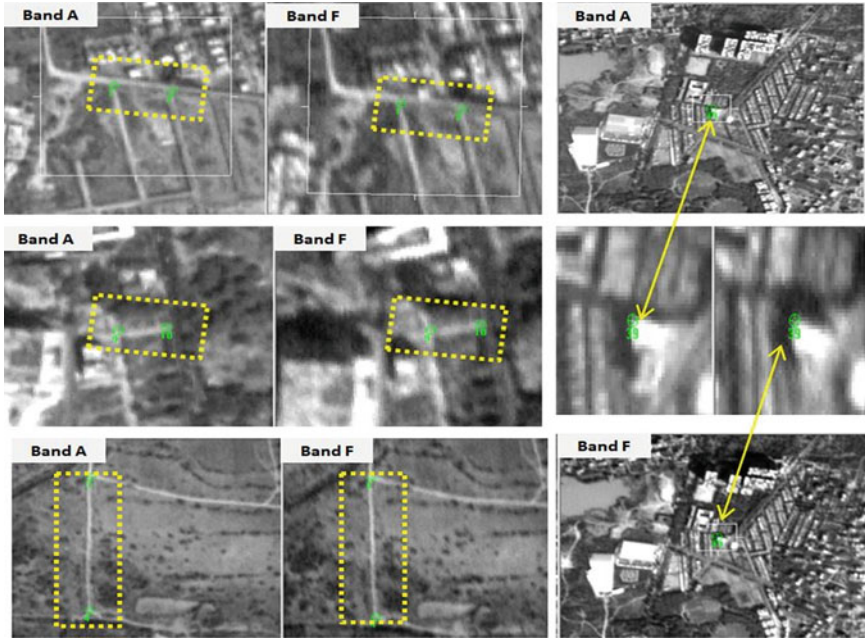


Fig. 4 Classic point measurements indicating same features in band A and band F images

Extraction ATE tool by using block checkpoints, GCPs, and Tie points whereas Ortho imagery is derived from the DSM product with respect to the positional accuracy and the orthorectified image is overlaid above the Digital Surface Model DSM to carryout Spatial Profile analysis. The obtained elevation surface models DSM and its quality image generated in Leica Photogrammetry software from ERDAS Imagine are shown in Fig. 4. It is observed from Fig. 5 that the elevation of the terrain in the current study area lies between 305 and 695 m shown as a symbolic stretch from black to white color, respectively.

3 Extraction of Building Heights

The profile analysis under panchromatic utilities in LPS is used to display relief of each drawn line along with the image and infers the quantitative assessment of heights in the form of plotted graphs. In the current study, each building height is evaluated with respect to the plain terrain by linking charts from the profile graphs. The input DSM obtained from the satellite imagery Cartosat 1 provides a compromising resolution to produce quality terrain outputs compared to very high-resolution datasets such as World View, Ikonos, and Quick Bird. Therefore, the difference in

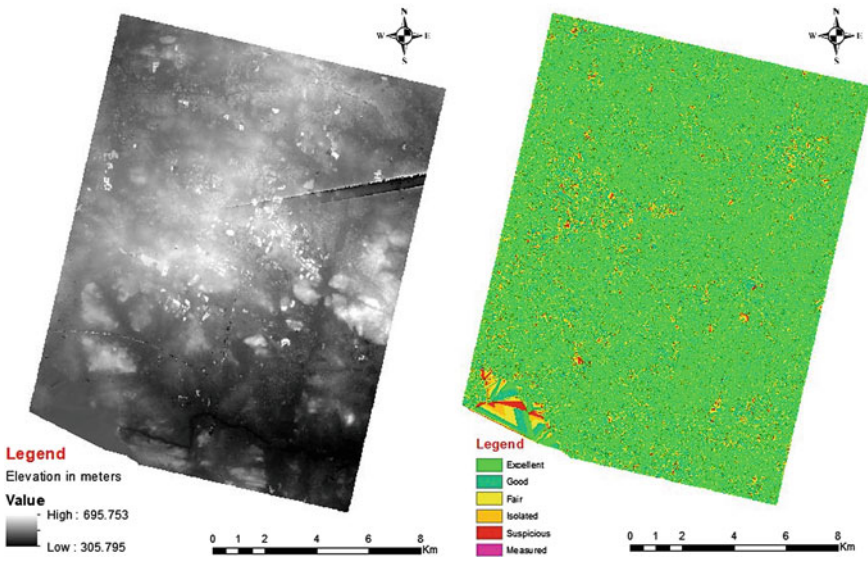


Fig. 5 Figure showing digital surface model and its quality image in LPS

heights is manually verified with the help of visualization techniques, and the accuracy assessment is performed by using 3D stereoscopic techniques. The height of sample building from profile analysis chart is shown in Fig. 6. The midway profile elevation is computed from the graph as 525 m and the ground elevation is 500 m which results in building height of 25 m.

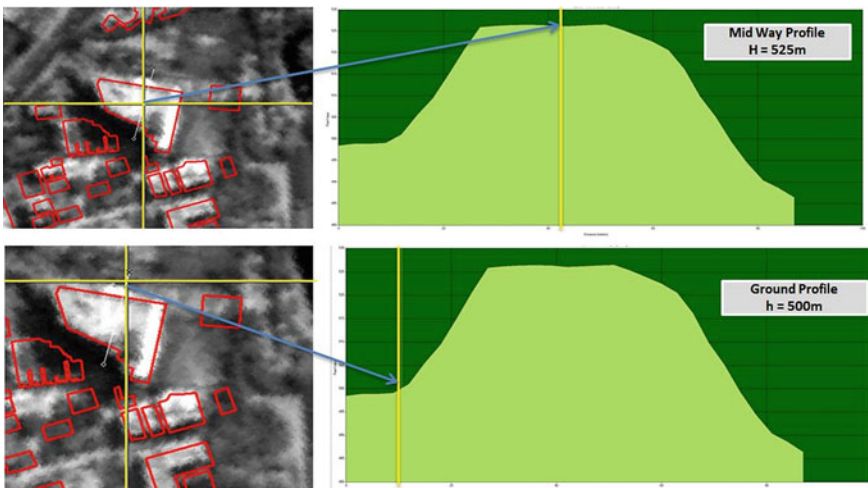


Fig. 6 Building height spatial profile graph

4 3D Building Modeling

The collaborative approach of various firms in Architectural, Engineering, and Construction management with an interdependency of each other helps for the planning and implementation of semantic rich building information models [27]. Building models are represented with varying levels of details LOD's with sequential design and structural refinement at each stage of development. Level of details articulates the planners a clear understanding of the geometrical models from least level of details to the highest. The study concentrates on the level of detail LOD-2, a generic system with particular shape and block height in advanced 3D modeling softwares such as city engine, Geo-Spatial data handling software such as QGIS, ArcGIS PRO, and feature translation software FME workbench.

4.1 Modeling Through City Engine

The City Engine Procedural Modeling tools are used with Computer-Generated Architecture CGA rules to convert the 2D footprint shapefiles with height attributes into 3D building blocks. The 2D footprint shapefiles from Arc GIS environment are imported to City Engine platform and it is observed that all the attributes are attached and reflected in 3D model parameters. In addition to building models, street networks and base maps are added from Get Map Data tool in City Engine and street can also be grown in the 3D scene containing auto-generated street segments and lines. Figure 7 illustrates the design of 3D modeling in City Engine software.

The building models in the study area are categorized into different classes such as Residential (Houses and Apartments), Commercial (Business), Assembly (Hospitals, Theaters, Malls), Religious structures, and Special type of buildings (Hotels, Restaurants, Exhibition halls) as shown in Fig. 8. A simple building rule with Façade partition CGA code is imported over the 2D footprints and the height attributes of these buildings are linked and connected to "ht." field from GIS shapefile obtained through DSM.

4.2 Modeling Through FME

Feature Manipulation Engine FME is data integration and automation software that streamlines the conversion of spatial and non-spatial data formats allowing simple and fastest feature integration through data interoperability. 2D drawing and digitized files such as .dwg, .dgn, .shp, etc. can be easily outlined to 3D design in FME workbench [28]. Initially, the source file (.dwg/.shp) is read in the FME reader along with the attribute schema entities. The height attribute excel or CSV file between reader file and the table, i.e., building ID in this case are merged together using feature

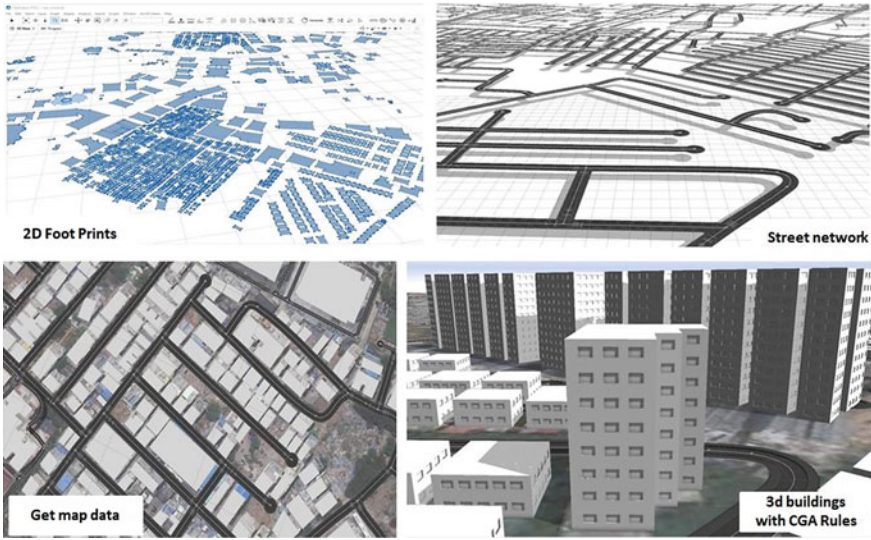


Fig. 7 Designing of buildings and streets (3D city modeling) in city engine

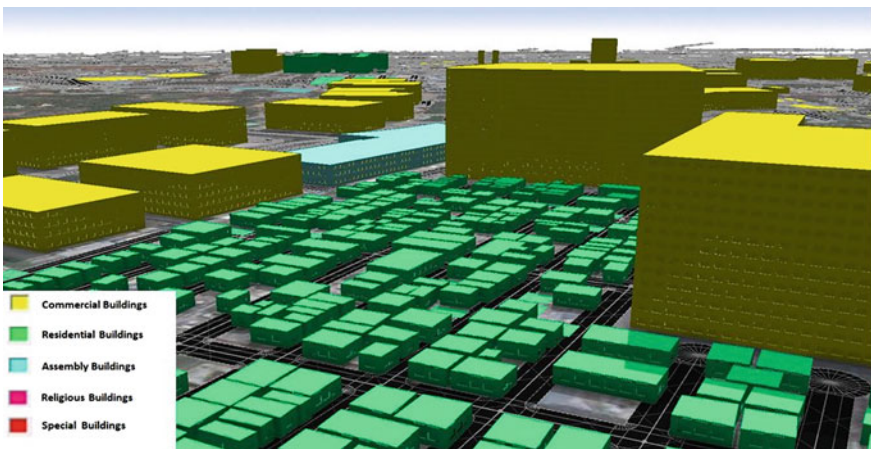


Fig. 8 LOD-2 building categories designed in city engine

merger translator in FME. Geometrical and Semantic extensions of the features are implemented by using extruder command that extrudes vertically along with the attached “ht.” attribute. The extruded output is re-projected to geographic coordinated system “LL-84” and the data attribution is performed in the output KML file. Figure 9 indicates the FME workflow and the KML file imported in Google Earth.

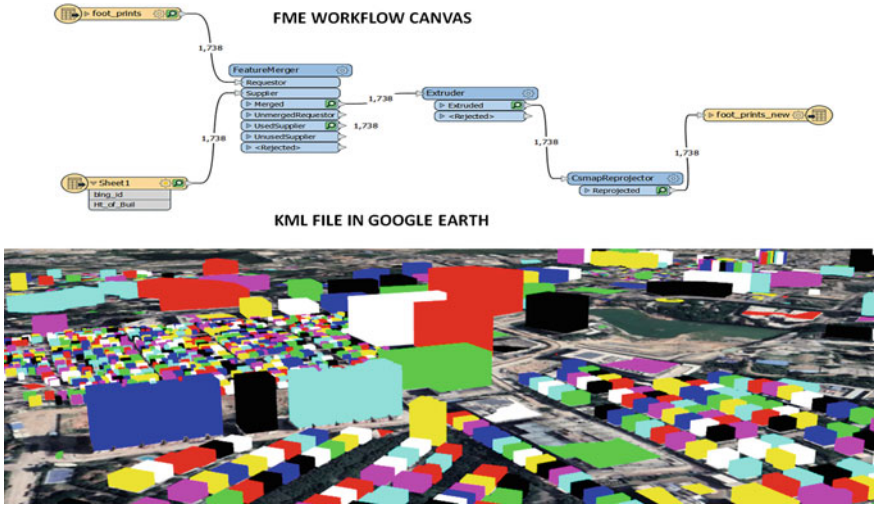


Fig. 9 FME Canvas (3D extraction from 2D footprints) and KML in Google Earth

4.3 Modeling Through QGIS

QGIS is an open-source GIS software that has the capability of handling both Raster and Vector datasets [29]. QGIS is essential for multidimensional data visualization, management, and efficient spatial analysis which provides great insight to the Decision Support System. QGIS is provided with numerous tiny programming functionalities called “plugins”. “QGIS2threejs” is one such plugin used for the visualization and generation of 3D buildings from simple 2D footprint shapefiles. A template file is displayed which allows to choose the height attribute style with multiplier and select the features to be extruded. GIS-based symbology is assigned to different building classes as shown in Fig. 10.

5 Conclusions

The current approach of 3D building generation from 2d input files using High-Resolution Stereo Pair Satellite data provides great insight into the interpretation and modeling. The level of details at each building construction phase is a virtual replica of real-time scenario which is helpful for visualization, planning, management, and monitoring. The future study would include further developments in the level of details that incorporate the interior structures and attribute tables. There are tremendous applications in the field of 3D city modelings such as multi-perspective data visualization, disaster management studies, indoor logistics, utility and facility management, urban planning, noise propagation studies,



Fig. 10 3D building Modeling generated in QGIS software overlaid on Open Street Map

and e-commerce. 3D building models when integrated with Geoinformatics, the stand-alone applications are supplemented into multiple domains.

Acknowledgements The project was funded by the Department of Science and Technology (DST), Government of India. We express our deep gratitude for the financial assistance. We are also thankful to NIGST, Survey of India, International Institute of Information Technology, Hyderabad (IIITH), and CGARD, National Institute of Rural Development (NIRDPR) for their consistent support and encouragement throughout the project tenure.

References

1. Alobeid A, Jacobsen K, Heipke C (2009) Building height estimation in urban areas from very high resolution satellite stereo images. In: Heipke C, Jacobsen K, Müller S, Sorgel U (eds) ISPRS workshop: high-resolution earth imaging for geospatial information, Hanover, Germany, vol 38
2. Hirt C (2014) Digital terrain models. In: Grafarend E (ed) Encyclopedia of geodesy. Springer, Heidelberg, pp 1–6. https://doi.org/10.1007/978-3-319-02370-0_31-1
3. Malinverni ES (2014) DEM automatic extraction on Rio de Janeiro from WV2 stereo pair images. Proc IOP Conf Series Earth Environ Sci 18:1–6. <https://doi.org/10.1088/1755-1315/18/1/012022>
4. Rufe PP (2014) Digital ortho imagery base specification V1.0. U.S. Geological survey techniques and methods, book 11, chap B5, p 13. <https://doi.org/10.3133/tm11B5>
5. Khoshelham K (2006) Automated 3D modeling of buildings in suburban areas based on integration of image and height data. In: Abdul-Rahman A, Zlatanova S, Coors V (eds) Innovations in 3D geo information systems, Lecture notes in Geoinformation and Cartography. Springer, Heidelberg, pp 381–393. https://doi.org/10.1007/978-3-540-36998-1_30
6. Rottensteiner F (2006) Consistent estimation of building parameters considering geometric regularities by soft constraints. Int Arch Photogr Rem Sens 36(3):8–13
7. Kabolzade M, Ebadi H, Mohammadzadeh A (2012) Design and implementation of an algorithm for automatic 3D reconstruction of building models using genetic algorithm. Int J Appl Earth Obs Geoinf 19:104–114

8. Arefi H, Reinartc P (2013) Building reconstruction using DSM and ortho rectified images. *J Remote Sens* 5(4):1681–1703. <https://doi.org/10.3390/rs5041681>
9. Crespi M, Barbato F, Vendictis LD et al (2007) CARTOSAT-1 stereo imagery: potentialities about orientation, DSM extraction and ortho rectification. In: Gomarasca MA (eds), *Geo information in Europe. Proceedings of 27th EARSeL Symposium, June 2007, Italy*, vol 36. IOS Press, Netherlands. <https://doi.org/10.3929/ethz-b-000006903>
10. Ribbens WB (2003) Aircraft instruments. *Encyclopedia of physical science and technology*, 3rd edn. pp 337–364. <https://doi.org/10.1016/B0-12-227410-5/00916-9>
11. Darrozes J, Roussel N, Zribi M (2016) The reflected global navigation satellite system (GNSS-R): from theory to practice. In: Nicolas B, Mehrez Z (eds) *Microwave remote sensing of land surface*, pp 303–355
12. Kostov GP (2011) Using of both fast static and RTK modes for GNSS determinations to obtain required high accuracy and productivity, according to the current possibilities of the IT. In: *Proceedings of the FIG working week, Marrakech, Morocco*
13. Trimble R10 GNSS Receiver (2014) User guide version 1.1, Revision B, p-11. <https://www.trimble.com>
14. Alkan RM, Ozulu IM, İlçi V (2017) Comparison of single baseline RTK and network RTK GNSS methods. In: *International symposium on modern technologies, education and professional practice in geodesy and related fields, Sofia*
15. Gregg W (2019) How GPS rovers improve construction project management. <https://www.forconstructionpros.com/equipment-management/article/21049278>
16. Indian Space Research Organization ISRO (2005) PSLV-C6/CARTOSAT-1. <https://www.isro.gov.in/spacecraft/cartosat-1>. Accessed 05 May 2005
17. Krishna Murthy YVN, Srinivasa Rao S et al (2008) Analysis of DEM generated using Cartosat-I stereo data over Mausanne Les Alphilles. *Cartosat Scientific Appraisal Programme (CSAP TS-5) ISPRS*, vol 37, pp 1343–1348
18. Toutin T (2004) DSM generation and evaluation from Quick Bird stereo imagery with 3D physical modelling. *Int J Remote Sens* 25(22):5181–5192. <https://doi.org/10.1080/01431160410001726030>
19. Stevens N, Garbeil H, Mouginis Mark P (2004) NASA EOS Terra ASTER: volcanic topographic mapping and capability. *J Remote Sens* 90:405–414
20. Nichol JE, Shaker A, Wong MS (2006) Application of high-resolution stereo satellite images to detailed landslide hazard assessment. *J Geomorph* 76:68–75
21. Fraser C, Baltsavias E, Gruen A (2002) Processing of Ikonos imagery for sub meter 3D positioning and building extraction. *ISPRS J Photogr Remote Sens* 56(3):177–194
22. Krishnan S, Sajikumar N, Suman KS (2016) DEM generation using Cartosat-1 stereo data and its comparison with publically available DEM. *J Proc Technol* 24:295–302. <https://doi.org/10.1016/j.protecy.2016.05.039>
23. Leica Photogrammetric Suite (2013) Hexagon safety infrastructure support. <https://support.hexagonsafetyinfrastructure.com>
24. Shragai Z, Even-Paz A, Klein I (2011) Automatic tie point extraction using advanced approaches. In: *Proceedings of the ASPRS annual conference, Wisconsin*
25. Gupta K, John S, Bhardwaj A et al (2017) Comparative evaluation of Pleiades, Cartosat- 2 and Kompsat-3 stereo data products for DSM and 3D model generation. *ACRS 2017*
26. Kayadibi O (2009) Recent advances in satellite technologies using to generate the Digital Elevation Model. *International Conference on Recent Advances in Space Technologies, Istanbul, Turkey 2009*:380–385
27. Chiu ML (2002) An organizational view of design communication in design collaboration. *J Des Stud* 23(2):187–210. [https://doi.org/10.1016/S0142-694X\(01\)00019-9](https://doi.org/10.1016/S0142-694X(01)00019-9)
28. Community Safe Soft (2020) 2D to simple 3D model: extrude building outlines. <https://community.safe.com/s/article/2d-to-simple-3d-model-extrude-building-outlines>
29. Srivas S, Khot P (2018) GIS based computational tools and techniques for multidimensional data analysis and visualization. *Int J Appl Eng Res* 13(15):11770–11775

Experimental Investigations on Flexural Behaviour of Steel Fibres Reinforced Quaternary Blended Self-compacting Concrete Slabs Using Mineral Admixtures



G. Sree Lakshmi Devi, C. Venkata Siva Rama Prasad, and P. Srinivasa Rao

Abstract The industry of construction has been witnessing a lot of amelioration, and one of the principal advancements in this regard is self-compacting concrete (SCC). It has lead to positive insight because of several considerations in terms of environment aspects like reducing the effects of noise pollution which are related to different vibrating techniques, in heavy reinforced areas where the pores present in the concrete can be minimize, reduction in time of completing the project, construction and assembling of the concrete members becomes quick and easier compare to conventional concrete (Jodeiri and Quitalg in *J Civ Eng Res* 2:100–107, 2012 [1]). However, cement content in SCC is more which obviously causes environmental impacts or degradation such as emission of CO₂ into the atmosphere is linked up with cement manufacturing and it is causing environmental pollution in terms of greenhouse gases, global warming and is associated with climatic changes globally. To reduce these effects due to production of cement, introducing high volume mineral admixture or supplementary cementitious materials as a partial replacement to cement minimizes the binder content and it improves the comparable properties with conventional self-compacting concrete leading to sustainable development in concrete industry (Devi and Rao in *i-Manager's J Civ Eng* 7(2), 2017 [2]). The current paper manifests the practical experimentation carried out on steel fibre quaternary blended self-compacting concrete (SFQBSCC) for the flexural behaviour with the incorporation of mineral admixtures or by-products from industries such as microsilica (MS), ground granulated blast furnace slag (GGBS) and fly ash (FA), along with the inclusion of steel fibres from 0% to 1.5% for 0.30 and 0.40 water-binder ratios and compared with SCC (Kukreja Chawla in *Ind Concrete J* 3(2)154 1989 [3]). Quaternary blended SCC mixes containing 40% cement, 25% FA, 25%

G. Sree Lakshmi Devi (✉)

Department of Civil Engineering, Vignana Bharathi Institute of Technology (Autonomous), Aushapur(V), Hyderabad, Telangana 501301, India

C. Venkata Siva Rama Prasad

Department of Civil Engineering, St. Peter's Engineering College (Autonomous), Dullapally, Maisammaguda, Medchal, Hyderabad, Telangana 500100, India

P. Srinivasa Rao

Civil Engineering, JNT University Hyderabad, Kukatpally, Hyderabad 500085, India

GGBS and 10% MS with w/b 0.40 and 0.30 ratios achieved consistency and strength w.r.t SCC of similar w/b ratios.

Keywords Steel fibres · Blended concrete · Reinforced quaternary blended self-compacting concrete slabs · Mineral admixtures · Construction techniques

1 Introduction

Concrete built with a cement system with many blends of ordinary Portland cement (OPC) is the rational choice for the construction industry in today's environment to meet the demands of sustainable construction [4]. Using supplementary cementitious materials (SCMs), it is one of the most effective ways to save Mother Nature's resources whilst also reducing environmental impact by using OPC as a partial or complete replacement for cement. Because most SCMs are pozzolanic in nature, they aid in improving concrete's long-term strength. Blending SCMs with cement has a number of benefits, including cost savings, the use of industrial by-products, improved microstructural characteristics of concrete and reduced environmental impact through lower greenhouse gas emissions. The cost of SCC will be reduced by SCMs especially if the mineral additive is an industrial by-product. SCMs have been shown to improve short- and long-term effects of concrete [1]. SCMs and natural pozzolans such as metakaolin (MK) and limestone powder are replaced with concrete partially and are one option for lowering the cost of SCC [5]. The use of blended cements is becoming ever more popular around the globe. But, the cements being used abroad and also the needs of nation industry norms, range. These observations have been made different societies, owing differences in standards which all depend upon environmental factors, location of construction and amp; availability of raw materials. With the addition of SCMs, multiple properties of concrete were improved. Using a large volume single type, SCM could have adverse effects on strength mixes such as strength and durability. With its microscopic particle diameter, silica fume likely to drain the water needed. Introducing 50% slag must provide effective shielding from alkali-silica [6]. This action might result in less protection to de-icer scaling. The inclusion of fly ash posed a drawback that reduces the early strength rate, setting time. Effective use of ternary blends enables influence of single SCM to make up the difference for the basic flaws of others. For e.g., silica fume added with slag can eliminate water gain on concrete surface. In similar way, by using quaternary blends which are also well known as high-performance green concrete by adding replacing cement with max amount of blended cements makes the structure more denser compare to conventional mixes [7, 8].

The previous research amongst many authors has shown that fibres can aid to overcome bending and fracture propagation in reinforced concrete [9]. Fibres in reinforced concrete might cause the initial fracture and collapse and can have enhanced as a result of this capacity to tensile strength in the case of flexural loading and stop extensibility and fractures [10].

2 Experimental Study

Steel fibre reinforced concrete's flexural behaviour built with water-binder ratios 0.30 and 0.40, quaternary mixed self-compacting concrete slabs is investigated in terms of load-deflections features in this work. The initial fracture load and ultimate load bearing capability of quaternary mixed SCC slabs characteristics are studied. The loads and deflections for SCC and fibre reinforced QBSCC mixtures are shown below. The flexural behaviour of SCC beams and QBSCC slabs using steel fibres addition from 0–1.5% is investigated. The under reinforced portion is made up of reinforced concrete slab specimens measuring 1200 mm × 1200 mm × 100 mm. 8 mm@150 mm c/c are the details of reinforcement used in the two directions, with fibres of steel which are crimped in nature are used, measuring 30 mm in length and 0.5 mm in diameter (L/d ratio—60) (Tables 1 and 2).

Figures 1, 2 and 3 show blended SCC and its flow properties. Figures 4, 5 also shows blended SCC and its flow properties (specimen and testing). Figures 6, 7 and 8 illustrate quaternary mixed fibre reinforced slabs that are casted for varying per cents of fibres and also evaluated after curing. This experiment makes use of a 500kN hydraulic jack. Deflection at the centre is measured with dial gauge having L.C deflection at 0.01 mm. Throughout the research, deflections were recorded at 20 kN intervals, and loading at the first crack was documented. The test results for ten slabs were averaged and summarized in Table 3. Load–deflection characteristics of quaternary mixed concrete made with 0–1.5% fibres and control SCC for slabs for water-binder ratios of 0.40 and 0.30 (Figs. 9 and 10; Table 4).

3 Conclusions

The outcome of the work can be used to derive the following conclusions.

1. From the obtained results, it has become evident that the concrete of self-compacting blended type's properties has fulfilled the requirements as per EFNARC with inclusion or without the inclusion of mineral admixtures.
2. Quaternary blended SCC slabs of water-binder ratios 0.40 and 0.30 had nearly same maximum flexural strength to reference SCC mixes whereas ordinary SCC slabs deflected more than QBSCC slabs with and without fibre 1.5% fibre reinforced QBSCC slabs have better deflection capabilities as compared to various % fibre reinforced QBSCC slabs.
3. Slabs with QBSCC of 1.5% steel fibre content had higher flexural strength at both 0.4 and 0.3 water-binder ratios.

Table 1 Materials necessary for 1 m³ concrete for water-binder ratio 0.30 for 100% cement—SCC and QBSCC

Admixtures (%)	Ratio of W/B	Cement content (kgs)	F.A content (kgs)	GGBS content (kgs)	M.S content (kgs)	FA content (kgs)	CA content (kgs)	Water (l)	SP (l)	VMA (l)
Without replacement in cement	0.40	420	–	–	–	991	840	170	5.04	0.42
	0.30	620	–	–	–	890	750	188	7.56	0.59
40% cement + 25% FA + 25% GGBS + 10% microsilica	0.40	168	105	105	42	991	840	170	5.04	0.42
	0.30	246	153	153	62	890	750	188	7.56	0.59

Table 2 Fresh properties as per the guidelines of EFNARC

S. No	Ratio of water-binder	Utilized mix	Recorded slump	T50 cm	L-box	U-box
1	0.4	SCC 1	712	4.3	0.90	28
2	0.4	QBSCC-1	724	4.1	0.92	29
3	0.3	SCC 2	675	3.9	0.83	26
4	0.3	QBSCC-2	715	3.0	0.85	23

Fig. 1 Blended SCC and its flow properties



Fig. 2 Blended SCC and its flow properties



Fig. 3 Blended SCC and its flow properties



Fig. 4 Blended SCC and its flow properties (specimen and testing)

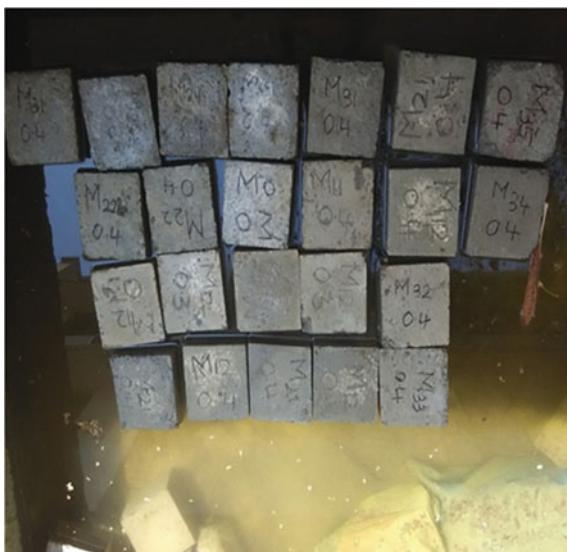


Fig. 5 Blended SCC and its flow properties (specimen and testing)



Fig. 6 Slab specimens after 28 days curing

Fig. 7 Slab specimen**Fig. 8** Slab testing

Table 3 Slabs's load-deflection characteristics after 28 days with a ratio of 0.4 W/B

S. No	SCC		% of QBSCC-0		% of QBSCC-0.5		% of QBSCC-1.0		% of QBSCC-1.5	
	Load (kN)	Deflection (mm)	Load (kN)	Deflection (mm)	Load (kN)	Deflection (mm)	Load (kN)	Deflection (mm)	Load (kN)	Deflection (mm)
1	20	0.61	20	0.64	20	0.56	20	0.44	20	0.47
2	40	1.10	40	1.21	40	1.72	40	0.93	40	0.95
3	60	2.65	60	2.32	60	2.16	60	1.61	60	1.05
4	80	3.40	80	3.63	80	3.26	80	2.95	80	2.43
5	100	4.65	100	4.78	100	3.93	100	3.25	100	3.04
6	120	6.15	120	5.32	120	4.87	120	5.52	120	4.32
7	140	6.98	140	7.43	140	7.41	140	6.65	140	5.85
8	160	8.56	160	8.72	160	8.23	160	8.42	160	7.42
9	180	9.23	180	9.72	180	9.54	180	9.32	180	8.76
10					200	9.93	200	10.62	200	9.43
11									220	9.72

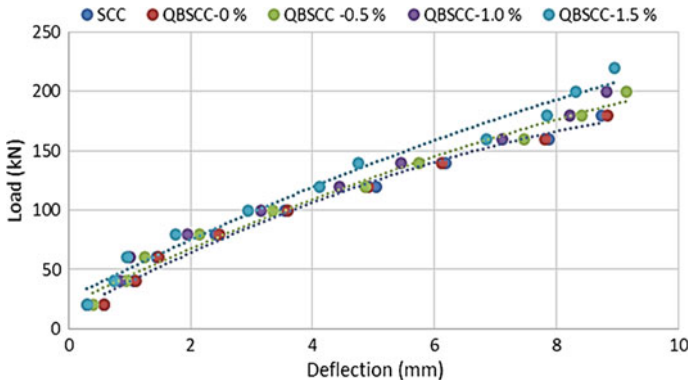


Fig. 9 Characteristics of load–deflection of slabs of water-binder ratio 0.40

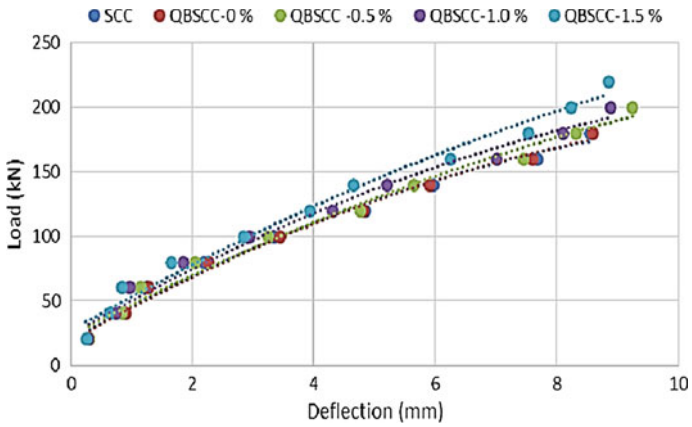


Fig. 10 Characteristics of load–deflection of slabs of water-binder ratio 0.30

Table 4 Slabs's load-deflection characteristics after 28 days with a ratio of 0.3 W/B

S. No	SCC		% of QBSCC-0		% of QBSCC-0.5		% of QBSCC-1.0		% of QBSCC-1.5	
	Load (kN)	Deflection (mm)	Load (kN)	Deflection (mm)	Load (kN)	Deflection (mm)	Load (kN)	Deflection (mm)	Load (kN)	Deflection (mm)
1	20	0.40	20	0.30	20	0.32	20	0.31	20	0.32
2	40	0.92	40	1.43	40	1.25	40	0.83	40	0.50
3	60	2.25	60	2.42	60	2.23	60	0.84	60	0.56
4	80	3.12	80	3.35	80	3.43	80	2.12	80	2.15
5	100	4.62	100	4.67	100	4.56	100	3.45	100	3.14
6	120	5.43	120	5.98	120	5.43	120	5.12	120	5.04
7	140	6.23	140	6.32	140	6.17	140	6.11	140	5.15
8	160	8.42	160	8.74	160	6.93	160	6.95	160	5.45
9	180	9.25	180	9.43	180	7.94	180	7.31	180	6.54
10					200	8.85	200	8.70	200	8.14
11									220	8.98

References

1. Jodeiri AH, Qaitlig RJ (2012) Effect of wirand FS7-II steel wire fibre on flexural capacity of reinforced concrete beam. *J Civ Eng Res* 2(6):100–107
2. Devi GSL, Rao PS (2017). Flexural behavior of quaternary blended fiber reinforced self compacting concrete beams using mineral admixtures. *i-Manager's J Civ Eng* 7(2):1
3. Kukreja CB Chawla S (1989) Flexural characteristics of steel fiber reinforced concrete. *Ind Concrete J* 3(2)154
4. Su N, Hsu KC, Chai HW (2001) A simple mix design method for self-compacting concrete. *Cem Concr Res* 31(12):1799–1807
5. Vejmelková E, Keppert M, Grzeszczyk S, Skaliński B, Černý R (2011) Properties of self-compacting concrete mixtures containing metakaolin and blast furnace slag. *Constr Build Mater* 25(3):1325–1331
6. Sabet FA, Libre NA, Shekarchi M (2013) Mechanical and durability properties of self consolidating high performance concrete incorporating natural zeolite, silica fume and fly ash. *Constr Build Mater* 44:175–184
7. Hamoush S, Picournell-Dardner M (2011) Freezing and thawing durability of very high strength concrete. *Am J Eng Appl Sci* 4(1):42–51
8. Devi GSL, Rao PS, Devi S (2015) Review on blended concretes. *Int J Res Eng Technol* 4(3):47–55
9. Devi GSL, Rao PS (2016) Effect of freezing and thawing on quaternary blended self compacting concrete using mineral admixtures. *i-Manager's J Civ Eng* 7(1):17
10. Su N, Hsu K-C, Chai H-W (2009) A simple mix design method for self-compacting concrete. *Cement Concrete Res* 31(2001):1799–180
11. Sree Lakshmi Devi G, Srinivasa Rao P (2017) Durability of quaternary blended self compacting concrete using mineral admixtures. *Special issue on self compacting concrete. Ind Concrete J* 4(1):70–77

Influence of Mineral Admixtures and M-Sand on Fresh and Hardened Properties of Self-Compacting Concrete



S. Bhavanishankar, N. Jayaramappa, C. V. Sai Nagendra,
and C. Venkata Siva Rama Prasad

Abstract Reduced production of energy-intensive materials and increased usage of industrial by-products are only two of the numerous possibilities in the conservation of a few natural resources. Industrial by-products are used to partially substitute cement in concrete to enhance its characteristics. Sand is also one of the vital ingredients which play an essential role in the construction field. In this research, an experimental study is done to determine the characteristics of self-compacting concrete produced by adopting the materials like flyash, GGBS, and silica fume as partial substitutes of cement and M-sand instead of river sand is used. This paper discusses a total of five mixes such as control mix, M-sand as fine aggregate with GGBS 20%, M-sand as fine aggregate with Flyash 20%, M-sand as fine aggregate with silica fume 10%, and M-sand as fine aggregate with GGBS 20%, Flyash 20% and Silica fume 20%. Results shown that the fresh properties of SCC were found to be maximum for the mix with M-sand, GGBS, Flyash, and Silica fume and minimum for the mix with M-sand and 10% silica fume. Finally, the specimens casted using M-sand as fine aggregate and 10% silica fume as cement had the highest Strength in Compression.

Keywords Strength in compression · Self-Compacting concrete · M-sand · GGBS · Flyash · Silica fume

1 Introduction

A new quite concrete that is compact solely by all of its weight and also into any corner of exterior sheathing, proposed by Okamura (1997). The self-compacting potential of this concrete can be greatly influenced by the material properties and

S. Bhavanishankar · N. Jayaramappa · C. V. Sai Nagendra (✉)
Department of Civil Engineering, UVCE, Bangalore University, Bangalore, Karnataka 560056,
India

C. Venkata Siva Rama Prasad
Department of Civil Engineering, St. Peters Engineering College (Autonomous), Dhulapally,
Maisammaguda, Medchal (Dt), Hyderabad, Telangana 500100, India

mix proportions. In his research, Okamura [1] recommended 50% solid and 40% mortar aggregate volume as coarse and fine, respectively, such that self-compacting ability could be readily achieved by simply altering the w/c ratio and admixture dose. The construction of a more fluid concrete had several benefits, including increased efficiency and reduced energy consumption, working environment quality. SCC has rapidly evolved in various areas of the construction industry, allowing it to be used for both in-situ and precast processing. In comparison to conventionally vibrated concrete, it requires no external apparatus for compaction and thereby decreases noise emissions at work locations [2].

SCC might be made in three ways: by raising the powder content by adding fines (through mineral admixtures) as cement, or using water binder ratio as 0.8 to 1 (EFNARC) as well as substituting fine aggregate, using SP and VMA as admixtures in the formulation of SCC mix with doses applied as a percentage of the total weight of cement integrating both natural and chemical admixtures with an ideal water binder proportion of 0.3–0.4 and optimal chemical doses [3].

Nowadays, Cement is commonly employed in the construction of concrete structures on a global scale. As a result, global cement demand has risen to nearly 5 billion metric tons. As a measure, a vast volume of production of cement necessitates the use of raw materials, resulting in a large amount of CO₂ released into the environment. About one ton of CO₂ gas emission can be observed During the manufacture of a ton of cement. SCMs as a tool of environmental protection is the subject of extensive investigation. Industrial wastes are being used to create cementitious materials with pozzolanic characteristics. Pozzolanic wastes of different industries, such as Silica Fume (SF), Rice Husk Ash (RHA), Ground Granulated Blast Furnace Slag (GGBS), Fly Ash (FA), and others, are being utilized as cement substitute materials [4].

The total annual global supply of coal ash is expected to be about 700 million tons, Fly ash accounts for at least 70% of that. The addition of FA to the mixture of concrete might enhance the slump while lowering the cost. It also lowers the demand for fine materials, which are all used in construction of buildings. The use of FA also decreases the requirement for viscosity-increasing chemical admixtures. The less water content in the concrete, the greater the longevity and mechanical integrity of the structure [5]. Venkata Kavyateja [6] studied the self-compacting concrete, which was developed by partial substitute of cement with flyash (25%) and alccofine (5, 10, 15%). At all curing ages, the mechanical characteristics of SCC increased for the mix containing 25% fly ash and 10% alccofine, according to the results. Mucteba Uysal [7] conducted studies on the impact of coarse aggregate form on self-compacting concrete with flyash addition. Among the various aggregates being basalt, granite, marble, dolomite, and sandstone. As compared to other blends, the blend containing basalt aggregate and flyash demonstrated the highest strength properties.

The iron and steel industries across the world create about 400 million tons of slag each year. Slag production is rapidly increasing as a result of growing demand for steel and iron across numerous sectors. The produced slag is deposited haphazardly and improperly into landfills and urban environments, damaging the local environment. To mitigate environmental emissions caused by slag, researchers have begun to look for an alternative way of reusing it by mixing slag in different ways into concrete

mixtures [8]. Ali Nazari et al. looked at the role of GGBFS in SCC. Increased split tensile strength is achieved by increasing GGBFS content to 45.0 wt%, and the amount of CaO required for Ca (OH)₂ and the resultant C–S–H gel is reduced when GGBFS concentration is more than 45.0%. [9].

Silica fume is a pozzolanic amorphous substance made up of ultra-fine particles (0.01 m) that is a by-product in electric arc furnaces producing elemental silicon or Ferrosilicon alloys [10]. The impact of admixtures (metakaolin and micro-silica) on the mechanical characteristics of regular grades of SCC was deduced by Seelapureddy [11]. In M30 and M40 concrete grades, 10% metakaolin was found to be ideal in terms of workability and strength. The substitution of cement in portion with metakaolin resulted in a decrease in workability. The use of appropriate doses of alaphadine, on the other hand, improves workability. Replacing 10% of the cement with silica fume resulted in a 24.5% enhancement in strength in 7 days and a 38.9% strength improvement in 28 days for M30 grade. Using silica fume to replace 10% of cement resulted in a 33.4% and 48.5% increase in strength in 7 and 28 days for M40 grade mix. Karthikeyan [12] investigated the effect of silica fume (2.5, 5, 7.5, and 10%) in self-compacting concrete. The flow properties are reduced at 10% replacement, but the compressive strength values are increased.

Vivek et al. [13] examined binary blend characteristics of fresh and hardened self-compacting concrete of high strength. He compared the obtained compressive strength values to the characteristic strength and suggested the appropriate percentage of supplementary cementitious materials to improve the properties of SCC, such as SF in the range 5 and 10% as a cement substitute, metakaolin should be used about 20 and 25% of the time, while GGBFS should be used between 25 and 50%.

Overpopulation and continuous mining of river sand have resulted in natural disasters and environmental hazards. River sand is drained from river beds for the development of large infrastructures and houses to satisfy the demands of population growth. The rise of globalization and the advanced technology needed to meet the demands of the national and international world markets has created a big problem for the preservation of river sand used as aggregate in the manufacture of concrete. Hence, it is appreciable to replace sand with some of the materials like M-sand, bottom ash, slag, etc. Manufactured sand is created by grinding a cubical granite stone with grounded sides. This M-sand has been cleaned and graded for use as a building material to replace river sand [14]. M-sand, rather than river sand, provides adequate strength, reduces environmental concerns, and is an environmentally acceptable material [15]. M-sand enhanced flexural and tensile strength in SCC by approximately 50% [16]. When 10% of the weight of cement is replaced with SCM's like metakaolin, GGBS silica fume in self-compacting concrete, M-sand, rather than river sand, provides higher strength properties.

Table 1 Physical characteristics of OPC

Property	Standard consistency	Fineness	Initial setting time	Final setting time	Specific gravity
Test value	29%	6.15%	80 min	500 min	3.14

Table 2 Physical characteristics of river sand

Property	Specific gravity	Fineness modulus	Percentage bulking	Bulk density	Zone
River sand -test value	2.68	2.8	24.8%	1513 kg/m ³ (Loose) 1660 kg/m ³ (Rodded)	II

2 Materials and Test Methods

Self-compacting concrete is made from a variety of materials, which are mentioned below along with their material characteristics.

2.1 Cement

Ordinary Portland cement of grade 43 Zuari brand according to IS 12269: 1987 was employed in this research. Table 1 lists the material's characteristics.

2.2 Fine Aggregate

Locally accessible fine aggregates were employed in this study, which included river sand and M-sand. Table 2 shows the characteristics of river sand.

2.3 Coarse Aggregate

For this project, Crushed granite aggregate with a size of 20 mm and a size of 12.5 mm that satisfied IS standards was used as coarse aggregate. Table 3 illustrates the characteristics of coarse aggregates.

Table 3 Physical characteristics of coarse aggregate

Property	Specific gravity	Fineness modulus	Percentage bulking	Bulk density
Test value	2.62	7.8	24.8%	1387.8 kg/m ³ (Loose) 1465 kg/m ³ (Rodded)

Table 4 Physical characteristics of mineral admixtures

Material	Fly ash	GGBS	Silica fume
Specific gravity value	2.16	2.70	2.12

2.4 Water

All of the mixtures were made with locally accessible potable drinking water.

2.5 Flyash

In this investigation, fly ash from Bellary thermal power station, Karnataka has been used. The properties of the material are tabulated in Table 4.

2.6 Ground Granulated Blast Furnace Slag

The current study employed slag from the Bellary Jindal steel mill in Bangalore, Karnataka. Table 4 lists the properties of GGBS.

2.7 Silica Fume

Table 4 lists the characteristics of silica fume received from local vendors in Bangalore.

2.8 M-Sand

Another fine aggregate in concrete is manufactured sand that falls within Zone II grade as defined by IS 383 and is purchased from local vendors. The physical characteristics are listed in Table 5.

Table 5 Physical properties of M-sand

Property	Specific gravity	Fineness modulus	Bulk density	Zone
Test value	2.65	3.1	1830 kg/m ³ (Loose) 1950 kg/m ³ (Rodded)	II

Table 6 Physical properties of super plasticizer

Particulars	Form	Color	Specific gravity	Chloride content
Value	Liquid	Light brown	1.2	<0.2%

Table 7 Mix proportions

Mix	Cement (kg/m ³)	Fine agg. (kg/m ³)	Coarse Agg. (kg/m ³)	GGBS (kg/m ³)	Flyash (kg/m ³)	Silica fume (kg/m ³)	Water (l)	SP (l)
CMIX	596.18	925.93	673.9	0	0	0	189.26	5.96
Mix1	476.14	925.93	673.9	102.2	0	0	189.26	5.79
Mix2	476.94	925.93	673.9	0	81.76	0	189.26	5.58
Mix3	536.55	925.93	673.9	0	0	80.24	189.26	5.76
Mix4	298.08	925.93	673.9	102.2	81.76	80.24	189.26	5.22

2.9 Super Plasticizer

In this study, Glenium B233, a commercially available superplasticizer produced by BASF building chemicals (India) Pvt. Ltd., is utilized to make self-compacting concrete. Table 6 lists all of the characteristics.

2.10 Mix Proportions

A total of five mixes were done including control mix by using okumara and Ozava method of mix design (Japanese method). Mix proportions or quantities are represented in Table 7.

2.11 Tests on Fresh Self-compacting Concrete

At the early stage (Fresh) of Self-compacting concrete, Slump flow test and T50cm test, V-funnel test and V-funnel test at T 5 min, L-Box test, U-box test, and J-Ring test are all performed for all mixes. Table 8 summarizes the test results.

Table 8 Fresh properties results

Mix	Slump value (mm)	V-Funnel time (s)	T50 time (s)	J-Ring slump (mm)	J-Ring H (mm)	L-Box H ratio	U-box H (mm)
CMIX	670	12	5	655	8	0.81	25
Mix1	665	11.4	4.4	660	9	0.82	26
Mix2	675	10.3	3.5	665	7	0.85	24
Mix3	660	11.8	5.0	650	10	0.80	28
Mix4	680	9.6	3.7	670	7	0.89	20
As per EFNARC	650–800	12	2–5	–	10	0.8–1.0	0–30

Table 9 Mechanical property of cubes test results

Mix	Compressive strength (MPa)	
	7 Days	28 Days
CMIX	25.50	32.10
Mix1	22.23	34.66
Mix2	22.67	32.88
Mix3	24.84	35.95
Mix4	19.61	29.30

2.12 Compressive Strength Test

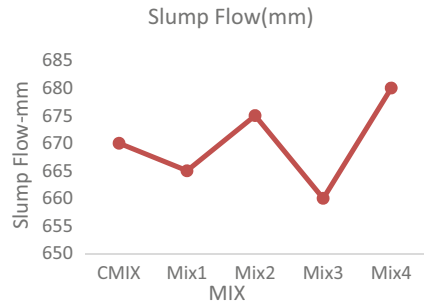
Compressive strength was evaluated on all self-compacting concrete samples. on a $150 \times 150 \times 150$ mm cube according to IS: 516-1959 standards. At room temperature, all of the concrete cubes were cast. All specimens at 7 and 28 days were used to assess compressive strength after curing, and the values are listed in Table 9.

3 Discussion of Test Results

3.1 Mineral Admixtures and M-sand Effect on SCC Fresh Properties

On fresh self-compacting concrete, various experiments are performed. According to the slump flow test data, mix 4 (casted with M-sand, GGBS, Silica fume, and Flyash) has a higher slump value of around 680 mm than the other mixes. The slump in the control mix was 670 mm, and by adding silica fume, the slump was reduced by around 1.470% relative to the control mix as shown in Fig. 1. For the T 50 cm test, the time required for Mix 2 (casted with M-sand and Fly ash) is 3.5 s, which is less

Fig.1 Slump flow value



than the time required for all other mixes, as seen in Fig. 2. Mix 4 takes 3.7 s, which is less than the control mix but more than mix 2. Control mix and mix 3 (silica fume and M-sand) have the same values, which are greater than mix 2 by around 30% as shown in Fig. 3. The percentage J -ring H test @ T50 cm is the lowest for a mix with flyash and the highest for a mix with silica fume. According to the J-Ring H test slump value, the mean slump value is obtained for mix 4 (M-sand, GGBS, Silica fume, and Flyash) around 670 mm and the minimum slump value is obtained for mix with silica fume around 650 mm, which is less than 2.98 percent. For control mix (scc using river sand) the value is about 655 mm which is less about 2.23% compared to mix 4 as shown in Fig. 7. Similarly, a V-funnel test is performed, and it is found that mix 4 (which contains both mineral admixtures and M-sand) has the shortest time, i.e., about 9.6 s, and the control mix (which contains river sand) has the longest

Fig. 2 T50 time (s)

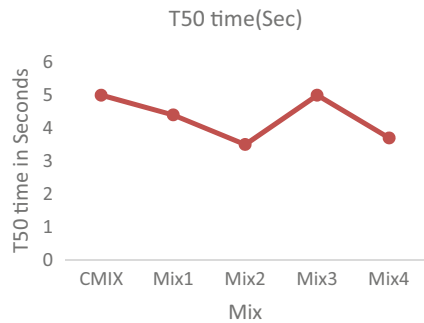


Fig. 3 J-ring H (mm) value

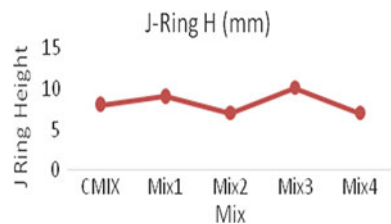


Fig. 4 V-funnel time (s)

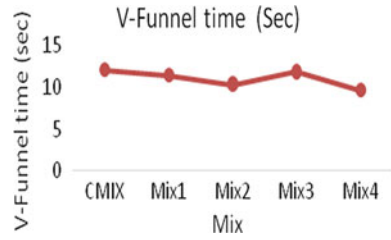


Fig. 5 L-Box H ratio

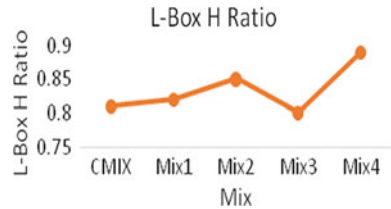
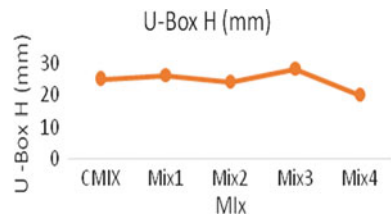


Fig. 6 U-Box H (mm)



time, i.e., about 12 s, as compared to the other mixes, as shown in Fig. 4. The time reduction is about 20% as compared to mix 4. For L-Box H ratio test the mix with minimum value is obtained for mix with silica fume about 0.8 and the maximum value is obtained for mix with all mineral admixture (mix 4) about 0.8 as shown in Fig. 5. The percentage difference in L-Box H ratio between control and mix 4 is approximately 8.98%. According to the results of the U-box survey, mix 4 has a lower value of about 20 mm, and mix with silica fume (mix 3) has the highest value of about 28 mm as compared to all other mixes, as seen in Fig. 6. The percentage difference in U-box H values between control and mix 3 is approximately 10.71%.

3.2 *Effect of Mineral Admixtures and M-sand on Hardened SCC Properties*

The results of the experiments on the influence of mineral admixtures and M- sand on strength properties are shown in Table 9. Based on these findings, it was found that at early ages, i.e., at 7 days, the mix’s compressive strength casted with river sand, i.e., the control mix is higher in comparison to all other mixes, with a value of

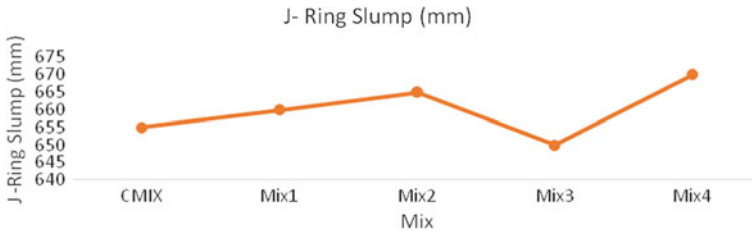


Fig. 7 J-Ring slump value

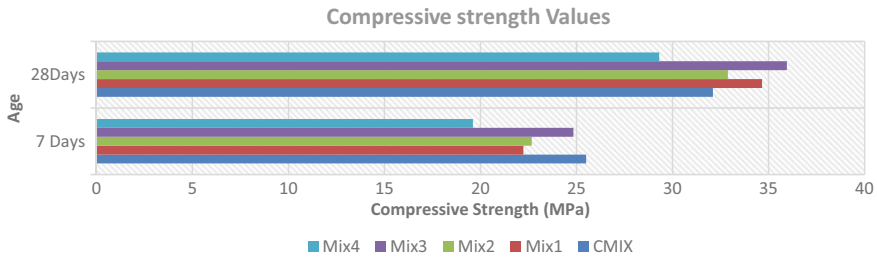


Fig. 8 Compressive strength of SCC mixes

around 25.5 N/mm². The collected intensity is smaller than that of other blends and is approximately 19.61 N/mm². Mix 4’s strength decreases by around 23.09 percent in comparison to the control mix. Many of the mixes performed better at 28 days after curing, with the exception of mix 4, which achieved 29.3 N/mm². As shown in Fig. 8, the specimens cast with silica fume and M-sand (Mix 3) had the highest compressive strength of about 35.95 N/mm² when compared to all other mixes. From the above values, it is observed that the silica fume and M-sand assists in attaining optimum strength in compression compared to control mix of SCC and the mix with all mineral admixture’s combination concludes that, the combination of all SCM’s did not help in enhancement of compressive strength of SCC at initial ages.

3.3 Relationship Between Fresh Properties and Hardened Properties Results

The linear relationship between the values of slump flow and fresh characteristics, as well as the slump flow and compressive strength, is computed and summarized in Table 10 depending on results of the tests obtained for all of the mixes.

Table 10 Equation and R² values for all tests

S. No	Slump test	V funnel	T50	J ring	L-Box ratio	U-Box	Compressive strength	Equation	R ²
1	x	y	-	-	-	-	-	$y = -0.11x + 84.72$	0.7121
2	x	-	y	-	-	-	-	$y = -0.07x + 51.22$	0.6162
3	x	-	-	y	-	-	-	$y = 0.9x + 57$	0.8100
4	x	-	-	-	y	-	-	$y = 0.0042x - 1.98$	0.8289
5	x	-	-	-	-	y	-	$y = -0.36x + 265.8$	0.9205
6	x	-	-	-	-	-	y	$y = -0.3016x + 253.05$	0.8756

4 Conclusions

1. Based on the results of the experiments, it suggests that manufactured sand can be used in lieu of river sand to improve SCC characteristics.
2. The compressive strength of 10% silica fume self-compacting concrete showed higher value of about 35.95 MPa than SCC alone with river sand and SCC with other admixtures and M-sand.
3. The combined addition of admixtures and M-sand in SCC is failed to enhance the strength property.
4. It was observed that based on fresh properties such as Slump Flow, J-Ring Slump Flow, J-Ring H value, and L-Box Ratio, 10% silica fume and M-Sand in SCC mix were poorly assisted to achieve the value, but the combination of admixtures and M-sand in SCC offered assistance to achieve optimum slump.
5. The other fresh properties like U-box H and T50 test, it was found that the mix with 20% flyash and M-sand in SCC was found to be minimum and maximum for 10% Silica fume and M-sand in SCC.
6. Finally, evaluating fresh and hardened properties, it is evident that the combination of admixtures and M-sand offers the best assistance in fresh properties but fails to increase SCC strength.

References

1. Okamura H (1997) Self-compacting concrete. *Concrete Int* 50–54
2. Petean AI, Nadasan L, Sabau M, Onet T (2013) Self-compacting concrete an innovative concrete. *Int J Eng Tome XI, Fascicule 3*. <https://doi.org/10.6084/m9.figshare.5443186>
3. Ramanathan P, Baskar I, Muthu Priya P, Venkata Subramani R (2013) Performance of self-compacting concrete containing different mineral admixtures. *KSCE J Civ Eng* 17(2):465–472
4. Malhotra V (2002) Introduction: sustainable development and concrete technology. *Concrete Int* 24(7):235–242
5. Yazici H (2008) The effect of silica fume and high-volume Class C fly ash on mechanical properties, chloride penetration and freeze–thaw resistance of self-compacting concrete. *Constr Build Mater* 22:456–462
6. Venkata Kavya Teja B, Guru Jawahar J, Sashidhar C (2020) Effectiveness of alccofine and fly ash on mechanical properties of ternary blended self-compacting concrete. *Mater Today Pro* <https://doi.org/10.1016/j.matpr.2020.03.152>
7. Uysal M (2012) The influence of coarse aggregate type on mechanical properties of fly ash additive self-compacting concrete. *Constr Build Mater* 37:533–540. <https://doi.org/10.1016/j.conbuildmat.2012.07.085>
8. Xue Y, Wu S, Hou H, Zha J (2006) Experimental investigation of basic oxygen furnace slag used as aggregate in asphalt mixture. *J Hazard Mater* 138(2):261–268
9. Nazari A, Riahi S (2011) The role of SiO₂ nanoparticles and ground granulated blast furnace slag admixtures on physical, thermal and mechanical properties of self-compacting concrete. *Mater Sci Eng A* 528:2149–2157
10. Malhotra VM, Bremner TW, Caratte GG (1992) Flyash, silica—fume, slag and natural pozzolana cement. In: 4th international conference, Turkey

11. Seelapureddy J, Bommisetty J, Seshagiri Rao MV (2020) Effect of metakaolin and micro silica on strength characteristics of standard grades of self-compacting concrete. Mater Today: Proc <https://doi.org/10.1016/j.matpr.2020.02.936>
12. Karthikeyan J, Arunkumar C (2013) Influence of silica fume in self-compacting concrete under its fresh and hardened state. In: Conference: 7th RILEM conference on self-compacting concrete, Paris, France
13. Vivek SS, Dhinakaran G (2017) Fresh and Hardened properties of binary blend high strength self-compacting concrete. Eng Sci Tech Int J 20:1173–1179
14. Ramesh D, Rajesh V (2018) Influence of m-sand and addition of steel fibres in self-compacting concrete. Int J Pure Appl Math 119(17):3305–3310
15. Hima Venkata Mahalakshmi S, Khed VC (2020) Experimental study on M-sand in self-compacting concrete with and without silica fume. Mater Today: Proc <https://doi.org/10.1016/j.matpr.2020.01.432>
16. Gokulnath V, Ramesh B, Priyadharsan K (2019) Influence of M-Sand in self-compacting concrete with addition of glasspowder in M-25 grade. Mater. Today: Proc <https://doi.org/10.1016/j.matpr.2019.08.188>

Experimental Investigation on Compressive Strength and Permeability of Pervious Concrete Pavement (PCP) with Alternative Mixes



Pala Gireesh Kumar, Abhirami Priyanka Pathivada,
and Velugoti Sasi Jyothshima Himaja

Abstract Sustainability has a monopolizing proportion over decades and the augmentation to the world of sustainable technology extends itself implying in various fields of transportation sectors like pavements. The present paper substantially explicates the concept of sustainable pervious concrete pavement (PCP) technology, meticulously analyzed for the behavioral dependency of PCP with constituent materials transposed. It clinched an optimum possible mix for PCP with all the aspects correlated. On top of the aforesaid, the properties such as void ratio, water-cement ratio, compressive strength, permeability, etc., were supervised for multifarious conditions, for the enhancement of the life span of the pavement. In furtherance with the priors, the behavior with variability of PCP's behavior was toiled along with the inclusion of admixtures. In the fullness of time, this paper bestows PCP at an intensified rate and endows results of all the aforementioned properties with graphitized analysis and thereby, proffering the sustainability of a previous pavement in terms of design life and permeability that acts as a beneficiary to the stormwater management.

Keywords Pervious concrete pavement (PCP) · Compressive strength · Permeability · Water-cement ratio · Void content

1 Introduction

Over decades, science and inventions have routed way into the new era of computers and technology. The leading edge has grown with time and finally led to the intellectual world that is automated and controlled with systems. In accordance, the wealth and global economy witnessed plenty of hikes. With an urbane living and a polished lifestyle, the quantum of risk has also grown with time. The quarter of climate, environment, and atmosphere, aroused the need for a tremendous check of

P. G. Kumar · A. P. Pathivada (✉) · V. S. J. Himaja
Department of Civil Engineering, Shri Vishnu Engineering College for Women (Autonomous),
Bhimavaram, West Godavari District 534202, India

these factors. Analogically, extreme ends of great infrastructure, intelligent transport systems, automatized maintenance techniques are witnessed in the course of civil engineering. With greater advancing aspects, the realm of sustainability needed prior enforcement. The term sustainability accords to the art perpetuating an eco-friendly environment within a sophisticated society at a balanced economical rate. In accordance, sustainability in terms of economy, infrastructure, and transportation steered intensively. In this regard, transportation has seen many revolutions and especially in the area of pavements. A lot of pavements with multifarious pros got introduced. Though pavement splits into rigid and flexible, we have come across the pavement of Hot Mix Asphalt, pavement of Fine or Coarse Grade Asphalt, pavement of Stone Mastic Asphalt, concrete pavement, composite pavement, pervious pavement, etc. Of all the available paving types, the one that juts above all is the pervious concrete pavement (PCP).

The appellation of pervious concrete pavement refers to the pavement being permeable. PCP embraces leading precedence for sustainability and has proven to be a better option regarding design life, maintenance, and eco-friendliness. The concept of stormwater management is one of the predominant factors that sympathizes with PCP and has proven to be one of the best alternatives for water conservation. The average annual precipitation is around 990 mm, and most of it is getting wasted and often seen stagnated in areas. In highly developed societies, roads are the most frequently occurring constructions, and with proper operational methods like the adoption of PCP, water can be conserved. In addition to stormwater management, PCP also assists in the lower urban heat island effect that eventually reduces variations due to temperature changes. Also, the emission of oxides of carbon and other gases is less in the case of PCP. Apart from the environmental considerations, PCP holds an advantage concerning economic aspects like lower utilization of cement content that leads to cut in pricing and easy maintenance is one among the economy factor. On top of all the aspects prevailing, the design life of PCP is accountable but, low strength is one of the backdrops that is dwindling the use of PCP as a replacement for existing paving methods. To emphasize PCP usage and to propose optimum mix design considerations, experimental works were carried upon various mixes with varying water-cement ratios along with void content. The results of admixtures inclusion are analyzed in this study along with the proposal of maintenance methods and remediation techniques.

2 Appraisal of Anterior Studies

Pavement being a capacious sector with a diversified area of study, PCP witnessed new research work proposals and advancements in various aspects. Few influencing facets of PCP are scrutinized thoroughly and presented in this paper.

Table 1 Previous studies of strength attribute of PCP

Author (Year)	Notable entries
Uma Mageswari and Narasimha (2013)	Strength altered from 10 to 26 MPa with inclusion of fines and reduction in aggregate size [1]
Mageswari et al. (2016)	PCP exhibited compressive strength up to 15 MPa for cement to aggregate ratio of 1:10 with W/C ratio of 0.36 [2]
Divya Bhavana et al. (2017)	Zeolite inclusion by 10% inferred compressive strength of 9.15 MPa whereas, for conventional mix, it is noted to be 8.5 MPa for cement to aggregate ratio of 1:4 [3]
AlShareedah and Nassir (2020)	Inclusion of fibers of polypropylene showcased an increase of compressive strength by 25% and flexural strength by 37% [4]
Tijjani et al. (2019)	PCP with Recycled aggregate exhibited 7% lower strength in comparison with granite PCP despite having greater permeability and void content [5]

2.1 Explication of Strength Attribute of PCP

Strength is one of the predominant characteristics that nearly define the worth of a pavement. It is considered as a deciding factor for paving a surface. Table 1 briefly explains the numerous studies carried out concerning the strength of the PCP mix.

2.2 Explication of Void Content and Permeability of PCP

PCP's usage is totally dependent on the percentage of void content that is maintained throughout its design life to incur permeability. More the void content, higher is the advantage of permeability. Table 2 explicates void content influence over PCP.

2.3 Explication of Aggregate Usage in PCP

The size of aggregate influences the attributes like strength, permeability, and infiltration rate. Under aggregates, the type of aggregates such as recycled aggregates or crushed aggregates implies the increment and decrement of PCP properties. Table 3 elucidates the predominant key factors from previous research.

Table 2 Permeability of PCP with regard to void content—notes from previous studies

Author (Year)	Notable entries
Jayasuriya and Kadurupokune (2008)	PCP exhibited a range of 60% lowered runoff when tested in the field which no other pavement type ever shown [6]
Kevern and Dan Sparks (2013)	It is identified that the cement slurry often led to decline of voids and eventually lowering permeability, therefore a good mix proportion is crucial for a good PCP [7]
Kamarul Zaman et al. (2019)	Cement to Aggregate ratio of 1: 8 showed an infiltration ranging between 1250 to 3250 L/m ² /min and 1:9 as 2300 to 2700 L/m ² /min [8]
Gagandeep et al. (2019)	Mix with no FA exhibited a flow rate of 820 in/ hr whereas a mix with 1 part of sand of C:A ratio 1:7 exhibited 950 in/h of flow rate [9]
Meng et al. (2019)	Placement of geogrids at variable depths exhibited 20% porosity and 640 in/h flow rate [10]

Table 3 Key observations concerning the aggregate usage in PCP

Author (Year)	Notable entries
Abd Halim et al. (2018)	CA of size 10 mm evaluated better results of permeability when compared to CA of 5 mm to 8 mm or low [11]
Yanya (2018)	Usage of recycled aggregate (RA) influenced the strength and permeability aspect. Inclusion of RA showcased rise in permeability and strength up to a point and started decreasing with increase in RA addition [12]
Ulloa-Mayorga et al. (2018)	Natural Aggregate exhibited better properties in comparison to RA but with increase in cement paste content, strength with RA is more than NA as the RA is able to absorb the slurry [13]
Galishnikova et al. (2020)	RA was replaced at a percentage of 0–100 which finally showed that at 50%, strength increment is noted [14]

2.4 Miscellaneous Study

Apart from the above-stated works, there are several studies on the aspects like maintenance methods of PCP involving pressure washing that restores around 80% of infiltration rate [15]. It is observed that a design life of 20 years can be achieved with proper maintenance [16] and the level of emission of greenhouse gases like carbon dioxide is less in PCP in comparison with other pavements [17]. An 8-year study revealed that a good PCP eventually dilutes harmful vehicular emissions with the installation of exhausts for air circulation [18]. Differential heating effects of PCP have proven to be one of the dominating traits that hold resistance to the urban heat island effect [19] thereby, ensuring a quality pavement that is environment friendly and easily maintained with minimal cost of maintenance [20].

Table 4 Properties of cement from the test results

Grade	OPC grade 43
Initial setting time	57 min
Final setting time	436 min
Standard consistency	31%
Specific gravity	3.21

3 Experiential Approach

The work is of two phases where casting cylinders for varying water-cement ratios and void content with cement & aggregate content kept constant comprises phase one. The cylinders are tested for 28 days of compressive strength and permeability. Of all the mixes of varying concerns, the mixes which yielded the maximum strength and permeability rate are considered for phase 2. The second phase appertions with the experimental approach based on the inclusion of admixture, Ground Granulated Blast-Furnace Slag (GGBS) in the mixes in varying percentages. Admixture is added to the mixes considered from phase 1 and then the cylinders are tested for compressive strength. Three specimens for each mix are cast in both the phases and the average of the three specimens is considered for every mix in every set. The tests are performed after 28 days for both phases.

3.1 Cataloging of Materials

As the constituent materials influence the pavement in terms of strength and other attributes, the detailing of the materials considered in the experimental program is stated vividly.

3.1.1 Cement

The cement utilized throughout the experimental work is ordinary Portland cement (OPC) of grade 43. The results of cement’s specific gravity, standard consistency, and setting time are tabulated in Table 4.

3.1.2 Coarse Aggregates

The coarse aggregates (CA) used are of rounded type about 10 and 20 mm sizes, tested for various properties and the results are stated in Table 5.

Table 5 Results of the tests on CA

Specific gravity	2.73
Impact value of aggregates (%)	23
Aggregate abrasion value (%)	33

3.1.3 Water

Water that is free from visible impurities is used in the work. As casting, curing, and testing require a hefty amount of water, an easy source of availability is taken into consideration.

3.1.4 Ground Granulated Blast-Furnace Slag (GGBS)

GGBS is used as a source of admixture in the phase two of the experimental work. GGBS is purchased from iron manufacturing unit where it is usually produced as a by-product during the iron manufacturing. The specific gravity of the GGBS used is stated to be 2.85 by the manufacturing unit and the GGBS exercised in the work is in powder form.

3.2 Material Mixing and Casting of Cylinders

Constituent tests for the materials are carried out and considering all the test results, the materials are used for mixing. A mixed proportion of cement to coarse aggregate ratio 1:4 is adopted for the experimental work. Cylinders of diameter 150 and 300 mm long are cast throughout the work. To avoid initial hydration due to the outside temperature, it is made sure that the casting is done on a shady day. Also, no mechanical vibrators are employed in the process as over-vibration results in loss of voids and thus fails the objective work. The cylinders are cast with varying W/C ratios and void content percentages. The specimens are demoulded after 24 h and cured for 28 days before testing for compressive strength and permeability.

3.3 Phase 1 Approach

As aforementioned, phase 1 considers casting of cylinders with varying ratios of water-cement and void content. A total of 27 cylinders were cast in phase 1. Three sets of cylinders are cast with a W/C ratio of 0.3 for set 1, 0.35 for set 2, and 0.4 for set 3. The casted cylinders are tested for compressive strength as per IS 516-1959 clause 5 with a gradual load from 140 kg/cm²/min increased without sudden shocks. In addition, the permeability is found using the constant head permeability method.

Table 6 Compressive strength and permeability values of set 1

Set 1 specimens	Cement content (kg/m ³)	CA content (kg/m ³)	W/C ratio	Void content (%)	Compressive strength (MPa)	Permeability (cm/s)
1a	330	1650	0.3	18	9.797	1.192
1b				20	8.908	1.299
1c				22	8.594	1.456

The permeability is calculated using the Eq. 1

$$K = \frac{QL}{Ah} \quad (1)$$

where,

K Permeability (cm/s).

Q Recorded discharge (cm³/s).

L Length of the cylindrical specimen (cm).

A Area of Cross- Section of the cylindrical specimen (cm²).

h Level height of constant head causing flow (cm).

3.3.1 Reported Values of Specimens with Water-Cement Ratio 0.3

The mix is designed for a W/C ratio of 0.3 where three levels of void content are maintained for three specimens each. The average of the three specimens of each mix is taken into account. The highest compressive strength of 9.797 MPa is recorded for the mix with 18% void content whereas highest permeability of 1.456 cm/sec is recorded for the mix with void content of 22%. Table 6 elucidates the mix details along with the test results obtained after 28 days for compressive strength and permeability of set 1.

3.3.2 Reported Values of Specimens with Water-Cement Ratio 0.35

The mix is designed for a W/C ratio of 0.35 with void content percentages maintained for three specimens. The average of specimens witnessed 11.546 MPa as highest compressive strength for the mix with 18% void content and 1.252 cm/sec as highest permeability for the mix with void content of 22%. Table 7 portrays the mix details of set 2.

Table 7 Compressive strength and permeability values of set 2

Set 2 specimens	Cement content (kg/m ³)	CA content (kg/m ³)	W/C ratio	Void content (%)	Compressive strength (MPa)	Permeability (cm/s)
2a	330	1650	0.35	18	11.546	0.795
2b				20	10.979	1.154
2c				22	9.940	1.252

Table 8 Compressive strength and permeability values of set 3

Set 3 specimens	Cement content (kg/m ³)	CA content (kg/m ³)	W/C ratio	Void content (%)	Compressive strength (MPa)	Permeability (cm/s)
3a	330	1650	0.4	18	14.2	0.629
3b				20	13.499	0.899
3c				22	12.287	1.130

3.3.3 Reported Values of Specimens with Water-Cement Ratio 0.4

A W/C ratio of 0.4 is used for the mixes in set 3 with the maintenance of void content differential for three specimens each. The experimental approach has seen the mix with 18% voids showcasing a high compressive strength of 14.2 MPa and 22% voids mix showing a high rate of permeability of 1.130 cm/sec which are the average values of three specimens. Table 8 manifests the mix details of set 3.

3.3.4 Analysis of Compressive Strength and Permeability Results from Phase 1 Approach

From the performed experimentation with varying void content percentages and W/C ratios, differential results are inscribed. The compressive strength from each mix of every set is represented graphically in Fig. 1 where it elucidates that the highest strength of 14.2 MPa is recorded for 18% void content at 0.4 W/C ratio. Likewise, the excessive permeability of 1.456 cm/sec is recorded 22% void content at 0.3 W/C ratio as shown in Fig. 2. It is evident that increase in W/C ratio enhances strength despite lowering permeability and vice versa.

3.4 Phase 2 Approach

From the experimental work performed and the graphical representation illustrated in 3.3.4, it is comprehensible that the mix 3a comprising of W/C ratio 0.4 with void

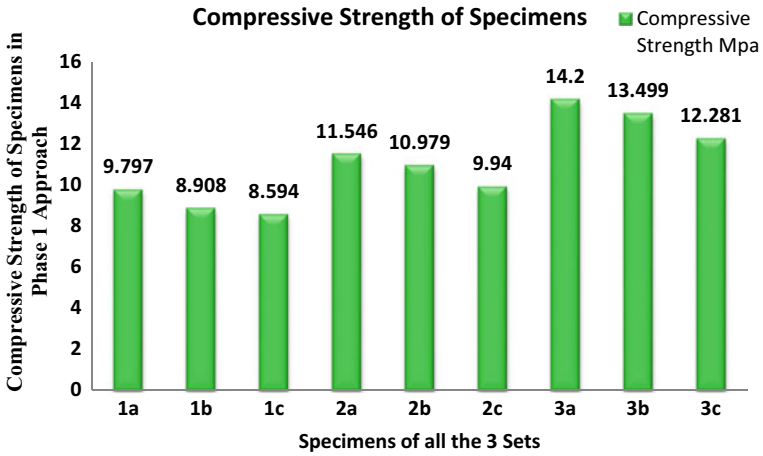


Fig. 1 Compressive strength of specimens in phase I approach

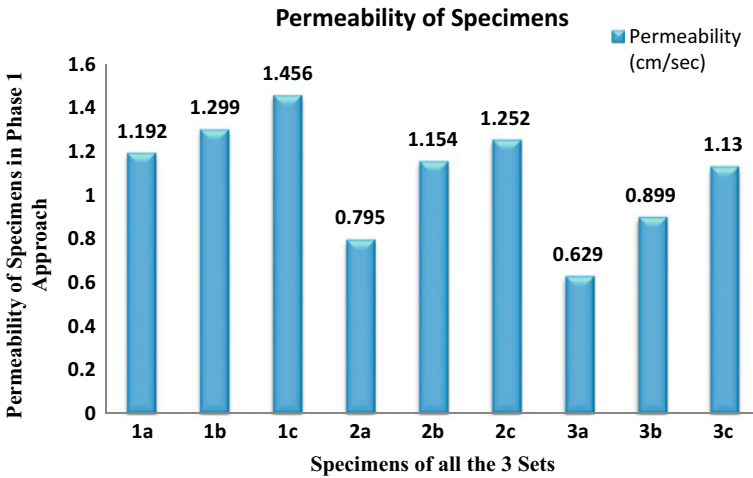


Fig. 2 Permeability of specimens in phase I approach

content 18% resulted in higher compressive strength of 14.2 MPa. Also, highest permeability of 1.456 cm/s is observed for mix 1c of 0.3 W/C ratio at 22% void content and thus, these two mixes are taken into consideration for phase two of the work where GGBS is added to the considered mixes in 10, 20, 30, and 50%.

Table 9 Compressive strength and permeability values of Mix 3a with the inclusion of GGBS

Set 4 specimens	GGBS inclusion (%)	Compressive strength (MPa)	Increment in strength with GGBS (%)	Permeability (cm/s)	Decline in permeability with GGBS (%)
4a	10	14.645	3.13	0.607	3.5
4b	20	15.140	6.62	0.590	6.2
4c	30	15.717	10.68	0.555	8.5
4d	50	15.790	11.19	0.534	12.1

Table 10 Compressive strength and permeability values of mix 1c with the inclusion of GGBS

Set 5 specimens	GGBS inclusion (%)	Compressive strength (MPa)	Increment in strength with GGBS (%)	Permeability (cm/s)	Decline in permeability with GGBS (%)
5a	10	8.872	3.24	1.409	3.26
5b	20	9.169	6.7	1.360	6.59
5c	30	9.494	10.47	1.324	9.1
5d	50	9.542	11.03	1.291	11.35

3.4.1 Results from the Addition of GGBS to Mix 3a

To elevate the compressive strength of the mix, GGBS is added in various percentages in powdered form. Cylinders are cast with the mix design of W/C ratio 0.4 and void content 18% inclusive of GGBS and are tested for compressive strength and permeability after 28 days. The results are tabulated in Table 9.

3.4.2 Results from the Addition of GGBS to Mix 1c

GGBS is added to the mix 1c in varying percentages of 10, 20, 30, and 50% where a W/C ratio of 0.3 and void content of 22% is used. The results of compressive strength and permeability are represented in Table 10.

3.4.3 Analysis of Compressive Strength & Permeability Results from Phase 2 Approach

With the inclusion of GGBS in various percentages, evident changes are observed in compressive strength as well as in permeability. With increase in inclusion of GGBS, the compressive strength in set 4 and set 5 have exhibited inclination in strength aspect whereas, a decline is observed in case of permeability. Figure 3 illustrates

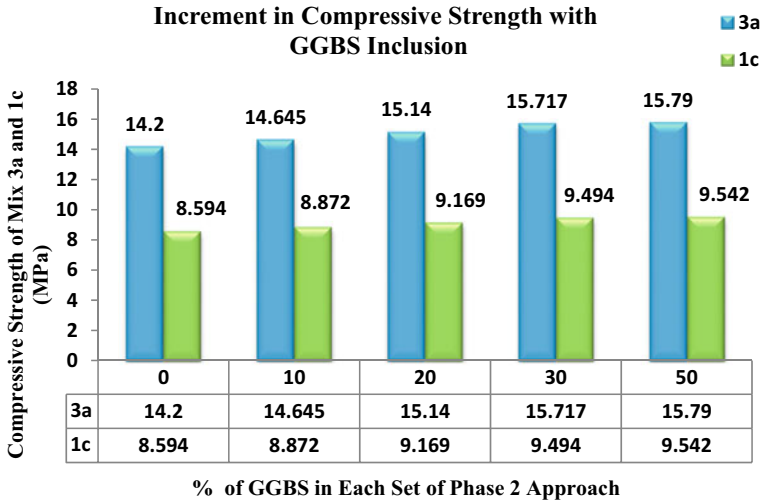


Fig. 3 Increment in compressive strength with GGBS inclusion

the incremental evidence recorded for compressive strength and Fig. 4 explicates the declination observed in permeability.

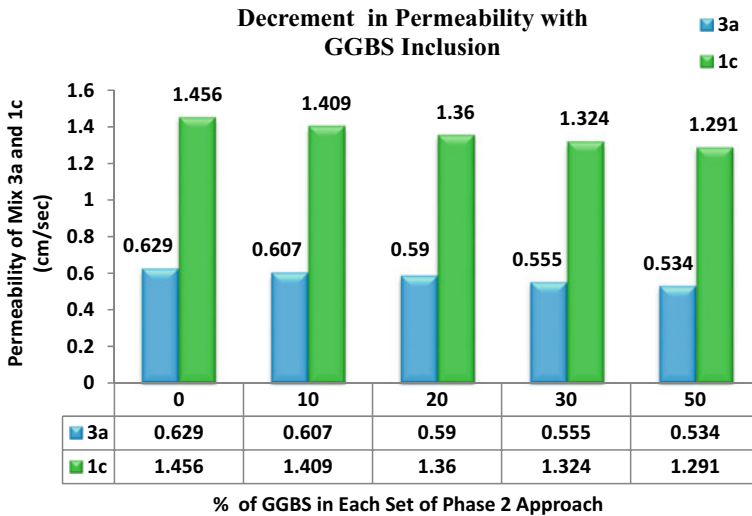


Fig. 4 Decrement in permeability with GGBS inclusion

4 Conclusions

From the performed experimental work, the results have cleared the way for the following conclusions,

- The compressive strength has witnessed an escalation with lower void content and a higher W/C ratio. However, the vice versa formulates the permeable behavior in the case of pervious concrete pavement. Thus, the extensive strength rate of 14.2 MPa is observed for a mix with a 0.4 W/C ratio where a void content of 18% is withheld. Despite a low permeability rate of 0.629 cm/s, it still falls under the optimal limitation to be used for paving of PCPs where rainfall intensity is of a lower level.
- In addition, the high permeability of 1.456 cm/s is recorded for a mix comprising a W/C ratio of 0.3 and void content of 22%. The compressive strength of 8.594 MPa makes it undesirable for heavy volume pavements whereas, it can be of high-performing paving material with heavy rainfall with low traffic volume.
- A mix with a W/C ratio of 3.5 and 20% void content resulted in the optimum values of compressive strength and permeability where the former reached is 10.979 MPa, and the latter is 1.154 cm/s.
- As the strength of PCP falls short in numerous circumstances, the inclusion of Ground Granulated Blast- Furnace Slag has proven to be one of the predominant choices.
- The inclusion of GGBS has shown incredible results where 10% of GGBS increased the compressive strength of the mix by 3, 20% of GGBS resulted in an increment of 6.5, and 30% of GGBS unconcealed an increase by 10.5%.
- The incorporation of 50% GGBS has not succeeded in producing sufficient increment in strength and, therefore, it is not suggestible to go for 50% of GGBS. Similar results and approximate increment is achieved through 30% inclusion as well.
- All in all, with the addition of GGBS in the mix, a decline in permeability is witnessed. Despite the flaw of decrease, the permeability rate can be preserved with simple maintenance methods thereby making it sustainable.
- With the results and analysis carried out, pavement of pervious concrete proves to be the best replacement for conventional concrete pavement as it deals with.
- Stormwater management and the sustainable maintenance of PCP makes it predominant in the sector of pavements.

Therefore, a mix of Cement to Coarse Aggregate ratios of 1: 4 with the inclusion of GGBS at 30% for a W/C ratio of 4 and void content of 18% proves to act as an optimal design mix for PCPs.

References

1. Uma Mageswari M, Narasimha VL (2013) Studies on characterization of pervious concrete for pavement applications. *Procedia Soc Behav Sci* 104:198–207
2. Mageswari M, Karthikeyan MP, Pavithran S, Rajkumar M, Govindarajan R (2016) High strength permeable pavement using no fines concrete. In: *SSRG Int J Civ Eng (SSRG-IJCE)* 3(3), ISSN: 2348-8352
3. Divya Bhavana T, Koushik S, Uday Mani Kumar K, Srinath R (2017) Pervious concrete pavement. *Int J Civ Eng Technol (IJCIET)* 8(4):413–442
4. Othman A, Somayeh N (2020) Pervious concrete mixture optimization, physical, and mechanical properties and pavement design: a review. *J Cleaner Prod* 288:125095. <https://doi.org/10.1016/j.jclepro.2020.125095>
5. Murtadha T, Wasiu A, Abideen G, Oluwole A (2019) Effect of aggregate type on properties of pervious concrete. *J Mod Technol Eng* 4(1): 37–46
6. Jayasuriya N, Kadurupokune N (2008) Impact of pervious pavements on drainage infrastructure. In: 11th international conference on Urban Drainage, Edinburgh, Scotland, UK
7. John K, Joseph S (2013) Low-cost techniques for improving the surface durability of pervious concrete. *Transp Res Rec J Transp Res Board* 2342:83–89. <https://doi.org/10.3141/2342-10>
8. Kamarul Zaman AB, Mustaffa Z, Anak Giri LDL (2019) Infiltration rate of pervious concrete on street curb application. *Int J Recent Technol Eng (IJRTE)* 8(2S2). ISSN: 2277-3878
9. Gagandeep AM, Rishi V (2019) Experimental study of construction of pervious concrete pavement. *Int J Basic Appl Res* 9(6)
10. Meng X, Chi Y, Jiang Q, Liu R, Kun Wu, Li S (2019) Experimental investigation on the flexural behavior of pervious concrete beams reinforced with geogrids. *Constr Build Mater* 215:275–284
11. Abd Halim NH, Nor HMd, Jaya RP, Mohamed A, Wan Ibrahim MH, Ramli NI, Nazri FM (2018) Permeability and strength of porous concrete paving blocks at different sizes coarse aggregate. In: *IOP Conference Series: Journal of Physics, Conference Series* 1049 012028
12. Yao Y (2018) Blending ratio of recycled aggregate on the performance of pervious concrete. *Frattura ed Integrità Strutturale* 12:343–351. <https://doi.org/10.3221/IGF-ESIS.46.31>
13. Ulloa-Mayorga VA, Uribe-Garcés MA, Paz-Gómez DP, Alvarado YA, Torres B, Gasch I (2018) Performance of pervious concrete containing combined recycled aggregates. *Ingeniería e Investigación* 38:34–41
14. Vera G, Shamseldin A (2020) Influence of silica fume on the pervious concrete with different levels of recycled aggregates. *Magaz Civ Eng* 93(1):71–82
15. Terhell S-L, Cai K, Chiu D, Murphy J (2015) Cost and benefit analysis of permeable pavements in water sustainability, *ESM* 121
16. VimyH, Susan T (2011) Evaluation of pervious concrete pavement permeability renewal maintenance methods at field sites in Canada. *Canadian J Civ Eng* 38:1404–1413. <https://doi.org/10.1139/111-105>
17. Liu C-M, Chen J-W, Tsai J-H, Lin W-S, Yen M-T, Chen T-H (2012) Experimental studies of the dilution of vehicle exhaust pollutants by environment-protecting pervious pavement 62(1):92–102
18. Radlińska A, Welker A, Greising K, Campbell B, Littlewood D (2012) Long-term field performance of pervious concrete pavement. *Adv Civ Engg Article ID* 380795, 9p
19. Haselbach L, Boyer M, Kevern JT, Schaefer VR (2011) Cyclic heat island impacts on traditional versus pervious concrete pavement systems. *Transp Res Rec J Transp Res Board*. <https://doi.org/10.3141/2240-1>
20. Kumar PG et al (2020), *IOP Conf Ser: Mater Sci Eng* 1006:012016

Evaluation of Functional Effectiveness of Speed Humps in Accordance to IRC Specifications



Satya Ranjan Samal, Malaya Mohanty, Pala Gireesh Kumar,
and S. Moses Santhakumar

Abstract Due to the mixed traffic environment in India, vehicles have different characteristics and there will not be a uniform behavior in the traffic stream. Hence, for the orderly movement of the traffic, speed humps are provided in developing countries like India. Speed humps are constructed according to the guidelines specified in Indian Road Congress 99–2018. The geometric features such as width and height of speed humps are 3.0 m 0.1 m respectively and the vehicles have to negotiate the speed humps at a speed of about 20 kmph. But, from the study it found that the majority of the speed humps are not constructed in accordance with IRC specifications. Most of the speed humps have less width, which results in road accidents due to the instant application of brakes. In addition to the entire traffic is also getting congested, which is responsible for the increase in fuel consumption of the vehicles and automatically increases the overall vehicle operating costs and maintenance costs. The study assessed the dimensions of the existing speed humps in various locations in the urban network. Also, congestion in the traffic stream has been analyzed in the urban network under mixed traffic environment.

Keywords Speed humps · Accidents · Speed · Congestion

S. R. Samal (✉) · M. Mohanty
School of Civil Engineering, KIIT Deemed to be University, Bhubaneswar, India
e-mail: satya.samalfce@kiit.ac.in

M. Mohanty
e-mail: malaya.mohantyfce@kiit.ac.in

P. Gireesh Kumar
Department of Civil Engineering, Shri Vishnu Engineering College for Women, Bhimavaram,
India

S. M. Santhakumar
National Institute of Technology, Tiruchirappalli, India
e-mail: moses@nitt.edu

1 Introduction and Background

Road accidents are considered as the 9th responsible factor for all the casualties in the world. Almost 1.3 million inhabitants died on the road way in every year and around 20–50 million people were adversely affected. In country like India around 1.5 lakhs lost their lives because of road crashes in every year [1]. The principal reason is exceeding the speed limit and careless driving behavior. To counteract the mentioned problem speed humps were used as traffic calming measures due to less in price and easy handling. The traffic in India is highly heterogeneous. In this complex scenario obtaining the traffic safety will be a very difficult task for the researcher and academician. The primary function of traffic calming measures to obstruct the flow up to certain extent. In normal practice the reduction of speed can be achieved by using traffic police, providing warning sign and obstructing the vehicle by any physical means. The last one is primarily used in India as the traffic calming measures in the form of vertical raised surfaces commonly known as humps.

IRC 99-2018 [2] is followed in India for the placement and design of traffic calming measures such as speed humps. Based on the guidelines laid by the code, the lowest chord length for a speed hump must be 3 m and the maximum height must be 0.1 m for achieving the speed of vehicles up to 20 kmph. However, from the field observation it noticed that most of the speed humps are not stratified by the codal provision. Due to the improper design of the speed hump there is chances that the vehicle may cross the speed humps more than the specified speed or very less speed as mentioned in the code. If the speed of the vehicle at the speed humps is more than the specified speed, the traffic safety will be a question mark. The purpose of providing speed humps will not be fulfilled. But from the field observation this type of phenomenon did not occur because majority of the speed humps have less chord length as per the codal provision. On other hand, if the speed of the vehicles are very less than the specified speed as per the code, all the vehicles have to reduce the speed drastically in a traffic stream, which results in traffic congestion in the roadway and may lead to rear-end collision. Due to the improper design of speed humps the roadway level of service (LOS) can be adversely affected.

The functional effectiveness of the speed humps has an important part to play on the traffic safety. However, in developing countries like India where mixed traffic environment making situation more complex, still very less studies have been conducted to observe the impact of speed humps on the various road users associated to reduction of speed and traffic safety. Thus the present study focuses on speed humps located in the urban network and compare the geometric aspects of speed humps according to the IRC guidelines. Also the reduction of speed in a traffic stream is monitored and the level of congestion due to faulty speed humps have been assessed.

1.1 Objectives of the Study

- To survey the speed humps placed on the urban road network.
- To compare the existing speed humps in accordance to the IRC guidelines.
- To examine the speed reduction profiles while vehicle approaches the speed humps as well as crossing the speed humps.
- To assess the level of congestion on the traffic stream and to examine the traffic safety of road users.

2 Literature Review

Dixon et al. [3] observed the behavior shown by motorists approaching a pedestrian crossing in the absence and presence of speed humps. They employed an experimental design to study the drivers' reactions. Pau [4] methodically classified the various issues faced by drivers caused by the erroneous installation of speed humps. He used the KV Laser (Sodi Scientifica Co. Italy) to collect the data for 30 chosen sites and visually analyzed the driver's actions during their approach toward the undulation. Jain et al. [5] proposed a smartphone operated early warning system (SWAS) which cautions the driver beforehand while approaching a speed-breaker. Another feature of the application continuously examines the smartphone accelerometer to discover previously uncharted speed-breakers. Afrin et al. [6] developed an arrangement that dynamically collected, detected and generated a notification for speed breakers ahead to warn the on-road vehicle drivers. Orden et al. [7] selected Burgos (North of Spain) for measurements in different zones with various types of traffic calming measures. They observed that raised crosswalks and lane narrowing were the most efficient traffic calming measures to lower speed. They also noted the best results when a combination of these measures was used. Abdel and Hashim [8] analyzed the impact of speed hump on pavement conditions. They collected data, covering a length of about 34 km. They determined the pavement condition index (PCI), near speed humps in both directions as well as features of each speed hump. Lav et al. [9] determined an optimal speed hump design. The main aim of the study was to design an ideal speed bump by gathering data and studying the dependent variables. They created simulation between a speed hump and a car wheel. Mohanty et al. [1] assessed the existing speed breakers in the urban area. They have observed the deceleration rate of the vehicles approaching the speed breaker. Samal and Das [10] concentrated on congestion indices to predict the congestion level. Kumar et al. [11] discussed about the level of service (LOS) of the selected road network by considering V/O ratio in Andhra Pradesh. Samal et al. [12] analyzed results of congestion and suggested mitigation measures. Samal et al. [13] analyzed impact of congestion on overall economy, health related issues and environment.

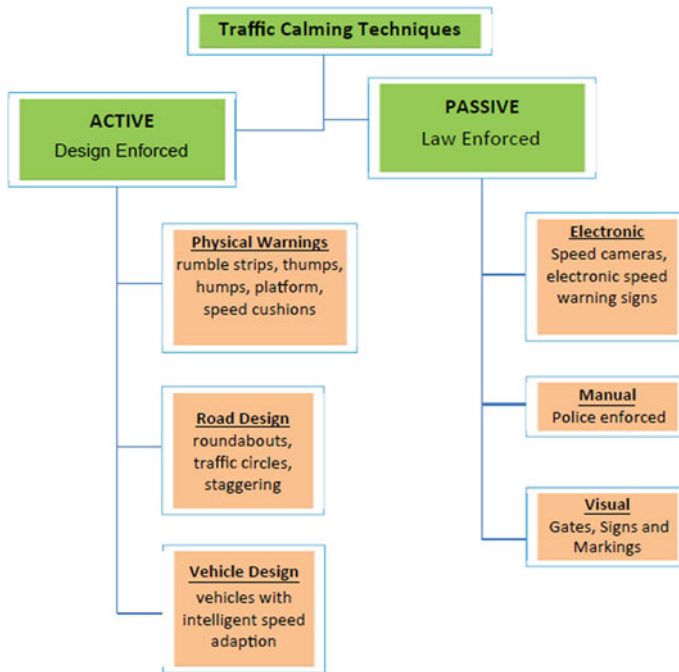


Fig. 1 Classification of traffic calming techniques according to IRC 99:2018

3 Traffic Calming Measures

According to IRC 99:2018, traffic calming techniques can be classified into various categories as shown Fig. 1.

The research is primarily concentrated on the circular speed humps on the urban road network. The geometric dimension such as length of the chord and height of the humps is the main parameters associated with the circular speed humps (Figs. 2 and 3).

4 Site Selection and Data Collection

Site selection is the one of the most important steps in the field of research. Site selection should be done in such a manner that there should not be any kind of obstructions during the collection of data. In the present study data is collected from the arterial roads of Bhubaneswar city. Video recording techniques is employed for the data collection. The geometric dimensions were measured on the field. The speeds of the different categories of the vehicle were noted down at different locations from the starting point of speed humps to a specified distance (Fig. 4).

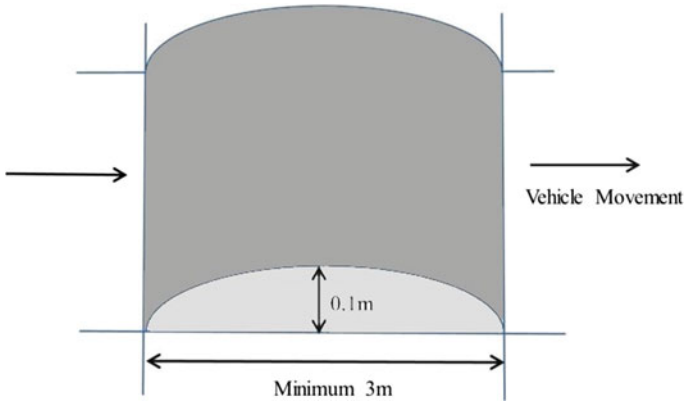


Fig. 2 Sectional prospect of a circular speed hump according to IRC 99:2018

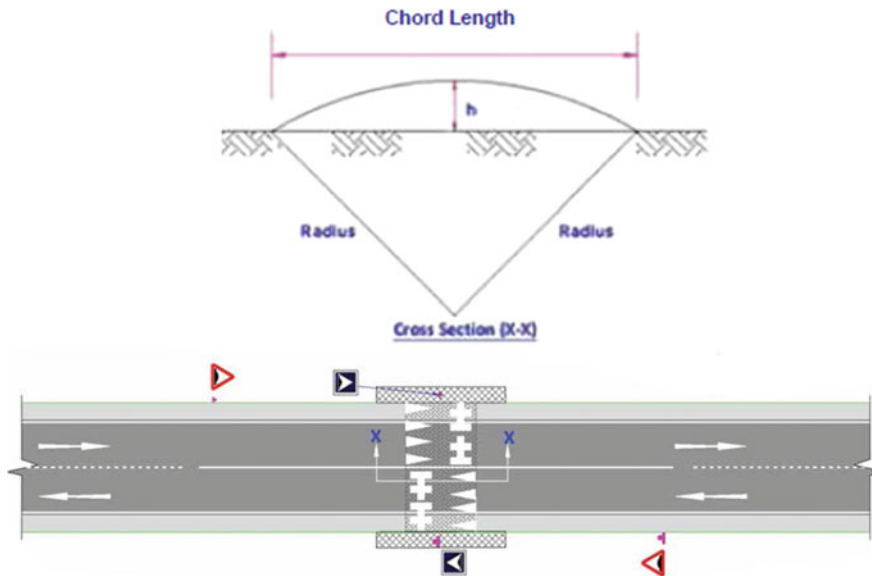


Fig. 3 Features of circular speed hump according to IRC 99:2018

5 Result Analysis

The geometric dimensions were measured on the field. The speeds of the various classes of the vehicle were noted down at different locations from the starting point of speed humps to a specified distance. In the research circular speed humps is taken into consideration in the specified road system in the Bhubaneswar city. 12 numbers



Fig. 4 Road network selection for the study area

of circular speed humps were observed. The geometric dimensions of the each speed humps were observed and the details are mentioned below (Table 1).

From the above data it can be identified that the chord length of circular speed humps ranged between 98 and 225 cm. The mean chord length of circular speed humps were obtained as 188 cm correspondingly, the height of circular speed humps ranges from 6 to 10 cm. The mean height is observed as 8 cm (Table 2).

According to IRC guidelines it can be understood that the least chord length of circular speed humps is 300 cm and the maximum height must be 10 cm. However, the data collected from the field shows that the circular speed humps installed on

Table 1 Details of the existing circular speed humps

S. No	Chord length (cm)	Height (cm)
1	170	7
2	197	8
3	220	8
4	127	8
5	98	7
6	204	7
7	223	10
8	225	8
9	225	7
10	188	8
11	215	6
12	160	7
Average	188	8

Table 2 Suggested chord length for circular speed humps according to IRC 99:2018 (maximum height: 0.1 m)

Desired speed (km/h)	Chord length (m)
20	3.0
25	3.5
30	4.0
35	5.0
40	6.5
45	8.0
50	9.5

Table 3 Mean vehicle speed while nearing the speed humps

Location from the upstream of speed humps (m)	Mean speed (kmph)
20–15	33
15–10	26
10–5	23
5–0	18
On speed humps	10

roads are not in accordance to IRC specifications. The height of the circular speed humps stick to codal provision (Table 3).

It clearly noticed that the mean speed of the vehicles negotiating speed hump is almost 10 kmph. It can be identified that there is immediate reduction of speed at a distance of 20 m from the upstream of the speed humps to the speed humps. The speed variation observed from 33 to 10 kmph. From the study it found that while the vehicle negotiating the speed hump the reduction of speed is about 50% less than the codal provision. That shows that there is a sudden slowing down of the entire traffic flow due to the faulty speed hump leading to congested traffic. Vehicles are compelled to reduce the speed more than the specified limit, which creates congestion and undesirable delay in the entire traffic stream (Fig. 5).

In the research work congestion analysis has been done to find the level of congestion occurring in the entire traffic stream due to the improper design and improper installation of speed humps. From the field study it observed that the existing speed humps were not constructed according to the IRC specifications. The present study tried to establish the correlation connecting the vehicle speed while negotiating the speed hump and the level of congestion in the traffic stream (Table 4).

Like level of service (LOS) the present study has tried to categorize the level of congestion in the urban road network. As per the result vehicle speed while negotiating the speed humps is almost 10 kmph, which coming in the category of congested traffic which signifies that the traffic quality is poor. That shows that there is a sudden slowing down of the entire traffic flow due to the faulty speed hump leading to congested traffic. Vehicles are compelled to reduce the speed more than the specified limit, which creates congestion and undesirable delay in the entire traffic stream.

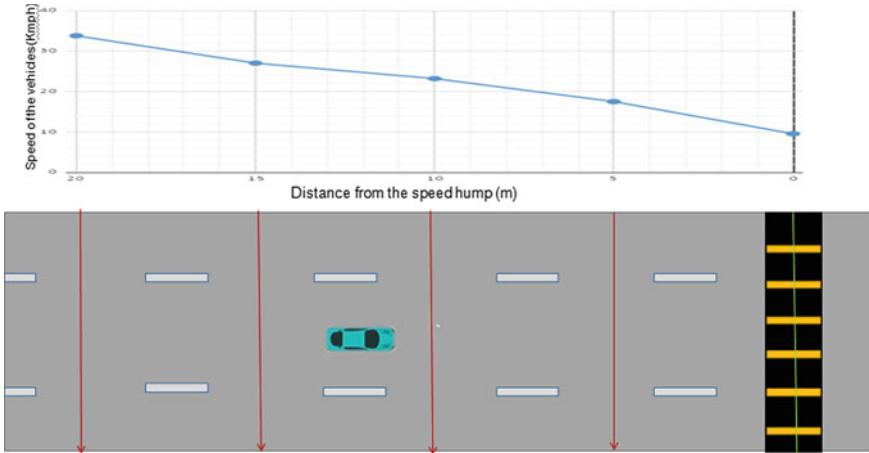


Fig. 5 Mean speed of vehicles while nearing speed humps

Table 4 Level of congestion with respect to vehicle speed while negotiating the speed humps

Vehicle speed while negotiating the speed humps (kmph)	Level of congestion	Traffic quality
>20	Free flow traffic	Excellent
20	Nearing to free flow traffic	Good
15	Moderate congestion	Satisfactory
10	Congested traffic	Poor
5	Forced flow traffic	Very poor
<5	Traffic jam condition	Critical

Due to the faulty speed hump, the vehicle decelerates at a higher rate, which creates further wear and tears alongside more chances of rear-end crash mainly at higher traffic volumes.

6 Conclusions and Recommendations

The research concentrates the analysis of the geometric features of speed humps and the adverse impact of the improper design on various road users. The traffic composition in India is basically under mixed flow condition. In the present study circular speed humps were taken for the analysis. From the field data it identified that none of the speed humps was constructed according to the codal provision. Shorter the chord length of the speed humps greater the discomfort to the drivers and greater the chances of accidents. It was identified that the mean speed of the vehicle

reduced from 33 kmph at 20 m to 10 kmph on the speed hump. In the research work congestion analysis has been done to find the level of congestion occurring in the entire traffic stream due to the improper design and improper installation of speed humps. The present study has tried to categorize the level of congestion in the urban road network. As per the result vehicle speed while negotiating the speed humps is almost 10 kmph, which coming in the category of congested traffic which signifies that the traffic quality is poor. There is a sudden slowing down of the entire traffic flow due to the faulty speed hump leading to congested traffic. Vehicles are compelled to reduce the speed more than the specified limit, which creates congestion and undesirable delay in the entire traffic stream. Due to the faulty speed hump, the vehicle decelerates at a higher rate, which creates further wear and tears alongside more chances of rear-end crash mainly at higher traffic volumes.

From the field data it identified that none of the speed humps was constructed according to the codal provision. The new speed humps going to construct should be in accordance with IRC specifications. The present study has tried to suggest some recommendations for the smooth movement of traffic with optimum safety for various road users. For the existing faulty speed humps if economy allows, all the faulty speed humps should be reconstructed or else warning signs should be placed on the upstream of speed hump showing faulty speed hump ahead and the speed limit of 10 kmph.

References

1. Mohanty M, Raj Y, Rout S, Tiwari U, Roy S, Samal SR (2021) Operational effects of speed breakers: a case study in India. *Eur Trans Int J Trans Econom Eng Law* 81:e1-e1
2. IRC:99-2018 Guidelines for traffic calming measures in urban and rural areas (First Revision) Indian roads congress
3. Dixon MA, Alvarez JA, Rodriguez J, Jacko JA (1997) The effect of speed reducing peripherals on motorists' behavior at pedestrian crossings. *Comput Ind Eng* 33(1-2):205-208
4. Pau M (2002) Speed bumps may induce improper drivers' behavior: case study in Italy. *J Transp Eng* 128(5):472-478
5. Jain M, Singh AP, Bali S, Kaul S (2012) Speed-breaker early warning system. In: NSDR
6. Afrin M, Mahmud MR, Razzaque MA (2015) Real time detection of speed breakers and warning system for on-road drivers. In: 2015 IEEE international WIE conference on electrical and computer engineering (WIECON-ECE). IEEE, pp 495-498
7. Gonzalo-Orden H, Rojo M, Pérez-Acebo H, Linares A (2016) Traffic calming measures and their effect on the variation of speed. *Transp Res Procedia* 18:349-356
8. Abdel-Wahed TA, Hashim IH (2017) Effect of speed hump characteristics on pavement condition. *J Traffic Transp Eng (English edition)* 4(1):103-110
9. Lav AH, Bilgin E, Lav AH (2018) A fundamental experimental approach for optimal design of speed bumps. *Accid Anal Prev* 116:53-68
10. Samal SR, Das AK (2020) Evaluation of traffic congestion parameters under heterogeneous traffic condition: A case study on Bhubaneswar city. In: *Transportation Research*. Springer, Singapore, pp 675-684
11. Kumar PG, Samal SR, Prasanthi L, Bhavitha V, Devi JM (2020) Level of service of urban and rural roads-a case study in Bhimavaram. In: *IOP conference series: materials science and engineering*, vol 1006, No 1,. IOP Publishing, p 012018

12. Samal SR, Kumar PG, Santhosh JC, Santhakumar M (2020) Analysis of traffic congestion impacts of urban road network under Indian condition. In: IOP conference series: materials science and engineering, vol 1006, No 1, p 012002. IOP Publishing
13. Samal SR, Mohanty M, Santhakumar SM (2021) Adverse effect of congestion on economy, health and environment under mixed traffic scenario. *Transp Devel Econom* 7(2):1–10

An Endeavor for Accomplishing GFRG Panel as a Load-Bearing Member in Civil Engineering



V. Johnpaul, N. Balasundaram, K. Ramadevi, M. Jemimah Carmichael, and S. Solai Mathi

Abstract The enormous need for building materials requires for all developing countries like India. The major problem faced by most of the people in India is the lack of affordable houses. It directed toward the new invention of construction methodology with reduced cost and less duration. The usage of the GFRG (Glass Fiber Reinforced Gypsum) panel as a load-bearing member might fulfil the desired need. The GFRG panel provides the solution of gypsum waste produced by fertilizer industries. The GFRG panel is the best green material and a better substitution for bricks that emits about 40% of carbon dioxide during the manufacturing process. Since we need some technological development to control pollution, which leads to global warming due to the massive emission of carbon dioxide, another big natural calamity is an earthquake that can destroy human life quickly. This GFRG panel can be used as a shear wall when filled with RCC in its cavities and can withstand the earthquake forces considerably. In this project, the axial load strength of the GFRG panel infilled with reinforced concrete is studied and compared with the various arrangement of reinforcement.

Keywords Axial load strength · GFRG panel · Gypsum fiber

1 Introduction

Lodging industrialization advancement in China has edified the analyst's energy to find better approaches to raising private structures in construction techniques. The

V. Johnpaul (✉) · N. Balasundaram · S. Solai Mathi
Department of Civil Engineering, Karpagam Academy of Higher Education Coimbatore,
Coimbatore, Tamil Nadu, India

K. Ramadevi
Department of Civil Engineering, Kumaraguru College of Technology Coimbatore, Coimbatore,
Tamil Nadu, India
e-mail: ramadevi.k.ce@kct.ac.in

M. Jemimah Carmichael
Department of Civil Engineering, Vignan's Lara Institute of Technology and Science, Guntur
Andhra Pradesh, India

college's multi-ribbed composite divider set forward should be utilized in tiny high-rise lodging structures. Exploring the thick-ribbed network beat shearing power fast-divider shows that it has enough horizontal solidness and is conceivable to be utilized in tiny high-rise private structures. Glass fiber fortified gypsum (GFRG) divider is a green item that can erect a structure quick in pre-assembled strategy. Showed up first in Australia in the mid-1990s, generous research and practices on GFRG dividers have been conveyed in Australia and a couple of Asian nations, for example, China, Malaysia, and India. GFRG dividers can be utilized in low structures as burden-bearing dividers in low-rise buildings or as upper story dividers in tall structures when loaded up with concrete in the empty centers.

A few investigations have discovered that gypsum is a rigid material; it very well may be utilized in parcel dividers. Specialists anticipated that a structure made of GRFG boards can have a life expectancy of 60 years and does not require bar and segments. A chemical ingredient has been endorsed as a green structure ingredient shown by the United Nations Framework on environmental change (UNFCCC). Board holes can either be incompletely or wholly loaded with fortified cement for achieving different qualities. They are working with a load-carrying framework, and a well manufactured fortified GFRG board can reach as high as 8–10 story is in low seismic zone regions. Likewise, board depressions were utilized for electrical wiring connections and funneling jobs. To show the innovation method, IIT has been fabricated twice—celebrated GFRG private structure to its grounds. Paul et al. [1] stated that GFRG panels are mainly used for building a cost-effective and for fast construction. Wei et al. [2] research shows these are mainly used to increase the rigidity of a small high-rise building. Shukla et al. [3] highlight the techniques to reduce the cost of housing in India. Singhal et al. [4] research highlight the use of GFRG for cost-effective, affordable building. He et al. [5] the research focused on experimental and theoretical analysis of the GFRG wall and its overall performance. Manjummekudiyil et al. [6] The research focused on both quality and cost-effective ways. Athira et al. [7] has studied the dynamic analysis on GFRG walls with ETABS. The present study analyzed the behavior of GFRG paneled and regular buildings when subjected to lateral forces.

2 Materials and Methods

2.1 Cement

The Ordinary pozzolana cement (zuari super grade) is used for the study. The physical properties like specific gravity, fineness, consistency, and initial setting time are tested as per IS 1489:1991 part I and are shown in Table 1.

Table 1 Chattels of cement

S. No.	Tests conducted	Results obtained
1	Specific gravity	3.12
2	Finesses	6%
3	Consistency	28
4	Initial setting time	34 in

Table 2 Properties of GFRG

S. No.	Parameter	Requirement	Results
1	Dimension		
	Length	520 mm	520 mm
	Height	250 mm	250 mm
	Thickness	124 mm	124 mm
2	Water content	Less than 1%	0.87%
3	Weight	40 kg/m ²	47 kg/m ²
4	Water absorption	5% by weight	2.4% by weight
5	Compressive strength	160 kN/m	165.33 kN/m

2.2 GFRG Panel

GFRG is a trust-worthy, accelerated wall panel used in building construction and its properties are shown in Table 2. It is comprised of chemical constituents such as calcinated gypsum, adhesives, Infiltrated glass fiber [8]. This type of wall construction is suitable for large-scale buildings. It was initially made in Australia and used since 1990 [9]. The wall panel was manufactured to a thickened density of 124 mm, long span dimension as 12 m, and depth of about 3 m were made precisely and restrained based on the site exposure conditions [10]. It consists of cavities that can be either filled or partly filled or unfilled with infiltrated concrete as mentioned in structural specifications. GFRG panel can also be used highly for non-load lifting wall, sandwiched with reinforced cement concrete beams and columns (wholly acted as a standard framed construction of the multi-story building) without any constraint in the number of stories of small-sized beams and reinforced cement concrete screed (acted on T-beam) were used for roof/floor slab [11].

2.3 Aggregate

Fine aggregate is washed and screened to eliminate deteriorious materials and oversized particles and conforming to zone II as per IS 383-1970 is used in the experimental works. Coarse aggregate which passes through 15 mm IS strainer and withheld

Table 3 Physical chattels of aggregate

S. No.	Tests conducted	Fine Agg	Coarse Agg
1	Relative density	2.62	2.68
2	Cumulative percentage withheld on each strainer to the total aggregate	5.13	6.84
3	Aggregate impact value	–	19.64%
4	Aggregate crushing value	–	17.04%

particles in 4.75 mm IS strainer is carried out in the experimental work. The physical properties like Relative density, cumulative percentage withheld on each strainer to the total aggregate, aggregate strength, and aggregate toughness were determined and values of those tests are indicated in Table 3.

2.4 Axial Load Strength

Breadth (B) of the sample was measured as shown in Figs. 1 and 2. The front and rear sides of the sample measurements are made by taking the mean value were used for computation [12]. In the experimental arrangement, sample was kept at the center of the plate. One has to ensure that in any situation, test sample should not be left out of the plate of the equipment. A minimum coat of rapid setting adhesive (such as dental gum) gets covered with the test sample, in order to hold and made a close touch with the plate. The design strength of the test sample should not be more than the applied adhesive strength when the test progresses [13]. Compressive load was applied gradually at a rate not exceeding 10 kN per minute before the attainment of ultimate load and then falls to a minimum 20% of the ultimate load. The ultimate load recorded in the testing equipment was noted as *F* (Table 4).

Unit strength of the sample is given by $P = F/B$ in kN/m,

Where, *F* is the ultimate load, in kN, and

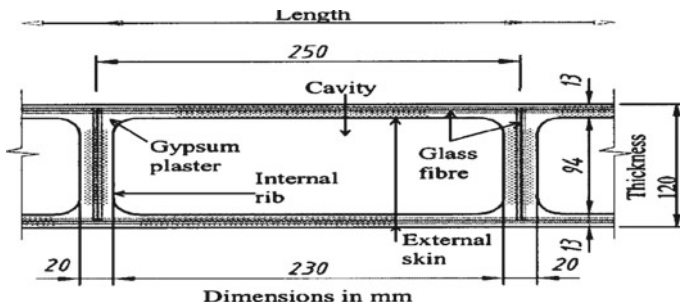


Fig. 1 Size used for testing

Fig. 2 Glass fiber reinforced GYPSM specimen



Table 4 Nomenclature of GFRG panels

S. No.	Test	Specimen	Specimen size	No. of specimen
1	Water absorption	W1	250 mm* 280 mm	3
2	Axial load test without concrete infilling	CS	250 mm* 520 mm	3
3	Axial load test with concrete infilling (No reinforcement)	A1, A2 and A3	250 mm* 520 mm	3
4	Axial load test with double 8 mm reinforcement	B1, B2 and B3	250 mm* 520 mm	3
5	Axial load test with single 10 mm reinforcement	C1, C2 and C3	250 mm* 520 mm	3
6	Axial load test with double 10 mm reinforcement	D1, D2 and D3	250 mm* 520 mm	3
7	Axial load test with single 12 mm reinforcement	E1, E2 and E3	250 mm* 520 mm	3
8	Axial load test with single 12 mm reinforcement	F1, F2 and F3	250 mm* 520 mm	3

B is the breadth of the waste sample in meter.

3 Experimental Result and Discussion

Table 5 gives the load acting vertically along a thrust line (axial load) of the GFRG panels for different reinforcement patterns is tabulated below.

The above shows the difference in the weight of the GFRG single panel varying from without infill with an average weight of about 8.28 and 35.8 kg for which having

Table 5 Test results of GFRG panel

S. No.	Test	Specimen	W1 (kG)	W2 (kG)	W3 (kG)	Mean (kG)
1	Water absorption	W1	4.92	4.95	4.93	4.933
2	Axial load test without concrete infilling	CS	8.25	8.5	8.1	8.28
3	Axial load test with concrete infilling (No reinforcement)	A1, A2 and A3	34.6	35.1	35.5	35.03
4	Axial load test with double 8 mm reinforcement	B1, B2 and B3	35.5	34.5	35	35.00
5	Axial load test with single 10 mm reinforcement	C1, C2 and C3	35.2	34.3	35.7	35.4
6	Axial load test with double 10 mm reinforcement	D1, D2 and D3	36.10	35.3	36.0	35.8
7	Axial load test with single 12 mm reinforcement	E1, E2 and E3	34.6	35.6	36	35.4
8	Axial load test with double 12 mm reinforcement	F1, F2 and F3	35.4	36.4	35.0	35.6

double 10 mm reinforcement of specimen size 250 mm * 520 mm. comparatively, this is less weight than commercial bricks[14].

The compressive strength tests of the seven different types of samples were examined for the study [15]. This double 12 mm reinforcement showed a better load-carrying capacity with compressive strength of 846.15 kN as shown in Table 6.

4 Conclusion

Based on the experimented results, GFRG panel building showed better behavior and is limited within the permissible values. The following parameters, such as a minimum number of story deformation, sideways between two adjacent stories, Natural periods were made in comparison with the typical building. It was observed that the deformation attained from time history analysis was more significant than response spectrum analysis. The natural period of standard building was high as compared to GFRG paneled building. The study concludes that the vertical load-carrying capacity of the GFRG panel increases enormously with infilling of reinforced cement concrete. It can be used in load-carrying members and also to resist lateral forces.

Table 6 Compressive strength test results

S. No.	Test	Specimen	Peak load F(kN)	Compressive strength <i>P</i>
1	Axial load test without concrete infilling	CS	80	162.00
2	Axial load test with concrete infilling (No reinforcement)	A1, A2 and A3	320	615.38
3	Axial load test with double 8 mm reinforcement	B1, B2 and B3	360	692.31
4	Axial load test with single 10 mm reinforcement	C1, C2 and C3	340	653.85
5	Axial load test with double 10 mm reinforcement	D1, D2 and D3	400	769.23
6	Axial load test with single 12 mm reinforcement	E1, E2 and E3	370	711.54
7	Axial load test with double 12 mm reinforcement	F1, F2 and F3	440	846.15

References

1. Paul S et al (2017) Sustainable, rapid and affordable mass housing using GFRG panels IJAMCE 4(3). ISSN: 2394-2827
2. Wei P et al (2021) Performance evaluation of a novel cross-laminated timber made from flattened bamboo and wood lumber. Bioresources 16(3):5187–5202
3. Shukla A et al (2016) A review of research on building system using glass fiber reinforced gypsum wall panels. IRJET 3(02). ISSN 2395-0056
4. Singhal S et al (2019) Comparative study on cost estimation of GFRG wall panel system with conventional building, pp 3394–3398
5. He W, Wang X, Wu Z (2020) Flexural behavior of RC beams strengthened with prestressed and non-prestressed BFRP grids. Compos Struct 246:112381. <https://doi.org/10.1016/j.compstruc.2020.112381>
6. Manjummekudiylil EM, Alias BP, Eldhose BK, Rajan S, Hussain T (2015) Study of GFRG panel and its strengthening 2:161–165 (2015)
7. Athira KB et al (2017) Contrast of seismic behavior of R.C.C and composite columns in G+15 storied Buildings with GFRG Infill. IJERT 6(06). ISSN: 2278-0181
8. Banu ST, Chitra G, Awoyera PO, Gobinath R (2019) Structural retrofitting of corroded fly ash based concrete beams with fibres to improve bending characteristics. Aust J Struct Eng 20:198–203. <https://doi.org/10.1080/13287982.2019.1622490>
9. Getuli V, Capone P, Bruttini A, Isaac S (2020) BIM-based immersive Virtual Reality for construction workspace planning: a safety-oriented approach. Autom Constr 114:103160. <https://doi.org/10.1016/j.autcon.2020.103160>
10. Singhal S et al (2019) Comparative study on cost estimation of GFRG wall panel system with conventional building 6(04). ISSN 2395-0056

11. Menon D (2014) Rapid affordable mass housing using glass fibre reinforced gypsum (GFRG) panels. *IJSER* 5(7)
12. Gao D, Jing J, Chen G, Yang L (2019) Experimental investigation on flexural behavior of hybrid fibers reinforced recycled brick aggregates concrete. *Constr Build Mater* 227:116652. <https://doi.org/10.1016/j.conbuildmat.2019.08.033>
13. Mandlik A, Sarthak Sood T, Karade S, Naik S, Phule S (2013) Pune University, lightweight concrete using EPS. *Int J Sci Res* 4:2319–7064. www.ijsr.net
14. Biswas A, Krishna AM (2017) Geocell-reinforced foundation systems: a critical review. *Int J Geosynth Gr Eng* 3:17. <https://doi.org/10.1007/s40891-017-0093-7>
15. Subhan Alisha S, Neeraja S, Akber S, Sai Manoj G (2016) Low cost housing by using GFRG panels 3:939–946

Comparative Study of Regular and Irregular Buildings Using Framed Tube Structure and Viscous Dampers



Abdul Rahman Khan and G. Sathya Prakash

Abstract Over time, we saw a continual rising population and a house is a basic human requirement, which is why engineers built vertical growth in place of expanding along the country. The reinforced concrete frame is subjected to lateral pressures as we ascend higher. It is therefore essential to resist pressure on the frame laterally. The side force of this study will be compared with two distinct structural systems, namely Framed Tube system and the Viscous Damper in the normal (rectangular) and irregular (L formed) structure with 50 storeys. A response spectrum analysis is carried out in order to come up with a solution in ETABS.

Keywords ETABS · Response spectrum · Framed tube structural system · Viscous dampers

1 Introduction

A tall structure's structural design process comprises of procedures including conceptual design, approximation analysis, preliminary design, and optimization, followed by detailed and final design. Limiting stresses, displacements, and accelerations are matched using codes. Architectural, mechanical, and electrical needs all impact the initial selection of a structural system. Several floor systems are investigated in conjunction with three to four lateral systems, yielding a variety of structural solutions for varied gravity and lateral combinations. Following that is preliminary design and optimization of multiple strategies, with drift and acceleration restrictions being met repeatedly.

Quakes are possibly the most unpredictable and annihilating of all apocalyptic events. They not only aim for unprecedented pulverization in terms of human losses, but they also have a significant monetary impact on the affected area. The worry about seismic dangers has prompted an expanding mindfulness and interest for structures

A. R. Khan (✉) · G. Sathya Prakash
Vidya Jyothi Institute of Technology, Hyderabad, India

G. Sathya Prakash
e-mail: sathyaprakashg@vjit.ac.in

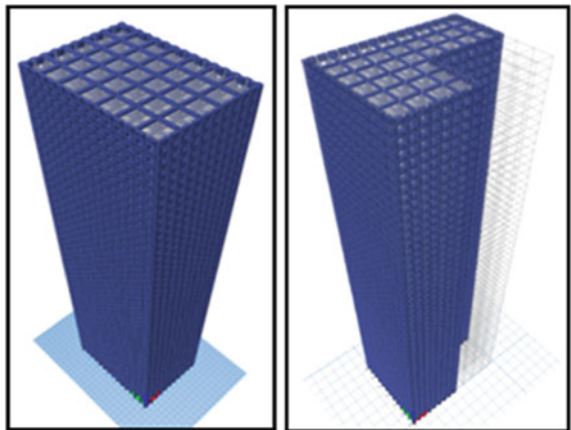
intended to withstand seismic powers. In this paper we will be doing an analytical research about Framed tube structural system applied on L shaped structure as well as Rectangular shaped and comparing it with Viscous dampers using ETABS program.

1.1 Framed Tube System

Braced frames and structural walls may not be sufficient to control the overall lateral displacement of tall structures, so the force demands on various structural elements. In such circumstances, more strong structural solutions are required, one of the most commonly utilized tube systems is the Framed Tube System. This method features a substantially stiffer exterior tube than the tube-in-the-tube system. This steep tube was created by separating the columns closely and connecting them to the stiff exterior shell with deep spandrel-beams. Depending on the construction, the column spacing is generally between 1.5 and 4.5 m and the depth of the beam can range between 0.5 and 1.2 m (Fig. 1).

The Framed tube system out performed when comparison was done with tube in tube structural system where parameters such as base shear, storey displacement and shear lag were compared [1]. Frame Tube Structure concept has significant advantages in comparison to Conventional Structure it efficiently reduces narrative drift and storey shear and in comparison to conventional structures and which is eligible when it comes under High rise committee criteria [2].

Fig. 1 3D representation of regular and irregular structures



1.2 Viscous Dampers

Damping is one of several strategies offered for allowing a structure to operate optimally when subjected to seismic, wind storm, or other forms of transitory shock and vibration disturbances. During the 1990s, the usage of dampers increased dramatically, to the point that they are now employed not just for military and defence constructions, but also for commercial constructions (Fig. 2).

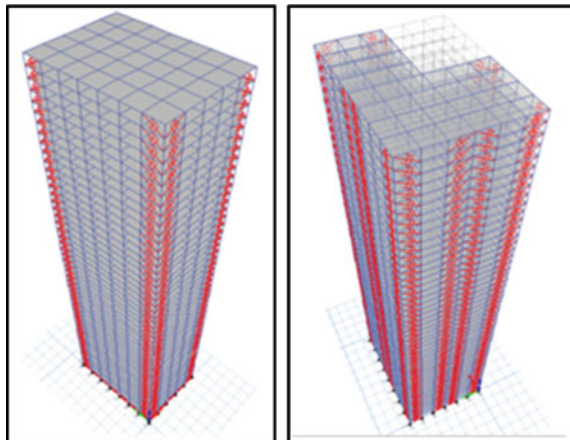
2 Objectives

- To analyse the structures and obtaining their responses through ETABS software.
- To study the behaviour of Framed tube system and viscous dampers on a G + 49 floor structure.
- To compare the results based on different parameters such as Base shear, Lateral displacement, storey drift, storey shear, and modal mass ratio.
- The analysis will be done by Response spectrum method.

3 Methodology

- Two types of structures are to be analysed Regular and L shaped. Both the structures are G = 49 floors, having 3 m floor height each with total height of 150 m.
- The loads considered are Gravity loads as well as Seismic loads i.e. dead load, live load, wind load, earthquake load.

Fig. 2 3D view of positioning of dampers at edges and at mid-bay



- Linear dynamic response spectrum method is done on both structures to obtain the results.
- The behaviour of structures will be compared on basis of following parameters base shear, storey shear, storey drift, lateral displacement, and modes.

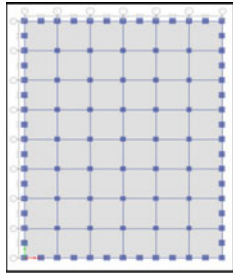
4 Model Data

- Building plan and its geometry
Dimensions of Structure = 48×36 m, Height of the structure = 150 m, Number of floors = 50, Number of bays in X direction = 6, Number of bays in Y direction = 8.
Bay width in X and Y direction = 6 m.
- Material properties
Grade of concrete = M40, Grade of Steel = Fe550.
- Section properties
Size of Column = $1 \text{ m} \times 1 \text{ m}$, Size of beam = $0.381 \text{ m} \times 0.609 \text{ m}$, Thickness of slab = 0.152 m Size of column for framed tube = 1.2 m, Deep beam = 0.381×1.5 m, Link properties = 250 kN.
- Gravity loads
Floor Finish = 1.5 kN/m^2 , Live Load = 2 kN/m^2 , Wall load 230 mm thick = 4.14 kN/m , Wall load 150 mm thick = 2.736 kN/m .
- Seismic loading
Zone factor—0.16, for zone III, Response reduction factor—5 [3], Soil Type—II.
Importance factor—1.5, No. of modes to be considered—15, Damping—5%.
- Wind loading
Wind speed—50 m/s, Terrain category—2, Risk coefficient, K_1 —1 [4], Topography factor, K_3 —1.

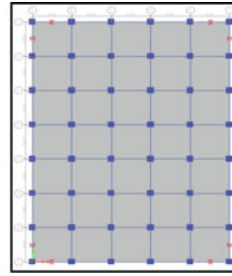
5 Analysis

We will be using the linear dynamic response spectrum approach in this study to calculate the seismic response of these two buildings. The seismic analysis response spectrum technique provides computational benefits for forecasting displacements and member forces in structural systems. After performing linear response spectrum analysis, modal response and modal shapes of the structures along with different parameters are checked.

- Model 1 (a)** Plan view of regular structure with Framed tube structural system.
(b) Plan view of regular structure with Viscous Dampers.



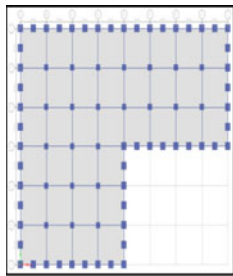
1(a)



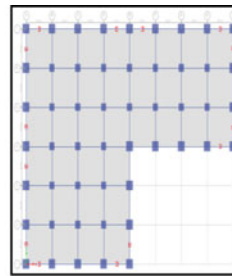
1(b)

Model 2 (a) Plan view of Irregular structure with Framed tube structural system (L shaped).

(b) Plan view of Irregular structure with Viscous Dampers (L shaped).



2(a)



2(b)

6 Results and Discussions

The results of these analysis will be calculated and compared based on Max storey displacement, Max storey drifts, Base shear, Modal reactions, and response of the structure.

6.1 Results of Regular Shaped Structure

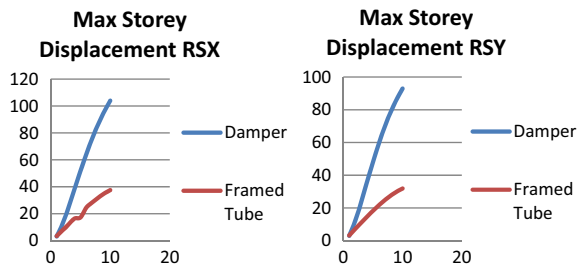
6.1.1 Max Storey Displacement

Table 1 shows that Viscous Dampers have a storey displacement of 103.95 mm in the X direction and 92 mm in Y direction and in Framed tube the displacement is way less i.e. 37 mm in X direction and 31 mm in Y direction (Fig. 3).

Table 1 Max storey displacement

Damper			Framed tube		
Story	X	Y	Story	X	Y
Story 5	3.09	2.968	Story 5	3.418	3.215
Story 10	12.456	11.838	Story 10	7.746	7.087
Story 15	24.779	23.344	Story 15	12.103	10.919
Story 20	38.198	35.699	Story 20	16.401	14.633
Story 25	51.66	47.917	Story 21	17.25	18.193
Story 30	64.499	59.39	Story 30	24.634	21.57
Story 35	76.276	69.727	Story 35	28.444	24.712
Story 40	86.731	78.707	Story 40	31.947	27.548
Story 45	95.843	86.337	Story 45	35.028	29.971
Story 50	103.953	92.968	Story 50	37.547	31.858

Fig. 3 Graphical representation of storey displacement in (RSX) and (RSY)



6.1.2 Maximum Storey Drifts

According to IS 1893:2002 Part 1 Clause 7.11.1, the storey drift must not be more than 0.004 times the storey height, or 0.012 (Table 2).

We can see that in the normal conventional frame, the storey drifts in the X and Y directions are 0.000217, 0.000143, which is 25% more than the storey drifts in the Normal RC frame with Framed tube structure, which are 0.000161, 0.000117. Storey drifts in an RC frame with VD are 72% greater in the X and Y directions than in a framed tube system (Fig. 4).

6.1.3 Base Shear

Table 3 compares the base shears of RC structure with a framed tube system, and a frame with viscous dampers. When compared to VD, the values of the framed tube system are 10,496.2 kN. This means that the VD absorbs or dissipates energy when an earthquake occurs, hence the base shear in VD is very low. Similarly, this can be seen the values of Y direction.

Table 2 Maximum storey drifts

Framed tube			Damper	
Story	X	Y	X	Y
Story 5	0.000283	0.000256	0.000418	0.0004
Story 10	0.000297	0.000263	0.000735	0.000692
Story 15	0.000304	0.000263	0.000876	0.000814
Story 20	0.000307	0.000261	0.000925	0.000848
Story 25	0.000306	0.000258	0.000917	0.00083
Story 30	0.000299	0.00025	0.000871	0.000778
Story 35	0.000286	0.000236	0.000801	0.000704
Story 40	0.000263	0.000212	0.000719	0.000623
Story 45	0.000218	0.00017	0.000635	0.00054
Story 50	0.000161	0.000117	0.000575	0.00048

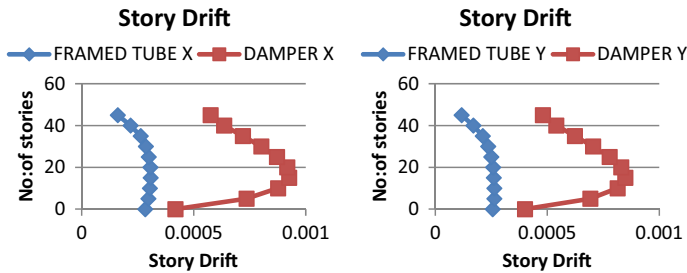


Fig. 4 Storey drifts (RSX and RSY)

Table 3 Base shear

	Framed tube	Damper
RSX	10,496.2	1349.91
RSY	12,814.1	1173.52

6.1.4 Modal Shape

The initial goal of the model study is to determine the elastic periods and vibration mode. The first three modes of vibration (translation in *x* and *y* directions, and torsion) are usually of particular interest because they account for the majority of the dynamic response however, this should be confirmed by looking into the modal participation factor (Table 4; Figs. 5 and 6).

The fundamental time period is 3.195 s in Mode 1, and in RC frame with Viscous Damper the fundamental time period is 5.595 s in Mode 1.

The total seismic mass of the structure has been engaged in 15 modes, with the first three modes accounting for 75% of the whole mass and the last three modes

Table 4 Modal data

Mode	Framed tube			Viscous damper		
	Period (s)	Mass ratio X	Mass ratio Y	Period (s)	Mass ratio X	Mass ratio Y
1	3.195	0.748	0	5.595	0.7084	0
2	2.619	0	0.7602	5.339	0	0.7158
3	1.638	0	0	4.056	0	0
4	0.995	0.1372	0	1.591	0.1289	0
5	0.832	0	0.1297	1.547	0	0.1226
6	0.545	0	0	1.092	0	0
7	0.537	0.0386	0	0.751	0.05	0
8	0.457	0	0.0371	0.742	0	0.0494
9	0.357	0.0254	0	0.483	0	0
10	0.325	0	0	0.431	0.0314	0
11	0.306	0	0.025	0.428	0	0.0312
12	0.22	0	0	0.263	0	0
13	0.188	0.032	0	0.213	0.042	0
14	0.162	0	0.0312	0.212	0	0.0419
15	0.117	0	0	0.129	0	0

Fig. 5 Modal participating mass ratio in RSX

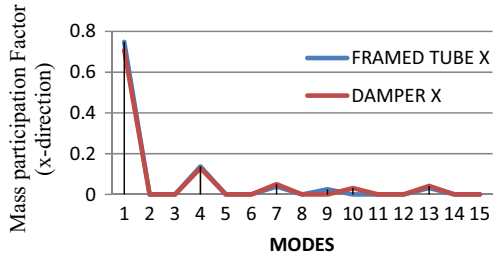
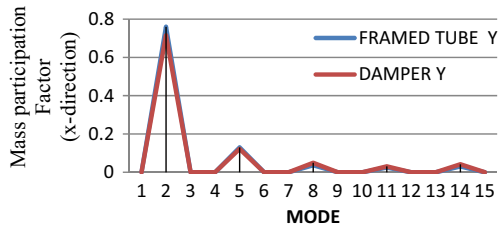


Fig. 6 Modal participating mass ratio in RSY



accounting for more than 90% of the whole mass. And in frame structure with viscous dampers 71% of the mass is participated in the X direction and 72% of the total mass of the structure is participated in the Y direction.

6.2 Results of Irregular Shaped Structure

6.2.1 Max Storey Displacement

Table 5 clearly shows that viscous dampers can be useful in RC tall constructions. The displacement in X direction in RC Frame after using VD is 43.175 mm, whereas the displacement in the framed tube structural system is 33.099 mm, and the displacement in the Y direction is 49.068 mm and 38.11 mm, respectively (Fig. 7).

Table 5 Max storey displacement in L shaped structure

Damper			Framed tube		
Story	X	Y	Story	X	Y
Story 5	1.735	1.653	Story 5	3.229	3.146
Story 10	5.938	5.776	Story 10	7.115	7.205
Story 15	10.955	10.883	Story 15	11.014	11.426
Story 20	16.147	16.376	Story 20	14.814	15.672
Story 25	21.271	22.011	Story 25	18.475	19.881
Story 30	26.236	27.678	Story 30	21.978	24.005
Story 35	30.984	33.306	Story 35	25.282	27.984
Story 40	35.435	38.805	Story 40	28.316	31.743
Story 45	39.496	44.067	Story 45	30.965	35.166
Story 50	43.175	49.068	Story 50	33.099	38.114

Fig. 7 Graphical representation of storey displacement (RSX) and (RSY)

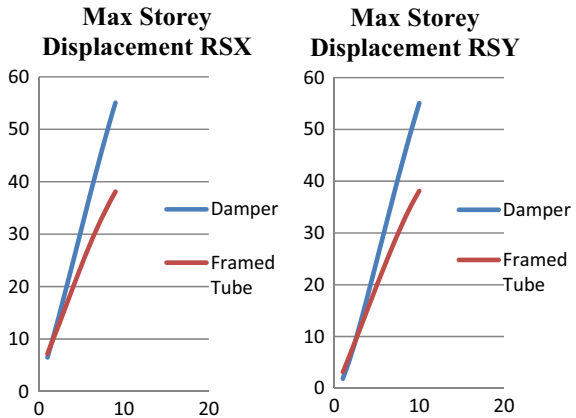


Table 6 Maximum storey drifts in L shaped structure

Viscous dampers			Framed tube		
Story	X	Y	Story	X	Y
Story 5	0.00021	0.000201	Story 5	0.000253	0.000258
Story 10	0.000314	0.000313	Story 10	0.000266	0.000284
Story 15	0.000349	0.000361	Story 15	0.000269	0.000297
Story 20	0.000359	0.000386	Story 20	0.000269	0.000306
Story 25	0.000363	0.000403	Story 25	0.000269	0.000311
Story 30	0.000361	0.000413	Story 30	0.000264	0.000311
Story 35	0.000351	0.000414	Story 35	0.000253	0.000303
Story 40	0.000327	0.000401	Story 40	0.00023	0.000285
Story 45	0.00029	0.000374	Story 45	0.000189	0.000246
Story 50	0.000258	0.00035	Story 50	0.000136	0.000194

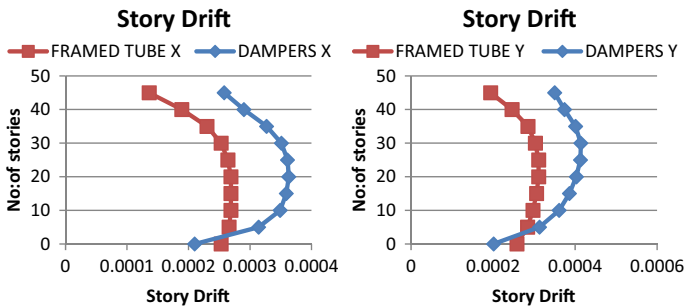


Fig. 8 Storey drifts (RSX and RSY)

6.2.2 Maximum Storey Drifts

The results on Storey drifts between, RC frame with framed tube structure system, and Frame with VD are shown in Table 6 (Fig. 8).

6.2.3 Base Shear

The base shear of an L-shaped structure with a framed tube system in X direction is 74% greater than that of a VD i.e. in a Framed tube structure it is 17054 kN and in a Frame with VD it is 4511 kN. Similarly, in Y direction (Table 7).

Table 7 Base shear of L shaped

	Framed tube	Damper
RSX	17,054	4021.28
RSY	13,341	3959.98

6.2.4 Modal Shape

As in the case of RC frame with Viscous Dampers we can observe that 97% of the total mass of the structure in being participated by 15 modes. Similarly, in RC structure with framed tube system also we can see that 98% of the total mass is being consumed in X direction where as in Y direction also 98% (Table 8; Figs. 9 and 10).

Table 8 Mode shape data

Mode	Framed tube			Viscous damper		
	Period (s)	Mass ratio X	Mass ratio (Y)	Period (s)	Mass ratio X	Mass ratio Y
1	2.99	0.0679	0.6562	2.935	0.0679	0.613
2	2.34	0.6673	0.0692	2.468	0.6316	0.0626
3	1.566	0.0105	0.0081	1.366	0.011	0.0126
4	0.89	0.0109	0.1415	0.757	0.0187	0.1442
5	0.732	0.1295	0.0064	0.697	0.1245	0.0151
6	0.517	0.0019	0.0015	0.417	0.002	0.0037
7	0.465	0.0015	0.0405	0.354	0.008	0.04
8	0.396	0.0375	0.0006	0.341	0.0365	0.0072
9	0.307	0.0007	0.0251	0.217	0.0008	0.0018
10	0.303	0.0007	0.0011	0.213	0.0086	0.0206
11	0.264	0.0246	0.0003	0.207	0.0198	0.0078
12	0.205	0.0005	0.0002	0.133	0.0005	0.0007
13	0.163	0.0008	0.0317	0.107	0.0106	0.0285
14	0.14	0.0301	0.0005	0.105	0.0276	0.0099
15	0.109	0.0006	0.0002	0.067	0.0007	0.0009

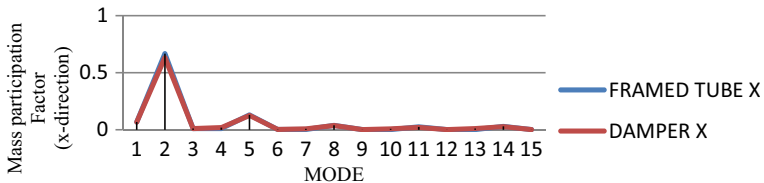


Fig. 9 Modal participating mass ratio in RSX

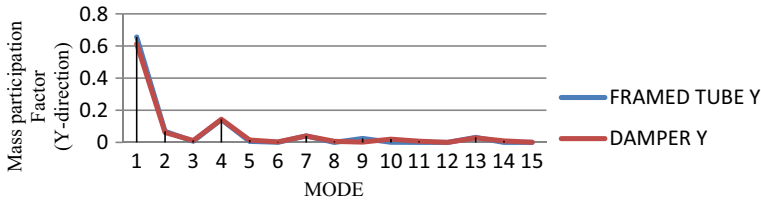


Fig. 10 Modal participating mass ratio in RSY

7 Conclusion

7.1 For Regular Structure

- The storey displacement of an RC frame with a framed tube system in regular structure is 63% less than frame with viscous damper. In Y direction, we can see that the displacement in Framed Tube system 65% less than that of the viscous dampers.
- When the response of storey drifts of RC Structure with Framed tube structural system is compared to viscous dampers, it has more outstanding values and may be employed for tall buildings.
- The base shear for Frame tube structure is comparatively more than RC frame with damper it is due to the rigidity of the peripheral columns which lets the structure to be stiff. The shear is 87% more from the Frame with Viscous dampers.
- When compared to the fundamental time period. The time required for the RC frame with tube structure is 3.195 s, which is 42% less than the time required for the Frame with viscous dampers. In addition, the modal mass participation ratio in the first modes is 98%. Where as in RC frame with viscous dampers the fundamental time period is 5.95 s.

7.2 For L Shaper Irregular Structure

- The displacement in the X direction in the RC Frame after using Viscous Dampers is 43.175 mm, whereas the displacement in the framed tube structural system is 33.099 mm, and the displacement in the Y direction is 49.068 mm and 38.11 mm, respectively, indicating that the framed tube structural system is more effective than Viscous Dampers.
- The drifts in RC frame with Framed tube structural system is 48.86% more effective in X direction as well as in Y direction.
- The base shear is 73% more than in the RC frame with Framed tube system when compared with the RC frame with viscous dampers or in X direction where as in Y direction the base shear is 66% more in RC frame with framed tube.

- The fundamental time period for RC frame with framed tube system is 2.99 s in the first mode with modal participation mass ratio of 98%, in three modes where as in RC frame with Viscous dampers the fundamental time period is 3.271 s.

Based on the comparison of two structural systems on parameters such as storey displacement, storey drift, base shear, and modal mass participating ratio, it can be concluded that an RC frame with framed tube is a better option when constructing tall buildings, whether they are regular or irregular structures.

References

1. Modakwar NP, Meshram SS, Gawatre DW (2014, June) Analysis of structures with irregularities. *IOSR J Mech Civ Eng*
2. Patel J, John RJ (2015, Dec) Seismic analysis of framed tube structure 6:12
3. Duggal SK, Earthquake resistant design of structures book
4. Indian Standard 1893 (part 1) 2016 and IS 1893 part 1 2002 code books. Criteria for earthquake resistant design of structures
5. Landi L, Diotallevi PP, Castellari G (2012, Dec) A procedure for the design of viscous dampers to be inserted in existing plan-asymmetric buildings
6. Hwang J (2013, Oct) Made a report on the topic Seismic design of structures with viscous dampers
7. Banne RA (2015, July–Sept) Analysis of framed tube structures with multiple internal tubes 2
8. Naveen GM (2016, 08 Nov) Study on regular and irregular building structures during an earthquake
9. Pavan Kumar Reddy A (2017, July) Analysis of G+30 highrise buildings by using etabs for various frame sections in zone IV and zone V 6(7)
10. Soltani M, Gholami H, Norouzi H, Shirvani-Dastgerdi H-R, Ostad-Ali-Askari K (2018) The influence of L-shaped structures on their behavior against earthquakes 4(4):1–8
11. Chopra AK, Elastic response spectrum: a historical note
12. Naveen S (2018) Analysis of irregular structures under earthquake loads. In: 2nd International conference on structural integrity and exhibition
13. Suraj S, Wadagule R (2019, 07 July) Comparative study of tube in tube structure and frame tube structure 06
14. Powale SA (2019, Aug) A comparative study of torsional effect of earthquake on ‘L’ And ‘S’ shaped high rise buildings 8(08)
15. Bhomaj S (2019, 09 Sept) Analysis and design of regular and irregular buildings 06
16. Khanal B, Chaulagain H (2020, 14 Jan) Seismic elastic performance of L-shaped building frames through plan irregularities
17. Tabara AM (2020, 23 May) Nonlinear response spectrum analysis of structures equipped with nonlinear power law viscous dampers
18. Hasnat A, Rifat Ibtesham Rahim M (2020, May) Response of building frames with vertical and stiffness irregularity due to lateral loads
19. IS 875 (part 1) 1987-code book for Dead loads
20. IS 875 (part 2) 1987-code book for Imposed loads
21. IS 875 (part 3) 1987-code book for Wind loads
22. IS 16700:2017 code book of criteria for structural safety of tall concrete buildings
23. Taylor devices Inc. North Tonawanda NY, 14120 for data of Viscous dampers

The Application of Statistics and Fuzzy Logic in Predicting Slope Stability



Arunav Chakraborty and Anasuya Goswami

Abstract In Civil Engineering Projects, natural slopes, filled slopes, and cut slopes have stability issues. Slope stability prediction is a complex engineering issue with multiple parameters. Computational methods such as regression analysis, neural networks, adaptive neuro-fuzzy interference, optimization methods, fuzzy logic, etc. can be used to understand the effect of these parameters on slope stability. These computational tools are advanced modelling methodologies capable of simulating extremely complicated functions. They are an effective modelling technique, particularly when the connections amongst the intrinsic data are unknown. It has the capability to recognize and comprehend the associated patterns that exist amongst input and the target data. In this research, regression analysis and fuzzy logic are used to estimate the factor of safety (FOS) of the slopes. GeoStudio, a limit equilibrium (LE) software, is used to examine 200 cases having varied geometry and shear strength characteristics. The prediction models are developed using the FOS values acquired by LEM. Further, a few cases have been taken along Assam-Meghalaya Border National Highway (NH-40). When compared to regression analysis, the results predicted by Fuzzy Logic showed a high degree of precision and accuracy.

Keywords Slope stability · Fuzzy logic · Regression analysis · Limit equilibrium · Factor of safety

1 Introduction

Geotechnical engineers are having a difficult time dealing with the problem of slope stability. Slope stability issues have arisen throughout history as men and women, as well as nature, have disturbed the delicate equilibrium of natural slopes, resulting in slope collapse being a regular natural tragedy that occurs all over the world. Slope stabilization procedures need a thorough understanding and accurate modelling of

A. Chakraborty (✉)
Tezpur University, Tezpur, India

A. Goswami
Sonitpur Polytechnic, Thelamara, India

specialized construction techniques. Understanding geology, hydrology, and soil characteristics is essential for effectively implementing slope stability concepts. When analysing the stability of slopes, geotechnical engineers must take into account the geology, groundwater conditions, and soil shear strength. To evaluate the results of analyses, judgements on acceptable risk or safety factors must be made. As a result, slope investigation and categorization are critical to the community's well-being [1–4]. The limit equilibrium methods (LEMs) viz., Fellenius Method, Bishop's Method, Janbu's Method, Morgenstern and Price's Method are widely used methods for slope stability [5]. Historically, these deterministic approaches were established much before the arrival of the computers and consequently more intricate computational methods followed thereafter. The accuracy of these computational techniques varies depending on how acceptable the simplifying assumptions are for the scenario at present. The most important concept in the application of LEMs of slope stability is the knowledge of mobilized shear strength and mobilized shear strength parameters [6, 7]. However, these deterministic approaches failed to account for uncertainties in soil characteristics, groundwater conditions, vegetation, and the slope's surroundings [8]. As a result, more stringent methods for evaluating the slope are necessary, which may account for the aforesaid uncertainties.

The probabilistic analyses of slope stability are highly capable of considering these uncertainties. These probabilistic approaches are capable of solving highly complex problems making them more powerful than the deterministic approaches and have gained popularity in the recent years. Some remarkable work on probabilistic slope stability analysis has been published in the last several decades. Slope stability prediction using machine learning encouraged many researchers to take highly complex and real estate problems into account. Habibagahi and Meidani employed fuzzy sets to cope with the uncertainties in the soil and on the basis of domain interval analysis a computer programme is developed to calculate the FOS [9]. The suggested reliability index provides a more complete picture of the failure risk than a traditional FOS. Sakellariou and Ferentinou [7] investigated the concept of prediction analysis and developed a relationship between the various slope parameters using an artificial neural network (ANN). The model findings were compared to those of Hoek and Bray [10] and reported to be strongly acceptable. Mohamed et al. [11] used the concept of fuzzy logic to predict the stability of slopes. The predicted outcomes were found to be quite close to the desired outcomes. Erzin and Cetin [12] studied the effect of seismic stresses by considering an artificial slope and used the concept of neural network and regression to determine the FOS and on comparing the results with the calculated ones, it was discovered that the ANN findings had a better degree of precision than the MLR results. In the Amiyani landslide area in Uttarakhand, Singh et al. [13] used a probabilistic method to conduct a slope stability study using FEM and LEM, and on comparing the results, the numerical simulations were found to match the field measurements.

The main objective of this research is to develop prediction models from 200 artificial slopes having varied slope geometry and soil parameters using multiple linear regression (MLR) and fuzzy logic (FL). Moreover, a few case studies have

been taken along Assam-Meghalaya Border National Highway (NH-40) to validate the prediction models.

2 Methodology

The methodology is adopted by considering 200 artificially simulated slopes having varied slope characteristics are examined and the FOS calculated using the Morgenstern-Price method. The prediction models from MLR and FL are developed by using these FOS values. In the prediction models, the input parameters include, slope height (H), cohesion (c'), internal friction angle (ϕ'), slope angle (β), and parameter “ m ” which is given by h/H where h is the water table depth measured from the ground surface. Alternatively, the FOS as the output parameter.

Regression is mainly a statistical method that predicts the nature of a connection between two or more variables. MLR’s overall goal is to learn more about the connection between a dependent and multiple independent or predictor variables [14]. The regression analysis has been conducted using XLSTAT. The FOS value can be expressed as:

$$\text{FOS} = f(H, c', \phi', \beta, m) \quad (2.1)$$

The idea of a fuzzy set is at the heart of fuzzy logic. A fuzzy set is one that lacks a sharp, well-defined border. It is based on fuzzy set theory, which states that a given item or variable has a degree of membership in a given set that might range from 0 to 1. This differs from traditional set theory, which relies on Boolean logic and states that a variable or object is either a member (logic 1) of a set or not (logic 0). A membership function is a function that specifies how each point or object in the discourse universe is allocated a degree of membership or a membership value between 0 and 1. Straight lines can be used to create the simplest membership functions, such as a triangular membership function, which is a collection of three points creating a triangle, or a trapezoidal membership function, which is a truncated triangle curve with a flat top. These membership functions are highly advantageous because of their simplicity. The prediction model is developed using MATLAB fuzzy logic toolbox. The model structure of fuzzy logic used here for prediction of slope stability is shown in Fig. 1. The model structure shows five input parameters, viz., height of the slope, cohesion, angle of internal friction, slope angle, and parameter “ m ” whereas factor of safety as the output parameter as discussed above.

In this research, triangular membership functions (trimf) are used for various input parameters along with 396 rules and 3 epochs. These membership functions can be chosen in terms of simplicity, ease, speed, and efficiency to fit the applications. A Microsoft Excel program is developed to generate the various rules. The different membership functions used for various input and output parameters are revealed in Figs. 2, 3, 4, 5, 6 and 7. For each of the input parameters shown (Figs. 2, 3, 4, 5 and 6), three different triangular membership functions are designed i.e., low, medium,

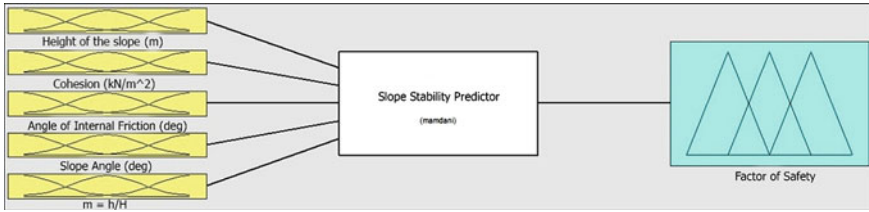


Fig. 1 Fuzzy logic model for prediction of slope stability

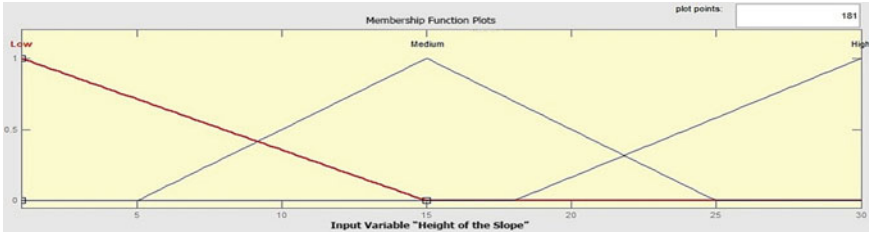


Fig. 2 Membership function for height of the slope (H)

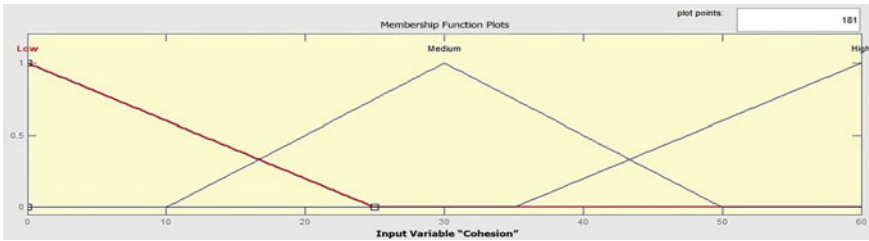


Fig. 3 Membership function for cohesion (c')

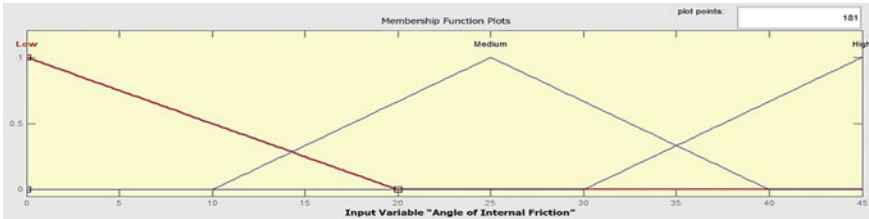


Fig. 4 Membership function for angle of internal friction (ϕ')

and high. In the same manner, the output parameter (Fig. 7) is also designed for three triangular membership functions, viz., unsafe, safe, and over-safe.

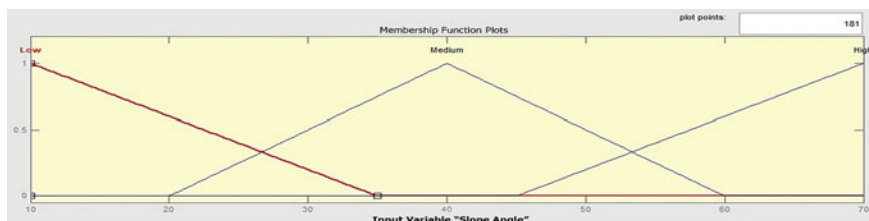


Fig. 5 Membership function for slope angle (β)

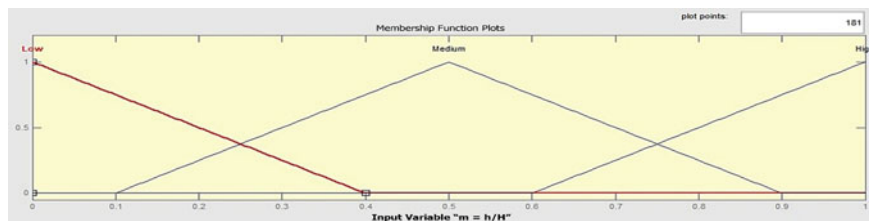


Fig. 6 Membership function for “m” parameter ($m = h/H$)

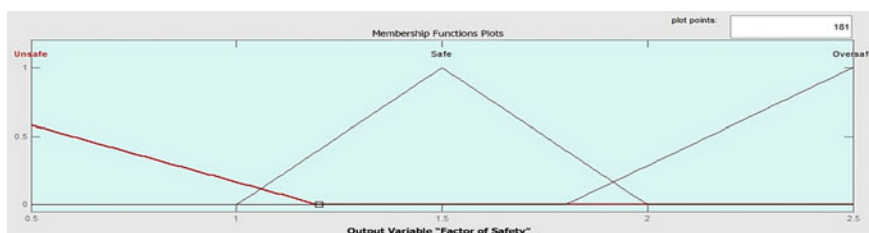


Fig. 7 Membership function for factor of safety of the slope (FOS)

3 Results and Discussions

The summary of the regression statistics used in this research is shown in Table 1. In

Table 1 Summary of the regression statistics

Parameters	Coefficients	Error	t	p
Intercept	1.7413	0.1079	16.1431	< 0.0001
H	-0.0497	0.0041	-12.0075	< 0.0001
c'	0.0278	0.0016	17.6278	< 0.0001
φ'	0.0176	0.0019	9.4931	< 0.0001
β	-0.0173	0.0015	-11.4164	< 0.0001
$m = h/H$	-0.9143	0.0524	-17.4317	< 0.0001

the table shown below, the error is the calculated standard deviation of the coefficient distribution. It's the difference between the coefficients in different instances. A coefficient that is significantly larger than its standard error suggests that the coefficient is not zero. The *t*-stat obtained by dividing the coefficient by the error. The larger the coefficient in relation to the error, the larger the *t*-Stat and the greater the likelihood that the coefficient is not zero. The *p*-value is calculated by comparing the *t*-stat to the *t*-distribution. A *p*-value of < 0.05 shows that the slope of the regression line is not zero, indicating that the dependent and independent variables have a significant linear connection, whereas, *p*-value > 0.05 implies that the slope of the regression line may be zero, and that there is insufficient evidence of a meaningful linear connection between the dependent and independent variables at the 95% level of confidence. The relation between the calculated and predicted FOS for 95% confidence level is shown in Fig. 8 and the variation of the standardized residuals with FOS is shown in Fig. 9.

Equation of the model:

$$\text{FOS} = 1.7413 - 0.0497(H) + 0.0278(c') + 0.0176(\varphi')$$

Fig. 8 Relation between calculated and predicted FOS for 95% confidence level

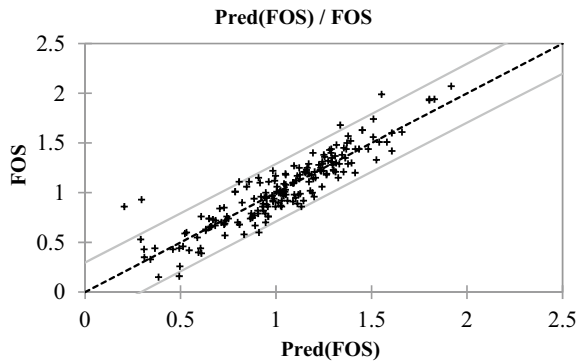
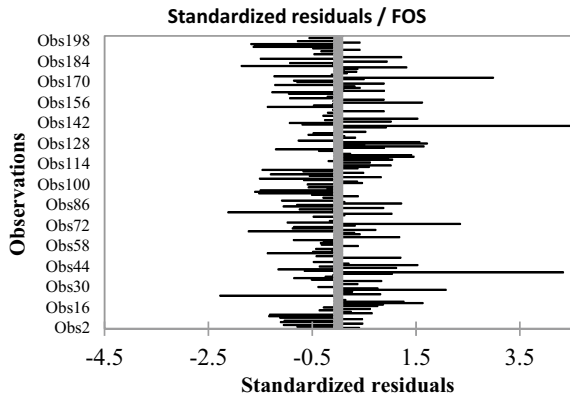


Fig. 9 Variation of the standardized residuals with FOS



$$-0.0173(\beta) - 0.9143(m) (R^2 = 0.83) \quad (3.1)$$

3.1 Case Study

The validity of the prediction models is checked by carrying out some case studies which are independent of the data used for model building. Moreover, the stability of the prediction models is also checked by calculating root mean square error (RMSE) and mean absolute error (MAE).

Meghalaya, which means “*cloud dwelling*” in Sanskrit, is a state situated in the north eastern part of India. On January 21, 1972, it was created by splitting away two districts from Assam: Firstly, the United Khasi Hills and Jaintia Hills, and secondly, the Garo Hills. Meghalaya is bounded to the south and west by Bangladesh and to the north and east by Assam. Shillong is the capital city of the state having latitude and longitude of $25^{\circ} 34' 32.00''$ N and $91^{\circ} 52' 23.00''$ E respectively. Because the National Highway linking Jorabat, Assam, and Shillong (NH-40) includes a lot of hill slopes, slope collapses are prevalent along the Jorabat-Shillong route. According to an investigation, the majority of the slopes are found to be either moist or wet condition, which causes serious problems, especially during the rainy season. During the past two decades, there have been several landslides occurring along these border roads. Moreover, the four laning and development of Jorabat-Barapani section of NH 40 by NHAI has worsen the situation. As a result, it's critical to keep an eye on these landslides. A total station survey is carried out along NH-40 for 18 vulnerable slopes between Jorabat ($26^{\circ} 05' 60.00''$ N; $91^{\circ} 51' 59.99''$ E) and Umling ($25^{\circ} 58' 24.09''$ N; $91^{\circ} 51' 31.18''$ E) over a distance of 25 km (shown in Fig. 10) to determine the different slope characteristics.

Undisturbed soil samples are collected by cylindrical samplers of length 20 cm and diameter 3.8 cm having an area ratio of 10%. At the beginning the in-situ unit weight of the soil is determined from the undisturbed samples and after that consolidated drained (CD) test is conducted to determine the shear parameters. The FOS is finally calculated for all the 18 vulnerable sites using finite element method (FEM). The summary of the test results for 18 slopes are shown in Table 2.

According to Smith [15], if a prediction model produces $R > 0.8$ and the error values are at their lowest, there is a very strong relationship between the predicted variables and the target variables. Figure 11 shows the comparison of results between the predicted and the calculated values of FOS. From Fig. 12, it is found that the RMSE and MAE values are comparatively low for FL and hence, the FOS values obtained by FL are at a much higher degree of precision.

From the present study it has been found that the major cause of the frequent landslides along NH-40 is precipitation. The majority of the hill slopes are found to be moist or wet, which becomes a threat during the rainy season. Long periods of rain soak, weaken, and erode the hill slopes, causing them to become unstable. Furthermore, water seeps into the soil mass through the fissures, weakening the

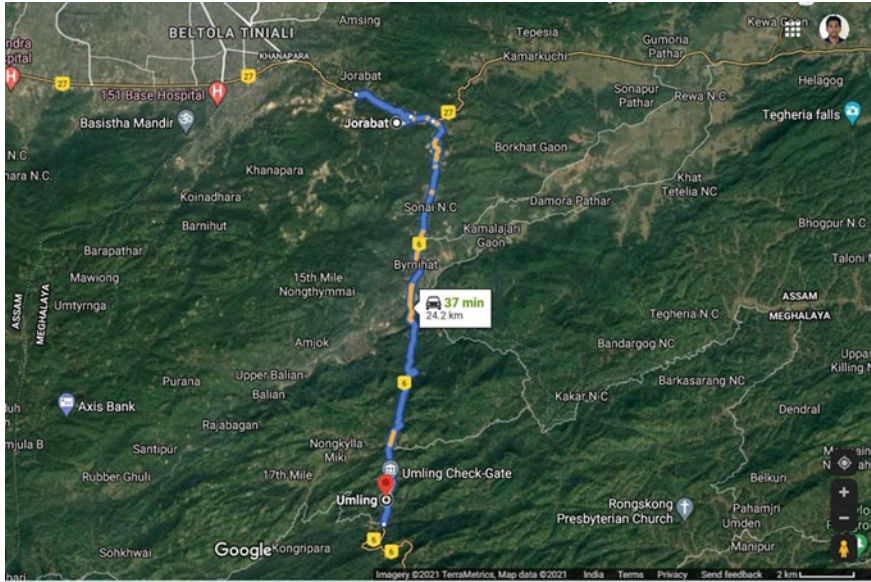


Fig. 10 A satellite-based picture map of NH-40

underlying soil layer and causing the slopes to collapse. It has also been observed in many places along NH-40 the lack of proper drainage facility. During heavy rainfall, water flowing at a high speed erodes the soil, causing slope failure.

The instability is also found to occur due to cutting of hill slopes to form steep slopes for four-laning by NHAI. The results of this research work would be highly valuable for the site engineers as the proposed methodology would help them in taking decisions for evaluating the stability of the entire study area and produce suitable landslide hazard assessment maps.

4 Conclusions

Limit equilibrium method is used to determine the FOS of 200 artificial slope cases having different slope geometry and soil parameters. The FOS values have been used for generating the prediction models. The input parameters include, the slope height, cohesion, friction angle, slope angle, and parameter “ m ” whilst, the FOS is taken as the output parameter. The validity of the prediction model is checked by considering some case studies from NH-40. From the above presented results the following conclusions can be made,

- a. For forecasting slope stability, regression analysis and fuzzy logic can be quite useful.

Table 2 Case study for 18 slopes along NH-40

Sl. No.	Site name	Height of slope (m)	Cohesion (kN/m ²)	Friction angle (°)	Slope angle (°)	Soil unit weight (kN/m ³)	Depth of water table (m)	FOS			
								$m = h/H$	FEM	MLR	FL
	H	c'	ϕ'	β	γ	h	m	FEM	MLR	FL	
1	Jorabat 1	21	39	30	48	17.6	13	0.62	1.15	0.91	1.21
2	Jorabat 2	22	40	32	50	17.3	10	0.45	1.10	1.04	1.12
3	Jorabat 3	18.5	38.2	31.5	58	17.7	12	0.65	1.21	0.97	1.15
4	Jorabat 4	24	39.5	30.5	60	17.9	10	0.42	1.18	0.92	1.25
5	Jorabat 5	18.7	35.6	31.2	55	17.3	8	0.43	1.15	1.01	1.20
6	Jorabat 6	22	39	31.5	50	17.3	11	0.50	1.25	0.96	1.32
7	Jorabat 7	30	38.5	30.7	47	17.5	10	0.33	1.48	1.20	1.52
8	Jorabat 8	27	37.9	30	45	17.3	11	0.41	1.15	0.89	1.20
9	Jorabat 9	22	38.5	29	55	17.5	15	0.68	1.24	0.98	1.18
10	Jorabat 10	21	39.2	29.7	58	17.5	12	0.57	1.37	1.17	1.41
11	Byrnihat 1	25	39	30	52	17.5	14	0.56	1.20	1.02	1.25
12	Byrnihat 2	31.5	39.8	31.3	45	17.8	11.5	0.37	1.45	1.11	1.50
13	Byrnihat 3	28.4	40	32	57	17.5	11	0.39	1.38	1.09	1.42
14	Byrnihat 4	25	38.5	31.5	49	17.5	11	0.44	1.29	0.98	1.25
15	Byrnihat 5	31	37.9	31.5	45	17.3	8	0.26	1.33	1.07	1.35
16	Umling 1	22	38.5	25	60	17.5	16	0.73	1.55	1.43	1.60
17	Umling 2	21	40	29.7	50	17.5	7	0.33	1.30	1.16	1.50
18	Umling 3	22.5	39	32.5	55	17.5	11	0.49	1.35	0.94	1.50

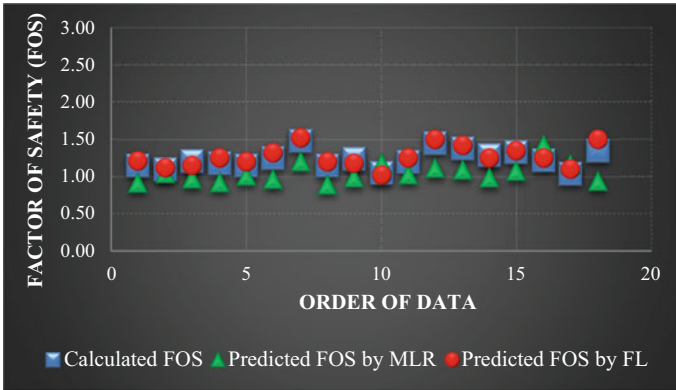


Fig. 11 Calculated FOS and predicted FOS

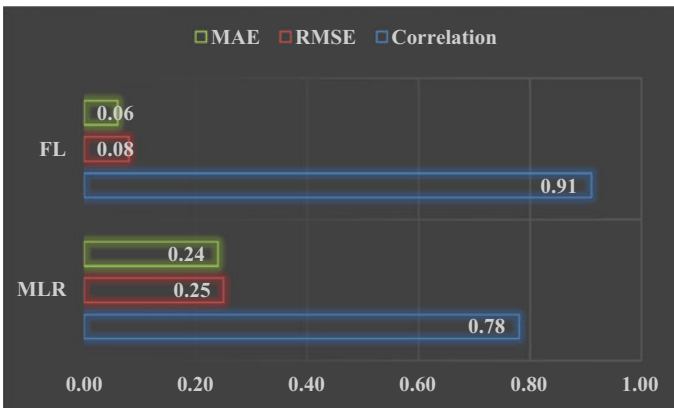


Fig. 12 Comparison of RMSE and MAE for MLR and FL

- b. The FOS produced by the suggested MLR and FL models agrees with the results of the FEM studies in most cases.
- c. However, the predicted results obtained by FL are found to have a correlation of 90.82% as against 78.50% with MLR.
- d. The FL technique is shown to have lower value of RMSE of 0.08 and MAE of 0.06 as against 0.25 and 0.24 respectively with MLR. Therefore, the predicted results of FL are found to be closer to the target values.
- e. Finally, it can be concluded that the present study would be highly beneficial for the planners and developers to estimate the stability for the whole study area by developing landslide hazard zonation maps.

References

1. Lee WA, Thomas SL, Sunil S, Glenn M (2002) Slope stability and stabilization methods, 2nd edn. Wiley
2. Vector Y (2008) Application of soil nailing for slope stability purpose. Thesis B.Sc., University of Technology
3. Choobasti AJ, Farrokhzad F, Barari A (2009) Prediction of slope stability using artificial neural network. Arab J Geosci 2(4):311–319. <https://doi.org/10.1007/s12517-009-0035-3>
4. Ping KZ, Zhi QC (2009) Stability prediction of tailing dam slope based on neural network pattern recognition. In: Proceeding of the international conference on environmental and computer science, pp 380–383
5. Chakraborty A, Goswami D (2016) State of the art: three-dimensional (3D) slope-stability analysis. Int J Geotech Eng. <https://doi.org/10.1080/19386362.2016.1172807>
6. Bromhead EN (1999) The stability of slopes, 2nd edn. Spon Press
7. Sakellariou MG, Ferentinou MD (2005) A study of slope stability prediction using neural networks. Geotech Geol Eng 23:419–445. <https://doi.org/10.1007/s10706-004-8680-5>
8. Chakraborty A, Goswami D (2018) Two-dimensional (2D) slope-stability analysis—a review. Int J Res Appl Sci Eng Technol (IJRASET) 6(II):2108–2112
9. Habibagahi G, Meidani M (2000) Reliability of slope stability analysis evaluated using a fuzzy set approach. In: 5th International conference on civil engineering, Ferdowsi University, Mashhad, Iran
10. Hoek E, Bray JW (1981) Rock slope engineering. Institution of Mining and Metallurgy, London
11. Mohamed T, Kasa A, Taha MR (2012) Fuzzy logic system for slope stability prediction. Int J Adv Sci Eng Inf Technol 2(2):38–42. <https://doi.org/10.18517/ijaseit.2.2.174>
12. Erzin Y, Cetin T (2012) The use of neural networks for the prediction of the critical factor of safety of an artificial slope subjected to earthquake forces. Sci Iranica 19(2):188–194. <https://doi.org/10.1016/j.scient.2012.02.008>
13. Singh R, Umrao RK, Singh TN (2012) Probabilistic analysis of slope in Amiyani landslide area, Uttarakhand. Geomatics Nat Hazards Risks 4(1). <https://doi.org/10.1080/19475705.2012.661796>
14. Yılmaz I, Yuksek A (2008) An example of artificial neural network (ANN) application for indirect estimation of rock parameters. Rock Mech Rock Eng 41:781–795. <https://doi.org/10.1007/s00603-007-0138-7>
15. Smith GN (1986) Probability and statistics in civil engineering: an introduction, Collins, London. Nichols Pub. Co, New York

Utilization of Red Mud as Sustainable Material: A State of Art Review



Akhilesh Buxi Pattanaik and Lasyamayee Garanayak

Abstract The management of natural resources for the development of a greener environment leads to the maximum utilization of industrial wastes. However, significant research is being conducted on waste material, in order to generate sustainable construction materials and meet the enormous demand in the construction industry. The aluminum industry's alkaline bauxite residue has been identified as a highly pollutant toxic material with a pH range of 10.5–13.5. It has several disadvantages, including the need for costly dumping precautions, breathing problems for living creatures due to the spread of dust particles in the air, and underground water pollution. The present study is based on identifying potential engineering applications for red mud in different aspects of the construction industry. It also discusses the physical, chemical, and mechanical properties of those red muds in terms of their mineral composition in order to compare cementitious properties and identify them as sustainable materials capable of resolving environmental pollution.

Keywords Red mud · High alkalinity · Leaching · Cementitious property

1 Introduction

Concrete demand in the construction sector leads to maximum utilization of ordinary Portland cement (OPC). It affects simultaneously the ecology and the economy due to the emission of high-volume of carbon dioxide (CO₂) for maximum consumption of natural resources during the manufacturing process of OPC [1]. It has been reported that 0.6–1 ton of CO₂ is released with the production of 1 ton of OPC, which is considered to be 5–7% of total CO₂ emissions worldwide [2]. Sand and aggregate, in addition to OPC, are essential components of concrete production, necessitating quarrying operations. As a result of this, a large amount of energy is expended, and

A. B. Pattanaik (✉) · L. Garanayak
Shiksha 'O' Anusandhan, Bhubaneswar, India

L. Garanayak
e-mail: lasyamayeegaranayak@soa.ac.in

a large amount of waste is created. Therefore, natural resource scarcity and long-distance transportation drive up the cost of construction materials production significantly [3]. All of these issues encourage the production of cement-free concrete or the development of sustainable materials for construction [3, 4]. Increasing the usage of industrial byproducts as a partial replacement to cement or as a new cement-free binder known as geopolymers is an alternative solution for bringing down the global carbon footprint [3]. The expansion of industries resulting in excessive emissions of industrial byproducts has a serious environmental impact. Multiple researches are going on to convert wastes from the industries like fly ash (FA), granulated blast furnace slag (GGBS), and red mud (RM) into useful construction material [5]. As the concrete industry has an enormous capacity to accommodate any kind of waste, utilizing red mud in cement or concrete manufacturing can be an effective idea for bulk utilization and curbing the negative environmental impact [6]. The current study attempted to find the research gap for the utilization of aluminum waste as a cement replacement generated from various sources in Odisha.

Global red mud production ranges between 120 million tons per year [7], with India accounting for 10% of global red mud production [8]. Red mud or alkaline residue refers to the solid waste produced after processing bauxite ores with caustic soda to produce alumina (Al_2O_3) [9]. The methods used to dispose of red mud differ from country to country. Which include marine discharge, lagoon, and dry stacking. Because of its alkaline nature and the availability of toxic materials, the disposal and storage of red mud have a significant environmental impact [10]. Priority research areas for red clay include (1) neutralization and recycling, (2) exploitation of the alkaline nature, (3) metal recovery, and (4) production of building material materials.

1.1 Generation of Red Clay

The Eastern Ghats of India is having the largest metallurgical grade bauxite belt, having about 2.4 billion tons of bauxite resources. From that Odisha and Chhattisgarh have a 49 and 8% contribution to the total bauxite reserve [11]. Presently available bauxite residue is 1817.2 million tons. In the upcoming 10 years with number of MNCs signing MOUs with Govt. of Odisha for exploration and exploitation of bauxite for setting up alumina refineries plants will increase. With the growth in industry and manufacturing expected quickly a significant increase in countries aluminum consumption will rise in the coming years. With increased consumption of aluminum more waste of red mud will be generated, which in turn will become a threat to our ecology and environment.

Environmentalists consider the treatment and disposal cost of red mud is 5% higher than the manufacturing cost of iron, which is a major impediment in the uptake of red mud. RM must be activated by adding amorphous silica when it has a low hydraulic activity [12] (Table 1).

Table 1 Production of red mud on a global scale

Sl. No.	Country	Yearly production (in million tons)	References
1	Australia	30	Sutar et al. [13]
2	Brazil	10.6	Lima et al. [14]
3	India	10	Vijaya et al. [8]
4	Greece	0.7	Sutar et al. [13]

1.2 Objective of the Paper

Red mud characterization and value utilization research is fragmented and deemed insufficient. Hence an analysis and synthesis of RM properties from various sources are presented in this paper along with an explanation of how these properties affect concrete's strength and durability characteristics. High alkalinity is a major limiting factor that hinders its value utilization. The paper concludes with a discussion of several engineering applications of bauxite residue from around the world.

2 Material Properties

2.1 Physical Properties

Physical properties have a significant role in analyzing the applicability of materials for practical application. Red mud typically has particle sizes ranging from 0.1 to 100 μm . Using a laser particle size analyzer, the X10, X50, and X90 particle diameters of red mud were determined to be 0.37, 1.57, and 56.88 μm , respectively. In contrast, the grain size of sintering red clay is 10 μm . Bayer red clay, on the other hand, is wider [15]. Particle size distribution greatly affects the microstructural properties and strength parameters. Finer grading of particles helps in achieving dense microstructure, improved strength, and durability [3]. Red mud contains fine particles with different shapes including flaky and spherical particles, according to research. When mixed with finer particles, red mud acts as a binder extender, increasing both workability and density [15]. Physical properties such as specific gravity, particle size distribution (PSD), specific surface area, and bulk density are important in determining the strength of concrete. Specific surface area, for example, influences the rate of dissolution reaction. Similarly, bulk density, which is related to packing density, influences hydraulic conductivity [16] (Table 2).

The presence of porous particles in red mud produces a high specific surface area which leads to absorption capacity and interfacial bonding [15]. The physical properties obtained from conducting experiments by several authors on bauxite residue are elucidated in the below table. Table 3 summarizes the physical Properties of RMs from different origins around the world. It is reported that the specific gravity of

Table 2 Physical properties of red mud collected from India and outside India [17]

Property	Indian red mud			UK	Spain	China	Jamaica
	Nalco, Odisha	Hindalco, Renukoot	Hindalco, Muri				
Specific gravity	2.85–3.45	2.85–2.97	3.27	3.05	3.7	3.44	2.7–3.7
pH	10.7–11.5	10.2–11	11.53	11.6	10.2		11.25–12.5
Surface area (m ² /g)	20.4–47.2				23.7		
Particle gradation							
% fraction							
Gravel	0	0	0	0	0	0	0
Sand	5–15	10–14	17	0	12	5	20–3
Silt	43–76	43–57	51	80	50	75	50
Clay	22–35	29–39	32	20	38	20	20–30
γ_{dmax} (Kn/m ³)	12.5–17.0	14.5–16.4	15.2–15.9	17.5	16.9	17	

Table 3 Typical composition of red mud/bauxite residue [21]

Composition	Weight %
Fe ₂ O ₃	30–60
Al ₂ O ₃	10–20
SiO ₂	3–50
TiO ₂	Trace–25
Na ₂ O	2–10
CaO	2–8

RM consistently varies in the range from 2.7 to 3.7, depending upon the source of origin. For river sand, the specific gravity value is 2.65–2.75 and for ordinary Portland cement, the value is 3–3.15. That indicates that the red mud is 1.3 times heavier than natural sand and 0.55 times heavier than OPC. Due to the presence of metallic compounds, particularly iron oxide, the (Gs) value of RM is evidently higher than that of RM [18]. High sp. gravity of RM leads to produce higher density of production materials [15]. However, the presence of finer particles helps in attaining high packing density which ultimately affects the hydraulic conductivity property of the hardened concrete [19]. Presence of finer particles sometimes helps in improving the hydration rate of pozzolanic material with high aluminum content it may be helpful in producing rapid hardening cement in combination with gypsum [20].

The presence of fine fraction, on the other hand, confers an advantage by making the material suitable for manufacturing dense concrete in which finer particle size helps in improving barrier for hydraulic conductivity. A concrete matrix governed by geometrical particle packing model will aid in greater resistance to chemical attacks [22]. This effect substantiated Rubinos' research, which investigated ability

of RM for liner applications and found that its fine fractions had significantly lower hydraulic conductivity than coarse fractions of RM [19].

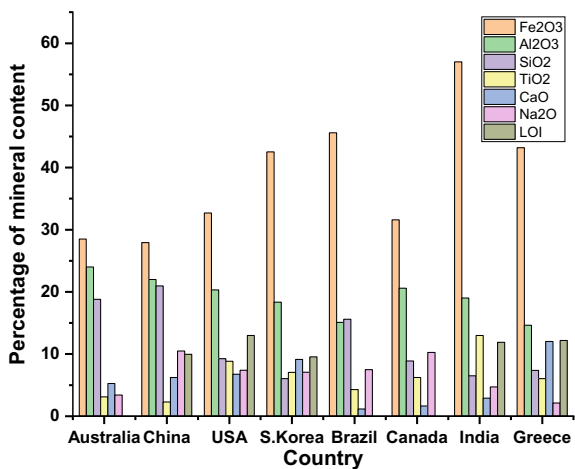
2.2 Chemical Properties

To effectively utilize red mud, it is imperative to become familiar with its chemical and mineral composition. The material properties of used product materials are better understood with this method. A mixture of minerals that have not been digested and minerals that have been transformed into new complex molecules during the refining process makes up red mud [23]. Types and quantities of chemical compounds vary depending on the ore characteristics and the production process (Fig. 1).

Major oxide components are Al_2O_3 (8.22%), Fe_2O_3 (5.46%), SiO_2 (5.25%), TiO_2 (2.5–17%), Na_2O (3–12%) and CaO (1–45%). Sintering and combined Bayer-sintering red mud exhibit high calcium percentages, i.e., more than > 20% in compared to Bayer red mud [15]. The high concentration of iron oxide in bauxite residue/red mud is what gives it its color and name [24]. Sintering red mud is rich in CaO and SiO_2 content which is good for concrete hydration. Whereas Bayer’s red mud lacks calcium oxide [23]. The percentage of CaO in Bayer’s red mud is less than 3%. Which makes it unfit for direct use in concrete manufacturing [21].

The above-collected global data revealed that there is a significant variation in oxides of RM found in India when compared to other countries all over the world. It is noticed that Indian red mud is rich in Al_2O_3 and Fe_2O_3 and SiO_2 content, which makes it suitable for the manufacturing of alkali-activated concrete, geopolymer blocks fired bricks, etc. Al_2O_3 and Fe_2O_3 are major constituents of brick manufacturing [25]. Hence if the major obstacles for bulk utilization like extreme fineness, poor setting

Fig. 1 Chemical composition of red mud different countries [11]



time, dewatering characteristics, and high alkalinity is controlled effectively this can be a material for future generation [26].

2.3 *Pozzolan Properties*

Clinker content in cement is the primary path for the reduction of CO₂ emissions. Here, red mud can be utilized as hydraulic and/or pozzolanic material [27]. Increased percentages of red mud on cement mortars were found as accelerating in the setting process with reduction of pozzolanic activity and mechanical strength [10]. So red mud can be utilized as silicate bonded bricks which are named geopolymers, and hollow building blocks [27]. It signifies that a higher percentage of its particle sizes are finely divided and they aid in forming cementitious compounds while reacting with Ca(OH₂) in presence of moisture (ASTM C595/C595M). It has little or no cementitious property, in contrast to hydraulic pozzolanic material [18].

In his research on the pozzolanic activity index of red mud found that it is not purely pozzolanic material. To be utilized as a building material directly RM obtained from the sintering process sounds cost-effective as it has a good amount of calcium oxide and silica oxide present in it [13]. But red mud obtained from Bayer's refining process cannot be used directly as it does not have these pozzolanic constituents [28]. But it can be used well along with fly ash and GGBS as Bayer's RM is rich in oxides of aluminum and iron. Hence the reaction rate will be faster. It was noticed that red mud with 4% gypsum and 35% fly Ash lowers the pH up to 10.28 and yields good strength [29]. Red mud solids have a water content of nearly 400 g/L, which is the major hindrance of RM as a raw material in the cement manufacturing process [26]. In the early age of strength development, the presence of aluminum oxide, titanium oxide, and silica oxide imparts greater importance [30].

2.4 *pH*

pH is a master variable that regulates the reaction kinetics forward and backward. For the availability of high pH value, red mud produces a major impact on the environment. It is varying from 9 to 12.5 [15]. The presence of Na₂CO₃ and NaAl(OH₄) in the liquid or the surface of the bauxite residue in the refinery before disposing of is the cause of its high alkalinity. Studies show that the pH of the waste, alkaline solids acts as a buffer. It will not decrease until these solids were completely digested by acids and reacting products were removed [16]. It is recommended to lower the alkalinity of red mud because it can conversely affect the use of additives in concrete.

Neutralization of RM can be done by acids, lime neutralization, biological neutralization, and seawater neutralization [24]. The use of supplementary cementitious materials (SCMs) like GGBS, Fly ash, etc. along with acids such as HCL or HNO₃ shows greater efficacy in lowering the pH of bauxite residue. The addition of 8%

gypsum lowers the pH up to 8.12, however, in post neutralization the pH is found to be increased. Acids have greater neutralizing capacity than SCMs. 0.1 M HCL or 0.1 M HNO₃ reduces the pH up to 6.59 and 7.54, respectively [29].

3 Mechanical Properties of RM Concrete

3.1 Compressive Strength

The study focuses on different mix proportions with different kinds of W/C ratios in combination with several replacement levels of RM to find the maximum replacement dosage. It is noticed that as the percentage of replacement increases, the compressive strength appears to rise. But by many authors, it is reported that for ordinary concrete the optimum replacement level is 10% [26]. Some researchers like Kang et al. investigate the effect of adding acid neutralized red mud on strength of concrete. The results were quite interesting as at a pH range of 6–7 excellent pozzolanic property is shown by red mud due to the fine particle size and great filling effect. The production of C–S–H gel accelerates with the inclusion of silica and free lime in RM concrete at later curing ages, which results in a higher strength enhancement at later curing ages. However, it can be inferred that when the RM concentration climbs to 10%, the strength increases. Although the strength reduces as the curing time progresses, it never falls below that of concrete [26].

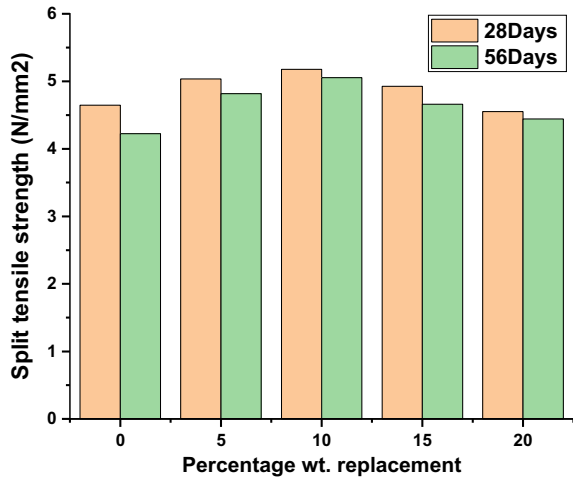
3.2 Split Tensile Strength

It has been shown by Kang et al. and Venkatesh et al. According to the analysis, a 10% replacement level yield an ideal strength of 5.7 MPa. As the microstructure of concrete is filled with red mud, it exhibits excellent pozzolanic properties and tensile strength is increased. While the strength slightly decreases above 10% replacement level, it is not a significant change. Figure 2 shows the development of split tensile strength with percentage replacement.

4 Durability Characteristics

Carbonation, chloride ingress, and sulfate attack are three critical factors that affect durability in harsh environments. Among these, chloride ion penetration is one of the main governing parameters that affect durability. The rate of penetration of chloride ion determines the time duration after which the passivity layer of the reinforcing bar brakes. This can major by the rapid chloride penetration test conforming ASTM

Fig. 2 Split tensile strength of red mud concrete



C 1202. With increasing red mud content, the time lag increases due to a decrease in the relative amount of capillary pores. Capillary voids in samples containing red mud become less interconnected, and the presence of sodium aluminum silicates (sodalite) reduces the flow of chloride ions [18].

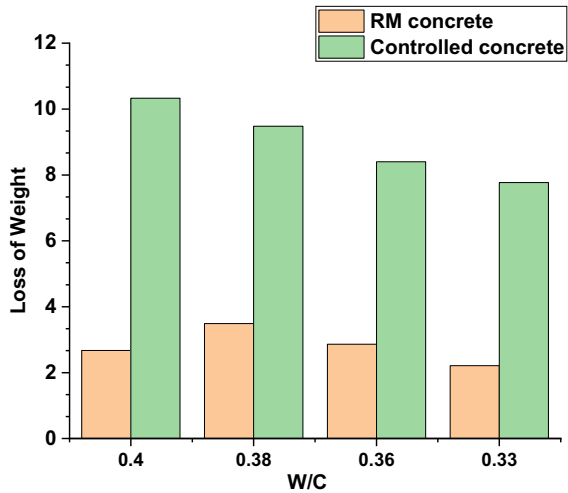
4.1 Effect of Accelerated Corrosion

Corrosion of steel bars is the most serious durability issue in RCC structures, reducing the structure's service life. RCC will lose service life due to corrosion-induced cracking. Because of its high alkalinity, red mud concrete indirectly protects the steel by forming a passivity layer. This protects the steel from harsh environmental conditions. Corrosion begins as a result of the breakdown of the passivity layer in concrete, which causes carbonation, or as a result of the acceleration of chloride ions in the microstructure [30–32]. From Fig. 3 it is evident that the loss of weight of steel due to accelerated corrosion is less in RM concrete than controlled concrete for all stages of replacement.

4.2 Sulfate Attack

The two types of sulfate attacks on concrete are physical salt attacks caused by salt crystallization and chemical sulfate attack caused by sulfates from the soil, groundwater, or marine water. Concrete can expand, crack, lose strength, and disintegrate

Fig. 3 Graph showing loss of weight of steel due to accelerated corrosion with respect to W/C ratio



as a result of sulfate attack. A highly alkaline environment does not aid with sulfate-related problems in concrete. This is a substantial advantage of RM concrete over regular concrete [33].

5 Availability of Red Mud for Construction Uses and Problems Associated

5.1 Geopolymer Concrete from RM

Some researchers like Shia et al., Cundi et al., He et al., Zhang et al., and Najar et al. researched the area of geopolymer concrete. In 1999 Shia et al. in their study found that calcined RM showed improved pozzolanic property than normal red mud. Its reactivity rate is also high. Cundi et al. in their study on geopolymer monoliths by using RM and pressure fluidized bed boiler ash as a raw material in an ambient curing condition. The results show the incorporation of pressure fluidized bed boiler ash accelerates solidifying of red mud. Natural pozzolanas such as rice husk ash have also been added by He et al. to form geopolymer composites at an ambient curing temperature. It is found that the compressive strength is found to be increased compared to Portland cement. The addition of fly ash in an oven curing condition of 23 °C for a different period at a relative humidity of 40–50% was investigated by Zhang et al. and observed that it shows good mechanical properties over a longer time. Design of single and multi-component mix used for developing products like flooring tile, Roof tile, and decoration products also aid in utilizing geopolymer as a building material done by combining RM with laterite and fly ash at an ambient curing temperature [25].

5.2 *Application of RM in Ceramics*

The addition of RM with sodium borate and sodium silicate along with fly ash shows better comprehensive properties. Roof tiles are manufactured by mixing RM and tile clay and firing at a temperature of 900–1020 °C. 30% addition of RM by weight is found acceptable for the manufacturing of roof tiles and bricks.

5.3 *Application of RM in Stabilized Bricks*

Red mud clay sintered at a temperature of 800–1100 °C for manufacturing bricks by Dodoo Arhin et al. (2013) shows improves mechanical properties at increased sintering temperature. It is found that RM along with fly ash at 1200 °C shows better performance at 50% weight replacement level [34]. Some researchers like manufactured high porosity bricks by combining RM with mine tailings. Non-fired bricks are also made by utilizing the chemical bonding properties of RM in combination with foundry sand and lime [35].

6 Conclusion

This review emphasizes the study of the characteristic of RM and its utilization as a sustainable material for building construction. Here are some important outcomes of the review.

The analysis of red mud is complicated by its complex mineralogical composition, extreme fineness, poor setting time, dewatering characteristics, and lack of easy supply are the key challenges toward its bulk utilization. This necessitates a thorough understanding of the properties and their impact on engineering behavior. Acid neutralization or the addition of SCMs to the waste can effectively neutralize it. The use of 0.1 M HCl or HNO₃ reduces the pH to 6.59. The addition of 8% gypsum lowers the pH to 8.12. However, after neutralization, the pH is found to be increasing. Examining the compressive strength reveals that at 10% replacement the strength is higher. However, as the replacement level increases, so does the strength. Rm concrete has substantial advantages over regular concrete against chemical attacks, accelerated corrosion, and other durability properties. Development of geopolymers from Rm aids in manufacturing floor tiles, building blocks, stabilized bricks, decoration products, etc. which makes it suitable for building purposes other than waste which creates environmental hazards. Hence, from the study, we can conclude that with the development of newer technology and extensive research in this area, this bauxite waste can become a boon to society.

References

1. Mermerdas K, Nassani DE, Manguri S, Oleiwi SM (2017) Effect of aggregate properties on the mechanical and absorption characteristics of geopolymer mortar. <https://doi.org/10.1016/j.jestch.2017.11.009>
2. Wardhono A, Gunasekara C, Law DW, Setunge S (2017) Comparison of long term performance between alkali activated slag and fly ash geopolymer concretes. *Constr Build Mater* 143:272–279
3. Part WK, Ramli M, Cheah CB (2015) An overview on the influence of various factors on the properties of geopolymer concrete derived from industrial by-products. *Constr Build Mater* 77:370–395
4. Ryu GS, Lee YB, Koh KT, Chung YS (2013) The mechanical properties of fly ash-based geopolymer concrete with alkaline activators. <https://doi.org/10.1016/j.conbuildmat.2013.05.069>
5. Demirbog R, Türkmen İ, Karakoc MB (2004) Relationship between ultrasonic velocity and compressive strength for high-volume mineral-admixed concrete. <https://doi.org/10.1016/j.cemconres.2004.04.017>
6. Bahraq AA, Maslehuddin M, Al-Dulajjan SU (2020) Macro-and Micro-Properties of engineered cementitious composites (ECCs) incorporating industrial waste materials: a review. <https://doi.org/10.1007/s13369-020-04729-7>
7. Kim SY, Jun Y, Jeon D, Oh JE (2017) Synthesis of structural binder for red brick production based on red mud and fly ash activated using Ca (OH) 2 and Na2CO3. <https://doi.org/10.1016/j.conbuildmat.2017.04.171>
8. Vijaya HM, Samuel T, Wesley PK (2018) Assessment of red mud as a construction material a review. *Indian J Sci Res* 17(2):473–478
9. Liu X, Zhang N (2011) Utilization of red mud in cement production: a review. <https://doi.org/10.1177/0734242X11407653>
10. Tang WC, Wang Z, Liu Y, Cui HZ (2018) Influence of red mud on fresh and hardened properties of self-compacting concrete. *Constr Build Mater [Internet]* 178:288–300. Available from: <https://doi.org/10.1016/j.conbuildmat.2018.05.171>
11. Rai S, Bahadure S, Chaddha MJ, Agnihotri A (2019) Disposal practices and utilization of red mud (Bauxite Residue): A review in Indian context and abroad. <https://doi.org/10.1007/s40831-019-00247-5>
12. Krivenko P, Kovalchuk O, Pasko A, Croymans T, Hult M, Lutter G, Vandevenne N, Schroyers W (2017) Development of alkali activated cements and concrete mixture design with high volumes of red mud. <https://doi.org/10.1016/j.conbuildmat.2017.06.031>
13. Sutar HK, Mishra SC, Sahoo SK, Maharana HS, Chakraverty AP (2014) Tribological aspects of thermally sprayed red mud-fly ash and red mud-Al coatings on mild steel. *American Chem Sci J* 4(3):255–279
14. Lima MSS, Thives LP, Haritonovs V, Bajars K (2017) Red mud application in construction industry: Review of benefits and possibilities. <https://doi.org/10.1088/1757-899X/251/1/012033>
15. Zhang J, Yao Z, Wang K, Wang F, Jiang H, Liang, M, Wei, J, Airey, G (2021) Sustainable utilization of bauxite residue (red mud) as a road material in pavements: a critical review. *Constr Build Mater* 270(2021):121419
16. Grafe M, Power G, Klauber C (2009) Review of bauxite residue alkalinity and associated chemistry. *CSIRO Doc DMR-3610 Proj ATF-06-3 Manag Bauxite Residues (May):51*
17. Reddy PS, Reddy NG, Serjun VZ, Mohanty B, Das SK, Reddy KR, Rao BH (2020) Properties and assessment of applications of red mud (bauxite residue): current status and research needs. <https://doi.org/10.1007/s12649-020-01089-z>
18. Ribeiro DV, Labrincha JA, Morelli MR (2012) Effect of the addition of red mud on the corrosion parameters of reinforced concrete. *Cem Concr Res* 42(1):124–133
19. Rubinos D, Spagnoli G, Barral MT (2015) Assessment of bauxite refining residue (red mud) as a liner for waste disposal facilities. *Int J Min Reclam Environ* 29(6):433–452

20. Khatib JM, Wright L, Mangat PS, Negim EM (2012) Porosity and pore size distribution of well hydrated cement-fly ash-gypsum pastes. <https://doi.org/10.5829/idosi.aejsr.2012.7.4.65131>
21. Borra CR, Blanpain B, Pontikes Y, Binnemans K, Van Gerven T (2019) Recovery of rare earths from bauxite residue (Red Mud). https://doi.org/10.1142/9789813271050_0016
22. Raj N, Patil SG, Bhattacharjee B (2014) Concrete mix design by packing density method. IOSR J Mech Civ Eng (IOSR-JMCE) e-ISSN: 2278-1684,p-ISSN: 2320-334X, 11(2):34–46
23. Wang L, Sun N, Tang H, Sun W (2019) A review on comprehensive utilization of red mud and prospect analysis. <https://doi.org/10.3390/min9060362>
24. Qi Y (2021) The neutralization and recycling of red mud—a review. <https://doi.org/10.1088/1742-6596/1759/1/012004>
25. Mohamed Najar PA et al (2019) Value added geopolymer products to offset expenditure on waste management and sustainability. In: Proceedings of 7th international conference & exhibition on aluminium, Bhubaneswar
26. Venkatesh C, Chand MSR, Nerella R (2019) A state of the art on red mud as a substitutional cementitious material. *Ann Chim Sci Des Mater* 43(2):99–106
27. Pontikes Y, Angelopoulos GN (2013) Bauxite residue in cement and cementitious applications: current status and a possible way forward. *Resour Conserv Recycl* [Internet] 73:53–63. Available from: <https://doi.org/10.1016/j.resconrec.2013.01.005>
28. Tsakiridis PE, Agatzini-Leonardou S, Oustadakis P (2004) Red mud addition in the raw meal for the production of Portland cement clinker. *J Hazard Mater* 116(1–2):103–110
29. Mishra MC, Gangadhara Reddy N, Hanumantha Rao B, Kumar Das S (2020) A study on evaluating the usefulness and applicability of additives for neutralizing extremely alkaline red mud waste [internet]. In: *Lecture notes in civil engineering*, vol 89. Springer International Publishing, Berlin, pp 139–149. Available from: https://doi.org/10.1007/978-3-030-51350-4_16
30. Rathan Raj R, PerumalPillaib EB, Santhakumai AR (2013) Effective utilization of red mud bauxite waste as a replacement of cement in concrete for environmental conservation. *Ecol Environ Conserv* 19(1):247–255
31. Venkatesh C, Nerella R, Chand MSR (2020) Comparison of mechanical and durability properties of treated and untreated red mud concrete. *Mater Today Proc* [Internet] 27(xxxx):284–287. Available from: <https://doi.org/10.1016/j.matpr.2019.11.026>
32. Venkatesh C, Ruben N, Chand MSR (2020) Red mud as an additive in concrete: comprehensive characterization. *J Korean Ceram Soc* [Internet] 57(3):281–289. Available from: <https://doi.org/10.1007/s43207-020-00030-3>
33. Singh S, Aswath MU, Ranganath RV (2016) Durability of red mud based geopolymer paste in acid solutions. *Mater Sci Forum* 866:99–105
34. Rai S, Lataye DH, Chaddha MJ, Mishra RS, Mahendiran P, Mukhopadhyay J et al (2013) An alternative to clay in building materials: red mud sintering using fly ash via Taguchi’s methodology. *Adv Mater Sci Eng*
35. Beulah M, Sudhir MR, Mohan MK, Gayathri G, Jain D (2021) Mine waste-based next generation bricks: a case study of iron ore tailings, red mud and ggbs utilization in bricks. <https://doi.org/10.1155/2021/9499613>

Usage of Polyacrylic Acid in Cold Mix Applications: A Review



Vikram Patel, Jayesh Juremalani, and S. Shankar

Abstract Last three decades have experienced substantial advancements in road construction and maintenance. However, urban and rural road maintenance is yet a challenge as once roads are constructed, maintenance is always overlooked. This review paper concentrates on minimizing cost of maintenance for roads so that urban roads are maintained at regular pace. Usually, the mixtures made of Cold Mix Asphalts (CMA) containing bitumen made of fossil fuels are laid on roads to fill potholes. Since fossil fuels are scarce and have known adverse environmental effects, an attempt is made to eradicate their usage. As Polyacrylic acid contains both adhesive and emulsion properties, it may be useful to replace fossil fuels. This paper researches the usage and results of Polyacrylic acid in road construction in different environmental conditions around the globe.

Keywords Asphalt · Polyacrylic acid · HMA · CMA

1 Introduction

Widening and strengthening of roads is also an important aspect of road maintenance and construction for infrastructure expansion. Hot Mix Asphalt (HMA) was largely used in traditional road construction which led to excessive emission of gases that affects the environment. Fuel consumption in preparation of HMA is high which does not help the sustainability of environment [1]. Hence, researchers and mix designers focused mainly on using CMA instead of HMA for its prominent disadvantages. The mix designs for bituminous mixes are reviewed in this paper.

V. Patel (✉) · J. Juremalani
Department of Civil Engineering, Parul University, Vadodara, Gujarat, India

J. Juremalani
e-mail: jayesh.juremalani@paruluniversity.ac.in

S. Shankar
Transportation Division, Department of Civil Engineering, National Institute of Technology, Warangal, India
e-mail: ss@nitw.ac.in

Investments involved in highway constructions incur huge amounts. The accurate highway design can help in saving capital and offer reliability when highway is in service. The flexible pavement design is the process of composition of mixture in a layered form. This review paper focuses on mix design studies conducted around the globe. The mix design of bitumen should add strength, fatigue resistance, eco-friendly, economical features to the highway. At first, the mix design sample is prepared in different proportions to check the fittest mix.

1.1 Polyacrylic Acid

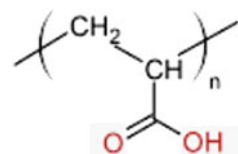
Polyacrylic acid is formed from large compound named as polymer. A polymer contains several repetitions of the smallest compound known as monomer. A collection of similar monomers constitute to form a polymer. Polymers are usually obtained from plastic or rubber wastes both in wet or dry states in order to use them in road construction. The chemical reactions can affect the length of polymer chain and its properties. Chemical structure of Polyacrylic acid is shown in Fig. 1 [2]. Polyacrylic acid compound is available in both liquid and powder form.

The Polyacrylic acid contains adhesive and emulsifying properties similar to conventional binders. Thus, researchers have tried to add this compound to bitumen to strengthen the mixture. As not many studies have been published that conforms use of Polyacrylic acid in cold mix asphalt, this review paper also provides background study of mix design proportions formulated by other researchers to form bituminous mix used in Cold Mix Asphalt (CMA). Later, two researches that agree on usage of Polyacrylic acid are thoroughly reviewed. The paper is organized into sections; first, provided brief introduction to the research. Second, concentrates on literature review of the past papers in regard to the bituminous mix design. Lastly, conclusion is drawn to list major findings of the review.

2 Literature Review

In India, road construction has continuously increased in last five years as shown in Fig. 2.

Fig. 1 Chemical structure of polyacrylic acid [2]



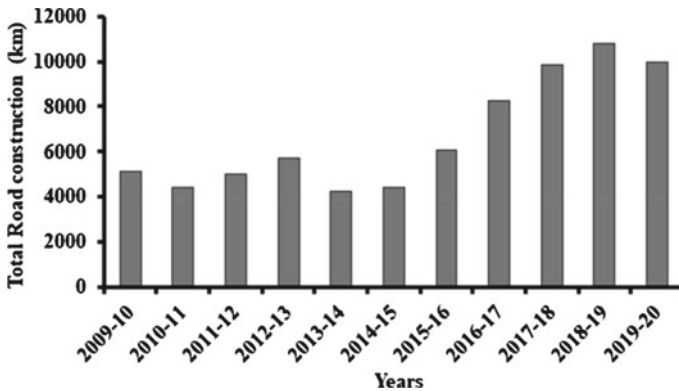


Fig. 2 Yearly road construction in India [3]

2.1 Background

In the 1900s, rural roads were first constructed using bituminous mix. The paving technique using bituminous mixture was first introduced so that fine dust particles were easy to remove. This process is called as dust palliative; originally, heavy density oils were added into the mixture. The required proportion of oil was estimated using pat test. With the proper quantity of oils, the bitumen mixture was prepared and patted in a shape of a cake. The strength was measured by pressing it against the brown paper; according to the stain it makes on the paper, the quantity of oil is adjusted.

The first method to prepare mix design was Hubbard field method that used sand asphalt mixture. However, large particles of sand were not offering promising results when mix was developed using Hubbard method [4].

2.2 Cold Mix Asphalts

Cold Mix Asphalt mixtures consist of aggregates and bitumen that are formed using oil. Usage of oil in asphalt helps in repelling water and makes asphalt soft to attain consistent coverage. Cold Mix Asphalt is ideally considered for filling potholes on rural roads where traffic is less. The CMA mixture is often termed as repair mixture that does not need heating procedures. Moreover, the oil in the mixture keeps it cool for longer period in every weather condition.

2.3 *Mineral Fillers*

Mineral fillers have been lately used in asphalt mixes to maximize the stiffness of the mortar mixtures. The mineral fillers increase the age of mixtures and make them moisture resistant. The mineral fillers act as a gap binder in a bituminous mixture, it can be a stone dust, Portland cement, fly ash, etc. [5].

Mogawer and Stuart [6] examined the characteristics such as performance, rutting, drain down of mastic, workability, cracking, moisture vulnerability, and gradation of asphalt mixtures.

Karrasahin and Terzi [7] made use of limestone in place of filler. The marble blocks as a waste from demolished property sites were chosen to be used as fillers in asphalt. The authors tested the property of the mix by using Marshall Test and it was observed that the mixture can be good to use [7].

Researchers back then focused on utilizing waste materials for sustainable development of infrastructure. Yongjie et al. [8] considered fly ash that replaced aggregates and mineral fillers partially. The fly ash was obtained from municipal solid waste incinerator (MSWI). The mixture hence formed was tested using Marshall Test [8].

Jony and Jahad [9] used waste glass pieces as filler and the mixture was examined using Marshall Test. The authors compared the performance of glass filler mixture with limestone and ordinary Portland cement. The glass filler mixture was observed to be performing well than the other mixtures under comparison [9].

2.4 *Binders*

In order to keep aggregates compact, a mixture must contain a binder so that it keeps the aggregates closer to avoid coarseness and make aggregates soft. This section describes selection of different binders by the researchers over the years.

In 1994, Brown and Mallick researched the properties of mixture that contained grade binder AC-20 [10]. The mixture was evaluated for its important properties such as rutting, viscosity, etc. In 1996, authors selected AC-20 binder for preparing the mixture but with different proportions. The results were observed to be acceptable [6].

Putman and Amirkhanian [11] examined the performance of mixture that contained performance grade binder PG 76-22. Moreover, the mixture used polymer-modified bitumen for enhancing the strength. The properties of bitumen were evaluated and found to be offering substantially better results over original bitumen mixture [11]. Sharma et al. added ordinary rubber fine particles in the bitumen with penetration ratio set at 80/100. The mixture so formed was named as Natural Rubber Modified Bitumen (NRMB). Sharma et al. [12] changed the bitumen grade to 60/70 and modified the bitumen and used PMB-40. The tests were performed on the mixture to support their research [12].

Chiu and Lu [13] checked the mixture properties when added asphalt rubber as binder in stone mastic asphalt. The ground tires rubber was blended with AC-20 asphalt to form asphalt rubber. The mixture did not contain fiber yet, it was found to be successful in preventing water from mixing with the bitumen mix [13]. Reddy et al. [14] compared use of Crumb Rubber Modified Bitumen (CRMB) in comparison to original bitumen mixture. It was found that the modified bitumen mix proves to be long in life, moisture susceptible and offers better performance in extreme temperatures too [14].

2.4.1 Cement as Binder

The binding agent in a bitumen mixture can keep the aggregates intact so that the mixture remains in place for longer period resulting in durability of repaired roads. The performance of cold mix asphalt has been increased when cement is used as a binder. Cement asphalt emulsion composite was used in pavement since 1970s [15, 16]. Schmidt et al. [17] proposed the idea of road maintenance by using asphalt emulsion. The quality of asphalt emulsions hence proposed by the authors was weak in bearing heavy loads. The water stability was less and the poor performance of asphalt emulsion was the reason why it was discontinued [17].

Schmidt et al. evaluated the effects of cement when mixed with cold mix asphalt. The cement and aggregates were found to be incorporated well with asphalt emulsions. The mix offers water-resistant as the MR hence created is strong enough to protect the mixture against water damage [17]. In 1974, Head [16] demonstrated that cement when added in 1% more quantity can improve the strength of mixture up to 300%.

Li et al. [18] studied various properties of CMA mixes by conducting stability tests. The samples were distinguished as cemented (cement immersed in water) samples and non-cemented ones. The cemented samples were seen to be tougher with flexible asphalt concrete and longer life span. Serfass et al. [19] observed the mechanical performance of two types of cold mix viz. grave-emulsion and dense wearing course mix after curing it for diverse situations.

Alvaro et al. [20] found the effect of cement content and prevailing humidity on the performance of asphalt emulsion and cement composites. A dense asphalt concrete mixture was used in this study. The quarry materials as aggregates were used to make cold mix asphalt concrete. The findings revealed that rigidity can be improved with the replacement of Portland cement as filler material with different curing environments. Basic limitation of this mix relates to duration of curing and preparation of mix [20].

Khodary et al. [21] proposed a novel method in order to improve bitumen properties such as chemical, physical and rheological. The nano materials-bitumen mixture was first ground in the size of 10–100 nm by using ball milling technique. The experiments demonstrated that the strength was improved as compared to unmodified mixture [21].

Serif et al. [22] studied the effect of cement on emulsified asphalt mixture. In their study, it was found that by adding OPC, the mechanical properties such as resilient modulus, susceptibility to temperature, creep, resistance to water, and resistance to permanent deformation can be substantially increased [22].

Pundhir and Nanda [23] studied the addition of 2% OPC on Semi dense bituminous concrete (SDBC) with cold mix and compared the stability value at different curing conditions. The modified mixture added with cement possessed higher stability value with respect to the specimen without cement [23].

2.5 *Natural Fiber and Polymers*

Anderson et al. [24] evaluated the rheological properties when polymers such as Neoprene, Styrene-Butadiene-Styrene (SBS), and Styrene-Butadiene-Rubber (SBR) are added to the cold mix. The study concluded that the results deviated from the experimental data [24].

Punith et al. [25] found that addition of polymers in considerably little amount improves the strength of road even in extreme temperatures.

Chavez et al. [26] showed that the compression strength of cold mix asphalt can be substantially increased (31%) by using polyvinyl acetate in comparison with unmodified cold mix.

Butt [27] studied the durability of mastic asphalt added with wax. Research concluded that 4% Montan wax enhances the performance of modified mastic asphalt at low temperatures. It was found that wax modification did not harm the storage constancy as well as crack susceptibility [27].

2.6 *Polyacrylic Acid*

As major cold mix asphalt manufacturing plants rely on kerosene or diesel at major that act as emulsion in the mixture and that the products are not easily available in India; the replacement needs to be found so that it becomes easy to produce cold mix asphalt. The oil used in most of the asphalt mixtures is kerosene or diesel which is imported and may become scarce in near future. Table 1 shows the projection of crude oil demand in India as per GDP percentage of 6, 7, or 8% [28]. It is projected that the demand is going to increase as increase in rates if GDP is lower to 4%. The figures in the tables are in unit of million tons. In order to avoid import of such a huge amount of crude oil which in turn is going to increase as India has increased cold mix asphalt pavement in last five years, usage of new substances that can be easily available in India to replace kerosene and diesel can be beneficial in wider sense.

In 2017, Guo et al., mixed Polyacrylic acid in cement. The construction sites before used cement-based on polymer additives and the performance was satisfactory. To examine how Polyacrylic acid can affect when added to cement, the authors

Table 1 Projection of crude oil demand in India [28]

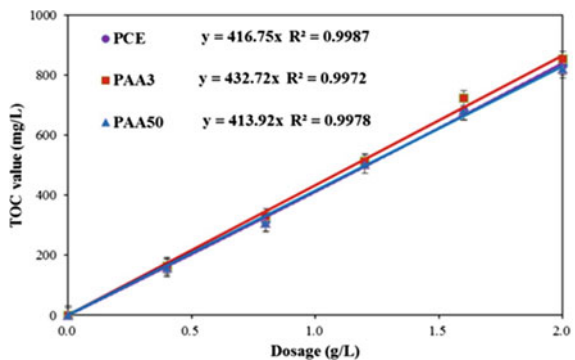
Year	6% real GDP growth			7% real GDP growth			8% real GDP growth		
	Growth rate of crude oil prices								
	4%	5.5%	7%	4%	5.5%	7%	4%	5.5%	7%
2020	215.85	204.59	193.85	235.18	223.02	211.43	256.03	242.92	230.40
2021	225.23	212.20	199.87	247.74	233.55	220.10	272.27	256.81	242.16
2022	235.00	220.10	206.07	260.97	244.58	229.13	289.53	271.50	254.51
2023	245.21	228.30	212.46	274.91	256.13	238.53	307.88	287.04	267.49
2024	255.86	236.80	219.05	289.60	268.22	248.31	327.40	303.46	281.13
2025	266.96	245.61	225.85	305.06	280.88	258.50	348.16	320.82	295.48

performed various tests on the mixture. The fluidity of mixture was examined; addition of Polyacrylic acid emulsion in less than 5% reduced the fluidity of the mixture [29].

Peng et al. [30], investigated the rheology of cement paste when added Polyacrylic acid (PAA) as emulsion and Polycarboxylate Superplasticizer (PCE) as plasticizer. Relation between concentration and total organic carbon (TOC) value of the mix is examined and the results are recorded in Fig. 3.

The tests including conductivity, X-ray photoelectron spectroscopy (XPS), and dynamic light scattering (DLS) were performed. The results illustrated that Polyacrylic acid can adsorb on the cement paste efficiently. The fluidity test was also performed on the mixture; the performance is as shown in Fig. 4. The amount of plasticizer, Polycarboxylate Superplasticizer (PCE) affects the adsorption performance; the plasticizer when added in more amounts, the more is the adsorption performance as shown in Fig. 5 [30].

Fig. 3 Relation between concentration and total organic carbon (TOC) value [30]



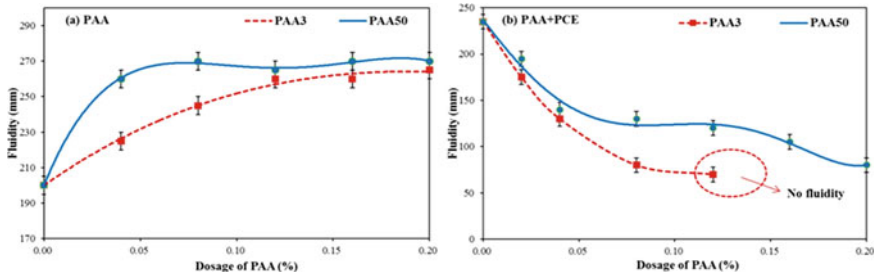
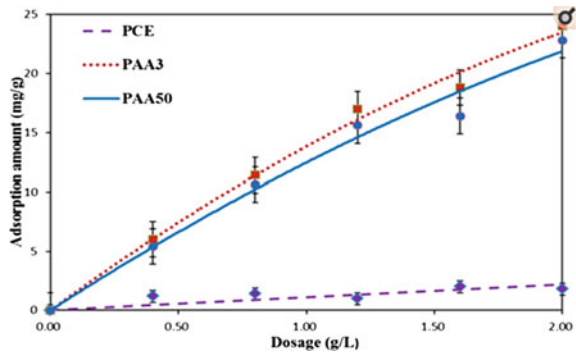


Fig. 4 Effect of polymers on fluidity performance of cement paste [30]

Fig. 5 Adsorption amount of PAA and PCE [30]



3 Summary

On the basis of key findings from the extensive literature review, following points were observed and summarized:

- (a) Polyacrylic acid with its adhesive properties has offered promising results when used with cement paste. However, the approach is novel and its behavior is yet to be explored with cold mix asphalt.
- (b) It is also observed that the different binders and stabilizing additives such as waste materials like plastic, lignin, and synthetic polymers have surprising effects on the strength and durability of flexible pavements.
- (c) The studies on modified emulsions were extensively conducted to obtain better road construction models. Engineering and mechanical properties of mixes were investigated using laboratory experiments. The results obtained proved that using additives can be beneficial for strength and performance of the roads.

4 Conclusions

There are limited investigations on generation of model that can help in filling potholes on urban roads in India. The models that used additives such as waste materials, lignin, and synthetic polymers for construction of complete roads have proved to be providing better results from the huge set of lab experiments. The study on Polyacrylic acid with cold mix asphalt is not addressed yet as use of this chemical compound is new in this domain. The compound has been tested with cement paste and has given promising results [29, 30].

Therefore, the present work is inspired by earlier research needs and involves a complete investigation of Polyacrylic acid used to prepare modified emulsion as a replacement of traditional emulsion which is prepared from fossil fuels in cold mix asphalt for the application of filling potholes on Indian roads.

References

1. Cline W (2004) Meeting the challenge of global warming, global crises. In: Global solutions 1st edn. Copenhagen Consensus 2004 project
2. Polyacrylic acid and super absorbents polymer properties database. <http://polymerdatabase.com/Polymer%20Brands/PAA.html>
3. National Highway Authority of India (NHAIa) (2019, April) Highway construction touched 30 km/day in 2018–2019
4. A Das M Deol S Ohri 2004 Evolution of non-standard bituminous mix – a study on Indian specification Int J Pavement Eng 5 1 39 46
5. Muniandy R, Huat, B (2006) Laboratory diametral fatigue performance of stone matrix asphalt with cellulose oil palm fibre. Am J Appl Sci 3(9)
6. Mogawer W, Stuart K (1996) Effect of mineral fillers on properties of stone matrix asphalt mixtures. TRR 1530 National Research Council 86-94
7. M Karasahin S Terzi 2007 Evaluation of Marbal waste dust in mixture of asphalt matrix Constr Build Mater 21 5 616 620
8. X Yongjie H Haobo Z Shujing 2009 Utilization of municipal solid waste incineration ash in stone mastic asphalt mixture: pavement performance and environmental impact Constr Build Mater 23 2 989 996
9. H Jony Y Jahad 2010 The effect of using glass power filler on hot asphalt concrete mixture properties Eng Technol J 29 1 44 57
10. Brown E, Mallick R (1994) Stone matrix asphalt properties related to mixture design. NCAT Report 94-02
11. B Putman S Amirkhanian 2004 Utilization of waste fibre in stone matrix asphalt mixtures Resour Conserv Recycl 42 3 265 274
12. G Sharma C Kamraj G Kumar 2004 Laboratory studies on the behaviour of stone matrix asphalt vis-à-vis dense graded bituminous mixes using natural rubber powder (wet process) Highway Res Bull IRC New Delhi 71 39 60
13. C Chiu L Lu 2007 A laboratory study on stone matrix asphalt using ground tire rubber Constr Build Mater 21 5 1027 1033
14. Reddy K, Palit S, Pandey B (2004) Laboratory evaluation of crumb rubber modified asphalt mixes. J Mater Civ Eng ASCE 45–53
15. Terrel R, Wang C (1971) Early curing behaviour of Portland cement modified asphalt emulsion mixtures. In: Proceedings of the AAPT, pp 110–131

16. Head R (1974) An informal report of cold mix research using emulsified asphalt as a binder. In: Proceeding of AAPT, pp 110–131
17. R Schmidt L Santucci L Coyne 1973 Performance characteristics of cement modified asphalt emulsion mixes Proc Assoc Asphalt Paving Technol 42 300 319
18. G Li Y Zhao S Pang 1998 Experimental study of cement-asphalt emulsion composite Cem Concr Res 28 5 635 641
19. J Serfass J Poirier J Henrat 2004 The influence of curing on cold mix mechanical performance Mater Struct 37 365 368
20. G Alvaro L Pietro N Manfred J Iwan 2013 The influence of cement content and environmental humidity on asphalt emulsion and cement composites performance Mater Struct 46 1275 1289
21. F Khodary M Abd El-Sadek H El-Sheshtawypaper 2013 Nano size cement bypass as asphalt modifier in highway construction to improve physical, chemical and rheological properties of bitumen Concr Eng Res App 3 6 645 648
22. O Serif C Fazil V Muhammet 2007 Effect of cement on emulsified asphalt mixture J Mater Eng Perform 16 5 578 583
23. N Pundhir P Nanda 2006 Development of bitumen emulsion based cold mix technology for construction of roads under different climatic conditions of India J Sci Ind Res 65 729 743
24. Anderson D, Christensen D, Roque R et al (1992) rheological properties of polymer-modified emulsion residue. Poly Mod Asph Bind. West Conshohocken, pp 20–34
25. V Punith R Sridhar S Bose 2004 Comparative studies on the behaviour of stone matrix asphalt and asphaltic concrete mixtures utilizing reclaimed polyethylene Highway Res Bull IRC New Delhi 71 61 76
26. V Chavez E Alonso A Manzano 2007 Improving the compressive strengths of cold-mix asphalt using asphalt emulsion modified by polyvinyl acetate Constr Build Mater 21 3 583 589
27. Butt A (2009) Low temperature performance of wax modified mastic asphalt. Master's thesis. Royal Institute of Technology, Stockholm, p 42
28. Agrawal P (2012) India's Petroleum Demand: Empirical Estimations and Projections for the Future. IEG Working Paper W319
29. Y Guo B Ma Z Zhi 2017 Effect of polyacrylic acid emulsion on fluidity of cement paste Coll Surf Physio Eng Asp 535 2 139 148
30. Y Peng M Baoguo T Hongbo 2018 Effect of polyacrylic acid on rheology of cement paste plasticized by polycarboxylate superplasticizer Mater MDPI 11 1081 1 19

Self-healing Concrete Based on Bacteria for Sustainable Infrastructure: A State-of-the-Art Review



Chiranjeevi Rahul Rollakanti and Kota Srinivasu

Abstract This study discusses the varieties of concrete bacteria and how they may be used for self-healing of cracks. This article also offers a brief overview of the many characteristics of cement that alter with the presence of microorganisms. Inherent in concrete are microcracks and promote concrete degradation due to the introduction into concrete of adverse chemicals, causing structural degradation. It has to be restored because of this fact. Self-healing strategies are employed to overcome these problems. Calcite precipitation happens in concrete by adding urease-causing bacteria together with the calcium supply. Techniques for biomineralisation lead to promising outcomes at concrete industry for the microcracks. By continuous hydration process, the newly formed microfractures may be screened in concrete. Two different types of bacterial concentrations such as *Bacillus pasteurii* and *Bacillus subtilis* have been considered for this study. The literature review indicated that the bacterial concrete has positive impact on crack healing and also enhancement of mechanical properties of concrete. Bacterial concrete at various bacterial concentrations demonstrates that the addition of bacteria may enhance concrete strength and durability properties. The research study recommends that the self-healing concrete with respective levels of bacteria can reduce the cost in terms of maintenance of concrete structures, through extending the life span of the structure ensuring sustainability.

Keywords Self-healing concrete · Biomineralization · *Bacillus pasteurii* · *Bacillus subtilis* · Crack healing · Sustainability

C. R. Rollakanti (✉)

Department of Civil Engineering, Dr. Y.S.R.A.N.U. College of Engineering & Technology, Acharya Nagarjuna University, Nagarjuna Nagar, Guntur District, Andhra Pradesh 522510, India

K. Srinivasu

NRI Institute of Technology, Guntur, Andhra Pradesh, India

1 Introduction

The concrete is the major component of the construction industry, and it is one of the building materials most frequently utilised. Cracks in concrete are unavoidable, and when cracks arise, the durability of the concrete constructions can be reduced. Different procedures of mending to cure cracks are accessible, but they are quite costly and time-consuming. The cracks in concrete are generally repaired using so-called self-healing concrete. At mixing, bacteria containing calcium lactate are placed in the concrete. As shown in Fig. 1, calcium carbonate precipitates when any cracks are generated in concrete microorganisms. The cracks are healed, and bacterial concrete strength enhances than typical concrete strength because concrete contains bacteria. The life span of the concrete structures will be strengthened by applying biotechnology which depends upon calcite precipitation. Cracks larger than 0.8 mm in diameter are harder to repair; however, cracks can be remediate with the use of bacteria and calcite precipitation [1]. The strength of bacterial-based materials is reduced by the use of lightweight materials without the use of fine aggregates. The strength of lightweight bacterial mortar was shown to be higher than that of conventional lightweights in this experiment. This can be used in instances where lightweight buildings are needed.

When considering the scenario of material, the concept of self-healing materials and utilisation of high quality of materials shall be incorporated to escalate the service life of concrete structure. The modest weight of these aggregates improves healing efficiency and structural sustainability as an efficient bacterium transport agent [2]. When the bacteria were added to rice husk ash concrete, the strength of the concrete is enhanced by stimulating the calcite precipitation, which can occur in life at all times [3]. If maximum calcium carbonate precipitation is reached, a maximum strength of

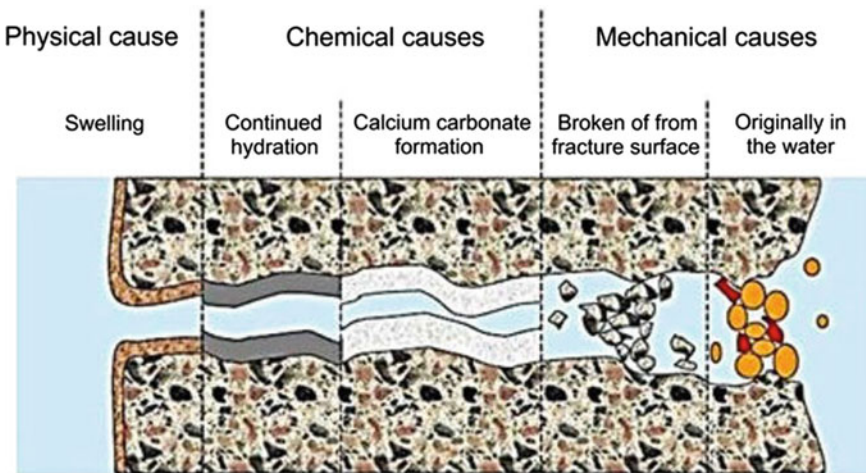


Fig. 1 Formation of calcium carbonate leads to self-healing concrete [1]

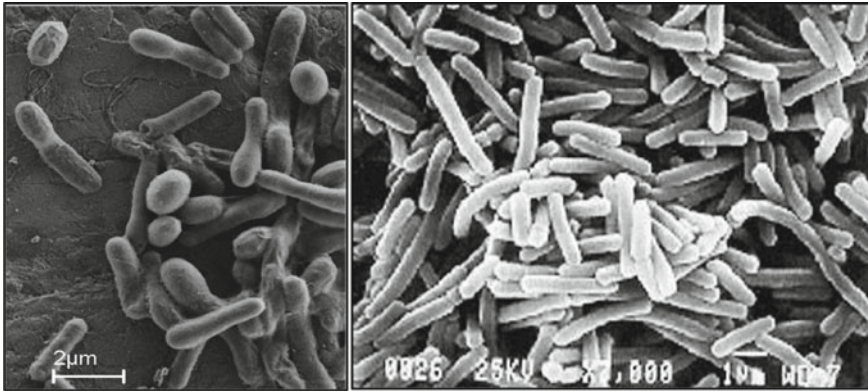


Fig. 2 *Sporosarcina pasteurii* bacterium [5]

M50 concrete can be enhanced by 24% [4]. The introduction of the *Sporosarcina pasteurii*, as shown in the Fig. 2, bacterium to fly ash concrete can improve concrete strength while simultaneously reducing porosity and permeability. This improves compression resistance by up to 22% and water absorption by up to four times with conventional concrete [5].

Positive results have been obtained in the earliest phases of crack repair [6]. The use of hydrogel encapsulation, capsules and vascular systems in concrete specimens for precipitation of calcite appears on the other hand to be a very efficient self-healing technology for building and research activities. Concrete cement elements can be incorporated and self-healing mechanisms devised. Bacterium can precipitate calcite from a number of calcium sources, depending on the source of calcium used. Concrete properties like as durability are improved by contemporary technologies.

2 Literature Review

The purpose of the literature review is primarily to understand the many tangible characteristics that affect the existence of microorganisms. Also, detailed are the species of microorganism application that is to precipitate CaCO_3 in concrete which is the majority extensively used structural substance, owing to the accessibility of its raw materials, affordability, robustness of the products and the compressive strength of its products, despite efforts to prevent the erosion and corrosion of numerous concrete structures, especially infrastructure. This is linked to water permeability, which reduces the effectiveness of the concrete [7]. A further factor in this deterioration is the production of micro- and macrocracks, which can lead to the entry of dissolved particles into the liquid, superfluous acidic gases and water penetration. These and supplementary toxic components, therefore, permeate the system.

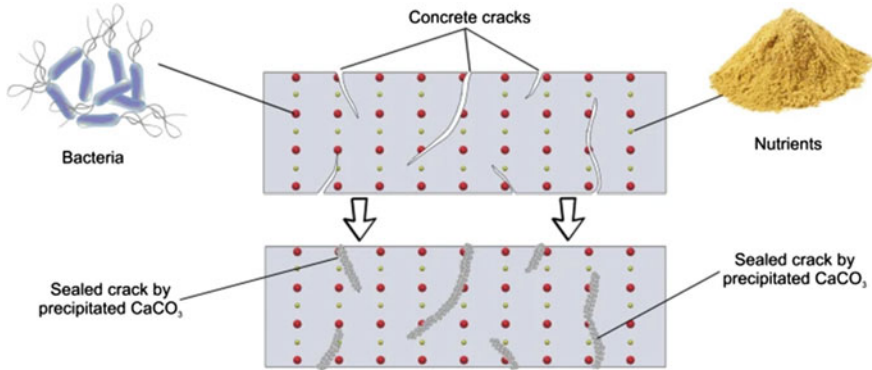


Fig. 3 Illustration of self-healing process in concrete matrix [9]

As a result, the strengthening will eventually change and its durability will be affected. The interaction between the concrete structures and the environment, hence, influences its long-term recital [8]. Water penetration into uncovered cement infrastructure often reduces the longevity of the structure and promotes the corrosion of steel reinforced bars, among other things [9]. Some cracks are not obvious and cannot be approached readily. The expansion, contraction and penetration of the material under examination lead to the growth of cracks. As a consequence, infrastructure inspection and maintenance measures are more explored throughout time.

Uninterrupted examination and continuance, particularly in the case of big infrastructure, might be difficult due to the considerable money needed to carry out the operation. The concept of autonomous repair of those cracks with low labour requirements and capital requirements in the structures concerned, also known as self-curing as illustrated in Fig. 3, is becoming increasingly interesting to academics. Due to the requirement of low labour and low capital expenses, the evaluation of the positive impacts of self-healing concrete using different approaches turns out to be fascinating. The positive impact of the self-healing concrete is, thus, tested using a number of ways [10]. The effectiveness of the self-healing of a cement base material is determined when a fracture of the necessary functionality and quality criterion has been repaired of the material's original shape.

Figure 4 refers to materials which can be repaired largely or fully after damage and, therefore, fully or partly [11]. Alternatively, self-healing material is described as material capable of detecting and healing itself. In this respect, the healing progression is carried out free of physical intrusion [12]. Nanotechnology and biotechnology are comparatively new accomplishments in the domain of concrete development, particularly in the areas of durability and other concrete qualities. To this objective, researchers will study all possibilities for the enlargement of bacterial concrete, intriguing the many tests and techniques used to evaluate the potency of the self-healing process. Self-healing concrete is a form of cement base material that is able

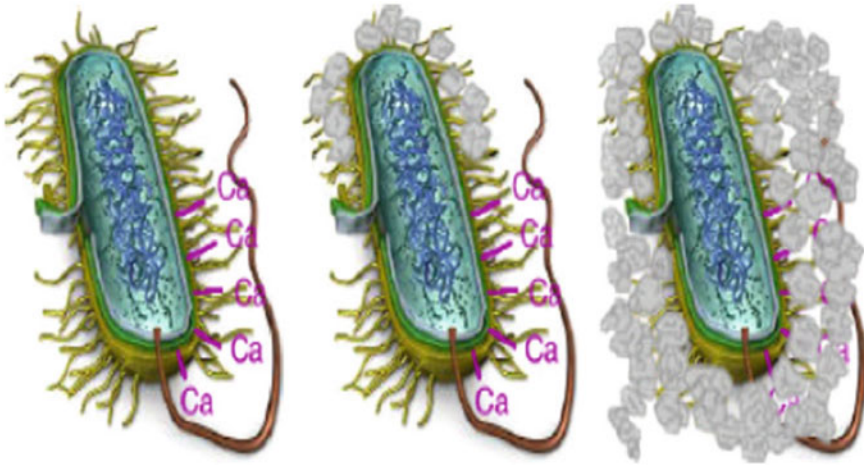


Fig. 4 Formation of calcium carbonates on the bacterial cell wall

to repartee its mechanical characteristics once a microcrack has occurred in the material [13]. Investigators have deliberated autogenous self-healing, autonomous self-healing and the incorporation of microorganism in bone replication concrete matrix processes to generate self-healing concrete material for sustainable development [14].

The use of chemical admixtures, polymers and geo-materials also showed that self-healing concrete is possible. Furthermore, it has been identified that the self-healing in concrete is responsible for the precipitating calcium carbonate bacteria [15]. When mixed with cemented materials and as well as integrated with addition of mineral and other admixtures, materials with increasing quality have the ability to boost the self-healing capacity of cemented materials. However, expansion in the presence of water as a result of a cement reaction must be prevented. Microfissure concrete may be used, as found in bulk water containing magnesium silicon ions and calcium. But, the cracks have not completely healed. The plugging operation only makes them small. In addition, attempts were made to produce damage by using tensile preloads in high-resistance concrete on the concrete [16]. As displayed in Fig. 5, autogenous healing in a manufactured crack has been proven in exposure to the environment and the presence of water [17].

The cemented composite material included synthetic fibres. As a consequence, cracks deliberately created have been corrected adequately. An additional concrete ingredient is used to boost the activity of self-healing of concrete fissures at the level of the micronutrient. The twin advantage of these materials is that they reduce the needed amount of cement and increase the number of concrete cracks that must be mended. Researchers have discovered that high-performance fibre can improve a cemented composite [18]. When alternative therapy regimes were tried, they had more influence than the earlier self-healing methods. Submersions in water, sea water and oil water were among the choices. Although the self-healing effect was observed, only cracks

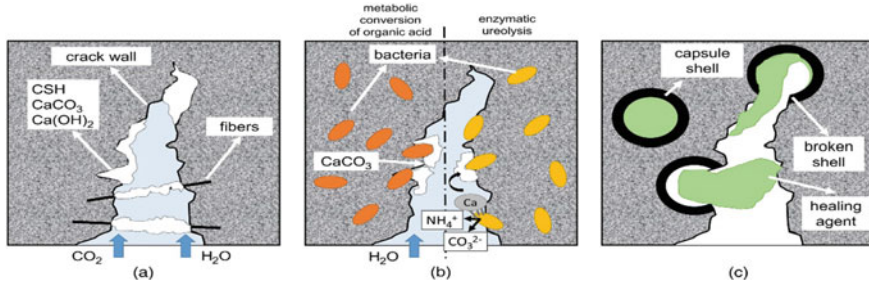


Fig. 5 Autogenous healing of self-healing concrete [17]

less than 50 μm were successfully filled. It was previously treated; however, broken concrete was constantly leaked by water rather than silent water [19]. This increased the self-healing performance. Self-treatment of concrete with retractable polymers has recently improved post-tension healing, which increases the effectiveness of the healing process. Various studies have investigated cement materials manufactured in this field. In their research, they found it to be a potential material for self-healing with superior self-healing abilities [20].

Calcareous particles were discovered in the proposed cement composite. They found that most of their functions could be recovered [21]. Various authors have recently examined and published in their findings on the significance of carbonated stainless steel slag as a concrete self-curing mediator. The crack healed up to an utmost length and width of 5 and 20 mm during the study. Many investigators have used eye observation methods to quantify the extent and effectiveness of filled cracks. For example light microscopic pictures, camera photographs and computed X-ray tomography are illustration techniques. Snoeck and colleagues have used a number of approaches to extend the lives of concrete buildings. It was chosen to put polymer in the concrete mix to provide a self-healing effect. Their efforts resulted in a positive outcome. Efficiency, on the other hand, relies on the type of polymer. Other elements affect efficiency, like the amount of polymers utilised, the type of cement used and the water-cement connection. As displayed in the Fig. 6, polymer was also united with supplementary components to increase the ability of the material to cure itself. Certain polymer-based self-healing compounds can recover their pressure to values above 100% of their initial value. Another study showed that polymers can improve self-healing by filling or healing around 65% of the effective crack width [22].

Researchers in recent times validated this in the study that revealing an increase of 16% in bending strength against the control specimens and a 16% increase in ultrasonic pulse speed. In addition, numerous ways to self-healing concrete have been researched. Their research has shown that self-healing concrete with encapsulation techniques is more promising to repair concrete cracks than to use superabsorbent polymers. Nanotechnology has made great progress over recent years and has proved to be an advantageous technology capable of reproducing natural attributes in the

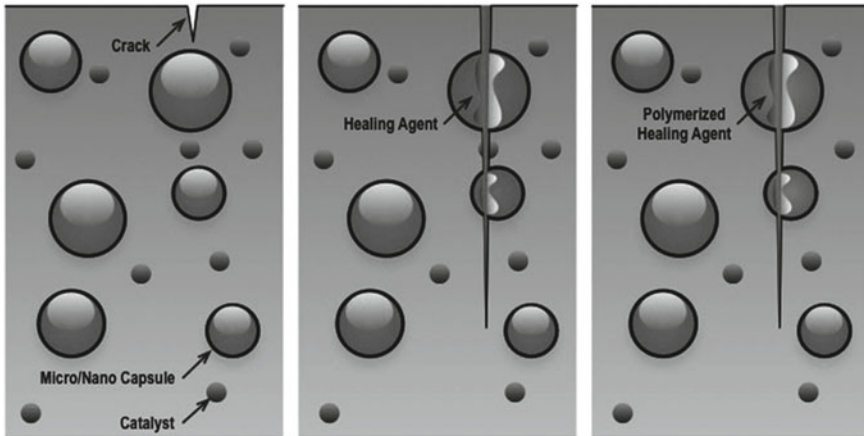


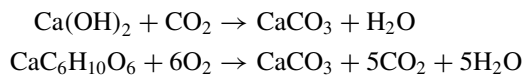
Fig. 6 Polymer-based self-healing mechanics by agent encapsulation [22]

construction and construction industry. Nanoparticles have in recent times been built-in into the concrete mix to form a new substance with several attractive properties. The nanoparticles can show exceptionally intense chemical reactivity. This allows a new material to be generated with the desired attribute. Nanotechnology is, therefore, applied to significantly boost concrete performance to generate more sustainable and new cement composites [23]. Perez and colleagues said that the possibilities of functionalised silica nanoparticles are studied and established in the production of self-healing concrete. More research in this sector is consequently necessary. Morsy et al. explored in their research the durability of cement-based materials on other nanoparticles. Muhammad et al. (Muhammad, etc.) recently issued a paper on the use of nanocomposites to progress the waterproofing capacities of concrete. It has been studied that microorganism can function as an independent concrete-healing agent. These conclusions were supported by numerous other research [24]. Every break in concrete from isolated bacterial crops and mixed bacterial culture was efficiently sealed in the cracked concrete. The precipitation triggered by the bacterial metabolism produced calcium carbonate.

3 Self-healing Mechanism of Bacteria in Concrete

An adequate self-healing organism should recognise the harm or crack that the healing element can release. Self-healing treatments are superior methods for concrete microcrack remedy. The autoheals show excellent results in the mending of microcracks on the concrete plane. The introduction of microorganisms will produce a preceding coating of concrete fractures that conform to calcium carbonate precipitation. A very alkaline substance, concrete, is able to resist the alkaline environment

with the injected bacteria. Calcium carbonate precipitation by microbiologically trigger facilitates to seal tiny cracks and link additional elements such as sand, gravel and cement. The microorganism's involvement in calcite precipitation can boost concrete's resilience [25]. Concrete can be filled with cracks of less than 0.2 mm in concrete. Self-healing concrete produces limestone biologically which can be able to heal cracks on the concrete surface. During the process of concrete mixing, particularly bacteria genus, bacillus, along with calcium lactate, has been added to the materials. When a crack develops in a concrete building, consequently water starts penetrating into the concrete through cracks. Further, the bacteria's spores germinate when they interact with water, nutrients or oxygen. Once it is activated, the bacteria tend to feed on calcium lactate [26]. In this process, when bacteria have consumed oxygen, consequently the soluble calcium lactate shall be converted to insoluble limestone. The limestone becomes hard and slowly fills up the fractured surface. Hence, oxygen is consumed by bacteria throughout the process, it inhibits corrosion of reinforcement, and hence, durability of steel is increased. As a result, calcium carbonate is evolved due to the chemical reaction of CO₂ which is present along with calcium hydroxide in the concrete matrix.



However, when cracks exceed the 0.2 mm thickness, concrete fails to heal itself and leads to harmful materials. The creation of cracks in self-healing concrete causes bacteria to activate from their state of hibernation. As displayed in Fig. 7, calcium carbonate precipitates in the fractures which repartee through the bacteria's metabolic activity through the process of self-healing [27]. When the cracks are fully stitched with calcium carbonate, the bacteria come back to the wintering stage. Whenever fractures develop, the bacteria will be triggered and the cracks will be plugged.

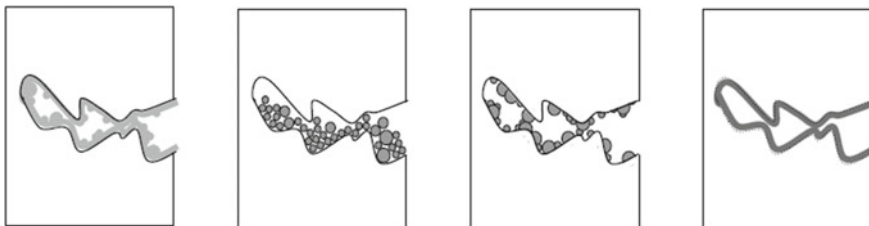


Fig. 7 Mechanism of natural self-healing in cementations materials

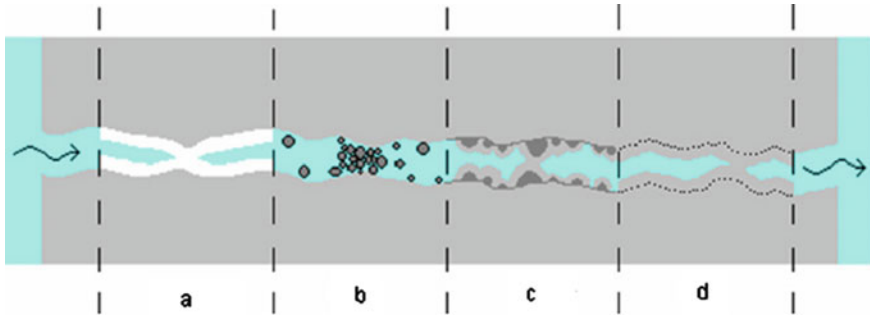


Fig. 8 Mechanisms of self-healing for cementitious materials

4 Mechanism of Self-healing for Cementitious Materials

The culturing of bacteria can be embedded into the concrete for the purpose of promoting self-healing. A bacterial culture has been sprayed in car-parking area to see how this would react on a damaged concrete plate surface. Due to the self-healing process, water permeability was significantly reduced. On the other hand, the compressive force did not improve significantly. To bypass this restriction, many studies using microorganisms were performed to recover the compressive strength of cement mortar and concrete. The compressive strength of the concrete was greatly boosted by the accumulation of bacteria and concrete admixtures [28]. In addition, a 36% improvement in compression strength was found.

Many research initiatives still actively involve microorganisms in the concrete to increase their strength and endurance. In cementitious materials, magnesium and sodium silicate (Na_2SiO_3) chemical compounds are utilised as healing agents according to Fig. 8. The utilisation of Na_2SiO_3 in cement-based products generates chemical reaction between the unhydrated particles of the $(\text{Ca}(\text{OH})_2)$ and Na_2SiO_3 [29]. Consequently, a new product of calcium-silica-hydrate (C-S-H) in the form of gel is formed, during the hardening of cement-based materials.

5 Conclusion

- (a) The significance of this paper is to know the use in the cure of cracks in concrete of urease producing bacteria such as *Bacillus subtilis*, species of *Bacillus pasteurii*. The study examined various bacterial types that can be used in the treatment of cracks.
- (b) This study also found that the compression strength in Portland cement mortar cubes and concrete is affected positively by bacteria. The benefits of bacteria can be mentioned as it can reduce the penetration of water and the permeability of chloride ions.

- (c) The results of this study suggest that “microbial concrete” can be a substitute high-quality, cost-effective, eco-friendly concrete sealant that eventually improves building material’s durability. This paper had reviewed a vast array of self-healing concrete design methods.
- (d) A taxonomy to cover possible design methods including natural, chemical and biological methods was suggested. This paper had examined the great potential of the biological method intensively using bacteria that can be used to precipitate calcite to help biological self-healing concrete develop.
- (e) Calcite precipitation forms calcium carbonate that helps to cure concrete cracks. This paper proposes a taxonomy that significantly contributes to the research of self-healing concrete by researchers in the biological sector.

References

1. Jonkers HM, Thijssen A, Muyzer G, Copuroglu O, Schlangen E (2010) Application of bacteria as self-healing agent for the development of sustainable concrete 36:230–235
2. Bollinger J, Britton J, Gisin N, Knight P, Kwiat P, Percival I (2001) Autonomic healing of polymer composites 409:1804–1807
3. Ghosh P, Mandal S, Chattopadhyay BD, Pal S (2005) Use of microorganism to improve the strength of cement mortar 35:1980–1983
4. Achal V, Mukerjee A, Reddy MS (2013) Biogenic treatment improves the durability and remediates the cracks of concrete structures. *Constr Build Mater* 48:1–5
5. Venkata Siva Rama Prasad C, Vara Lakshmi TVS (2018) Use of crushed rock sand as an alternative to river sand in bacterial concrete. *i-Manager’s J Civ Eng* 9(1):1
6. Achal V, Mukherjee A, Reddy MS (2011) Microbial concrete: way to enhance the durability of building structures 23:730–734
7. Chahal N, Siddique R, Rajor A (2012) Influence of bacteria on the compressive strength, water absorption and rapid chloride permeability of concrete incorporating silica fume. *Constr Build Mater* 37(1):645–651
8. Venkata Siva Rama Prasad C, Vara Lakshmi TVS (2018) Effect of *Bacillus subtilis* on abrasion resistance of bacterial concrete. *Int J Appl Eng Res* 13(16):12663–12666
9. De Belie N (2016) Application of bacteria in concrete: a critical review, pp 56–61
10. Venkata Siva Rama Prasad C, Vara Lakshmi TVS (2020) Experimental investigation on bacterial concrete strength with *Bacillus subtilis* and crushed stone dust aggregate based on ultrasonic pulse velocity. *Mater Today Proc* 27(Part 2, 2020):1111–1117. <https://doi.org/10.1016/j.matpr.2020.01.478>
11. Reddy MS (2009) Lactose mother liquor as an alternative nutrient source for microbial concrete production by *Sporosarcina pasteurii*, pp 433–438
12. Dong B, Han N, Zhang M, Wang X, Cui H, Xing F (2013) A microcapsule technology based self-healing system for concrete structures 7(3):1–11
13. Luo M, Qian C (2016) Influences of bacteria-based self-healing agents on cementitious materials hydration kinetics and compressive strength. *Constr Build Mater* 121:659–663
14. Venkata Siva Rama Prasad C, Vara Lakshmi TVS (2018) Effect of *Bacillus subtilis* on mechanical behavior of bacterial concrete. *ARPN J Eng Appl Sci* 13(18)
15. Tziviloglou E, Wiktor V, Jonkers HM, Schlangen E (2016) Bacteria-based self healing concrete to increase liquid tightness of cracks. *Constr Build Mater* 122:118–125
16. Siddique R, Singh K, Kunal M, Corinaldesi Singh V, Rajor A (2016) Properties of bacterial rice husk ash concrete. *Constr Build Mater* 121:112–119

17. Hung CC, Su YF (2016) Medium-term self-healing evaluation of engineered cementitious composites with varying amounts of fly ash and exposure durations. *Constr Build Mater* 118:194–203
18. Venkata Siva Rama Prasad C, Vara Lakshmi TVS (2019) Effect of crushed sand and *Bacillus subtilis* on the Cantabro loss of bacterial concrete. *Int J Technol* 10(4):753–764
19. Wang JY, Snoeck D, Van Vlierberghe S, Verstraete W, De Belie N (2014) Application of hydrogel encapsulated carbonate precipitating bacteria for approaching a realistic self-healing in concrete. *Constr Build Mater* 68:110–119
20. Chahal N, Siddique R, Rajor A (2012) Influence of bacteria on the compressive strength, water absorption and rapid chloride permeability of fly ash concrete. *Constr Build Mater* 28:351–356
21. Anne S, Rozenbaum O, Andreazza P, Rouet J (2010) Evidence of a bacterial carbonate coating on plaster samples subjected to the calcite bioconcept biomineralization technique. *Constr Build Mater* 24(6):1036–1042
22. De Muynck W, Debrouwer D, De Belie N, Verstraete W (2008) Bacterial carbonate precipitation improves the durability of cementitious materials. *Cem Concr Res* 38:1005–1014
23. Wang J, Dewanckele J, Cnudde V, Van Vlierberghe S, Verstraete W, De Belie N (2014) X-ray computed tomography proof of bacterial-based self-healing in concrete. *Cem Concr Compos* 53:289–304
24. Wu M, Johannesson B, Geiker M (2012) A review: self-healing in cementitious materials and engineered cementitious composite as a self-healing material. *Constr Build Mater* 28(1):571–583
25. Andalib R, Abd Majid MZ, Hussin MW (2016) Optimum concentration of *Bacillus megaterium* for strengthening structural concrete. *Constr Build Mater* 118:180–193
26. Qian C et al (2015) Self-healing and repairing concrete cracks based on biomineralization 630:494–503
27. Luo M, Qian CX, Li RY (2015) Factors affecting crack repairing capacity of bacteria based self-healing concrete. *Constr Build Mater* 87:1–7
28. Santhosh K, Ramachandra VR et al (2001) Remediation of concrete using microorganisms. *ACI Mater J*
29. De Belie N, Wang J (2015) Bacteria-based repair and self-healing of concrete, vol 373

Digital Concrete for Sustainable Construction Industry: A State-of-the-Art Review



Chiranjeevi Rahul Rollakanti, C. Venkata Siva Rama Prasad,
and Adams Joe

Abstract Recent research and industry have seen a great deal of digital production techniques with concrete and cemented materials, and the advanced techniques of industrialisation such as the 3D printing. 3D printing is an attention seeking technology in recent times, which in future years can have huge social and economic effects. The building industry and research projects around the world have focused on automatic construction systems. The possibility of revolutionising building is not only through cost reduction but also through enhanced sustainability and usefulness. There are major challenges, including understanding the early age hydration, and regulating the connection to rheology, the integration of strengthening and the overall connection between the processing, material and performance, both in structural and in terms of durability. This research article describes a state of the art 3D concrete printing with historical knowledge and progress with equipment, materials and computer modelling. This paper presents current progress, modern and up to date approach. It is essential to interdisciplinary action since the subject combines many different areas and is led thus far by areas such as architecture. The literature review examines the state of the art in the recent advancements of construction industry of digital concrete manufacture guiding the research difficulties so far.

Keywords Digital concrete · 3D concrete printing · 3D printers · Sustainable construction

C. R. Rollakanti (✉) · A. Joe
Department of Civil Engineering, Middle East College, Knowledge Oasis Muscat, Al Rusayl,
Muscat, Oman
e-mail: rahul@mec.edu.om

A. Joe
e-mail: adams@mec.edu.om

C. Venkata Siva Rama Prasad
Department of Civil Engineering, St. Peters Engineering College (Autonomous), Dhulapally,
Maisammaguda, Medchal, Hyderabad, Telangana 500100, India

1 Introduction

Concrete is one of the world's widely utilised building construction materials, both in terms of volume and in application. The use of concrete gives a number of distinct advantages in building construction sector and also regarding various types of structures. The concrete is commonly used for its high strength, durability and fire resistance, amongst other things. The second argument is that concrete fundamental elements may be available practically everywhere around the world [1]. Moreover, concrete is a versatile material which enables architects to make fantastic use of their designs. The enormous manufacturing and use of concrete affects our ecology, which we have to fight with. Portland cement production techniques utilise considerable energy and emit a large quantity of greenhouse gases into the atmosphere. Concrete will continue to be in high demand as a key building material for a long time to come. In order to ensure that concrete remains a competitive building material in the future, the durability of concrete structures is vital for the long term. In the current building sector, there are major long-term viability issues. The majority of construction procedures and materials in use presently have detrimental consequences on the environment [2]. Much greenhouse gas is emitted and huge quantities of energy are consumed throughout the construction process, such as on-site production, material transportation, installation, assembly and on-site building.

Recent studies suggest that formwork occupies a significant proportion of total construction projects expenditure. This is indeed a regular practise for concrete construction throughout the world. Another problem to tackle is the huge volume of waste produced throughout the building process. Formwork is a key source of trash as it is abandoned at some stage in the building construction process and it increases waste generated in the construction sector as a whole [3]. It has been proven that the building industry is responsible for the world's bulk of overall waste, which is incredible. The general procedure of concrete casting inside the formwork has limited the freedom of engineers and architects to construct structures in numerous methods, unless extremely costly tailor-made forms are achieved for the project. Concrete building frequently comprises numerous operations, including in-site manufacture, transport and production, and every stage takes a large amount of time. Furthermore, in the current concrete building sector, there is a lot of work and safety difficulties. Most of the construction fatalities are falls from height [4]. In addition, the safety of workers in the local concrete industry is becoming a big concern. In particular, qualified work is required for the insertion and connection of the reinforcing operation and the construction in casting geometries. Workers' safety is continually endangered with accidents and injuries at work.

The labour and working staff shall be shifted to technology-oriented workforce. Hence, accidents, fatalities, injuries and loss of life might be minimised. In future, more capable and technologically aware workers will replace unskilled workers. This would greatly reduce deaths and serious injuries. As discussed above, construction time and labour can be reduced with concrete printing, as no formwork is required. With today's technology advent and substantial breakthroughs in the area of additive

manufacturing, which is generally known as 3D Printing (3DP). This task automation of the construction sector is observed to be increased in the future ahead [5]. 3DP has different advantages over the typical concrete construction technology. 3DP is also an environmentally favourable and sustainable building technique. Accurate control of the production process and optimisation of the use of materials should limit building waste. As mentioned in several studies, 3DP is going to be a future trend in the construction field and it could lead to be a low-CO₂ way for producing concrete if properly implemented.

This technological application might open the way for shorter construction durations as well as for more distant locations to be created and designs to be adaptable, so that 3D concrete printing not only can be a novelty of technological developments but can also revolutionise the building industries. It also offers a number of other environmental advantages that are not available in traditional buildings [6]. A new study shows that construction materials and human needs could be considerably minimised if automated 3D press technologies are further refined to improve their efficiency compared to present building methods. Construction Industry and scholars worldwide have recently paid great attention to 3D concrete printing. The additive manufacturing technology is used to create 3D products that incorporate the construction of subsequent layers of material under computer supervision. Additive Manufacturing (AM) for the printing of a broad and sophisticated structure employing quick prototype procedures with acceptable mechanical and structural integrity has been developed and standardised. The use of additive concrete production seems to be a practical way to tackling the issues facing today's concrete industry. Compared to subtractive manufacturing techniques, additive production describes the process for connecting materials to build things of 3D model data. In the last three decades, commercial application of additive manufacture (AM) was also taken place in the areas of aerospace, medical research and other fields. Recent deployments of additive manufacturing technology in the building sector, namely contour crafts, D-shape and concrete printing, illustrate the promise that large-scale AM techniques will be adopted [7].

3D printing is about to change the building industry and will impact the use by architects, engineers and designers of concrete in its design. In more than a dozen new technical papers on 3D concrete, a wide variety of issues were covered, including the different technologies of printed 3D concrete as well as elements of combining design and functionality of printed concrete material. However, in the literature just a few research papers on 3D concrete printing were published. The major objectives of the research and literature review paper are to showcase the current state-of-the-art computer modelling and 3D printing problems of cement-based materials.

2 Development of the 3D Printing Technology

During the period of mid-1980's, 3D printing has become more popular in the areas of biomedical industries and as well as manufacturing sectors. Users were able to use

their computers to turn digital models into real three-dimensional products. In the earlier times, the 3D printers were being able to print little objects, however research and development activities eventually escalated to large-scale printing products such as cars due to technical improvements. Maybe it's the point when other companies began thinking of 3D printing [8]. Layered construction process is a new manufacturing approach, first established in the mid-1990s and known as Contour Crafting (CC). The 3DP technology got its patent in 2010. The technology, devised as the process of extruding ceramic pastes but cementitious materials were recently developed to generate large-scale structural components, and even whole equipment such as a printed building [9].

The major components of this technology are concrete tank, a hose, pumping mechanism, nozzle and robot arm. The robotic arm can steer the nozzle in three different directions up, down and diagonally. The concrete is poured layer-by-layer on the nozzle, and the concrete layers are healed and they are strong enough required to provide the support for the new layers. The pulling method, for example, employs pneumatic pressure which is required to transfer the material from a bucket to surface of the concrete sheet. One of the disparities between shotcreting and sculpting of contours. The substance exits faster than when the extrusion operation is carried out, using a piston pump mechanism comparable to a syringe, than the injection approach. In the mid-1990s a second manufacturing additive, known as Selective Aggregation has been developed, involving the preparation and targeted deposition of the cement on the sand matrix. A strong and dense material was created as a result of this process, which could be automated with computer-assisted design and analysis models. Mountain construction techniques were developed to combine the mountains by merging sand grains [10]. A device named "D-Shape," which is based on this principle of sand grain combination, appears to be invented. The grains were coupled with a sand binding agent, which originally was a polymer material and was then converted into an inorganic binder due to the difficulty of attaching the polymer binder to the machine. The selective throwing of the grains into the sand matrix.

Originally a technique like the fabrication of contours but changing the design of the extruder was described with the phrase "freeform building" or "concrete printing." It was utilised in the first decade of the twenty-first century. The dust used in this method may be printed in various resolutions, including enormous expansions and fine details. In terms of enormous structural components, the focus on increasing additive production in the construction sector was uncommon as compared to other technologies. It also provided additional functionality to structural components like sound, heat and ventilation [11]. Moreover, current 3D printing is being built for more than 25 years. Despite significant improvements, it is far from possible to print by merely pressing the "PRINT" button on a computer. 3D printers are still being developed in practical applications; nonetheless, laboratories and manufacturers still seek to improve existing 3D printers or create new printers.

3 3D Concrete Printing (3DCP) Technologies

Different technologies have been developed in recent years for the application of additive manufacture in concrete buildings. Three 3D printing processes are now used in the building sector: extrusion-based layering and powder bed technology. Extrusion-based layering is the most often used technology in construction (selected material deposition via extrusion). This is comparable to Fused Deposition Modelling (FDM) in which layer by layer combinations of specified materials have been deposited via extrusion printer head, the command of the crane, robot or arm of a 6- or 4-axis 3D printer with computer-supported design tools. The powder-based technologies are off-site processes designed to be developed on site for big and complex geometric structural printing. These massive, sophisticated geometric masterpieces are made using a number of printing methods, including Stereo-Lithography [12]. The production procedures and types of materials used in contour production, concrete printing and 3DCP are all quite comparable. Various studies on 3DCP are selected through literature review, this study summarises the major aspect of concrete printing technologies. The primary 3DCP experiments are now selected. The following sections discuss the methodologies and similarities and differences, advantages and disadvantages of various 3DCP technologies.

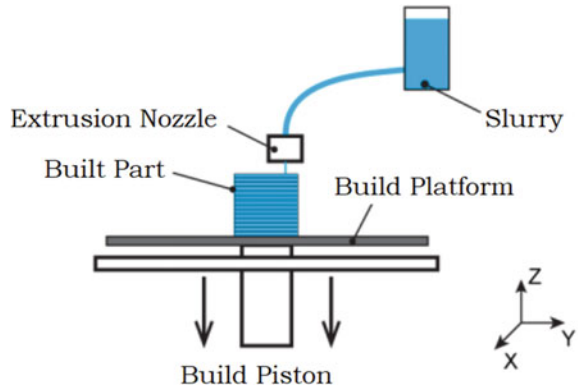
3.1 *Extrusion-Based Layering*

The extrusion-based technique is symmetrical to FDM technology which is also used for layer printing by layer structures using a cemented material extruded from nozzle mounted on a gantry, shutters to print a layer-by-layer of the structure. By addressing some of the construction site applications such as comprehensive building structural components with complex geometry, this technology can make an essential and useful contribution to the construction industry [13]. The Contour Crafting (CC), Concert Printing (CP), and CONPrint3D extrusion-based laying processes may be used to print concrete constructions using cemented materials or aggregates and fibre strengthening. Concrete printing and the manufacturing of contours are typically instances of additive manufacturing, both components of a comparable technology called inkjet and mixed material extruded via boxes to build up vertical components. Figure 1 shows the schedule for the powder-based approach in action.

3.1.1 **Contour Crafting**

The Contour Crafting (CC) technology was created by Dr. Behrokh Khoshnevis of University of Southern California and is a fully on-site technology. With the vertical extrusion of the layers this printing technology can be strengthened manually by strengthening bands to allow the final product to be strengthened. The vertical

Fig. 1 Extrusion-based technique [13]



concrete form is constructed utilising an extrusion method which transforms two layers of a cemented mixture into a vertical concrete covering. A shape contour maker has a large printing area with a working surface of $5\text{ m} \times 8\text{ m} \times 3\text{ m}$. This technology gives a good quality of the surface, is easy to produce and can be printed on a variety of materials [14]. It is quite difficult for the CC machine to insert the reinforcement links between layers manually. Smooth extruded surfaces with fins similar to Trowel-like fins are added to the printed head. Figure 2 depicts a CC machine-made concrete wall shape for a concrete foundation.

The major benefits of CC technology are higher surface smoothness and the much more rapid speed at which CC is manufactured. The ability to link with different robotics procedures for the installation of internal components like pipelines, electrical drivers and enhancer modules is the another essential characteristic of CC [15].

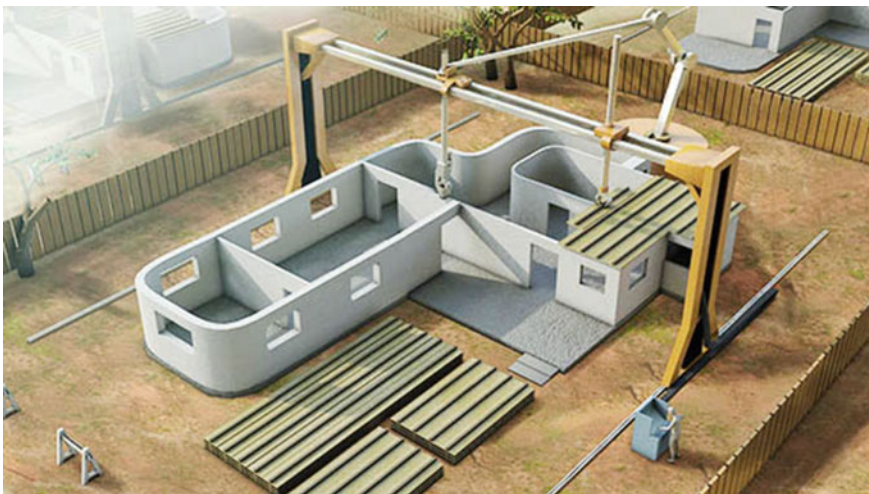


Fig. 2 Contour Crafting (CC) technology [15]

Vertical parts are currently mainly manufactured in CC compression. If you require a door or a window, a lintel is fitted to conceal the gap and allow the wall to be built above it. Hence, the problem is not large-scale. Due of this limitation, vertical extrusion is the only printing process of the CC type. The initial forming and trowel method might also be hard for manufacturing, depending on the size and shape of the printed object. A further advantage is that the sequential casting in form of the concrete is distorted because of hydro statistic pressure of the extruded concrete, making CC technologies very difficult to print.

3.1.2 Concrete Printing

Concrete printing at the University of Loughborough is invented by means of a $4\text{ m} \times 1.6\text{ m} \times 1.50\text{ m}$ dimension printing press with a printing area of roughly 132 m^2 . This technology allows the use of high-performance ground and fibre-reinforced concrete, which offers improved mechanical performance in printed components. The study found that coarse aggregates up to 9.5 mm and concrete of C30 were used for printing concrete mixtures. Concrete Printing is a new construction material created by a United Kingdom team from the University of Loughborough. The technique is based on extrusion-based technology and is comparable to CC technology [16]. In contrast, concrete printing technique was designed to maintain 3D freedom whilst reducing deposit resolution in order to further regulate the internal and external geometries of the printed structures. Figure 3 displays the full bench which is typically made by means of the concrete printing technology. The bench is also provided with an example of a reinforcement strategy which is intended to plan voids as pipes for reinforcement following installation.

Concrete Printing permits freeform components and overhangs, but requires additional support. A second material is employed in a technique similar to the FDM process. This technique is detrimental since the second material requires an additional

Fig. 3 Full scale bench manufactured by the Concrete Printing [16]



deposition device, leading to a higher maintenance, cleaning and control instruction and the need to clean the secondary structure throughout the subsequent processing operations [17]. In comparison with the intended industrial application, the advantages of the concrete printer technology are that the trade-offs needed to preserve its dimensionality are quite slow.

3.1.3 CONPrint3D: Concrete On-Site 3D Printing

Contrary to their numerous technological advantages, the production of contours and concrete printing have certain intrinsic constraints such as the necessity for new and sophisticated technology and small sized mineral particles. This limitation is overcome by a novel on-site 3DCP technology developed by CONPrint3D, Technical University of Dresden, Germany. The high geometric flexibility of CONPrint3D is one of the technological benefits that makes it possible to use the standard equipment and rely little on a well-trained workplace [18]. CONPrint3D is majorly focused on creating a time and resource efficient building process but also on producing a commercially viable new process whilst gaining greater acceptance from existing industries' professionals. This is achieved by the utilisation of current construction and manufacturing processes by adapting a new methodology to the site restrictions. The key component of the project strategy is to autonomously and accurately adapt a concrete boom pump to transport material to certain locations using a custom printed head installed on the boom as shown in Fig. 4.

Moreover, as the contour-building and concrete printing methods are only confined to vertical extrusion and require original shape, one of the major problems such as hydrostatic pressure control, further operation and maintenance could result in complexity, depending on the structural geometry to be printed.

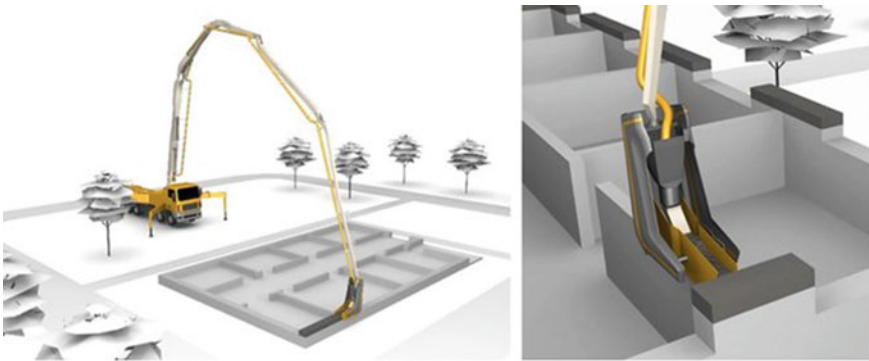


Fig. 4 CONPrint3D technology [18]

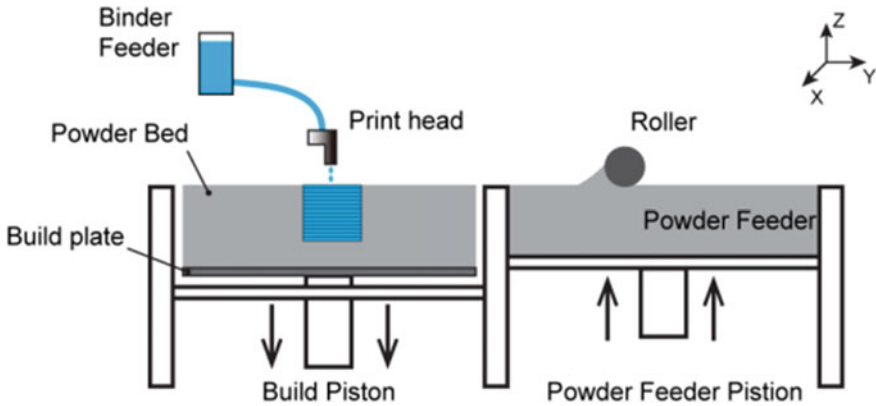


Fig. 5 Powder-based technique [19]

3.2 Powder-Based Methods

The powder-based approach is one more typical additive process in which precise structures of difficult geometry are produced by selectively depositing the liquid binder (or “ink”) in the powder bed into a binding powder where the bed is struck to form a strong structure. This method is also well known as an off-site process which is majorly for precast concrete component fabrication. Powder-based technology is particularly suitable, according to the scientists, for tiny building components for example panels and on-site interior structures [19]. Figure 5 shows a diagram of the powder technique in action. Starting with the first powder layer (about 3 mm thick), a roller with the print head spreads out the powder which is required to cover the base of the building plate. The roller then disperses a thin layer of powder (approximately 0.1 mm in thickness) over the surface of the powder sheet, which is adjusted according to the setting of the thickness required for the 3D printer above the layer. The binder solution shall be transported from binder feeder towards the printed head, blasted into the powder layer by the help of nozzle, which makes it possible for polished particles to bind to each other and form a firm bond. Repeating the preceding techniques, the created item is finished and then it was removed after a specific period of drying and then loose powder shall be removed by using a blower.

3.2.1 D-shape

The D-shape approach has been explored by Enrico Dini. He had used a powder-based technology to harden a huge sand bed, similar to that used in concrete making, by depositing a binding agent. Sand is used as a construction material, whilst in the construction of the structure magnesium-oxychloride cement is used as a binding agent. Shiro Studio paired up with a D-shaped pavilion that sized 3 m by 3 m by 3 m

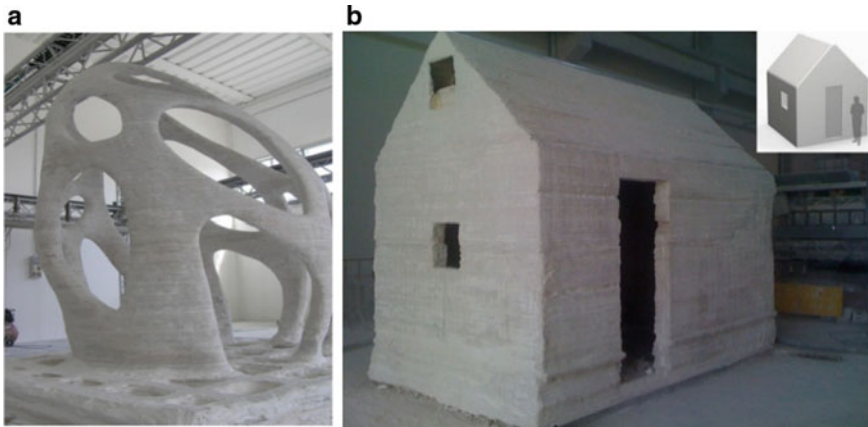


Fig. 6 **a** Radiolaria Pavilion, **b** Ferreri house printed by D-shape [20]

in 2008 [19]. The Radiolaria Pavilion was developed to demonstrate the capacities of D-shape technology by using sophisticated geometry (Fig. 6a). In 2010, D-shaped Ferreri house, measuring 2.4 m × 4 m has completed in one single procedure was also 3D printed (Fig. 6b). It took only three weeks for the house to be printed [20].

3.2.2 Powder-Based 3DCP Using Geopolymer

Construction components can be made utilising by a powder-based production process, with fine details and elaborate forms. When it comes to building components, there is a large demand for those that can only be created with costly coating using the existing building methods. To address this industrial demand, powder-based manufacturing techniques are capable of producing robust and durable parts at an acceptable speed [21]. Although this technology has a significant potential for use in the building industry, it does not fully meet its promise because of the extremely limited choice of cement-based printing materials accessible in commercially available 3D-based powder printers. In a study, the authors have recently succeeded in inventing a unique methodology for the adoption of geopolymer-based material (Fig. 7) in order to satisfy the demands and the need for widely existing powder-based 3D printers [22]. Geopolymer is an eco-friendly alternative material to OPC. Geopolymer provides greater mechanical, chemical and thermal characteristics compared with polypropylene whilst producing less carbon dioxide.

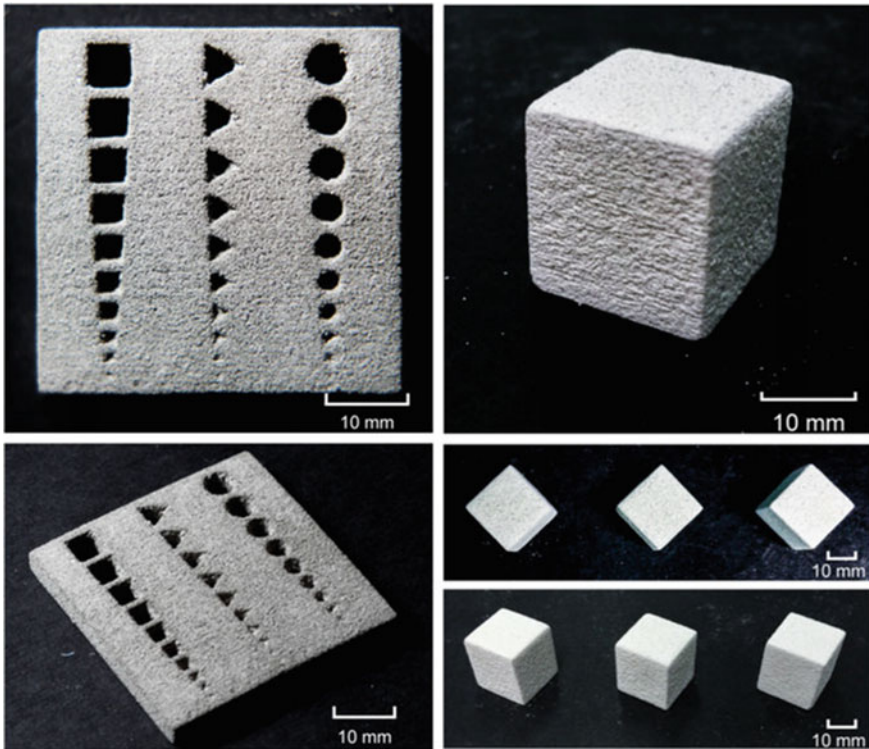


Fig. 7 3DP components by geopolymer-based material

4 Conclusion

Whilst additive printing is a relatively new notion for manufacturing components, it may give a new approach to develop architectural and structural components. The adoption of 3D printing technology by the construction sector can address various challenges such as time-consuming and inefficient construction procedures, amongst others. Whilst 3D printing is still in its early stages, many scholars think that it presents new chances for establishing new trends that ultimately lead to cost-effective, sustainable and time-efficient construction approaches. Worldwide researchers did studies to maximise capacity, bond strength and also the utilisation of 3D printed concrete reinforcement. Further attempts are being made to create 3D imprinted concrete standards and specifications in order to launch code-based designs of 3D imprinted concrete structures and to progress the technology further.

This research paper shall provide an overview of state-of-the-art 3D concrete (3DCP) technology, in particular extrusion and powder-based techniques in addition to already available 3DCP technology. We analyse the similitudes, differences and advantages of the different 3DCP technologies. The latest state-of-the-art extrusion,

powder-based elements and structures were also discussed. Even though 3DCP is a relatively new technique, encouraging examples of this study demonstrate that the technology is rapidly evolving so that 3D printing of concrete structures is going to be a reality in the very near future. 3D printing will have to be deployed by a staff who are equipped with integrated knowledge about the materials to be used, structures, robotics systems, computer software and hardware in the building industry. To equip future personnel to address the difficulties arising from this new technology, an entirely new academic programme is required in institutions.

References

1. Glavind M (2009) Sustainability of cement, concrete and cement replacement materials in construction. In: Sustainability of construction materials. Wood Head Publishing in Materials. Cambridge, UK, Great Abington, pp 120–147
2. Rollakanti CR, Venkata Siva Rama Prasad C, Poloju KK, Al Muharbi NMJ, Venkat Arun Y (2021) An experimental investigation on mechanical properties of concrete by partial replacement of cement with wood ash and fine sea shell powder. *Mater Today Proc* 43:1325–1330
3. Yan H, Shen Q, Fan LC, Wang Y, Zhang L (2010) Greenhouse gas emissions in building construction: a case study of One Peking in Hong Kong. *Build Environ* 45(4):949–955
4. Venkata Sai Nagendra C, Venkata Siva Rama Prasad C, Rukmini Florence KN (2019) An experimental investigation on properties of concrete by partial replacement of cement with dolomite and sand with crushed sea shell. *Int J Sci Technol Res* 8(10):1610–1614
5. Sree Lakshmi Devi G, Srinivasa Rao P, Venkata Siva Rama Prasad C (2021) Experimental investigation on compressive strength of quaternary blended concrete using different mineral admixtures. *Mater Today Proc* 46:783–785
6. Shakor P, Sanjayan J, Nazari A, Nejadi S (2017) Modified 3D printed powder to cement-based material and mechanical properties of cement scaffold used in 3D printing. *Constr Build Mater* 138:398–409
7. Lim S, Buswell RA, Le TT, Austin SA, Thrope T (2012) Developments in construction scale additive manufacturing process. Civil and Building Engineering, Loughborough University, Loughborough, LE11 3TU, UK
8. Bos F, Wolfs R, Ahmed Z, Salet T (2016) Additive manufacturing of concrete in construction: potentials and challenges of 3D concrete printing. *Virtual Phys Prototyping* 11(3):209–225
9. Sakin M, Kiroglu YC (2017) 3D printing of buildings: construction of the sustainable houses of the future by BIM. *Energy Proc* 134:702–711
10. Buswell RA, Leal de Silva WR, Jones SZ, Dirrenberger J (2018) 3D printing using concrete extrusion: a roadmap for research. *Cem Concr Res* 112:37–49
11. Shakor P, Nejadi S, Paul G, Malek S (2019) Review of emerging additive manufacturing technologies in 3D printing of cementitious materials in the construction industry. *Front Built Environ* 4
12. Li VC, Fischer G, Lepech MD (2009) Shotcreting with ECC. In: Shotcrete conference, 2009 Alpbach—Tyrol Austria, pp 1–16
13. Gardiner JB (2011) Exploring the emerging design territory of construction 3-d printing—project led architectural research, School of Architecture Design, RMIT University
14. Bos F, Wolfs R, Ahmed Z, Salet T (2016) Additive manufacturing of concrete in construction: potentials and challenges of 3D concrete printing. *Virtual Phys Prototyping* 11:209–225
15. Khoshnevis B, Hwang D, Yao K-T, Yeh Z (2006) Mega-scale fabrication by contour crafting. *Int J Ind Syst Eng* 1(3):301–320

16. Lim S, Buswell RA, Le TT, Austin SA, Gibb AGF, Thorpe T (2012) Developments in construction-scale additive manufacturing processes. *Autom Constr* 21:262–268
17. Wangler T, Roussel N, Bos FP, Salet TAM, Flatt RJ (2019) Digital concrete: a review. *Cem Concr Res* 123
18. Nerella VN, Krause M, Näther M, Mechtcherine V (2016) CONPrint3D—3D printing technology for onsite construction. *Concr Aust* 42(3):36–39
19. Nematollahi B, Xia M, Sanjayan J (2017) Current progress of 3D concrete printing technologies. In: ISARC. Proceedings of the international symposium on automation and robotics in construction, 34, Vilnius Gediminas Technical University, Department of Construction Economics & Property
20. Cesaretti G, Dini E, De Kestelier X, Colla V, Pambaguian L (2014) Building components for an outpost on the Lunar soil by means of a novel 3D printing technology. *Acta Astronaut* 93:430–450
21. Al-Qutaifi S, Nazari A, Bagheri A (2018) Mechanical properties of layered geopolymer structures applicable in concrete 3D-printing. *Constr Build Mater* 176:690–699
22. Xia M, Sanjayan J (2016) Method of formulating geopolymer for 3D printing for construction applications. *Mater Des* 110:382–390

Identification and Ranking of Construction Productivity Factors in Construction Projects in Wilayat A'Seeb



Salim Abdullah Salim Al Sinaidi and Kiran Kumar Poloju

Abstract As the construction industry and technology advance, it is a challenge to maintain the project requirements in terms of quality, time, and cost. To make sure the project budgeting plan stays on track, it is essential to reach development on time so that the cash flow can be maintained for the project. However, many factors influence this, including construction productivity. Many external and internal factors must be taken into consideration to maintain a uniform production rate during construction. For example, material shortages, poor construction supervision, payments delays, and omissions in drawings are some of the internal factors. Condition of the weather and political stability are some of the external factors. To find the factors that affect productivity, the construction company must first determine their importance and the degree of their influence on the output. As a result, project planning and scheduling will reduce the chances of losing productivity. In this study, factors that affect construction productivity will be identified and ranked, and the context will be confined to the few construction companies in Oman. The participants were given a questionnaire to complete to rate the listed productivity factors according to their relative importance.

Keywords Productivity factors · Advancement technology · Scheduling project · Construction companies

1 Introduction

Workers are still the main drivers of industrial development, notwithstanding significant breakthroughs in construction technology. Because of the unfavorable influence of the current economic situation on the global building industry. As a result, improving labor productivity has become more critical than ever. The labor cost ratio accounts 30–50% of the project's overall cost. As a result, it is a clear and accurate

S. A. S. Al Sinaidi (✉) · K. K. Poloju
Department of Civil Engineering, Middle East College, Muscat 124, Oman

K. K. Poloju
e-mail: kpoloju@mec.edu.om

picture of the construction process' efficiency and success [1]. According to the report, a 10% boost in labor efficiency might result in annual savings of one billion pounds for the British economy. Concerns concerning labor productivity are justified due to the significance and role of this effect. The building business in the Sultanate of Oman is one of the most prominent areas where labor productivity is declining. Despite the existence of contractors, equipment, modern tools, and building supplies, high construction expenses are seen, creating significant delays in project completion and many projects surpassing their budgets. The research aims to find out productivity of labor and rank factors which affect medium firms to disseminate the information gathered to companies so that they may plan better risk assessments. Many earlier productivity-related studies defined the concept of productivity. For instance [2], according to the US Department of Commerce, productivity is defined as "output per person-hour of labor input", whereas [3] defined productivity as "the performance accomplished by operatives". Productivity has been "the ratio of outputs of goods and/or services to inputs of basic resources" was defined by [4, 5] interpreted productivity as "the quantity of work produced per man-hour, equipment-hour, or crew-hour". Several studies have looked into the elements that affect productivity: Management, technological, labor, and external variables are the four basic categories in which these factors are categorized. The worldwide ranking system has considerable consistency. This classification system can be used to categorize the factors that influence labor productivity. However, the researcher needs that this to be accomplished. These organizations may be able to preserve their dominance, but they are tough to defend. This is since the geographical and ecological zones are different. In addition, the impact of elements varies depending on the construction location. As a result, a partial literature analysis was carried out to keep up with regional research achievements in the field of construction productivity [6]. In the Yemeni construction business, factors impacting labor productivity were investigated. To collect the data, a questionnaire survey was sent out, and 103 replies were received and analyzed. The study found that among the top productivity factors are labor experience, material availability, leadership capabilities, political and security situations, and communication efficiency [7]. The elements that affect labor productivity in Bahrain's construction sector were investigated. A study approach comparable to that used in the Qatari building sector was used. A survey method was distributed, and 59 participants completed and returned it. Poor labor skills, a lack of coordination among design disciplines, a lack of labor supervision, errors and omissions in design drawings, and a delay in replying to requests for information were discovered to be among the top productivity factors, according to the study [8]. Researched the elements that influence employee productivity in the construction business in Saudi Arabia. In order to measure the trends of productivity growth elements in construction, we administered a questionnaire survey with five scales ranging from Not Important to Very Important. The study found that the cost of materials is the most significant factor affecting building productivity. In the second step of the design process, materials and equipment were analyzed. Finally, research in the Kingdom of Saudi Arabia identified administrative aspects as less essential. Because the study must be successful, realistic, and extend over a long time, one of the

most significant and challenging procedures that the researcher faced was the selection of experts specializing in the subject of construction [9]. Has chosen the years of expertise of the specialists as a criterion for researching the topic of construction and urbanization in Iraq. Years of experience were also taken into account when working on large-scale projects. In addition, a questionnaire research was conducted to assess the most significant factors that affect labor productivity in the Iraqi construction industry, and it was discovered that ineffective construction site administration, difficulty entering or getting to the construction site, the dangerous project site where any attack could occur, and the contractual worker's financial situation were the most important factors [10]. A study looked at factors affecting labor productivity in Iran's construction industry. There were several construction experts participating in this study who had between five and seven years' experience in the field. As a result, 200 questionnaires have been distributed, contains a total of 157 responses. The results of the survey were collected, and the most common causes were working that was returned, plans that were not completed, and construction accidents, a shortage of equipment or tools, and late payment of dues [11]. Investigated and classified the elements that may have a detrimental impact on the productivity of Jordanian construction employees. A questionnaire was issued to specialists who took part in a structured survey to collect data. In addition, numerous approaches were used to limit the questionnaire, such as a phone call, a personal interview, and submitting the questionnaire via e-mail. The influential elements were found and sorted after receiving the responses: project planning, management-worker relationships, experience, developments and equipment, and motivational motives. Safety and financial borrowing, on the other hand, are the least important variables evaluated.

2 Methodology

A closed-ended structured questionnaire survey was used in this quantitative study. To put it another way, the data gathering instrument is quantitative, with constrained questions and limited responses to yield statistically relevant data. From the literature, 20 factors were selected as the most critical productivity determinants. There are four categories in Table 1 to categorize the factors investigated: management, technological, labor, and external. Contractors classified as small and medium-sized construction companies based in Wilayat A 'Seeb, Sultanate of Oman, were sent the questionnaire survey by the Oman Tender Board (OTB). A total of 90 contractors are classified as small and medium companies [12]. Survey materials were distributed in two parts where first section contains basic information on the respondents and second section contains a list of the 20 most important productivity factors that were surveyed. Five-point Likert scales are used in this section; the higher the number, the greater the impact on productivity.

Table 1 The determinants of productivity were explored, and the related groups under which they were grouped

S. No.	Productivity factors	Groups
1	Delay in payment	Management
2	Unrealistic work planning	
3	Accident (safety matters)	
4	Supervising incompetently	
5	Site selection for the project	
6	Condition of the soil	
7	Omissions from drawings	Technological
8	Clarity of project specification	
9	Complexity of design	
10	Rework	
11	Delay in replying to requests for information	
12	Changes in construction orders	
13	Labor availability	Labor
14	Expertise and skill in labor	
15	Motivating labor	
16	Condition of the weather	External
17	An overcrowded project site	
18	Permits delayed	
19	Regulations change frequently	
20	The public holiday	

2.1 Sample Size

This study examined the construction companies located in A ‘Seeb, Oman. As outlined in the authors’ [13] article, Equation 1 was used to generating sample of the population:

$$n = \frac{m}{1 + \left(\frac{m-1}{N}\right)} \tag{1}$$

The sample sizes of the limited, limitless, and accessible populations are addressed by n , m , and N , respectively, whereas m is computed by Eq. 2:

$$m = \frac{z^2 \times p \times (1 - p)}{\varepsilon^2} \tag{2}$$

where,

z Value of the statistic given for 90, 95 and 99% are 1.64, 1.96 and 2.57 respectively.

p Proportion of the population [14], obtained to be 0.50.

$$m = \frac{(1.960)^2 * 0.500 * (1 - 0.500)}{(0.050)^2} = 385$$

2.2 Data Collection

This study gathered information from 90 Oman Tender Board-registered consulting firms, and it was limited to the A ‘Seeb, Oman. A large test of the specialists and locomotive engineers selected for this study had excellent work experience, including 7–10 years of experience in construction and consulting projects. Considering this, the sample size required for a representative sample of the population is the following:

$$n = \frac{385}{1 + \left(\frac{385-1}{90}\right)} \approx 74$$

A total of 90 questionnaires were disseminated through phone and email. Furthermore, 79 questionnaires received responses, accounting for approximately 87.77% of the total of 90 questionnaires submitted. As a result, four surveys were deleted due to incompleteness, leaving 75 surveys valid for use in this study, or 83.33%, exceeding the needed sample size and ensuring the reliability of the respondents’ responses.

2.3 Data Analysis

The following are the five points The Likert Scale is interpreted as follows: 1 (Zero Effect) 2 (Minimal Effect) 3 (Moderated Effect) 4 (Substantial Effect) to 5 (Extreme Effect). The relative relevance of the productivity factors was quantified using the Relative Importance Index (RII), as illustrated in Eq. 3.

$$RII = \frac{5(n5) + 4(n4) + 3(n3) + 2(n2) + n1}{5(n1 + n2 + n3 + n4 + n5)} \tag{3}$$

where n is the number of the respondent.

The average value of the relative relevance index for all group formation elements was used to calculate the rank of each group. In other words, when the RII group’s average value rises, the group’s influence is seen as strong.

3 Results and Discussion

The information gathered from 75 respondents was analyzed and reported. The relative relevance index for each surveyed productivity component and every group of factors is also displayed.

3.1 Management Group

Table 2 shows the relative relevance indexes and ranks of the six elements grouped within the management group. Supervising incompetently was identified as the most important factor influencing worker productivity in the study, with an RII of 0.8. Not just in this gathering, but also among the 20 elements analyzed, and thus regarded as the most important factor determining Wilayat Seeb's development work efficiency. The effect of delay in payment is ranked second within this party, with RII score of 0.7256, and second, in the whole factors investigated. The effect of postponing fees was categorized and shown to be among the last elements, based on prior studies that involved large corporations. It was ranked second in this research and a survey poll that involved small and mid-businesses, indicating that it is extremely significant. As a result, the factors affecting worker productivity in construction may differ in rank between large and small-medium-sized businesses. With a relative relevance index of 0.725, the third-ranked factor is unrealistic to work planning, which is also placed third among the factors surveyed. The impact of condition of the soil is ranked fourth in this category and twelfth out of the 20 categories studied. Furthermore, under the RII of 0.618, the industrial accident factor, which accumulated against security issues, is placed fifth part in its significance in the managing group and fourteenth in general. Site selection for the project is the sixth and last rated factor in this category, with an RII of 0.589 and a rank of sixteenth overall among the factors analyzed.

Table 2 The management group, factors affecting productivity, and the relative relevance of indicators and ranks

Factors	Relative importance index (RII)	Rank
Supervising incompetently	0.8	1
Delay in payment	0.726	2
Unrealistic work planning	0.725	3
Condition of the soil	0.631	4
Accident (safety matters)	0.618	5
Site selection for the project	0.589	6

Table 3 The relative relevance of indicators and ranks in the technological group, as well as productivity variables

Factors	RII	Rank
Omissions from drawings	0.724	1
Rework	0.723	2
Changes in construction orders	0.706	3
Delay in replying to requests for information	0.675	4
Complexity of design	0.622	5
Clarity of project specification	0.607	6

3.2 Technological Group

As shown in Table 3, six technological parameters that influence the efficiency of agents on building sites have been proposed and considered. With a relative importance value of 0.724, incomplete drawing is placed first in this group and fourth overall out of the 20 factors examined. This finding supports [15] and is thus seen as the most important element impacting the productivity of construction work in A ‘Seeb, with the reason for falling into this category perhaps being an omission in the designs. Its impact could cause the project’s completion to be delayed. Furthermore, under the RII of 0.723, the rework factor is placed second in its effect in this group and sixth overall. As a result, the project’s delivery may be delayed as a result of its influence. Changing orders during construction is placed third in the technology group and sixth overall, with an RII of 0.706. With relative relevance ratings of 0.675, delays in responding to information requests are placed fourth in this collection and seventh overall. The complexity of design and clarity of the project specifications, with RIIs of 0.622 and 0.607, are placed fifth and sixth in this group, respectively, and twelfth and fifteenth out of the 20 criteria investigated.

3.3 Labor Group

Table 4 shows the relative relevance indexes and ranks of the three elements classed within the labor group, and it can be observed that they have an impact on worker efficiency on construction sites. According to the survey of the questionnaire that was completed, the expertise and skill in labor factor were rated first in the labor

Table 4 The relative relevance of indicators and ranks in the labor group, as well as productivity variables

Factors	RII	Rank
Expertise and skill in labor	0.705	1
Availability of labor	0.684	2
Motivating labor	0.621	3

Table 5 The relative relevance of metrics and ranks in the external group, as well as productivity variables

Factors	RII	Rank
Permits delayed	0.673	1
Condition of the weather	0.536	2
Regulations change frequently	0.505	3
The public’s holiday	0.484	4
An overcrowded project place	0.463	5

group and taken the seventh place among all the allotted factors, along with an RII of 0.705. Furthermore, a worker’s lack of experience and expertise at job may reduce the productivity of the construction procedures. As well as being the outcome of poor practical judgment and possibly without merit. Also, these mistakes can cost money in terms of time, repairs, and rework. Within RII 0.684, labor availability is ranked second in terms of influence in this group and eighth out of the 20 factors investigated. With an RII of 0.621, the motivating labor factor is ranked third in this category and thirteenth overall. This effect could be natural and part of our makeup.

3.4 External Group

Table 5 shows how the relative relevance indices and ranks of the five factors surveyed are grouped within the external group. With a relative importance value of 0.673, delays in obtaining construction permits are placed first in this group and inside the top ten of the 20 factors examined. Condition of the weather was also ranked second in this group, with an RII of 0.536. As a result, Oman is a huge country in the Middle East that experiences a variety of conditions of the weather throughout the year. Its atmosphere differs from one city to the next. Summer in the Wilayat of Seeb is quite hot, with temperatures reaching the fifties in June, July, and August [16]. It’s worth noting that the government is encouraged to prevent operating in open locations, for instance building places, in the summer months when the heat is extreme. In comparison, other seasons are mild and have no effect on the weather. Furthermore, with RII values of 0.505, 0.484, and 0.463, regulations change frequently, the public holiday, and overcrowded at the project site are placed 3rd, 4th, and 5th within the external collections, respectively, as well as last among the whole factors investigated.

3.5 Productivity Factors in A ‘Seeb—Ranking Based on Relative Importance

Table 6 shows the total effects of the factors that were examined. The following

Table 6 Overall, the relative importance of productivity indices determines and ranks the components

Productivity factors determinants	RII	Group	Rank
Supervising incompetently	0.8	Management	1
Delay in payment	0.726		2
Unrealistic work planning	0.725		3
Omissions from drawings	0.724	Technological	4
Re-work	0.723		5
Changes in construction orders	0.706		6
Expertise and skill in labor	0.705	Labor	7
Labor availability	0.684		8
Delay in replying to requests for information	0.675	Technological	9
Permits delayed	0.673	External	10
Condition of the soil	0.631	Management	11
Complexity of design	0.622	Technological	12
Motivating labor	0.621	Labor	13
Accident (safety matters)	0.618	Management	14
Clarity of project specification	0.607	Technological	15
Site selection for the project	0.589	Management	16
Condition of the weather	0.536	External	17
Regulations change frequently	0.505		18
The public holiday	0.484		19
An overcrowded project location	0.463		20

are the top 10 ranking factors for worker efficiency in the Seeb Wilayat: (1) Supervising incompetently, (2) Delay in payment, (3) Work planning that is unrealistic, (4) Omissions from drawings, (5) Re-work, (6) Changes in construction orders, (7) Expertise and skill in labor, (8) Labor availability, (9) Delay in replying to requests for information and (10) Permits delayed. Seven of the ten ranking factors are due to engineers and designers, which is worth recognizing and paying attention to.

3.6 The Average of the Productivity Factor Groupings Overall

As shown in Table 7, according to this classification, construction labor productivity is influenced by four groups. An RII of 0.682, the average for the first rank of the managers, appears to have a broad impact on supervisory effectiveness in the Sultanate of Oman. With a rise of 0.676 and 0.670, respectively, the technological and labor groups come in second and third, proving the relevance of drawing clarity, motivation, experience, and skills. With an average RII of 0.532, the external group

Table 7 The average of the productivity factor groupings overall

Group of productivity	Average of RII	Ranking
Management group	0.680	1
Technological group	0.675	2
Labor	0.671	3
External	0.533	4

finishes in fourth. In contrast, the indices of relative relevance of the quantitative average of the elements correlated with the four groups categorized, indicate nearly identical effects on worker productivity and show both the legitimacy and realism of the factors and outcomes studied.

4 Conclusion and Recommendations

This study was able to uncover 20 factors affecting construction labor productivity in the Sultanate of Oman, with a particular focus on the Wilayat of Seeb which were divided into four categories: management, labor, technology, and external factors. (1) incompetent supervisor, (2) Delays in payments, (3) unrealistic work planning, (4) drawings omissions, and (5) reworks were identified to be extremely critical variables affecting work productivity in construction projects in A 'Seeb.

The results of the overall average of the relative importance indices among all four classed categories, on the other hand, showed that the management group came out on top, followed by the labor, technological, and external groups, in that order.

The findings of this study contribute to our understanding of the causes and reasons that influence employees' efficiency in the construction industry, as well as filling a difference in boosting capacities and information on the elements that influence labor productivity in Al-Seeb.

Other research papers on labor productivities and its consequences in different regions of the Sultanate of Oman are advised because the study has shown that these elements fluctuate depending on the needed location. As a result, these studies will help enterprises better understand the elements that influence labor productivities and growth in Oman.

References

1. Horner R, Talhouni BT, Thomas H (1989) Results of major labour productivity. In: Proceeding the third Yugoslavian symposium of construction management, pp 18–28
2. Adrian JJ (1987) Construction productivity improvement (19th edn). Person College Div
3. Peles CJ (1987) Productivity analysis—a case study. Transaction of the American Association of Cost Engineers, 31st Annual Meeting, Atlanta

4. Handa VK, Abdalla O (1989) Forecasting productivity by work sampling. *Constr Manag Econ* 7(1):19–28
5. Fink MR (1998) A better way to estimate and mitigate disruption. *J Constr Eng Manag* 124(6):490–497
6. Alaghbari W, Alsakkaf A, Sultan B (2019) Factors affecting construction labour productivity in Yemen. *Int J Constr Manag* [online] 19(1):79–91. Available from <https://doi.org/10.1080/15623599.2017.1382091>
7. Jarkas A, Al Balushi R, Raveendranath P (2015) Determinants of construction labour productivity in Oman. *Int J Constr Manag* 15(4):332–344
8. Almathami KY, Trigunarsyah B, Coffey V (2017) Factors influencing productivity in construction. In: ISEC978, pp 4–8
9. Al-Rubaye Z, Mahjoob A (2020) Identify the main factors affecting labor productivity within different organizational structures in the Iraqi construction sector. *Mater Sci Eng* 745:231–244
10. Rad K, Kim (2018) Factors affecting construction labor productivity: Iran case study. *JSTTCE* 42:165–180
11. Hiyassat M, Hiyari M, Sweis GJ (2016) Factors affecting construction labour productivity: a case study of Jordan. *Int J Constr Manag* [online] 16(2):138–149. Available from <https://doi.org/10.1080/15623599.2016.1142266>
12. Oman Tender Board (2021) Electronic tendering services [online]. Available from https://etendering.tenderboard.gov.om/product/ReportAction?callValue=&eventFlag=SearchVendPublic&category=Z1&subCategory=101&grade=-1&companyName=&vendType=2>B_CRNo=&pageNo=&prevPageNo=&CTRL_STRDIRECTION=LTR&PublicUrl=1&WF_MTxnNo1=&procCode=&callVal=&securityFlag=1&randomno=&encparam=eventFlag%2CCTRL_STRDIRECTION%2CPublicUrl%2CsecurityFlag%2CpnoVal%2CchidMax%2Ccategory%2CsubCategory%2Cgrade%2CvendType&hashval=6e8f3278da2a38cdf429e1f837f4bfc03cdfc37d4b207d805e0b5987f590d0d7&pnoVal=1&hidMax=67
13. Hogg R, Tennis E (2009) Probability and statistical inferences (Eight editions). Prentice-Hall, Upper Saddle River
14. Sincich T, Levine D, Stephan D (2002) Practical statistics, 2nd edn. Prentices Hall, Upper Saddle River
15. Jarkas AM, Bitar C (2012) Factors affecting construction labour productivity in Kuwait. *Res Gate* 138(7):811–820
16. Seeb Climate Oman (2021) Climate Data ORG [online]. Available from <https://en.climate-data.org/asia/oman/muscat/seeb-957557/>

Performance of Pervious Concrete as a Sustainable Alternative toward Green Infrastructure Using Marginal Aggregates



Barnali Debnath and Partha Pratim Sarkar

Abstract Pervious concrete is a Low Impact Development technique that can easily retrofit the urban drainage by shifting the conventional sewer amenities to a sustainable drainage facility, which is an essential part of green infrastructure. The present study presents the performance of pervious concrete pavement made with marginal aggregates. Some north-eastern states of India are facing a scarcity of natural aggregates and these are being imported from other states/countries which increases the cost of construction. To mitigate this shortage of construction material, an attempt has been taken in this study to use commonly accessible waste over-burned brick aggregates in pervious concrete.

Keywords Pervious concrete · Marginal aggregates · Green infrastructure · Brick

1 Introduction

The drastic change in the natural climatic conditions and its adverse effect is motivating the developers and designers to think beyond the norm and to look for a sustainable solution. Currently, the designers are not only looking forward to an economical project but also they are checking the impact that the projects would have on the livelihood of the human being and the natural environment. Environmental Protection Agency (EPA) is now enforcing to use the Low Impact Development (LID) and sustainable infrastructures in order to reduce environmental pollution [1]. Pervious concrete (PC) is a kind of sustainable construction technique, which not only controls the hydrological issues but also counteracts several environmental threats. It is an emerging technique that can easily retrofit the traditional drainage system and can act as a sustainable stormwater management practice [2–9]. Pervious concrete is somewhat similar to normal concrete but contains a high amount of voids

B. Debnath (✉)
NIT, Agartala, India

P. P. Sarkar
Department of Civil Engineering, NIT, Agartala, India

that permit water to flow through it and thus it can upgrade the current sewer facilities to a sophisticated drainage facility [10]. Several works have been conducted on PC considering its performances, design, application, etc. [9]. However, the present study uses a new concept and mainly emphasizes the characterization of PC using waste over-burned brick as the coarse aggregate.

The idea behind the application of waste bricks in pavement construction came from the shortage of regular materials as well as from the waste consumption point of view. From the last few decades, the massive growth of infrastructures and urbanizations have caused a huge escalation in the production of waste materials and thereby causing a negative impact on the environment. Therefore, measures are being taken into consideration to minimize the load of waste materials in nature, and solutions are being sought to re-use these waste materials. While considering the civil engineering construction material, over-burned brick aggregate (OBBA) is also a waste material that is obtained during the manufacture of bricks. These over-burned bricks are generally obtained due to the irregular circulation of the temperature inside the brick kiln [11]. For construction purposes, bricks are mostly utilized in masonry work where the proper shape and regular size of bricks are most important, but the over-burned bricks are mostly of uneven and irregular shapes which cannot be used for masonry purposes. That is why, these over-burned bricks are considered waste materials, although they possess comparatively higher strength than the normal bricks. It is reported in the literature that almost 13% of bricks are over-burned during the burning process and these are discarded as waste material which creates a massive problem in brick industries [12]. The present study mainly focuses on these waste bricks to use as an alternate construction material for pavement construction. Due to the inaccessibility of stone aggregates in some north-eastern states of India, constructors are now thinking to use any cost-effective material as a replacement for stone. In this regard, waste bricks can come up as a convenient solution to be used as a replacement for stones [13, 14]. In this study, these waste bricks are utilized as coarse aggregates in the porous concrete mixes (PC). The main objectives of the research are to identify the suitability of using OBBA in pervious concrete and to develop a new method for selecting a mix proportion of PC using OBBA. The mechanical properties of PC such as its compressive, flexural, tensile strength, etc. are evaluated, and the hydrological behavior of PC mixes is evaluated by estimating its porosity and permeability. The effect of aggregate gradation and water/cement ratio is chosen as the variables for mix design. Finally, a comparison is also carried out with natural stone aggregates.

2 Materials and Methodology

2.1 Materials

Crushed over-burned bricks are taken as aggregate and OPC (Ordinary Portland Cement) 43-grade cement is used as a binding material. From the physical property

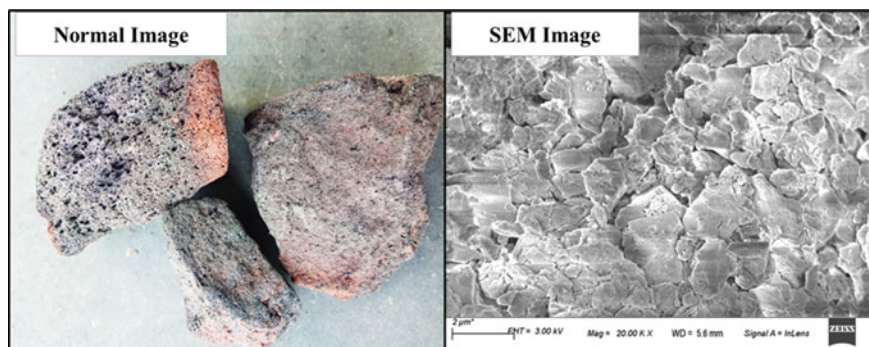


Fig. 1 Normal and SEM image of OBBA

test of crushed over-burned brick aggregate (COBBA), the crushing strength, impact value, and abrasion values are found to be 38, 36, and 44%, which are slightly higher as compared to the natural aggregates as observed in previous literature [6, 11]. The specific gravity is found as 1.898, which is slightly lesser, and the water absorption is 13%, which is much higher as compared to the natural aggregates. The reason for this high water absorption can be understood from SEM (Scanning Electron Microscope) images of COBBA, where it is clear that the surface texture of COBBA is highly porous and contains dispersed grains or weakened crusts (Fig. 1).

2.2 Mix Design

As the utilization of bricks in pervious concrete is relatively new, there are no standard guidelines available for the mix design of PC with COBBA. American Concrete Institute (ACI) has recommended one guideline for the design of PC and it is mentioned to use the dry rodded density of aggregate [15]. But it is very difficult to obtain the dry rodded density for brick aggregate due to its low strength and no standard method is also available. Therefore, IS 10262 [16] and IRC 44 [17] are also employed in this study for the mix design of PC with OBBA. A new mix design process has been formulated in this study and the steps of the design are shown in Fig. 2. For normal concrete mixes, the common method is to choose a target strength first and then develop a suitable mix design to achieve the selected target strength. However, for pervious concrete mix, it is important to have a sufficient amount of voids inside the specimens so as to obtain the required porosity and permeability. Therefore, unlike normal concrete, the first step for designing a PC is to choose a target void first and then develop a suitable mix design to achieve the selected target void.

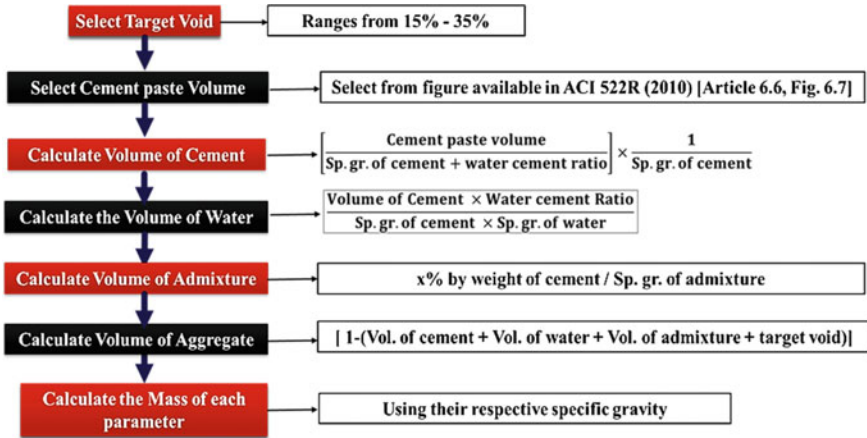


Fig. 2 Steps of mix design

2.3 Sample Preparation

Samples are prepared by varying the grades of aggregate and water/cement ratio (*w/c* ratio). Three single-size aggregates are taken for OBBA such as 13.2–12.5 mm (designated as Grade-1), 12.5–9.5 mm (designated as Grade-2), and 9.5–4.75 mm (designated as Grade-3). Four types of *w/c* ratios are also taken such as 0.28, 0.3, 0.32, and 0.35. The selected proportions of mixes are mentioned in Table 1. As the surface of COBBA is having crushed grains attached to it, it is very much essential to wash the aggregates properly before making the samples. To avoid the water absorption by the aggregate, SSD (saturated surface dried) aggregates are used for PC mixes. For different types of tests, different types of samples are prepared, and the size and shape of the samples are mentioned during the discussion of respective test results.

Table 1 Mix proportions of PC

Mix name	OPC (kg/m ³)	Coarse agg (kg/m ³)	Fine agg (kg/m ³)	Water (kg/m ³)	<i>w/c</i> ratio
Mix-1	467.73	1085.43	158.69	130.96	0.28
Mix-2	452.52	1085.82	158.75	135.76	0.30
Mix-3	438.26	1086.18	158.80	140.24	0.32
Mix-4	418.49	1086.68	158.87	146.47	0.35

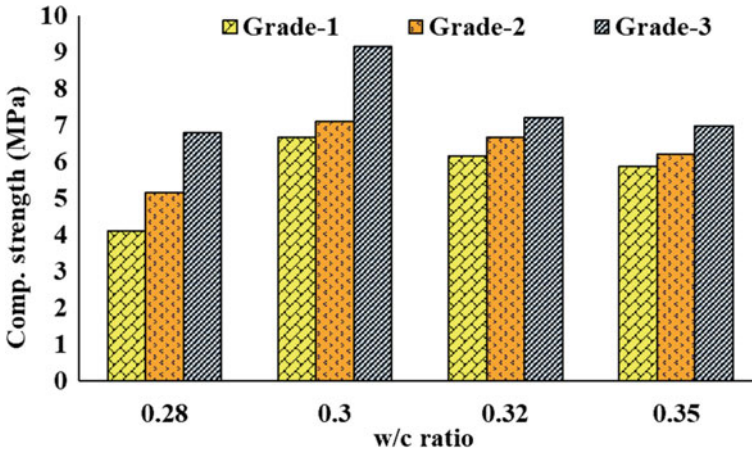


Fig. 3 Comp. strength versus w/c ratio

3 Result and Discussion

3.1 Compressive Strength Test

Compressive strength (CS) test is conducted in a compressive testing machine (CTM) with a uniform loading rate of 4 tons/min. 15 cm × 15 cm × 15 cm cube samples are prepared for every mix type. The variation of CS with w/c ratio is presented in Fig. 3. It is perceived that the comp. strength of PC increases with w/c ratio and then decreases showing a peak value at $w/c = 0.3$. At $w/c = 0.28$, the water content was too low to attach all the aggregates, and hence the mix shows a low strength. When the w/c ratio is more than 0.3, the water content exceeds the required limit, and the excess water makes the cement paste too thin. This thin layer of cement paste cannot provide adequate strength to the PC mixes. Considering the aggregate gradation, Grade-3 has shown maximum strength than the other two gradations. As the aggregate size for Grade-3 is comparatively smaller than Grade-2 and Grade-3, the available voids between the two aggregates are also smaller. This is why Grade-3 gradation can provide better bond strength and hence it has shown maximum comp. strength.

3.2 Tensile Strength Test

The tensile strength (TS) of pervious samples are conducted on a cylindrical sample having a height of 30 cm and a diameter of 15 cm. For conducting the tensile test, the samples were diametrically placed on the machine and it was evaluated using Eq. 1.

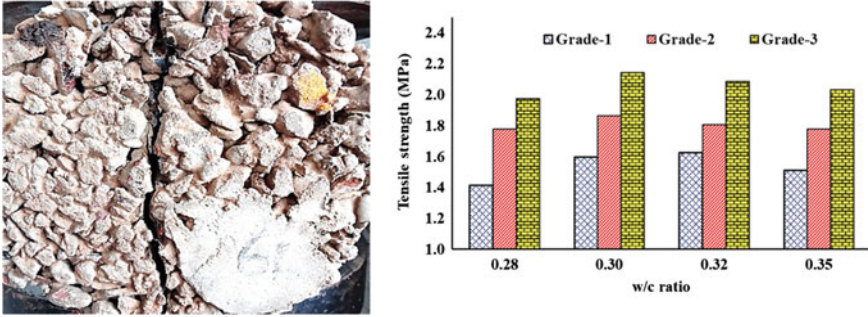


Fig. 4 Crack generated during the tensile strength test

$$TS = \frac{2P}{3.14dL} \tag{1}$$

where P = applied load on the sample, L = the length, and d = diameter of specimen. Figure 4 is showing the crack generated during the tensile test and the crushed sample after the tensile test. The change of tensile strength with aggregate gradation and w/c ratio are also represented in Fig. 4. The deviation of TS with w/c ratio and grades of aggregate is quite similar to the results of CS, where the maximum value of TS is obtained at $w/c = 0.3$. The tensile strength behavior of PC is mostly controlled by the cement matrix and the strength of aggregate. The path for tensile failure passes from aggregate to aggregate through the layer of cement paste and hence it is greatly dependent upon the thickness of cement paste and therefore, w/c ratio also becomes a vital factor. For smaller aggregates, as the pores are limited, the failure path can easily transform from one aggregate to another and does not generate any crack for low load. This is why, smaller aggregates have shown high TS, as compared to bigger aggregates.

3.3 Flexural Strength Test

This flexural strength (FS) is carried out on a four-point bending test for each case. 10 cm × 10 cm × 50 cm beam specimen was made, and the load is applied at four different points. The flexural strength was found from the following formula.

$$FS = \frac{PL}{bh^2} \tag{2}$$

where, P = load, L , b and h = the length, width, and depth of the specimen. It is obtained from Fig. 5 that FS also depends upon the w/c ratio and the grade of aggregates. Flexural strength is mostly controlled by the interfacial transition zone (ITZ) of any specimen, and this ITZ is dependent upon the cement paste thickness.

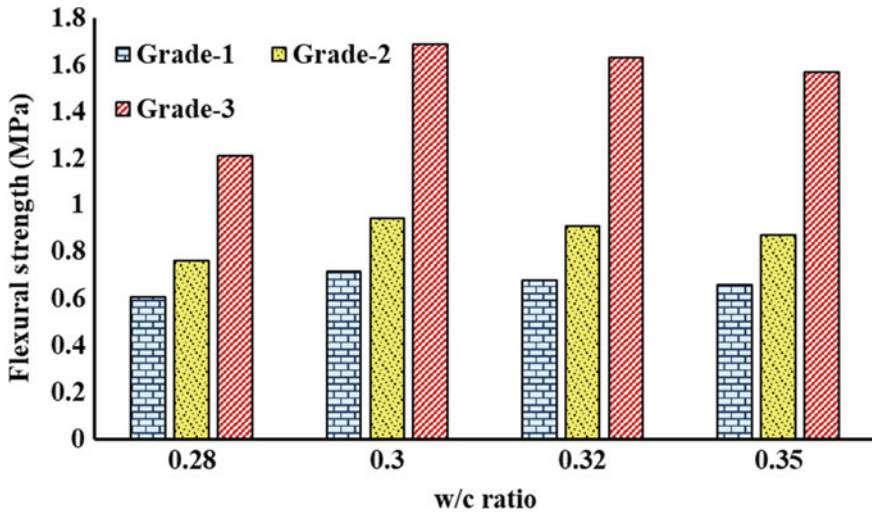


Fig. 5 Flexural strength versus w/c ratio

The high or low amount of w/c ratio makes weaker cement paste and hence ITZ increases and flexural strength reduces. Considering aggregate gradation, the smaller size aggregates develop lesser voids inside the mix which increases the flexural strength.

3.4 Permeability and Porosity Test

The porosity of PC and its permeability is assessed by using cylinders of height 20 cm and diameter 10 cm according to ASTM C1754 (2012). The porosity can be calculated using Eq. 3. The coefficient of permeability is evaluated from the falling head permeability test as developed by Debnath and Sarkar [18].

$$n = \left[1 - \frac{K \times (A - B)}{\rho_w \times D^2 \times L} \right] \times 100 \tag{3}$$

where, n = porosity of specimen (%), A = dry mass (g), B = submerged mass (g), ρ_w = density of water at a temperature of the water bath (kg/m^3), D = diameter (mm), L = average length (mm), $K = 1,273,240$ in SI units. The change of permeability and porosity is presented in Fig. 6, where it can be identified that both the pore parameters are continuously dropping with the decrease in the aggregate size. The pore space among a group of aggregates decreases with the size of OBBA and hence the pore parameters of the mixes also reduce for smaller aggregates. The change in CS with permeability and the porosity is shown in Fig. 7, and it is observed that CS

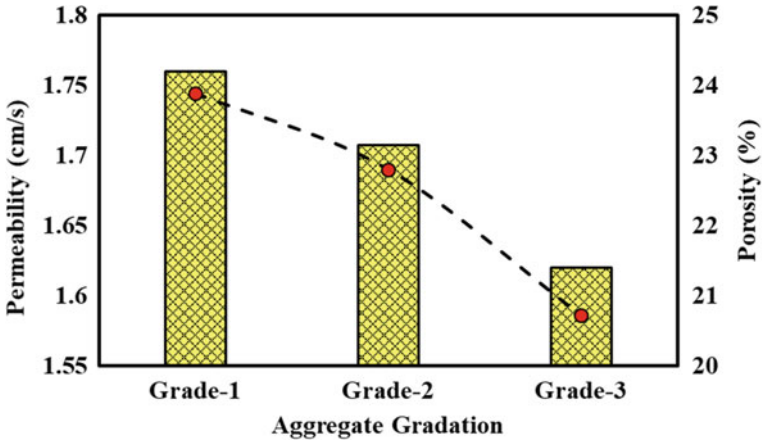


Fig. 6 Permeability and porosity versus aggregate gradation

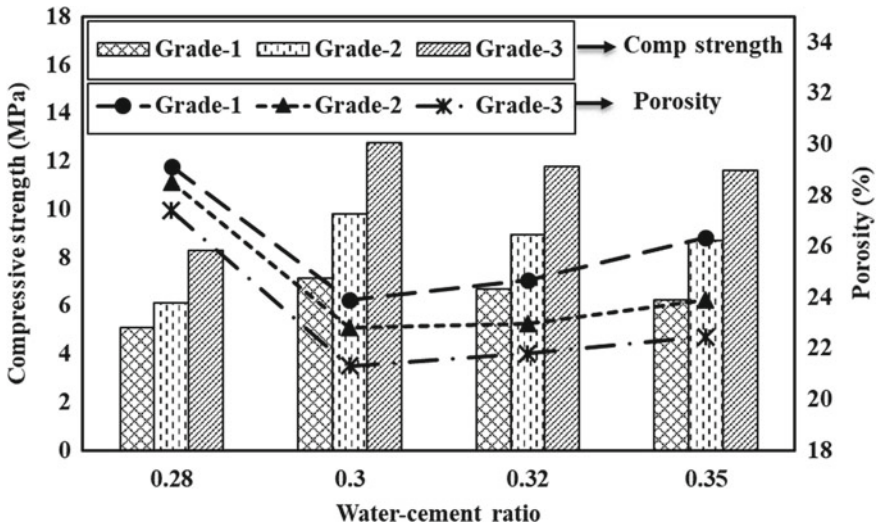


Fig. 7 Change in comp. strength and permeability with porosity

decreases with porosity. There exists a reciprocal correlation between porosity and CS, whereas permeability varies almost linearly with porosity.

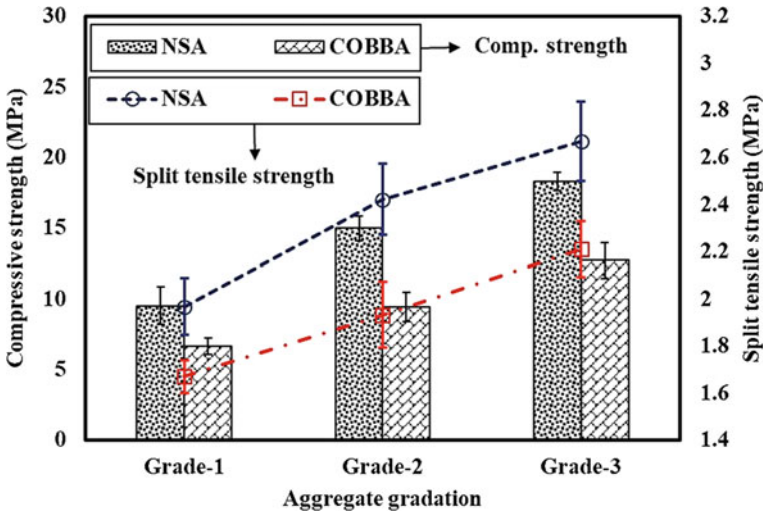


Fig. 8 Comparison of PC mixes made with COBBA and NSA

4 Comparison of OBBA and Natural Aggregate in PC Mix

The current study mainly concentrates on the development of PC mixes with marginal aggregates (here OBBA), and several test results of PC mixes with COBBA are mentioned in the earlier contexts. However, it is important to check the variation in test results of PC mixes prepared with COBBA and natural aggregates. Therefore, natural stone aggregates (NSA) of similar sizes are also used in this study only for comparing the test outcome. The comparison of CS and TS for both OBBA and NSA are presented in Fig. 8. It is found that the strength of PC-OBBA is somewhat lesser than that of the NSA mixes. The poorer strength quality of OBBA make the PC specimens more susceptible to failure and PC made of OBBA is unable to endure heavy loads. However, according to ACI522R [15], the lower limits of CS and TS are 3 and 1 MPa, respectively. In this respect, the average value of CS and TS for PC mix with OBBA is coming to 9.5 and 1.9 MPa, respectively, i.e., the values of CS and TS for PC-OBBA are about 3.2 and 1.9 times higher than the minimum requirements.

5 Conclusion

This study was conducted to alleviate the shortage of construction material and to discover a waste material that can be used as a substitute for conventional aggregates. The primary target of this study was to identify the suitability of waste OBBA as a substitute to the natural aggregates. This study mainly portrays the experimental investigations of prominent factors on the mechanical strengths and pore properties

of PC made with COBBA. After extensive experimental tests, the whole features can be concluded as

- i. Water/cement ratio is an essential factor to control the mechanical strength of PC. Too high or too low w/c ratio may reduce the compressive strength as well as tensile and flexural strength of PC. A limiting range of w/c ratio is selected as 0.3–0.32.
- ii. The size of OBBA has a vital consequence in mechanical properties as it is seen that the smaller-sized aggregates possess better strength in comparison to bigger aggregates.
- iii. The pore properties such as porosity and permeability are also inherently dependent upon the w/c ratio and aggregate gradation. It is also observed that the porosity has a reversible relationship with the compressive strength of PC.
- iv. From the comparison of PC mixes for COBBA and NSA, it is found that the COBBA mixes show little lesser strength as compared to NSA mixes. However, the obtained results are higher than the minimum requirements suggested in the guidelines. From all these observations, it can be said that the waste COBBA can be used as an alternate coarse aggregate in PC.

References

1. EPA (1999) Storm water technology fact sheet porous pavement, EPA 832-F-99-023, Environmental Protection Agency, Office of Water, Washington D.C., Sept 1999
2. EPA (2010) Storm water phase II final rule: an overview, EPA 833-F-00-001, Fact Sheet 1.0, U.S. Environmental Protection Agency, Office of Water, Washington, D.C., Jan 2000
3. Tennis P, Leming M, Akers D (2004) Pervious concrete pavements. Portland Cement Association
4. Obla K (2007). Pervious concrete for sustainable development. In: Recent advances in concrete technology. National Ready Mixed Concrete Association (NRMCA)
5. Ibrahim A et al (2014) Experimental study on Portland cement pervious concrete mechanical and hydrological properties. *Constr Build Mater* 50:524–529
6. Debnath B, Sarkar PP (2020) Characterization of pervious concrete using over burnt brick as coarse aggregate. *Constr Build Mater* 242:118154.
7. Zhong R et al (2016) Influence of pore tortuosity on hydraulic conductivity of pervious concrete: characterization and modelling. *Constr Build Mater* 125:1158–1168
8. Wu H et al (2016) Experimental investigation on freeze–thaw durability of Portland cement pervious concrete (PCPC). *Constr Build Mater* 117:63–71
9. Debnath B, Sarkar PP (2020) Pervious concrete as an alternative pavement strategy: a state-of-the-art review. *Int J Pave Eng* 21(12):1516–1531
10. Haselbach LM, Valavala S, Montes F (2005) Permeability predictions for sand-clogged Portland cement pervious concrete pavement systems. *J Environ Manage* 81:42–49
11. Sarkar D, Pal M, Sarkar AK, Mishra U (2016) Evaluation of the properties of bituminous concrete prepared from brick-stone mix aggregate. *Adv Mater Sci Eng* (Article ID 2761038). <https://doi.org/10.1155/2016/2761038>
12. Mazumder AR, Kabir A, Yazdani N (2006) Performance of over burnt distorted bricks as aggregates in pavement works. *J Mater Civil Eng* 18(6):777–785
13. Lanham MD, Sobhan MA, Zakaria M (2001) Experimental behaviour of bituminous macadam mixes with brick aggregate. *J Civil Eng* 29(1):115–123

14. Debnath B, Sarkar PP (2020) Prediction and model development for fatigue performance of pervious concrete made with over burnt brick aggregate. *Mater Struct* 53:86
15. ACI Committee 522R (2010) Report on Pervious concrete, American Concrete Institute Committee 522, Technical Committee Document, Farmington Hills, MI
16. IS: 10262 (2009) Concrete mix proportioning—guidelines, 1st revision
17. IRC 44 (2017) Guidelines for cement concrete mix design for pavements, Indian Road Congress
18. Debnath B, Sarkar PP (2019) Permeability prediction and pore structure feature of pervious concrete using brick as aggregate. *Constr Build Mater* 213:643–651

A Study on Urban Heat Island Using Geospatial Techniques



N. Haripavan, Nisha Radhakrishnan, and D. Kannamma

Abstract Global warming poses a threat to the earth's climatic system. The rise in long-term temperature of the earth's surface is a significant consequence of global warming. Urban areas are more susceptible to abnormal rises in temperatures. The higher temperatures in urban areas, generally defined as Urban Heat Island (UHI), pose a severe threat to the fastest-growing cities. Several aspects cause UHI's, such as replacing natural surfaces with built-up areas, changes in air quality, and anthropogenic heat. UHI is a key driver in the transformation of climate. This article reviews recent trends followed in determining and analyzing UHI and providing thoughtful validation strategies. The elements analyzed in this article include different data products used for identifying various methodologies for determination and analysis of UHI temperature-independent spectral-indices (TISI), Temperature emissivity separation (TES), and Normalized Difference vegetative Index-based emissivity method (NBEM) methodologies. The discussion of this research resembles the study of different algorithms used for multiple Thermal Infra-Red sensors like Landsat 7, 8 and the use of open-source technologies like QGIS. The current study also lists various validation techniques and elaborates the requirement of T-Base, R-base, and inter-comparison techniques for UHI studies. This study is helpful for researchers for identifying the problem and for professionals to take responsible decision-making during urban planning.

Keywords Global warming · Urban heat Island · Land surface temperature

N. Haripavan (✉) · N. Radhakrishnan
Department of Civil Engineering, National Institute of Technology, Tiruchirappalli, India
e-mail: 403918055@nitt.edu

N. Radhakrishnan
e-mail: nisha@nitt.edu

D. Kannamma
Department of Architecture, National Institute of Technology, Tiruchirappalli, India
e-mail: kanama@nitt.edu

1 Introduction

An increase in the population and rapid globalization raises the movement of people from rural to urban areas for their socio-economic growth, leading to rapid urbanization [1]. Urban areas are increasing in a fast phase with the continuous development and industrialization of new towns and cities [2]. With the rapid increase of urbanization, the population density and the concrete structures have been increased to cater to the increased population's needs. In contrast, it reflects on the environmental parameters of the urban area, causing an urban heat island [3]. When the city experiences a higher temperature than the surrounding villages, especially at night time, it is stated as urban heat island; the temperature difference is based on different parameters like green cover, land use pattern, precipitation, density of population, and materials used in construction and anthropogenic heat [4].

Cities constitute less than 2.5% of the earth's surface, but they absorb 75.5% of the world's energy resources. The temperature rise caused by the heat island reduces the need for heating in the winter but increases the cooling demand in the summer [5]. Cities exhibit their microclimate based on the land use patterns mainly from the modification of land use patterns and surface properties, which absorbs more solar radiation and reduced convective cooling and evaporation [6]. The evaporative-based cooling influences both the green and blue covers on the surface, which are primarily relevant for earth's canopy layer. The tree-dominated area offers more heat stress relief. Projection of climatic changes over a short period reflects the heat stress and the severity of the extreme effects of weather change [7]. The distribution of LST exhibits high in hardscape areas and low in the vegetative area [8]. The increase of non-evaporating surface or anti-infiltration surface and decreased vegetative cover influenced the land surface temperature [9]. Inadequate planning, execution, and uncontrolled land use management exhibit a tremendous impact on the urban environment [10]. Higher urban density helps in reducing CO₂ emissions, reduces the consumption of resources, helps revitalize historic buildings, and boosts the efficient use of infrastructure [11]. Reliable quantification of UHI can help in assessing the heat risk. Warmer air is caused by the heat stress of urban residents, which increases urban mortality. The higher temperature increases the consumption of more resources due to the use of air conditioners [12].

2 Retrieval of Land Surface Temperature

2.1 LST from Landsat 5 TM

LST from Landsat 5 TM is calculated based on Grover and Singh [1, 13]. Every object discharges thermal electromagnetic energy, which is received by sensors and stored in the form of a digital number (DN) and further transformed into spectral radiance ($L\lambda$).

$$L\lambda = Mt * Qcal + At \tag{1}$$

$L\lambda$ is the spectral radiance, Mt, At are the band-specific multiplicative and band-specific additive rescaling factors, $QCal$ is the digital number of the given pixel [1, 13].

Depending on the type of the land cover, value of 0.95 for vegetative land, and 0.92 for non-vegetative land were added as rectifications need for emissivity [1, 13]. Surface temperature was derived by using Eq. 2 after modification.

$$B_T = \frac{K_2}{\ln\left[\left(\frac{K_1}{L_\lambda}\right) + 1\right]} - 273.15 \text{ }^\circ\text{C} \tag{2}$$

TB is the brightness temperature, L denotes the radiance of spectral band in and K_1, K_2 are two calibration constants.

$$\text{Land surface emissivity } (\varepsilon) = "0.004 * Pv + 0.986" \tag{3}$$

$$Pv = \left(\frac{NDVI - NDVI_{min}}{NDVI_{max} - NDVI_{min}}\right)^2 \tag{4}$$

$$LST = TB/1 + [(\lambda * TB/\rho) * \ln \varepsilon] \tag{5}$$

2.2 Land Surface Temperature from Landsat 8 TIRS

Split-window (SW) algorithm is used for deriving LST from Landsat 8 having thermal bands (bands 10 and 11). In order to estimate LST for a certain place. Equations 6 and 7 explains the algorithms in depth about LST and LSE [1, 13].

$$LST = "TB10 + C1 (TB10 - TB11) + C2(TB10 - TB11)2 + C0 + (C3 + C4W)(1 - \varepsilon) + (C5 + C6W)\Delta\varepsilon" \tag{6}$$

LST is Land surface temperature, TB10, TB11 are the brightness temperature values of band10 and band11, ‘ ε ’ represents the mean of LSE, ‘ W ’ is the atmospheric water vapor content; $\Delta\varepsilon$ represents the variance in LSE and $C0$ to $C6$ are the split window coefficients [1, 13].

$$LSE = "\varepsilon_s(1 - FVC) + \varepsilon_v * FVC" \tag{7}$$

where ε_s and ε_v are the emissivity values of the corresponding bands band10 and band11 for soil and vegetation, respectively. FVC is the fractional vegetation cover

estimated over a pixel by using Eq. 8.

$$FVC = (NDVI - NDVI_s) / (NDVI_v - NDVI_s) \quad (8)$$

The NDVI is reclassified into soil and vegetation to obtain $NDVI_s$ and $NDVI_v$ and the classified data is used to find out FVC [1, 13].

$$\varepsilon = (\varepsilon_{10} - \varepsilon_{11}) / 2 \quad (9)$$

$$\Delta\varepsilon = \varepsilon_{10} - \varepsilon_{11} \quad (10)$$

where ε means fractional vegetation cover and $\Delta\varepsilon$ means LSE difference between band10 and band11 [1, 13].

The final LST obtained is converted into degree Celsius by using the relation $0^\circ = 273.15$ K.

3 Determination of LSE

Surface emissivity affects parameter measurements from thermal remote sensors like the LST [14]. Emissivity is a surface attribute that exists independently of irradiance. Water elements, chemical composition, surface structure, and coarseness are all elements that influence it [1]. However, computations are frequently problematic since natural surfaces do not emit energy in the same way that a black body does, necessitating correction using standard emissivity numbers [1]. For various TIR sensors, several approaches for estimating emissivity have been proposed [15]. The surfaces must then be inspected during both day and night under similar observing conditions, such as viewing angle [1].

3.1 Normalized Difference Vegetative Index-Based Emissivity Method

As previously stated, Landsat TM has a mono window for thermal data. Because of their simplicity, NDVI-based approaches have gained favor [17, 18]. The fractional cover mixture model is one such approach [1, 8, 16]. After logarithmic adjustment, the data indicated a high association ($R^2 = 0.94$) [18]. The relationship can be represented as follows:

$$"E = a + b \ln(NDVI)" \quad (11)$$

$a = 1.0094$, $b = 0.047$ which were derived from regression analysis.

3.2 Temperature Emissivity Separation Method

Gillespie et al. created the TES algorithm [20]. Even though it was built for ASTER thermal photography, Sobrino has demonstrated that a three-band (8.9–12 m) arrangement can achieve identical results to a four or five-band setup [16].

NEM Module: To calculate N ground temperatures, NEM approach, which considers a constant emissivity for all N channels (TG) [20]. In the TES algorithm, this approach is employed as a distinct module. Iteratively, the reflected sky irradiance is eliminated. At 340 K, the temperature transmitted to the succeeding module is between ± 3 K, and at 273 K, it should be within ± 2 K [1].

Ratio module: To determine emissivity ratios, the NEM module’s temperature T is employed in Eq. 12 [1].

$$\beta_i = \frac{R_i \overline{B(T)}}{\overline{R} B_i(T)} \tag{12}$$

$$\overline{R} = \frac{1}{N} \sum_{i=1}^N R_i \quad \text{and} \quad \overline{B(T)} = 1/N \sum_{i=1}^N B_i(T) \tag{13}$$

β_i ratio ranges within 0.7–1.4

MMD = $\max(\beta_i) - \min(\beta_i)$ is the maximum-minimum difference among the emissivity ratios β_i .

$$E \text{ min} = 0.994 - 0.687 \cdot \text{MMD} \tag{14}$$

Regression analysis is used to identify a relationship between emissivity from lab data and a field experiment [1]. The MMD is usually between 0.0 and 0.4.

$$E_i = \beta_i [E \text{ min} / E \text{ min}(\beta_i)] \tag{15}$$

TES could restore LST to ~ 1.5 K and emissivity to 0.015 K, according to numerical modeling [20].

4 Influence Factors of UHI Effect

The outdoor climatic conditions are determined by elements such as temperature, humidity, air movement, and radiation. In general, thermal and humidity index, relatively stress index are used to assess weather adaptability, with THI being the most extensively utilized [22].

$$\text{THI} = "T - (0.55 - 0.0055H) \times (T - 14.5)" \tag{16}$$

T represents maximum temperature and H represents relative humidity.

The residents in UHI areas suffer from nervous system disorders, which manifests themselves as sleeplessness, irritability, sadness, and memory loss [23].

5 Source Heat

The heat in an area can be calculated using the SEB equation [14, 24]:

$$Q^* + QF = QE + \Delta QS + \Delta QA + QH \quad (17)$$

Q^* represents net all-wave radiation, and QF , QE , QH , ΔQS , ΔQA , represents various heats releases like anthropogenic heat release, turbulent sensible, turbulent latent heat flux densities, sensible heat storage, and net heat advection, respectively [21, 23, 24].

5.1 Net All-Wave Radiation (Q^*)

The long and short waves absorbed by an area are represented by section of the energy balance [23, 24]. Using appropriate measuring instruments, both forms of radiation could be measured, and the net all-wave radiation could then be determined as the difference between the entering and exiting components [23–25]. In extreme circumstances, attenuation has been observed to be as high as 33% [23] and it has also been linked to Urban Cool Island [26]. According to reports, the majority of the diminished part is diffused and received again, with a difference of no more than 5% between urban and rural locations [24].

5.2 Net Heat Advection (ΔQA)

The inaccurate measurement caused by a spatial change in temperature, humidity, and wind is known as net heat advection. According to Christen and Vogt (2004), the impacts of advection could be insignificant if care is used while determining the measurement height [27].

5.3 Anthropogenic Heat (QF)

Anthropogenic heat is the heat created by a region's stationary and mobile sources. Anthropogenic heat has a lesser influence than albedo and vegetation cover, according

to Taha (1997), and is negligible in business and residential districts [28]. In the winter, however, Offerle et al. (2006) consider it to be a substantial input [29]. It appears that the term might be significant or negligible depending on the location and its energy use, and it could have varied diurnal, seasonal, or even weekly trends [23, 28, 29].

6 LST Validation

LST is required for climate change, surface energy budgets, and urban climate studies [1]. As a result, accurate geographical and temporal LST estimates are essential [15]. For estimating the LST, many techniques have been suggested and developed. The key objective of this study is to make necessary recommendations for adopting suitable LST validation methods for medium spatial resolution sensors. The precision of the ground-truth LSTs and their description at the satellite pixel size are key components of this technique. The T-based technique is generally limited to homogeneous surfaces, such as water bodies and densely vegetated areas because the LST fluctuates greatly over place and time [30]. LST derived from satellite data is only compared with an authenticated LST result from another satellite in the inter-comparison approach [5, 30–32].

7 Conclusions

The present study has been chosen to review the concepts, recent methods, and methodologies in understanding, generation, determination, and validation of UHI. It also discusses various algorithms required for determination of LST based on the datasets of Landsat series like TISI, TES, NBEM methods. This study also discusses the influencing factors like THI and RSI on UHI and also study regarding heat generation using the energy balance equation which includes net all-wave radiation, heat fluxes, heat advection and anthropogenic heat. It also gives a comprehensive knowledge on the importance of validation and techniques and methods used for validation of results acquired for different data sets like ASTER, MODIS, Landsat series by considering “T-based, R-based” and inter-comparison methods. In order to do comparative studies more datasets are needed and ground data should be available to get the reliable results. In view of standing challenges using low resolution remotely sensed thermal data, this review has highlighted the potential of existing medium-resolution images in determining thermal changes of an urban area. It was also concluded that there is a need to in development of more methodologies for determining the UHI reduction with a change in the design and planning parameters required.

References

1. Mohamed AA, Odindi J, Mutanga O (2017) Land surface temperature and emissivity estimation for urban heat island assessment using medium- and low-resolution space-borne sensors: a review. *Geocarto Int* 32(4):455–470. <https://doi.org/10.1080/10106049.2016.1155657>
2. Kotharkar R, Bahadure P, Sarda N (2014) Measuring compact urban form: a case of Nagpur city, India. *Sustainability (Switzerland)* 6(7):4246–4272. <https://doi.org/10.3390/su6074246>
3. Lilly Rose A (2010) Impact of urbanization on the thermal comfort conditions in the hot humid city of Chennai, India. In: Proceedings of the international conference on “recent advances in space technology services and climate change—2010, RSTS and CC-2010, May, pp 262–267. <https://doi.org/10.1109/RSTSCC.2010.5712856>
4. Sahana M, Ahmed R, Sajjad H (2016) Analyzing land surface temperature distribution in response to land use/land cover change using split window algorithm and spectral radiance model in Sundarban Biosphere Reserve, India. *Model Earth Syst Environ* 2(2). <https://doi.org/10.1007/s40808-016-0135-5>
5. Cardoso RDS, Dorigon LP, Teixeira DCF, de Costa Trindade Amorim MC (2017) Assessment of urban heat islands in small- and mid-sized cities in Brazil. *Climate* 5(1). <https://doi.org/10.3390/cli5010014>
6. Xie Q, Zhou Z (2015) Impact of urbanization on urban heat island effect based on tm imagery in Wuhan, China. *Environ Eng Manag J* 14(3):647–655. <https://doi.org/10.30638/eemj.2015.072>
7. Ahmed S (2018) Assessment of urban heat islands and impact of climate change on socio-economic over Suez Governorate using remote sensing and GIS techniques. *Egypt J Remote Sens Space Sci* 21(1):15–25. <https://doi.org/10.1016/j.ejrs.2017.08.001>
8. Guha S, Govil H, Dey A, Gill N (2018) Analytical study of land surface temperature with NDVI and NDBI using Landsat 8 OLI and TIRS data in Florence and Naples city, Italy. *Eur J Remote Sens* 51(1):667–678. <https://doi.org/10.1080/22797254.2018.1474494>
9. Khan A et al (2019) Step-wise land-class elimination approach for extracting mixed-type built-up areas of Kolkata megacity. *Geocarto Int* 34(5):504–527. <https://doi.org/10.1080/10106049.2017.1408704>
10. Triantakostas D, Stathakis D (2015) Examining urban sprawl in Europe using spatial metrics. *Geocarto Int* 30(10):1092–1112. <https://doi.org/10.1080/10106049.2015.1027289>
11. Bhargava A, Lakmini S, Bhargava S (2017) Urban heat island effect: it’s relevance in urban planning. *J Biodivers Endangered Species* 05(02):1–4. <https://doi.org/10.4172/2332-2543.1000187>
12. Kotharkar R, Bagade A (2018) Local climate zone classification for Indian cities: a case study of Nagpur. *Urban Clim* 24:369–392. <https://doi.org/10.1016/j.uclim.2017.03.003>
13. Grover A, Singh R (2015) Analysis of urban heat island (UHI) in relation to normalized difference vegetation index (NDVI): a comparative study of Delhi and Mumbai. *Environments* 2(4):125–138. <https://doi.org/10.3390/environments2020125>
14. Voogt JA, Oke TR (2003) Thermal remote sensing of urban climates. *Remote Sens Environ* 86(3):370–384. [https://doi.org/10.1016/S0034-4257\(03\)00079-8](https://doi.org/10.1016/S0034-4257(03)00079-8)
15. Li Z-L et al (2013) Land surface emissivity retrieval from satellite data. *Int J Remote Sens* 34(9–10):3084–3127. <https://doi.org/10.1080/01431161.2012.716540>
16. Sobrino JA et al (2008) Land surface emissivity retrieval from different VNIR and TIR sensors. *IEEE Trans Geosci Remote Sens* 46(2):316–327. <https://doi.org/10.1109/TGRS.2007.904834>
17. Valor E, Caselles V (1996) Mapping land surface emissivity from NDVI: application to European, African, and South American areas. *Remote Sens Environ* 57(3):167–184. [https://doi.org/10.1016/0034-4257\(96\)00039-9](https://doi.org/10.1016/0034-4257(96)00039-9)
18. van de Griend AA, Owe M (1993) On the relationship between thermal emissivity and the normalized difference vegetation index for natural surfaces. *Int J Remote Sens* 14(6):1119–1131. <https://doi.org/10.1080/01431169308904400>
19. Liang S, Zhang X, Xiao Z, Cheng J, Liu Q, Zhao X (2014) Longwave emissivity. In: Springer briefs in earth sciences, pp 73–121. https://doi.org/10.1007/978-3-319-02588-9_4

20. Gillespie A (2014) Land surface emissivity. In: Njoku EG (ed) *Encyclopedia of remote sensing*. Springer, New York NY, pp 303–311. https://doi.org/10.1007/978-0-387-36699-9_77
21. Abteu W, Melesse A (2013) Spatially distributed surface energy flux modeling. In: Abteu W, Melesse A (eds) *Evaporation and evapotranspiration: measurements and estimations*. Springer Netherlands, Dordrecht, pp 141–159. https://doi.org/10.1007/978-94-007-4737-1_10
22. Yang L, Qian F, Song DX, Zheng KJ (2016) Research on urban heat-island effect. *Proc Eng* 169:11–18. <https://doi.org/10.1016/j.proeng.2016.10.002>
23. Rizwan AM, Dennis LYC, Liu C (2008) A review on the generation, determination and mitigation of Urban heat island. *J Environ Sci* 20(1):120–128. [https://doi.org/10.1016/S1001-0742\(08\)60019-4](https://doi.org/10.1016/S1001-0742(08)60019-4)
24. Oke TR (1988) The urban energy balance. *Prog Phys Geogr Earth Environ* 12(4):471–508. <https://doi.org/10.1177/030913338801200401>
25. Brotzge JA, Crawford KC (2003) Examination of the surface energy budget: a comparison of Eddy correlation and Bowen ratio measurement systems. *J Hydrometeorol* 4(2):160–178. [https://doi.org/10.1175/1525-7541\(2003\)4%3c160:EOTSEB%3e2.0.CO;2](https://doi.org/10.1175/1525-7541(2003)4%3c160:EOTSEB%3e2.0.CO;2)
26. Sang J, Liu H, Liu H, Zhang Z (2000) Observational and numerical studies of wintertime urban boundary layer. *J Wind Eng Ind Aerodyn* 87(2):243–258. [https://doi.org/10.1016/S0167-6105\(00\)00040-4](https://doi.org/10.1016/S0167-6105(00)00040-4)
27. Christen A, Vogt R (2004) Energy and radiation balance of a central European city. *Int J Climatol* 24(11):1395–1421. <https://doi.org/10.1002/joc.1074>
28. Taha H (1997) Urban climates and heat islands: albedo, evapotranspiration, and anthropogenic heat. *Energy Build* 25(2):99–103. [https://doi.org/10.1016/S0378-7788\(96\)00999-1](https://doi.org/10.1016/S0378-7788(96)00999-1)
29. Offerle B, Grimmond CSB, Fortuniak K, Klysik K, Oke TR (2006) Temporal variations in heat fluxes over a central European city centre. *Theoret Appl Climatol* 84(1–3):103–115. <https://doi.org/10.1007/s00704-005-0148-x>
30. Tang J, Di L, Xiao J, Lu D, Zhou Y (2017) Impacts of land use and socioeconomic patterns on urban heat island. *Int J Remote Sens* 38(11):3445–3465. <https://doi.org/10.1080/01431161.2017.1295485>
31. Bernard J, Musy M, Calmet I, Bocher E, Keravec P (2017) Urban heat island temporal and spatial variations: empirical modeling from geographical and meteorological data. *Build Environ* 125:423–438. <https://doi.org/10.1016/j.buildenv.2017.08.009>
32. Equere V, Mirzaei PA, Riffat S (2019) Definition of a new morphological parameter to improve prediction of urban heat island *Sustain Cities Soc* 56 (July 2020). <https://doi.org/10.1016/j.scs.2020.102021>

A Comprehensive Study on Vehicular Pollution and Predictive Simulation—A Review



Pala Gireesh Kumar, Abhirami Priyanka Pathivada, and Musini Tejaswi

Abstract With a shift of lifestyle and living from villages to cities, the rate of urbanization has grown rapidly in recent times. Eventually, the volume of traffic has escalated at a faster pace resulting in pollution of air. With the increased use of vehicles and the rise in the release of toxic gases from vehicles, it has become a necessity to emphasize the behaviour of these gases and prevent further complications. The resultants of the toxic gases have devastating and adverse effects and it has to be considered as a posing threat to humans and the environment. Concerning the culmination of vehicular pollution, standard regulations were imposed by air quality control organizations. Despite the rules and revised regulations, it has become difficult to have vehicular pollution under control. With emphasis over the contaminants and possible approaches for subduing the pollution are under experimentation using simulating models. The present paper deals with the strategies adopted for regulating and managing the contaminated toxins and thereby, overriding the hazardous threats using Operational Street Pollution Model (OSPM).

Keywords Vehicular populace · Toxin · Air quality · Environment

1 Introduction

Environment is fundamental in each part of life. Natural environment consists of all living and non-living things. All the components required for survival of living organisms are gained from environment. One of the major problems that disturbing is pollution. Pollution is the introduction of foreign substances into the natural environment. That creates imbalance lead to adverse changes (Us EPA, Terms of environment). In urban Asian congregations India as well encountering one such genuine ecological worries as air contamination. Air contamination was positioned in the group of 10 main executioners on the planet, furthermore, the global burden of disease (GBD) has set India as sixth biggest executioner in south Asia as reported. GBP assessed

P. Gireesh Kumar · A. Priyanka Pathivada (✉) · M. Tejaswi
Department of Civil Engineering, Shri Vishnu Engineering College for Women (A), Bhimavaram
534202, India

that air contamination causes more than 620,000 unexpected passing yearly in India and triggered as fifth driving reasons for the transience of life. Ravindra et al. [17]. Other than wellbeing impact air contamination additionally adds to huge monetary misfortunes, particularly in the budgetary assets which are prerequisite in according medicinal help to the agonized individuals. Likewise, an extensive urban area was forced to contend with the quick urbanization and major part of the nation's populace will live in urban communities within the traverse of next two decades, Jha et al. [9].

Quick urbanization has likewise brought about huge increment in the quantity of engine vehicles and even multiplied in a few urban areas in the most recent decades. As the quantity of vehicles proceed to develop and consequently start building up, vehicles are currently turning into the principle wellspring of air contamination in urban regions Jha et al. [9]. Confining to India vehicles often considerably more old, also in this progressing world for the most part adjudged as antiquated innovations. Like in progressed nations, the establishments in charge of overseeing civic air standard are not created profoundly (CPCB 2010).

2 Vehicle Pollution in India

In the wake of expanding urbanization in India there has been augmentation of the vehicle contamination at an alarming rate. And in gigantic civic communities, the air pollution from vehicles varying spatially across the reserve has come to be a paramount predicament. Kavyashree et al. [13]. So the purpose instigating the problem in civic India over the extending vehicular contamination are likewise takes after (CPCB 2010).

- High denseness of vehicles in Indian civic locals.
- Predominance of private vehicles specially cars and 2 wheelers, following the deplorable communal transport system.
- Non-appearance of sufficient land utilization and arrangement for the improvement of urban territories there by provoking increase in travel as well as fuel utilization.
- Scanty reviews and mediocre servicing of vehicles.
- Defiled fuel in addition to the fuel production.
- Unacceptable traffic administration framework besides street surroundings.
- Deprivation in the effective mass rapid transport system and intra-railway network.

3 Environmental and Health Effects of Vehicles Pollution

See Table 1.

Table 1 Wellbeing impacts related with contaminations

Pollutant	Wellbeing Impacts Related With Contaminations
Co	Affects cardio vascular system, might as well peculiarly effect embryo, sick, anemia also little ones, impact on nervous system impairment co-ordination, perception plus shrewdness
No _x	Intensified proneness to infection, pulmonary diseases, imbalance of lung functioning, eye, nose including throat irritation
So _x	Deleterious influence on lung functioning
PM	Finely comminuted PM, likeliness to be noxious in self or be able to convey lethal remnant of substances furthermore able to transmute the immune system. And these comminuted particulates penetrate way down into the respiratory system
Lead	Impairs liver and kidney, triggers brain mutilation that precipitates decreased IQ in children
Benzene	Both toxic and carcinogenic
Hydrocarbon	Potential to causes cancer

4 Air Quality Modelling

A numerical model is a get together of ideas or wonders as at least one scientific conditions, which inexact the conduct of a characteristic framework or marvels. They are generally utilized to foresee the effects or centralization of parameters under various sorts of present or future situations, utilizing promptly accessible or measured information. Joining impacts of provenance quality including meteorology in portraying the subsequent surrounding air fixations, scientific prototypes may as well utilized in deciding the ecological effects of the current or in creating ventures. Air contamination demonstrating otherwise called air contamination scattering displaying is the scientific reproduction to what extent or degree the air toxins scatter inside the encompassing environment. PC programs were executed that are read as scattering prototype which tackle numerical conditions including calculations that re-enact the poison scattering. To evaluate or to anticipate the downwind grouping of air poisons discharged from various provenances say mechanical plants as well vehicular movement, these scattering prototypes were utilized. To entrust securing besides dealing with the surrounding air standards as in administrative organizations similar prototypes are essential. And these prototypes aid in the outline of successful curbing procedures with diminishing discharges of destructive air toxins. A scattering prototype is a PC re-enactment that utilizations numerical conditions to foresee air contamination fixations in light of climate, geology and discharges information.

- Emission criterion: provenance class, tempo of emission, locus, elevation, temperature, etc.
- Topography: countryside or civic locale, altitude of terrain, obstacle elevation as well as breadth if any.
- Receptor locus (altitude, farness of the root, etc.).

- Meteorological context: orientation plus velocity of wind, Atmospheric temperature, Atmospheric constancy, Cloud cover, solar radiation, etc.

Present Scenario tells that, the cities experience the problem of high volumes traffic on their main arteries: this huge amount of motor vehicles on the road emits pollutants which hold a substantial influence on air standards. Making of sky scrapers to provide accommodation for the growing urban population, further leads to the reduction of air standards within civic thoroughfares, as canyons having intense aspect ratios that lower the rate of air transfer between rooftop along with road in line So et al. [21], Li et al. [15]. The recirculation of traffic generated pollutants and its contribution to the overall street level concentration is modelled taking into account of street canyon effect in the plight of wind orientation virtually vertical to the street canyon. Speaking of the receptor locus within the bounds of leeward posse is influenced by the immediate tuft indicating impressively higher focuses than in windward posse being presented in the barely thought recycling air. The model utilized for displaying should represent mechanical turbulence delivered by the moving vehicles (Traffic Produced Turbulence) which acts notwithstanding the turbulence made by the rooftop level breeze. This prompts a quicker scattering of the immediate tuft yet in addition to enhance the air trade particularly rooftop level in the middle of road canyon along with the surrounding air.

5 Operational Street Pollution Model (OSPM)

For re-enacting the scattering of toxins subsequent to road gorge, the Operational Street Pollution Model is a climatic disseminating model. The National Environmental Research Institution of Denmark, Division of Environmental Science, Aarhus University produced this OSPM. To compute the accumulations of vehicular pollutants about the road gorge on one and the other leeward as well as windward views, OSPM is exercised which is averred as a parameterized, semi-empirical configuration. Figure 1 interprets OSPM of the fundamental principles employed in it. OSPM works out from the involvement of (i) direct vehicular wear out (ii) on grounds of vortex formation recirculation of pollutant inside gorge, including (iii) concentration at its genesis. Gaussian plume subject has been employed to evaluate the direct involvement from vehicular wear out whilst on the contrary recirculation is patterned by making use of box model approach in OSPM. Both wind rough currents as well as traffic actuated violence were modelled in OSPM taking into account of street tempestuousness. OSPM incorporate the following particulars: Traffic extensiveness, provenance ascendancy, meteorological particulars for instance wind velocity plus orientation at 10 m altitude, solar radiation information, canyon geometry like linear measurement, breadth including direction of the road furthermore, elevation of structures neighbouring the road as well as close thought of genesis. OSPM contemporary variants able to anticipate hourly concentration of CO, NO besides particulate matters, etc.

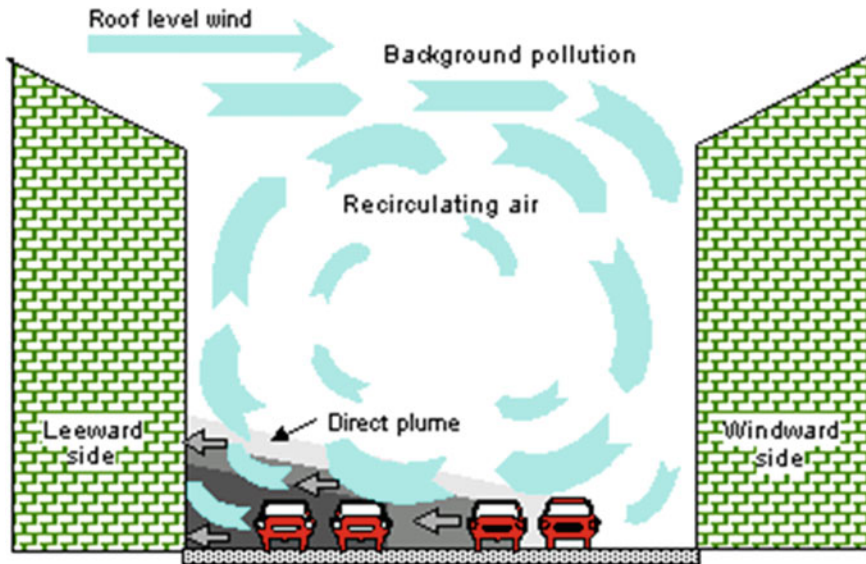


Fig. 1 Schematic delineation of essential model standards utilized as a part of OSPM demonstrate (Image source: <http://envs.au.dk/en/knowledge/air/models/ospm/ospm-description>)

6 State of the Art

Anjaneyulu et al. [1], carried out studies on the concentration of vehicular emission in Calicut city. Study area is divided in to 15 links and concentration of each link was evaluated. The performance of each model like CALINE, IITLS and Linear regression models is compared. Concludes, that the Linear regression model gives a good result than other two models.

Aquiline Noel and Alfred Micallef [2], mooted sensitivity anatomization along with gauging of semi-empirical exemplar called OSPM. Here the study period was two years. Model was used for simulating the concentration of CO. Co-relation coefficient of 0.90 was obtained between the modelled & measured concentration.

Dhyani *et al.* [3], delved in concern to the special diffusion of PM 2.5 in Delhi city, furthermore assessed with the help of CILINE 4 models. In 24 h monitoring of the study period, immoderate results were achieved in excess of the advocated national ambient air quality standards.

Dubey *et al.* [4], Performed a modelling for Dhanbad city in prevising the accumulation of CO of vehicles subjected to varied categories. They chose co for the line source modelling. They carried out vehicles counting at different road network on various traffic intersection and road links. The data obtained used in (CALIN E 4) for evaluating the suitability to the line source modelling. The performance of the model by using various statistical parameters is also evaluated.

Fallah *et al.* [5], expounded the wielding of dispersion models, a mock-up of traffic appertain to air pollution. Integrated modelling chain was used for simulating NO₂ concentration. Furthermore, the whole lot of dispersion model was testified to the assessed concentration of the generated hybrid disposition of street canyon and Gaussian models. The results revealed appreciable amelioration in the upshot of individual model by dint of hybrid modus operandi.

Fu *et al.* [6], developed a dispersion model of large resolution urban scale traffic pollutants. From the study they observed that human subjection to traffic pollutants within the inhabited civic areas is tremendously influenced by canyon geometry. Also building height and street width effect pollution inside and outside canyon.

Hennigner and Sascha [7], carried appropriation of CO₂ fixation inside the urban shelter layer of the city of Germany. Versatile measuring technique is utilized to decide the air quality markers, and these strategies guarantee a profoundly frequented Special and also fleeting thickness of territory covering with in an urban situation. Be that as it may, the outcome was not the correct centralization of CO₂ but rather the entire contamination fixation was measured.

Holmes and Morauska [8], has given a brief report appertain to the dispersion of various pollutants employing dispersion modelling with its praxis. Also discussed about the various Gaussian models which are available. CALIN B 4 and HIWAY 2 (US BPA) models encounter instinctual limitation of Gaussian equation to civic dispersion modelling apropos of small extents as well as intricate environment, for these models emanate from Gaussian plume model. Moreover for the modelling confined to subside wind rapidity, these models display total contempt. But these were exploited preponderantly for research including modulation purposes regardless of these stumbling blocks owing to their facileness of work, timesaving and curtailed use of computer. Gaussian plume model along with a box model for undeviating contribution and recirculating past of air respectively wielded in OSPM, a semi empiric model. For bye the model is unfitted to represent the sporadic fluctuation of wind flow, ergo inexpedient in evaluating concentration for a time scale less than one hr in the wake of postulation that the roof level wind speed is at the street level.

Jha *et al.* [9], Investigations were carried out on more contemporary approach and the time series analysis. Tests are conducted using different fundamental methods and results of each technique were analysed. Concludes, the result obtained from time series analysis is more accurate than the Trend line analysis and economic analysis.

Kavyashree *et al.* [10], inquired into the modelling of air pollutant concentration for a road way, passing through Mysore city. The concentration of particulates over two sampling station has been studied. Collected the meteorological data, traffic data and wind rose diagram during this period and was plotted. (CALLNE 4) line source model applied to Pm (10). Concludes that the model exhibits better correlation against actually monitored data.

Khandar *et al.* [11], recounted the study of vehicular pollution within the bounds of civic area along with its effect on human haleness plus environment. Total emission of 90% is contributed from the vehicles and transport section. Study summarizes the emission from different type of vehicles conditional on the class, effectiveness as

well as type of fuel consumed and inferred that the prime fount of CO were the two wheelers.

Kukkonen *et al.* [12], carried out studies on measuring the hourly concentration of CO_x, NO₂, and O₃ on the street and roof level. Study period was for two months. OSPM model is used for calculating the street concentration and the result was compared with the measurement. Model predicts the CO and NO₂ concentration well but, over predicted the NO₂ concentration. The performance of the model is evaluated by using the statistical parameters.

Kumar *et al.* [13], US EPA model AIRMOD is used for studying the pollutant concentration of Mumbai city. The result of the AIRMOD mainly depends on the reliability of the input data. To garner the Meteorological deets, Weather Research and forecasting (WRF) model is exercised and the results were presented in comparison of modelled and experimental data.

Lazic *et al.* [14], carried out investigation on dispersal of air pollutants enclosed by urban street canyon. Hourly concentration of NO_x, NO₂, O₃, CO and PM10 was anticipated by employing OSPM during the 10 week summer duration deemed to five streets in Serbia. At each verge of the street at 4, 8, 9 and 16 m height model receptors were stowed besides the used mass bag bio monitors were simultaneously exposed at 4 and 16 m heights. The result of both bio-monitoring and modelling shows a dwindling tendency of air pollutants in respect of elevation.

Ottosen *et al.* [16], analysed OSPM model particulars besides unpredictability of model variable. They expounded the pertinent technique for composing of data, chronicled the upshot of exertion, also under the aegis of explorative data anatomization he inquired into the merits of this methodology in connection with the work.

Sathe *et al.* [18], done examinations on the assessment of the execution of Danish Operational road contamination display. Comparison for the performance of the model by using both quantitative and statistical method is also carried out. From the results it was found that, the OSPM model is good for predicting the concentration of particulates than the NO₂ Concentration.

Shuhaili *et al.* [19], studied the quantification including anatomization of air standards encompassing various exalted traffic roads surrounded by Selanyor (Malaysia). During January 2012, one and all the week's field dossier including traffic data were garnered. From the division of environment Malaysia, contemporary statistics anent to CO, MO, HC, PM and additional imperative data were acquired. Following this, on the basis of traffic software or operative street pollution model is employed for carrying out simulation anatomization. It unfolded the quality of the precise location is affected conspicuously attributable to moving vehicles. The juxtaposition of measured and model data results indicate that OSPM likely be utilized inside Malaysian cities to anticipate the quantified indication of air pollution.

Solazzo *et al.* [20], assayed OSPM for street canyon by employing hourly co-concentration particulars. The all-embracing effectuation of the model was evaluated from statistical analysis by utilizing six unassociated databases. Hence, for low winds as well as prevailing winds disparate anatomization was executed.

Venegas *et al.* [22], elucidated and proposed street canyon effect mechanism in semi empirical urban street model (SEUS). The SEUS model is studied to analysis the hourly concentration of NO_x and NO_2 . Evaluated righteous consistency with distinguished hourly concentration were evinced from the statistical analysis of the results. The model has a good performance under wind speed greater than 3 m/s.

Wang Guangyi *et al.* [23], decision-making on human health and air quality analysis are primary aims which are considered for the study carried. Dispersion model like OSPM is used for getting the pollution concentration based on various data base. The study area of Netherland is divided into 4 plots. In the time of 2016, NO_2 as well as PM_{10} were specified as the pollutants. The pollution concentration was finally visualized in 3D GIS environment. Hence, both horizontal and vertical distribution of the pollutants using GIS technique was given.

Wang *et al.* [24], carried out studies on the prediction of PM_{10} concentration from vehicular emission. The road side measurement was taken in a street canyon of china. The mass concentration of PM_{10} was measured by Dust Track dust monitor and recorded for every 30 min and measurements were carried out for peak hours. The source strength was then estimated by OSPM.

Adriana Simona Mihaita *et al.* [25], garnered data at first regarding the traffic patterns and nitrogen oxide accumulation diurnally with hourly stretch. Then making use of the factual information, 3D mesoscopic traffic simulation model has been forged. Later, a model has been fabricated to predict the nitrogen oxide concentrations. Finally, the comparison between the estimated results and the real data were discussed. The paper also includes the human & economic impacts due to harmful emissions.

Kiran Mantripragada *et al.* [26], shows the pollution source detection system, which detects a geographic position of vehicle and also the pollution. The system includes a back-end system, which measures the gradient of the concentration of pollution and it also helps to reduce the pollution.

Rafeqet Ali *et al.* [27], estimated the repercussion of urbanization in Pakistan solitarly on carbon dioxide effusions. Two different models such as Auto Regressive distributed lag (ARDL) and VECM are used for long time and short time analysis respectively. This paper states that CO_2 emissions are increasing due to urbanization and it can be reduced by promoting the use of public transportation and educating people how different human actions lead to environment degradation.

Grange *et al.* [28], the important sources for the Nitrogen oxide emissions are Diesel-powered road vehicles. The higher NO_x emissions resulted in the lower temperature emanated from vehicle effusion remote sensing information. Gasoline Powered vehicles don't have this feature. This leads to 'low temperature NO_x emissions penalty' in Europe. The paper concludes that, at present Light-Duty Diesel Vehicles emit less NO_x gases when compared with other vehicles.

Ha. imei Wang *et al.* [29], this paper mainly focuses on the Volatile Organic Compound (VOCs) which are emitted from the parts of a vehicle. Initial emittable concentrations (Co), diffusion coefficient (Dm) also partition coefficient (K) were the three pivotal effusion variables divulged in the study. Tests have been performed for six different VOCs. The ascendancy of temperature on the pivotal variables was

comprehended in the study and concludes that major pollutants were contributed from a car seat.

Qianru Zhang *et al.* [30], carried out research within the bounds of Beijing-Tianjin-Hebei (BTH) region, China on the influence of vehicle effusion constraint stratagems. For the diminution of prime pollutants they commanded that new vehicle emission standards would be the preponderance effectual approach. The paper pointed in view of the atmospheric circumstances within BTH region that in the diminution of PM_{2.5} as well as O₃ pollution, season along with locality—definite vehicle effusion constraint stratagems were indispensable.

7 Conclusion

Meteorological data like wind speed, wind direction, temperature, street geometry and emission data are vital input to the model. To extract the meteorological data for the study area can take advantage of Weather Research and Forecasting Model (WRF). Spatial distribution of particulates PM₁₀ and PM_{2.5} is done by using GIS techniques like Universal kriging method. Spatial distribution analysis helps in better understanding of pollutant dispersion. After the modelling done based on the both observed and predicted values by model it is possible to predict that model is under predicting or over predicting the values. The statistical parameters like correlation coefficient r value can calculated for PM₁₀, PM_{2.5}. Street Canyon effect can also be related with aspect ratio. In future work, the model can be exploited for sparing by way of devising the traffic variables along with air standard levels for the forthcoming time period.

References

1. Anjaneyulu MVL, Harikrishna M, Chenchuobulu S (2006) Modelling ambient carbon monoxide pollutant due to road traffic. *World Acad Sci Eng Technol* 17:103–106
2. Noel A, Micallef A (2004) Evaluation of the operational street pollution model using data from European cities. *Environ Monit Assess* 95(1):75–96
3. Dhyani R, Sharma N, Maity AK (2017) Prediction of PM 2.5 along urban highway corridor under mixed traffic conditions using CALINE4 model. *J Environ Manag* 198:24–32
4. Dubey B, Pal AK, Singh G (2013) Assessment of vehicular pollution in Dhanbad city using CALINE 4 model. *Int J Geol Earth Environ Sci*. ISSN 2277-2081
5. Fallah-Shorshani M, Shekarrizfard M, Hatzopoulou M (2017) Integrating a street-canyon model with a regional Gaussian dispersion model for improved characterisation of near-road air pollution. *Atmos Environ* 153:21–31
6. Fu X, Liu J, Ban-Weiss GA, Zhang J, Huang X, Ouyang B, Popoola O, Tao S (2017) Effects of canyon geometry on the distribution of traffic-related air pollution in a large urban area: implications of a multi-canyon air pollution dispersion model. *Atmos Environ* 165:111–121
7. Henninger, Sascha (2011) A mobile measuring methodology to determine near surface carbon dioxide within urban areas. In: *Air quality-models and applications*

8. Nicholas SH, Morawska L (2006) A review of dispersion modelling and its application to the dispersion of particles: an overview of different dispersion models available. *Atmos Environ* 40(30):5902–5928
9. Jha K, Sinha N, Arkatkar SS, Sarkar AK (2013) Modelling growth trend and forecasting techniques for vehicular population in India. *Int J Traffic Transp Eng* 3(2)
10. Shree MK, Krishna BM, Kumar BM (2015) Monitoring and prediction of PM10 dispersion from vehicular pollution in Mysuru
11. Khandar C, Kosankar S (2014) A review of vehicular pollution in urban India and its effects on human health. *J Adv Lab Res Biol* 5(3):54–61
12. Kukkonen J, Valkonen E, Walden J, Koskentalo T, Aarnio P, Karppinen A, Berkowicz R, Kartastenpää R (2001) A measurement campaign in a street canyon in Helsinki and comparison of results with predictions of the OSPM model. *Atmos Environ* 35(2):231–243
13. Kumar A, Dikshit AK, Fatima S, Patil RS (2015) Application of WRF model for vehicular pollution modelling using AERMOD. *Atmos Clim Sci* 5(2):57
14. Lazić L, Urošević MA, Mijić Z, Vuković G, Ilić L (2016) Traffic contribution to air pollution in urban street canyons: integrated application of the OSPM, moss bio monitoring and spectral analysis. *Atmos Environ* 141:347–360
15. Li X-X, Liu C-H, Leung DYC (2007) 12.3 large-eddy simulation of flow field and pollutant transport inside urban street canyons with high aspects ratios
16. Ottosen T-B, Ketzel M, Skov H, Hertel O, Brandt J, Kakosimos KE (2016) A parameter estimation and identifiability analysis methodology applied to a street canyon air pollution model. *Environ Model Softw* 84:165–176
17. Ravindra K, Sidhu MK, Mor S, John S, Pyne S (2015) Air pollution in India: bridging the gap between science and policy. *J Hazardous Toxic Radioactive Waste* 20(4):A4015003
18. Sathe Y, Ayare A, Kulkarni G (2013) Urban air quality modelling and simulation: a case study of Kolhapur (MS), India
19. Shuhaili AF, Ihsan SI, Faris WF (2013) Air pollution study of vehicles emission in high volume traffic: Selangor, Malaysia as a case study. *WSEAS Trans Syst* 12(2):67–84
20. Solazzo E, Vardoulakis S, Cai X (2007) Evaluation of traffic-producing turbulence schemes within operational street pollution models using roadside measurements. *Atmos Environ* 41(26):5357–5370
21. So ESP, Chan ATY, Wong AYT (2005) Large-eddy simulations of wind flow and pollutant dispersion in a street canyon. *Atmos Environ* 39:3573–3582
22. Venegas LE, Mazzeo NA, Dezzutti MC (2014) A simple model for calculating air pollution within street canyons. *Atmos Environ* 87:77–86
23. Guangyi W, Van den Bosch FHM, Kuffer M (2008) Modelling urban traffic air pollution dispersion. In: ITC
24. Wang Y, Huang Z, Liu Y, Yu Q, Ma W (2017) Back-calculation of traffic-related PM10 emission factors based on roadside concentration measurements *Atmosphere* 8(6):99
25. Mihaita AS, Ortiz MB, Camargo M, Cai C (2018) Predicting air quality by integrating a mesoscopic traffic simulation model and simplified air pollutant estimation models
26. Mantripragada K, Mello U, Nemote RH, Sultanum NB, Real LCV (2018) System and method for tracking pollution
27. Ali R, Bakesh K, Yasin MA (2019) Impact of urbanization on CO₂ emissions in emerging economy: evidence from Pakistan
28. Grange SK, Ferren NJ, Vaughan AR, Rose RA, Carslaw DC (2019) Strong temperature dependence for light-duty diesel vehicle NO_x emissions
29. Wang H, Zheng J, Yang T, Cantle Z, Zhang P, Liu X (2020) Predicting the emission characteristics of VOCs in a simulated vehicle cabin environment based on small-scale chamber tests: parameter determination and validation
30. Zhang Q, Tong P, Liu M, Lin H, Yun X, Zhang H, Tao W, Liu J, Wang S, Tao S, Wang X (2020) A WRF-chem model-based future vehicle emission control policy simulation and assessment for the Beijing-Tianjin-Hebei region, China

Intelligent Traffic Control System for Smart Transportation—A Way Forward



Pala Gireesh Kumar, Gudimetla Likhitha, Inapagolla Teja Sahithi, Bandi Lavanya Reddy, and Poliseti Sunyuh

Abstract Transportation is an important field in everyone's day-to-day life where traffic congestion is one of the major issues faced in India. The number of vehicles on roads keeps increasing continuously, making the management of traffic flow more challenging. The present paper intends to explore the call for major improvements and innovations in the existing Traffic Signaling System. Current traffic light systems use a fixed time delay for different traffic directions and do follow a particular cycle whilst switching from one signal to another. This creates unwanted congestion during peak hours, loss of man-hours, and eventually a decline in productivity. This study emphasizes providing a clear solution for the snag of congestion. Forwarding the aspect of the study, solutions for the problem faced by ambulances moving towards the traffic signal during high-density traffic are majorly focused. Different ways have been proposed to make the traffic system smarter and reliable. This paper also discusses the various approaches made to enhance the traffic system across the globe. The hitches like the delay of signal lights, long-duration traffic jams, and improper routing of ambulances stuck in jams were given supreme importance, and the possible ameliorations were propounded by using smart transportation.

Keywords Traffic signaling system · Congestion · Delay time · High-density traffic · Smart transportation

1 Introduction

The tremendous problem faced by both developed and developing countries is that traffic congestion, the management of traffic flow is complicated in that cases when the count of vehicles keeps on rising. The causes may be a delay of the signal lights, improper roads, etc., India is the second-most populated country in the world and is a fast-growing economy. As we see there is no effective traffic control system available, it is facing horrible congestion problem in its cities. The delay of signal lights is

P. Gireesh Kumar (✉) · G. Likhitha · I. Teja Sahithi · B. Lavanya Reddy · P. Sunyuh
Department of Civil Engineering, Shri Vishnu Engineering College for Women, Bhimavaram,
West Godavari District 534202, India

hardcoded in the Traffic lights, which don't use any real-time traffic information. So, the demand for managing traffic arises. This work mainly aims at providing a solution for the problems faced by the congestion. In the last few years, to provide effective road transportation wireless networks are extensively used. To give the moderation of roads to the road users, it is important to have real-time traffic information [6]. The negative impact on traffic congestion can be reduced when we use Intelligent Traffic Control Systems to manage the flow of traffic. Intelligent traffic control systems use real-time traffic information to manage the traffic flow. Due to a lack of traffic information, people are facing crises like, sending their office hours in traffic or maybe sometimes if there is no traffic on the road but still, they need to wait for the signal to change.

This lack of traffic information might be a cause for an ambulance or any other emergency vehicle, stuck in the traffic [5]. Data collection, data transmission, data analysis are the main functions of an intelligent traffic control system. The whole system is dependent on the sensors and microcontroller which collect the information required. The technique is Intelligent Traffic Control System makes complete automation in the monitoring system from the information collection to the information transformation [10].

As we know Ambulances are the most important medical means of transport in any country as they carry patients to the nearby hospitals. We often see ambulances facing difficulties whilst passing through traffic signals. We can solve this problem by using sensors. When an ambulance arrives in a particular lane, the corresponding lane signal becomes green, and all the other lanes become red. This can be done by using RF transmitters and receivers. Also, we can manage the traffic density by using a microcontroller. For this, we also use IR sensors. IR transmitters and receivers are mounted on the sides of the roads. IR transmitters transmit the signal when the vehicle passes between the sensors. And the microcontroller counts the number of vehicles passing on the road and manages the traffic lights accordingly. Using the same concept of IR Sensors, we can provide passage to priority vehicles. In this system we use IR transmitters connected in a vehicle when a vehicle comes in the line IR receiver is placed at a distance from the traffic light, it passes the signal to the microcontroller and then a particular lane becomes green [4]. The collection of data is an important factor of intelligent traffic control system, which is responsible for the management of public transportation.

The rest of the paper is organized as follows. Why transportation is important and about the influence of intelligent traffic control systems on controlling traffic congestion. Followed by the challenges that are faced. Then come the different smart traffic control systems that are used in different countries like the UK, Australia, and Russia. Next, comes the discussion on various ways that are inaugurated to overcome traffic congestion. Finally concludes with the benefits of smart traffic control systems.

1.1 Why Smart Transportation is Important?

Migration of people from rural to urban causes growth in the urban population which increases the number of vehicles on the road. So, a developing country like India is also working on an intelligent traffic control system as a solution. In Indian metropolitan cities like Mumbai, Chennai, and Delhi, the matter of traffic management has become a critical issue compared to other cities. Intelligent traffic control systems count the number of vehicles passing on a road and manage the flow of traffic. For this, the system uses sensors to get the data required to control the traffic. Traffic lights changed based on the data collected by sensors. Intelligent traffic control systems use modern and arising technologies to formulate moving around a city more convenient and safer. It is being implemented today in various communities with its successes and failures being used to enhance systems in new locations. Intelligent Traffic Control Systems can reduce crimes and enhance security. A fair traffic management schedule can effectively alert drivers. The information of traffic flow can be known to the driver, so the drivers can plan their trip without any delay. They can also reduce the speed by knowing the traffic information. This will also minimize traffic delays.

2 Influence of Intelligent Traffic Control System on Controlling Traffic Congestion

The advantages they bring to transportation within smart cities are multiple. Intelligent Traffic Control Systems are more efficient and better managed. This system intends for achieving traffic efficiency by deducting traffic problems. To operate the network based on traffic congestion, an intelligent traffic control system enables traffic signal lights to regulate in real-time conditions. Developing these systems helps to reduce the number of road accidents and reduce waiting time. The fortunate traffic management can reduce the pollution. People can save fuel by travelling in a limited time. Using RFID-based vehicle positioning, stolen vehicles can easily be detected. The location of the stolen vehicle through SMS will be sent to the owner when that vehicle passes a junction.

2.1 Challenges Faced

As the collection of data is an important component of intelligent traffic control systems, the data which is collected needs to be recorded. Recording the data is more difficult. To solve the drastic traffic congestion, the conventional traffic system needs to be upgraded. This system is very big which includes many units i.e., sensors, microcontrollers etc., which make the system very complex. Understanding this

system will not be that easy at the start. After getting the required data it may be hard to categorize priority vehicles if any emergency vehicles present in opposite lanes.

3 State of Art

Extensive research work has been done to implement intelligent traffic control systems all over the world, to reduce the manual work and to implement the signaling systems. Smart Transportation systems involve many research areas and therefore, this paper focuses on those which are most relevant. The main purpose is to study, how this smart transportation is helpful in various ways. Few such literature reviews concentrating on Intelligent Traffic Control Systems are as follows,

Swarup Suresh Kulkarni et al., by using the AVR system-on-chip we can read the RFID tags that are attached to the vehicles which is helpful to control the heavy traffic, also we can provide passage for priority vehicles. GSM SIM900 is used for message sending towards the police control room or it can be used to send the data of patients to the hospitals. The manual effort on the part of the traffic policeman is saved. When a stolen vehicle is detected, the signal spontaneously changes red and helps the police to take immediate action if that vehicle is present at that crossing [1].

Hitiyaremye Eric et al., this research paper concentrated on the impact of intelligent road track control in a technologically connected vehicle environment and the requirements in developing cities. It is the connection of connected vehicle to infrastructure {allows to share information} to the vehicle to vehicle {allows the automobile to communicate each other} to a vehicle to device {consists in an exchange of information between vehicle and any electronic device connected to vehicles itself} to Connected environment is regarded in this [2].

Linganagouda et al., this project is the real-time scenario of a four-way crossing. Using the concept of RFID, the crisis that is faced by ambulance is lessened. That particular lane in which the ambulance passes will become green. IR transmitter and receiver are used to make passage for Priority vehicles. And lastly, it concentrates on the reduction of traffic density. IT transmitters and receivers are used to control the signal duration based on the traffic density accordingly [3].

Jadhav et al., this complete system works based on microcontroller AT89c51. This uses the concept of RFID (RADIO FREQUENCY IDENTIFICATION) to trace the vehicles. By collecting the traffic information, the proposed system will help in the reduction of congestion troubles at the crossings [4].

Diksha Bhawe et al., in this paper, the proposed system was based on arising vehicular communication. The system acquires higher reliability and valid information. The sensors are fixed in certain locations are utilized in monitoring the traffic based on real-time data. The data required is collected with the help of GPS [5].

Arman Syah Putra et al., IoT (Internet of Things)-based intelligent traffic monitoring systems are proposed to estimate the speed of the motorist. This intelligent

traffic monitoring system uses tools such as RFID, Sensors, IP address, QR Barcode to conduct surveillance [6].

Laisheng Xiao et al., this system uses an unusual EPC code to specify the vehicles rather than the license plates. And the positioning data of the vehicles is collected using GPS technology. The data from the mobile objects are transmitted easily by high-speed wireless IP service which is provided by the GPRS techniques [7].

Saili Shinde et al., this paper provides a review on the importance of intelligent Traffic Control systems that are used to reduce traffic flow and all the methods that have been used to develop an intelligent traffic control system. There is a necessity to minimize the congestion. The Inadequate potential of roads, huge red-light delays, etc. are some of the reasons for traffic congestion on the road. The signals do not use any real-time data and that doesn't count on the quantity of traffic density, which is the major problem [8].

Roxanne Hawi et al., this paper is a review of the implementation of Smart Traffic Control systems and the different types of systems used for traffic control. From this manuscript, it is obvious that smart systems are the means of controlling traffic. This system takes priority-based decisions using real-time data to control the traffic. The existing conditions on the roads are collected based on the advanced information based on sensors and RFID tags. The information that is provided such as the count of vehicles on the road. The systems take decisions and change the single accordingly. The system uses AI systems in sensors networks [9].

Venkata Sri et al., in this, with multiple junctions, the complexity increases as the state of one light node influence the flow of traffic towards many other nodes. These include IoT technology which constantly sends the congestion information into the server for the user convince and for traffic analysing purposes. Sensors are used to measure traffic density. They have used IR sensors to sense the traffic on road. Those sensors are interfaced with a microcontroller. Using the data collected traffic is being controlled. The road for which the sensors are active is given a green signal and a red signal to all other paths. IoT technology is included in this project for better applications. By using mobile we can see the traffic congestion in a particular area by using the Internet of Things, where the microcontroller sends the data to mobile [10].

Chitragar et al., this system will help in coping with the traffic at crossings and emergencies. The multidisciplinary systems were controlled using PLC or Programmable logic controller. The density of traffic at crossings is collected using smart systems and makes the changes in the signal correspondingly. Specific procedures are accomplished to select the lane that is to be serviced first relying on certain priorities [11].

Mandhare et al., this paper provides a review of the various sensors based on, reliability, accurateness, price, conserve energy, and expenditure. The main purpose of this Intelligent Traffic Control System is to analyse, develop, and incorporate the sensors, to boost environmental integrity. The gathered information will be very accurate. The transportation system can be well-organized with Intelligent Traffic Control Systems [12].

Satya Priya Biswas et al., this work illustrates the distinct approaches made to enhance the traffic system across the world. It also includes methods for prioritizing the lane. If the number of vehicles on a lane increase it might be a cause for traffic congestion. The microcontroller collects data from the IR sensors. Whenever a vehicle is present on the road, it is sensed by the sensors placed on either side of the road. By using a simple algorithm that is based on the extent of traffic to manage the flow of traffic. The time which is allotted to a particular lane will be influenced by the length of the traffic. The extent of the traffic is determined by the proximity sensors [13].

Bilal Ghazal et al., the proposed system that can overcome the omissions in the control of traffic is a simple, low price, and real-time smart traffic control system. All the operations such as observing the traffic density and the flow of traffic, altering of signals are accomplished by the PIC microcontroller. To provide a path for an emergency vehicle the system uses an XBee wireless system. IR sensors are used to rate the traffic density on the roads [14].

4 Smart Traffic Control Systems used in Developed Countries

Different country has a different set of rules that need to be followed to control the traffic. The formal methods of controlling traffic are keeping traffic policemen, traffic lights, traffic signals. In these years of increasing technology, intelligent traffic control systems should be used to control traffic. Flexible instructions are used to control the traffic. Data collection, Data Transmission, Data Analysis are the important functions of intelligent traffic control systems. Developed countries like Australia, Russia, and the UK have acquired a smart traffic management system and are as follows:

In the UK, traffic monitoring is crucial for traffic architects to stimulate effective traffic management and enhance traffic flow planning and likewise helps to lower congestion and pollution. It also regulates and assesses modifications created by sustainable transportation activities and criteria. In smart transportation systems, the sensors work based on the demand and regulate the flow of traffic. A central control system, traffic signal lights, queue detectors are the main components of the smart transportation system (Fig. 1). The information regarding the current traffic flow was collected by queue detectors and transferred to the control system. The control system then computes and analyses the time required to maintain the flow of traffic. This uses real-time data every two seconds and decides the phasing of the lights. Installing these systems in the city will help in the reduction of day-to-day congestion by managing the traffic flow in response to the real-time information, in reduction of pollution throughout the city.

Sydney is the capital city of the state of New South Wales, and the most populated city in Australia. The traffic control system that is used there is Sydney Coordinated Adaptive Traffic System [SCATS] which is an intelligent traffic control system. In

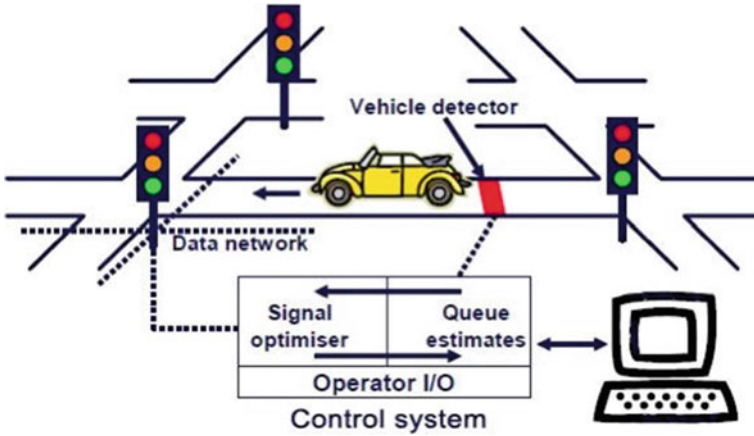


Fig. 1 Traffic control system used in the UK

response to the data received from the detectors, the SCATS system chooses a plan and monitors the traffic based on real-time information. Various sensors are used to sense the existence of vehicles at traffic signals. The sensors are installed in the pavements (Fig. 2). The collected information is then computed by SCATS and takes necessary actions. SCATS got recognized worldwide in the transportation systems. In around 40 countries these Sydney Coordinated Adaptive Traffic Systems [SCATS]

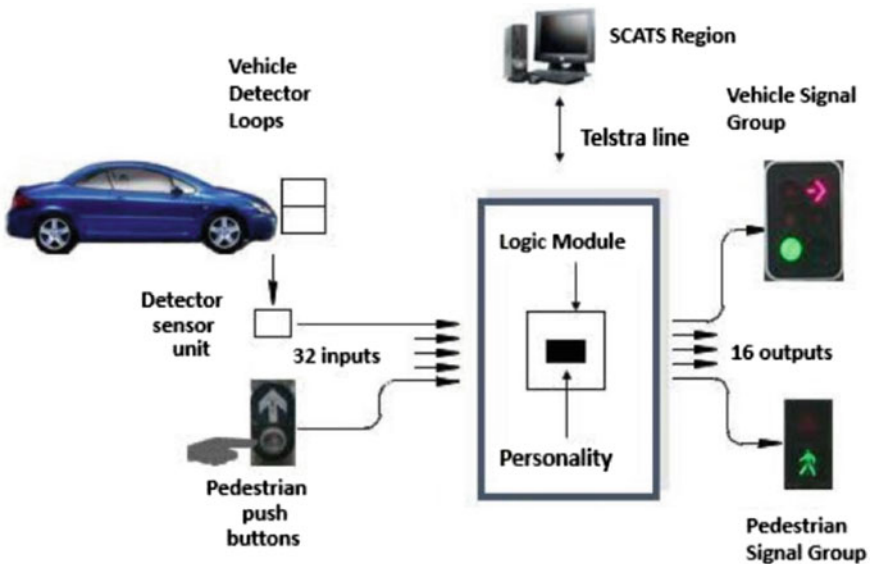


Fig. 2 Traffic control system used in AUSTRALIA



Fig. 3 Traffic control system used in RUSSIA

were introduced. SCATS were also adopted in Central New Jersey, New Zealand, Hong Kong, Shanghai.

In Europe, with 16 million people during the daytime and multiple automobiles the city Moscow is the largest metropolitan city that is growing promptly and results in a very high density of traffic. Amongst the world's major cities, the city Moscow was rated number one in the congestion index. Implementation of Smart Transportation Systems was started to tackle its huge traffic congestion problems and to smoothen the flow of traffic (Fig. 3). This system uses all-in-one cameras for the optimization of timings of traffic signals. This works by detecting the waiting and approaching vehicles.

4.1 Various Ways that are Inaugurated to Overcome Traffic Congestion

Mostly all over the world, the traffic rules are the same, the technologies used may be slightly different. The mainly used traffic control system is the light will be operated based on the preset timing system. It doesn't use traffic density to control. If intelligent traffic control systems are installed in India it will be beneficial for the Indian economy. Multiple classifications of vehicles have been expanded. Particularly the growth of countless innovative vehicles is due to the advantages in sensing, wireless communication technology and machine learning (Table 1).

Table 1 Various ways that are inaugurated to overcome traffic congestion

Approaches	Illustration
Manual Traffic Control Management	One of the most conventional methods of monitoring traffic is that manual traffic control management. This method includes humans, and it is the simplest form of traffic management. Using signboards, a traffic policeman stands at each crossing to control the flow of traffic
Automatic Traffic Management Technique	This method is also a type of traditional method to control the traffic. This system works based on fixed time delay. Depending on the maximum traffic density in a junction, the time for a particular light is hardcoded. The time given for green light is 120 s where the traffic is more, whereas in an area where the traffic is less will be less than 120 s. It depends on traffic density in that area of the city. To indicate to the vehicles that the signal is about to change, yellow light glows for 20 s
Intelligent Traffic Management Technique Based on Image Processing	Intelligent Traffic Management technique based on image processing is one of the modern technologies introduced. In this system cameras and computers are used to calculate the time for red and green signals to control the traffic. The cameras are used to capture the image of high-density traffic on the road. The calculated information then transfers to the traffic signal. Based on the data received red and green signals will changes accordingly
Traffic Management System Using Wireless Technologies	Traffic management systems using wireless technologies are also modern technology that has been developed and developing in different countries. This system uses RF-transmitters and RF-receivers to control the traffic. RF-transmitters are connected to the emergency or priority vehicles. And RF-receivers are connected near the signal poles. By this when a vehicle in which RF-transmitter has connected passes on the road the transmitter transmits the signal to the RF-receiver at the signal poles and changes the signal

5 Conclusion

From this theoretical study, using Intelligent Traffic Control Systems will be favourable, which increases safety and convenience of people, ambulance services will not be impacted and our current traffic system becomes more convenient. As a result, the roads with high density will get greater importance than the roads with

low density. This work presents a review of the existing research performed in the field of transportation and attempts to formulate a system suitable for developing countries. To solve the troubles faced by ambulances, monitor and control the traffic density and provide a freeway to the extreme priority (VIP and Police cars) are the main motives of this project. Thus, a safer place to travel can be attained by this proposed traffic control system.

References

1. Kulkarni S, Raut R (2017) Intelligent traffic control system implementation for traffic violation control, congestion control and stolen vehicle detection. *Int J Rec Contrib Eng Sci IT (IJES)* 5(2):57–71
2. Eric H, Baptiste MJ, Gilbert U (2018) Impact of intelligent road traffic control in a technologically connected vehicle environment. *Int J Comput Sci Trends Technol (IJCSST)* 6(3)
3. Linganagouda R, Raju P, Patil A (2016) Automatic intelligent traffic control system. *Int J Adv Res Electr Electron Instrum Eng* 5. <https://doi.org/10.15662/IJAREEIE.2016.0507013>
4. Jadhav AD, Madhuri LB, Ketan LT (2014) Intelligent traffic light control system [ITLCS]. In: *Proceedings of 4th international conference*
5. Bhav D, Shinde S, Shukla S, Solanki R (2017) Intelligent traffic monitoring system. 7(4). *ISSN(O) 2349-3585*
6. Putra AS (2018) Intelligent traffic monitoring system (ITMS) for smart city based on IoT monitoring. In: *INAPR international conference*
7. Xiao L, Wang Z (2011) Internet of Things: a new application for intelligent traffic monitoring system. *J Netw* 6(6)
8. Shinde S, Jagtap S (2016) Intelligent traffic management systems: a review. *IJIRST Int J Innov Res Sci Technol*. *ISSN 2349-6010*
9. Hawi R, Okeyo G, Kimwele M (2015) Techniques for smart traffic control: an in-depth review. *Int J Comput Appl Technol Res* 4:566–573. *ISSN 2319-8656*
10. Venkata Sri AS, Chowdhary IP, Surya S, Kumar NA, Pavan YR (2020) Solar based smart traffic control systems and traffic analyzer system using IOT. *Int J Res Anal Rev (IJRAR)*. 2004082
11. Chitragar NR, Ramesh GB (2004) Smart traffic control system based on vehicle density using PLC. *Int J Innov Res Electr Electron Instrum Control Eng*. *ISSN 2321*
12. Mandhare PA, Kharat V, Patil CY (2018) Intelligent road traffic control system for traffic congestion: a perspective. *Int J Comput Sci Eng*. *E-ISSN 2347-2693*
13. Biswas SP, Roy P, Patra N, Mukherjee A, Dey N (2015) Intelligent traffic monitoring system. *Conference Paper*
14. Ghazal B, ElKhatib K, Chahine K, Kherfan M (2016) Smart traffic light control system. *ISBN 978-1-4673-6941-1*
15. David O, Ese, Okhueigbe E, Ighodalo (2017) An intelligent system for traffic control in smart cities: a case study. *Am J Artif Intell*
16. Chattaraj A, Bansal S, Chandra A (2009) Intelligent traffic control system using RFID
17. Srivastava MD, Purna, Sachin S, Sharma S, Tyagi U (2012) Smart traffic control system using PLC and SCADA. *Int J Innov Res Sci Eng Technol*. *ISSN 2319-8753*
18. Won M (2020) Intelligent traffic monitoring systems for vehicle classification: a survey
19. Hussian R, Sharma S, Sharma V, Sharma S (2013) WSN applications: automated intelligent traffic control system using sensors. *Int J Soft Comput Eng (IJSCE)*. *ISSN 2231-2307*
20. Chinyere OU, Francisca OO, Amano OE (2011) Design and simulation of an intelligent traffic control system. *Int J Adv Eng Technol*. *ISSN 2231-1963*

Performance Evaluation of Potassium Based Additives for Black Cotton Soil Stabilization



N. Mallikarjuna and K. S. R. Prasad

Abstract The black cotton soil covers more than a quarter of India's geographical area. This black cotton soils retains features like highly shrinking and swelling character and low bearing capacity depending on the changes in moisture content present in atmosphere and this is because of montmorillonite mineral that is present in black cotton soil. In order to control these issues that are associated with black cotton soils, wide variety of techniques are available. Chemical stabilization is the most widely used stabilization technique all over the world due to its high efficiency. In present study investigates about the efficiency of soil stabilization by potassium chloride in black cotton soils is investigated. The binder percentages of 5, 10, 15 and 20% were considered basing on the earlier literature. The experimental findings of index, engineering and microstructures properties of the KCL blended soils at different percentages are presented in this paper. The results showed the increase of 5% blended samples of curing periods compressive strength in different intervals of days as 0, 7 and 28 days respectively. In curing times from 5 to 20% ranges there is decrease with increase in blinder content for Unconfined Compressive Strength (UCS). Hence an optimum binder content of 5% is selected as the optimum binder dosage for stabilization. The microstructure changes occurred in 5% blended sample which are analyzed by XRD patterns. The strength of soil of black cotton is increased successfully because of the conversion of montmorillonite to illite mineral as this is the main aim of our work. This current study clearly represents the efficiency of KCL in treating and stabilization of black cotton soil.

Keywords Stabilization · KCL · UCS · Illite

N. Mallikarjuna (✉) · K. S. R. Prasad

Department of Civil Engineering, VR Siddhartha Engineering College, Vijayawada 520007, India

K. S. R. Prasad

e-mail: ksr466ce@vrsiddhartha.ac.in

1 Introduction

The expansive soil is spread over a large part of India and it covers various states all over the country mostly in the states of Madhya Pradesh, Gujarat, Andhra Pradesh, Maharashtra, Tamil Nadu and Karnataka. It also covers few other states of our country. Moreover greater than twenty percentage of geographical area in India is covered with expansion soil [1, 2]. As this expansion soil is black in color it is popularly known as black cotton soil and it is highly sustainable for growing cotton. Basing on the moisture content in soil these expansive soil shrink when there is decrease in moisture level and it swells when there is high amount of moisture in the soil. The main cause for this feature in soil mass is because of montmorillonite minerals [3].

This feature of shrink and swell of black cotton soil basing on presence of moisture in soil is because of montmorillonite mineral. Almost in every continent these expansive soils are present. Many countries reported the issues that lead to destruction because of these expansive soils. These expansion soils are also known as black cotton soils which are covered over large area in India. Entire Deccan Plateau is mostly covered with these black cotton soils, they are covering the large area of south Vindhya range. Suitable remedial measures are to be taken before construction in the expansive soils. There are numerous solutions available to minimize the swelling characteristic of soil. For instance we have various techniques to overcome this issue such as maintenance of water wells under the foundation, removing the soil up to certain depth and soil reinforcement.

Stabilization of expansive soils can be performed is a well-known technique that involves modification of characteristics of black soil by adding up of chemical mixtures in it. As an effect of this chemical stabilization the shrinkage and swelling properties of expansive soil is reduced to some extent. Chemical stabilization involves treatment of expansion soil with electrolytes such as ferric chloride, potassium chloride calcium chloride or sea water are utilized in various studies [4–8]. Even though we have many types of electrolytes for soil stabilization, soil stabilization with the help of potassium chloride (KCL) is the most effective one. Furthermore mixing of electrolyte in non-uniform proportion is a major drawback in the use of electrolytes as it could give rise to unpredictable outcomes. In [9] Katti et al. explained different kinds of additives such as KCL, $MgCl_2$, $BaCl_2$ and $CaCl_2$ for stabilization of the expansive black cotton soil. Out of all these additives potassium chloride (KCL) is observed to be efficient for stabilization when compared with remaining additives. In [10] it is observed that potassium chloride reduced the expansive activity of soil to great extent. In [11] it is found that the KCL has reduced the plasticity index, liquid limit, OMC and free swell of soil.

2 Literature Survey

The usage of river sand was introduced by the early literature on black cotton soil stabilization. Due to the rapid growth in the industries for construction [12] there is a huge demand for sand has kept increasing tremendously which leads to deficiency in choosing appropriate river sand in all over the globe. Hence crush sand [13] is replaced with the river sand as it is easily available in many areas.

2.1 Stabilization of Soil

Generally for enhancement of physical properties this soil stabilization method is practiced. Soil stabilization is used for permanent modification in properties chemical and physical of soil. The main reason for stabilization of soil is to improve the shear strength of soil which in turn reduces the shrink and swell properties of expansion soils. It also improves the load bearing capacity of subgrade soil. Subgrade materials are stabilized in wide range by using the particles of soil due to granule material [14].

2.2 Advantages of Soil Stabilization

The main advantage of soil stabilization is achieving of high resistance value. The plasticity, permeability and pavement thickness [15] are reduced considerably. Soil stabilization also eliminates the excessive excavations, soil handling and material hauling. This is highly beneficial in aiding compaction and it improves the access of project sites in any weather conditions.

2.3 The Principles of Stabilization

The soil stabilization of main intent is as follows. The principles involving in soil stabilization are.

- a. The soil properties are to be evaluated.
- b. By using the effective and economic methods of stabilization the deficiency and the properties that are lacking in soil can be supplemented.
- c. The stability and durability values of soil are intended for designing the stabilization of soil mix [16].
- d. The plastic limit and liquid limit must be reduced for improving the shrink and swell properties of expansion is stabilized.

2.4 Chemicals Used for Soil Stabilization

Generally three kinds of commercial grade chemicals are used for stabilizing the soil such as potassium chloride (KCl), calcium chloride (CaCl_2) and ferric chloride (FeCl_3) are compared in various studies earlier. The chemical which is found to be more efficient in soil stabilization is observed as potassium chloride (KCl). It is very important to measure the quantity of chemical that is mixed with the expansive soil. It ranges from 0 to 1.5% by considering the dry weight of expansion soil that is to be stabilized.

Usually electrolytes like KCl, CaCl_2 and FeCl_3 are added to the expansive soils in different proportions. In our current study we used potassium chloride for stabilizing the expansion soil as it is the effective additive compared with other chemicals. The physical properties such as plastic limit, liquid limit, shrinkage limit and OMC and MDD % of stabilized expansive soils are estimated in order to estimate the influence of electrolytes in the expansion soil and its physical properties are determined by this method. Engineering properties such as compaction, permeability, Unconfined Compressive Strength (UCS) and shear strength of stabilized soil are influenced by the percentage of electrolytes that are added to the expansion soil.

3 Proposed System

As per Indian standards Unconfined Compressive Strength (UCS) and condensing properties of soil of virgin can be estimated. Soil stabilization is performed for different levels of KCl content ranging from 5 to 15%. This chemical KCl is mixed thoroughly into the soil. This mixture is observed at different intervals of time such as 0, 7 and 28 days therefore the shrinkage limit, liquid limit and plastic limit, were estimated for the stabilized soil. The thread rolling method is used for estimating the liquid limit and plastic limit by using Casagrande percussion method.

IS Standard code prescribes a procedure for estimation of compaction parameter in the expansive soil that is stabilized. Potassium chloride KCl was mixed thoroughly to the soil and then the mixture was compacted in the proctor mold. Soil was compacted in three layers of equal height. After compaction, soil was removed from the mold. Three soil samples, from top, middle and bottom were collected in each test for estimation of moisture content in the soil. On an average of three samples were considered as OMC for observing the soil stabilization. This soil stabilization is conducted at different levels of KCl content treated with the soil at 0, 5, 10 and 15% of potassium chloride electrolyte added to the expansion soil. For each sample dry density is estimated after calculating the water content in soil sample at different percentages. Depending on these observations the graphs are plotted.

For these soil stabilization samples of KCl treated soil for 0, 7, and 28 days are used for determining the Unconfined Compressive Strength (UCS) and strength of the soil is tested as per instruction. A metallic split sampler, having height of 76 mm

Table 1 Proposed system of BC soil stabilization with KCl

BC SOIL	Index properties: LL, PL, grain size analysis, pH, specific gravity, CEC Strength properties: UCS Mineralogical studies: XRD Morphological studies: SEM
BC SOIL + KCL	Index properties: LL, PL, grain size analysis, pH, specific gravity, CEC Strength properties: UCS Mineralogical studies: XRD Morphological studies: SEM

height and diameter of 38 mm is utilized for preparing the samples for testing UCS. Initially, tests were conducted for basic black cotton soil and its index properties are determined before treating the BC soil with KCl and later tests were repeated for BC Soil + KCl for added 5, 10 and 15% of added potassium chloride and its index properties are determined in the tests conducted. The following tabular gives clear representation on the composition and properties of BC soil before stabilization and after stabilization with KCl basing on mineralogical and morphological studies is shown in Table 1 as follows.

4 Material Used for Stabilization (KCL)

4.1 Physical Properties

- KCl electrolyte of weight 74.5513 g per molecule is added to the stabilized soil.
- The density of KCl in the crystalline solid form is of 1.984 g per cm³.
- The electrolyte KCl has the melting point of 104 °K and its boiling point is 169 °K respectively.
- At 0, 20 and 100 °C, the KCl solubility range in water is observed to be 217.1 g/L, 253.9 g/L and 360.5 g/L respectively.

4.2 Chemical Properties

- The metallic sodium is heated with KCl up to 850 °C for achieving the chemical properties.
- Here KCl is ionized completely in to K⁺ and Cl⁻ ions in H₂O, hence high electrical conductivity values are obtained in resulting aqueous solution.

5 Result

Basic soil samples of black cotton soil are collected and properties of those soil samples are classified such as liquid limit, plastic limit, plasticity index and specific gravity of the soil samples are tested for determining their values in percentage and respective IS Standards of each property are represented in the following Table 2.

After treating this black cotton soil with KCl and stabilizing it at different percentages of 0, 5, 10, 15%, the soil is tested for its physical and chemical properties for an interval of 0, 7, 28 days and various tests such as OMC (%), MDD (%), and UCS tests are conducted. They are represented in Table 3 along with its respective IS Standards.

Tests were performed on virgin expansive soil and potassium chloride mixed soil. Amount of potassium chloride were varied from 0 to 15%. Effect of potassium chloride on Atterberg limits, namely, liquid limit, plastic limit and shrinkage limit are shown in Fig. 1. Addition of potassium chloride in expansive soil caused a reduction

Table 2 Geotechnical properties of basic black cotton soil

Property	Value	IS standards
Liquid limit (%)	54	IS: 2720 (Part 5)-1985
Plastic limit (%)	30	IS: 2720 (Part 5)-1985
Plasticity Index (%)	24	IS: 2720 (Part 5)-1985
Specific gravity	2.68	IS: 2720 (Part 3)-1980
Soil classification	CH	IS: 1498-1970 (IS classification)
MDD (%)	1.64	IS: 2720 (Part 7)-1980
UCS (kPa)	121	IS: 2720 (Part 7)-1980

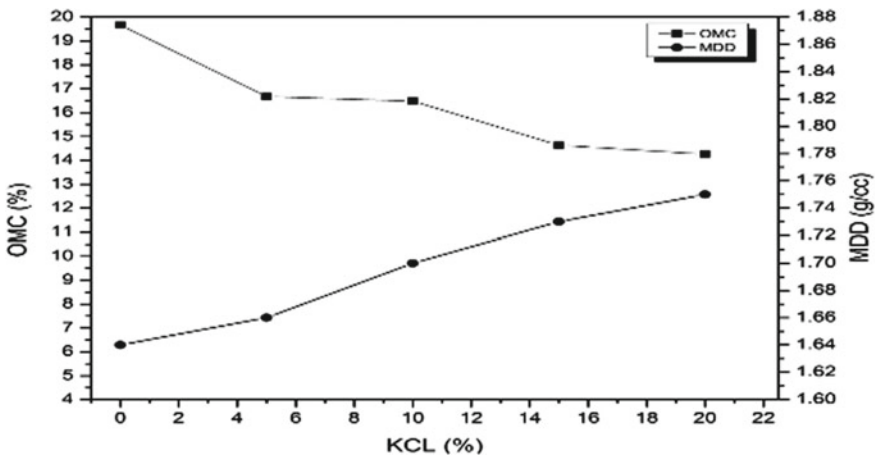


Fig. 1 Compaction characteristics of soil at different levels of KCl contents

in the liquid limit of soil. Reduction in the liquid limit is more substantial at 5–7% of potassium chloride and mixing of additional amount leads to decrease in the efficiency of potassium chloride. Change in the plastic limit of potassium chloride added soil is insignificantly up to 5% of KCl, but further more addition of KCl caused an increase in the plastic limit. Shrinkage limit is increased with increase in the amount of added potassium chloride. The increase in the shrinkage limit is significant up to 10% of potassium chloride, beyond 10%, rate of increase in the shrinkage limit becomes insignificant.

Here BC Soil when stabilized with KCl, we classified the compaction characteristics of soil for presence of OMC (%) and MDD (%) at different levels of KCl content in the soil. It is represented in Fig. 1.

The black cotton soil after treating with KCl, it is observed for the strength improvement in soil for Unconfined Compressive Strength (UCS) for different time intervals such as 0, 7, 28 days at different levels of KCl like 0, 5, 10, 15% of KCl (%) and the observation showed that strength improvement is optimal at 5% KCl content which is represented clearly in Fig. 2.

The black cotton soil is stabilized with KCl at 5% the following characteristics that is a mineral called Sanidine mineral. This Sanidine mineral helps in raising the efficiency of BC soil by maintaining the liquid limit and plastic limit in required standards, as shown in Fig. 1. The black cotton soil when treated with 5% of KCl in it, the soil forms a new mineral called Sanidine mineral which works effectively in reducing the liquid limit and plastic limit of the BC soil by converting the montmorillonite mineral to illite mineral that improves the strength of the black cotton soil and improves its efficiency for its usage in construction. It is represented in Fig. 3 as follows.

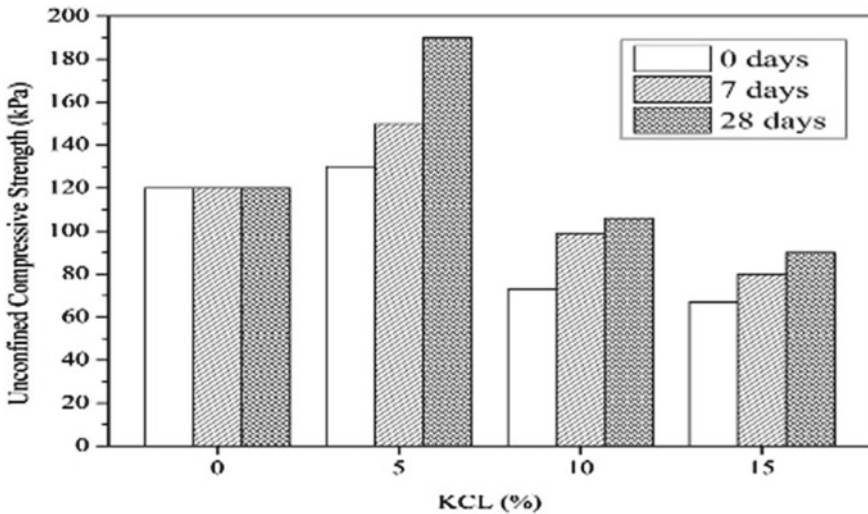


Fig. 2 Strength improvement in BC Soil + KCl analyzed for UCS at different curing periods

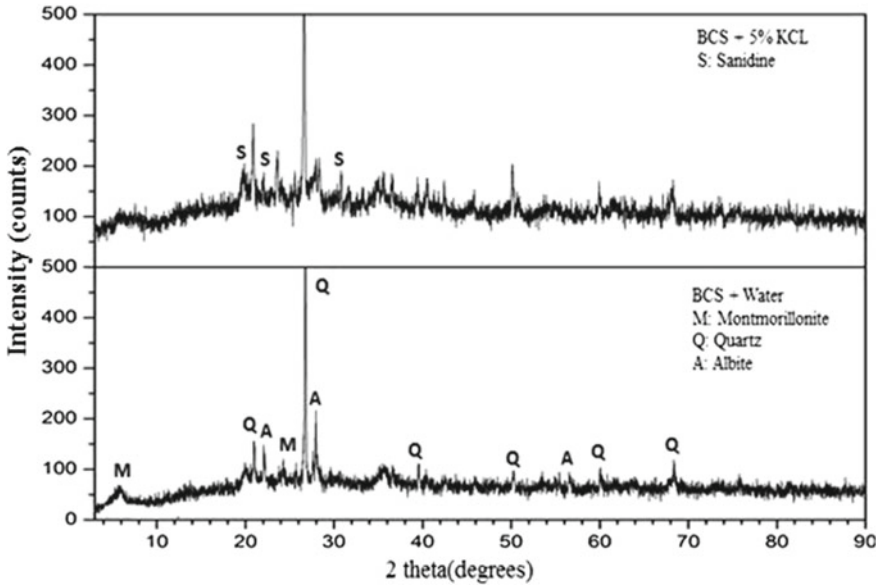


Fig. 3 XRD analysis for BC soil and 5% KCL treated soil

In the process of soil stabilization with KCl the black cotton soil is analyzed for measuring the liquid limit and plastic limit at different levels of KCl content for soil stabilization at observed and their intensity in the soil that is given in Fig. 4 as follows.

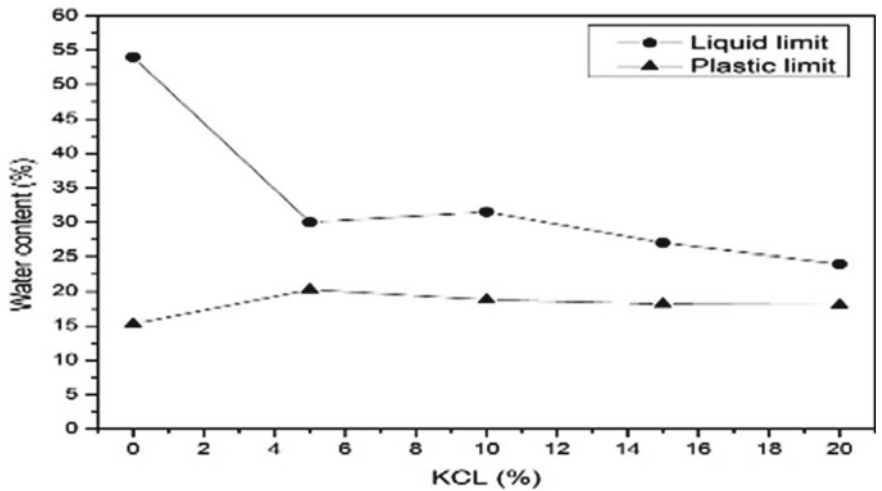
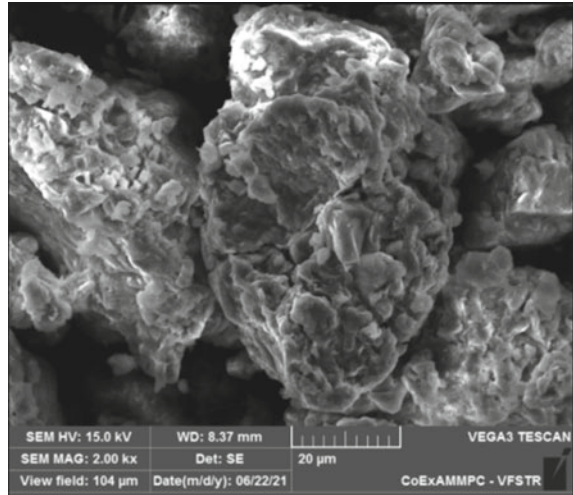


Fig. 4 Variation in liquid limit and plastic limit in black cotton soil at different levels of KCL content

Fig. 5 SEM analysis for untreated black cotton soil representation

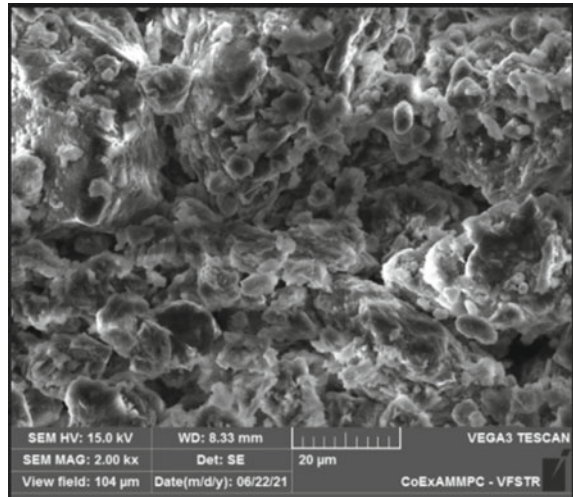


The BC soil treatment with KCl works effectively. The untreated BC soil is hard and it has expansive properties which swell when there is moisture and it shrinks during summer which may lead to breakages. The untreated soil is represented in Fig. 5 as shown.

After stabilization of BC Soil with KCl, the properties of soil are analyzed by using XRD patterns. In this XRD method the black cotton soil is tested for the presence of Quartz minerals in the soil.

After treatment of BC soil with KCl its properties are enhanced as montmorillonite mineral is converted to illite mineral the production of Sanidine also improves the physical and chemical properties of basic soil which in turn reduces the liquid and plastic limits of untreated soil. Here in our survey the stabilization electrolyte KCl plays a key role in soil stabilization. This KCl chemical fills the gaps between the soil particles by reducing its liquid and plastic limit range in the soil in treated soil. Hence strength of our basic black cotton soil is improved as observed in SEM analysis as depicted in the below figure. The resultant treated black cotton soil is suitable for its usage in construction without causing any breakage in walls with change in moisture content in the soil. This enhancement of basic soil is mainly observed at a rate of 5% KCl mixture treated with the soil. Before treatment of soil there are gaps in between the soil which is the biggest drawback in black cotton soil as observed in SEM analysis in Fig. 5. We can observe the change by comparing both the figures. The following Fig. 6 represents the treated soil as shown.

Fig. 6 SEM analysis for treated black cotton soil with potassium chloride at 5%



6 Conclusion

Unconfined compressive strength tests (UCS) and compaction tests are conducted according to Indian standards. Mixing of KCl caused to substantial reduction in the OMC, plasticity index and liquid limit of BC soil. Shrinkage limit, dry density to maximum limit and unconfined compressive strength are improved with addition of KCl. Mixing excessive amount of potassium chloride has adverse effect on soil characteristics. Excessive amount not only reduced the cations exchange capacity but also increased the water absorption, and consequently it reduced the efficiency of potassium chloride. In this paper we observed the optimal results at 5% of KCl content treated with black cotton soil at different intervals of time 0, 7 and 28 days respectively. It is advised that optimum amount of KCl is to be determined before using it for ground improvement in expansive soil. This 5% of KCl content in BC Soil works efficiently in the conversion of montmorillonite to illite mineral in black cotton soil which is the main aim of our project. Hence in our paper we clearly presented the properties of BC Soil before and after stabilization, its physical and chemical properties. BC soil reduces its liquid limit, plastic limit, plasticity index in best proportions by adding 5% of KCl. The BC soil is improved and it is useful in construction. We conducted XRD test, MCC and OMC tests are conducted on treated soil at different percentages of KCl and final results are clearly mentioned in this paper.

References

1. Nicholas Wallis JA (2020) Intensified systems of farming in the tropics and subtropics the

- international bank for reconstruction and development, Washington, D.C., U.S.A.
2. Ranjan G, Rao ASR (2020) Basic and applied soil mechanics. New Age International (P) Ltd, New Delhi
 3. Chen FH (2019) Foundations on expansive soils. Elsevier Scientific Publishing Co., Amsterdam, IEEE explorer
 4. Sastry MVBR, Srinivasulu Reddy M, Gangaraju ChP (2018) Comparative study of the effect of addition of rice-husk-ash and cinder-ash to soil-lime mixtures. *Indian Highways* 14(8):5–14
 5. Prasad Raju GVR (2017) Evaluation of flexible pavement performance with reinforced and chemical stabilization of expansive soil subgrades. Ph.D thesis, Kakatiya University, REC, Warangal
 6. Katti RK, Kulkarni RR, Radhakrishnan (2016) Research on expansive soils without and with inorganic additives. *IRC Road Res Bull* 1–97
 7. Frydman S, Ravina I, Ehrenreich T (2015) Stabilization of heavy clay with potassium chloride. *Geotechnical Engineering*, South East Asian Society of Soil Engineering
 8. Al-Omari RR, Ibrahim SF, Al-Bayati IK (2015) Effect of potassium chloride on cyclic behavior of expansive clays. *Int J Geotech Eng* 4:231239
 9. Al-Ashou O, Al-Khashab MN (2014) Treatment of expansive clay soil with potassium chloride. *Al-Rafidian Eng J* 1(2)
 10. Al-Omari RR, Oraibi WK Cyclic behavior of reinforced expansive clay. *Soils Found* 40(2):1–8
 11. Shukla RP, Parihar N, Tiwari RP, Agrawal BK (2013) Black cotton soil modification using sea salt. *Electron J Geotech Eng* 19:8807–8816. Bundle Y
 12. Shrivastava SK, Jain D (2012) Stabilization of natural soil with sand and cement. 3(10). ISSN 2321-0613
 13. Louafi B, Bahar R (2012) SAND: an additive for stabilization of swelling clay soils. *Int J Geosci*
 14. Tejaswi N, Divya Kanthi P, Satyanarayana B, Shyam Chamberlin K (2011) Stabilization of clayey soil using cement kiln waste. *International J Adv Struct Geotech Eng* 02
 15. Lal NB, Kadyali LR (2010) Highway engineering, 5th ed. Khanna Publishers, Delhi
 16. Jain SR (2009) Improvement of sub grade strength by partial replacement of M-sand. *Am J Eng Res* 5(7). ISSN 2320-0936

Possible Utilization of Expansive Soil Incorporated with Bagasse Ash and Bagasse Fibre



J. Harisha Deepthi and S. Satish

Abstract In today's world, the major geographical areas of India are covered with expansive soil that possess poor strength which cause undue settlements. The soil used in construction has to sustain adverse climatic conditions and different loads. To enhance the engineering parameters of sub grade soil one effective technique is soil stabilisation. In this paper, agricultural wastes like bagasse ash and bagasse fibre are used at varying percentages, like 2% to 8% and 0.5% to 2% respectively are used to treat. To evaluate the properties, laboratory tests like Atterberg limits, compaction properties, unconfined compression, and Soaked California bearing ratio test have been performed on untreated and treated samples. In addition to that micro structural study was conducted using scanning electron microscopy and X-ray diffraction to examine the structure growth of untreated and treated soil. The results indicate that an improvement in maximum dry, California bearing ratio and compressive strength of up to 1.16, 4.55 and 2.55 times are observed with 2 + 0.5% bagasse ash and fibre.

Keywords Bagasse ash · Bagasse fibres · California bearing ratio · Unconfined compressive strength · SEM and XRD analysis

1 Introduction

In civil engineering structures, different types of soil are employed [9]. However, some soil deposits are appropriate for construction in their natural state, while others, such as expansive soils, are unsuitable without treatment. Wetting and drying of a sub grade layer made up of expansive soil causes pavement failure in the form of settling and cracking [14]. The natural ground is either removed or replaced with good quality of soil from other sources. Instead of borrowing soil or removing the poor soil the properties can be enhanced through various stabilisation techniques. Many agricultural and industrial (agro industrial) waste products include rice straw, steel slag, cement kiln dust, fly ash, sugarcane bagasse, blast furnace slag, bagasse fibre, and textiles [8] etc. can be used as these agro-industrial wastes are growing in

J. Harisha Deepthi (✉) · S. Satish
Department of Civil Engineering, VR Siddhartha Engineering College, Vijayawada, India

number, posing a dilemma for disposal land space as well as for resident communities near disposal sites. Sugarcane is the largest crop in the world, yet it is also being wasted in large quantities, so it is being used as a sustainable resource. A study was undertaken throughout our project to use agricultural waste (sugarcane bagasse ash and bagasse fibre) to stabilise expansive sub grade soil.

The by-products of sugarcane combustion in sugar refineries include bagasse ash [4] and bagasse fibre. After sugarcane juice extraction the fibrous material left over is bagasse fibre [2]. It can be used in various applications like bio-fuel as well as in the manufacture of pulp and paper products, and also building materials. When bagasse is burnt, it produces ash with a high silica [3] concentration, and bagasse fibres are moderately strong, cost-effective, and environmental friendly. These materials are used as reinforcement in various geotechnical works, such as pavements, to enhance properties of expansive soil. Utilizing natural ingredients for reinforcing materials is indeed economical and eco-friendly, resulting in a cleaner and greener environment [5].

2 Literature Review

Many researchers have studied the utilisation of waste products in geotechnical applications. Some of the studies on waste-based soil stabilisation are highlighted here.

The stabilisation of sub grade soil utilising rice husk, SCBA, and cow dung ash mixed with alluvial soil was discussed in this article [1]; the unsoaked and soaked CBR, UCS increased. In this study [18], sugarcane bagasse ash, rice husk ash, and ground nut shells of 3–15% are used to improve the sub grade soil properties. Bagasse fibres of 0.25–1% are used by Anees Raja et al. [5]; at 0.75 and 1% fibre content, that UCS increased considerably. The MDD was decreased from 1.46 to 1.38 g/cc, and the UCS improved from 183 to 292 kPa and an increase in OMC at 4 and 6% cement ratio with a 0–10% rise in bagasse ash. This suggests that bagasse ash could be used as an additive in cement-stabilised lateritic soil. In this study [19], red soil was mixed with 1–4% cement content and 2–8% bagasse ash. The plasticity and grain size distribution characteristics of bagasse ash on cement-treated lateritic soil were also investigated in the study. The plasticity values as well as the Atterberg limits were found to be decreasing, while the plastic limit was increasing. Sisal fibres 0.25–1% [12]; the MDD was reduced and the OMC increased by 0.75–1%.

Table 1 Engineering properties of soil

Parameter	Result
Colour	Greyish black
Specific gravity	1.72
Free swelling, %	100
Liquid limit, %	87
Plastic limit, %	38
Plasticity index, %	49
Maximum dry density, kN/m ³	13.04
Optimum moisture content, %	32.14
California bearing ratio, % (soaked)	0.52
Compressive strength, kN/m ²	115.42

3 Materials and Methodology

3.1 Expansive Soil

Soil sample was collected at a depth of approximately 18 m at Tadigadapa 100 feet road, Vijayawada, Krishna district, Andhra Pradesh, and primary tests were performed and results are presented in Table 1.

3.2 Preparation of Bagasse Ash

Sugarcane pulp (Fig. 2) is allowed to air dry and then burnt in a kiln as shown in Fig. 3. The temperature inside the kiln is around 1000 °C. The use of fuels like kerosene was avoided to set the fire so that we could obtain pure bagasse ash. The Deval's abrasion equipment shown in Fig. 4 is used to make the ash finer. 200 g of sample obtained from kiln taken along with initial charge of 5 spheres and 200 revolutions is performed and preceded further by sieving through 425 micron sieve [10] until the weight is constant. The ideal number of charge as well as the revolutions, required to obtain fine ash is found to be 400 revolutions and 5 spheres. The processed bagasse ash in Fig. 1 having a specific gravity of 2.50 is used for experimentation further.

3.3 Bagasse Fibre

The bagasse fibre was procured from Vuyyuru sugar factory, Vuyyuru, Krishna District is allowed for drying in air until there is no change in weight the fibre is

Fig. 1 Bagasse ash**Fig. 2** Bagasse fibre**Fig. 3** Burning of sugarcane bagasse

dried and sieved through a 4.75 mm sieve [5] as shown in Fig. 2. The fibre which was retained on the sieve was used for further experiments.

Fig. 4 Making of fine ash using Deval's abrasion



Table 2 The following is a list of the mixes were used in this research

Blend No	Bagasse ash (BA) %	Bagasse fibre (BF) %	BA + BF (BAF) %
1	0	0	0
2	2	0.5	2 + 0.5
3	4	1	2 + 1
4	6	1.5	2 + 1.5
5	8	2	2 + 2

3.4 Experimental Programme

- Laboratory tests such as Atterberg limits, Swell, dry density, CBR and UCS are performed on base soil according to IS code specifications.
- The stabilization is done by adding bagasse ash [15] percentages of (2, 4, 6, and 8%) and bagasse fibre [16] (0.5, 1, 1.5, and 2%) to untreated soil and then the optimum percentage is determined.
- The % variations where laboratory studies were conducted are shown in the list below (Table 2).

4 Discussions and Observations

4.1 Liquid Limit

The liquid limit varies with the addition of BA % and the results are illustrated in Fig. 5. It can be seen as the proportion of ash increases, the liquid limit increases

Fig. 5 Alterations of liquid limit with the addition of BA

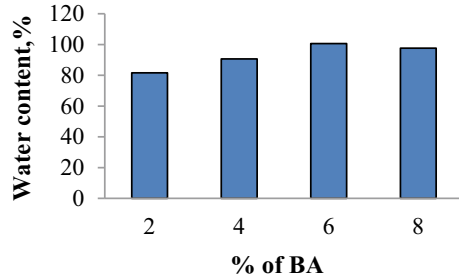
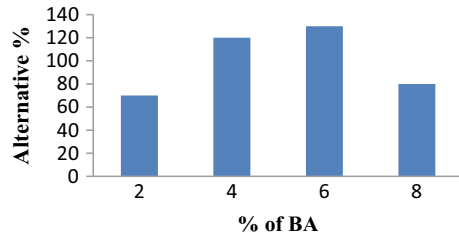


Fig. 6 Effect of free swelling by adding of BA



up to 6% and then decreases. The liquid limit value is reduced from 87% with untreated soil to 81.59% when the soil is amended with 2% BA. The reality is that the interaction produces cementing chemicals, such as calcium silicate with clay minerals, contributes to the BA combination’s overall moisture content reduction.

4.2 Free Swelling

The findings demonstrate that when the bagasse ash concentration increase, the free swell climbed up to 6% before decreasing. The highest reduction occurred when the expansive soil was treated with 2% BA, the free swell value decreased from untreated soil values of 100–70%. This is due to cation exchange, flocculation, and soil particle agglomeration. This is also owing to the volume previously occupied by montmorillonite minerals being replaced by BA (Fig. 6).

4.3 Compaction Characteristics

This test was conducted with varying percentages of BA, BF, and BAF. Firstly, the untreated soil is treated with BA and BF. After getting the optimum percentage of BA, it is mixed with varying percentages of BF. MDD increased and then decreased for all mixes from an untreated soil value of 13.04–13.53 kN/m³, 14.51 kN/m³, and 15.2 kN/m³ with the addition of 2% BA, 1.5% BF, and 2 + 0.5% BAF as shown in

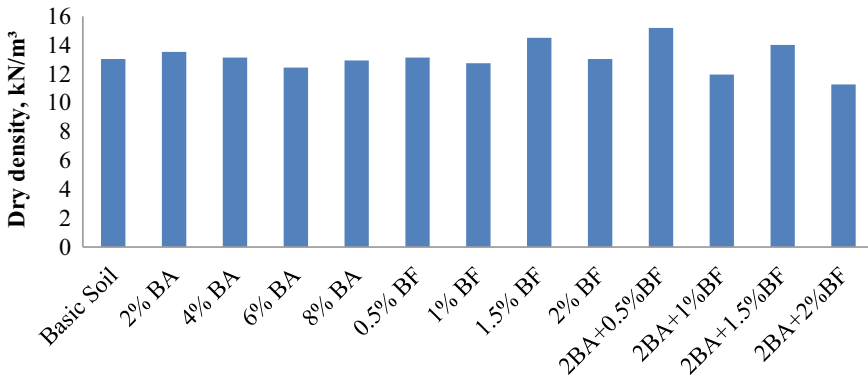


Fig. 7 Effect of MDD on BA, BF and BAF

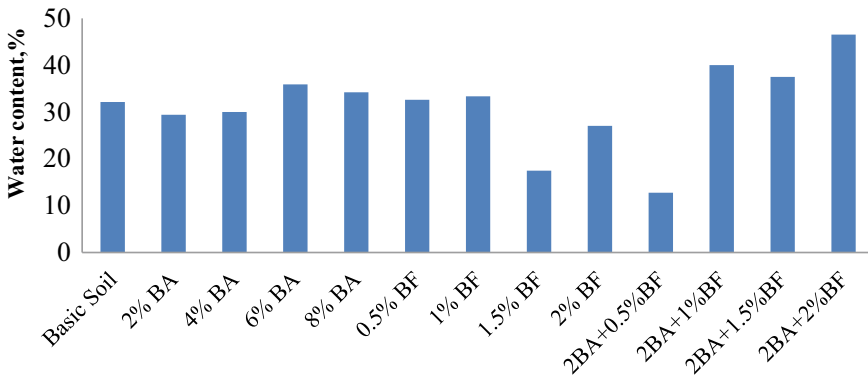


Fig. 8 Effect of OMC on BA, BF and BAF

Fig. 7. The drop in MDD is due to the fact that topsoil has a lower specific gravity than bagasse ash.

The variations of OMC with BA, BF, and BAF are shown in Fig. 8. From the fig, for untreated soil the OMC decreases for all mixtures from a fundamental soil value of 32.14–29.41%, 17.465 and 12.77% with the addition of 2% BA, 1.5% BF and 2 + 0.5% BAF. The OMC decreased and then increased because the ash absorbed more water. So the compaction is easy with wet soil [15].

4.4 California Bearing Ratio

Various percentages of BA, BF, and BAF were used in performing CBR. Figure 9 depicts the results. CBR percentages climbed to 6% BA, 1.5% BF, and 2 + 0.5% BAF values of 6.73%, 1.98%, and 2.37%, respectively, as compared to basic soil.

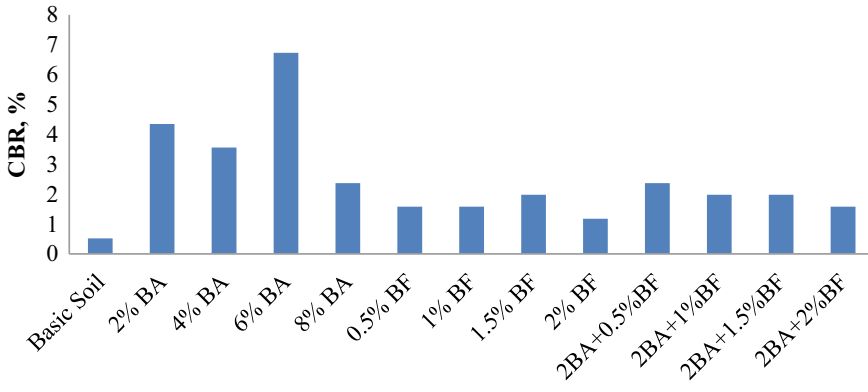


Fig. 9 Effect of CBR on BA, BF and BAF

The pozzolanic interactions of bagasse ash with soil are the cause of this increase in strength [1]. It causes the montmorillonite crystals to aggregate, resulting in increased strength. The lack of calcium needed for the creation of CSH, which is the most important component of strength gain, might be the cause of the bigger gains in strength.

4.5 Unconfined Compressive Strength

Figure 10 shows how UCS values change when BA, BF, and BAF are added to expansive soil. At 2% BA, 1.5% BF, and 2 + 0.5% BAF, treated maximum UCS readings of 163, 362.85, and 294.57 kN/m² were obtained. The contact and locking mechanisms among soil particles, ash, and the fibre surface produced during the

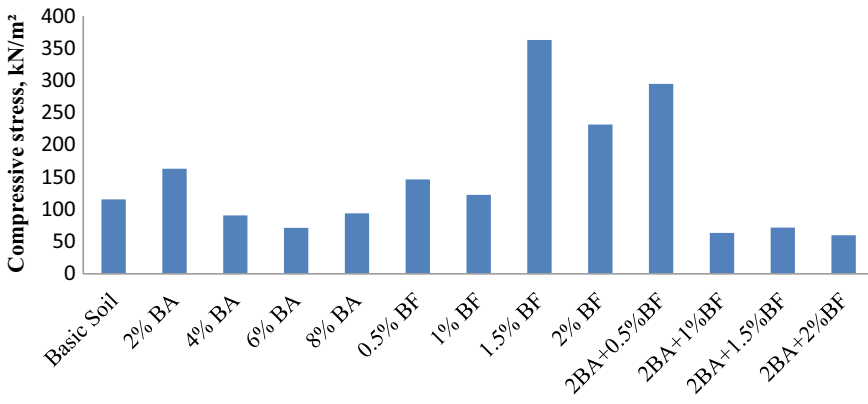


Fig. 10 Fluctuations in UCS with the addition of BA, BF, and BAF

sample preparation by compression load might be related to the strength development of BAF treatment with expansive soil. The combination of BAF boosts the soil's strength significantly.

4.6 Performance Improvement

Performance ratios are computed as follows

$$R_t = \text{Treated with admixture/Untreated value} \quad (1)$$

$$R_{tm} = \text{Treated MDD value with admixture/Untreated MDD value} \quad (2)$$

$$R_{to} = \text{Treated OMC value with admixture/Untreated OMC value} \quad (3)$$

$$R_{tc} = \text{Treated CBR value with admixture/Untreated CBR value} \quad (4)$$

$$R_{tu} = \text{Treated UCS value with admixture/Untreated UCS value} \quad (5)$$

4.6.1 Presentation of Liquid Limit and Free Swell

The performance improvement ratio for liquid limit and free swell, R_t . The R_t was found to increase from 0.93 to 1.15 and then decrease with BA. For free swell, the R_t was found to increase from 0.7 to 1.3 and then decrease with BA.

4.6.2 Presentation of OMC and MDD

The performance improvement ratio for MDD, R_{tm} and OMC, R_{to} . The R_{tm} was found to decrease from 1.03 to 0.95 and then increase; the R_{fo} increased by 0.91–1.11 times with BA. The R_{tm} was found to increase from 1.00 to 1.11 and then decrease. The R_{fo} decreased from 1.01 to 0.54 times with BF. The R_{tm} was found to decrease from 1.16 to 0.86; the R_{fo} increased from 0.39 to 1.44 times with BAF.

4.6.3 Presentation of CBR

The performance improvement ratio for CBR, R_{tc} . The R_{tc} was found to increase from 8.36 to 12.94 and then decrease with BA. The R_{tc} was found to increase from

3.03 to 3.80 and then decrease with BF. The R_{tc} was found to decrease from 4.55 to 3.03 times with BAF.

4.6.4 Presentation of UCS

The performance improvement ratio for UCS, R_{tu} . The R_{tu} was found to decrease from 1.41 to 0.61 and then increase with BA. The R_{tu} was found to increase from 1.26 to 3.14 and then decrease with BF. The R_{tu} was found to decrease from 2.55 to 0.51 times with BAF.

4.7 XRD and SEM Analysis

The SEM and XRD analyses done on optimal percentage samples using a high revolution scanning microscope at a 10 kV excitation wavelength are shown in the figures above. All normal and modified samples taken were dried in an oven for 24 h prior to testing. Several SEM pictures were acquired at various magnifications to assess sample micro structural change as well as the development of cement-based compounds in the soil properties (Figs. 11, 12, 13, 14, 15 and 16).

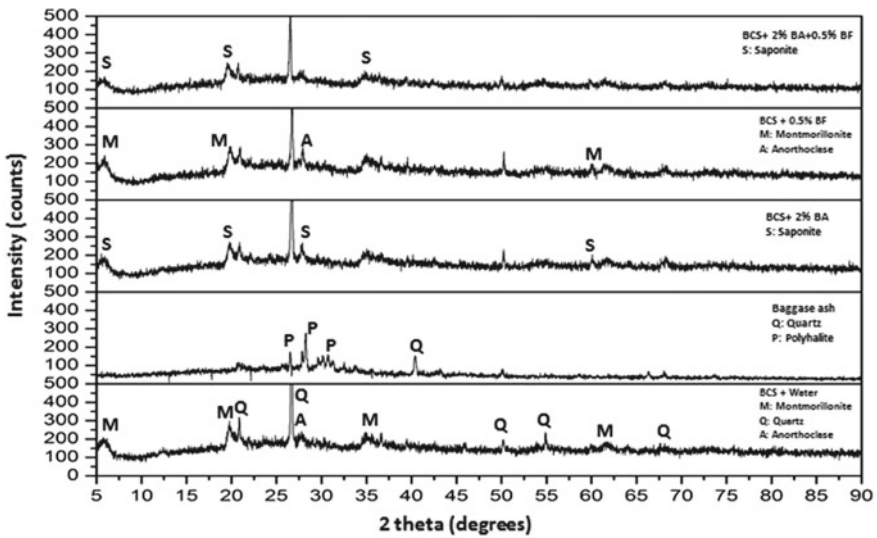
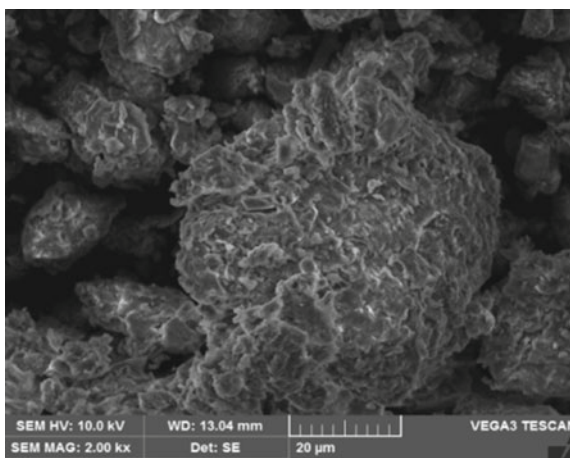
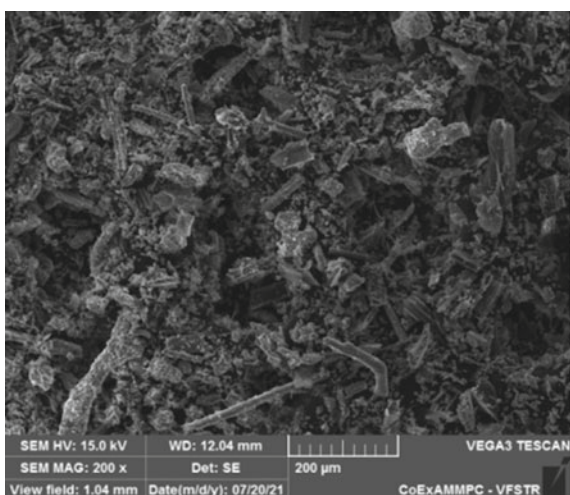


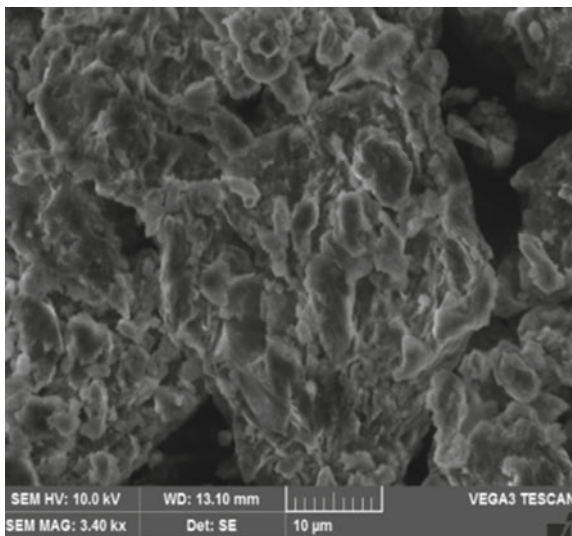
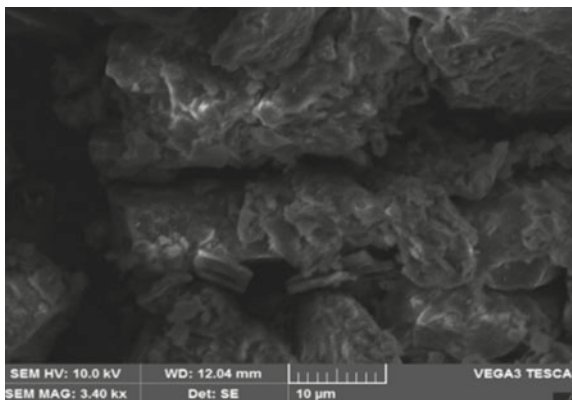
Fig. 11 Comparison of XRD with Basic soil, BA, 2% BA, 0.5% BF, 2 + 0.5% BAF

Fig. 12 Basic soil**Fig. 13** BA

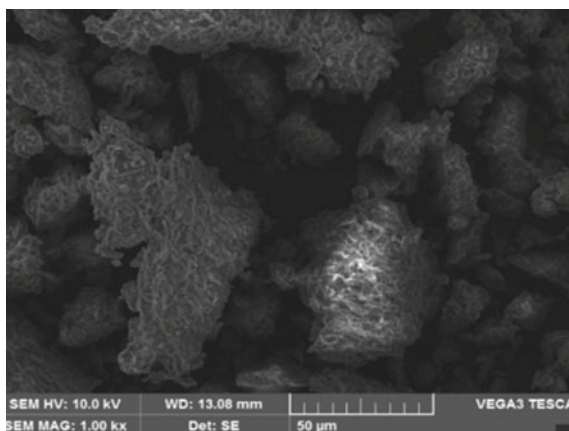
5 Conclusions

The addition of BA and BF to a soil increased its properties, according to the results of the tests. From the research, the findings could be derived.

- The liquid limit and free swell of the treated sample decreased by 6.21 and 30% with 2% BA.
- The MDD increased by 3.6, 11.27, and 16.56% at 2% BA, 1.5% BF, and 2 + 0.5% BAF.
- The CBR value increased by 1197, 280, and 355% at 6% BA, 1.5% BF, and 2 + 0.5% BAF.

Fig. 14 Soil + 2% BA**Fig. 15** Soil + 2 + 0.5% BAF

- The UCS values increased by 41.2, 214, and 155% at 2% BA, 1.5% BF, and 2 + 0.5% BAF.
- We obtained maximum fine percentage of ash at 400 revolutions and 5 balls in the Deval's abrasion equipment.

Fig. 16 Soil + 0.5% BF

References

1. Yadav AK, Gaurav K, Kishor R, Suman SK (2017) Stabilization of alluvial soil for sub grade using rice husk ash, sugarcane bagasse ash and cow dung ash for rural roads. *Int J Pavement Res Technol* 254–261
2. Kharade AS, Suryavanshi VV, Gujar BS, Deshmukh RR (2014) Waste product bagasse ash from Sugar Industry can be used as stabilizing material for expansive soil. *Int J Res Eng Technol* 3(3)
3. Sabat AK (2012) Utilization of bagasse ash and lime sludge for construction of flexible pavements in expansive soil areas. *Int J Res* 17
4. Manikandan AT, Moganraj M (2014) Consolidation and rebound characteristics of expansive soil by using lime and bagasse ash. *Int J Res Eng Technol* 3(4)
5. Raja A, Kumar A (2018) Use of bagasse as natural fibre for soil reinforcement. *Int J Sci Res Sustain* 1(1)
6. Lima A, Varum H, Sales A, Neto V (2012) Analysis of the mechanical properties of compressed earth block masonry using the sugarcane bagasse ash. *Constr Build Mater* 35
7. Abd El-Halim AA (2017) Image processing technique to assess the use of sugarcane pith to mitigate clayey soil cracks. *Soil Tillage Res* 169
8. Bahurudeen A, Santhanam M (2015) Influence of different processing methods on the pozzolanic performance of sugarcane bagasse ash. *Cem Concr Compos* 56:32–45
9. Ikeagwuani CC, Nwonu DC (2019) Emerging trends in expansive soil stabilisation a review. *J Rock Mech Geotech Eng* 11:423e440
10. Hasan H, Dang L, Khabbaz H, Fatahi B, Terzaghi S (2016) Remediation of expansive soils using agricultural waste bagasse ash. In: *The 3rd international conference on transportation geotechnics*
11. Danso H (2017) Properties of coconut, oil palm and bagasse fibres: as potential building materials. In: *3rd international conference on natural fibres*. *Procedia Eng* 200:1–9
12. Prabakara J, Sridhar RS (2002) Effect of random inclusion of sisal fibre on strength behaviour of soil. *Constr Build Mater* 16(2)
13. Geotech J (2013) Unconfined compression strength of reinforced clays with carpet waste fibres. *Geoenviron Eng*
14. Kiran RG, Kiran L (2013) Analysis of strength characteristics of black cotton soil using bagasse ash and additives as stabilizer. *Int J Res Eng Technol* 2(7)
15. Osinubi KJ, Bafyau V, Eberemu AO, Adrian O (2008) Bagasse ash stabilization of lateritic soil

16. Dang LC, Fatahi B, Khabbaz H (2016) Behaviour of expansive soils stabilized with hydrated lime and bagasse fibres. In: The 3rd international conference on transportation geotechnics
17. Wei L, Chai SX, Zhang HY (2011) Mechanical properties of soil reinforced with both lime and four kinds of fibre. *Constr Build Mater* 172
18. Chittaranjan M (2011) Agricultural wastes as soil stabilizers. *Int J Earth Sci Eng*
19. Abdullahi M (2007) Evaluation of plasticity and particle size distribution characteristics of bagasse ash on cement treated lateritic soil. *Leonardo J Sci*
20. Osinubi KJ (1998) Permeability of lime-treated lateritic soil. *J Transp Eng* 124(5):465–469

Improving the Geotechnical Properties of Silty Sands by Using GGBS and Coir Fibre



G. Hima Bindu and V. Mallikarjuna

Abstract The construction of any infrastructure over a weak or cohesion less soil, which experiences, low shear strength, high compressibility, differential settlements, low stiffness, and ductility is one of the key constraints faced by geotechnical engineering. In case high rise of buildings and pavements built on cohesion less soils, improving the load bearing capacity of soil is critical. In the past, various methods like stabilisation, ground improvement techniques, and the use of reinforcement were used to improve the load bearing capacity of soil. The laboratory output of Silty sands admixed with GGBS and reinforced with coir fibres is investigated in this paper. The Silty sands have been considered by using percentages of GGBS such as 5, 10, 15, 20% and 2, 4, 6, 8% of coir fibres. The optimum values increased at 15% of GGBS and 6% of coir fibres, and the effect of curing time was considered for 3, 7, 14 days to investigate the compressive strength through unconfined compression test. To pavements, California bearing ratio test is performed under soaked and unsoaked conditions. In this paper, the key use of GGBS and Coir fibres is for improving soil properties and utilising the industrial waste material and natural waste material to reduce cost effective process.

Keywords Silty sands · GGBS · Coir fibres · Unconfined compression test · C.B.R

1 Introduction

Nowadays, there is a significant expansion of roadways and railways taking place all over the world, and one of the main technical and economic engineering challenges is preparing for suitable pavement thickness for construction. Most problems with Silty sands are caused by liquefaction. The type of soil most prone to liquefaction is one where deformation resistance is mobilised by particle friction. Liquefaction is

G. Hima Bindu (✉)

Geotechnical Engineering, Department of Civil Engineering, VR Siddhartha Engineering College, Vijayawada, India

V. Mallikarjuna

Department of Civil Engineering, VR Siddhartha Engineering College, Vijayawada, India

more common in saturated clean sands and Silty sands with a relative density of less than 50%. “In dry soils, liquefaction will not occur Liquefaction occurs when high excess pore water pressures are induced under cyclic earthquake loading, resulting in severe loss of strength and stiffness”. Various materials are used to control problems and develop the geotechnical qualities of soils such as fly ash, pond ash, lime, coal ash, alluvium, natural pozzolans, polymers, acids, and different types of fibres are admixed with silty sands. The investigation in this paper was conducted on ground granulated blast furnace slag and coir fibres. The GGBS consists silica fume as part of binder and it develops the cohesion between particles. The by-product of steel production, ground granulated blast furnace slag, is now frequently utilised as a partial replacement for conventional Portland cement. It has a lower carbon footprint than OPC and produces very little sulphur dioxide and nitrogen oxides. Therefore, repurposing this waste product can help without negatively impacting the environment. The use of GGBS material is beneficial, increases the soil’s resistivity whilst also acting as a binding agent and promoting particle cohesion. Coir fibre is abundant, non-toxic, low in density, and inexpensive. It gains in strength, durability, and static performance, and there are no catastrophic breakdowns.

1.1 Review of Literature

Using different engineering approaches, a variety of materials are added to improve the qualities of soil based on past study. Palm fibres are used by Marandi et al. [2]; to assess strength and ductility. Sliding failure strength, rather than rupture failure strength, was employed to manage the specimen’s breaking phenomenon. MDD and OMC both decrease by 0.5 and 1%. The permanent and robust stresses, as well as the resilient modulus, are investigated by Mahipal Singh et al. [1]; Experiments using 30% fly ash and 70% sand mix were repeated several times. In their study, Joyanta Maity et al. [3]; address the benefits of employing natural fibres like jute, coir, and sabia grass composite as a subbase road material. For all types of sand, the value of MDD decreases as fibre is added, but the value of OMC increases. The maximum fibre length for all-natural fibres with a C.B.R of 1.5% is 5 mm. Nithin et al. [7]; investigated those silty sands used coir fibres and fly ash in different percentages as 5, 10, 15, 20% and 0.5–5% done and the optimum value is found in fly ash is 15 and 4% coir and UCS improvement is 20%, 31%, and 26% respectively. Singh et al. [8]; tested local silty sand with various concentrations of coal ash and coconut fibre. OMC values rise as coal ash levels rise, whilst MDD values fall when coir, 80% soil, and 20% coal ash are added. Naderabbasi et al. [21]; investigated the effects of lime and natural pozzolan on silty sands using 20 treatments in which lime was added at a rate of 0, 1, 3, 5, 7%. Increases OMC and decreases MDD. Smitha et al. [24]; the experimental investigation was carried out by using agar biopolymer treated on silty sands to undrained shear strength improvement in the soils. A series of triaxial tests were done. According to Sargent et al. 2020; activated slag and alluvium are handled

by soil stabilisation and gain stiffness through hydration and pozzolanic reactions, with a considerable proportion of the clay minerals.

2 Materials

2.1 Soil

The soil was gathered from the environs of Vijayawada (AP). According to the Indian standard soil classification, it is classed as Silty sand (SM). The soil sample is sieved and sedimentation analysis is done in accordance with IS:2720 (Part 4)-1984. The sample's water-content dry density relationships are determined using the standard proctor test, index properties, UCS, and CBR, and the findings are given in Table 1.

2.1.1 GGBS

The Ground granulated blast furnace slag used in this investigation was obtained from the Vadeswaram VNS ready mix plant, which is located near Vijayawada (AP). It's made by cooling molten blast furnace iron slag in water or steam, which results in a glassy, granular product that's dried and ground into a fine powder. It is a pozzolanic material that is non-crystalline and slightly cementitious material. The physical and chemical properties are described in detail (Tables 2 and 3).

2.1.2 Coir

Coconut fibres are used to make coir. Coir fibre is a natural fibre obtained from the coconut husk. Coir is the most dense and durable of all commercial natural fibres.

Table 1 Properties of the soil

S. No	Properties	Value
1	Classification as per Indian Standard	SM
2	Specific gravity (G)	2.63
3	Optimum moisture content (%)	12.90
4	Maximum dry density (g/cc)	1.59
5	Silt size (0.002–0.075 mm)	48%
6	Sand size (0.075–4.75 mm)	37.8%
7	Clay size (<0.002 mm)	14.2%
8	C.B.R (%) (Unsoaked)	14.0
9	C.B.R (%) (Soaked)	10.30
10	Typical name of soil classification	Silty sand

Table 2 Physical properties of GGBS

Ingredient	Unit of measurement	Requirement as per 16,714-2018	VNS-GGBS
Specific gravity	2.85–2.95	Not mentioned	2.9
Fineness	400–600 kg/m ²	320	380
Bulk density	1050–1375 kg/m ³	Not mentioned	1200
Colour	–	Not mentioned	Off white

Table 3 Chemical properties of GGBS

Ingredient	Percentage mass	Requirement as per 16,714- 2018
Calcium oxide Cao%	40	–
Silica SiO ₂	35	–
Alumina Al ₂ O ₃	10	–
Magnesia (MgO)	8	MAX 17
Glass content %	95- - 100	MIN 85

The ability to make durable items with a low disintegration rate is a fundamental benefit. Coir fibre ropes from the early nineteenth century have been discovered. The exceptional strength of coir fibre has been the primary cause of rope manufacture for generations. It is made up of white fibres, whereas fully ripe coconuts are made up of brown fibres. In this study, the coir is gathered from the industrial region of Vijayawada, and it is cut into little pieces of around 2 cm, with each single fibre having a diameter of 0.25 mm and taken as 2, 4, 6, 8% and admixed with Silty sands.

3 Experimental Work

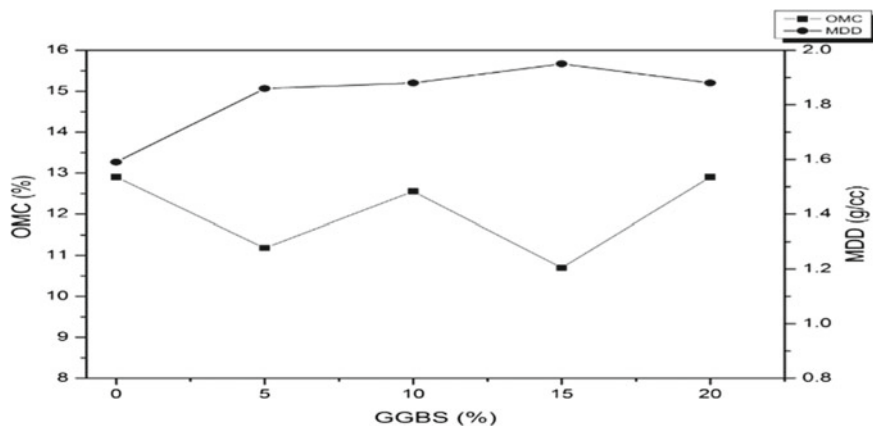
California Bearing ratios, standard proctor tests, and unconfined compression testing are all done individually with different % of GGBS 0, 5, 10, 15, 20, and Coir fibres 2, 4, 6, 8. The tests are carried out in parallel, with the best GGBS % taking precedence. The GGBS contains silica fume as part of the binder, and its self-cementing properties can develop particle cohesion in a wide range of stabilisation applications. Under dry conditions, the Coir is coupled with these GGBS and Silty sands, with intriguing results.

4 Compaction Test

The association between optimum moisture levels and maximum dry density was determined in the current study using a traditional proctor test with a % of 0, 5, 10,

Table 4 Results of standard proctor test with GGBS and coir fibres separately

GGBS (%)	OMC (%)	MDD (g/cc)	COIR (%)	OMC (%)	MDD (g/cc)
0	12.90	1.59	0	12.90	1.59
5	11.18	1.86	2	14.89	1.27
10	12.55	1.88	4	10.69	1.57
15	10.70	1.95	6	16.67	1.48
20	12.90	1.88	8	11.97	1.32

**Fig. 1** Graph for standard compaction test with GGBS of all % mixed in Silty sands

15, and 20. For all % of enhanced maximal dry density, the ideal percentage of GGBS was 15%. Furthermore, the optimum maximum dry density is increased from 2, 4, 6, and 8–4% when coir fibres are mixed with Silty sand. The following are the findings and graphs of standard proctor test with GGBS and Coir fibre (Table 4 and Figs. 1, 2).

Various percentages of Coir fibres are blended using the optimal value of the standard proctor test with GGBS and Silty sands at 15% GGBS, and moisture content increases as the proportion of Coir fibres increases. Simultaneously, the maximum dry density in this paper decreases by combining the two materials reports stated. GGBS = G, COIR = C (Table 5 and Fig. 3).

5 Unconfined Compression Test

The UCS test's main purpose is to swiftly determine the compressive strength of fine-grained soils that have enough cohesion to allow testing in an open setting. The UCS is the load per unit area that a cohesive soil's cylindrical specimen bears when

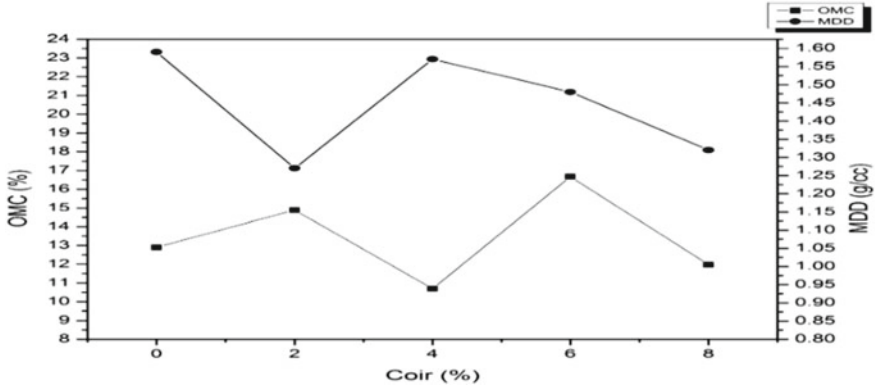


Fig. 2 Graph for standard proctor test with coir fibres mixed in Silty sands

Table 5 Results of standard proctor test with coupled GGBS and coir fibres

Percentage (%)	Optimum moisture content (%)	Maximum dry density (g/cc)
15% GGBS	10.70	1.95
15% G + 2% C	14.43	1.37
15% G + 4% C	14.59	1.49
15% G + 6% C	18.70	1.60
15% G + 8% C	22.41	1.42

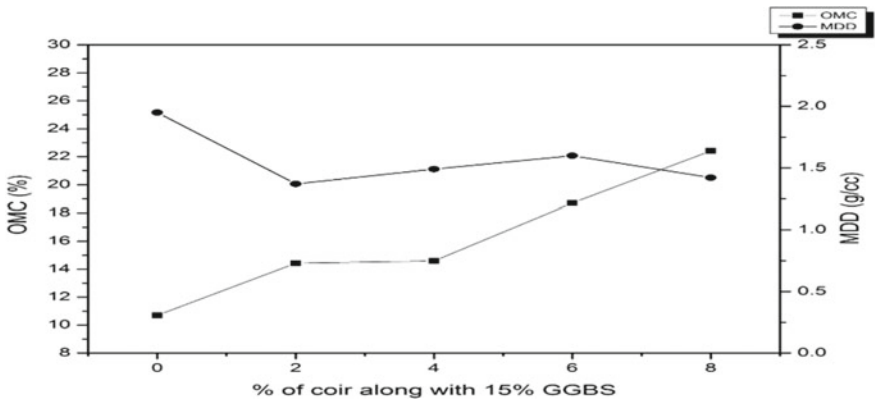


Fig. 3 Graph for compaction test with 15% GGBS and all % of coir fibres

compressed. The specimen is made with L/d ratios of 76 mm and a diameter of 38 mm. The proving ring is used to measure the applied load, whilst dial gauges are used to measure the deformation. The % of maximum is calculated by taking the 5, 10, 15, and 20% of GGBS. The % with the highest strength is regarded as the ideal,

and work is continued by combing Coir percentages based on the associated OMC and MDD values.

6 Results and Analysis

6.1 Effect of Curing with GGBS

For various amounts of GGBS, UCS is performed, and the specimens are cured for 3, 7, and 14 days, respectively. The specimens are made up of GGBS and Silty sands in various proportions. The cementing property of GGBS and the presence of silica and alumina, which reacted during the curing period of the sample. Therefore, the strength increased and also the presence of silica, Alumina improves particle bonding. The UCS values increased as the percentage of GGBS increased up to 15%, after which the UCS values declined by 20%. The data and graph clearly show that the curing period of 3, 7, 14 days causes an increase in strength (Table 6 and Fig. 4).

Table 6 Results of curing with GGBS in 3, 7, 14 days

GGBS (%)	3 days	7 days	14 days
5	0.42 kg/cm ²	0.52 kg/cm ²	0.59 kg/cm ²
10	0.54 kg/cm ²	0.77 kg/cm ²	1.26 kg/cm ²
15	0.948 kg/cm ²	1.36 kg/cm ²	2.059 kg/cm ²
20	0.785 kg/cm ²	0.904 kg/cm ²	1.811 kg/cm ²

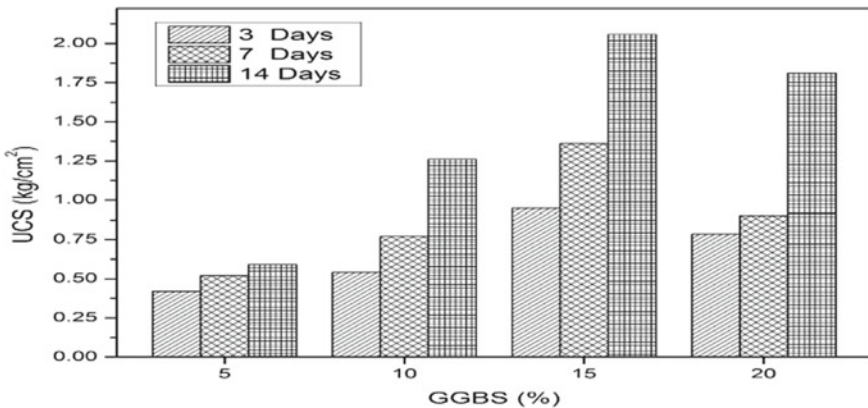


Fig. 4 Stress strain relationship with GGBS and Silty sands

Table 7 Results of curing with coupled GGBS and coir in 3, 7, 14 days

COIR (%)	3 days	7 days	14 days
2	5.99 kg/cm ²	7.60 kg/cm ²	9.27 kg/cm ²
4	8.52 kg/cm ²	8.90 kg/cm ²	10.64 kg/cm ²
6	10.62 kg/cm ²	11.22 kg/cm ²	12.686 kg/cm ²
8	9.84 kg/cm ²	10.26 kg/cm ²	11.43 kg/cm ²

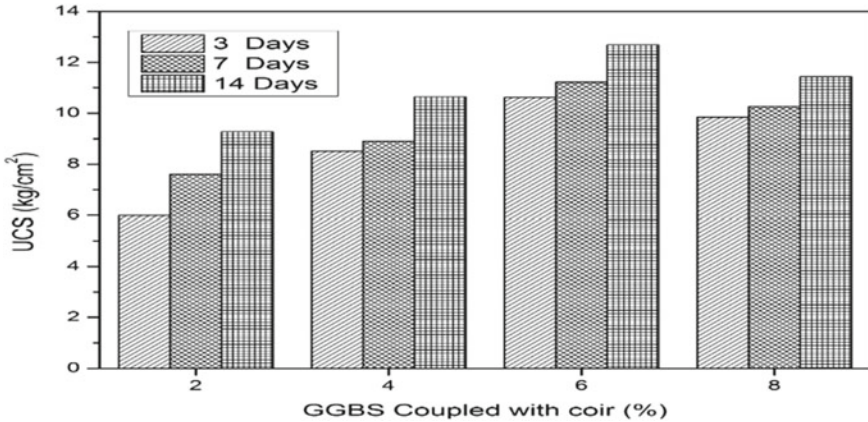


Fig. 5 Unconfined compression test with coir fibre and Silty sands

6.2 Effect of Curing with Optimum GGBS and Coir Fibre

By incorporating coir fibres, which were cut into 0.5 cm pieces and mixed as a %, the strength increases. As the % of coir fibres increases, the strength increases. When compared to GGBS, the addition of coir fibres increases strength by up to 6%, but the relationship between stress strain and strength decreases by 8% through the specimens. It has been discovered that the elasticity of coir fibres increases during the curing process, resulting in increased strength. Furthermore, when 6% coir is combined with GGBS and silty sands, the coir increases compressive strength through UCS after curing for 3, 7, 14 days (Table 7 and Fig. 5).

7 California Bearing Ratio

The California bearing ratio test is a penetration test used to assess the subgrade strength of roads and pavements as well as the thickness of pavements by component layers. The cylindrical mould measures 150 mm in diameter and 175 mm in height. C.B.R is performed with 3 layers of 56 blows in both dry and wet situations. In

Table 8 Results of C.B.R with GGBS in soaked and unsoaked conditions

GGBS (%)	Unsoaked (%)	Soaked (%)
0	14.0	10.36
5	24	15.23
10	27.35	18.6
15	32.23	22.35
20	28.42	19

Table 9 Results of C.B.R with coupled GGBS and coir fibre in soaked and unsoaked condition

Optimum GGBS + Coir	Unsoaked (%)	Soaked (%)
15% G	32.23	22.35
15% G + 2% C	16.74	13.23
15% G + 4% C	18.89	17.24
15% G + 6% C	26.49	24.23
15% G + 8% C	22.38	18.58

drenched conditions, the soaking lasts for four days. Various percentages of GGBS were tested independently, with the optimum percentage of GGBS mixed with coir being taken at the same time. A total of 16 samples were tested in both soaked and unsoaked situations. Strength does not improve when coir is added to the GGBS whilst it is unsoaked, but it does improve when it is soaked, increasing from 22.35 to 24.23%. However, in soaked condition increased this may be due to increase in elasticity of the coir fibres. According to studies, from Singh et al. [8] inclusion of coal ash with 0.25% coir fibre the C.B.R values increases from 14.6 to 19.4%. Whether due to coir have a water-retaining property and GGBS has a binding nature and a higher water absorbance property, the problem of liquefaction can be managed by increasing strength in wet situations. The water content of the coir is absorbed, and GGBS develops cohesion between the Silty sands. As a result, natural and industrial waste can be used to reduce pavement thickness without increasing the cost of stone aggregates and without negatively impacting the environment, lowering the cost of pavements. According to UCS and C.B.R, the optimum percentages for Silty sands in this paper are 15% GGBS and 6% coir (Tables 8, 9 and Figs. 6, 7).

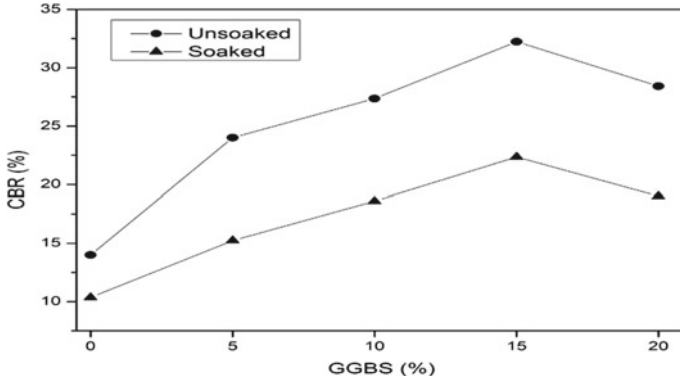


Fig. 6 C.B.R test with coupled GGBS on Silty sands under soaked, unsoaked condition

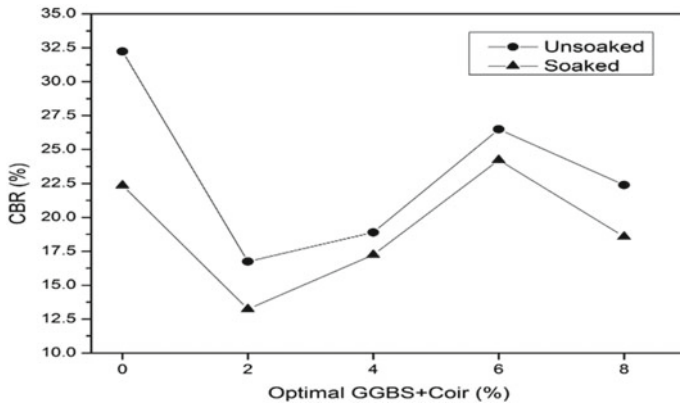


Fig. 7 C.B.R test with coupled GGBS and coir fibres on Silty sands under soaked, unsoaked conditions

8 Conclusions

The current research represents laboratory experiments conducted on Silty sands on the addition of GGBS, an industrial waste, and Coir fibre, a natural waste, for the strength properties of subgrade pavements. The conclusions are highly encouraging.

- i. The findings of the compaction tests show that optimum moisture levels rise with the GGBS percentage increased whereby maximum dry density was reduced from observations.
- ii. According to the stress strain relationship, adding GGBS increases strength; the maximum value for Silty sands (SM) is 2.059 kg/cm². Simultaneously, the mixing of Coir fibres results in a significant raise in unconfined compression strength of up to 12.686 kg/cm².

- iii. The results of the strength and pavement thickness tests, as reported by C.B.R, show that adding GGBS increases strength in unsoaked conditions, whilst adding coupled GGBS and Coir fibres increases strength in wet conditions by 22.35–24.23%. It is critical to enhance the soaking state so that the materials may be used to reduce the thickness of the pavements.
- iv. The inclusion of binder and coir fibres increased relative strength and penetration resistance by up to 15% GGBS and 6% Coir fibres, resulting in the most significant improvement in UCS and C.B.R. More than these percentages, it is found that by adding materials, the strength of the structure could deteriorate.
- v. It has been determined that the best percentages of GGBS and Coir fibres for Silty sands (SM) in this current paper based on experimental work are 15% GGBS and 6% Coir fibre. These can be utilised for flexible pavements with low economic cost and without environmental impact. As a result, GGBS and coir fibres are utilised to minimise pavement thickness, and there is also a control in liquefaction damage under saturated circumstances, which may not affect these pavements are concluded.

References

1. Chauhan MS, Mittal S, Mohanty B (2008) Performance evolution of silty sand subgrade reinforced with fly ash and fiber. Elsevier Sci Direct Geotext Geomembr 26(5):429–435
2. Marandi SM, Bagheripour MH, Rahgozar R, Zare H (2008) Strength and ductility of randomly distributed palm fibers reinforced silty sand soils. Am J Appl Sci (3):209–220
3. Maity J, Chattopadhyaytopadhyay BC, Mukherjee SP (2012) Behavior of sands mixed randomly with natural fibers. EJGE 17(2012), Bund.L
4. Verma D, Gope PC, Shandilya A, Gupta A, Maheshwari MK (2013) Coir fiber reinforcement and application in polymer composite: a review. J Mater Environ Sci 4(2)
5. Bongarde US, Shinde VD (2014) Review on natural fiber reinforcement polymer composite. Int J Eng Sci Innov Technol 3(2)
6. Vibhakar NN, Natha S (2014) Study of the effect of coir fiber reinforcement on the strength parameters and CBR value of clayey soil. Int J Eng Res Tech 3(4)
7. Nithin S, Sayida MK (2014) Stabilization of silty sand using fly ash and coir fiber. Research conference paper, 18 May 2014
8. Singh SK, Arif SM (2014) Inclusion of coconut fiber in soil mixed with coal ash. Int J Res Eng Tech 3(11)
9. Maurya S, Sharma AK, Jain PK, Kumar R (2015) Review on stabilization of soil using coir fiber. Int J Eng Res 4(6):296–209
10. Anggraini V, Asadi A, Huat BBK, Nahazanan H (2015) Performance of chemically treated natural fibers and lime in soft soil for the utilization as pile supported earth plat form. Int J Geosyn Ground Eng
11. Akinyemi BA, Omoniyi TE, Adeyemo MO (2016) Prospects of coir fiber as reinforcement in termite mould clay bricks. Actatechnol Agric (3)
12. Darsana P, Abraham R, Joseph A, Jasheela A, Binuraj PR, Sharma J (2016) Development of coir fiber cement composite roofing tiles. Procedic Technol 169–178
13. Prabhakar K, Reddy KR (2016) Strength characteristics of coir fiber and fly ash on soil. Int J Eng Sci Comput 6(10)
14. Alex S, Vinu T (2016) Effect on resin on strength characteristics of thonnakkal clay. Int J Eng Res Appl 6(7)-part (2)

15. Mohan NS, Shettar M, Bhat R (2017) Fabrication and investigation of epoxy resin-based glass fiber-coconut fiber hybrid composite material. In: International conference on mechanical and automobile engineering (ICMAE), 21 December 2017
16. Giridhar V, Kumar PSP, Naveena G (2017) Behavior of black cotton soil using soil tech MKIII polymer as a stabilizer. IJIRSET 6(2)
17. Bansal S, Ramachandran M, Raichurkar P (2017) Comparative analysis of bamboo using jute and coir fiber reinforced polymeric composites. Elsevier Material Today 4:3182–3187
18. Bhagat VK, Prasad AK, Lal Sri Vastava AK (2017) Physical and mechanical performance of luffa coir fiber reinforced epoxy resin-based hybrid composites. IJCTET 8(6)
19. Kumar MB, Kumar TK (2017) Strength characteristics of expansive soils using epoxy resin and silty soil. IJSR 6(8)
20. Liu J, Feng Q, Wang Y, Zhang D, Jihong W, Kanungo DP (2018) Experimental study on unconfined compressive strength of organic polymer reinforced sand. Int J Polym Sci 8
21. Abbasi N, Mahdih M (2018) Improvement of geotechnical properties of silty sand soils using natural pozzolan and lime. Int J Geo-Eng 9. Article no 4
22. Kumar BTH, Sanjay SJ (2018) Study on effect of different sizes of footings resting on treated coir mat and coir fiber reinforced sand. IJSTE 4(11)
23. Rishap AS, Amrutha B, Padmanaban I, Sri Vidya V (2018) Subgrade modification using natural coir fibers. IJLEMR 3(2)
24. Smitha S, Swamy KR, Skreerthi D (2019) Triaxial test behaviour of silty sand treated with agar bio polymer. Int J Geotech Eng
25. Kuppusamy J, Krishnamurthy M (2020) Effect of polymer resins on geotechnical properties of black cotton soil. IJRTE 8(5)

Mode Choice Model Development for the Effect of Road Transport Service on Air Travel Demand—A Case Study from Jumla to Nepalgunj, Nepal



Vidya Rajesh, Yagendra Dharala, Prabesh Adhikari, and Sathees Kumar

Abstract Air transport was the only mode of transportation to reach Nepalgunj from Jumla before the construction of highway. Nowadays people can choose either air transport or road transport according to their interest. An attempt has been made to study the effect of air trips due to operation of highways in study area and develop mode choice model for the effect of road transport service on air travel demand from Jumla-Nepalgunj. The study area is Jumla Highway, linking Surkhet, Dailekh, Kalikot, and Jumla districts. The study follows the analytical and descriptive approach considering the responses of concerned key personnel. The logit model was developed and observed that large number of trip makers were students who have low income. Privacy is minor factor when compared to cost, time, health, comfort, and safety while choosing transport modes. Increasing ages and income of the passengers is contributing toward the increasing number of the plane users. The model was developed with 95% confidence interval. The study has concluded that there is no effect of road transport service on air travel demand from Jumla to Nepalgunj as the growth rate of air traffic is nearly equal before and after operation of road.

Keywords Air travel demand · Air transport · Mode choice · Travel characteristics · Travel preference

V. Rajesh (✉)

School of Civil Engineering, SASTRA Deemed University, Tanjavur, India
e-mail: vidya@civil.sastra.edu

Y. Dharala

Infrastructure Development Office, Mugu, Ministry of Physical Infrastructure Development, Surkhet, Karnali Province, Nepal

P. Adhikari

Civil Aviation Authority of Nepal, Kathmandu, Nepal

S. Kumar

Department of Civil Engineering, Mohammed Sathak Engineering College, Kilakarai, Tamil Nadu, India

1 Introduction

Transportation system in Nepal is yet to be well developed as it is constituted by rugged mountains and valleys. The Road transport is considered to be cheap mode and dominated transport [11]. Roads and airports continue to play an important role in Nepal's transport infrastructure and economic development [3]. Air transport is a product itself that can be delivered as intermediate product for other Industries [2]. Airways was the only mode of transportation to reach Nepalgunj from Jumla before the construction of major feeder road. After the construction of road people can choose either plane or bus according to their interests. Jumla district had access to Nepalgunj only through Jumla Airport till 2010 AD. Now this district is connected to Nepalgunj by highway. However, the demand for both modes has never been studied. It is known fact that the economics of air service does not permit frequent services if there is insufficient demand. Without understanding the traveler's needs and preferences, upgrading of transportation system will be wastage of resources. Introducing a new access mode (e.g., road) can substantially change the access mode shares. Transportation between Jumla to Nepalgunj is divided into highway and air transport.

The main challenge facing is the lack of number of passengers due to newly constructed highway which will curtail the airlines schedules from Jumla to Nepalgunj. This problem is made worse by declining aviation passengers and makes unsustainable to aviation industry of Jumla district.

1.1 Objectives of the Study

This study was to assess the development of mode choice model for the effect of road transport service on air travel demand from Jumla to Nepalgunj. The specific objectives are as follows,

- (i) To study the existing transportation situation prevailing in area of study and explore its travel characteristics.
- (ii) To find the preferred modes of transport from Jumla to Nepalgunj and examine the survey of travel preference of trip mode.
- (iii) To explore the factors affecting the mode choice and develop mode choice model from Jumla to Nepalgunj.

2 Literature Background

Road transport in Nepal occupies major share of passenger and freight movement with 11.8 km per 100 km². The deficiency of which leads to lesser economic growth [13]. At present the Strategic Road Network has altogether 12,494 km (51% blacktop,

13% gravel and 36% earthen roads) [9, 10]. Among modes of all transport, highest growth rate of aviation is found to be highest. Annual global growth rates of air passengers were approximately 6% in the 1990s and had values of 8% in the 2008 [16]. Average growth of vehicles is about 5.6% worldwide from 1970 to 2008 [7].

2.1 Trend of Air Transport in Nepalgunj Airport

Nepalgunj Airport is the regional hub airport of the mid-western region of Nepal. Plane service started in this airport in 1961 AD. This airport also has a night landing facility. Presently it has flights to Kathmandu, Humla, Jumla, Rara, Dolpa. The runway of this airport has 1554 m in length and 30 m in width. The growth of air passengers from 2009 to 2018 AD was found to increase about 13.17% annually [4].

2.2 Comparison Between Air Transport and Road Transport

Transportation systems are affected by special constraints. Usually, the land transport infrastructures are built where there are fewer physical impediments [15]. The high-value transport, that deteriorates over time, is particularly effective by air.

2.3 Effect of Socio-demographic Variables on Mode Choice

Many previous works have emphasized that the selection of mode of travel and trip frequency are affected by socio-demographic variables [6].

2.4 Factors Affecting Mode Choice

Typical mode choice attributes like cost, time, transfers made it easier to use in travel models. [5, 14] Investigated those sound systems with devices of safety coupled with navigation costs more. Multilogit Models Developed [1].

3 Study Area

The area for this study is Jumla, (one out of ten districts), a mountainous district of Karnali province. The topographical setup includes hills, plains, rivers, and mountains. The district is divided into one municipality and seven rural municipalities.

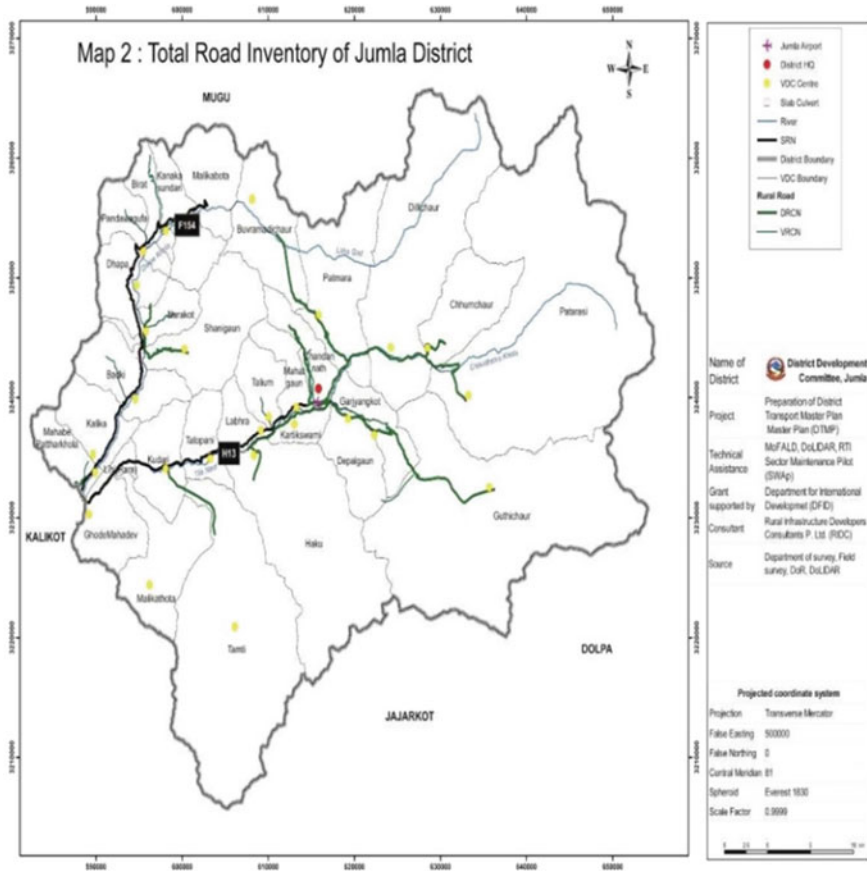


Fig. 1 Area of study [8]

Karnali highway is 233 km starting from Birendranagar, surkhet and connected to NPJ by Ratna Highway (113 km). The Karnali Region is the most remote and least developed zone in Nepal. The Karnali Highway is already considered to be one of the most dangerous roads in the world by many, though is important connection between Nepal’s two regions. Figure 1 depicts the study area [8].

3.1 Sample Size Determination

$$D = n \div [1 + (\tilde{n} \div N)] \tag{3.1}$$

where, N is a total number of populations; D is a sample size from finite population; n is a sample size from infinite population; (Eq. 3.1) [12]. The sample size from

infinite population can be calculated using the following Eq. 3.2

$$n = S^2 / se^2(\bar{x})^2 \tag{3.2}$$

where,

S^2 is the variance of the population element.

$se(\bar{x})$ is the standard error of sampling population.

For 95% confidence level and 10% error the sample size can be calculated as a function of coefficient of variation CV.

$$Se(\bar{x}) = 0.1 \mu / 1.96 = 0.051 \mu$$

$$\bar{n} = \left(\frac{S}{.051 \mu} \right)^2 = 384 CV^2 \tag{3.3}$$

As the value of n is very small compared with N thus the ratio of (n/N) is very small. So, the sample size of finite population can be taken as the same value of n . For $CV = 1$ the minimum sample size is 384 as per Eq. 3.3. Questionnaires were distributed and about 401 numbers responded which is more than the minimum sample size obtained [12]. This study uses random sample method.

3.2 Primary Data

Collected data includes both quantitative and qualitative data. The questionnaire survey with the people of study area were conducted and key informant interviews with the relevant agencies. The questionnaire survey was carried out with 401 people in Khandabari, Jumla, and Chainpur of Jumla district. All these places are accompanied by the major settlement of Jumla district. The questionnaire had divided into three parts:

- Demographics, the questioner item correspondent to village they live, age, gender, job, family size, and income.
- Travel behavior, Travel mode, frequency, travel cost, and travel time are the trip characteristics considered in study zone giving importance to travelers' choice for their modes for trips from study zone to Nepalgunj. Added variables are: travel time, comfort, health status, security, and trip privacy.
- The major information from the key informant survey includes the existing transportation situation of Jumla district, travel trend before and after the operation of highway, status of existing road conditions as well as the views and opinions for the future of the airline and road transport service in Jumla.

3.3 Secondary Data

Air traffic data between Jumla Airport and Nepalgunj Airport was collected directly from section of Nepalgunj Airport civil aviation office. Road transport data was collected from the transport entrepreneurs of the Jumla district. SPSS software was used in the study for analysis and development. The dependent variables and independent variables are mentioned below:

- (i) Dependent variable:
 - Plane
 - Bus
- (ii) Independent variables:
 - Gender: Male and Female
 - Age
 - Income
 - Education: Slc, Inter, Bachelor, Master and No study
 - Profession: Agriculture, Student, Business and Service
 - Trip frequency: Once a year and more than one time in a year
 - Easiness to get plane ticket: Easy and Difficult
 - Convenient season: winter and any time
 - Trip purpose: Study, Business, visiting doctors/clinic and Visiting friends/relatives

The equation is as given in 3.4

$$\begin{aligned}
 U = & a0 + a1[\text{Gender}] + a2[\text{Age}] + a3[\text{Income}] + a4[\text{Education}] \\
 & + a5[\text{Profession}] + a6[\text{Trip frequency}] \\
 & + a7[\text{Easiness_to_get_plane_ticket}] \\
 & + a8[\text{Trip Purpose}] + a9[\text{Convenient Season}]
 \end{aligned}
 \tag{3.4}$$

4 General Analysis of Data

4.1 Gender of Respondents

It is found that about 72.82% of the respondents are male and 27.18% are female. It indicates that male is the active trip maker than female. Majority of respondents are male because of the social belief that females should not leave home and males should leave home to manage their family. Male are comparatively educated, creative, and more skillful than females.

4.2 Age of Respondents

It was found that respondents' % for age 25 or less, age between 26 and 35 years, 36–45 years, 46–55, and more than 55 were 14.46%, 38.91%, 26.18%, 17.8%, and 2.65% of the total samples, respectively. The large percentage of respondents lies in the age category of 26–35 because of higher education, visiting doctors/clinics, visiting friends/relatives, and business.

4.3 Job of Respondents

Regarding the nature of respondent's job, 24.69%, 3.49%, 19.95%, 1.25%, 2.5%, 42.39%, 2%, 3.73%, pertains to agriculture, business, civil service, technician, NGO, students, politician and trekking, respectively.

4.4 Average Monthly Income of Respondents

No income is about 54.36% of the whole sample. Similarly, 9.48% respondents have NRS 10,000.00–20,000.00, 9.23% respondents have NRS 20,000.00–30,000.00, 10.22% people have monthly income less than NRS 10,000.00 and 16.71% of respondents have NRS above 30,000.00. The results show the majority of respondents are a student and some respondents so they have no monthly income and they are depending on their family income for their trip.

4.5 Level of Education

The analysis shows that 38.9% of them are from SLC, which means that majority of respondents are SLC level. 36.2% are from intermediate level, 16.96% from bachelor, 4.24% from masters, and 0.7% respondents are from above the master's level, and close to 2.99% have no education.

4.6 Family Size of Respondents

The collected data is categorized into three categories. The result shows that the majority of people have a family size between 4 and 6 members which represents about 57.1% of the whole sample. While the people with a family size bigger than seven members represent about 36.5% of the sample. The average family size of

the respondents is about 6. Most of the people in Jumla district have joint families of large size. The majority of people have a family size between 4 and 6 members because people have low education and lack of awareness and knowledge.

4.7 Travel Characteristics in Influence Area

Travel characteristics suggest how individuals and households may affect travel patterns on the basis of questionnaire survey. This describes the annual family trips to Nepalgunj, purpose of trip to Nepalgunj, mode of transport use, ticket availability, and willingness to pay for bus and airlines fair charge and travel trend before and after operation of highway.

4.8 Number of Family Trips to Nepalgunj

One-fifth of the respondents (21.44%) in the sample never go to Nepalgunj. About 12.95% of respondents make more than three trips to Nepalgunj in a year 24.2% visit once in a year, 21.2% travels 2 times in a year, 16.45% travels 3 times in a year, and 3.75% of the respondents visit Nepalgunj every month.

4.9 Purpose of Trip to Nepalgunj

The distribution of respondents' purpose of trip to Nepalgunj shows that 25.43% of the respondents go to Nepalgunj for higher study, 8.72% for service, 11.22% for business, 13.96% for visiting relatives and friends, 9.22% represent mixed and 21.48% were non-responsive.

4.9.1 Easiness to Get Plane Ticket

The distribution of the easiness to get plane tickets by the respondents shows that about 7% stated that it was easy, 49.88% responded to be neither easy nor difficult, 28.90% said it was difficult, 7.73% responded that they did not know and 6.0% people did not respond the questions.

4.9.2 Convenient Season to Reach Nepalgunj by Bus

Response showed that the people (74.31%) expressed that the convenient time to travel by bus is winter season. Majority of passengers seem to prefer to travel in

winter season by bus due to the bad condition of road in rainy season. 3.49%, 6.73%, 12.46%, and 3% preferred to travel in monsoon, dashai, any time, respectively. Close to 3% were non-responsive. In winter season people have free time so they visit their friends/relatives and visit doctors/clinics.

4.9.3 Travel Trend from Study Area to Nepalgunj

More than 50% of the passengers 52.1% used to go Nepalgunj once in a year before operation of highway followed by twice a year 20.5%, 4.5% thrice a year, 0.6% more than three times in a year, and 22.3% of the respondents did not respond the question.

4.10 Important Factors Choosing Transportation Modes

Firstly, respondents stated that comfort, health status, and safety were the most important when choosing a plane. Half of the people think that comfort (56.2%), Health status (52.8%), and safety (51.9%) are the major factors for preferring planes. This is particularly relevant on highway when travelers have to go through rough pavement for continuous day and night travel without having sound sleep. Obviously, travel cost influences choice, however, only 39.5% of respondents think that it is of high importance for plane while only 21.2% of people think travel cost is highly important for bus. Around half of the respondents had expressed that the cost factor is important for bus mode (53.2%) and plane (45.1%). One of the key informants said that the people having high economic status usually go to Nepalgunj by plane. The actual travel cost from Jumla to Nepalgunj by airlines was about NRS 5500.00 (Source: Yeti airlines rate, 2018 AD) and NRS 1800.00 for bus transport (Jumla to Surkhet = NRS 1500.00 and Surkhet to Nepalgunj = NRS 300.00). It indicates that the travel cost for plane is more than the travel cost of road users. Each respondent was asked to express his/her importance of travel time for each mode. They could choose from the three options, less importance, importance, and high importance. The traveling times for plane is high importance expressed by 47.6% compared with the bus mode expressed by 25.4%. Similarly, 26.8% people have given less important to travel time for bus and 14.0% for plane. People have to travel continuously for 24 h from Jumla to Nepalgunj.

As per Table 1, acceptance of high importance of comfort factors in plane is more than bus. 56.2% of respondents think that comfort factor is of high importance for choosing plane while only 28.7% respondents feel high importance for bus. More people (30.5%) choose comfort as less important for bus compared to 3.7% choosing it for plane. There was another question about comfort in which two-third people (71.3%) prefer plane, giving consideration to the convenience. Another major factor affecting mode choice is health status. Health status is of high importance (52.8%) for choosing plane while 21.5% people think it is high important for choosing bus mode. As in comfort factors, more people have chosen health status as less important

Table 1 Important factors choosing transportation modes

Factors	Less importance (%)		Importance (%)		High importance (%)	
	Bus	Plane	Bus	Plane	Bus	Plane
Travel cost	25.6	18.0	53.2	45.1	21.2	39.5
Travel time	26.8	14.0	47.8	38.4	25.4	47.6
Comfort	30.5	3.7	40.8	40.1	28.7	56.2
Health status	28.0	3.6	50.5	44.1	21.5	52.8
Safety	32.4	8.2	42.9	39.9	24.7	51.9
Privacy	40.1	36.5	36.2	37.1	23.4	26.4

for choosing bus mode compared to plane (3.6%). Key informants had also said that people usually go to Nepalgunj by plane for health checkups. As per Table 1, 51.9% of people thought that safety factor is the high importance and 8.2% people thought that it is less important for choosing plane. About 24.7% of people considered that it is of high importance and 32.4% felt that it is less important for choosing the bus mode. There was another question regarding safety concerns in which two-thirds of people (75.3%) considered that the plane is safe mode. Privacy factor is less important than other factors for choosing modes. Only 26.4% people (for plane) and 23.4% people (for bus) thought that privacy is of high importance for choosing modes. More people considered (36.5% for plane and 40.1% for bus) this factor is less important for choosing modes.

5 Model Development

The model is found to be significant at the confidence interval of 95% and it is reliable with R^2 values of 0.684, and 0.931, respectively. Likelihood Ratio Test and R^2 value test for model and estimation of parameters are presented in Tables 2 and 3, respectively.

The utility equations of model for Plane users is presented in Eq. 5.1

$$\begin{aligned}
 U_{plane} = & -4.113 - [0.839 * Gender] + [0.076 * Age] + [0.029 * Income] \\
 & - [2.638 * Easiness\ to_get_plane_ticket] - [2.659 * Trip_frequency] \\
 & - [1.778 * Convenient_season] - [1.679 * Purpose(study)] \\
 & + [1.046 * Purpose(business)] + [0.494 * Purpose(visiting\ doctor/clinic)]
 \end{aligned}
 \tag{5.1}$$

Table 2 Likelihood ratio test and R^2 value test for model

Step	-2 log-likelihood	Cox and Snell R^2	Nagelkerke R^2
1	46.598	0.684	0.931

Table 3 Estimate of various parameters

	B	S.E	Wald	df	Sig	Exp(B)	95% C.I. for EXP(B)	
							Lower	Upper
							Gender (1)	-0.839
Age	0.076	0.32	5.707	1	0.047	1.079	1.014	1.148
Income	0.029	0.058	15.014	1	0.045	1.023	1.000	1.000
Trip_Purpose			2.818	3	0.039			
Trip_Purpose (study)	-1.679	1.473	1.299	1	0.044	0.039	0.299	96.117
Trip_Purpose (business)	-1.046	0.946	1.225	1	0.038	0.848	0.446	18.171
Trip_Purpose (visiting doctor/clinic)	0.494	1.038	0.227	1	0.034	0.610	0.080	4.664
Easiness_to_Get_PlaneTicket (1)	-2.638	0.798	10.942	1	0.001	0.071	0.015	0.341
Convenient_Season (1)	-1.778	0.696	6.524	1	0.011	0.169	0.043	0.661
Trip frequency (1)	-2.659	0.759	12.279	1	0.046	0.072	0.016	0.310
Constant	-4.113	1.940	4.498	1	0.034	0.016		

5.1 Validation of Model

The final model needs to be validated against the data that were not used to develop the model. Hence for the validation process, the data from travel preference survey (nearly 30%) is taken. The value of “p” in the above equation determines the probability of the using plane. A cut point of 0.5 is used to separate the plane users from the bus users. This means that the value of “p” below 0.5 is termed as a bus user and the value of “p” above 0.5 is termed as plane users. A total of 150 users were used out of which 49 users failed which means that the accuracy of the model is 67.33%.

5.2 Result from Model

5.2.1 Age Effect

The exponent of the coefficient of the variable “Age of users” is 1.079 which means that the ratio of the odd of the plane users to the odd of the bus users is 1. 079. This shows that the odd of the plane users increased by 7.9%.

5.2.2 Income Effect

The exponent of the coefficient of the variable “Age of users” is 1.023 which means that the ratio of the odd of the plane users to the odd of the bus users is 1.023. This shows that the odd of the plane users increases by 2.3%. This can also be stated as for every 10 years increase in the age of the users, the odd of the plane users increases by 23%.

5.2.3 Effect of Easiness to Get Plane Ticket

Since this is the categorical variable and it has two categories, one is used as a base category and another one is stated on the basis of this base category. In this case, the “difficult” is used as the base variable. The exponent of the coefficient of the dummy variable “easy” is 0.071 which means that the odd of the plane user is 92.9% difficult.

5.2.4 Effect of Trip Purpose

Since this is the categorical variable and it has four categories, one is used as a base category and others are stated on the basis of this base category. In this case, the “visiting friends/relatives” is used as the base variable. The exponent of the coefficient of the dummy variable “study” is 0.039 which means that the odd of the plane users for the “study” is 96.1% less than that of the plane users for “visiting friends/relatives”. The exponent of the coefficient of the dummy variable “business” is 0.848 which means that the odd of the plane users for the “business” is 15.2% more than that of the plane users for “visiting friends/relatives”. The exponent of the coefficient of the dummy variable “visiting doctors/clinic” is 0.61 which means that the odd of the plane users for the “visiting doctors/clinic” is 39% more than that of the plane users for “visiting friends/relatives”.

5.2.5 Effect of Trip Frequency

Since this is the categorical variable and it has two categories, one is used as a base category and another one is stated on the basis of this base category. In this case, the “once a year” is used as the base variable. The exponent of the coefficient of the dummy variable “more than one time in a year” is 0.072, which means that the odd of the plane user is “more than one time in a year” 92.8% less than “once a year”.

5.2.6 Effect of Convenient Season

Since this is the categorical variable and it has two categories, one is used as a base category and another one is stated on the basis of this base category. In this case,

“any time” is used as the base variable. The exponent of the coefficient of the dummy variable “winter” is 0.169 which means that the odd of the plane user in “winter” is 83.1% less than in “any time”.

5.2.7 Gender Effect

Since this is the categorical variable and it has two categories, one is used as a base category and another one is stated on the basis of this base category. In this case, the “female” is used as the base variable. The exponent of the coefficient of the dummy variable “male” is 0.332 which means that the odd of the plane user by “male” is 66.8% less than “female”.

6 Conclusions

During the period of collection of primary data and general analysis of primary and secondary data, few findings have been made which are summarized as follows.

- Economic status has been significantly enhanced in this zone after the operation of highway. But the result from the studies shows that the present situation of road maintenance is very poor due to lack of adequate resources and weak management.
- They expressed that winter season is the preferred time than rainy season for bus users due to bad condition of road in monsoon period. Also expressed that road transport is unsafe and dangerous and air transport has not fixed scheduled.
- Male is the active trip maker than female in this study area. Though students have low income and sometimes no income, however, they are the frequent trip maker than other professionals for better education. Bus users’ decrease as the age increases because old people prefer to have comfortable and safe modes of transport which are not possible in road transport.
- Travel cost for plane is more important factor so that rich people frequently use it. Study shows that low-income people have less importance for time factor. Comfort is the major factor while choosing modes. Two third of the people think that they choose plane, giving consideration to comfort. Health is another major factor in choosing transport modes. Usually, old people and patients use plane for health checkups. Study has concluded that privacy is minor factor compared with other factors while choosing transport modes.
- Both the increasing ages of the passengers and that of the income is contributing toward the increasing number of the plane users.
- The chances of plane users are the highest by “business” followed by the “visiting doctors/clinic”, “visiting friends/relatives”, and “study”, respectively.

Number of air passengers has been increased as previous trends after the operation of road. Study has concluded that there is no effect of road transport service on air

travel demand from Jumla to Nepalgunj as the growth rate of air traffic is nearly equal before and after operation of road.

References

1. Ashalatha R, Manju VS, Zachari AB (2013) Mode choice behavior of commuters in Thiruvananthapuram City. *J Transp Eng* 139(5). [https://doi.org/10.1061/\(ASCE\)TE.1943-5436.0000533](https://doi.org/10.1061/(ASCE)TE.1943-5436.0000533)
2. Braathen S (2011) Air transport service in remote region. Leipzig, Molde University Collage, Norway
3. CAAN (2012) Civil aviation report 2011–2012. CAAN Publication Civil Aviation Authority of Nepal. Available via <https://caanepal.gov.np/publication/caan-report>. Accessed 14 Jan 2020
4. CAAN (2018) Civil aviation report. Civil Aviation Authority of Nepal. Available via <https://caanepal.gov.np/publication/caan-report>. Accessed 14 Jan 2020
5. Choo S, Mokhtarian PL (2004) What types of vehicles do people drive? The role of attitude and lifestyle in influencing vehicle type choice. *Transp Res Part A: Policy Pract* 38(3):201–222. <https://doi.org/10.1016/j.tra.2003.10.005>
6. Curtis C, Perkins T, Perth WA (2006) Travel behaviour: a review of recent literature. *Urbanet* (3)58
7. Dargay J, Gately D, Sommer M (2009) Vehicle ownership and income growth, worldwide: 1960–2030. *Energy J* 143–170
8. DTMP (2013) District Transport Master Plan. Department of Local Infrastructure Development and Agricultural Roads (DOLIDAR) District Development Committee Mugu. Available via <https://dccmugu.gov.np/wp-content/uploads/2016/06/DTMP-Final-Report-Mugu.pdf>
9. DoLIDAR (2015) Local Road Network (LRN) Department of Local Infrastructure Development and Agricultural Road. Available via http://archive.rapnepal.com/sites/default/files/reportpublication/lrn_review_report_dfid_gon_format.pdf
10. DoR (2018) Strategic road network of Nepal. HMIS Unit: Department of Road
11. Gajurel DP (2011) Structure-performance relation in Nepalese banking industry. *Int Proc Econ Develop Res* 2:25–31
12. Kish L (1965) Survey sampling. Wiley, New York
13. MoPIT (2015) Ministry of physical infrastructure and transport. Available via http://mopit.gov.np/noticefile/Notice_inviting_REOI_for_RSSP_1558853388.pdf
14. Outwater M, Sana B, Perdous N, Woodford B, Lobb J (2014) TCRP report 166: characteristics of premium transit services that affect choice of mode. Transportation Research Board. Washington D.C. (201 National Cooperative Highway Research Program (NCHRP) special report 2884)
15. Rodrigue J-P (ed) (2013) *The geography of transport systems*, 3rd edn. Routledge, London, 416pp. ISBN: 978-0-415-82254-1
16. Whiteleg J (2009) *Aviation: the social, economic and financial*. Ashden Trust, London

Analyzing the Demand and Pattern of Electric-Rickshaw Trips: En Route to Sustainable Travel Option



Sandeep Singh and S. Moses Santhakumar

Abstract Electric rickshaws' operation is an environmentally sound and clean mode of transportation. University campuses have always been favored locations to emphasize sustainability and to help remodel society's transportation systems. This study utilizes the electric rickshaws' trip data collected in the National Institute of Technology Tiruchirappalli (NITT), India, using perception and origin–destination surveys via in-person questionnaires. The study explores the travel demand and travel pattern of electric rickshaw riders inside the NITT campus. The aim of the study is to evaluate the various factors influencing the travel demand and pattern of electric rickshaws'. Also, an attempt is made to optimize the location of charging stations by minimizing the dead kilometre constraint. We find a higher demand for the electric rickshaws within the campus' proximity, mainly for educational trips with an average trip frequency of 10 minutes. Results of the study imply that majority of the trip destination lies near the academic and administrative areas, where the charging stations need to be located. The findings from the survey would provide essential inputs for the planning of electric rickshaw services. Additionally, the study results can be used as a case-study example for strategically placing the charging stations in an educational campus. This type of transport mode would help promote sustainable mobility and accessibility within the campus.

Keywords Electric rickshaw · Dead kilometre · Charging station · Sustainability

1 Introduction

The present exploitation of natural resources for fossil fuels requirements has led humanity to look into an impending energy crisis. Such looming calamity would cause near fatality for a developing country such as India [1]. A significant chunk

S. Singh (✉) · S. M. Santhakumar

Transportation Engineering and Management, Department of Civil Engineering, National Institute of Technology Tiruchirappalli, Tiruchirappalli, Tamil Nadu, India

S. M. Santhakumar

e-mail: moses@nitt.edu

of this supply goes to the transport sector in petrol and diesel emissions. India's urban traffic is dominated by fossil-fuel based two-wheelers and passenger cars, while Electric Vehicles (EVs) represent a tiny share. Among the different vehicles, public buses, taxi fleets, two-wheelers, and three-wheelers are expected to be the first adopters of EVs in India.

Electric Rickshaws (e-rickshaw) are eco-friendly battery-operated three-wheelers with better economies and lower operational cum maintenance costs. This e-rickshaw does not emit toxic pollutants into the air during operation and does not have any tailpipe. These vehicles have gained popularity among Indian rickshaw drivers and commuters. They resemble the pedal-powered cycle-rickshaw of yore, but instead of pedals, they run on rechargeable lead-acid batteries. The retrofitted e-cycle rickshaws or e-rickshaw come with an accelerator, a headlight, a tail-light, indicators, and even windshields. There is an exponential increase in adopting EVs as a supplant to conventional vehicles, especially inside university campuses [2]. The tendency of colleges and universities to embrace newer technologies to benefit future generations makes them an opt fit for implementing EVs. In light of the above circumstances, the National Institute of Technology Tiruchirappalli (NITT), India, adopted three e-rickshaws' operation on a pilot basis to cater to the travel demand of students. Due to the positive feedback received from students and faculty, the institute is planning to adopt an e-rickshaw on campus. The study regarding the travel demand, travel patterns, the optimal location of charging stations, and so on, have been looked at in detail in this study.

Furthermore, as EVs demand increases, due emphasis is required for developing the infrastructure, i.e., charging stations for the EVs. A scientific approach to decide on the number and location of the charging station is necessary to have a sustainable and economic system. Hence, this study aims to provide a systematic approach to optimize the location of the charging station and identify the number of EVs required to meet and satisfy the demand with due importance to users' perception regarding modal preferences.

2 Review of Literature

Numerous studies were done on stages of transportation planning, selectively on trip generation, trip attraction, modal split, and route assignment. As per research, the trip demand and pattern in the university campus are distinct compared to the trip pattern in a city. Understanding the trip characteristics and optimum location of charging stations is vital for solving EVs' operation in university campuses.

Residential campuses have complete control over their transport network and hence can initiate policies to offset the negative impacts of the increasing population of students and staff. Carlos [3] surveyed pedestrian and bicycle characteristics in the university campuses in the USA to display the importance of modal shift. He concludes that educational places are the best places to practice sustainability. Rastogi and Doley [4] studied the trip characteristics inside a university campus in India. A

paper questionnaire survey was conducted, and the results were analyzed to develop trip generation models for educational and recreational trips. They noted a difference in the perception of e-rickshaw usage by a student and other users. Nisha and Samir [5] described the evolution of e-rickshaws based on the design concepts that can be accepted socially to reduce human drudgery. Yousefi et al. [6] stated that finding the optimal routes to reach the destination is considered a significant challenge. They have proposed a mechanism that includes two phases to investigate the optimal route choice from an Origin and Destination (OD) matrix. Inês et al. [7] presented research on the charging station locations for e-vehicle in Lisbon, Portugal. The methodology adopted a maximal covering model for optimizing the demand. The model was useful for the planning of electric mobility systems. Christina et al. [8] proposed a methodology considering the integrated design for allocating charging infrastructure.

Chandra and Minal [9] addressed different perspectives of issues faced by EVs in the Indian scenario. The significant problems include the intermittent availability of electricity and the high upfront cost of EVs in its wider adoption. The study discussed the prospects in the EVs market in the Indian economy. This literature review summarizes that the main barrier to the adoption of EVs is the economic and socio-technical barriers to consumers. Nevertheless, these findings pertain to a specific region or a city. Only limited studies have been conducted on planning the flexible routes of EVs inside the educational campus, especially in India. The research related to the trip pattern and demand and the optimum location of charging depots still needs to be explored, which is carried out in this study.

3 Study Methodology and Data Collection

Competitive methodologies with a significant focus on travel patterns in the NITT campus are incorporated to get accurate output. The first type of analysis carried out is on the perception survey data. It elaborates the trip characteristics, which explains the demand, frequency, and use of e-rickshaw by a person. The second type of analysis is based on the Origin–Destination (OD) survey. The research focuses on the trips generated, trips attracted, and trip characteristics. The second analysis is the zoning of the study area. Further, the link flows are identified in each route to implement e-rickshaw inside NITT-Campus. The overview of the methodology is represented in Fig. 1.

The data analysis was done using Power BI, Microsoft Excel, and Arc GIS softwares to obtain the major routes, dead kilometres, location of charging stations, and the number of e-rickshaw required.

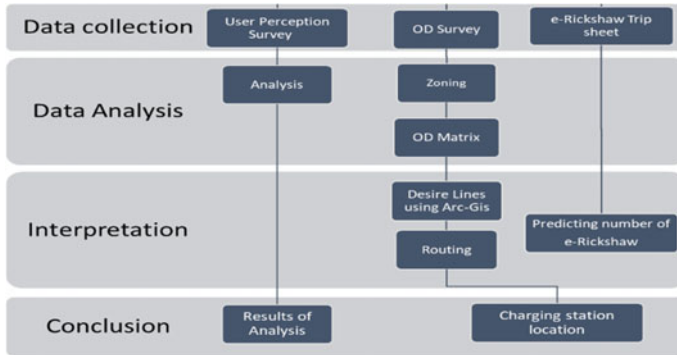


Fig. 1 Study methodology flow chart

3.1 Study Area Characteristics

The NITT campus is considered the study area. NITT has 800 acres of land cover. It is located on the National Highway (NH-83). The campus had educational buildings, labs and lecture rooms, libraries, residential areas, and hostels. The sports complex, NSO playground, and SAC building encase most of the sports and extracurricular activities on the campus. The whole campus is well connected through proper roads that make access to any part of campus feasible via electric vehicles. The research work consists of the analysis of operation of an e-rickshaw designed by Transvahan Technologies India Pvt Ltd. A typical image of the e-rickshaw being operated in the NITT is shown in Fig. 2.



Fig. 2 Picture depicting e-rickshaw operation in NITT campus

3.2 *Detail Surveys for Data Acquisition*

The data collection stage involves conducting perception surveys to collect information regarding preference in implementation of e-rickshaw inside the NITT campus and the factors which can possibly affect it. It also involves the OD survey conducted through an in-person questionnaire method. The e-rickshaw trip sheet is used to collect information regarding the trips and kilometres traveled per day. Different types of surveys are conducted as a part of data acquisition; namely, perception survey, OD survey, and the data were also collected using the e-rickshaw trip datasheet. A sample size of 4% of the population is fixed for the OD survey. The OD survey data is collected from 240 campus residents. The data is collected from 4:00PM to 9:00PM to cover the travel data from the entire day. Additionally, the perception survey is done on campus by circulating Google forms. A total of 700 data entries were obtained through Google form survey over a week, contributing to 10% sample data from the entire population. The in-person questionnaire survey method is adopted for this purpose. The e-rickshaw trip sheet questionnaire containing the fields related to the origin, destination, e-rickshaw occupancy, etc., are used to survey e-rickshaw drivers.

4 Data Analysis and Results

4.1 *Analysis of Perception Survey Data (E-rickshaw Demand Over Time)*

Perception analysis is used to find the level of satisfaction of the passenger while using a particular mode of transport [10]. The analysis is based on the 548 (78%) male students and 151 (22%) female residents of the NITT campus. The time-series graph shows the demand for e-rickshaw through a typical weekday which is illustrated in Fig. 3. The survey revealed that males and females show a similarity in peak hour demands. A peak in demand is observed at 08:00–09:00 and 12:00–14:00. This peak demand corresponds to the commencement and ending times of classes. The demand is significantly low during class hours (09:00–12:00 and 14:00–17:30). However, the evening hours (post-class hours) see a slight increase in the demand corresponding to the rise in shopping and recreational trips.

4.1.1 *Frequency of Service and Rate Per Trip*

The raw data from the Google form response is cleaned to change the data type from text to number to carry out further analysis. Figure 4 represents the stacked bar chart for the frequency of e-rickshaw services required by users based on gender. The analysis shows that close to 60% of users prefer the services to be provided at intervals of every 10 min, irrespective of gender. Around 22% of the respondents

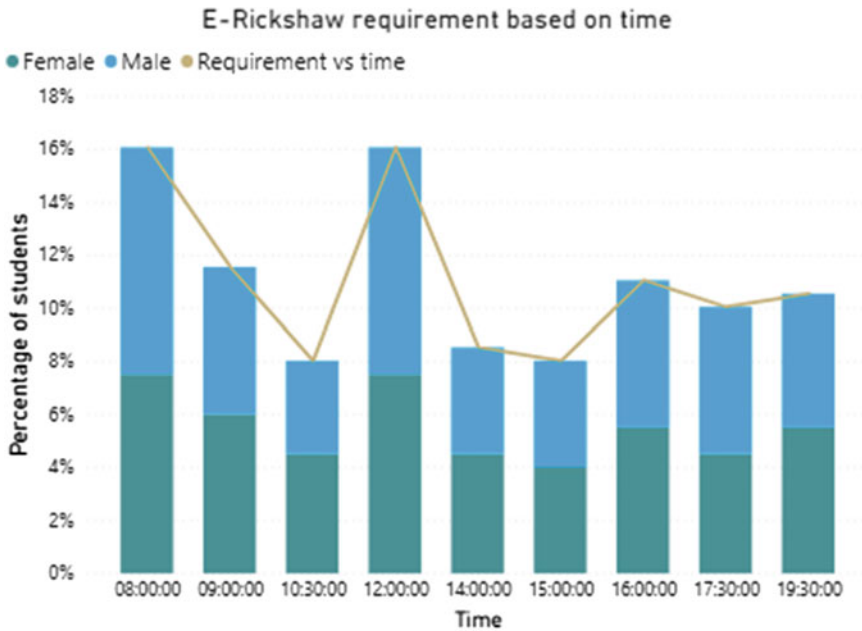
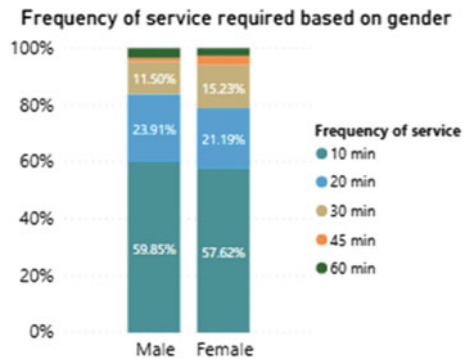


Fig. 3 E-Rickshaw demand versus time

Fig. 4 Frequency of service requirement



feel a frequency of 20 min is required. A negligible percent of respondents feel that a frequency of more than 30 min is sufficient. The average frequency of service required is found to be 17 min. Based on the peak hour demand, it is optimal to provide e-rickshaw services at 10 min intervals during peak hours and at an interval of 20 min during off-peak hours.

The prediction of the future demand for e-rickshaw can be made based on assessing the currently used mode of transport [11]. The willingness of users to pay for the e-rickshaw services inside the NITT campus revealed that 41% of the respondents are willing to pay up to Rs. 5 per trip, followed by 25% of users willing to pay up

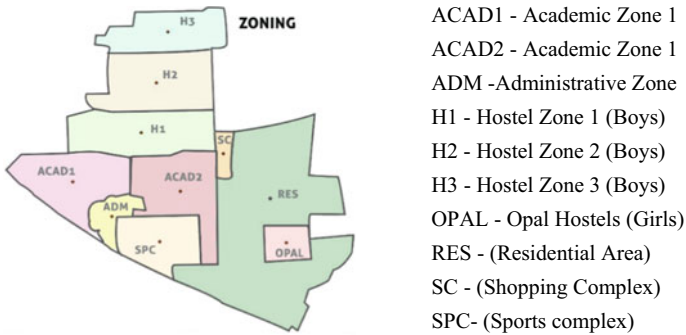


Fig.5 Zones inside NITT

to Rs. 10 per trip. As per the analysis, the average amount a user is willing to pay per trip is Rs. 5.5. The price for the trip is fixed based on the willingness to pay and expenses incurred in the e-rickshaw operation.

4.2 Zoning the Study Area

The predetermined study area is subdivided into smaller areas called zones. In this study, the zones are mainly divided based on location proximity and the nature of trips. The zonal division is done along the existing boundaries and roads. The study area is divided into ten main zones, as shown in Fig. 5.

The OD matrix is a matrix in which each cell represents the number of trips from the origin (row) to the destination (column). An OD matrix helps design an efficient transportation system [12], in our case, establishing the e-rickshaw transport system on campus. The Power BI software is used to generate an OD matrix by using the OD survey data. The OD matrix neglects the intra-zonal trips. From the observations, the maximum travel demand is from the ACAD1 zone as it comprises 196 trips. It is inferred from the analysis that the nature of trips is mostly academic-based. Table 1 shows the OD matrix.

4.3 E-rickshaw Trip Data Analysis (Desire Line Diagram)

The optimized use of e-rickshaw can lead to energy demand reduction and management [13]. With full battery capacity, the e-rickshaw can travel 60 km as per the company’s technical specifications. Thus, a reduction in dead kilometre travel is required to make it more cost-efficient. The desire lines are the graphical representation of the flow of traffic between two zones. The thickness of the traffic line indicates the traffic volume flowing from one zone to another. The desire lines help in

Table 1 Origin–destination matrix

Destination origin	ACAD1	ACAD2	ADM	H1	H2	H3	NITH	OPAL	RES	SPC	Grand total
ACAD1	0	19	5	57	19	38	20	34	0	2	194
ACAD2	10	0	7	26	23	23	6	15	0	3	113
ADM	2	6	0	5	5	6	2	5	0	2	33
H1	63	26	5	0	10	12	3	0	1	10	130
H2	19	17	1	10	0	72	2	0	0	1	122
H3	49	24	8	9	60	0	4	0	0	8	162
NITH	2	9	2	8	4	4	0	14	0	0	43
OPAL	51	12	5	0	0	0	4	0	1	2	75
RES	0	0	0	1	0	0	0	1	0	0	2
SPC	0	0	0	12	2	6	2	6	0	0	28
Grand total	196	113	33	128	123	161	43	75	2	28	902

the scheduling of different modes of transport to suit the demands of the commuters. The home interview method is used for the plotting of desire lines. Figure 6 illustrates the desire line diagram for e-rickshaw trips inside NITT.

Around 240 campus residents are interviewed at their hostels. The demand and movement of EVs on campus can also be validated using this desire line diagram. The ArcGIS software is used to obtain the centroid of each zone’s desire lines originating from each zone’s centroid, coded in different colors to make it easily recognizable. As seen earlier, the maximum trips are observed from ACAD1 to H3, followed by ACAD1 to OPAL. This again indicates that most of the trips carried out on campus are academic-oriented.

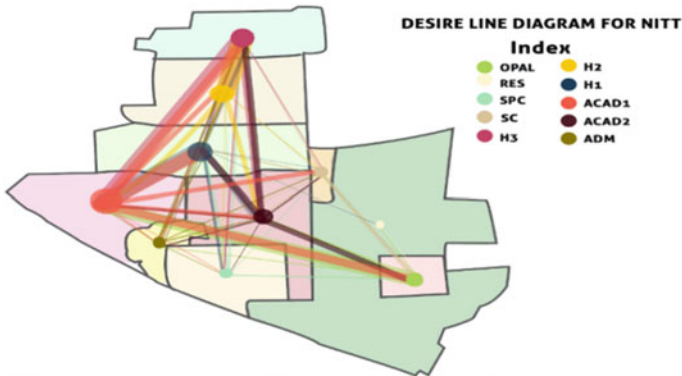


Fig.6 Desire line diagram for e-rickshaw trips inside NITT

Table 2 Inter-zonal trips inside NITT

Zone I	Zone II	Inter-zonal trips	Zone I	Zone II	Inter-zonal trips
H2	H3	172	ACAD1	ACAD2	29
H1	ACAD1	120	OPAL	ACAD2	27
H3	ACAD1	87	ACAD1	SC	22
OPAL	ACAD1	85	H1	SPC	22
H1	ACAD2	52	H1	H2	21
H3	ACAD2	47	H1	H3	21
H2	ACAD2	40	OPAL	SC	18
H2	ACAD1	38	-	-	-

4.4 Routing and Charging Station Location

4.4.1 Routing the E-rickshaws Inside NITT

The goal of transport routing is to create the most effective route by minimizing the distance. Routing is done in a more generalized way due to certain constraints in the study. As discussed in the previous sections, the study area is divided into ten different zones, and further desire lines diagrams are generated based on the OD matrix. The thickness of the desire line directly depicts traffic volume, i.e., the thicker the line, the more volume of people tend to move from one zone to another. Table 2 Inter-Zonal Trips inside NITT.

Table 2 derived from the OD matrix, shows the top 15 inter-zonal trips. The top 10 trips are considered for determining the routes, and routing is done. The endpoints are fed as inputs, and the output is the shortest path connecting the two endpoints, that is, the route. Intra-zone routing is done considering all major trip generation areas of the destination zone’s origin zone and trip attraction areas. Since H3:H1 and ACAD2:ACAD1 are part of the routes H3:ACAD1 and OPAL:ACAD2, those two routes are omitted. Thus, eight routes are finalized:H1:ACAD1; H1:ACAD2; H2:ACAD1; H2:ACAD2; H3:ACAD1; H3:ACAD2; OPAL:ACAD1; OPAL:ACAD2. The result of the routing is shown in Fig. 7.

4.4.2 Optimum Location of Charging Station

The location of the charging stations is optimized by considering various locations based on routing. Charging stations are considered along the routes already assigned. The possible locations for setting up charging stations are Depot, MM1, MM2, Main Gate, ECE dept, SC, Hostel Office. Three locations from the boys’ hostel area are considered which include the Hostel Office, MM1, and MM2. Two locations from the academic area considered are Main Gate and ECE dept. From the girls’ hostel area, the existing depot is considered as the charging station location. As decided

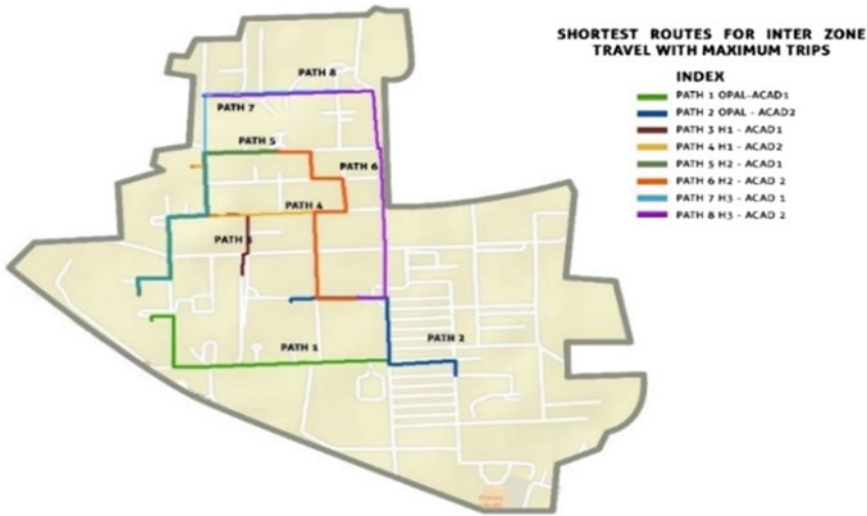


Fig.7 Routing of e-rickshaws inside NITT

by the NITT transport section authority, the number of charging stations is three. Hence, there are nine possible combinations. However, only six cases are considered to maximize the distance between the charging stations. The optimal combination of the location of charging stations in the three areas is determined by the following objective function. It uses the dead kilometre as the primary parameter and is shown in Eq. 1.

$$\text{Objective function : } \text{Min}Z(n) = [\Sigma(X(i))] \tag{1}$$

The objective function is to find the location of the charging station in each of the three locations ($n = 1, 2, 3$) by minimizing the sum of the dead kilometres for each route ($X(i)$). The dead kilometres from each route endpoint to the charging station are determined as the shortest route between them. The dead kilometre factor is equal to the maximum of the two dead kilometres of the endpoints of the route ($Y(i, 1), Y(i, 2)$), where $Y(i, k)$ is the dead kilometre for i th routes k th endpoint. It is expressed as shown in Eqs. (2) and (3)

$$X(i) = \text{Max}[Y(i, 1), Y(i, 2)] \tag{2}$$

$$Y(i, k) = \text{Min}[\text{Distance from route}(i) \text{ End points}(k) \text{ to Charging station}(j)] \tag{3}$$

whereas, the route number and ranges from 1 to 8, j is the charging station location number and ranges from 1 to 7, k is the endpoint number of the i th route, and ranges from 1 to 2.

Table 3 Dead kilometre calculation

Three charging stations at Depot, ECE department, and MM2		
Endpoint of route (<i>i</i>)	Charging station location	Dead kilometer [$X_{(i)}$]
Amber	MM2	0.350
Lyceum	ECE dept	0.140
Aqua	MM2	0.950
Orion	MM2	0.700
LHC	ECE dept	0.350
MM1	MM2	0.400
OPAL	Depot	0.300
Orion	ECE dept	0.850
Total [$Z_{(i)}$] = 4.040		

Table 4 Summary of calculated Z value

Charging station	Sum of dead Kms [$Z_{(i)}$]
Depot, MM1, main gate	5.1
Depot, hostel office, main gate	4.7
Depot, MM2, ECE dept	4.04
Depot, MM2, SC	4.44
Depot, MM1, SC	5.59
Depot, MM2, main gate	5.45

Table 3 shows a sample of dead distance calculation for the case of charging locations at Depot, ECE department, and MM2. The maximum of two dead kilometres from the endpoint of each route to the nearest charging station is calculated in column three. The sum of dead kilometres provides the Z value of the specific combination.

Table 4 gives a summary of the six trial combinations. The combination with the minimum value of [$Z_{(i)}$] is the optimal combination.

By minimizing the dead kilometres, the cost spent on the extra charging requirement and the idle timing for charging is reduced. From Table 4, minimum dead kilometres can be achieved by locating the stations at the Depot, MM2, and the ECE department. It has a minimum sum of a dead kilometre of 4.04 km. Figure 8 depicts the location of the charging station.

4.4.3 Comparison with the Current System—One Charging Station

Currently, there is only one charging station located at the depot. The dead kilometre calculation is shown in Table 5.

The dead kilometre is equal to 14.3 km. By introducing three charging locations, the dead kilometre is reduced to 4.04 km. There is a 71.7% reduction in the dead

Fig. 8 Location of charging station

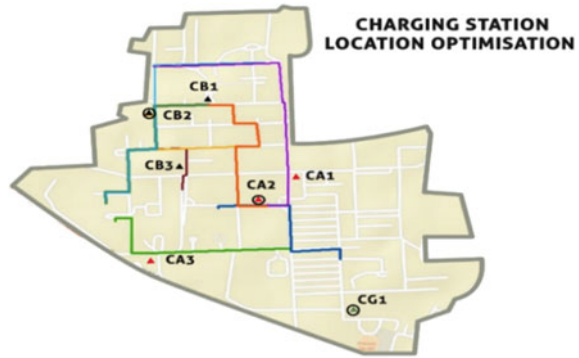


Table 5 Z value for one charging station

One charging station at depot		
Endpoint of route (<i>i</i>)	Charging station location	Dead kilometer [$X_{(i)}$]
Mech Dept	Depot	1.2
Orion	Depot	1.6
Amber	Depot	2.1
Aqua	Depot	1.8
MM1	Depot	1.8
MM2	Depot	2.0
MM2	Depot	2.0
MM1	Depot	1.8
Total [$Z_{(i)}$] = 14.3		

kilometre traveled by e-rickshaws. Though the initial one-time expense in the erection of stand and provision for 3-phase supply is high, having three stations will prove to be economical in the long run.

5 Summary and Conclusion

The study aimed to find the number of e-rickshaw required to satisfy the current demand as e-rickshaw was being used on a pilot basis. Based on the data collected from the OD survey and understanding the daily requirement of e-rickshaw, the data is extrapolated to find the number of e-rickshaw required to cater to the demand on the campus. By doing so, the number of necessary e-rickshaw was calculated as eight. The expected average frequency of e-rickshaw service is approximately 17 min. Most of the users are willing to pay up to Rs. 5.5/trip. Major routes are identified based on the desire line diagram. The location of the charging station is optimized by

minimizing the dead kilometres. The due focus is given to find the optimal location of the charging stations by minimizing the dead kilometres and maximizing the distance between them. The optimal location is found to be Depot/Transport Section, MM2, and ECE department. Introducing three charging stations at the locations mentioned above reduces the dead kilometre wastage by 71.7% instead of the current system of one charging station. Furthermore, the major share of trips inside the campus is educational trips by students, and the most preferred mode is bi-cycle followed by the walk. Hence routes should focus between hostel/residential zones to academic zones. Thus the e-vehicle transport systems (e-rickshaw service) can be successfully implemented in the NITT campus. Additionally, the users' safety and comfort-related concerns and safe driving practices for drivers need emphasis and improvement. Based on the analysis and findings, various policies can be suggested to maintain efficient e-rickshaw service inside NITT. The study can be extended to several other locations to develop an effective route-based model. Further new search algorithms like chaos harmony algorithm, the genetic algorithm, etc., can be considered to develop an more efficient models to optimize the location of charging stations.

Acknowledgements The authors would like to thank the National Institute of Technology Tiruchirappalli for supporting this research work. Also, the authors acknowledge and appreciate the efforts taken by Mr. Deepak, Ms. Rama devi, Ms. Keerthy, and Mr. Sidharth (B.Tech students of Civil Engineering Department, NITT) in data collection process.

References

1. Singh S, Prathyusha C (2021) System dynamics model for urban transportation system to reduce fuel consumption and fuel emission. In: Jana A, Banerji P (eds) *Urban Science and Engineering*. Lecture Notes in Civil Engineering, vol 121. Springer, Singapore. https://doi.org/10.1007/978-981-33-4114-2_31
2. Singh S, Priyadarshini B, Prathyusha C, Santhakumar SM (2021) Assessment of the electric rickshaws' operation for a sustainable ecosystem. In: Muthukumar P, Sarkar DK, De D, De CK (eds) *Innovations in Sustainable Energy and Technology*. Advances in sustainability science and technology. Springer, Singapore. https://doi.org/10.1007/978-981-16-1119-3_29
3. Carlos JLB (2003) Sustainable transportation planning on college campuses. *Transp Pol* 10:35–49
4. Rastogi R, Doley G (2015) Sustainable transport option for university campus. Paper presented at the 16th international conference on urban transport entitled energy, climate and air quality challenges—the role of urban transport policies in developing countries.
5. Nisha C, Samir KB (2015) Technology, knowledge, and markets: connecting the dots—electric rickshaw in India as a case study. *J Frugal Innov* 1(3):1–10
6. Yousefi S, Abbasi T, Anvari Z (2014) Routing in urban environments using updated traffic information provided through vehicular communications. *J Transp Sys Eng Info Tech* 14(5):23–36
7. Inês F, Anabela R, Gonçalo G, António PA (2011) Optimal location of charging stations for electric vehicles in a neighborhood in Lisbon, Portugal. *Transp Res Rec* 2252(12):91–98. <https://doi.org/10.3141/2252-12>
8. Christina I, Ioannis T, Konstantinos K, Grigorios B (2019) Electric transit route network design problem: model and application. *Transp Res Rec* 2673(8):264–274

9. Chandra S, Minal S (2019) Challenges of electric vehicle adoption in India. *Indian Highways* 47:42–45
10. Prathyusha C, Singh S, Shivananda P (2021) Strategies for Sustainable, Efficient, and Economic Integration of Public Transportation Systems. In: Jana A., Banerji P (eds) *Urban Science and Engineering. Lecture notes in civil engineering*, vol 121. Springer, Singapore. https://doi.org/10.1007/978-981-33-4114-2_13
11. Singh S, Shukla BK (2021) A comparative study on the sustainability of public and private road transportation systems in an urban area: current and future scenarios. In: Ashish DK, de Brito J, Sharma SK (eds) *3rd international conference on innovative technologies for clean and sustainable development. ITCSD 2020. RILEM Bookseries*, vol 29. Springer, Cham. https://doi.org/10.1007/978-3-030-51485-3_12
12. Singh S, Priyadarshni B, Prathyusha C, Santhakumar SM (2021) Investigating the characteristics and choice of electric scooter users: a case study of Tiruchirappalli city. In: Muthukumar P, Sarkar D.K., De D., De C.K. (eds) *Innovations in Sustainable Energy and Technology. Advances in sustainability science and technology*. Springer, Singapore. https://doi.org/10.1007/978-981-16-1119-3_15
13. Hasan ASMM (2020) Electric rickshaw charging stations as distributed energy storages for integrating intermittent renewable energy sources: a case of Bangladesh. *Energies* 13:6119. <https://doi.org/10.3390/en13226119>

Compressive Strength of Quaternary Blended Self-Compacting Concrete Made with Supplementary Cementitious Materials Through Regression Analysis



G. Sree Lakshmi Devi, C. Venkata Siva Rama Prasad, and P. Srinivasa Rao

Abstract Concrete is a widely utilized material in the building sector and it is a major source of pollution across the globe. The use of SCMs in concrete has been increasingly common in recent years, growing in tandem with the expansion of the concrete industry (Su et al. in *Cem Concr Res* 31:1799–1807, 2001) [1], as a result of discussions about issues such as raw material extraction, CO₂ emissions, and so on. These consequences created demands to reduce usage of cement-making raw materials by utilizing supplemental cementitious materials such as fly ash, micro silica, and so on. The waste materials from industries aid sustainable growth in the current environment (Jodeiri and Quitlig in *J Civ Eng Res* 2:100–107, 2012) [2]. The development of SCC resulted in a good perception of its numerous benefits such as reduced noise pollution. Construction time and power consumption are reduced as a result of vibration through the use of supplementary materials. By integrating maximum cement content with mineral admixtures, characteristics and self-compacting concrete are improved. For the concrete data gathered from the laboratory experimental work done in this study, a mathematical analysis employing statistical approaches for prediction of 28 days of strength of concrete was undertaken. The mix proportioning elements were the variables in the prediction models (Sabet et al. in *Constr Build Mater* 44:175–184, 2013) [3]. Multiple non-linear regression models produced high correlation coefficients for compressive strength prediction at various curing ages (28, 56, and 91 days) and for various modifications, such as using FA, GGBS, and Microsilica as partial substitutes for cement. In this paper, an experimental work was carried out on Compressive Strength of Quaternary Blended Self-Compacting Concrete (QBSCC) with mineral admixtures for 0.30 and 0.40 water-binder ratios with A simple mathematical model is used to estimate the concrete compressive

G. Sree Lakshmi Devi (✉)

Department of Civil Engineering, Vignana Bharathi Institute of Technology (Autonomous), Aushapur(V), Hyderabad, Telangana 501301, India

C. Venkata Siva Rama Prasad

Department of Civil Engineering, St. Peter's Engineering College (Autonomous), Dullapally, Maisammaguda, Medchal, Hyderabad, Telangana 500100, India

P. Srinivasa Rao

Civil Engineering, JNT University Hyderabad, Kukatpally, Hyderabad 500085, India

strength based on the results of early age tests (Devi and Rao flexural behavior of quaternary blended fiber reinforced self compacting concrete slabs using mineral admixtures. In: IOP conference series: materials science and engineering, vol 1006, No 1, IOP Publishing, pp 012020, 2020) [4].

Keyword Concrete · Blended concrete · Quaternary blended concrete · Sustainable concrete

1 Introduction

Concrete is the most frequently utilized construction material in use today due to its availability, flexibility of handling, and capacity to give shape to any desired form. One of the most essential engineering qualities of concrete is its compressive strength [5]. In construction projects, 28 days is a too long time to wait, yet it is necessary to analyze concrete quality certification and cannot be avoided. As a result, waiting 28 days is required for validation of the concrete quality control procedure which represents steps involved in concrete manufacturing, i.e., batching, mixing, placing, curing, and so on and as well as the desired strength [6, 7]. Today, research is focusing on strategies for using industrial waste as a source material for the expansion of development areas all over the world [8, 9]. This utilization would not only be practical, but it might also result in a feasible and taint-free situation [10]. Usage of blended concretes in cement as complete or partial replacement can reduce the utilization of raw materials in concrete industry, which can obviously lead to sustainable development in terms of environmental friendliness, preservation of raw materials which are chosen for cement manufacturing and also leads to reduction in pollution in the atmosphere which is the main cause of global warming and greenhouse gas effects which in turn resulting in increase in global temperature [11, 12]. The concrete compressive strength must be employed while designing a concrete construction. The mechanical properties of a concrete sample that has been cured for 28 days and is evaluated by the standard strength test in Universal Testing Machine are referred to as the concrete's characteristic strength. In this research, mineral admixtures are used as partial replacement of cement with chemical admixtures to modify the workability of the mix as well as strength to achieve quality of concrete as that of SCC made with 100% cement. One of the most extensively used statistical procedures for establishing relationships between dependent and independent variables in regression analysis [13]. Regression is the process of fitting models to data in general. The behavior of the dependent variable is expressed as a function of the independent variable, which is responsible for that behavior. The 28-days compressive strength is the dependent variable in this study, while the 7-day compressive strength is the independent variable.

2 Experimental Study

Mathematical models based on concrete mix test data, i.e., experimental results, are the most accurate, dependable, and scientific. By decreasing the odds of failure, they enable rapid and reliable concrete strength prediction without full-scale testing [14, 15]. Through correlation analysis, statistical analysis can also provide insight into the major elements determining 28-day compressive strength. As a result, concrete compressive strength prediction has been a hot topic of study, with a large number of experiments being conducted. In this study, an attempt is made to construct a link between the 7-day compressive strength and the 28-day compressive strength of Binary, Ternary, and Quaternary mixed Self-Compacting Concrete, and to represent this relationship with a mathematical model that can be easily implemented [16]. The analytical models were developed utilizing data from Binary, Ternary, and Quaternary mixed Self-Compacting Concrete compressive strengths, which were then confirmed using the strong results from the current investigation. The models were kept as simple as possible. The use of models in concrete buildings eliminates the need to wait 28 days to determine the concrete strength.

Study involves the strength properties of concrete like compressive strength for water-binder ratios 0.3 and 0.4. Specimens of Binary, Ternary, and Quaternary Blended Self—Compacting Concrete were cast and tested for compressive strength at 28 days of curing for 0.40 and 0.30. A mathematical model have been proposed to predict 28 days strength w.r.t 7 days Tables 1 and 2 shows the mix proportions, Tables 3 and 4 represents workability similarly Tables 5, 6 and 7 represents compressive strength, Tables 8, 9 and 10 represents Percentage increase in strength at 28 days and Tables 11 and 12 represents Experimental and Predicted strength of different concrete specimens for 0.30 and 0.40 w/b ratios (Figs. 1, 2, 3, 4, 5, 6 and 7).

The empirical equation of predicted compressive strength at 28 days is $Y = 0.92 * X + 11.37$ (N/mm²).

Tables 11 and 12 Gives the % variation of experimental compressive strength and predicted compressive strength of binary, ternary and quaternary blended self-compacting concrete of w/b ratio 0.3 and 0.4 with respect to 7 days strength.

3 Conclusions

Based on the experimental the following conclusions can be drawn:

- The combination of 50% cement +50% GGBS performed the best of 0.4 and 0.3 w/b ratios in compressive strength of all mix combinations of binary blended self-compacting concrete.
- The combination of 60% cement + 30% GGBS + 10% Micro Silica performed the best 0.4 and 0.3 w/b ratios in compressive strength of all mix combinations of Ternary blended self-compacting concrete.

Table 1 Mix proportions for ordinary, binary, ternary and quaternary blended self-compacting concrete for W/B ratio 0.30 and 0.40

S. No.	Mix	Cement Kg/m ³	Fly ash Kg/m ³	GGBS Kg/m ³	Micro silica Kg/m ³	Fine Agg Kg/m ³	Coarse Agg Kg/m ³	Water Lts	Super plasticizer Lts	VMA Lts
1	M0	614	0	0	0	884	749	177	7.36	0.61
2	M11	307	307	0	0	884	749	177	7.36	0.61
3	M12	307	0	307	0	884	749	177	7.36	0.61
4	M21	461	123	0	31	884	749	177	7.36	0.61
5	M22	430	123	0	62	884	749	177	7.36	0.61
6	M23	307	154	154	0	884	749	177	7.36	0.61
7	M24	400	0	184	31	884	749	177	7.36	0.61
8	M25	369	0	184	62	884	749	177	7.36	0.61
9	M31	246	154	153	62	884	749	177	7.36	0.61
10	M32	154	154	246	62	884	749	177	7.36	0.61
11	M33	92	154	307	62	884	749	177	7.36	0.61
12	M34	154	246	154	62	884	749	177	7.36	0.61
13	M35	92	307	154	62	884	749	177	7.36	0.61

Table.2 Quantities of materials required per 1 m³ of ordinary, binary, ternary and quaternary blended self-compacting concrete for w/b ratio 0.40

S. No.	Mix	Cement Kg/m ³	Fly ash Kg/m ³	GGBS Kg/m ³	Micro silica Kg/m ³	Fine Agg Kg/m ³	Coarse Agg Kg/m ³	Water Lts	Super plasticizer Lts	VMA Lts
1	M0	420	0	0	0	884	749	177	5.04	0.42
2	M11	210	210	0	0	884	749	177	5.04	0.42
3	M12	210	0	210	0	884	749	177	5.04	0.42
4	M21	315	84	0	21	884	749	177	5.04	0.42
5	M22	294	84	0	42	884	749	177	5.04	0.42
6	M23	210	105	105	0	884	749	177	5.04	0.42
7	M24	273	0	126	21	884	749	177	5.04	0.42
8	M25	252	0	36	42	884	749	177	5.04	0.42
9	M31	168	105	105	42	884	749	177	5.04	0.42
10	M32	105	105	168	42	884	749	177	5.04	0.42
11	M33	63	105	210	42	884	749	177	5.04	0.42
12	M34	105	168	105	42	884	749	177	5.04	0.42
13	M35	63	210	105	42	884	749	177	5.04	0.42

Table 3 Workability of ordinary, binary, ternary, and quaternary blended mixes for w/b ratio 0.30

S. No.	W/B ratio	Type of mix	Slump flow	T50cm slump flow	L-box	V-funnel	U-box
1	0.3	Ordinary	680	3.5	0.83	7.2	28
2		Binary	690	3.3	0.85	7.2	27
3		Ternary	700	3.2	0.86	7.3	26
4		Quaternary	710	3.0	0.88	7.3	25

Table 4 Workability of ordinary, binary, ternary, and quaternary blended mixes for w/b ratio 0.40

S. No.	W/B ratio	Type of mix	Slump flow	T50cm slump flow	L-box	V-funnel	U-box
1	0.40	Ordinary	700	3.2	0.85	6.5	22
2		Binary	710	3.0	0.87	6.4	21
3		Ternary	720	2.7	0.90	6.3	20
4		Quaternary	740	2.5	0.92	6.3	20

Table 5 Compressive strength of ordinary and binary blended self-compacting concrete at 7 and 28 days

S. No.	w/b ratio	Mix	Compressive strength (N/mm ²)	
			7 Days	28 days
1	0.3	M0	59.65	68.48
2		M11	51.53	59.34
3		M12	55.76	63.94
4	0.4	M0	41.36	50.98
5		M11	35.16	43.10
6		M12	37.89	46.48

Table 6 Compressive strength of ternary blended self-compacting concrete at 7 and 28 days

S. No.	w/b ratio	Mix	Compressive strength (N/mm ²)	
			7 days	28 days
1	0.3	M21	62.38	70.74
2		M22	55.95	63.56
3		M23	52.10	58.86
4		M24	61.82	70.29
5		M25	62.81	70.80
6	0.4	M21	46.60	54.94
7		M22	42.36	50.04
8		M23	38.12	44.71
9		M24	46.65	54.92
10		M25	47.52	55.93

Table 7 Compressive strength of quaternary blended self-compacting concrete at 7 and 28 days

S. No.	w/b ratio	Mix	Compressive strength (N/mm ²)	
			7 days	28 days
1	0.3	M31	58.46	67.16
2		M32	56.29	64.02
3		M33	52.02	57.53
4		M34	56.30	64.86
5		M35	52.27	58.09
6	0.4	M31	40.83	48.73
7		M32	37.86	45.83
8		M33	35.99	42.89
9		M34	38.35	46.35
10		M35	35.62	43.51

Table 8 Percentage increase in compressive strength of ordinary and binary blended self-compacting concrete at 28 days

S. No.	w/b ratio	Mix	% increase w.r.t 7 days
1	0.3	M0	14.80
2		M11	15.15
3		M12	14.67
4	0.4	M0	23.25
5		M11	22.58
6		M12	22.67

Table 9 Percentage increase in compressive strength of ternary blended self-compacting concrete at 28 days

S. No.	w/b ratio	Mix	% increase w.r.t 7 days
1	0.3	M21	13.40
2		M22	13.60
3		M23	12.98
4		M24	13.70
5		M25	12.72
6	0.4	M21	17.89
7		M22	18.13
8		M23	17.29
9		M24	17.73
10		M25	17.69

- The combination of 40% cement + 25% fly ash + 25% GGBS + 10% Micro Silica performed the best of the w/b ratios 0.4 and 0.3 studied in terms of compressive strength among the mix combinations of QBSCC.

Table 10 Percentage increase in compressive strength of quaternary blended self-compacting concrete at 28 days

S. No.	w/b ratio	Mix	% increase w.r.t 7 days
1	0.3	M31	14.88
2		M32	13.73
3		M33	13.59
4		M34	15.20
5		M35	14.13
6	0.4	M31	19.34
7		M32	21.05
8		M33	19.17
9		M34	20.86
10		M35	21.15

Table 11 Experimental and predicted compressive strength of binary, ternary, and QBSCC for 0.3 w/b ratio

S. No.	Mix	7 days strength	28 days strength	Predicted 28 days strength	% variation
1	M0	59.65	68.48	66.24	-3.26
2	M11	51.53	59.34	58.67	-1.13
3	M12	55.76	63.94	62.66	-2.01
4	M21	62.38	70.74	68.75	-2.80
5	M22	55.95	63.56	62.84	-1.13
6	M23	52.1	58.86	59.30	0.75
7	M24	61.82	70.29	68.24	-2.91
8	M25	62.81	70.8	69.15	-2.32
9	M31	58.46	67.16	65.15	-2.99
10	M32	56.29	64.02	63.15	-1.35
11	M33	52.02	57.53	59.22	2.94
12	M34	56.3	64.86	63.16	-2.61
13	M35	52.27	58.09	59.45	-2.34

- The empirical equation that shows the relationship between 7 days strength and 28 days strength of binary, ternary, and QBSCC is $Y = 0.92X + 11.37$ (N/mm²).
- Percentage variation between experimental compressive strength and predicted compressive strength for Binary, Ternary, and QBSCC for w/b ratio 0.3 is less than 5%.
- Percentage variation between experimental compressive strength and predicted compressive strength for Binary, Ternary and Quaternary blended self-compacting concrete for w/b ratio 0.4 is less than 5%.
- Overall, in strength aspects, concrete mixes with lower Water-binder ratio (i.e., 0.30) performed best compared to water-binder ratio of 0.40.

Table 12 Experimental and predicted compressive strength of binary, ternary, and QBSCC for 0.4 w/b ratio

S. No.	Mix	7 days strength	28 days strength	Predicted 28 days strength	% variation
1	M0	41.36	50.98	49.42	-3.06
2	M11	35.16	43.1	43.71	1.43
3	M12	37.89	46.48	46.22	-0.56
4	M21	46.6	54.94	54.24	-1.27
5	M22	44.02	50.04	51.87	-3.65
6	M23	38.12	44.71	46.44	3.86
7	M24	46.65	54.92	54.28	-1.16
8	M25	47.52	55.93	55.08	-1.52
9	M31	40.83	48.72	48.93	0.43
10	M32	37.86	45.83	46.20	-0.81
11	M33	35.99	42.89	44.48	3.7
12	M34	38.35	46.35	46.65	0.65
13	M35	35.62	43.51	44.14	1.44

Fig. 1 Shows flow properties of self-compacting blended concrete

Fig. 2 Shows flow properties of self-compacting blended concrete



Fig. 3 Shows flow properties of self-compacting blended concrete



Fig. 4 Shows flow properties of self-compacting blended concrete

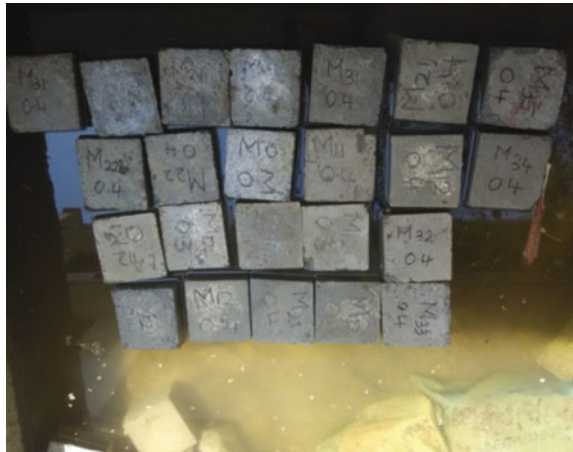


Fig. 5 Shows flow properties of self-compacting blended concrete

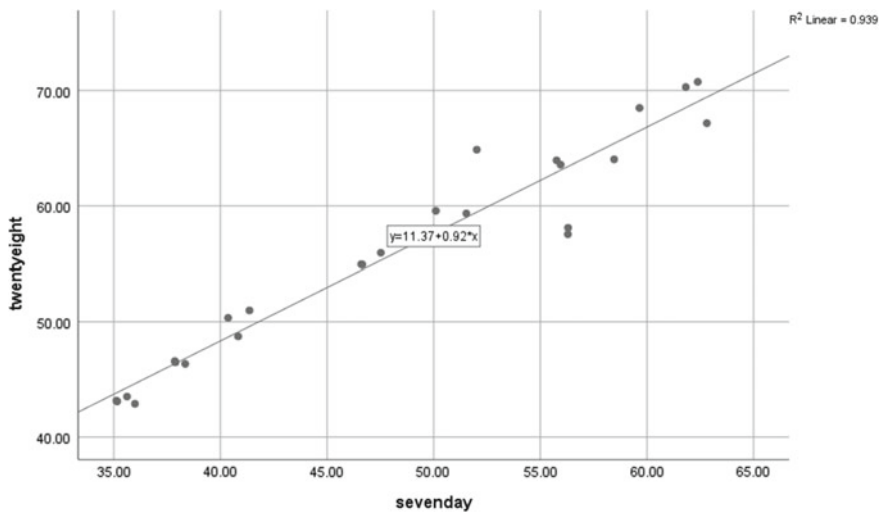


Fig. 6 Relationship between seven days and 28 days compressive strength through regression analysis of binary, ternary, and quaternary blended self-compacting concrete

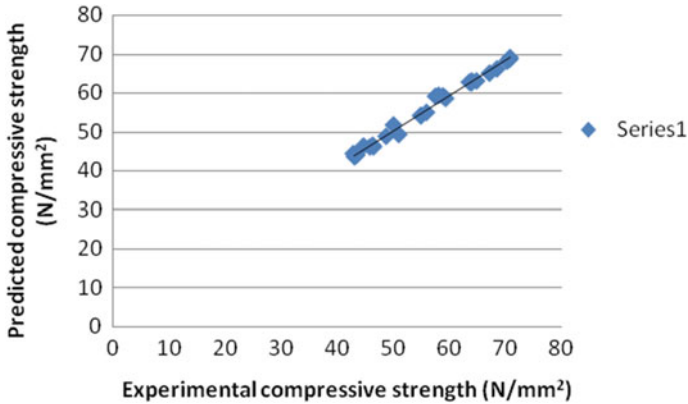


Fig. 7 Relationship between predicted seven days and 28 days compressive strength of binary, ternary, and quaternary blended self-compacting concrete

References

1. Su N, Hsu KC, Chai HW (2001) A simple mix design method for self-compacting concrete. *Cem Concr Res* 31(12):1799–1807
2. Jodeiri AH, Qaitalg RJ (2012) Effect of wirand FS7-II steel wire fibre on flexural capacity of reinforced concrete beam. *J Civ Eng Res* 2(6):100–107
3. Sabet FA, Libre NA, Shekarchi M (2013) Mechanical and durability properties of self consolidating high performance concrete incorporating natural zeolite, silica fume and fly ash. *Constr Build Mater* 44:175–184
4. Devi GSL, Rao PS (2020) Flexural behavior of quaternary blended fiber reinforced self compacting concrete slabs using mineral admixtures. In: *IOP conference series: materials science and engineering*, vol 1006, No 1. IOP Publishing, pp 012020
5. Rollakanti CR, Prasad CVSR, Polaju KK, Al Muharbi NMJ, Rollakanti YVA, Rahul C, Prasad CVSR, Polaju KK, Al Muharbi NMJ, VenkatArun Y (2021) An experimental investigation on mechanical properties of concrete by partial replacement of cement with wood ash and fine sea shell powder. *Mater Today: Proc* 43:1325–1330
6. Devi GSL, Rao PS, Prasad CVSR (2021) Experimental investigation on compressive strength of quaternary blended concrete using different mineral admixtures. *Mater Today: Proc* 46:783–785
7. Rollakanti CR, Prasad CVSR, Polaju KK, Al Muharbi NMJ, Arun YV (2021) An experimental investigation on mechanical properties of concrete by partial replacement of cement with wood ash and fine sea shell powder. *Mater Today: Proc* 43:1325–1330
8. Hamoush S, Picournell-Dardner M (2011) Freezing and thawing durability of very high strength concrete. *Am J Eng Appl Sci* 4(1):42–51
9. Prasad CVSR, Lakshmi TV (2018) Effect of *Bacillus subtilis* on abrasion resistance of bacterial concrete. *Int J Appl Eng Res* 13(16):12663–12666
10. Lulseged A, Mehantharaja K, Prasad CVSR (2016) A study on using plastic coated aggregate in bituminous mix for flexible pavement. *Int J Sci Eng Technol Res* 5:0933–0936
11. Devi GSL, Rao PS (2016) Effect of freezing and thawing on quaternary blended self compacting concrete using mineral admixtures. *i-Manager's J Civ Eng* 7(1):17
12. Prasad CVSR, Lakshmi TV (2020) Experimental investigation on bacterial concrete strength with *Bacillus subtilis* and crushed stone dust aggregate based on ultrasonic pulse velocity. *Mater Today: Proc* 27:1111–1117

13. Sree Lakshmi Devi G, Srinivasa Rao P (2017) Durability of quaternary blended self compacting concrete using mineral admixtures. *Indian Concr J* 91(4):70–77 (Special issue on Self compacting concrete)
14. Devi GSL, Rao PS (2017) Flexural behavior of quaternary blended fiber reinforced self compacting concrete beams using mineral admixtures. *i-Manager's J Civ Eng* 7(2):1
15. Duchesne J (2021) Alternative supplementary cementitious materials for sustainable concrete structures: a review on characterization and properties. *Waste Biomass Valor* 12(3):1219–1236
16. Okamura H, Ouchi M (2003) Self-compacting concrete. *J Adv Concr Technol* 1(1):5–15

Analysis and Comparison of RCC and Steel–Concrete Composite High Rise Buildings



Mahmoud Magdi Eldeib and Kiran Kumar Poloju

Abstract Use of concrete-steel composite buildings is rare in Oman and many Asian countries. This work aims to clarify the comparison between RCC and Steel–Concrete composite high-rise buildings. Steel and concrete composite buildings are constructed by attaching the concrete slab to the steel beam plate using steel shear connectors that act as a single unit. In the current work, the ETABS software was used to conduct an analysis and design of RCC and steel–concrete composite high-rise buildings 2B+G+30 floors. The Euro codes 2 and 4 were used in the design, and seismic zone II and wind loads with the loading conditions were applied to the structure due to the location of Oman in this region. Furthermore, it is vital to ensure that the building’s design is efficient and error-free to assure the building’s safety. The comparison was focused on analysis of the linear static in the structural parts, the composite buildings outperform RCC buildings because they combine the benefits of concrete and steel, this enhances its structural capabilities. Furthermore, the composite buildings are much better than RCC buildings in resisting the parameters in bending moment, the shear force, and the axial forces, thus gives them a great advantage to be an alternative to concrete buildings, and the size of the structural elements can be smaller than those in the RCC building while maintaining the integrity of the building in addition, they require less time to construct than RCC structures.

Keywords RCC buildings · Composite buildings · ETABS · Multistory buildings

1 Introduction

There is abundant information about RCC buildings today, and as a result, RCC structures are still commonly utilized today, but they are also one of the key issues

M. M. Eldeib (✉) · K. K. Poloju
Department of Civil Engineering, Middle East College, Rusayl, Oman
e-mail: 16F16206@mec.edu.om

K. K. Poloju
e-mail: kpoloju@mec.edu.om

impeding the development and growth of building productivity [1]. It necessitates an increase in population and urbanization to high-rise buildings in order to provide a place to live in addition to giving cities an aesthetic and architectural shape, and because the fast life in cities has become large. In order to keep up with this rapid progress, modern construction technologies and methods are required [2]. As a result, steel and concrete composite building systems have become one of these alternatives, and due to their significant benefits over RCC construction, they have lately gained popularity and in recent years, it has become increasingly popular [3]. Because composite construction incorporates the qualities of both steel and concrete, it has various advantages. Furthermore, it saves a significant amount of time, resulting in a reduction in the number of working days and, as a result, a reduction in the cost of the daily wage for laborers [4]. Steel absorbs earthquake energy in composite constructions because of the ductility it imparts to the structure. Furthermore, it is regarded as a critical component in the resistance to fire and shocks [5]. The composite slab technology lowers the structure's tensile strength and serves as permanent molds for the concrete slab on-site, providing support in the form of rolled steel sheets. Composite floors are employed in high-rise structures because they mimic the structural characteristics of a reinforced concrete slab [6]. When compared to non-composite building (RCC structures), the major purpose of combining composite floors with side steel roofs is to save between 30 and 50% of the weight of steel [7]. This project aims to shed light on tall structures made of steel and concrete composites by analyzing engineering structures using ETABS to analyze vertical and horizontal loads as well as earthquake-loads on the structural and studying the benefits of replacing RCC structures with structures made of steel and concrete composites. In light of what has been noted, the majority of the structures used in the Sultanate of Oman are typical structures. As a result, this project will demonstrate the benefits and drawbacks of steel and concrete composite high-rise constructions, if any exist. It will also provide a proper design and analysis of the composite structure which can be used in the construction sector and industry.

2 Description of Structures Design Data Details

The (RCC and Steel–concrete composite) high-rise buildings are designed as a commercial building. The study was conducted on the same plan for both buildings, as the same loads were kept in both buildings, but the only difference was the materials used. The following Table 1 shows the construction data that was used in each of the buildings (Fig. 1).

Table 1 Description of design data details for RCC and steel–concrete high-rise buildings

Description of design data details	RCC		Steel–concrete composite	
Slab thickness (mm)	Basement 1 & 2		200	
	Ground floor + 30 floor		150	
Column size (mm)	B (1&2)	1200 × 1200	B (1&2)	650 × 650 with W 18 × 60 embedded
	G-10th floor	1000 × 1000	G-10th floor	650 × 650 with W 18 × 60 embedded
	10th–20th floor	800 × 800	10th–20th floor	650 × 650 with W 18 × 60 embedded
	21st–30th floor	600 × 600	21st–30th floor	650 × 650 with W 18 × 60 embedded
Beam size (mm)	B (1&2)	800 × 300	B (1&2)	500 × 300
	G-10th floor	800 * 300	G-10th floor	I Beam W 18 × 50
	10th–20th floor	700 × 300	10th–20th floor	I Beam W 24 × 76
	21st–30th floor	600 × 300	21st–30th floor	I Beam W 24 × 76
Height of floor (m)	B1 + B2		5.5	
	G		3.6	
	1–10th floor		3.2	
	11th–20th floor		3	
	21st–30th floor		2.8	
Concrete grade	M30			
Concrete density	25 KN/m ³			
Seismic-zone	II			
Speed of wind	35 m/s			

3 Result and Discussion

The ETABS software is used to conduct a linear static analysis to assure the structure’s stability and flexibility, as well as its ability to avoid falling or collapsing [8]. Bending Moment, Axial Force, Shear Force, and Displacement are all included in linear static analysis.

3.1 Bending Moment

3.1.1 The Maximum Bending Moment (BM) in X Direction in the Column

Table 2 shows that in the composite column the maximum bending moment is

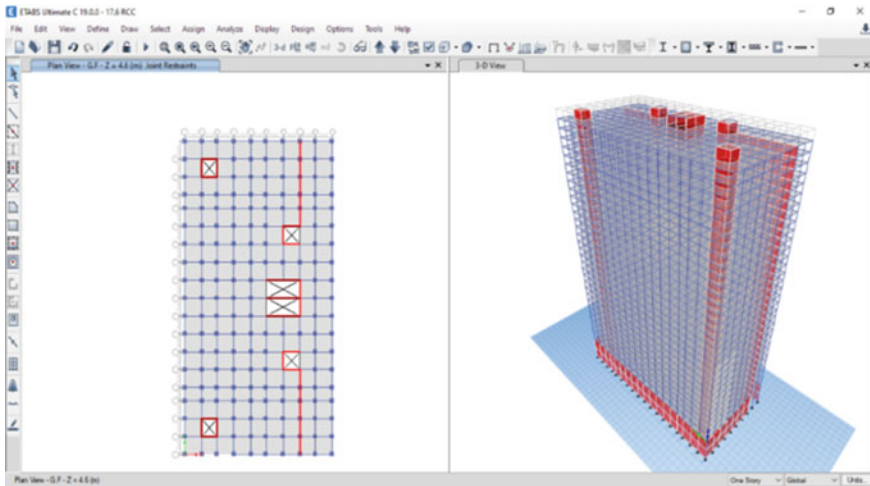


Fig. 1 The high-rise building modeling in ETABS software

Table 2 In X direction the max bending moment in the column (KN-m)

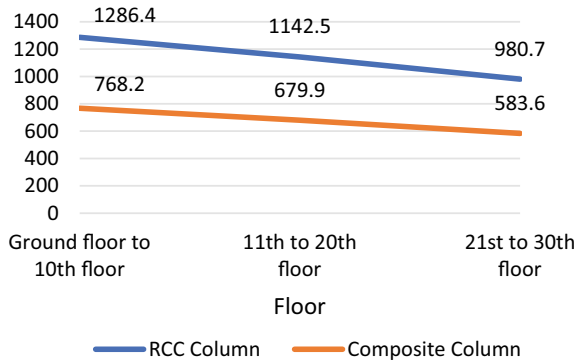
Floor	RCC	Composite	Note
G-10th	1054.3	732.4	The composite column reduces the moment by 30.52%
10th-20th	893.6	682.4	The composite column reduces the moment by 23.64%
21st-30th	710.3	605.6	The composite column reduces the moment by 14.74%

decreased on an average of 30.52% compared to the RCC column from the ground-10th floor, as comparing of bending moment in the 11th–20th floors, the composite column showed a 23.64% reduction in bending moment compared to the RCC column, also in the last tenth floors, the value of bending moment is decreased by an average of 14.74% in composite column especially in comparison to RCC column. That is to say composite column is superior to RCC column in bearing and resistance to compressive bending moment and building weight, thus it does not bend as much as a RCC column does. The maximum values of bending moments decrease in the X direction at the height of the floors and that happen in the composite and RCC columns. It can be concluded that the composite shafts have a low bending moment, which indicates their strength, according to these studies. As a result, composite columns are believed to be superior to RCC columns in terms of resistance to bending moment.

3.1.2 In Y Direction the Maximum Bending Moment in the Column

The results of the maximum bending moment in the Y direction in both composite and RCC columns are shown in Fig. 2. 1286.4 KN m is the maximum bending

Fig. 2 The maximum bending moment-BM-(KN-m) in the column at Y direction



moment in the RCC at ground to tenth floor, according to these results, on either hand, 768.2 KN m is the maximum bending moment in composite column in the same floors. Whenever comparing the outcomes, of the bending moments in the floors 11th–20th and 21st–30th respectively, composite column has a 40.3% decrease in bending moment compared to its RCC column. The rate of bending moment dropped by 40.5% composite column compared to the RCC column, 1142.5 KN m is the result of bending moment in the RCC column at floors 11th–20th, from floor 21st–30th the bending moment was equal 980.7 KN m. In the floor 11th–20th the bending moment was equal 679.9 KN m in the composite column, whereas on the 21st–30th floors it is 583.6 KN m. The bending moment in composite column is lower than the RCC column as showed in the Fig. 2, and that mean the composite column can help to reduce required materials in the building because it does not require as many materials to be safe, in contrast to a RCC column does. It shows that composite columns have a low bending value in the vertical direction, indicating rigidity of it and that they are superior to RCC columns.

3.1.3 The Maximum Bending Moment in the Beam

Table 3 compares the results of the bending moment in RCC and composite beams in the floors, through the results in Table 3, a decrease can be observed in the value of the bending moment in composite beams compared to RCC beams, with the average bending moment in composite beams decreasing by 15% from the ground to the 10th floor compared to RCC beams. In the floor from 11th to 20th, the bending moment

Table 3 In the beam, represent the maximum bending moment in (KN m)

Floor	RCC	Composite	Note
G-10th	704.3	598.6	The moment is reduced by 15% in the composite beam
11th–20th	593.5	432.8	The moment is reduced by 27.1% in the composite beam
21st–30th	487.4	332.4	The moment is reduced by 31.8% in the composite beam

fell by 27.1%, and in the 21st–30th floor, the bending moment decreased by 31.8% in composite beams compared to RCC beams. From the previous findings, it is possible to infer that composite beam are more effective than RCC beams because they can bear a lot of loads without bending. As a result, composite beams is better than RCC beams in high-rise and ordinary building because it can bear the loads on the building and it can gave more rigidity in it, which ensures the building’s safety from collapse.

3.2 Axial Force

The 23,061.3 KN is the maximum axial force in the RCC column on the ground floor to tenth floor, while in same floors in the composite column had 17,432.5 KN as maximum axial force, indicating that the composite column is subjected to 24.4% less axial force than the concrete column. 16,402.5 KN is the highest axial force in the RCC column, while 12,243.1 KN is the maximum axial force in the composite column and that happens in the 11th–20th floors, indicating a decrease by an average of 25.4% in the composite column in comparison to RCC column. On the 21st–30th floors, 9,760.9 KN is the largest axial force in the RCC, compared to its composite column, which had the greatest axial force on 6,963.4 KN, implying a 28.7% reduction in the composite column’s axial force compared to the RCC column. According to the previous findings and the graph in Fig. 3, the composite column’s maximum axial strength is significantly lower than that of the RCC column. As a result of the axial force, the composite column requires a smaller footing or foundation than the RCC column, whereas the RCC column requires a greater foundation to resist the axial force.

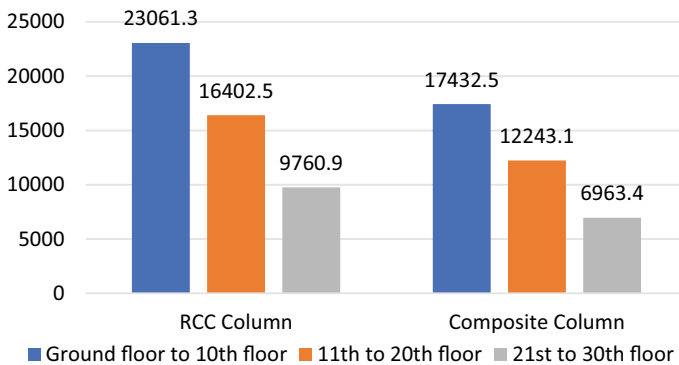


Fig. 3 Show the max. axial force in the column (KN)

Table 4 The maximum shear force on the beam (KN)

Floor	RCC	Composite	Note
G-10th	420.15	380.6	The maximum shear force is reducing in composite beam by 9.4%
11th–20th	396.5	320.7	The maximum shear force is reducing in composite beam by 19.12%
21st–30th	323.2	234.9	The maximum shear force is reducing in composite beam by 27.3%

3.3 Shear Force

Table 4 shows the results of shear force in the composite and RCC beams. The maximum shear force in the RCC beams from G-10th floor is 420.15 KN, whereas the shear force in the composite beam is 380.6 KN, and that represents a decrease in shear force by 9.4% at the composite beams compared to the RCC beams. 396.5 KN is the maximum shear force at floors 11th–20th in the RCC beams and on the other side 320.7 KN is the maximum shear force in composite beams. In floors 21st–30th the maximum shear force in both of RCC beams is 323.2 KN, whereas the maximum shear force in the composite beams is 234.9 KN, and this indicates the maximum shear force fell by 27.3% in these floors. Based on the preceding findings, composite beams outperform RCC beams in terms of shear force, allowing them to be smaller, allowing for more architectural space without causing structural damage.

3.4 Displacement

The term “displacement” is widely used in high-rise buildings to describe how far the building has moved away from its foundation. The side loads that the structure is subjected to, such as wind and earthquakes, have a direct impact on the displacement. In order, in both directions (*X* and *Y*), Fig. 4 shows a result of comparison in the displacement in the RCC and composite buildings, 0.0532 mm is the highest displacement in the RCC building *X* direction and in *Y* direction equal 0.0529 mm, while in composite building the highest displacement was 0.153 mm in the *X* direction and 0.153 mm in the *Y* direction, that is to say to a 65.23% increase in displacement percentage in the *X* direction and a 65.42% in the *Y* direction when compared to an RCC structure. The RCC building compared to composite structure has good resistance to displacement. But the findings of displacement results will haven't an impact in all circumstances because the values of it within the allowable displacement limitations in Euro code 2 and 4 [9].

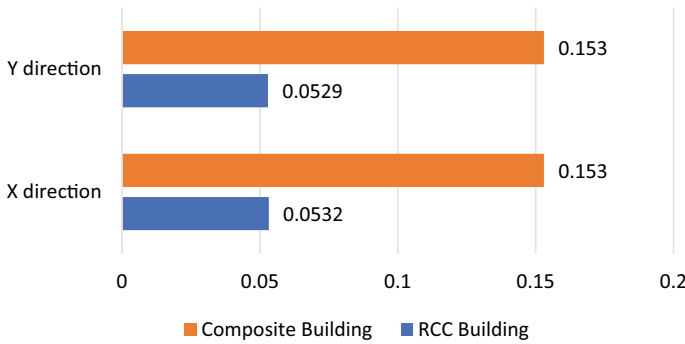


Fig. 4 Show the maximum displacement in the floors (mm)

4 Reviews for Composite Beam and Composite Column

See Table 5.

Table 5 Shows some details about for composite beam and composite column

Composite beam	Composite column
<p>Composite beams can be made out of a variety of materials, but the most frequent ones are concrete and steel. Other materials, such as pre-stressed concrete and wood, can also be employed. Steel beams are frequently used in reinforced concrete slabs, along with cast and prefabricated elements [10]</p>	<p>The steel concrete composite column is built composed of a hollow in the center of hot rolled steel or concrete-encased hot rolled steel. The interaction of concrete and steel in the composite column resists external loading on the structure through friction and bonding. It is feasible to construct a high-rise building by combining a composite column with a composite beam to give resistance, rigidity, and the ability to withstand large loads [11]</p>
Advantages of composite beam	Advantages of composite column
<ul style="list-style-type: none"> • Corrosion and fire resistance • As the structure’s weight decreases, the foundation cost will decrease • Provide design and fabrication freedom • Kept the loading and span the unchanged: steel is more cost-effective and appropriate for construction • Assist in the earthquake resistance • The criteria for long-span construction is met • Greater stiffness and hardness than equivalent steel, resulting in less deflection • In busy areas, it’s simple to schedule the construction [12] 	<ul style="list-style-type: none"> • The cross-sectional strength has improved • Increase the rigidity, which reduces the slenderness and increases the bulking resistance • The concrete-encased columns are fire resistant • The enclosed columns are protected • Alternatives to reinforced concrete and pure structural steel are particularly cost-effective • High-rise building construction • Formwork is necessary in the concrete-filled tubular [13]

5 Conclusion and Recommendation

According to the findings, buildings with composite columns resist the bending moment in the columns better than buildings with RCC columns, the bending moment in the *X* direction was reduced by up to 30.52% using composite columns and the bending moment in the *Y* direction by up to 40.5%. This means that composite columns can lower the bending moment value, making them more cost-effective in terms of materials as compared to RCC columns, to sustain the high bending moment, extra reinforcing and concrete may be required. In terms of beams, the bending moment of a composite can be reduced by up to 31.8%, this indicates that the ability of the composite beams is better in resisting bending moment compared to its counterpart RCC. RCC beams will be required to resistance of the bending moment more reinforcement and concrete and that lead to an increase in cost. In terms of axial force, the composite columns outperformed the RCC columns, with a resistance to axial forces of up to 28.7%. And through this result it does not require a big base in the composite building to withstand axial forces, as does its RCC counterpart which requires a big base to withstand to prevent it from collapsing. The composite beams were able to reduce shear force by up to 27.3%, indicating that composite beams are superior to RCC beams in resisting it. Since the huge distances between the columns, they will require more beams to resist and withstand shear forces, which composite beams can provide. The RCC building outperformed the composite building in terms of displacement, resisting displacement by up to 65.42%, however the displacement outputs in both buildings were within the Eurocode 2 and 4 allowable regions. Hence, this outcome will have no bearing on the structural analyses' preference for composite buildings. As a result of the preceding, it can be determined that composite structures resist both the bending moment, the shear force, and the axial forces far better than RCC buildings, giving them a significant advantage as a concrete alternative. Because composite structures feature both concrete and steel elements that can withstand tensile and compressive pressures, they perform better in structural analysis than RCC buildings. The composite building are combines the advantages of concrete and steel. As a result of the previous reason, it is possible to use smaller structural elements in the composite buildings compared to these structural elements in the RCC building, because the composite building can withstand the structural parameters, whereas the RCC building requires an increase in the dimensions of its elements to be able to resist the structural parameters and ensure the building is in safety position, as it is in this project, as result, the composite building is more better architecturally than the RCC building since it provides more interior space. It was found through the results that the composite high-rise building is superior to the RCC high-rise building in terms of design and structural analysis. In addition to that the composite structure does not require a large number of workers or a long period of time to create, as opposed to a concrete structure, which requires a large number of personnel and a long period of time to construct.

References

1. Muthulingam M, Vignarajah M (2017) Practical finite element analysis linear static and dynamic analysis. https://www.researchgate.net/publication/323026605_Practical_Finite_Element_Analysis_Linear_Static_and_Dynamic_Analysis
2. Singh DK (2021) Shear forces and bending moments. In: Strength of materials. Springer, Cham, pp 143–206. https://www.researchgate.net/publication/347588808_Shear_Forces_and_Bending_Moments
3. Robert L, Joseph A (2021) Shearing forces and bending moments in beams. https://www.researchgate.net/publication/351705644_Shearing_Forces_and_Bending_Moments_in_Beams
4. Shweta A, Wagh et al (2014) Int J Eng Res Appl 4(4):369–376. ISSN: 2248-9622. https://www.ijera.com/papers/Vol4_issue4/Version%201/BI044369376.pdf
5. Computers and Structures, Inc. CSI (2021) <https://www.csiamerica.com/products/etabs>
6. CADbull (2019) <https://cadbull.com/detail/988/Apartment-design>
7. SGetIntoPC.com (2020) <https://getintopc.com/software/3d-designing/csi-etabs-ultimate-2017-free-download/>
8. Mechanika (2021) Non-linear analysis. <https://mechanika-ltd.com/non-linear-analysis/>
9. Muley P, Radke A (2019) Performance of high rise building under seismic and wind excitation for the different plan configurations of same area. https://www.researchgate.net/figure/shows-analysis-of-all-twenty-one-models-in-ETABS-for-displacement-at-each-level-due-to_fig1_337943131
10. Ujjwal B, Kumar P, Singh A, Shivam V, Yatendra B (2018) Design and analysis of a residential building using ETABS integrated with green building concept. <https://www.semanticscholar.org/paper/Design-and-Analysis-of-a-Residential-Building-using-Bhardwaj-Kumar/69cfc394ac661745f8505ac1ab50513fc08b8955>
11. Wave City (2021) High-rise buildings—advantages and benefits. <https://www.wavecity.in/blog/high-rise-buildings-advantages-benefits>
12. Farouk A (2011) High rise buildings and how they affect countries progression. <https://www.g-casa.com/conferences/zagreb/papers/Akram1-HighRise.pdf>
13. Akshay Dashore (2020) 10 construction challenges in high-rise buildings. <https://theconstructor.org/building/construction-challenges-high-rise-buildings/45779/>

A Study on Deformation Characteristics of Splice Connection in Steel Structures



V. Ramana Kollipara, T. D. Gunneswara Rao, and P. Sridhar

Abstract The local failure of the connections in a steel framed structure affects the serviceability criteria of the whole structure. Hence, it is necessary to understand the behaviour and failure mechanisms of the connections that are used in steel framed structures. In view of this, the present paper describes the investigations conducted on the performance of splice connections for hollow tubular sections (HTS). In both experimental and numerical studies, a parametric variation is also considered in the dimensional properties of the connection components, such as end plate thickness, thickness of HTS member, and bolt diameter. Splice connections with different end plate configurations are subjected to pure bending to study the failure mechanism. Later, a comparison of load-deflections curves, initial stiffness and energy absorption values of the splice connections obtained from both experimental and numerical approaches was done. It was concluded that the proposed FE model is able to predict the performance and failure mechanism of splice connection joining HTS members accurately.

Keyword Energy absorption · Hollow tubular sections · Initial stiffness · Pure bending · Splice connections

1 Introduction

Nowadays, there is an increase in usage of hollow tubular sections (HTS) as a moment resisting component in steel framed structures to reduce the total weight and also to minimize the maintenance cost of the structures [1]. The performance of any steel framed structure depends mainly on the strength and deformation capacities of its

V. Ramana Kollipara (✉)

Associate Professor, Lakireddy Balireddy College of Engineering, Mylavaram, India

T. D. Gunneswara Rao

Professor, NIT Warangal, Hanamkonda, India

e-mail: laxmansaty@student.nitw.ac.in

P. Sridhar

Assistant Professor, Shri Vishnu Engineering College for Women, Bhimavaram, India

connections/joints. End plate connections show better performance than the regular connections due to high strength, more ductility, etc. These additional benefits lead to increase in the utilization of splice connections for the assembly of various joints in the main steel framed structures. The significant research available on the extended end plate connections is mostly limited to the fabrication of regular joints only, whereas the research on Splice connections joining tubular sections is scarce.

Initially, Krishnamurthy et al., conducted a theoretical and numerical study on end plated connections by varying the thickness of end plate. Design equations are proposed to calculate the capacity of splice connection, and the same proposed equations were validated by comparing with the numerical results in both 3D and 2D models [2]. The dimensional parameters of the connection components influence the behaviour of the connection. Due to this parametric variation, the connections may show either semi rigid or fully rigid type behaviour [3, 4]. Dessouki et al. performed both analytical and numerical studies on the splice connections joining I-beams as beam-beam and beam-column joints with and without stiffeners. It was concluded that the performance of splice connection depends on the both material and geometric non-linearity of the connection [5]. Design yield moment equations are developed for a splice connection of hollow tubular sections, and the proposed equations are validated through the appropriate experimental programme. Finally, it was concluded that the mechanical properties of the splice connection depends on the dimensional parameters of its connection components [6]. Abidelah et al. studied the behaviour of splice connection of I-beams with and without end plate stiffeners. The properties like stiffness, load carrying capacity and energy absorption of the connections may vary based on the stiffeners provided to the connection and these stiffeners are also helpful for the equal distribution of applied load to all the fasteners of the connection [7]. End plate connections show reserve strength in it when the connection reaches to the strain hardening state [8]. Research on joining of hollow tubular sections using end plate connections is limited to the column-column splice connections, which are subjected to various types of loading conditions [9, 10]. Kabanda conducted a comparative study on bending capacities of two different hollow tubular sections (Rectangular and Polygon) and concluded that the proposed polygon hollow tubular sections have more bending capacity than regular rectangular hollow sections [11]. Theoretical design equations are established to compute the moment capacities of a splice connection for square HTS members, and the validation of theoretical equations is done using the experimental results [12].

2 Experimental Programme

The present experimental programme is devoted to study the influence of connection components (like end plate, bolt and weld) on the performance of beam-beam splice connection of square HTS members. For this three end plate connection configurations are considered (as shown in Fig. 1) having the variation in number and

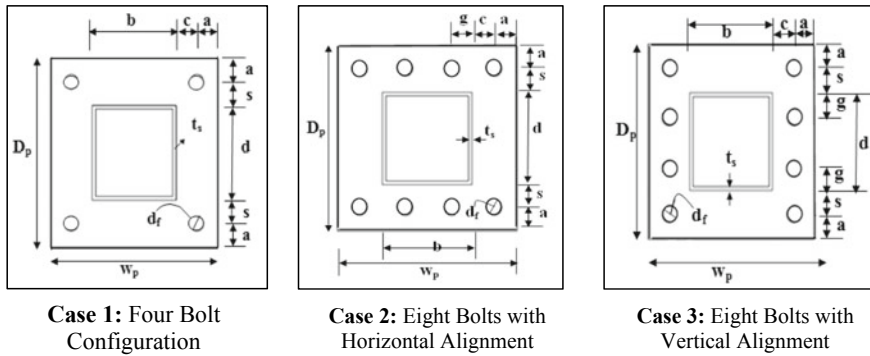


Fig. 1 Detailed layout of end plate connection configurations [12]

alignment of bolts in the connection. The first case comprises a four-bolt configuration in which bolts are arranged in two rows on top and bottom side of the section flange. In second and third cases, eight number of bolts are adopted for the connection fabrication with two different alignment of bolting i.e., horizontal alignment and vertical alignment. In addition to the variation in number and position of the bolts, a parametric study is also conducted by varying the dimensions of the end plate, diameter of the fasteners and the dimensions of HTS members. All members are tested under four-point loading arrangement.

In this experimentation, mild steel square shape HTS with two different thicknesses are adopted with the projected yield strength of 210 MPa. The details of sections are given in Table 1. The dimensions (W_p , D_p) and thickness (t_p) of end plate are different for each test of three connection configurations. The experimentally predicted yield and ultimate strengths of end plate are 250 MPa and 410 MPa respectively which are conforming to E250 (Fe410W) A grade according to IS: 2062. The diameter of fasteners is considered as another parametric variation in the present study. Mild steel of 8.8 grade material bolts with two different diameters are chosen according to IS: 1367 (Part3). The yield and ultimate strengths of bolts are 640 MPa and 800 MPa respectively. The contact between the end plate and HTS member is developed using two different thicknesses (3 and 5 mm) of fillet weld. Table 2 gives the dimension details of the connection components for each case.

Based on the parametric variation considered, a notation is given for each test specimen of three connection configurations as follows: ‘Case 1a’, ‘Case 1b’ and ‘Case 1c’ are indicating the four-bolt connection configuration, ‘Case 2a’, ‘Case 2b’ are for eight-bolt connection configuration with horizontal alignment of bolting,

Table 1 Dimension details of HTS [6]

S. No.	Section	Breadth ‘b’(mm)	Depth ‘d’(mm)	Thickness t_s (mm)	Yield stress (MPa)
1	HTS1	50	50	1.2	210
2	HTS2	50	50	2	210

Table 2 Details of the connection configurations with parameters

S. No.	Case	Type of section	End plate dimensions (mm)			Position of fastener w.r.t. the flange or web of section (mm)				No. of bolts in the splice connection	Dia. of bolt, d_b (mm)
			w_p	D_p	t_p	a	c	s	g		
1	Case 1a	HTS1	75	110	6	10	0	20	...	4	6
2	Case 1b	HTS2	75	110	6	10	0	20	...	4	6
3	Case 1c	HTS2	100	140	5	20	0	20	...	4	12
4	Case 2a	HTS2	90	120	6	15	10	20	10	8	6
5	Case 2b	HTS2	90	120	4	15	10	20	10	8	6
6	Case 3a	HTS2	120	90	6	15	20	10	10	8	6
7	Case 3b	HTS2	120	90	4	15	20	10	10	8	6

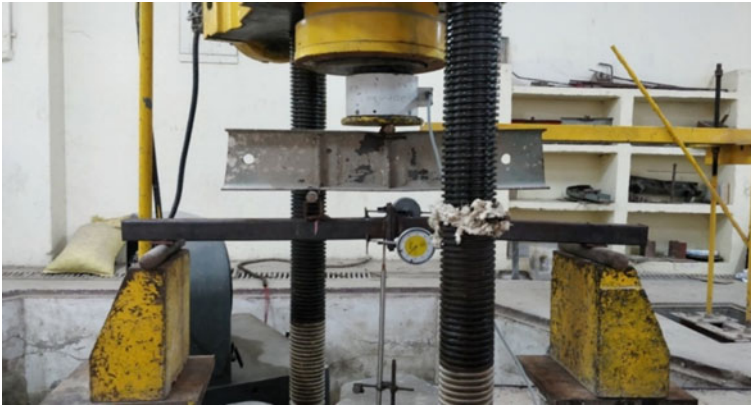


Fig. 2 Four point loading test setup [6]

and ‘Case 3a’, ‘Case 3b’ specifies eight-bolt connection configuration with vertical alignment of bolting. The edge distance is indicated as ‘a’. Position of fastener from the face of section flange and web is denoted by ‘c’ and ‘s’ respectively. The position of interior bolt w.r.t. the section flange or web is designated as ‘g’. In this experimental programme DAC system (which is having a load cell and LVDT) was used to measure the applied load and corresponding deflection of the specimen. The following Fig. 2 shows the four-point arrangement.

3 Numerical Study

In this approach, the test specimens are modelled and analyzed under the loading of pure bending using the finite element package ANSYS. A nonlinear elastic–plastic model is used for the prediction of performance of the steel material in the simulation process. It was adopted for HTS members, end plate, and a bilinear model is adopted for the fasteners. The components of splice connection i.e. HTS members and end plate are modelled with sharp edges.

3.1 Description of FE Model

Three-dimensional finite element models are prepared for each case of beam-beam splice connection in ANSYS. For all numerical models, both material and geometric non linearities are considered in the simulation process and are selected from the standard ANSYS library. 8-noded hexahedral solid brick elements are used to model the main components (HTS member and End plate) of the splice connection, and are meshed with 10-noded tetrahedral brick elements. Surface-surface contact property

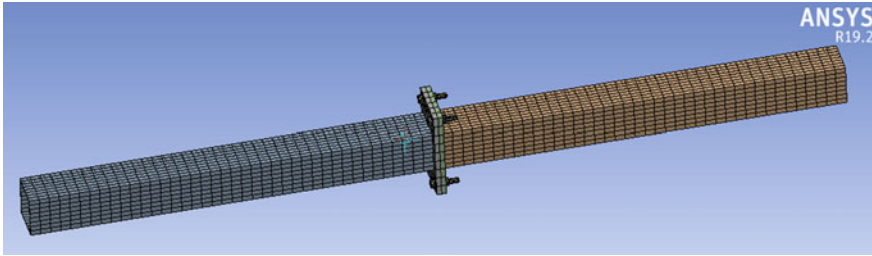
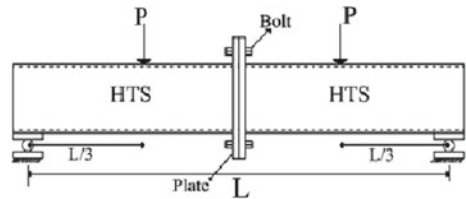


Fig. 3 Finite element modelling of the splice connection members

Fig. 4 Schematic diagram of four point loading [6, 12]



is adopted for developing the interaction between the all connection components (end plate, HTS member, bolt and nut). Bonded contact with a frictional coefficient of 0.15 is assigned for the interactions of end plate and HTS member, and bolt and nut. Frictionless contact is adopted for the development of interaction between end plate and end plate; end plate and nut; and bolt and nut. A fine mesh with structural meshing method is used to attain the proper element shape. The following Fig. 3 shows the finite element model of the proposed end plate connection configuration.

All finite element model specimens are subjected to four-point bending test and to simulate the model the both ends of the members are given as simply supported boundary conditions. The total load is divided into two-point loads and are applied on either side of splice connection at an equal distance (as shown in Fig. 4). Constant increment of loading is adopted for the simulation process.

4 Results and Discussions

Various failure modes of the splice connections of the proposed end plate configurations were observed corresponding to its parametric variation. For each case, a comparison was done between the experimental and numerical failure modes, and it was observed that similar type of failure has occurred in both the approaches. In four-bolt connection configuration, a total of three cases are considered and for each case a different failure mode was observed. Figures 5, 6 and 7 are showing the mode of failures occurred in the four bolt connection configurations. In 'Case 1a' specimen, observed failure mechanism may be caused due to the lesser thickness

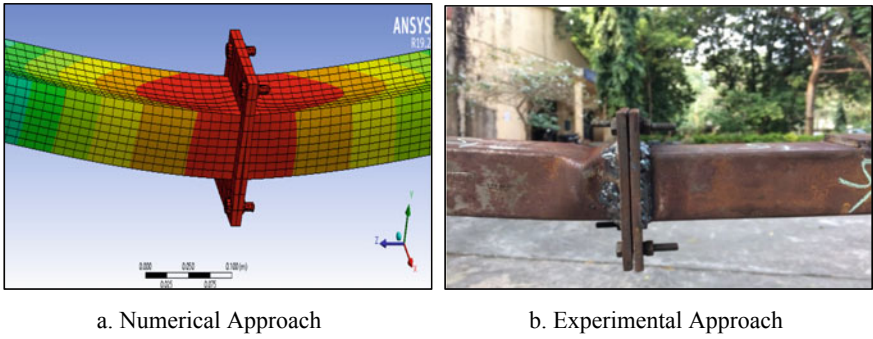


Fig. 5 Failure mechanism in the splice connection of 'Case 1a'

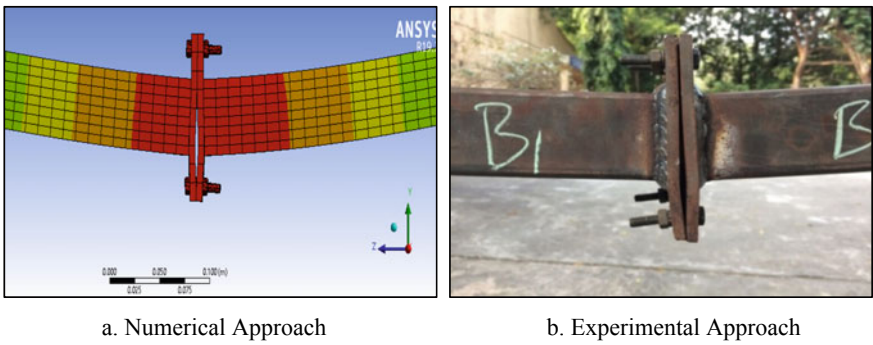


Fig. 6 Failure mechanism in the splice connection of 'Case 1b'

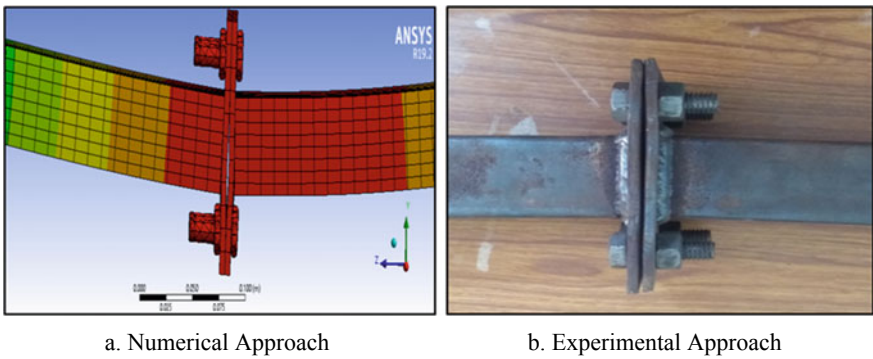


Fig. 7 Failure mechanism in the splice connection of 'Case 1c'

of HTS member. The failure of the splice connection in ‘Case 1b’ is majorly due to the bending of tensile bolts, and also a small amount of yielding of end plate in the connection was observed. Higher yielding of end plate is occurred in the splice connection of ‘Case 1c’ during the loading which is termed as end plate failure mechanism.

In eight bolt connection configuration two cases are considered for each alignment (horizontal and vertical) of bolting and Figs. 8, 9, 10 and 11 show the observed failure mechanisms in the splice connection for both alignments. For all cases, the failure of the splice connection occurred due to the yielding of end plate alone. In case of vertical alignment of bolting, yielding of the end plate is occurred at the bottom of connection which is in the direction perpendicular to the plane of the splice connection. It may be caused due to the higher gauge distance between the two vertical rows of bolts in the connection.

For each case, load versus deflection curves are developed and a comparison is given between both experimental and numerical approaches. Figure 12 illustrates the comparison of load versus deflection curves for all cases. From these curves, connection properties like energy absorption capacity and initial stiffness are calculated and compared for both the approaches. Table 3 gives the details of values of the

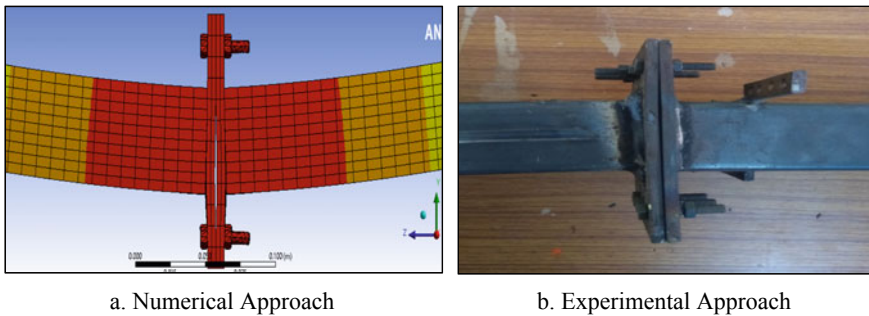


Fig. 8 Failure mechanism in the splice connection of ‘Case 2a’

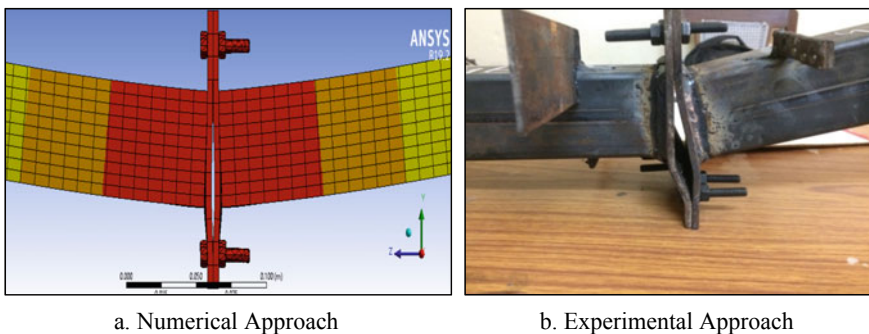


Fig. 9 Failure mechanism in the splice connection of ‘Case 2b’

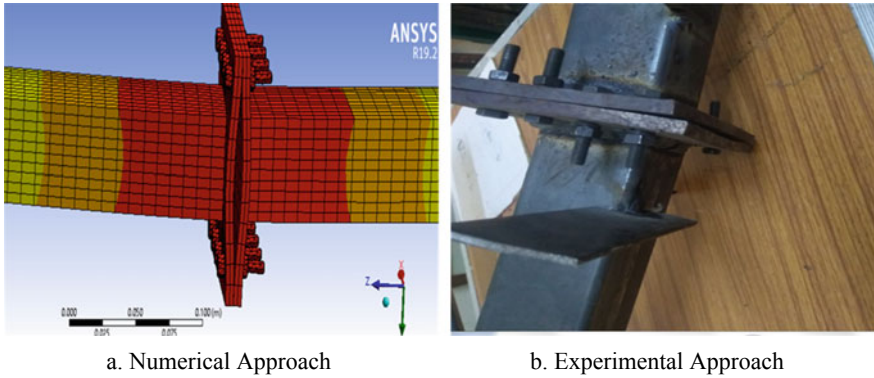


Fig. 10 Failure mechanism (bottom side) in the splice connection of ‘Case 3a’

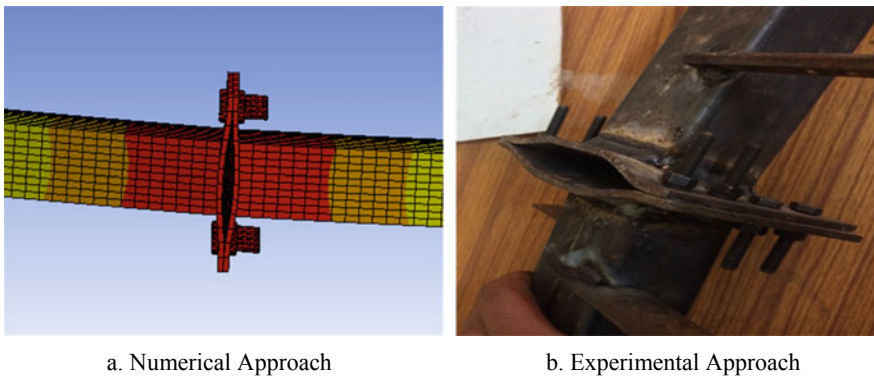


Fig. 11 Failure mechanism (bottom side) in the splice connection of ‘Case 3b’

connection properties. A good correlation is observed between both experimental and numerical results.

5 Conclusions

The present paper describes the experimental and numerical investigations on the behaviour of splice connections for tubular sections. A total of three splice connection configurations are considered along with a dimensional parametric variation. Based on the observed failure modes in the splice connections and obtained results, the conclusions are summarized as below:

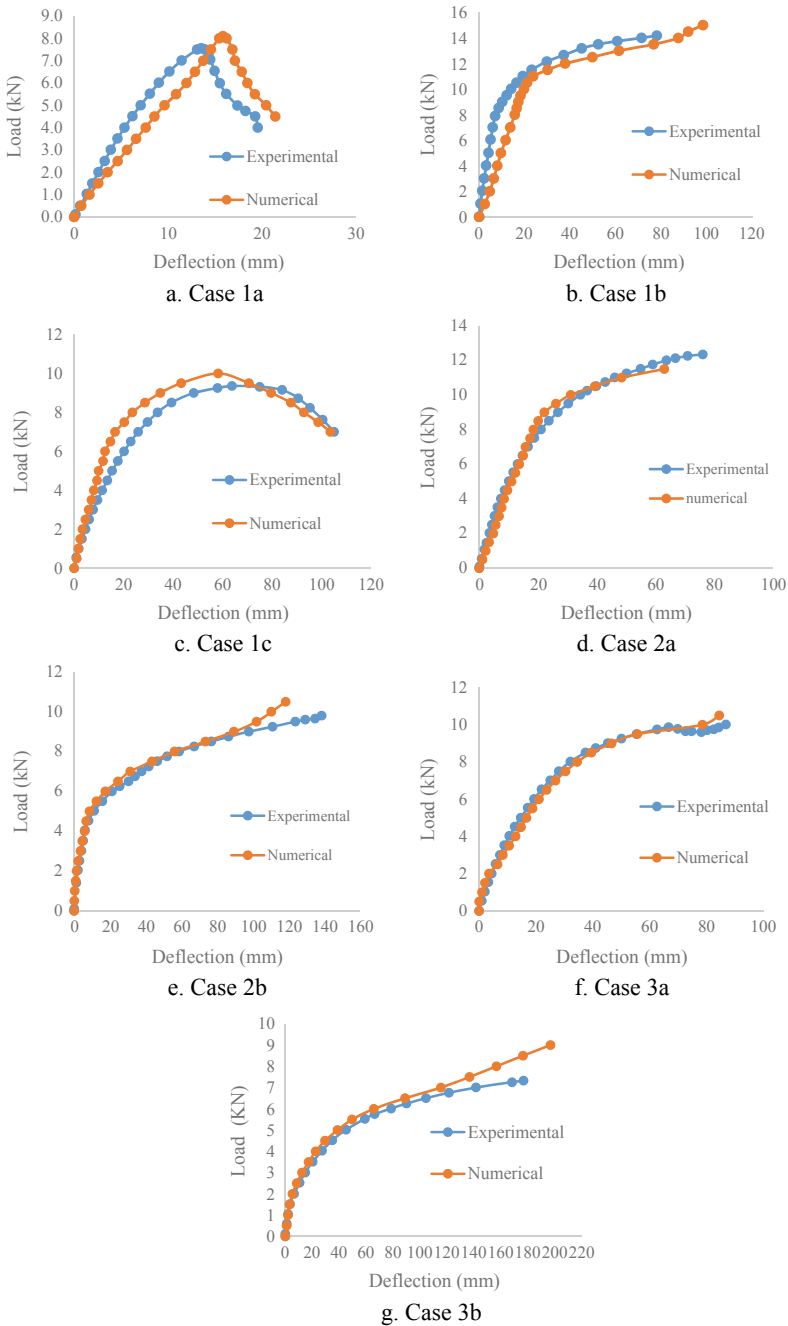


Fig. 12 Comparison of load versus deflection curves

Table 3 Comparison of connection parameters

S. No.	Case No.	Mode of failure	Ultimate load (kN)		Energy absorption capacity (kN mm)		Stiffness of the connection (kN/mm)	
			Experimental	Numerical	Experimental	Numerical	Experimental	Numerical
1	Case 1a	Specimen	7.5	8	94.7	99.41	0.711	0.803
2	Case 1b	Bolt	14.18	15	916.167	1044.24	1.352	1.538
3	Case 1c	End plate	9.35	10	795.29	838.26	0.334	0.385
4	Case 2a	End plate	11.5	12.33	701.377	617.21	0.552	0.478
5	Case 2b	End plate	9.8	10.5	1081.62	930.65	0.656	0.761
6	Case 3a	End plate	10	10.5	720.34	627.23	0.345	0.306
7	Case 3b	End plate	8.10	9	1019.39	1172.96	0.138	0.157

- A sudden failure in the member, and drop in the values of energy absorption and initial stiffness of the splice connection are observed in the case of lesser thickness of HTS member.
- With an increase in the thickness of end plate, the ductile nature of the connection increases, which leads to the increment in the values of energy absorption and initial stiffness.
- The obtained results indicate that the stiffness of splice connection increases with an increase in the diameter of bolts. Also, the number of bolts used for the fabrication also influences the performance of the splice connection.
- The connections having horizontal alignment of bolting shows better performance than the vertical alignment, which may be due to the higher gauge distance between the bolts in the vertical alignment.
- The percentage variation between the results obtained from both experimental and numerical approaches are in the considerable range. So, it was concluded that the FE model is able to accurately predict the performance/failure mechanism of the end plate splice connection joining HTS members.

References

1. Willibald S (2003) Bolted connections for rectangular hollow sections under tensile loading. Doctoral dissertation, Verlag nicht ermittelbar
2. Krishnamurthy N, Graddy DE (1976) Correlation between 2-and 3-dimensional finite element analysis of steel bolted end-plate connections. *Comput Struct* 6(4–5):381–389
3. Mashaly E, El-Heweity M, Abou-Elfath H, Osman M (2011) Behaviour of four-bolt extended end-plate connection subjected to lateral loading. *Alex Eng J* 50(1):79–90
4. Seradj H (1997) Ductile end-plate connections utilizing plate yielding. Doctoral dissertation, University of Oklahoma
5. Dessouki AK, Youssef AH, Ibrahim MM (2013) Behaviour of I-beam bolted extended end-plate moment connections. *A Sha Eng J* 4(4):685–699
6. Kollipara VR, Rao TG (2019) Experimental and analytical study for plastic moment capacity of beam-beam splice connection. *Int J Ste Str* 19(4):1202–1208
7. Abidelah A, Bouchaïr A, Kerdal DE (2012) Experimental and analytical behaviour of bolted end-plate connections with or without stiffeners. *J Con Ste Res* 76:13–27
8. Agerskov H, Bjørnbak-Hansen J (1985) Bolted connections in round bar steel structures. *J Str Eng* 111(4):840–856
9. Kato B, Mukai A (1985) Bolted tension flanges joining square hollow section members. *J Con Ste Res* 5(3):163–177
10. Kato B, Mukai A (1991) High strength bolted flange joints of SHS stainless steel columns. *Els Ap Sci Pub Ltd* 107–115
11. Kabanda JS (2017) Comparison of the moment rotation capacities of rectangular and polygonal hollow sections. *J Con Ste Res* 137:66–76
12. Kollipara VR, Rao TG (2019) Theoretical approach to the moment capacities of beam-beam splice connection for SHTS. *J Con Ste Res* 160:332–339

A Comparative Study on Strength Characteristics of Fiber Reinforced Geoactivator Activated Geopolymer Concrete



S. Jagandas, G. Mallikarjuna Rao, and M. Venu

Abstract This paper presents the behavioural comparison of plain and fibers added geopolymer concrete (GPC) prepared by fly ash-ground granulated blast furnace slag (GGBFS) based and activated with geo activator with silica modulus (M_s) of 2.92, test specimens cured under normal temperature curing conditions. The production of carbon dioxide is approximately 8%, experimental work is done in this research to develop a field construction binder that replaces the OPC and reduces the emission of carbon dioxide (CO_2), producing green and sustainable concrete. Any earth crust materials which are rich in silica (Si) and alumina, to activate the source materials combination of sodium or potassium-based activators are used by many researchers but it requires high concentration and oven heat curing at $60^\circ C$ for 24 h, to get better strength making it an uneconomical and still it is inconclusive for field construction. In this research, a single reagent alkaline-based solution, geo activator (neutral grade sodium silicate) was used to develop the fiber-reinforced GPC (FRGPC). This research work is done to understand various mechanical properties with geo activator and checked the workability before going to cast the specimens. The results of this paper are useful for construction industries and also future researchers.

Keywords Geopolymer concrete · Geoactivator · SFRGPC · GFRGPC · Fly ash · GGBS

1 Introduction

According to knight frank India-2021 only in 3 months, 76,006 building constructions are started, compared to last year the increment is 38% more. Concrete is the most popular modern composite construction material, today, second only to water,

S. Jagandas (✉) · G. Mallikarjuna Rao · M. Venu
Department of Civil Engineering, Vardhaman College of Engineering, Hyderabad, India

G. Mallikarjuna Rao
e-mail: mallikarjuna@vardhaman.org

M. Venu
e-mail: venucivil@vardhaman.org

concrete is the most consumed composite material with three tons per annum used for each person within the world. Twice the maximum amount of concrete is employed in the construction world as all other building materials combined. The materials required to make concrete are cement, aggregate, and water but cement is the artificial material made by burning the natural limestone at high temperature, release high carbon dioxide, and consuming 4GJ of energy per one ton. Nowadays, fast increases in the construction activity to meet the rapid increase in the development of infrastructure in countries like India and China. Day by day the consumption of cement is increasing, expected to reach 500 million tons by 2030. The OPC binder used in traditional concrete releases approximately 8% of CO₂ which affects the ozone layer and human health and creates climate problems. To overcome this need to plant 2.62 billion acres of forest land which is equal to island and cement is highly energy-intensive. The available limestone to make the OPC is sufficient for the next 50 years only. To overcome this need to develop alternative geopolymer cement that replaces the OPC and produces green and sustainable concrete material. Finding the necessary substitute to OPC and thus reducing the CO₂ emission. In the modern era, with rapid industrialization and urbanization, world global demand for construction materials increases every year from county to country. The increased demand for construction needs more natural by-products of cementitious materials which bind aggregate 70% of the total volume of concrete. At present, ground granulated blast furnace slag (GGBS), red mud, fly ash, silica fume, metakaolin, graphene powder have been using the partial substitute or additional materials to OPC for better physical and durable properties than OPC concrete. Complete replacement of these materials is not fit based on their mechanical properties and economy. There is a necessity to search for an alternative to OPC paste which is of lower CO₂ emission, make use of the waste by-products. In this context, geopolymer concrete has reached considerable attention from both academics and the concrete industry. Besides environmental friendliness, excellent plastic properties and other properties such as superior resistance against thermal stability chemical attack, or even smartness were extensively reported.

Davidovits [1] produced a geopolymer binder by polymeric reaction combining alkaline reagent with the silica and alumina in the source material of earth crust or by-product material as given in the above paragraph [2] stated that geo activator is used to develop a cast in situ construction concrete which is also called neutral grade sodium silicate, is a single alkaline activator solution not required in the combination of activators instead of water geo activator is used. This project work is done to understand the behavior for fly ash-ggbs mixer-based field geopolymer concrete activated with a single hardener-based activator by conducting a fresh test and harden test, on GPC specimens.

2 Literature Review

Davidovits et al. [3] stated that geopolymer concrete is a by-product inorganic polymer composite produced from the alkaline chemical reaction of aluminosilicate compounds to yield an amorphous to semi-crystalline 3-D structures consisting of repeating Si–O–Al. Further, these monomers are poly-condensed to form a rigid three-dimensional (3-D) structure of silicates and aluminates. Mallikarjuna Rao et al. [4] studies suggested that a combination of fly ash 70% and, GGBS 30% used geopolymer concrete and hardener consisting of mixer sodium hydroxide and metasilicate of few different molarities (16, 12, 8 M). The ratio of metasilicate sodium to sodium hydroxide considered or concluded in this work is 2.5 to 2.6. Mallikarjuna Rao et al. [4] studies suggested geo activator used fly ash-ggbs based combination GPC gives better strength at normal temperature compared to OPC. Vikas Gugulothu et al. [5] different GGBS percentages, activated with geoactivator, concluded that, good workability and good mechanical properties than OPC.

3 Experimental Study

This research paper presents the comparative study of mechanical properties of GPC and FRGPC, prepared by fly ash-GGBS based and activated with a single solution-based activator. Prepared and cured in normal temperature about $28^{\circ}\text{C} \pm 2$.

3.1 Materials

Fly ash: Indian low calcium class-F fresh dry fly ash used, taken from the silos of rank ready mix concrete plant near Hyderabad outer ring road (ORR) Shamshabad, was used as one of the main base material up to 70%.

GGBS: Waste product from the fresh blast-furnaces manufacturer to make iron. Blast-furnaces became powder at high temperatures of more than $1,600^{\circ}\text{C}$. It is a pozzolanic material with higher percentages of calcium oxide. GGBS took from Toshali cement powder Pvt. Ltd India. The biochemistry of materials fly ash-GGBS is mentioned in Table 1.

Fine aggregate: Locally available best quality Indian fresh sand was used with a specific gravity of 2.62. As per the test sieve analysis, the fine sand material was declared to be in zone II, and conforming to IS 383:1970 it's cleaned from dust, dried from moisture content, and stored in a fresh place before going to use.

Coarse aggregates: Locally available CA are taken and cleaned, dried before going to use. Different sizes of coarse aggregates such as 4.75, 12, 16, and 20 mm are used, from each size, 25% of aggregates are taken for experimental work.

Table 1 Chemical composition of materials pulverised fuel ash & GGBS

Oxide	Percentage (by weight)	
	Fly ash	GGBS
SiO ₂	61.93	36.3
Al ₂ O ₃	28.11	16.6
Fe ₂ O ₃	4.13	1.6
CaO	0.88	34.8
Na ₂ O	0.37	0.2
K ₂ O	0.8	0.5
Other oxides	3.3	9.6
Loss of ignition	0.47	0.4
Amorphous content	82(35% of SiO ₂ and 46% of mullite)	

Geo activator or Geo hardener: In this study, a single alkaline hardener was used with specific gravity 2.1 and silica modulus SiO₂:Na₂O (Ms) = 2.92:1 with 28.98% SiO₂, 9.92% Na₂O by mass, which was produced and transported from Chennai, KIRAN GLOBAL Ltd, India.

Steel fiber: End hooked steel fibers (Sf) were used in this work with 0.16 mm dia and 50 mm height and aspect ratio of 60. The fiber dosage was taken at 0.5, 1 and 1.5% on volume fraction (V_F).

Glass fiber: Synthetic macro glass fiber (Gf) is used with 0.1 mm dia and 6 mm height.

Superplasticizer: Naphthalene Conplast-430 based superplasticizer is used to improve the workability of fibers added to GPC.

3.2 Mix Design

The binder to solution ratio is fixed at 0.55. Binder content is fixed at 450 kg/m³ for every trail of mixing the fly ash content and GGBS content is fixed, i.e., 70% and 30% for set 1 and 50% and 50% for the second set of total binder content. Workability consideration is not required because the workability is excellent by geo activator alone for plain GPC in case of HFRGPC superplasticizer used (Table 2).

4 Results and Conclusions

4.1 Workability

Geo activator used fly ash-ggbs based GPC workability is better than OPC concrete. The viscosity of the geo activator is more than the water and the geo activator is like an oily gel, it increases the cohesion between particles to particles. Even though adding

Table 2 Mix proportion of field geopolymer concrete

S.NO	Binder content (kg/m ³)	FA:GGBS ratio	alkaline/binder ratio	Fine agg. (kg/m ³)	Coarse agg. (kg/m ³)	Alkaline liquid(kg/m ³)	Steel fiber (%)	Glass fiber (%)	SP (kg/m ³)
Mix A	450	70:30	0.55	760	972	247.5	NIL	NIL	NIL
Mix B	450	50:50	0.55	760	972	247.5	NIL	NIL	NIL
Mix C	450	70:30	0.55	760	972	247.5	0.5	0.25	2.25
Mix D	450	70-30	0.55	760	972	247.5	1	0.50	4.5
Mix E	450	70-30	0.55	760	972	247.5	1.5	0.75	6.7
Mix F	450	50-50	0.55	760	972	247.5	0.5	0.25	2.25
Mix G	450	50-50	0.55	760	972	247.5	1	0.50	4.5
Mix H	450	50-50	0.55	760	972	247.5	1.5	0.75	6.7

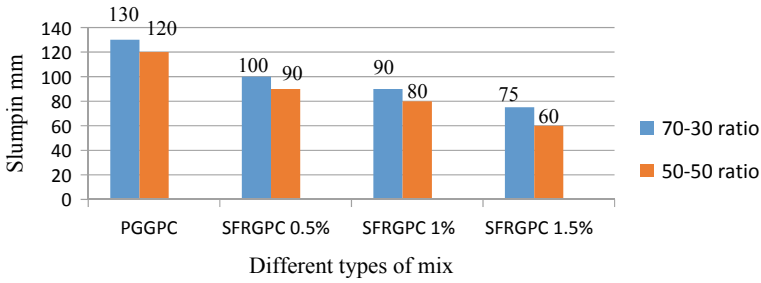


Fig. 1 Workability for SFRGPC

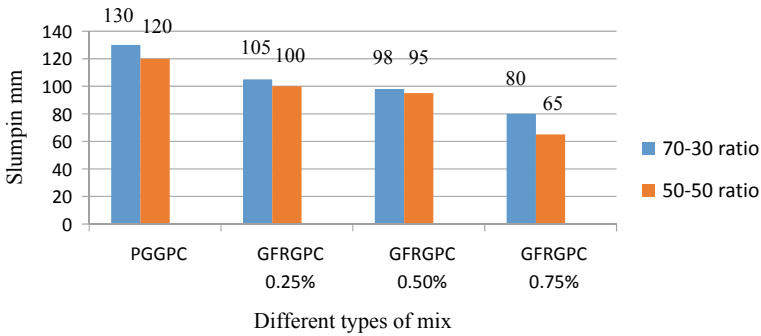


Fig. 2 Workability for GFRGPC

fiber up to 1% the slump is better than OPC slump because fibers are not absorbing activator-like conventional concrete because the solution has oily gel behavior, so obviously workability is better than OPC. The workability is better in the pan mixer compared to the hand mixer. The slump is 130 mm for the fly ash-GGBS combination ratio 70–30 and 125 mm for the 50–50 ratio given in Figs. 1 and 2. Workability is slightly decreased by increasing the GGBS percentage because the shapes of the GGBS particle are angular but still, it is workable. By adding steel fibers 1.5% to GPC workability is reduced to 60 mm, to achieve better workability naphthalene-based superplasticizer is used on the mass of binder content. Sometime extra geo activator were added to improve the workability because in the case of 50–50 ratio concrete settled within a minute. Workability is not too different between SFRGPC compared to GFRGPC however workability is better in GFRGPC because the cluster formed by glass fiber is smaller than steel fibers. As shown in Figs. 3 and 4 in each mix workability has decreased approximately 1% from 70–30 to 50–50 ratio because 20% GGBS has increased. Increment of GGBS percentage leads to decrement in workability.

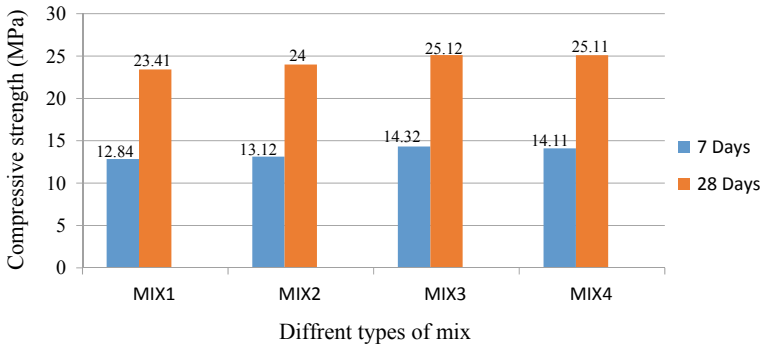


Fig. 3 Comparison compressive strength of SFRGPC between 7 and 28 days

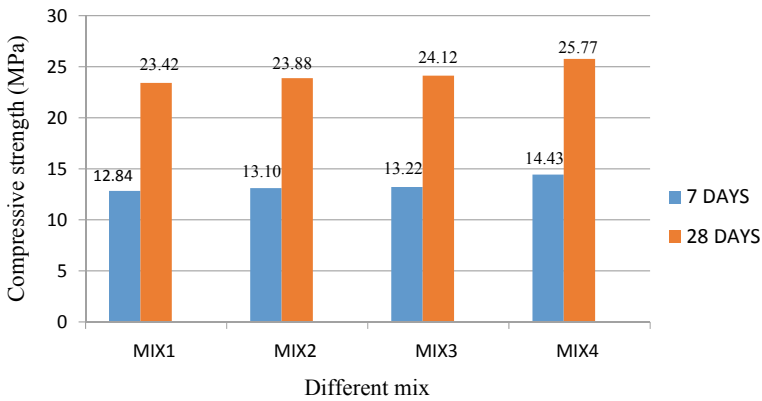


Fig. 4 Comparison compressive strength (MPa) of GFRGPC at 7 days and 28 days

4.2 Compressive Strength

Figure 3 shows that the comparison of compressive strength of fly ash-GGBS is 70–30 ratio based SFRGPC for 7 days and 28 days. Mix1 is plain GPC without steel fiber, strength at 7 and 28 days 12.84 and 23.41. There is an increment in strength by increasing steel fiber dosage 0.5 and 1% but at 1.5% small decrease in the strength. The increment between 7 to 28 days is approximately 50%. It is the same in the case of steel fiber added GPC also. The strength variation is more different between 7 and 28 days. The main observation done in the experiment is that fast increment of strength when specimens are directly exposed to the sun rays but specimens kept in the lab the polymerization process slows down as well as by increasing activator content also increases in the strength. In the case of geo activator-based GPC at 7 days, 64% strength is achieved and at 28 days 117% strength is achieved. Compared to OPC 17% more strength is achieved but in the case of 0.5 and 1% steel dosage mix1,

mix2 strength is increased but at 1.5% strength is decreased. In the first 3 mixes, 7 days to 7 days strength is increased approximately 1% and 28 days to 28 days is also approximately 1% increased but in mix4 0.5% strength is decreased.

Figure 4 is analyzed by comparing the compressive strength of fly ash-GGBS to a 70–30 ratio-based GFRGPC for 7 days and 28 days. Mix1 is plain GPC without steel fiber, strength at 7 and 28 days 12.84 and 23.42. There is an increment in strength by increasing glass fiber dosage 0.25, 0.50 and 1%. The increment between 7 and 28 days is approximately 50%. It is the same in the case of steel fiber added GPC also for all mixes. The strength variation is more different between 7 and 28 days. The main observation done in the experiment is that fast increment of strength when specimens are directly exposed to the sun rays, but specimens kept in the lab the polymerization process slows down as well as by increasing activator content also increase in the strength in glass fibers added GPC also. In mix1 the increment of strength is more than the OPC concrete, in the case of geo activator-based GPC at 7 days 64% strength is achieved, and at 28 days 117% strength is achieved. Compared to OPC 17% more strength is achieved but in the case of 0.25, 0.50 and 0.75% micro glass fiber dosage in all mixes compressive strength is increased. In all the 4 mixes compressive strength increased 7 days to 7 days and 28 days to 28 days is approximately 1%.

Figure 5 shows that the comparison of compressive strength of fly ash-GGBS is 50–50 ratio based on SFRGPC for 7 days and 28 days. Mix1 is a plain GPC without steel fiber, strength at 7 and 28 days, 15.64 and 26.13. There is an increment in strength by increasing steel fiber dosage 0.5 and 1% but at 1.5% small decrease in the strength. The increment between 7 to 28 days is approximately 59%. It is the same in the case of steel fiber added GPC also. The strength variation is more different between 7 and 28 days. The main observation done in the experiment is that fast increment of strength when specimens are directly exposed to the sun rays but specimens kept in the lab the polymerization process slows down as well as by increasing activator content also increase in the strength. In mix1 the increment of strength is more than the OPC concrete, in the case of geo activator-based GPC at 7 days 78% strength is

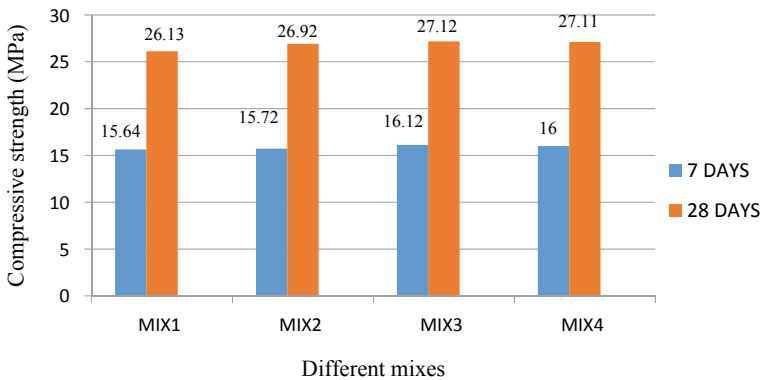


Fig. 5 Comparisons of SFRGPC of 7 days and 28 days

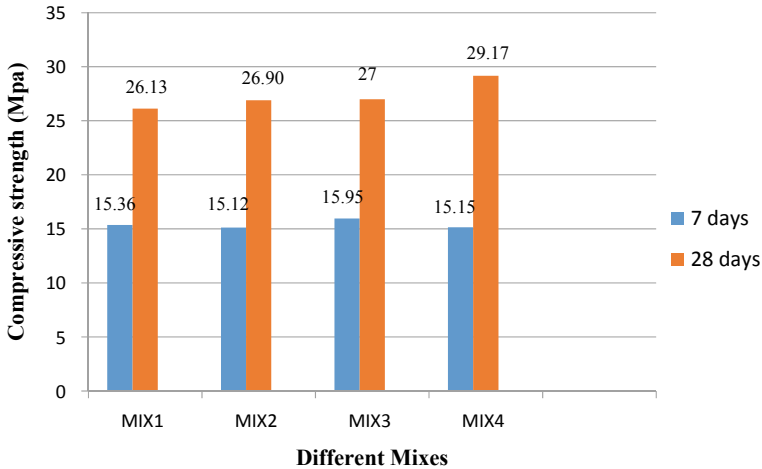


Fig. 6 Comparisons of GFRGPC between 7 and 28 days

achieved, and at 28 days 130% strength is achieved. Compared to OPC 30% more strength is achieved, but in the case of 0.5 and 1% steel dosage mix1, mix2 strength is increased but at 1.5% strength is decreased. In the first 3 mixes, 7 days to 7 days strength is increased approximately 1% and 28 days to 28 days is also approximately 1% increased but in mix4 0.5% strength is decreased.

Figure 6 concludes that the comparison of compressive strength of fly ash-GGBS is 50–50 ratio based on GFRGPC for 7 days and 28 days. Mix1 is plain GPC without steel fiber, strength at 7 and 28 days is 15.36 and 26.13. There is an increment in strength by increasing glass fiber dosage 0.25, 0.50 and 1%. The increment between 7 to 28 days is approximately 58% it is slightly in the case of steel fiber added GPC also for all mixes. The strength variation is more different between 7 and 28 days. By increasing activator content also increases the strength in glass fibers added to GPC also. In mix1 the increment of strength is more than the OPC concrete, in the case of geo activator-based GPC at 7 days 76% strength is achieved, and at 28 days 130% strength is achieved. Compared to OPC 30% more strength is achieved, but in the case of 0.25, 0.50 and 0.75% micro glass fiber dosage in all mixes compressive strength is increased. In all the 4 mixes compressive strength increased 7 days to 7 days and 28 days to 28 days is approximately 1%.

4.3 Split Tensile Strength

Figure 7 shows that the split tensile strength of the geo activator used by is giving better tensile strength for both cases. Split tensile strength is slightly more in the 50–50 ratio compared to the 70–30 ratio. In both cases by increasing the fiber content

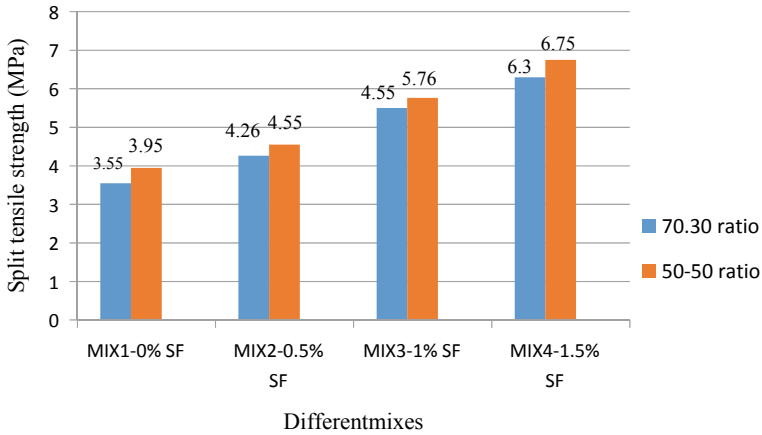


Fig. 7 Comparison of split tensile strength SFRGPC of 70–30 and 50–50 ratio

tensile strength is increasing irrespective of a percentage added but at 1.5% of steel fiber, there is an increment in tensile strength but decrement in compressive strength. We stopped at 1.5% and fixed 1.5% as the optimum dosage.

Figure 8 concluded that the split tensile strength of the geo activator used by GPC is giving better tensile strength for both cases. Split tensile strength is slightly more in the 50–50 ratio compared to the 70–30 ratio. For all the mixes in both cases, by increasing the glass fiber content tensile strength was increased. The ultimate strength for the 70–30 ratio is 5.37 and for the 50–50 ratio is 6.43 at 0.75% of glass fiber dosage.

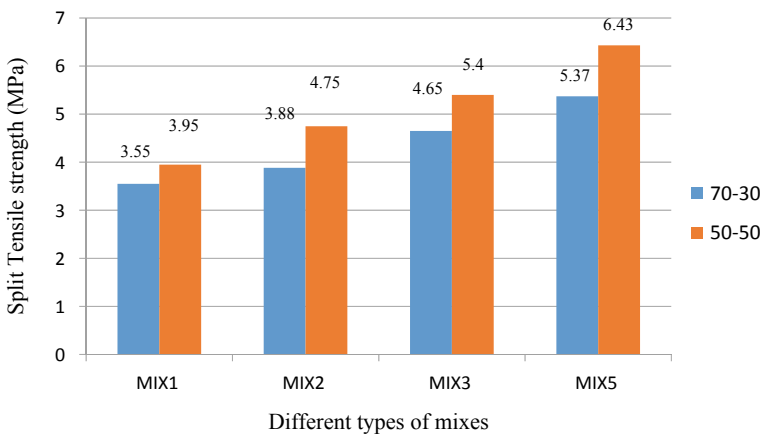


Fig. 8 Comparison of split tensile strength GFRGPC of 70–30 and 50–50 ratio

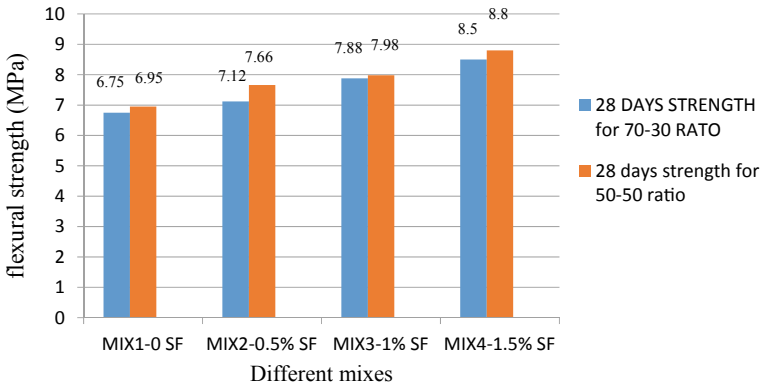


Fig. 9 Comparison of 28 days flexural strength between 70–30 and 50–50 ratio SFRGPC

4.4 Flexural Strength

Figure 9 states that comparative study between 28 days strength of fly ash-GGBS 70–30 and 50–50 ratio. The flexural strength of the 50–50 ratio is slightly more than the 70–30 ratio. The flexural strength of SFRGPC increased the same as tensile strength. By increasing, fiber dosage strength is increased. The strength is increased approximately 1% in each fiber dosage compared to its previous value.

Figure 10 concluded that the flexural strength of the 50–50 ratio is slightly more than the 70–30 ratio. The flexural strength of GFRGPC increased the same as tensile strength. By increasing, fiber dosage strength is increased. The strength is increased approximately 1% in each fiber dosage compared to its previous value.

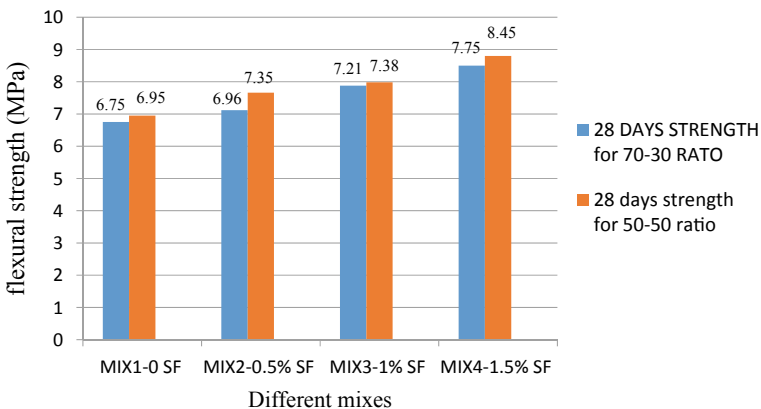


Fig. 10 Comparison of 28 days flexural strength between 70–30 and 50–50 ratio GFRGPC

5 Conclusions

- The slump value of the fresh fly-ash-GGBS base materials used in geopolymer concrete is better than the OPC concrete and it increases with the increased additional extra geo activator to the mixture.
- Mechanical properties are satisfied at ambient curing by using a single hardener activator solution.
- The combination of fly ash 30% and GGBS 70% is a better combination with a single solution geo activator to produce a geopolymer concrete for outdoor usage conditions.
- The compressive strength is approximately 50% increased 7 days to 28 days in both cases.
- The compressive strength is increased by adding steel fiber up to 1% and slightly decreased at 1.5% and by adding glass fibers the strength is increased up to 0.75% in all the mixes.
- Compressive strength is decreased by increasing fiber more than 1.5% but flexural and split tensile strength was increased.
- The geo activator-based GPC concrete got better workability even though adding 1% steel fiber.

References

1. Davidovits J (2008) In: Geopolymer Chemistry and applications. Geopolymer Institute
2. Rao GM, Rao TG (2015) Final setting time and compressive strength of fly ash and GGBS-based geopolymer paste and mortar. Arab J Sci Eng 40(11):3067–3074
3. Davidovits J (1978) Synthetic mineral polymer compound of the silico-aluminate family and preparation process US patent 4472199
4. Rao GM, Kumar KS, Poloju KK, Srinivasu K (2020) An Emphasis of Geopolymer Concrete with Single Activator and Conventional Concrete with Recycled Aggregate and Data Analyzing using Artificial Neural Network. In: IOP Conference Series: Materials science and engineering (Vol. 998, No. 1, p. 012060). IOP Publishing
5. Gugulothu V, Gunneswara Rao TD (2020) Effect of Binder Content and Solution/Binder Ratio on Alkali-Activated Slag Concrete Activated with Neutral Grade Water Glass. Arab J Sci Eng 45:8187–8197

Stone Crushers: A Technical Review on Significant Part of Construction Industry



Shubhangi Gurway and Padmanabh Gadge

Abstract Adoption and implementation of innovative solutions is the need of an hour & with the advent of time, this need give driving force to various development projects. Construction industries are those over which major emphasis should be given as they contribute enormously to country's economic development. Increasing the number of construction projects will demand high quality of work which is in direct concern with associated factors and equipment used. Crushers are one of the essential quarrying machines used in foresaid industries which are generally used to reduce the size of large size rocks into small stones, sand dust and gravels. Enormous amount of work has been performed beforehand to improve the performance of stone crushers. To take this research forward we tried to give a thorough review of all the designs and performed on different stone crushers. Present focus is on primary and secondary crushers used in stone crushing, because in tertiary crushing process combination of primary and secondary crushing were used according to the specific application. Consequential findings and outcomes of experiments and fabrication work of stone crushers in recent years are deeply reviewed with the objective of finding out the scope for application of Taguchi Optimization to improve performance.

Keywords Stone crusher · Jaw crusher · Cone crusher · Impact crusher · Aggregate production

1 Introduction

Crushers are widely used equipment to reduce the large size rocks into stones finer than about 50–100 mm in size [1]. In infrastructure industry, these equipment are available in different capacities ranging from 0.1 ton/hr. to 50 ton/hr. They can be classified according to extent to which they can break and fragment the starting

S. Gurway (✉) · P. Gadge

Department of Mechanical Engineering, G.H. Rasoni University, Saikheda, M. P., India

P. Gadge

e-mail: padmanabh.gadge@ghru.edu.in

material and the type of forces they apply. Based on the mechanism and the type of forces applied crushers are basically classified into three types namely Jaw crusher, Cone crusher and Impact crushers. However, the performance of all the crushers according to specific areas of application is the major point of concern in the research field [2]. The present work aims to provide the basic concept of crushers used in construction industries and various analytical and experimental work carried out on it in recent years.

1.1 Motivation of the Work

As foundation of society truly built on the crushed rocks and related materials, we could not even imagine our infrastructures without stones and subsequent materials right from construction of buildings to modes of transport. Continuous maintenance of demand-supply chain of these rock materials ores and minerals is thus necessary for improvement of the standard of living and to foster the infrastructure development of the country. Despite their significant role in development, these materials are taken for granted and people get unaware of their rising demand in upcoming future. In real scenario, the research and development of the equipment used for processing these materials are underestimated and not much attention is paid to their production, unless it is directly related to one's everyday life. With a developing interest and an expanding concern for manageability, the requirement for performance improvement and rise in productivity of rock pulverizers are day by day getting progressively significant [3]. The importance of crushers in the mining industry declined with the introduction and resultant dominance of AG and SAG based circuits, but the recent move to consider more energy-efficient circuits has caused the industry to reconsider the role of crushers [4]. To showcase its importance in infrastructure development, we are trying to give a brief overview of the work carried out earlier and efforts taken in development and analyze its performance in Table 1.

1.2 Effect of Various Parameters on Crusher Performance and Efficiency

For optimum performance of this equipment some of the major factors like breakage modes, number of crushing zones and compression ratio plays a significant role. For a given crusher, these factors depend on eccentric speed, closed side setting, rock material breakage characteristics and feed size distribution [4]. Similarly, various parameters like number of crushing stages, type of stone to be crushed, eccentric speed, feed rate or throw affect its performance. Similarly, when it comes to efficiency, the crusher relies on delivering crushing energy into the material contained within the crushing chamber or cavity. Many factors influence the effectiveness of the crushing

Table 1 Summary of experimental and analytical work carried out on stone crushers (2011–2021)

Sl. no	Type of crusher consider in work	Crusher specification	Type of study	Summary/remark	Publication year	Author/ reference	Country
1	Secondary crusher	Cone crusher model Svedala H6000	Design + Analysis	The cone crusher performance is analyzed by using bonded particle method to study rock breakage mechanics. DEM is used as a tool for the analysis	2012	Quist [20]	Sweden
2	Primary crusher	Jaw crusher	Expt. + Nume	FEM analysis can be used as a powerful tool for analyzing the failure of the component in jaw crusher	2013	Rusiński et al. [16]	Poland
3	Primary crusher	Jaw crusher	Expt. + Nume	Regression analysis was done in order to find out the effect of mechanical properties of rock on the specific power utilization of jaw crusher	2014	Korman et al. [11]	Croatia

(continued)

Table 1 (continued)

Sl. no	Type of crusher consider in work	Crusher specification	Type of study	Summary/remark	Publication year	Author/ reference	Country
4	Primary Crusher	Gyratory Crusher	Analytical + Design	Control system was designed and added to the crusher for controlling the charge level. Simulation was done to monitor the work. Productivity increased	2015	Lindstedt et al. [14]	Sweden
5	Primary crusher	Jaw crusher	Design	Lighter weight swing jaw plate of jaw crusher was designed using CatiaV5R15 and Finite element analysis of the same was done by ALGOR V19	2016	Patel et al. [10]	India
6	Primary crusher	Jaw crusher	Design + Analysis	Dynamic and kinematic analysis of all parts of the crusher has been done to improve its performance	2016	Abdulkarim et al. [15]	Iraq

(continued)

Table 1 (continued)

Sl. no	Type of crusher consider in work	Crusher specification	Type of study	Summary/remark	Publication year	Author/ reference	Country
7	Secondary crusher	Cone crusher	Expt	Experimental analysis of cone crusher using RMT-150B rock mechanics testing system	2016	Yanjun Ma [21]	China
8	Secondary crusher	Cone crusher	Expt. + Analysis	Simulation of The laboratory crusher Morgårdshammar B90 has been done using DEM and the results are compared with laboratory experiments. MATLAB image analysis is used to find out the performance parameters	2016	Johansson[22]	Sweden
9	Primary	Single toggle jaw crusher	Analysis	Kinematic analysis has been done in order to find the effect of any kind of alteration on the performance of the Single toggle jaw crusher	2017	Moses Frank Oduori et al. [12]	Kenya

(continued)

Table 1 (continued)

Sl. no	Type of crusher consider in work	Crusher specification	Type of study	Summary/remark	Publication year	Author/ reference	Country
10	Primary crusher	Jaw crusher	Analysis	Adaptive neuro-fuzzy interference system (ANFIS) was used to predict the specific power consumption of the jaw crusher with 96% of accuracy when compared with regression model	2019	Khaled Ali Abuhasel [9]	Saudi Arabia
11	Primary crusher	Jaw crusher	Design + Analysis	New design of jaw plate involving toothed profile was designed using CATIA software and Finite element analysis was done using ANSYS	2019	Ashok et al. [13]	India

(continued)

Table 1 (continued)

Sl. no	Type of crusher consider in work	Crusher specification	Type of study	Summary/remark	Publication year	Author/ reference	Country
12	Aggregate type	Granite stone crusher	Design + Analysis	The design of stone crusher for crushing particle size between 25–135 mm to about 24–20.2 mm was done. ANSYS software is used to find out high region stress area as major factor for safe working of proposed equipment	2020	Tauyanashechikuku et al. [24]	Zimbabwe
13	Secondary crusher	cone and horizontal shaft impact (HSI) crushers	Comparative study	Statistical Analysis was used to compare the performance parameters of both crushers. Pearson Correlation matrix was used to correlate the variables with performance	2020	Ekin Köken et al. [17]	Turkey, China

(continued)

Table 1 (continued)

Sl. no	Type of crusher consider in work	Crusher specification	Type of study	Summary/remark	Publication year	Author/ reference	Country
14	Secondary crusher	Inertia cone crusher	Design	Modeling of real-time dynamic model of inertia cone crusher using EDEM software. For model verification, the industrial-scale experimentation was performed on a GYP1200 inertia cone crusher	2020	Cheng et al. [18]	China
15	Secondary crusher	Cone crusher	Analytical	The evaluation of size reduction process was done by using analytical method. Crushability test was conducted using Bonded particle method	2020	EkinKoken [25]	

(continued)

Table 1 (continued)

Sl. no	Type of crusher consider in work	Crusher specification	Type of study	Summary/remark	Publication year	Author/ reference	Country
16	Secondary crusher	C900 cone crusher	Analysis and design	The effect of various parameters on the crusher performance has been analyzed. Similarly, DEM simulation has been used to monitor the performance of the crusher. The optimization of the performance has been done	2021	Yanjun Ma et al. [19]	China

in the chamber and the amount of size reduction achieved. The factors can be- Feed Material Variables (FMV), Mechanical Design Variables (MDV), Machine Operating variables (MOV), and Machine limits like maximum feed size, capacity, Power, Force and interaction with other equipment.

2 Concept of Stone Crusher

Stone Crusher is a sort of pulverizer which is utilized to compress or break out assortment of enormous stones. It normally highlights a huge crushing rate and high return and is utilized as an essential equipment in primary, secondary, and tertiary stages of crushing. Right from hard stones to delicate minerals, stone can incorporate slag, limestone, quartz, rock, iron metal, sandstone, copper metal, marble, concrete and that is just the beginning. Since crushers can be utilized on a wide scope of materials, they can be used in huge applications in ventures like mining, for the pounding of quarried stone in development that was significantly utilized as building materials and in destruction, to squash garbage abandoned by the destruction of structures, streets, extensions, channels and different designs [5]. The basic stepwise procedure of stone crushing is described below:

- Large size rocks as raw materials are fed into primary crushers like jaw crushers or gyratory crushers for primary crushing via the hopper of vibrating feeder.
- The primarily crushed stones are then sent to the secondary crushing chamber by means of belt conveyor and sent to the vibrating screen of separation of unqualified parts from the qualified one.
- After separating, qualified materials will be screened and filtered as final products, while unqualified stones will send back to previous crushing chambers again for recrushing. These finally crushed stones are again crushed according to the requirement of the customer.

A single type of crusher is not sufficient enough to convert the large size rock into required size stone. So, the crushing process involves primary, secondary and tertiary crushers during the whole crushing cycle to achieve the required dimension. Figure 1 shows different stages of crushing which have been discussed earlier. In these stages, the stone can be crushed from 1000 to 4 mm.

2.1 Primary Crusher

Primary crushers are heavy duty rugged machines used for crushing Run-of-Mines ore (–) 1.5 m and convert them into stones of size 100–200 mm in dimension to make them suitable for further crushing process. Most commonly used primary crushers are gyratory and jaw types. These types of crushers generally find their applications in crushing of brittle rocks like quartz and ready mix concrete sites. The crushing

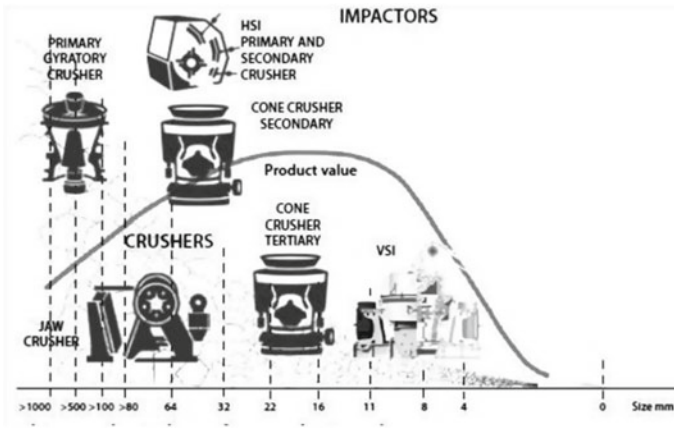


Fig. 1 Different stages of crushing. See ref [6]

process in these crushers involves feeding large size rocks into its crushing chamber through hopper which form an acute angle between the fixed jaw plate and a swing jaw plate hinged at the top. The crushing sequence is obtained by compressive force created between fixed and movable jaw plate and the process continues until the stones are small enough to get out of the passage which facilitates desired space for crushed stones to move out as shown in Fig. 2.

Another type of primary crushers commonly used by quarrying industries is the gyratory crushers which consist of long length conical shaped, hard steel crushing elements suspended from top. It rotates and sweeps out in a conical path within the round, hard, fixed crushing chamber (Fig. 3.) The optimum crushing action is

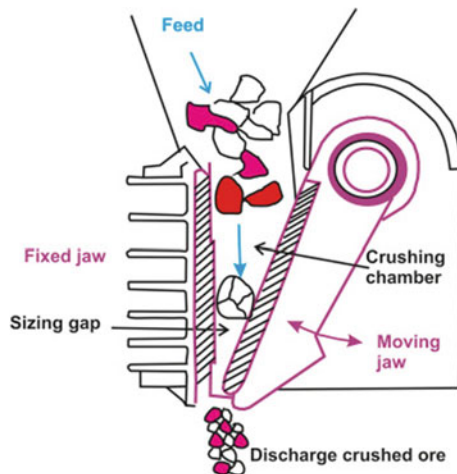


Fig. 2 Primary crushing through jaw crusher. Source taken from reference [7]

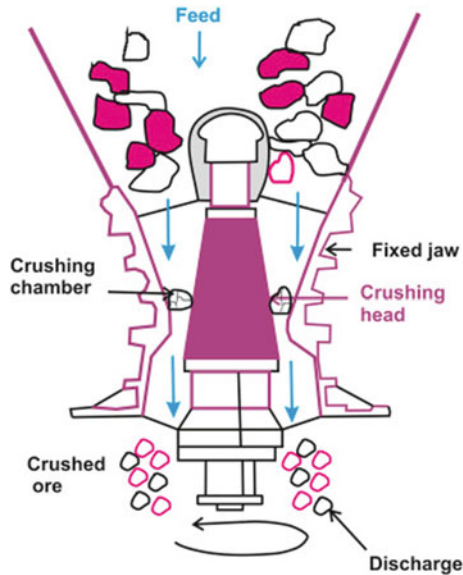


Fig. 3 Working of gyratory crusher. *Source* taken from reference [7]

achieved by reducing the gap between the hard crushing surface attached to the spindle and the concave fixed liners mounted on the mainframe of the crusher. The passage opening and closing are done by an eccentric drive provided at the bottom of the spindle which leads to gyration of central vertical spindle [7]. These types of crushers are used in stone crushing plants for creating abrasive materials and quarried stones.

2.2 Secondary Crusher

The secondary crushers are used as a subsidiary equipment of the stone which have been previously crushed in primary crusher. These types of crushers are generally used to reduce the previously crushed stones into as small as 5–20 mm in dimension and make them suitable for direct application like aggregate for road construction and maintenance purposes. They are lighter in weight and smaller in size compared to primary crushers. The commonly used secondary crushers are cone, roll, and impact types.

The cone crusher is shown in Fig. 4. Are somewhat similar to gyratory type in construction. It has larger diameter crushing surface and very short spindle relative to its vertical cross-section. The spindle is not swinging as in the gyratory crusher. The eccentric motion of the inner crushing cone is almost similar to gyratory type [7].

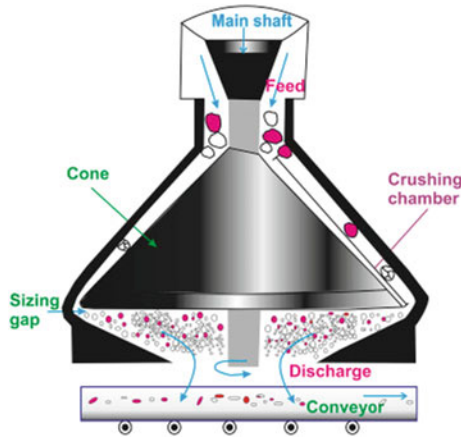


Fig. 4 Components of cone crusher. *Source* taken from reference [7]

The **roll crusher** is another secondary crusher that consists of a pair of horizontal cylindrical spring rolls as shown in Fig. 5. These rollers rotate contrarily to each other. The semi crushed stones are fed into the gap between the two rollers which are then squeezed and crushed. The finally crushed ores are then sent through the discharge section. Some advanced roll crushers are designed with two varying diameters and rotating speed cylindrical roller out of which one is fixed and other is moving. It improves the grain structure of minerals in the processed ores. Roll crushers are usually used in crushing of phosphate, chalk, limestone, coal and other types of soft ores and in construction industries they are used in creating rock aggregates and recycling [7].

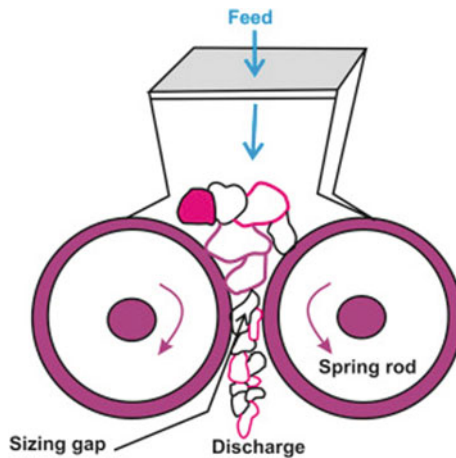


Fig. 5 Basic components of roll crusher. *Source* taken from reference [7]

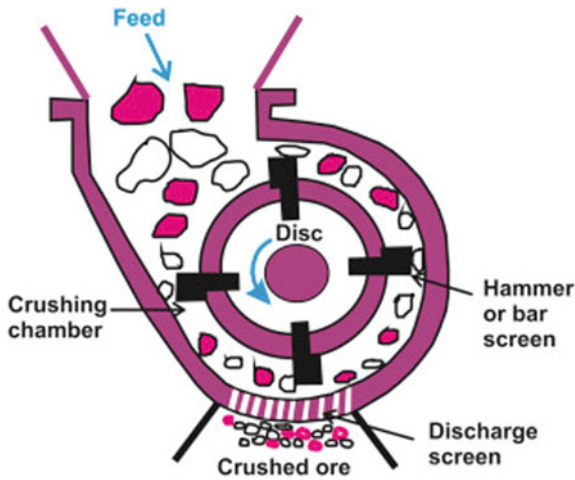


Fig. 6 Basic components and operation of an impact crusher [7]

Impact crushers are most commonly used in stone quarrying industry for making fine-grained stones used in road and building materials. The **impact crusher** as shown in Fig. 6 feed the material into the crushing chamber where a rotating disc containing hammer is working. The rotating action of the hammer apply heavy blow over the feed and break the stones to uniform size. Mesh type discharge screen is present at the bottom of the machine which separates the fine stones from oversized ones. The unqualified stones are swept around for further crushing until they are fine enough to meet the required specification and move out of the discharge gate. These crushers are normally employed for secondary or tertiary crushing [7].

2.3 Tertiary Crushing

In case of extra hard material which has not been possible to crush in previous stage or for extra fine material like sand gravels and sand dust, recrushing is suggested. The unqualified stones after processing of secondary crusher are collected in a bin and conveyed for tertiary crushing through conveyor belt in close circuit [7].

3 Analytical, Numerical and Experimental Research Conducted on Different Types of Crushers

Several experimental and numerical analysis has been performed by researchers in improvement areas of crushers in estimating the energy consumption, designing of

components to avoid failure, productivity improvement, etc. which is briefly reported in this section.

3.1 Experimental and Numerical Analysis of Primary Crushers

Analytical and experimental results are the backbone of the conducted studies which show promising results in estimating the energy consumption of jaw crushers. Input parameters like closed site setting [8], gap, stone strength and target reduction ratios can be a useful parameter in determining the energy consumption of jaw crushers [9]. Similarly different mechanical and physical properties of stone-like strength [10] put have major impact on power consumption of jaw crushers [11]. As it is not feasible to use jaw plate with different stiffness properties with different strengths of stones, some other properties like compressive strength, weight should be considered while designing a plate [10]. For improving the performance parameters of jaw crusher modified design and modeling can be a possible solution. Kinematic analysis and modeling can be used to estimate the design performance by considering different operating parameters like velocity, position and displacement of various links [12]. In one of the new design suggested by author [13] jaw plate can be designed with specialized tooth profile so that when failure occurs the respective tooth which is subjected to damage will be replaced instead of complete jaw plate replacement, which directly saves cost. Designing of lighter weight jaw plate using point load deformation failure relationships with interactive failure of rock particles as a model was the main objective to model a high strength jaw plate toggle which nicely interacts with different rock strength and low power consumption rate [10]. In one of the designs and analytical studies [14] crusher failure is analyzed and model for automatic control of charge level is designed. Simulation was performed before implementation to verify and adjust the algorithm. In order to test the algorithm on the crushing stage, a separate control box was developed based on a Crusher Controller Unit (CCU).

Several case studies have also been conducted by different researchers which showcase the real-world scenario of stone crushing plants. In one of the case study [15] Mathematical modeling, formulation and analysis of different parameters like crusher capacity, coefficient of fluctuation of energy, critical speed has been done and experimental results show that by controlling the distance between the lower gaps of the crusher different sizes of stone could be achieved. Case study in [16] witnessed the failure of support structure of jaw crusher in very short span of their installation due to higher amount of dynamic crushing forces. Experimental results show the presence of resonance effect during working. Author proposed a modified design of supporting structure having longitudinal bracings which increase its strength. Research study [14] again represent the failure of supporting structure of crusher at early stage of installation but this time controlling of charge level according to different properties of stones has been observed as a reason of failure as it creates different deforming

forces. As a solution, automatic control of the steady-state setting of charge level by developing a mathematical model and designing different control algorithms has been proposed. The proposed design was tested at different levels of the analysis.

3.2 Experimental and Numerical Analysis of Secondary Crushers

Quality of stone is directly concerned with the process performed in secondary crushing [17] as primary crushers are only meant for facilitating the crushing process because its output (stone size 100–50 mm) does not have direct application in any construction work. In one of the case studies conducted by researcher in 44 crushing plants several results have been witnessed which shows different aspects of energy consumptions related to cone crusher and HIS type crusher [17]. The parameters like displacement, power draw, product size distribution, amplitude and throughput capacity for analyzing and optimizing the performance parameter of cone crusher and by varying a drive speed for different selected parameters we can simulate the performance result [18]. Some key structural parameters like bottom angle of mantle, eccentric angle, length of parallel zone have also put major impact on the crushed material quality and equipment productivity [19]. Cone crusher liner is one of the parameters that influences power draw, linear wear and hydraulic pressure.

Like primary crushers, several designing, modeling and simulation studies have been conducted by researchers. Analysis of the impact of some key structural parameters in order to optimize the performance and productivity of cone crusher has been done. In [19] a specific chamber was taken into consideration for the optimization. DEM method was used as a simulation tool for performance analysis and the results were consistent with the numerical analysis results. Again in one of the research work modeling and simulation of cone crusher using bonded particle approach of designing have been applied for designing rock breakage mechanics where spheres with bi-model size distribution are bonded together in a cluster shape according to 3D scanned rock geometry. The scale is calibrated using laboratory single particle breakage test. The model is analyzed using Discrete Element Method as one of the simulating tools for analyzing the behavior of particle systems [20]. A wear prediction model with different time parameters is designed to improve the performance of cone crushers by considering different parameters and simulation has been performed to validate the performance result [21].

Experimental and analytical studies conducted also show the scope for further improvement in performance of the secondary crushers. In one of the experiments conducted, several mineralogical, physiological and mechanical properties of rock have been considered in evaluating the size reduction process of different rock aggregates and sieve analysis has been used to analyse the particle size distribution of crushed and uncrushed stones. The determined PSDs are hence used to quantify the

degree of rock crushability (DRC). The result witnessed that variation in size reduction ratio and P_{10} , i.e., theoretical aperture square mesh aperture should be majorly focused to quantify the PSD [22]. While designing the vibrating cone crusher, analysis of different technological and operating parameters has been done where it was founded that the value of the ratio of crushing force to driving force and the frequency of force oscillations of additional vibration device was among the most significant parameters which need to be analyzed and solved during design [23].

4 Gap Analysis and Future Scope

From the summary of work carries out in last decade shown in Table 1 it is observed that subsequent amount of work has been done in analysis and experimentation of the crusher especially for improving the energy efficiency, but none of the work has been carried out related to optimization of crushing parameters like closed -side-setting (CSS), throw, particle size distribution (PSD), eccentricity, etc. which may give promising results in crusher's performance improvement. In future Taguchi Optimization method can be effectively applied by selecting number of input parameters that actually affect the crushing sequence, with the objective function of improving the quality of finally crushed stones or reducing the rejection rate.

5 Conclusion

With the aid of reviewed research work in past few years, it is observed that it is not possible to optimize the whole crushing plant by concentrating on single crusher type as it involves three stages of crushing with different types of crushers. So, after reviewing the recent work carried out by various researchers, some of the conclusions have been drawn which are discussed below:

- The operating parameters like eccentric speed of jaw crusher, throw, power draw, closed Side Setting in cone crusher affect the energy efficiency of crushing plant.
- Stone properties may affect the performance of crusher.
- The crusher performance can be improved by applying different experimental, analytical and numerical techniques.

Further development in the optimization crushing parameters is yet to be studied and is planned for future research. Similarly, on-site study which gives real instinct of the performance parameters is planned for future work.

References

1. Neikov OD (2009) Mechanical crushing and grinding. In: Handbook of non-ferrous metal powders
2. Ojha A, Pandey A, Goswami RB (2020) study on construction technology machine jaw crusher. *Int J Recent Technol Sci Manage* 5(11):8–13
3. Lee E (2012) Optimization of compressive crushing, Thesis for the degree of doctor of Philosophy in product and production development, Chalmers University of Technology Goteborg, Sweden
4. Bearman R, Munro S, Evertsson M (2011) Crushers—an essential part of energy efficient comminution circuits. <https://www.researchgate.net/publication/268250199>
5. Stone Crusher Manufacturers | Stone Crusher Suppliers (pulverizers.net)
6. Balasubramanian A (2017) Size reduction by crushing method. <https://www.researchgate.net/publication/315487098>. <https://doi.org/10.13140/RG.2.2.28195.45606>
7. Haldar SK (2018) Mineral processing. In: Mineral exploration (Second Edition) Principles and Applications. pp 259–290
8. Pothina R, Kecojevic V, Klima MS, Komljenovic D (2007) Gyrotory crusher model and impact parameters related to energy consumption. In: Minerals and metallurgical processing, August 2007, Society for mining, metallurgy, and exploration, Inc. 24(3):170–180
9. Abuhasel KA (2019) A comparative study of regression model and the adaptive neuro-fuzzy conjecture systems for predicting energy consumption for jaw crusher. *Appl. Sci.* 9(18):3916. <https://doi.org/10.3390/app9183916>
10. Patel KS, Qureshi U (2016) Design and finite element analysis of swing jaw plate of jaw crusher with stiffener. *Int J Adv Eng Res Developm* 3(9):53–59
11. Korman T, Bedekovic G, Kujundzic T, Kuhinek D (2015) Impact of physical and mechanical properties of rocks on energy consumption of jaw crusher. *Physico Chem Problems Mineral Process* 461–475. <https://doi.org/10.5277/ppmp150208>
12. Oduori MF, Munyasi DM, Mutuli SM (2016) Analysis of the single toggle jaw crusher kinematics. *J Eng* 1578342:1–9. <https://doi.org/10.1155/2016/157834E>
13. Ashok, Narasimha Rao LNV (2019) Design and analysis of jaw plate with various tooth profiles using FEM. *Int J Basic Appl Res.* ISSN 2249–3352 (P) 2278–0505 (E)
14. Bolander SLA (2015) Automation and optimization of primary gyratory crusher performance for increased productivity. Master thesis in Master of Science in Engineering Technology Mechanical Engineering submitted to Luleå University of Technology
15. Abdulkarim JM et al. (2016) Development design for jaw crusher used in cement factories. *Int J Scientif Eng Res* 7(6):445–456. ISSN 2229-5518
16. Eugeniusz, Moczko P, Pietrusiak D et al. (2013) Experimental and numerical studies of jaw crusher supporting structure fatigue failure. *J Mech Eng* 556–563. <https://doi.org/10.5545/sv-jme.2012.940>
17. Köken E, Qu J (2020) Comparison of secondary crushing operation through cone and horizontal shaft impact crushers In: International multidisciplinary scientific geoconference surveying geology and mining ecology management, SGEM. 2020 August, 1.1:789–796. <https://doi.org/10.1016/j.mineng.2010.07.013>
18. Cheng J et al (2020) (2020) A dynamic model of inertia cone crusher using the discrete element method and multi-body dynamics coupling. *Minerals* 10(10):862. <https://doi.org/10.3390/min10100862>
19. Wu F et al. (2021) Chamber optimization for comprehensive improvement of cone crusher productivity and product quality. In: Mathematical problems in engineering 5516813:13. <https://doi.org/10.1155/2021/5516813>
20. Quist J (2012) Cone crusher modelling and simulation. Mater thesis submitted to Department of Product and Production Development, Chalmers University of technology, Goteborg Sweden. Available online via <https://publications.lib.chalmers.se/>
21. Ma Y et al (2016) (2016) Prediction of cone crusher performance considering liner wear. *Appl Sci* 6(12):404. <https://doi.org/10.3390/app6120404>

22. Johansson M et al (2016). Cone crusher performance evaluation using DEM simulations and laboratory experiments for model validation. In: 10th international comminution symposium. article in minerals engineering, September 2016. Available online at www.researchgate.net
23. Gerasimov MD, Chetverikov BS, Lubimyi NS et al. (2020) Method of forming technological parameters in the design of vibrating cone crushers. In: Buidintech BIT 2020. IOP conference series: materials science and engineering, vol 945. IOP Publishing, pp 012063. <https://doi.org/10.1088/1757-899X/945/1/012063>
24. Tayanashechikuku, Mushongo RN et al. (2020) Design of a small-scale granite stone crusher. In: 30th CIRP design 2020 (CIRP Design 2020). Available via www.sciencedirect.com
25. Köken E 2020) Evaluation of size reduction process for rock aggregates in cone crusher. In: Bulletin of engineering geology and the environment., vol 79. pp 4933–4946. Available online via www.springer.com
26. Evertsson CM (2000) Cone crusher performance. Thesis for the degree of Doctor of philosophy, Machine and Vehicle Design, Chalmers University of technology Goteborg, Sweden. ISBN 91-7197-856-9

3D Concrete Printing in Construction Industry—A State of the Art



Harika Sesetti, Muthina Venu Lalithya, and Pala Gireesh Kumar

Abstract The construction industry is likely to undergo considerable changes in order to enhance its productivity, optimize material usage, and improve workmanship. In the recent few decades, various automation technologies like 3D Concrete Printing (3DCP) have been introduced in the construction industry to automate the construction process. 3D Concrete Printing is an emerging method that can be used for fabricating the building and building components straight from a digital model into consecutive layers devoid of the use of any temporary supports or subsequent vibration. It is necessary to examine the existing processes, potentials, and limitations associated with 3DCP, and identify future research aspects to understand its applications in the construction industry. The primary goal of this study is to summarize the previous works of literature from both technical and non-technical aspects. Hence, this article provides a state-of-the-art analysis of recent accomplishments in the field of 3D printing of civil structures and construction components as well as recommendations for future research.

Keywords 3D Printing · Fabrication · Powder-based technology

1 Introduction

In comparison to the other industries, construction industry is said to produce a large amount of wastage. As a result, a new construction process that can minimize

H. Sesetti (✉) · P. G. Kumar

Department of Civil Engineering, Shri Vishnu Engineering College for Women (Autonomous), West Godavari, Vishnupur, Bhimavaram 534202, Andhra Pradesh, India

e-mail: harikacivil@svecw.edu.in

P. G. Kumar

e-mail: gireeshcivil@svecw.edu.in

M. V. Lalithya

Shri Vishnu Engineering College for Women (Autonomous), West Godavari, Vishnupur, Bhimavaram 534202, Andhra Pradesh, India

© The Author(s), under exclusive license to Springer Nature Singapore Pte Ltd. 2022

P. G. Kumar et al. (eds.), *Recent Advances in Civil Engineering*, Lecture Notes in Civil Engineering 233, https://doi.org/10.1007/978-981-19-0189-8_32

385

material waste and be sustainable is needed. The construction industry is a labor-intensive industry. It is because of the low technical advancements and robotic usage [1]. Hence a new construction process that can save laborious work is needed to be developed. Also, there is a need to develop a construction process that can be fast and accurate as well as cost-efficient. Hence it is significant to develop a new construction process that can automate the construction industry. 3D Concrete Printing is one such technique.

3D Concrete Printing is a form of an Additive Manufacturing (AM) process, wherein the buildings and construction components are fabricated layer-by-layer straight from a 3D digital model by successively depositing materials through a 3D printer's nozzle [2]. Unlike traditional construction methods, 3D Concrete Printing allows the fabrication buildings and construction components in previously unimaginable shapes. 3D Concrete Printing reduces the wastage generated in the construction process since the 3D printer will print the material only wherever it is necessary. Hence, it also reduces the in-situ construction time and cost. 3DCP also reduces labor usage, since the 3D printer will carry out the whole process.

Although the application of 3D Concrete Printing is still in its infancy, this technology has become possible in the past few decades due to its advances both in computer and materials technologies in the recent decades [3]. Many new pieces of research have been going on to explore and overcome the limitations of 3D Concrete Printing. Hence, a critical analysis of all the previous works of literature is needed. Therefore, this study intends on providing: (1) The history of 3D Concrete Printing in the construction industry; (2) The current status and existing processes and techniques of 3D Concrete Printing; (3) And current potentials and challenges of 3DCP.

2 History of 3D Concrete Printing

The first developments of 3DCP in the construction industry are made in the year 1995 by Dr. Behrokh Khoshnevis at the University of Southern California. He produced a complicated 3D ceramic part by using stereo lithography technology.

In 2000, Dr. Behrokh Khoshnevis's team had developed a new 3DCP technique called Contour Crafting using a Cartesian machine with a concrete extruder. This team has aimed of using concrete for printing large-scale concrete construction elements and has made the first important steps in the development of construction 3D printing.

In 2005, an Italian civil engineer named Enrico Dini has developed D-Shape 3DCP technology. This technology employs powder bonding techniques that used epoxy resin binder and were later adapted to use an inorganic binder.

In 2008, Richard Buswell and others of Loughborough University had started research on switching from a gantry-based system to an industrial robot in business applications. In 2014, they eventually accomplished in licensing this technology to the Skanska.

In 2015, a Chinese company named Winsun 3D printed 10 residences within 24 h to demonstrate 3DCP capability. To display the architectural flexibility of 3DCP, Winsun also 3D printed a six-story building. This company prints the buildings and construction components in a warehouse, and then the printed structures are assembled altogether in the construction site [4].

In 2017, another company called XtreeE 3D printed a wall with windows integrated in it. This wall was printed with robotic arms that can work together simultaneously while placing the window frames. In the same year, the first concrete bridge was 3D printed by TU Eindhoven in Eindhoven, Netherlands. The bridge was 3D printed in three pieces within a warehouse. The pieces of the bridge were then assembled together in the construction site [4].

In 2018, a company named ICON 3D printed the first building in Texas, United States. The 3D printed building is a one-family single-story house with a timber roof that was built on-site using a mobile gantry printer [4]. This company aimed to print affordable housing, especially for poor populations.

In 2019, a start-up company founded by the alumni of IIT-Madras called Tvasta Manufacturing Solutions has broken the record by 3D printing a single-storey house in India for the first time. The 3D printed house was built within 5 days and is of area 600 sq-ft. It was the first 3D printed house in India.

Later the L and T Constructions has 3D printed a two-storey building (G + 1) of 700 sq-ft at their Kanchipuram facility, India. It was the India's first 3D printed two-storey (ground plus one) building with reinforcement. This company said that as the country is vigorously pursuing the objective of building 60 million houses under Housing for All by 2022 programme, this achievement will stimulate the mass housing segment in India.

In the last few years, the popularity of employing 3DCP technology in the construction industry significantly increases with many new construction applications. This led to several important landmarks in the construction industry, for instance the first ever 3D printed house, the first ever 3D printed building, the first ever 3D printed bridge, and the first ever 3D printed office, etc.

3 Present 3D Concrete Printing Technologies

Various 3DCP technologies have been introduced into the construction industry during the last few decades. These technologies are mainly of two types. They are: (1) Extrusion-Based techniques and; (2) Powder-Based techniques. Again, they are subdivided into various types of techniques. All these 3D Printing techniques are briefly explained in the following sub-sections along with their similarities and differences as well as the pros and cons of using these techniques.

3.1 Extrusion-Based Techniques

In the extrusion-based technology, the nozzle placed on a six-axis robotic arm, gantry, or a crane extrudes the cementitious materials layer-by-layer to print the required structure [5]. The extrusion-based technique has the ability to create a notable and beneficial impact to the construction industry, and it was developed with the purpose of printing large-scale building applications with intricate geometries directly at the construction site [6]. In the recent few decades, various extrusion-based techniques have been introduced in the construction industries which are explained below. Figure 1 depicts an illustrative representation of the extrusion-based process.

3.1.1 Contour Crafting

Behrokh Khoshnevis of the University of Southern California, USA, introduced the Contour Crafting (CC) which is an extrusion-based technology. In the Contour Crafting process, the nozzle extrudes the cementitious mix layer by layer to build the required structure [7]. Here in this technique, the external shell of a wall is printed first and then the void is filled with pouring the concrete mix. While the Contour Crafting machine is continuously extruding the layers, it is possible to insert specially made reinforcement ties uniformly between the layers using this technique. It is also possible to insert internal parts such as electrical conductors, pipes, etc. in the CC process by integrating other robotic methods [8]. The main advantages of using this technique are the greatly improved speed of fabrication and the superior surface finish. And for the time being, this technique is only applicable for vertical extrusion. In addition, Contour Crafting mainly generates vertical components in compression at the moment. Therefore, when a window or doorway is needed, a lintel is used to bridge the gap between them, and the wall is then erected on top of it. Hence, it avoids the cantilever problem [6]. The CC technique is depicted schematically in Fig. 2.

Fig. 1 An illustration of the extrusion-based technique [5]

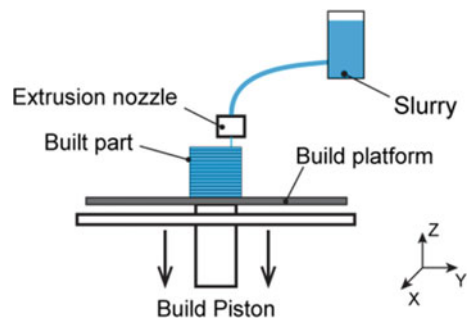
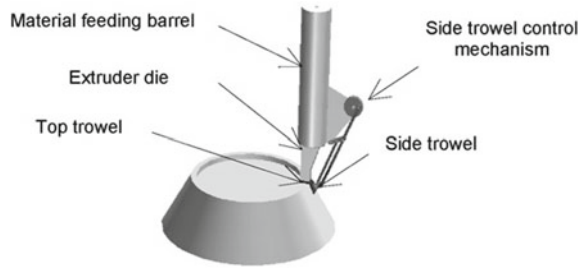


Fig. 2 Contour Crafting [7]

3.1.2 Concrete Printing

A research team at Loughborough University, UK, developed the Concrete Printing technology which is an extrusion-based technique. According to Behzad Nematollahi et al., this technology is similar to Contour Crafting technology to some extent; Concrete Printing, on the other hand, has been developed to maintain architectural flexibility and has slighter deposition persistence, allowing for more control over interior and exterior geometry [9]. The printing material used in the Concrete Printing technique is a high-performance fiber-reinforced fine-aggregate concrete, which has better material properties than those utilized in Contour Crafting technology. Although the main aim of this technology is the production of 3D topologies rather than 2.5D topologies, the usage of second material for additional support to create overhangs or other freeform structures results in reducing the flexibility and the efficiency of the process while raising its material cost [6]. There are few drawbacks in concrete printing technology like (1) the commutation essential to ensure the dimensional precision makes the process extremely slow; (2) the size and possibilities of shape and design depends on the size of the printing frame [6].

3.1.3 CONPrint3D: Concrete On-Site 3D Printing

Although the usage of CC and Concrete Printing technologies has various advantages, there are still some built-in drawbacks like the limited size of 3D printed parts, small aggregate sizes, and the need of using new advanced machines, etc. To overcome these drawbacks the TU Dresden, Germany has developed a new 3DCP technology called CONPrint3D which is abbreviated as Concrete On-site 3D Printing that intends to introduce 3D printer directly into construction sites. The main advantages of this technology are low reliance on skilled labor, usage of frequently used construction machines, and high architectural flexibility [6]. CONPrint3D's aim was to not only build a labor, resource, and time-efficient innovative construction process but also to build a new construction process which is economically feasible while gaining greater recognition from the existing industry professionals.

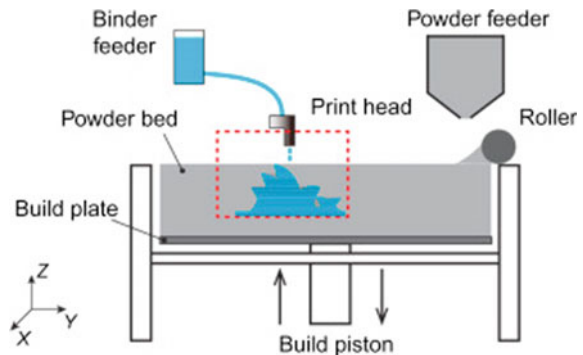
3.1.4 Large-Scale 3D Concrete Printing Using Ultra-High Performance Concrete

Another innovative 3DCP technique has been developed in the construction industry by a research team in France after considering the limitations of Contour Crafting and Concrete Printing technologies i.e., Large-scale 3D Concrete Printing using ultra-high performance concrete. In this technology, the extrusion print head placed on a six-axis robotic arm extrudes ultra-high performance concrete layer by layer to get the desired structure. The main advantages of using this technology are fully exploring the capabilities of 3DCP by printing layers with altering thickness, allowing the fabrication of large-scale 3D printed intricate geometries without any formwork, and enabling geometrical complexity as well as enabling multi-functionality for 3D printed parts by taking the benefit of the complex geometry [6].

3.2 Powdered-Based Techniques

Another type of additive manufacturing technique that creates accurate structures with intricate geometries is the Powder-Based technology. In powder-based techniques, a liquid binder is selectively jetted on the layers of powdered materials to bind the materials wherever it is necessary to get the required structure [10]. Later an air blower is used to get rid of the unbound printing material. This technique is mainly applicable for fabricating small-scale construction components that can be later assembled together at the construction site. Hence this technique is an off-site process [6]. A representation of powdered-based technique is shown in the below Fig. 3.

Fig. 3 A schematic of the powder-based technique [10]



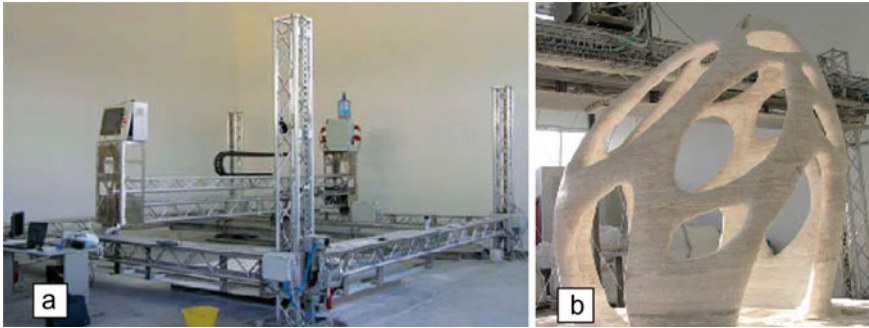


Fig. 4 The D-shape printer and the final 3D printed structure by D-Shape [11]

3.2.1 D-Shape

The D-Shape technique is a powder-based technique which has been developed by an Italian civil engineer, Enrico Dini in 2004. Enrico aimed to use the locally available materials to form 3D printed structures and has tested a wide range of crushed stone aggregates [9]. He utilized epoxy resin as the binder in the first 3D printed structure of the D-Shape printer. Later he changed the binder to a magnesium-based binder after experiencing problems with epoxy resin, which is currently being used. In D-Shape technology, the liquid binder is selectively deposited on a large-scale sand-bed to selectively harden the printing material. Then the loose powder can be removed using an air blower once the hardening is complete, and the hardened model can be pulled apart [11]. The main disadvantage of D-shape technology is that they require more cleaning, control, and maintenance and the final structure must be cleaned from remaining dust to form the post-treatment shape [9] (Fig. 4).

3.2.2 Emerging Objects

The Emerging Objects technique is another type of powder-based technique, which has been developed in the USA. In Emerging Objects technology, the binding agent is selectively deposited to selectively solidify a proprietary cement composite formulation [6]. This technology was used to construct the Bloom. Bloom is a self-supporting tempietto that measures 2.74 m tall and has a footprint of 3.66 m \times 3.66 m [12]. And it is made up of 840 custom-made 3D printed blocks [6]. Every block is 3D printed with a proprietary cement composite formulation that is mainly made up of iron oxide-free OPC. This technology is also used to manufacture a small-scale 3D printed prototype building known as Shed, which is constructed with Picoroco blocks [13] (Figs. 5 and 6).

Fig. 5 Shed printed by emerging objects [13]



Fig. 6 Bloom printed by emerging objects [12]



3.2.3 Powder-Based 3D Concrete Printing Using Geopolymer Powder

The Powder-based 3DCP technology has the ability to produce strong and long-lasting construction elements with fine details and complex geometries at a sensible pace to meet industrial demand. On the other hand, the use of cement-based printing materials in commercially available powder-based 3D printers is extremely limited which prevents the powder-based 3DCP technology from functioning at its full potential in the construction industry. To overcome this shortcoming, a new powder-based 3DCP technology is developed to adopt geopolymer-based printing materials [6]. Geopolymer is a sustainable substitute to OPC and has superior thermal, chemical, and mechanical properties, and also has 80% fewer carbon emissions compared to OPC.

4 3DCP Process

3D Concrete Printing Process of any building or construction components is generally carried out in five steps. They are (1) Designing; (2) Slicing; (3) Printing; (4) Post-processing and; (5) Final product. In the 3DCP process, a 3D digital model was created which specifies spatial coordinates of the civil structure to be printed. This 3D digital model is developed using 3D design software. This process of designing a house or any construction component is known as computer-aided design [4]. The developed 3D CAD model is then saved as a standard 3D data exchange format file. One of the most common and most popular formats in the 3D printing industry is the STL format (Standard Tessellation Language format). Later the designed structure is sliced into layers by using slicing software. To trace out and print the physical objects, the 3D printer reads these sliced layers as machine code. There are various mechanisms such as gantries, robotic arms, and construction cranes, etc. for the tracing of the coordinate system. Since the computer design has the spatial coordinates of the structure, the machine can print the material exactly in the specified locations by turning on and off the extrusion [4]. Once the 3D printing of the designed structure is completed, curing is carried out. After curing surface finishing is also done. Once all the above steps are completed, the final product is obtained i.e., the designed structure to be printed is obtained. This process of construction is known as computer-aided manufacturing (CAM) [14] (Fig. 7).

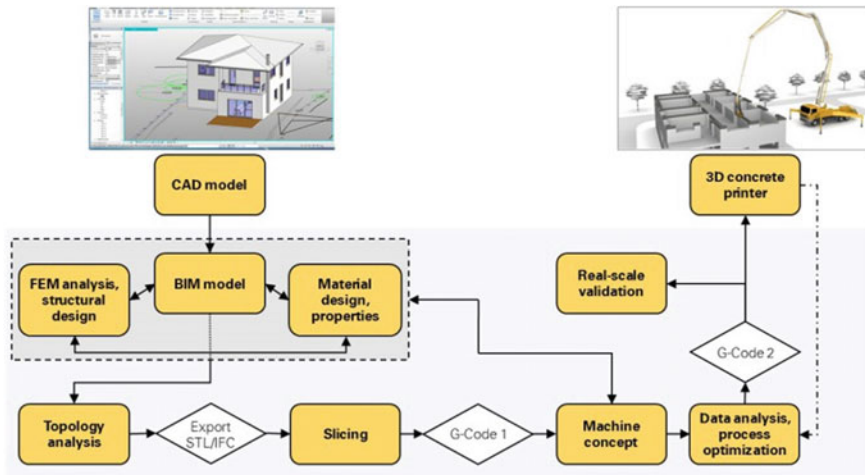


Fig. 7 3D concrete printing process [14]

5 Current Potentials and Challenges of 3DCP

5.1 Potentials of 3DCP

One of the biggest benefits of this technique is that the use of 3D Concrete printing reduces the on-site injuries of construction workers. Since the 3D printer will carry out the whole printing process. This technique also reduces material wastage, since we print the material only in the areas wherever it is necessary, unlike traditional construction methods. Hence, this method is more sustainable, environmentally friendly way to build compared to conventional methods. 3D printers are very fast and accurate that they can construct continuously. This technique is time and cost-efficient as the only input is the printing material. This technique also reduces the cost of laborers, since the 3D printer will carry out the whole printing process. This technique also reduces the chances of errors. This technology also creates new high-end technology-based jobs. And there are many more advantages of using 3DCP instead of conventional methods in the construction industry.

5.1.1 Significance of 3DCP in the Current Pandemic Situation

In the pandemic situations like covid-19, the application of 3DCP plays a significant part in the construction industry. As the 3D printer will carry out the whole 3D printing process, there is no need for the construction workers to work in the pandemic situations like this. As a result, this technology helps in preventing the transmission of viruses while still allowing for the construction of the necessary civil structures. As the 3D printers are very fast and accurate as well as labor independent, the application of 3DCP in the construction industry during these pandemic situations is easier and safer compared to the traditional construction methods.

5.2 Challenges of 3DCP

One of the biggest challenges of 3DCP is printing large-scale construction components or structures. The size of the 3D printed model is directly associated with the size of 3D printer, as the 3D printer cannot print any model larger than the printer. Even when this technology developed, most of the 3D printers used were small. And this technology remained unclear that whether it can build large-scale models or not. But in the recent few years, there are many large-scale 3D printed applications that are built using large-scale 3D printers.

Developing appropriate new materials for the 3D printing process is another significant challenge of 3DCP. Because the printing materials must meet certain requirements such as: (1) When the material mix is poured, the mix ought to be able to sustain its own mass as well as the mass of each consequent layer to obtain the

final design without any distortion [2]; (2) The material mix must be flowable in the system while also being buildable and be able to hold itself and each consequent layers after pouring; (3) The extruded material should set as fast as possible but not fast enough to ensure proper bonding with the consequent layer.

Poor surface finishing is another challenge of 3DCP which is caused due to the improper control and excess deposition of materials, and insufficient material which results in forming voids [2]. Hence proper care must be taken while printing the 3D model as well as after printing for better surface finishes. In order to improve the surface finish to some extent in some printers, trowels are integrated with the nozzle orifice.

Another challenge of 3DCP is reinforcing the 3D printed parts. For enhanced structural integrity as well as mechanical properties, reinforcements are needed for 3D printed structures [2]. But it is difficult to include reinforcements in the 3D printed structures. Therefore, it is necessary to develop a printing system capable of printing both reinforcement and concrete. Some 3D printers are using the steel fibers as reinforcement by including them in the mix. Some 3D printers are using steel screw-type reinforcements. And a Chinese company named Winsun had introduced another possibility of adding the reinforcements to the 3D printed structures by printing around the pre-installed reinforcements with the help of a specially developed extruder [2].

6 Conclusion

From the performed theoretical study, we can conclude that 3DCP is an emerging technology that can bring significant changes to the construction industry. 3DCP is a computerized layer-by-layer fabrication process which has lots of potentials and can be used to achieve various benefits. The major benefits of using 3DCP are the capability of printing without any formwork; architectural freedom; reduction in cost and; minimizing the wastage generated in the construction process, etc. Although there are various benefits of using 3DCP in construction industry, its application is still in its infancy because of the limitations associated with it. Many researchers are working to overcome these limitations. The current achievements of 3DCP application in the construction industry had significantly increased, proving its importance in the construction industry. Hence it is hard to assume so far that, in the next few years 3DCP could replace traditional construction methods. But it is more possible that both methods will be available in the construction industry and 3DCP may be employed along with the traditional construction methods, sustaining each other, particularly in the case of more complicated civil structures.

References

1. Hossain MA, Zhumabekova A, Paul SC, Kim JR (2020) A review of 3D Printing in construction and its impact on the labor market. *Sustainability* 12(20):8492. <https://doi.org/10.3390/su12208492>
2. Biranchi P, Tay, YWD, Paul SC, Tan MJ (2018). Current challenges and future potential of 3D concrete printing. *Materialwissenschaft und Werkstofftechnik* 49(5):666–673. <https://doi.org/10.1002/mawe.201700279>
3. Alzarrad MA, Elhouar S (2019) 3D printing applications in construction from the past and into the future. Paper presented at creative construction conference 2019 (CCC 2019), Budapest, Hungary, 29 June-2 July 2019
4. Truong, Andrew (2019) State-of-the-Art Review on 3D Printing Technology Applications in Construction. <https://escholarship.org/uc/item/4m27c4xs>. Accessed 2019
5. Image referred from: <https://www.researchgate.net/profile/Behzad-Nematollahi/publication/318472250/figure/fig1/AS:613936437141553@1523385261709/Schematic-of-extrusion-based-technique.png>
6. Nematollahi B, Xia M, Sanjayan J (2017) Current progress of 3D concrete printing technologies. Paper presented at 34th international symposium on automation and robotics in construction (ISARC 2017), Center for Sustainable Infrastructure, Swinburne University of Technology, Melbourne, Australia, June 2017
7. Image referred from: <https://3.bp.blogspot.com/-EknBZeEK3bo/V2JIODdpFnI/AAAAAAABABKs/hmljwmw7pBAXzP2kqTQevnpwunlrFMAsgCLcB/s1600/2.jpg>
8. Tay YWD, Panda B, Paul SC, Mohamed NAN, Tan MJ, Leong KF (2017) 3d printing trends in building and construction industry: a review. *Virtual and Phys Prototyping* 12(3):261–276
9. Tarhan Y, Sahin R (2019) Developments of 3d concrete printing process. Paper presented at international civil engineering and architecture conference 2019 (ICEARC19), Karadeniz Technical University, Trabzon/Turkey, 17–20 April 2019
10. Image referred from: <https://ars.els-cdn.com/content/image/3-s2.0-B9780128154816000117-f11-01-9780128154816.jpg>
11. Image referred from: <https://www.researchgate.net/profile/Yi-Wei-Daniel-Tay/publication/316926620/figure/fig5/AS:682986483752961@1539848075378/a-D-shape-printer-and-b-final-printed-component-with-all-the-excess-raw-material.jpg>
12. Image referred from: <https://www.digitalengineering247.com/images/rapid-ready/Bloom.jpg>
13. Image referred from: <http://emergingobjects.com/wp-content/uploads/2013/09/shed01.jpg>
14. Image referred from: https://www.bft-international.com/imgs/1/2/6/7/8/2/1/11_1_Mechtcherine_Abb_800_450-fe1ba91e78efcfff.jpeg

Effect of Steel–Polyester Fiber Combination on the Fresh and Mechanical Properties of Concrete



S. Sathish, C. Chella Gifita, and K. Sharmila Devi

Abstract Concrete is good in compression, and its poor tensile capacity is the major problem in conventional concrete. Fiber reinforced concrete is an effective measure to improve the tensile characteristics of concrete, and hybrid fiber reinforced concrete is the recent technology in which the fibers are added in combination in the same system. This article mainly explores the strength aspects of M30 grade hybrid fiber reinforced concrete. Compressive strength, split tensile strength, flexural tensile strength, and impact strength tests were conducted to understand the influence of single and combinations of fibers in the concrete. In addition to the strength criteria dry density, fresh properties like slump flow and micro structural characteristics are also examined. HyFRC compressive strength increases in the range of 8–12% when compared to control concrete. Split tensile strength and impact strength results show excellent performance in HyFRC. Among all strength values, the improvement in flexural strength is dominant in hybrid FRC series and this composite is exclusively suitable for the performance-based design of structures and special applications.

Keywords Fiber reinforced concrete · Steel fiber · Polyester fiber · Compressive strength · Split tensile strength · Flexural strength impact strength

1 Introduction

Concrete is widely used construction material, and it is the second most consuming materials in the earth. Nowadays, there are different types of concrete available and they are known for its special properties and applications. Concrete is good in compression, and it is classified as a brittle material because of its low-energy absorption capacity and tensile strength [1]. They are more prone to early age cracking due to the usage of mineral admixtures, shrinkage, volume instability, and different types

S. Sathish · K. Sharmila Devi
Under Graduate Student, Department of Civil Engineering, National Engineering College,
Kovilpatti, Tuticorin, India

C. Chella Gifita (✉)
Faculty of Civil Engineering, National Engineering College, Kovilpatti, Tuticorin, India

of stresses at its visco-elastic stage. Hence, to overcome this serious shortcoming in concrete, small discrete fibers are added to reinforce the brittle materials like concrete and cement and this composite is known as fiber reinforced concrete, which is practiced for few centuries in civil engineering applications [2]. FRC composite is high performance concrete and they improved the strength and ductility properties associated with the plain concrete. Short discrete fibers can transfer the stress and prevent the propagation of cracks. ACI 544-1R recommends the fibers are steel, glass, natural, and synthetic, and their function depends on the fiber material and its geometry [3]. Nowadays, to take the advantages of each fiber simultaneously, the concept of fiber hybridization has been taken into consideration. Hybrid fiber reinforced concrete consists of two or more fibers differ in material and geometry are combined to form a system. The optimum fiber combination could provide improved performance when compared to FRC made with single fibers [4]. Among many fiber combinations, steel-polymer is the most popular and many researchers have shown their interest in characterizing this composite. Deng et al. noticed the multiscale cracking resistance of steel-polypropylene fiber reinforced material and large aspect ratio improved the stiffness degradation and toughness [5]. Hybrid composite made with the combination of steel-glass fibers shows better mechanical and durability properties and glass fiber reinforced self-consolidating concrete shown good acid resistance [6]. Meng et al. studied the damage behavior and stiffness degradation of hybrid composite made with steel and polypropylene fibers [7]. Studies were done to assess the damage evolution rate of hybrid FRC reported the restrained effect offered by the confinement and the addition of fibers. Past literatures focused mainly on the mechanical properties and durability performance of single fiber reinforced concrete and the studies related to hybrid fiber reinforced concrete are limited. Rashid tested the prestressed concrete girders made with steel and polypropylene fibers concluded that the combination of fibers played a prime role in improving the durability by their binding action [8]. Ganesan et al. understood the influence of steel fibers on durability parameters such as water absorption, resistance to chemical attack, resistance to abrasion, and alternate wetting and drying cycles [9]. Test results show that the steel fiber reinforced geopolymer concrete possess better durability characteristics when compared to control concrete. Synthetic fibers were effective in bridging the cracks and lower the permeability at high stress levels, and among the three synthetic fibers, polyolefin performs better in durability aspects [10]. PVA and coir fiber combination improve the strength and durability characteristic of light weight foam concrete, and maximum strength was reported when 0.3% PVA, and coir fibers are added in the composite [11]. Iman Sadrenejad has reported the concrete beams reinforced with two different fibers polyolefin and polypropylene show reduced corrosion of steel reinforced in RC beams and high-volume fraction produced negative results in terms of strength [12]. Slag-based concrete with the incorporation of steel fibers showed improved performance in terms of abrasion resistance, drying shrinkage, and freeze-thaw resistance [13]. Extensive review of literature shows that the mechanical properties of single fiber composites are well established, and hybrid FRC-related properties are under investigation. To fulfill this objective, this paper focused on the mechanical properties of steel-polyester hybrid fiber reinforced concrete of

M30 grade. Compressive strength, split tensile strength, flexural tensile strength, and impact strength are the mechanical properties considered and presented in the paper. The research findings of this experimental investigation explore the steel–polyester hybrid FRC as a promising material with enhanced strength and toughness characteristics.

2 Experimental Program

2.1 Materials

Locally, available 53 grade portland cement was used in this study. Fly ash class C obtained from Tuticorin thermal power plant is used as a supplementary cementitious material in the development of concrete mixture, and based on the literature information, it is replaced up to 10%. Natural coarse aggregate of size 20mm and 12.5 mm conforming to IS 383: 2016 codal specification was employed in this study [14]. Manufactured sand smaller than 4.75 mm size was used as a fine aggregate. Both coarse and fine aggregates were tested as per IS 2386 (Part-3) [15], and the properties are listed in Table 1. High range water reducing polycarboxylic ether-based admixture master ease super plasticizer was used to obtain the desired workability. This water reducing admixtures are added to reduce the water content with the improved workability and also it increases the compressive strength up to 20%–30%. Potable tap water with pH value 7.8 is used in the mixing of concrete. Locally, available hooked end steel and polyester fibers are used in the study and its properties are given in Table 2. Figure 1 shows the steel and polyester fibers used for the experiments.

Table 1 Physical properties of aggregates

Physical properties	Fine aggregate	Coarse aggregate	
		12.5 mm	20 mm
Specific gravity in SSD condition	2.62	2.92	2.76
Water absorption in SSD condition in %	2.41	1.12	1.30
Fineness modulus	3.54	4.39	
Dry rodded density in kg/m ³	1509.31	1574.30	1731.69

Table 2 Fiber characteristics

Fiber type	Geometry	Density in kg/m ³	Length (mm)	Diameter (microns)	Specific gravity	Tensile strength (MPa)	Modulus GPa
Steel fiber	Hooked end	7850	30	300	7.8	1700	200
Polyester fiber	Filaments	1340	12	12 to 15	1.34	450	5



Fig. 1 Steel and polyester fibers

2.2 Mix Design and Mixing

Based on the properties of raw materials, M30 grade concrete mix proportioning is done as per IS 10262: 2009 method. Water cement ratio of 0.4 is assumed for mild exposure condition, and the final mix proportion is arrived after several trials. The detailed mixture proportion used in the current study is shown in Table 3. In the development of hybrid fiber reinforced concrete, the sequence of correct mixing is very essential in order to obtain the uniform mix composite. First, the dry coarse and fine aggregate samples are added to the 40 L capacity pan mixer and it is thoroughly mixed for 1 min. Secondly, the binder materials like cement, fly ash and then 80% of total mixing water is added along with the high range water reducing admixture and mixed thoroughly for 2 min. Third, in case of single and hybrid fiber reinforced concrete mixture, the discrete steel and polyester fibers are sprinkled manually and mixed continuously for another 2 min. Finally, the remaining amount of water is added to the mix until the homogenous mix is arrived. Fibers addition does not affect

Table 3 Mixture proportion in kg for one cubic meter

Cement	Fly ash	Fine aggregate	Coarse aggregate		Water	Super plasticizer
			20 mm	12.5 mm		
360	39	711	733	489	159	3.2

the workability of concrete, because the addition of PC-based admixture makes the concrete more workable, and the slump values are in the range of 90–120 mm in all the FRC mixture series.

2.3 Sample Preparation

Freshly, concrete mix was poured in the steel molds and it is vibrated externally by the table vibrator. Totally, five series of specimen were prepared in this experimental program. Table 4 shows the details of fiber hybridization adopted to explore the mechanical properties of single and hybrid fiber reinforced concrete. Control concrete specimens were also made for comparison purpose. To predict the hardened concrete properties, the specimens of various size were made, demolded after 24 h, and cured for 28 days time period. Figure 2 shows the pan mixer and mixing of ingredients in the making of concrete.

Table 4 Fiber hybridization

S. no	Mix series	Steel %	Polyester %
01	M00	–	–
02	0.2P	–	0.2
03	0.3P	–	0.3
04	SP1	0.5	0.2
05	SP2	0.5	0.3



Fig. 2 Pan mixer and mixing process

Table 5 Slump test results

S.No	Mix series	Slump value in mm
01	M00	200
02	0.2P	90
03	0.3P	100
04	SP1	110
05	SP2	90

2.4 Testing Methods

2.4.1 Fresh Properties of Concrete

Slump flow test is conducted to examine the workability properties of fresh concrete immediately after the preparation of fresh mixture. Fresh concrete mix is placed in the slump cone in three layers and compacted as per the guideline given in IS: 1199–1959. Then, slump cone is vertically lifted up and the mix is allowed to spread freely on the surface. The spread diameter is noted as the slump flow diameter in mm. The addition of fly ash necessitates the effective dispersion of fibers in both single and hybrid combination and slump test results of control, single, and hybrid fiber reinforced concrete are portrayed in Table 5. Slump test results indicate the addition of fibers have made a remarkable effect on the slump characteristics, and steel fibers should be added slowly to avoid the balling effect. Polyester fibers do not impose any balling effect but their workability decreases if they are not well distributed while mixing.

2.4.2 Mechanical Properties of Hardened Concrete

Compressive strength is an important qualitative index to determine the strength of the hardened concrete. Test is conducted on 150 mm size concrete cube specimens as per IS 516:1959 guidelines [16]. All the series of specimens are tested in a compression testing machine of 2000kN capacity at the age of 28 days. On the day of testing cube, specimens were removed from the curing tank and it is surface dried before testing. Crushing failure load is noted, and the compressive strength is calculated for all the five series M00, 0.2P, 0.3P, SP1, and SP2, respectively.

Split tensile strength is calculated on 100×200 mm long cylinders in the compression testing machine after 28 days curing period as per IS 5816:2004 specifications [17]. Specimen was placed horizontally in between the two loading strips kept on top and bottom of the specimens, and the diagonal compressive load is applied, and the failure load is noted. Based on the ultimate load, the split tensile strength is calculated to understand the influence of single and combination of fibers in concrete composites.

Flexural tensile strength of concrete is calculated in beams of suitable size $100 \times 100 \times 500\text{mm}$. Flexural strength single and hybrid fiber series were compared with the control concrete. Two point flexural loading test is employed for the determination of flexural strength of the concrete in a 25kN universal testing machine. The flexural strength of the specimen is expressed as the modulus of rupture in N/mm^2 .

Impact strength of single and hybrid fiber reinforced concrete specimens is determined by conducting drop weight impact test on concrete disc specimens of size 100 mm diameter and 50 mm thick. Disc specimen was kept firmly in between the three lugs and impact hammer of 14 kg are allowed fall freely from a height of 380 mm repeatedly. The number of blows required to cause first crack (N1) and ultimate crack failure (N2) is noted, and from the blow counts, the impact energy for the first crack and ultimate failure is calculated. Energy absorbed by the disc specimen is calculated by.

$$E = m \cdot g \cdot h$$

- E Impact energy, (joule)
- g Acceleration due to gravity, (m/s^2)
- h Height of fall, (m)
- m Weight of hammer, (kg).

Compression, split tension, impact test, and flexural tension setup are shown in Fig. 3a–d

3 Results and Discussion

3.1 Compressive Strength

Figure 4 shows the compressive strength results of control concrete, single FRC, and hybrid FRC series. The test results are 38.41, 39.85, 40.22, 41.48, 43.04 MPa for M00, 0.2P, 0.3P, SP1, and SP2 series, respectively. When compared to control concrete, the addition of single polyester fiber increases the compressive strength ranges from 3.7%–4.7% and in case of hybrid FRC, the improvement is up to 12.05%. Fibers are effective in bridging across the micro cracks and increase the compressive strength by transferring the compressive stress from the cement matrix to the fibers in the composite [18]. Among all five series, hybrid combination with 0.5% steel fibers and 0.3% polyester fibers possess maximum compressive strength. It is observed that the confinement due to hybrid combination of fibers increases the compressive strength due to the increase in volume fraction of fibers. As stated earlier in hybrid combination, fibers of different type and different length offer different restrain conditions [19]. Also, the increase in fiber content slows down the occurrence of cracks due to intercept across the cracks in hybrid FRC [20].



Fig. 3 a-d Test setup for compression, split tension, impact, and flexural tension

Fig. 4 Compressive strength results

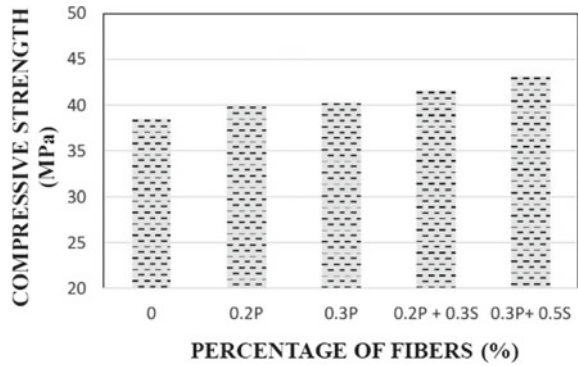
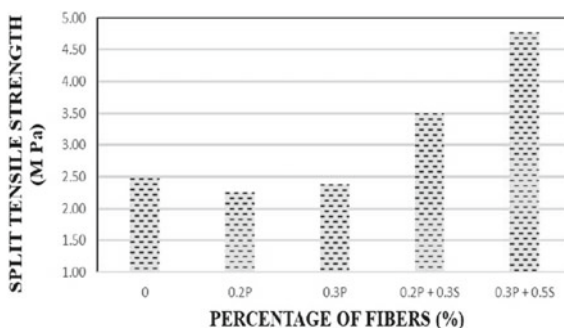


Fig. 5 Split tensile strength results

3.2 Split Tensile Strength

Figure 5 describes the indirect tensile strength of control concrete, single, and Hybrid FRC, and it is understood that the addition of fiber combination improves the post cracking behavior of the composite. The synergetic effect between two fibers bridging across the cracks and delayed the propagation of cracks. Both the hybrid combination series SP1 (0.5% steel + 0.2% polyester) and SP2 (0.5% steel + 0.3% polyester) show greatest split tensile strength than single polyester series. The high modulus of elasticity and hooked end anchorage of steel fibers increases the split tensile strength of the concrete when compared to single polyester FRC. Split tensile strength of mono fiber reinforced concrete series such as 0.2 P and 0.3P polyester fiber series decreases by 9.27% and 3.62% when compared with the reference concrete mixture.

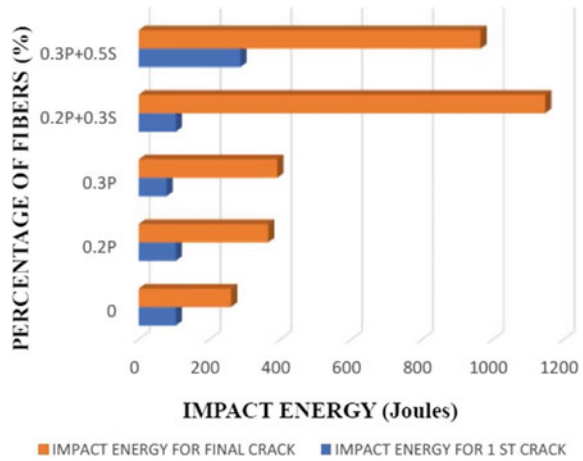
3.3 Flexural Tensile Strength

Table 6 shows the flexural tensile strength results of control, single, and hybrid fiber reinforced concrete. Table 6 exhibits drastic increase in modulus of rupture (MOR) of polyester FRC and hybrid FRC compared to control concrete. When compared to pure concrete sample without fiber, the increase in volume fraction of 0.2% and 0.3% polyester fiber increases the flexural strength by 11.49% and 20.22%. But the

Table 6 Flexural strength in MPa

S. no	Mix series	Flexural strength in MPa
01	M00	4.35
02	0.2P	4.85
03	0.3P	5.23
04	SP1	5.89
05	SP2	5.96

Fig. 6 Impact strength results



amount of increase is high when it is combined with 0.5% steel fibers. It increases by 35.40% and 37% in SP1 and SP2 series.

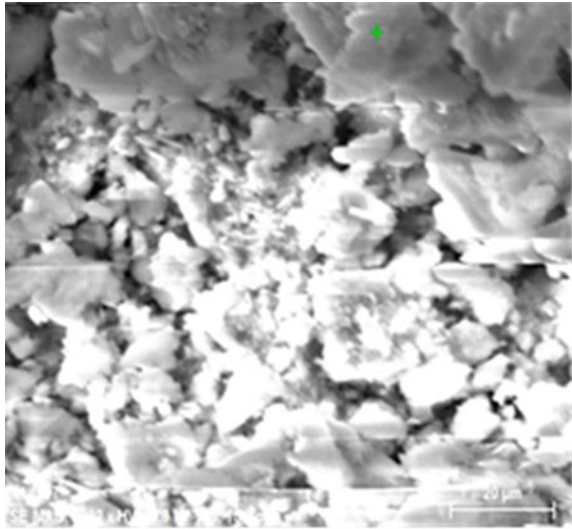
3.4 Impact Strength

Impact test results indicate the addition of fibers in two different size influence the impact energy than the single polyester fiber alone. Hybrid mix series SP2 shows maximum energy at first crack failure, and the impact energy enhances by 2.76 times than the control concrete. Excess polyester fiber content reduces the impact energy at first crack because of the entrained air, reduced stiffness, and shorter length of polyester fibers. But the same polyester fiber when combined with steel, the impact energy at ultimate crack increases 4.4 folds greater than the control concrete. Hooked end steel fibers provide enough anchorage, good tensile strength, and their bonding action with the concrete surface prevents the specimen to undergo large amount of cracking when subjected to impact loading. The knitting action of two fibers with different modulus resulted a very strong interface between the fibers and the matrix delayed the fracture process. Also the short discrete polyester fibers are effective in distributing the stresses and thereby enhanced the energy absorbing capacity of hybrid FRC. Test results are shown in Fig. 6

4 SEM Examination

Microscopic structure of the hardened fracture surface of a specimen hybrid series 0.3P + 0.5S reinforced with 0.3% polyester fibers and 0.5% steel fibers in the

Fig. 7 SEM image of hybrid series with 0.3 polyester and 0.5 steel fibers



composite is shown in Fig. 7. The hydrated cement products are compact and look like quasi-amorphous, and the fiber surface is not visible as it is covered by the hydrated cement products, and this ensures good bond between the fiber and cement matrix. The mechanical interlocking between the aggregates and paste is improved due to the overlapping and insertion of the hydration products in the composite. Addition of binders such as fly ash enhances the bond between the aggregate–paste interface, and from Fig. 7, it is seen that the fly ash particles are covered by the C-S-H gel and also it improves the cohesiveness of interfacial transition zone (ITZ) between the aggregate and matrix.

5 Conclusions

This study represents the behavior of hybrid fiber reinforced concrete, and the following points are drawn.

- The influence of single and combination of steel and polyester on M30 grade concrete is understood through the experimental observations. High water reducing admixture added to the concrete makes the composite more workable, and fibers inclusion does not make any adverse effect on the fresh properties.
- Steel and polyester fibers in combination played a prime role in binding the concrete matrix together. Compressive strength values increase in the range of 8% to 12% when compared with no fiber concrete
- The trend of increasing split tensile strength is observed when the volume fraction of fibers is increased but, however, the addition of polyester fibers alone shows a negative effect.

- The improvement in flexural strength of all hybrid series is higher than the increase in compressive strength and split tensile strength.
- High tensile strength and high modulus of steel fibers combined with polyester show excellent performance in impact strength.

Acknowledgements Authors would like to thank Department of Civil Engineering National Engineering College for their extensive support in doing this research work.

References

1. Mohammadhosseini H, Tahir M (2018) Durability performance of concrete incorporating waste metalized plastic fibers and palm oil fuel ash. *Constr Build Mater* 180:92–102
2. Soylev TA, Ozturan T (2014) Durability, physical and mechanical properties of fiber-reinforced concretes at low-volume fraction. *Constr Build Mater* 73:67–75
3. ACI Committee 544 Fiber Reinforced Concrete
4. Qian CX, Stroeven P (2018) Development of hybrid polypropylene-steel fiber reinforced concrete. *Cem Concr Res* 30:63–69
5. Deng F, Chi Y, Xu L et al (2021) Constitutive behavior of hybrid fiber reinforced concrete subject to uniaxial cyclic tension: Experimental study and analytical modeling. *Construct Build Mater* 295:123650
6. Gantaa JK, Rao MVS, Mousavi SS et al (2020) Hybrid steel/glass fiber-reinforced self-consolidating concrete considering packing factor: mechanical and durability characteristics. *Structures* 28:92–102
7. Meng K, Xu L, Chi Y (2021) Experimental investigation on the mechanical behavior of hybrid steel-polypropylene fiber reinforced concrete under conventional triaxial cyclic compression. *Construct Build Mater* 291:123262
8. Rashid MU (2020) Experimental investigation on durability characteristics of steel and polypropylene fiber reinforced concrete exposed to natural weathering action. *Construct Build Mater* 250:118910
9. Ganesan N, Ruby A, Deepa SR (2015) Durability characteristics of steel fiber reinforced geopolymer concrete. *Constr Build Mater* 93:471–476
10. Poorsaheli HB, Behravan A, Seyed Taha T (2021) Durability performance of hybrid reinforced concretes (steel fiber+ polyolefin fiber) in a harsh marine tidal zone of Persian Gulf. *Construct Build Mater* 266:121176
11. Raj B, Sathyan D, Mini KM, Raj A (2020) Mechanical and durability properties of hybrid fiber reinforced foam concrete. *Construct Build Mater* 245:118373
12. Sadrinejad I, Ranjbar MM, Madandoust R (2018) Influence of hybrid fibers on serviceability of RC beams under loading and steel corrosion. *Constr Build Mater* 184:502–514
13. Papachristoforou M, Anastasiou EK, Papayianni J (2014) Behavior of self compacting concrete containing ladle furnace slag and steel fiber reinforcement. *Mater Des* 59:454–460
14. IS 383—1979 Specification for coarse and fine aggregates from natural sources for concrete. BIS India
15. IS 2386 (Part III) —1963 Indian standard methods of test for aggregates for concrete. BIS India
16. IS 516—1959 Method of Tests for Strength of concrete, BIS India
17. IS 5816—2004 Splitting tensile strength of concrete—Method of test, BIS India
18. Aslani F, Hamidi F, Valizadeh A et al (2020) High-performance fiber-reinforced heavyweight self-compacting concrete: analysis of fresh and mechanical properties. *Construct Build Mater* 232:117230

19. Chen B, Liu J (2004) Residual strength of hybrid-fiber-reinforced high-strength concrete after exposure to high temperatures. *Cem Concr Res* 34:1065–1069
20. Sukontasukkul P, Pongsopha P, Chindapasirt P et al (2018) Flexural performance and toughness of hybrid steel and polypropylene fiber reinforced geopolymer. *Constr Build Mater* 161:37–44

Modal Analysis of Bridges with New Concretes: Replacing the Regular Construction Material Under the Action of Seismic Load



Nilanjan Tarafder, Endow Mazumder, and L. V. M. Prasad

Abstract In the current study, new concrete materials are introduced to the bridge structures. An effort has been made to replace the traditional conventional concrete (CC) with self-compacting concrete (SCC) and fiber reinforced self-compacting concrete (FRSCC). This is to evaluate the behavior of the bridge under a seismic event, whether new concretes perform better or not with quantitative calculation. Three-dimensional (3D) finite element model (FEM) was prepared for each condition with CSiBridge platform and static nonlinear analysis was performed. To entertain this, pushover analysis was performed as per IS: 1893–2016 with following the guidelines of IRC. Several mode shapes were analyzed and deflection behavior of the bridge in vertical direction was evaluated for each and every case. The results showed promising outcomes and FRSCC improved the strength of the bridge by a great amount and the deflection that occurred for the seismic event was reduced by 67% compared to the bridge made with CC. The demand-capacity ratio (D/C Ratio) was also improved by 3% and 16%, respectively with SCC and FRSCC replacements, respectively. SCC also improved the bridge's performance under seismic load up to a certain limit but FRSCC improved the performance greatly.

Keywords Bridge · Pushover analysis · Demand-capacity ratio · Mode shapes · Deflection

1 Introduction

Bridge is a vital form of structure. Under a seismic event, bridges can be a critical structure and it may also reach some severely damaged conditions [1]. Constructional concrete also plays a big role in the strength of the bridge. The new concretes: self-compacting concrete (SCC) and fiber reinforced self-compacting concrete (FRSCC)

N. Tarafder (✉) · E. Mazumder · L. V. M. Prasad
NIT Silchar, Silchar, India

L. V. M. Prasad
e-mail: mlvprasad@civil.nits.ac.in

are already proved to be better than the regularly used concrete in general constructions. And nowadays regular conventional concrete (CC) is showing many problems on huge scale (like collapse of bridges in many places). This work is carried out to understand the effect of these new concretes on the bridges. Practically seismic condition is considered a severe natural disaster that affects the structures in many ways. Mode shape analysis or modal analysis is a good process to understand the behavior of bridges under these seismic events.

Currently, seismic study of the bridge structures has drawn significant appeal among the researchers as a vital form of engineering and response of the bridge to an earthquake plays a critical part in this respect. Kulkarni et al. found the ductility could be highly improved by applying the response reduction factors [2]. Babazadeh et al. simulated a 3D FE model of a bridge structure and thereby predicted the intermediate damage limits for a reinforced concrete (RC) bridge column, which lead to a strain index limit of 0.005 for spalling [3]. Tegos et al. simulated a bridge disabling seismic displacement model in the transverse direction, but the setup proved very useful for precast I-beam type bridges only [4]. Biao analyzed multiple bridges with pushover analysis, and results were compared with inelastic time history analysis to understand the seismic effects on the bridges, concluding, pushover analysis is well suited for bridges' seismic analysis [5]. A study with FRC showed that fibers' use increased the compressive and flexural strength, and residual strength, energy absorption ability and ductility was also improved [6]. The simple RC column was compared with the FRC column and axial deformation control. The ultimate strength was improved by 199 and 92% with fibers in the regular RC column [7]. A fuzzy-based neural network also proves the improvements of FRC instead of using RC [8]. Our group has conducted a performance study to quantify the effects of bridge pier type under seismic conditions. Base shear capacity and drift results showed single and double pier bridge behavior in longitudinal and transverse directions. It was found that, based on the performance level requirements, bridge pier type has to be selected [9]. There is a necessity to focus and move to the novel internal concrete materials to achieve the desired target fully. A new material called self-compacting concrete (SCC) was well investigated by the authors in their previous works. SCC can be easily prepared with the proportions prescribed by Meesaraganda et al. The SCC has the property of filling any highly congested reinforcement setup very easily without external vibration [10, 11]. A modal analysis study indicates that the method of modal combinations provides a basis for estimating the potential contributions of higher modes when determining inter-story drift demands and local component demands in multistory frame buildings subjected to seismic loads [12]. One study identified the modal parameters of an RC building using Bhuj earthquake data [13]. Yu et al. indicated that the modal pushover analysis is a perfect method to analyze a structure for its seismic evaluation [14]. Hence, it is worth examining the performance of bridges using new concrete types: SCC and FRSCC, under disastrous seismic situations as the traditional concrete is causing nearly as well as total collapse to the bridges under severe seismic condition.

As there is a well-research gap about using the new concrete materials in the bridge structure, current study was done to fill the gap. The SCC and FRSCC are

new types of concretes that have the property to flow under its own weight because of which it is very significant material for bridges. These two new materials can fill the congested reinforcement areas of the bridge without any requirement of external vibrational forces—reducing sound pollution and saving electrical power. SCC and FRSCC are eco-friendly materials and taken under consideration as replacement concretes in place of traditionally used CC. Mode shape analysis was carried out in order to understand the behavior of the bridges with the new concretes under seismic conditions.

2 Bridge Modeling and Materials

The bridge structure is modeled in CSiBridge software and a geometric sketch model is shown in Fig. 1. CSiBridge is a specialized software for bridges created by Computer and Structures Inc. (CSI). The software can render any bridge model as practical appearance along with actual bridge’s elements, which is not possible with other software by CSI. The bridge is a two span t-beam bridge and the base of the pier is kept fixed. 3 models are rendered with CC, SCC and FRSCC as the material inside the bridge. Table 1 shows the detailed cross-sectional dimensions of the bridge under consideration. The reinforcement used in the model was kept same

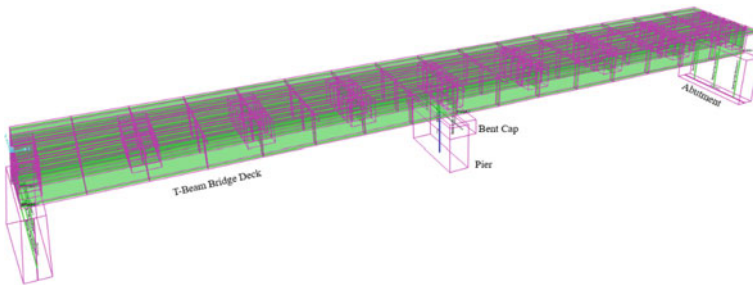


Fig. 1 Geometric sketch of the bridge

Table 1 Cross-sectional properties of 3D FE bridge model

Bridge component	Length (m)	Width (m)	Height (m)
Each span	24	6.4	2.1
Abutment	6.4	1.3	3.55
Bent cap	6.2	1.8	1
Pier	5.3	1.3	3.55
Top slab per span	24	6.4	0.2
T-Beam flange	24	2.1	0.2
T-Beam web	24	0.4	1.9

Table 2 Reinforcement details for each model

Element	Longitudinal reinforcement	Transverse reinforcement	Clear cover
Abutment	44 Φ 20 at top and bottom	Φ 12 @ 150 mm c/c at top and bottom	40 mm
Bent Cap	16 Φ 20 at top and bottom	Φ 16 @ 150 mm c/c at top and bottom	40 mm
Pier	32 Φ 25 with Φ 12 @ 150 mm c/c confinement	10 Φ 25 @ with Φ 12 @ 150 mm c/c confinement	50 mm

Table 3 Mix proportion of CC, SCC and FRSCC

Concrete Type	Cement (Kg)	Fly ash (Kg)	CA (Kg)	FA (Kg)	Water (Lt.)	SP (%)	VMA (%)	Glass Fiber (Kg)
CC	440	–	1024	572	150	–	–	–
SCC	415	137	717	934	190	1.30	0.20	–
FRSCC	415	156	717	934	190	1.50	0.25	1

Table 4 Basic concrete properties with its strengths

Concrete type	Elasticity modulus	Poisson's ratio	Compressive strength (MPa)	Split tensile strength (MPa)	Flexural strength (MPa)
CC	31.60	0.18	35.12	2.47	3.13
SCC	35.05	0.21	41.21	3.08	4.11
FRSCC	39.21	0.25	50.09	3.62	4.67

for all three models in order to evaluate the structures' behavior without unnecessary factor changes. The details about the reinforcements used in the study are shown in Table 2. For the concrete materials, OPC 53 grade cement, normal river sand as fine aggregate and maximum 20 mm size of coarse aggregate was considered. Experimental study was also performed by the authors and the mix proportions of every concrete, i.e., CC, SCC and FRSCC are shown in Table 3. The detailed basic concrete properties, as well as compressive, split tensile, and flexural strength properties which are used in the modeling (manually) of the bridges, are shown in Table 4.

3 Analysis

The analysis was performed in the CSiBridge software for all the models with the aforesaid boundary conditions keeping constant. 3D finite element method was used

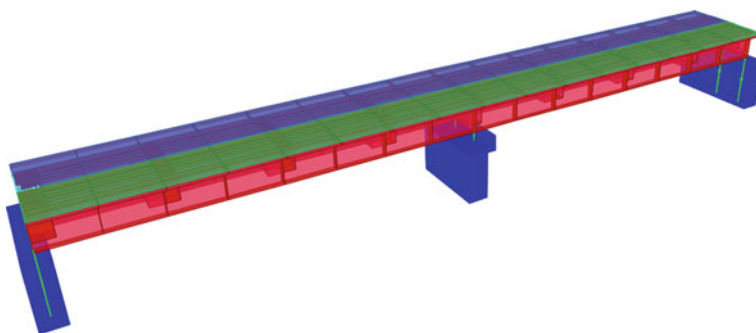


Fig. 2 3D FEM model of the bridge

Table 5 Detailed loading condition

Load pattern	Load type	Magnitude of load
Dead load	Dead–full structure	5 kN/m [IS: 456–2000]
Barrier load	Dead–line load	3 kN/m [IS: 456–2000]
Sidewalk load	Dead–area load	1.5 kN/m ² [IS: 456–2000]
Pedestrian load	Pedestrian live–area load	1.5 kN/m ² [IS: 456–2000]
Asphalt load	Wearing surface–area load	1.5 kN/m ² [IS: 456–2000]
IRC class a load	Vehicle live–moving load	As per IRC 6[12]
Pushover load	Seismic response spectrum	As per IS: 1893–2016 [13]

to analyse the structure. A 3D model is also shown in Fig. 2. The loading condition on the bridge is selected as per the IRC 6, section II, 2017 [12]. Pushover analysis was performed on the models for the seismic analysis purpose and as per IS: 1893–2016 was used in this regard. For seismic severity, zone V was considered including soil type 2 which is average for a construction purpose [13]. The detailed loading conditions are tabulated in Table 5.

4 Result and Discussion

The analysis results for each model were evaluated in-depth and a clear comparison has been produced between the traditional concrete behavior and new concrete

materials' behavior under a seismic event. Considerable amount of increment in the strength of the bridge was found by replacing the CC with SCC and FRSCC.

4.1 Demand-Capacity Ratio

It is the ratio of the structural member force after the sudden removal of a column to the member strength (capacity), as a benchmark to determine the failure of major structural members by the linear static analysis procedure. The ratio is a very important factor to evaluate the bridges' vulnerability due to the seismic force. If the D/C ratio is found to be 0, which means bridge takes no damage and if the ratio is 1, it implies that the bridge is on the verge of failure. Figures 3 and 4 show the demand-capacity ratio for the bridges in longitudinal and transverse directions. The first figure shows the behavior of the bridges with different concrete materials in the longitudinal direction. From the graph, it is visible that using SCC instead of regular CC, performs better and if the CC is replaced by FRSCC, the results are even better. With each replacement, the D/C ratio of the bridge is coming near to zero which indicates less damage was taken by the bridge for the same earthquake condition. The SCC reduced the damage on the bridge by 2.75% which further reduced by 15.84% while adding fibers to the concrete. Similarly, Fig. 4 shows the behavior of the bridge in transverse direction under same earthquake condition. Here also the replacements reduced the D/C ratio of the bridge which indicates less damage for the bridge with new materials as a constructional built. With the replacement of SCC

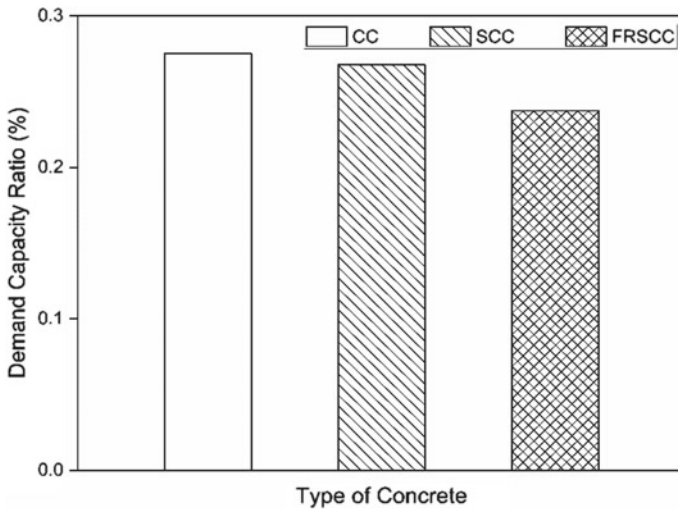


Fig. 3 Demand-capacity ratio for pushover load in longitudinal direction

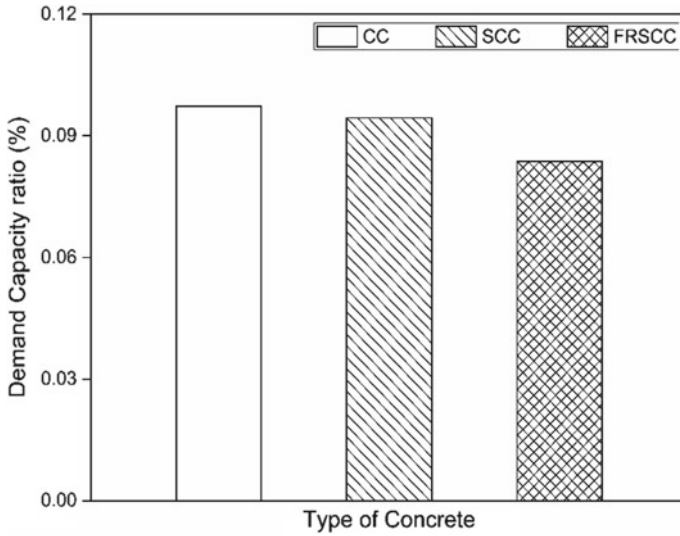


Fig. 4 Demand-capacity ratio for pushover load in transverse direction

and FRSCC instead of CC, the reduction of damage against the bridge is 3.14 and 16.36%, respectively.

4.2 Mode Shapes

Mode shape is a very important property in seismic analysis of a structure. It shows the vibration type of the structure under natural or external frequency. Pushover analysis was performed to evaluate the vibrational shapes of the structure for 12 mode shapes and these are discussed here in detail. Figures 5, 6, 7, 8, 9, 10, 11, 12, 13, 14, 15 and 16 shows all the vertical deflection of the bridges due to the 12 mode shapes, respectively. It can be seen that mode shapes 1 & 2, that is the seismic frequency types 1 & 2 have no effect on the bridges made with CC, SCC and FRSCC (see Figs. 5 and 6). But the mode shapes 3, 4 & 5 does affect the bridge structures (see Figs. 7, 8 and 9). In Fig. 7, where there is a deflection of the bridge span of more than 55 mm, that is reduced to 40 mm by using SCC and it can be greatly reduced to 20 mm by using FRSCC in place of CC. Also by using FRSCC, the deflection is distributed throughout the full length of the span of the bridge which reduced the failure chances greatly. But with CC and SCC there is still a chance for crack generation in the middle length of the bridge span. In Figs. 10, 11, 12 and 13, it is seen that these mode shapes have no effect on the bridge structure, indicating these frequencies are safe for the bridge due to 6th, 7th, 8th and 9th mode shapes. Figures 14 and 15 shows the deflection of the bridge under the action of 10th and 11th mode shapes. These mode shapes affect the structure higher than the previous

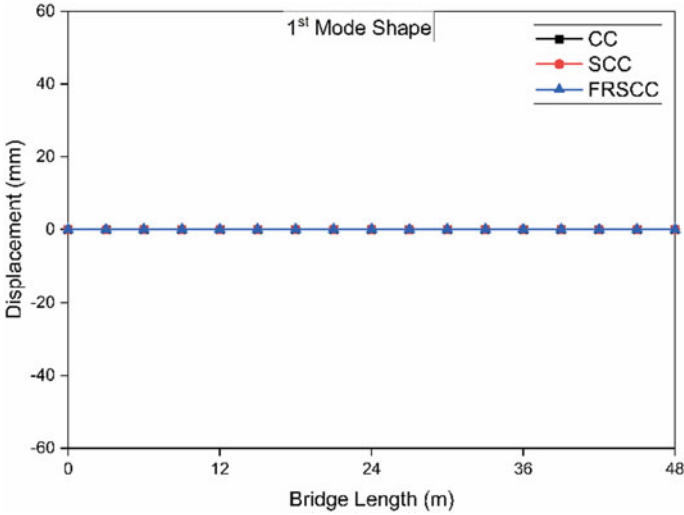


Fig. 5 Vertical deflection of the bridge for 1st mode shape

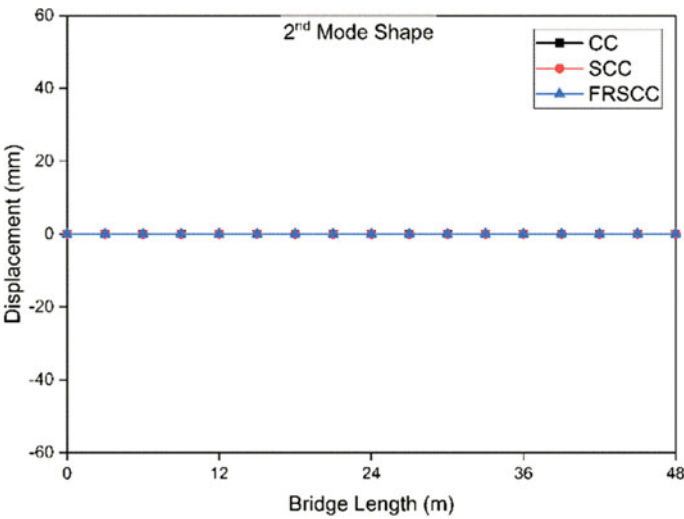


Fig. 6 Vertical deflection of the bridge for 2nd mode shape

mode shape frequencies. Both of these mode shapes caused the bridge to have a rapid deflection of nearly 60 mm with CC as constructional material. But FRSCC reduced this deflection by 67% which is a great improvement for the bridge under seismic severity situation. The last mode shape's (12th mode shape) vibrational frequency does not affect the bridge and hence the structure shows no deflection in this scenario

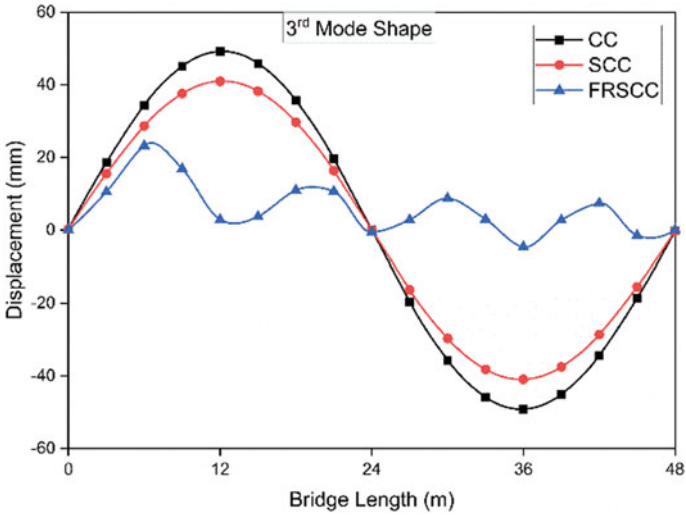


Fig. 7 Vertical deflection of the bridge for 3rd mode shape

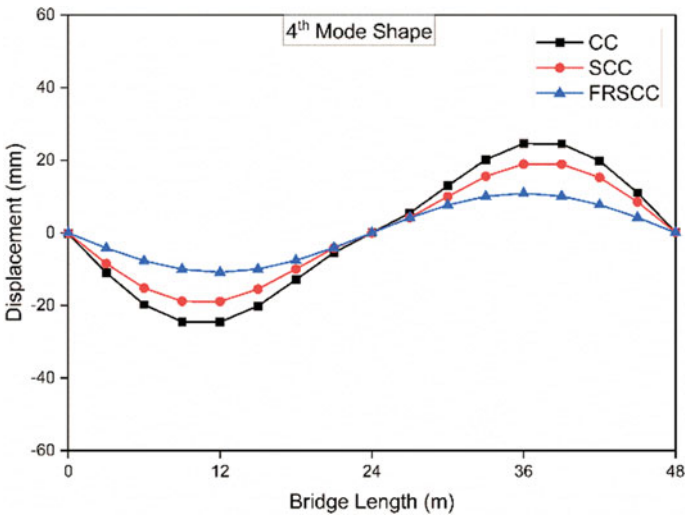


Fig. 8 Vertical deflection of the bridge for 4th mode shape

as can be seen in Fig. 16. Along with the modal shapes explanation, modal loading period and frequencies are also presented in Table 6.

Along with the graphs, for clear visualization of the bridge deflection type, deformed shapes are presented in Figs. 17, 18, 19, 20, 21, 22, 23, 24, 25, 26, 27 and 28 for each and every mode shape.

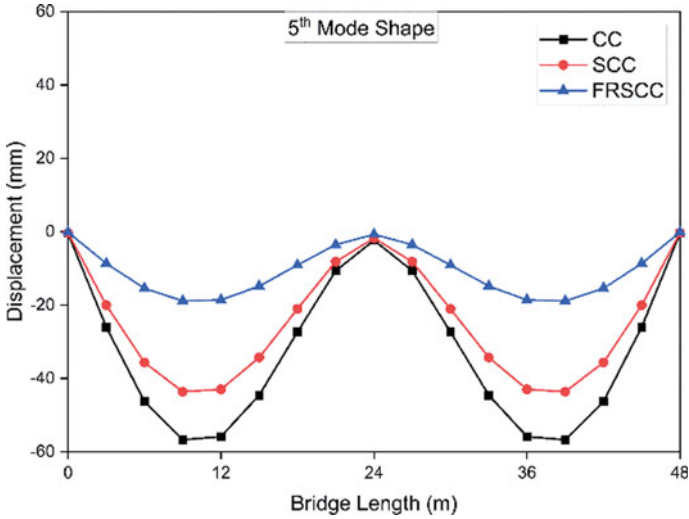


Fig. 9 Vertical deflection of the bridge for 5th mode shape

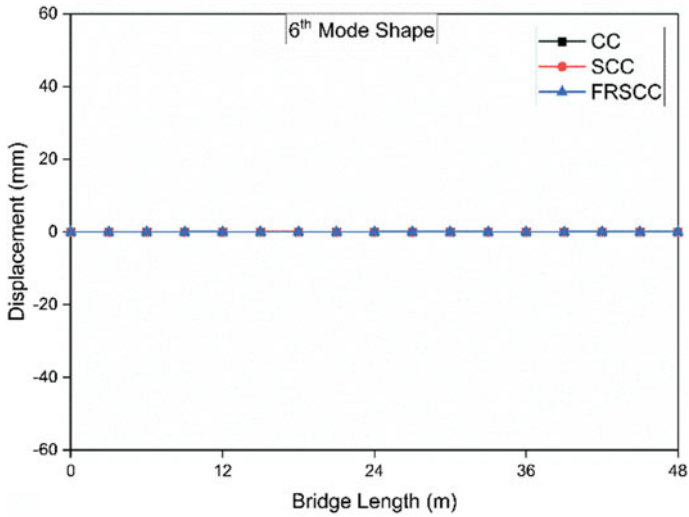


Fig. 10 Vertical deflection of the bridge for 6th mode shape

5 Conclusion

The current study was conducted to evaluate the behavior of the bridge under a severe seismic event by replacing the regular conventional concrete with SCC and FRSCC. The hypothesis was that the replacement will improve the bridge strength and behavior. After the analysis and evaluation the following conclusion is concluded:

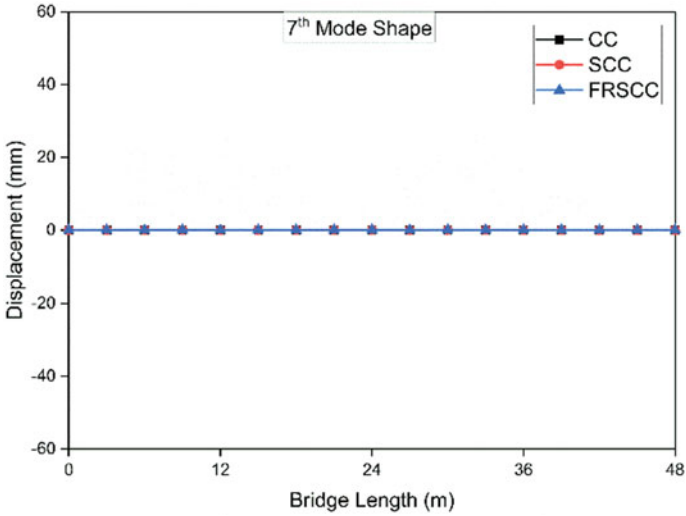


Fig. 11 Vertical deflection of the bridge for 7th mode shape

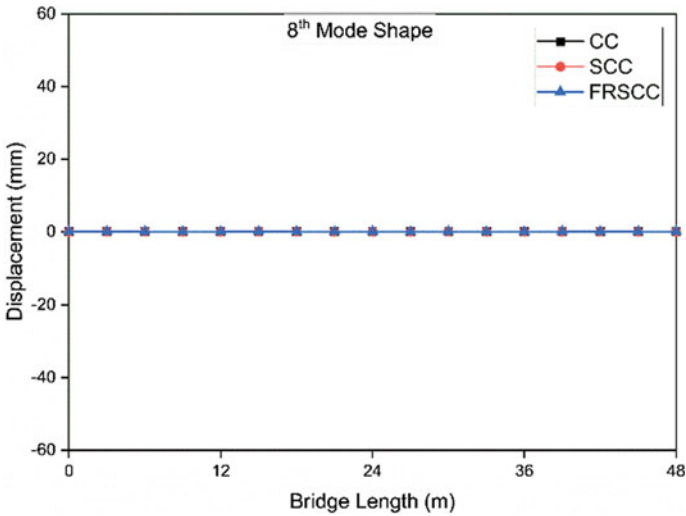


Fig. 12 Vertical deflection of the bridge for 8th mode shape

- SCC and FRSCC both is more suitable for construction purposes of bridge structures and they are also eco-friendly which reduces sound pollution, saves traditional raw materials of construction. Demand-Capacity Ratio was reduced by 3% and 16% using the new replacement concrete types, respectively, which improved the strength of the bridge structure against seismic loads leading to withstand in the situation much longer.

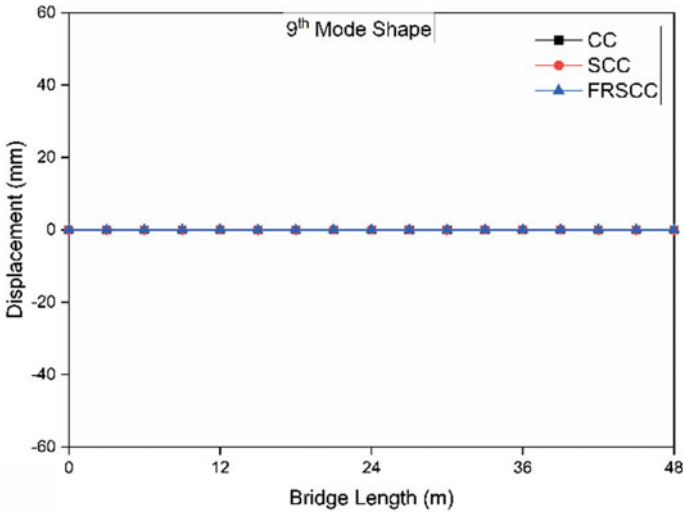


Fig. 13 Vertical deflection of the bridge for 9th mode shape

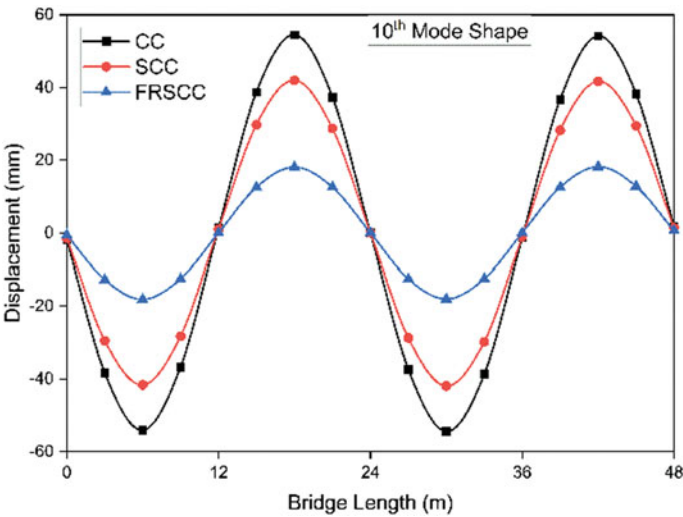


Fig. 14 Vertical deflection of the bridge for 10th mode shape

- The new concrete replacements proved to be better than the currently used construction method in the strength point of view as well as safety. SCC improved the strength of the bridge by reducing the deformation by 50% but with fiber addition in the SCC, which is with FRSCC the safety limit is increased by reducing the deformation to 67% from the bridge made with CC. The analysis and results supported the initial hypothesis and proved its importance and advantage.

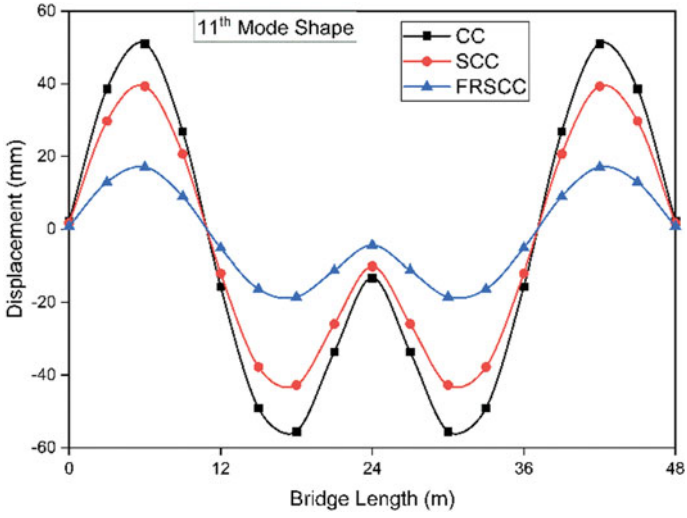


Fig. 15 Vertical deflection of the bridge for 11th mode shape

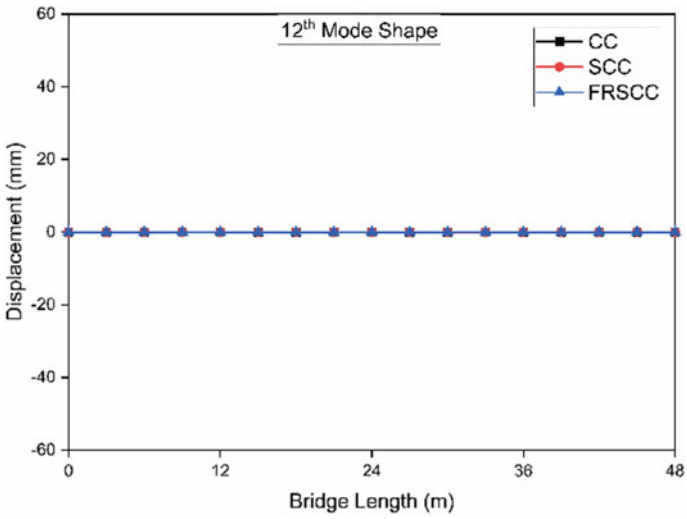


Fig. 16 Vertical deflection of the 12th mode shape

Table 6 Modal periods and frequencies

Mode shapes	Period (Sec)	Frequency (Cyc/sec)
1st mode shape	0.921	1.086
2nd mode shape	0.254	3.934
3rd mode shape	0.199	5.001
4th mode shape	0.133	7.531
5th mode shape	0.126	7.952
6th mode shape	0.094	10.613
7th mode shape	0.087	11.432
8th mode shape	0.082	12.268
9th mode shape	0.054	18.372
10th mode shape	0.050	20.167
11th mode shape	0.043	23.185
12th mode shape	0.040	24.756

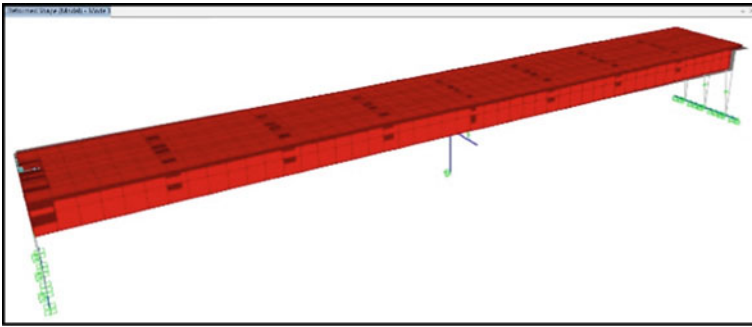


Fig. 17 Deflection pattern for 1st mode

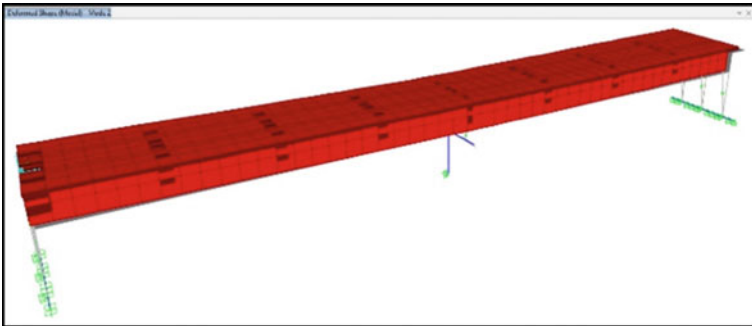


Fig. 18 Deflection pattern for 2nd mode

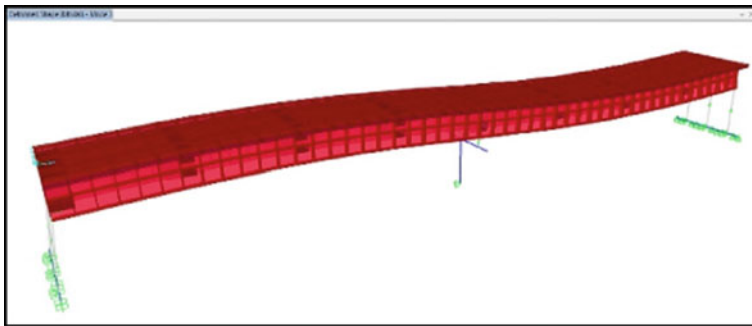


Fig. 19 Deflection pattern for 3rd mode

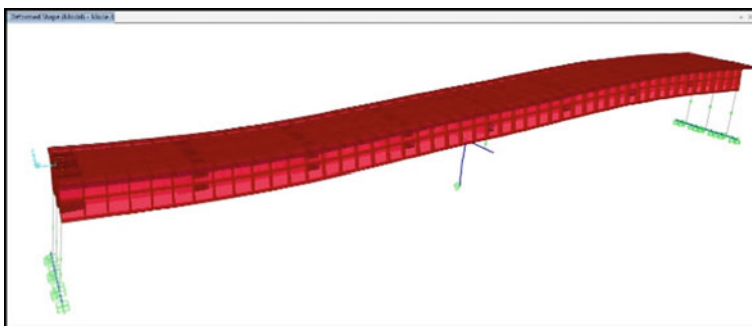


Fig. 20 Deflection pattern for 4th mode

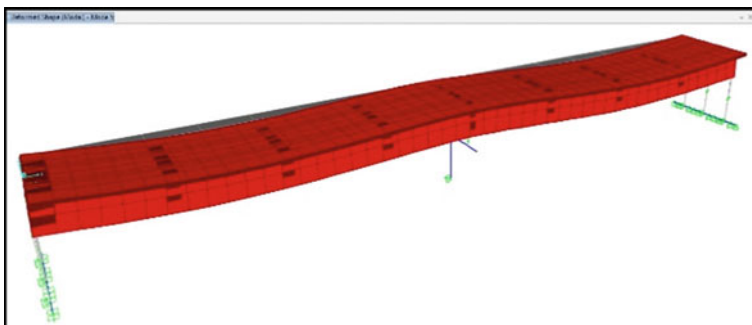


Fig. 21 Deflection pattern for 5th mode

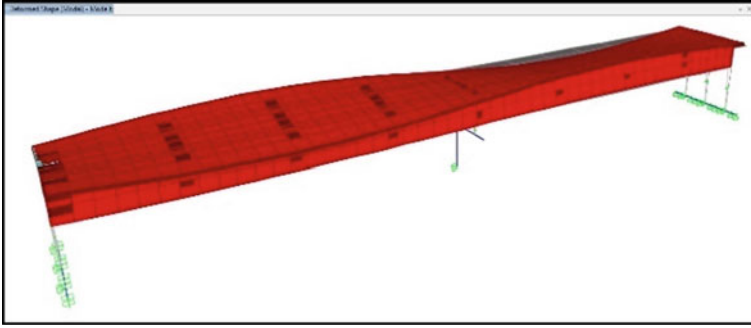


Fig. 22 Deflection pattern for 6th mode

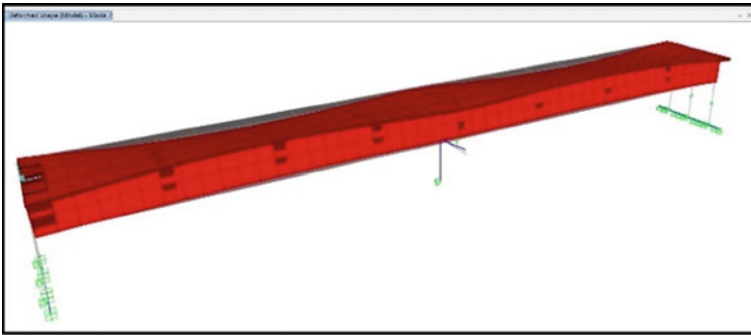


Fig. 23 Deflection pattern for 7th mode

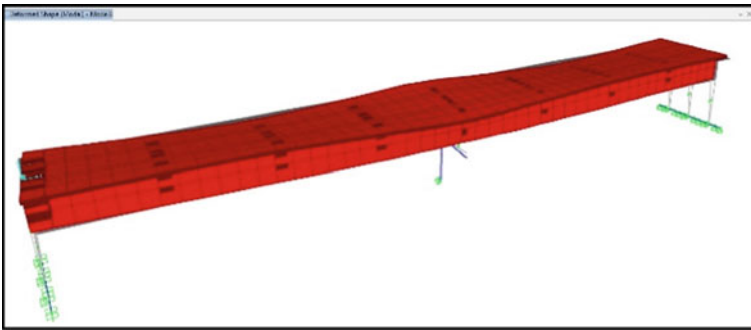


Fig. 24 Deflection pattern for 8th mode

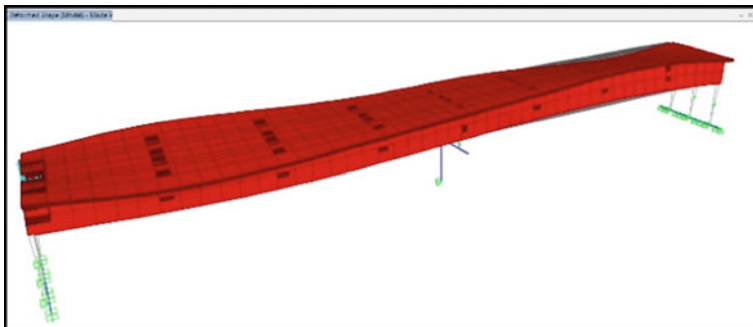


Fig. 25 Deflection pattern for 9th mode

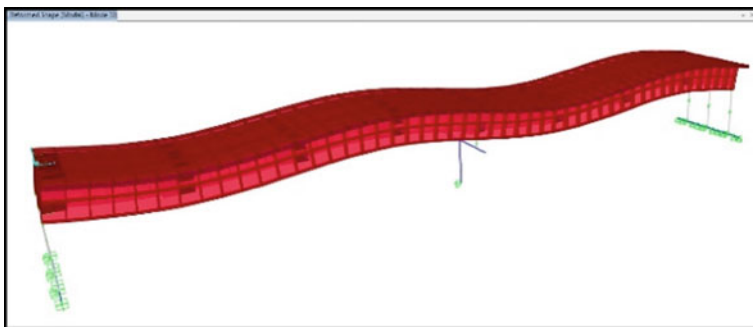


Fig. 26 Deflection pattern for 10th mode

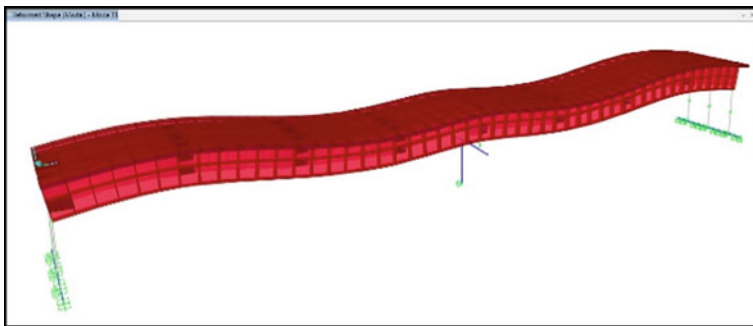


Fig. 27 Deflection pattern for 11th mode

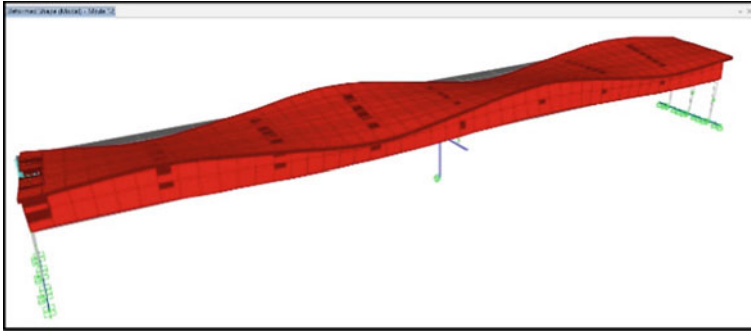


Fig. 28 Deflection pattern for 12th mode

References

1. El-Sheikh A (1996) Development of a new space truss system. *J Constr Steel Res* 37(3):205–227
2. Kulkarni R, Adhikary S, Singh Y, Sengupta A (2016) Seismic performance of a bridge with tall piers. *Proc Inst Civ Eng Bridg Eng*. 169(1):67–75
3. Babazadeh A, Burgueño R, Silva PF (2015) Use of 3D finite-element models for predicting intermediate damage limit states in RC bridge columns. *J Struct Eng (United States)*. 141(10)
4. Prof IT, Tegou S, Eng C, Markogiannaki O, Tegos I, Tegou S et al (2013) Seismic Design of Precast I-Beam Bridges Based on Ductility. 23(2):176–186
5. Wei B (2018) Study of the applicability of modal pushover analysis on irregular continuous bridges. 21(2):233–237
6. Hasani M, Moghadas F, Sobhani J, Chini M (2021) Mechanical and durability properties of fiber reinforced concrete overlay: experimental results and numerical simulation. *Constr Build Mater* [Internet]. 268:121083 <https://doi.org/10.1016/j.conbuildmat.2020.121083>
7. Vasumathi AM, Rajkumar K, Prabhu GG (2014) Compressive behaviour of RC column with fibre reinforced concrete confined by CFRP strips. *Adv Mater Sci Eng* 2014:10
8. Mehrabi P, Honarbari S, Rafiei S, Jahandari S, Bidgoli MA (2021) Seismic response prediction of FRC rectangular columns using intelligent fuzzy-based hybrid metaheuristic techniques. *J Ambient Intell Humaniz Comput*
9. Tarafder N, Prasad LVM (2020) Seismic performance of box girder bridge with non-linear static pushover analysis. *Int J Emerg Technol* 11(2):897–904
10. Meesaraganda LVP, Tarafder N (2019) Durability studies of environmental friendly self compacting concrete with and without fiber. *Key Eng Mater* 803
11. Kassimi F, Khayat KH (2021) Mechanical properties of fiber-reinforced concrete with adapted rheology. *Cem Concr Compos* 118:103958
12. Kunnath SK, Kalkan E (2004) Method of modal combinations for pushover analysis of buildings. In: 13th World conference earthquake engineering, vol 2713. pp 15
13. Singh JP, Agarwal P, Kumar A, Thakkar SK (2014) Identification of modal parameters of a multistoried RC building using ambient vibration and strong vibration records of Bhuj earthquake, 2001. *J Earthq Eng* 18(3):444–457
14. Yu Q, Pugliesi R, Allen M, Bischoff C (2004) Assessment of modal pushover analysis procedure and its application to seismic evaluation of existing building. *World Conf Earthq Eng* [Internet]. (1104). <http://scholar.google.com/scholar?hl=en&btnG=Search&q=intitle:Assesment+of+modal+pushover+analysis+procedure+and+its+application+to+seismic+evaluation+of+existing+buildings#6>

15. IRC:6–2017. Standard specification and code of practice for road bridge, Section: II, Load and Load Combinations, 7th rev. New Delhi, India, pp 1–55
16. IS 1893 (Part 1):2016. Criteria for earthquake resistant design of structures, 6th rev. New Delhi, India, pp 1–44

Effect of Speed Calming Measures on Vehicular Speed for Rural Roads



Kuldeep, Akshata Badiger, M. R. Archana, and V. Anjaneyappa

Abstract The vehicular speed plays major role in road accidents. The speed calming measures like speed bumps/humps, rumble strips help to reduce the speed of vehicles in the locations where the speed reduction is necessary. The effectiveness of trapezoidal humps, circular humps, and rumble strips on the speed of different types of vehicles of 2-wheelers, 3-wheelers, cars, LCVs, HCVs, and buses are studied on rural highways in Karnataka. Geometric features of speed calming measures (SCM) and spot speeds of different vehicle classes are collected. The performance of SCM's on vehicles speed is analyzed and presented. Circular humps are more effective in curve sections compared to trapezoidal humps by 24% and trapezoidal humps are 65% more effective at village limits in comparison with rumble strips. Highest speed reduction is observed for HCVs and buses.

Keywords Vehicular speed · Trapezoidal hump · Circular hump · Rumble strips

1 Introduction

India's road network is second largest in world with length of 58.98 lakh km [1]. The road accidents are one of world's leading causes of death with around 1.35 million people dying each year [2]. The factors that influence the road safety can be divided into two parts as objective and subjective factors. The subjective factors mainly include the influence of drivers and pedestrians and objective factors include cross-section of road, road alignment, and sight distance. The other objective factor

Kuldeep (✉) · A. Badiger · M. R. Archana · V. Anjaneyappa
RV College of Engineering, Bengaluru, India
e-mail: kuldeep.cht19@rvce.edu.in

A. Badiger
e-mail: akshatab.cht19@rvce.edu.in

M. R. Archana
e-mail: archanamr@rvce.edu.in

V. Anjaneyappa
e-mail: anjaneyappa@rvce.edu.in

is traffic safety facilities which contains traffic signs, road lightings, traffic flow, and environmental factors [3]. Speed control becomes necessary when vehicles approach zones like hospitals, schools, curves, and villages [4]. Traffic enforcement and physical warnings like speed calming measures (speed humps, rumble strips) are used to reduce the speed [5]. The impact of SCM's on vehicular speed is dependent on physical and geometric properties of road [6].

The size and shape are the two important factors in design of SCM's [7]. The speed limit of road will decide the geometrics of SCM's to reduce the speed effectively [8]. The major difference between speed bumps and humps is length of speed bump is shorter compared to speed hump with approximately same height [9]. Speed humps, speed bumps, and crosswalks have helped to reduce the accident rate by 60%, injuries by 63%, and number of fatalities by 82% on Lithuanian roads [10]. The installation of speed humps study in New York has shown number of total fatal accidents reduced by 33% [11]. A 3 and 5 cm height bump decreased the mean speed by 15.7 and 30.8%, respectively [12]. Tabletop hump reduced the speed of vehicles up to 71.6% [13]. The reduction in 85th percentile speed was from 81 to 54 kmph, 74 to 44 kmph, and 84 to 45 kmph for hump, bump, and double bumps, respectively [14]. The reduction in speed of vehicle depends upon the spacing between the humps placed [15]. As per IRC areas where the NH and SH roads travel through the villages, to counter the speed of vehicles a buffer zone with well-defined boundaries should be constructed [16].

2 Study Area and Field Studies

A rural road of Bengaluru rural district of Karnataka is chosen for the study. The geometry of roads consists of divided four-lane and undivided two-lane carriage way, mostly consisting of bituminous overlays. A total of 36 speed calming measures were identified consisting of Circular hump, Trapezoidal hump, and Rumble strips. Speed of vehicles is measured at 36 locations of having speed calming measures on the rural roads.

2.1 Geometry of Speed Calming Measures

Different types of speed calming measures of circular humps, trapezoidal humps, and rumble strips are selected for studies. The height, width, and length of speed calming measures are shown in Table 1.

Table 1 Details of speed calming measures

Road stretch	Height (m)	Width (m)	Length (m)	Type of SCM
SH-96	0.1	1	5.5	Trapezoidal
	0.1	1	5.5	
	0.1	1	5.5	
SH-104	0.08	2	5.5	Circular
	0.08	1.5	5.5	
	0.08	1.5	5.5	
SH-9	0.01	0.15	7	Rumble strip
	0.01	0.3	7	
	0.01	0.3	7	
	0.01	0.3	7	
	0.01	0.3	7	
	0.01	0.3	7	
	0.01	0.2	7	
	0.01	0.2	7	
	0.01	0.3	7	
	0.01	0.2	7	
SH-82	0.1	3	5.5	Trapezoidal
	0.1	3	5.5	
	0.1	3	5.5	
	0.1	3	5.5	
	0.1	3	5.5	
	0.1	3	5.5	
	0.1	3	5.5	
SH-35	0.1	3	5.5	Trapezoidal
	0.1	3	5.5	Trapezoidal
	0.1	1	5.5	Trapezoidal
	0.01	0.3	5.5	Rumble strip
	0.04	0.6	5.5	Rumble strip
	0.1	0.7	5.5	Trapezoidal
SH-74	0.08	1	5.5	Trapezoidal
	0.05	2	5.5	Circular
	0.07	1.2	5.5	Circular
	0.07	3	5.5	Circular
Hessaeghatta to Nelamangala	0.1	1	5.5	Circular
	0.1	1	5.5	
	0.1	1	5.5	

2.2 Spot Speed

Spot speed studies at the identified 36 locations where humps and rumble strips are placed, along with the in-service road stretches are considered for study. The studies were carried out during off-peak time of weekdays (between 12 to 4 pm) when the vehicular speed was evidently higher. It was ensured to collect the speed data in day-light and good weather conditions to avoid discrepancies in data collection due to weather conditions. Radar gun is used to measure spot speed of different vehicle classes at various SCM's, which measured the spot speed at an accuracy of ± 2 kmph. The measurement was made on either side of SCM's at a distance of 30 m before and after SCM's.

3 Result and Discussion

3.1 Effect of SCM on Speed at Curve Sections

The average speed of different types of vehicles at trapezoidal hump, circular hump, and rumble strips at curve section is represented in Fig. 1, 2, and 3. The figures illustrate the reduction in vehicle speed at speed calming measures at curve sections. The average speed reduced by 44, 58.3, and 23.5% at trapezoidal hump, circular hump, and rumble strips, respectively.

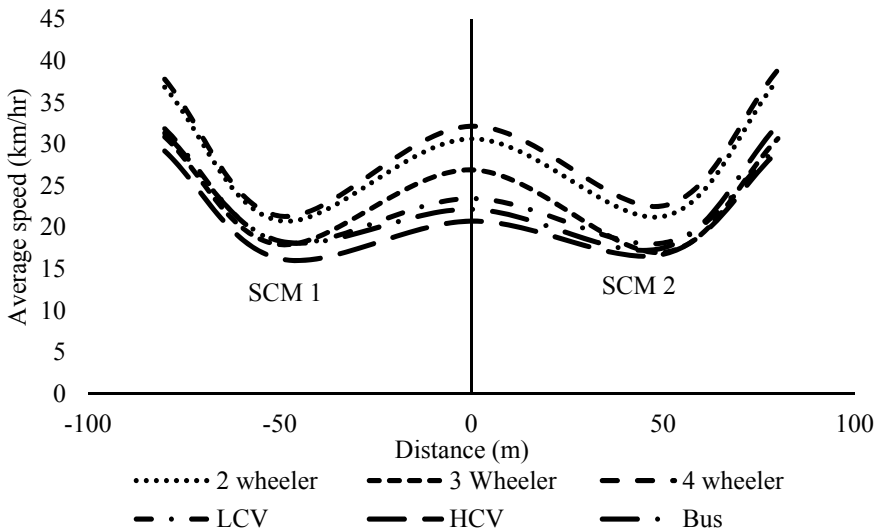


Fig. 1 Average speed at trapezoidal SCM at curve

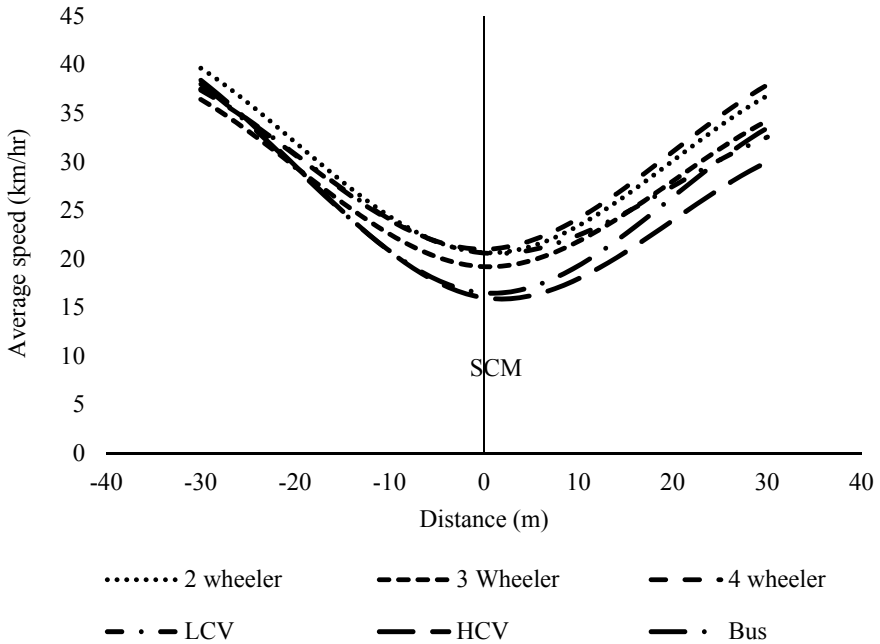


Fig. 2 Average speed at circular SCM at curve

3.2 Effect of SCM on Vehicle Speed at Village Limits

The average speed of different types of vehicles at trapezoidal hump and rumble strips at village limits are represented in Figs. 4 and 5. The average speed reduced by 42.7 and 25% at trapezoidal hump and rumble strips, respectively.

3.3 Effect of Types of SCM on Speed for Different Vehicles

Figure 6 shows the average speed of different vehicles at the approach of circular humps are more effective in reducing speed compared to rumble strips by 33.6, 34.3, 28.9, 31.5, 36.1, 32.4% for cars, two-wheelers, auto-rickshaws, LCVs, HCVs, buses, respectively. Compared to trapezoidal humps the speed reduction is by 28.9, 28.1, 25, 27.1, 29.9, and 24% for cars, two-wheelers, auto-rickshaws, LCVs, HCVs, and buses, respectively.

Figure 7 represents the average speed of different vehicles at the SCM, Speed reduction at circular humps compared to rumble strips are 51.6% for cars, 48.6% for two-wheelers, 48.5% for auto-rickshaws, 51.4% for LCVs, 56.4% for HCVs, and 56.4% for buses. In comparison with trapezoidal humps, the speed reduction in

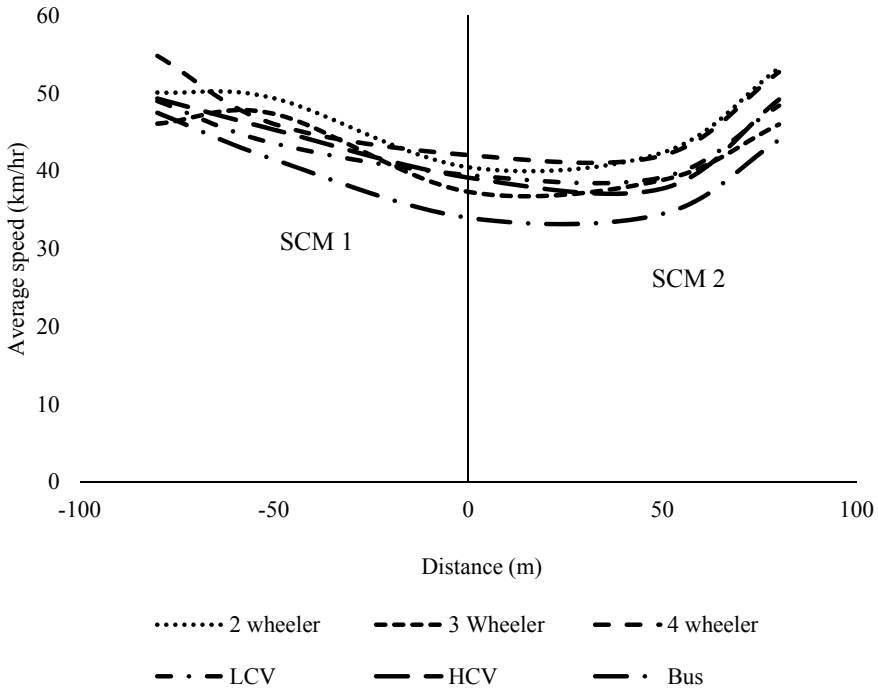


Fig. 3 Average speed of rumble strips at curve

circular humps is 0.69% for cars, 6.6% for two-wheelers, 5.2% for auto-rickshaws, 5.1% for LCVs, 7.5% for bus and increase in speed by 3.1% for HCVs.

The average speed of vehicles after passing the SCM, As shown in Fig. 8 the speed reduction in circular humps compared to rumble strips are 17.3% for cars, 21.4% for two-wheelers, 18.2% for auto-rickshaws, 21.8% for LCVs, 27.1% for HCVs and 16.1% for buses. In comparison with trapezoidal humps, the speed reduction in circular humps is 4.1% for cars, 9.1% for two-wheelers, 2.1% for HCVs, 3.5% for buses but there was increase in speed by 0.09% for auto-rickshaws and 0.35% for LCVs.

3.4 Regression Analysis

The relationships are developed between the average speed of different type’s vehicles and geometry of speed calming measures. The relationships developed are presented in Eqs. 1–6. The relationship between speeds of various vehicle types with various parameters related to speed calming measures was found to yield the best relationship for logarithmic values of the independent variables. Hence the equations were developed with logarithmic values of dependent variables to obtain best

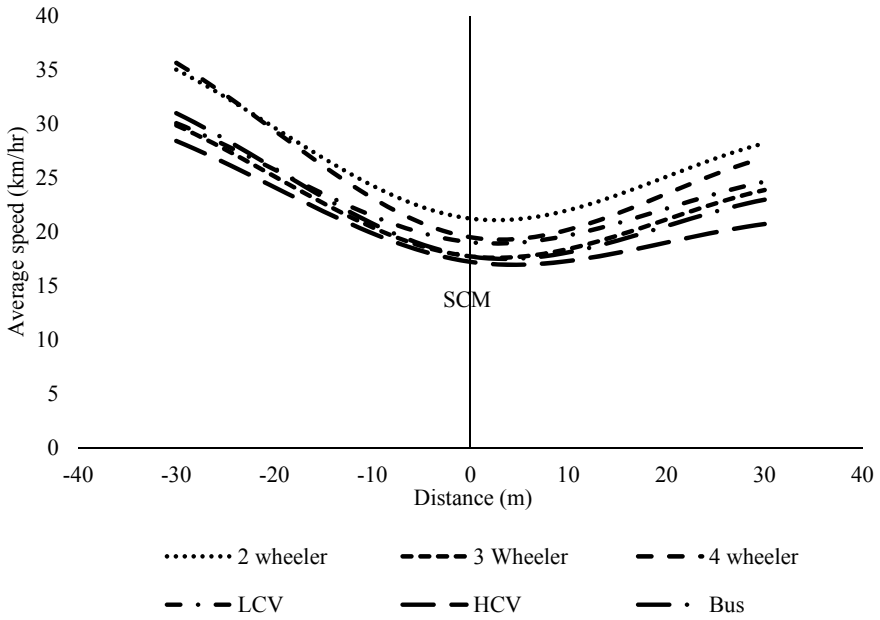


Fig. 4 Average speed of trapezoidal hump at village limit

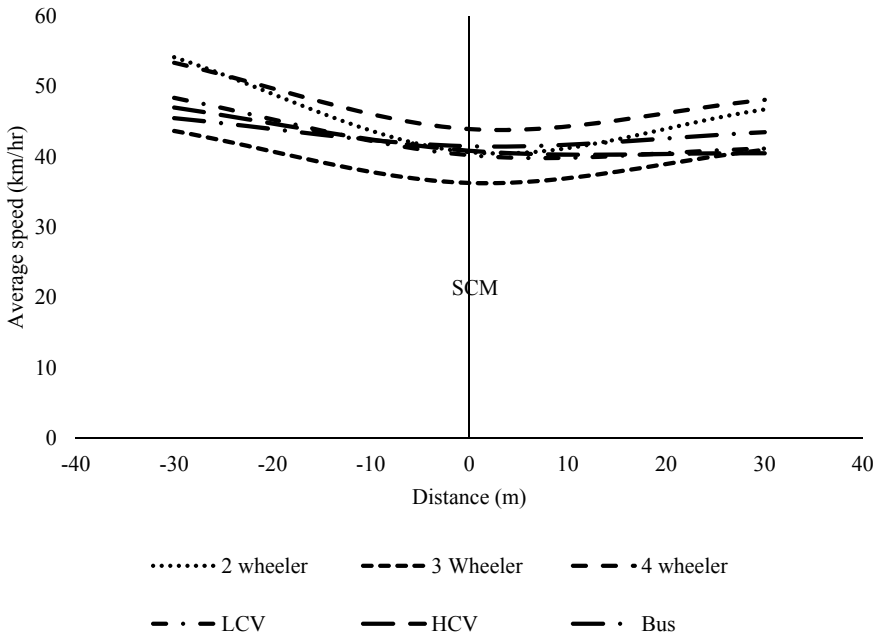


Fig. 5 Average speed of rumble strips at village limit

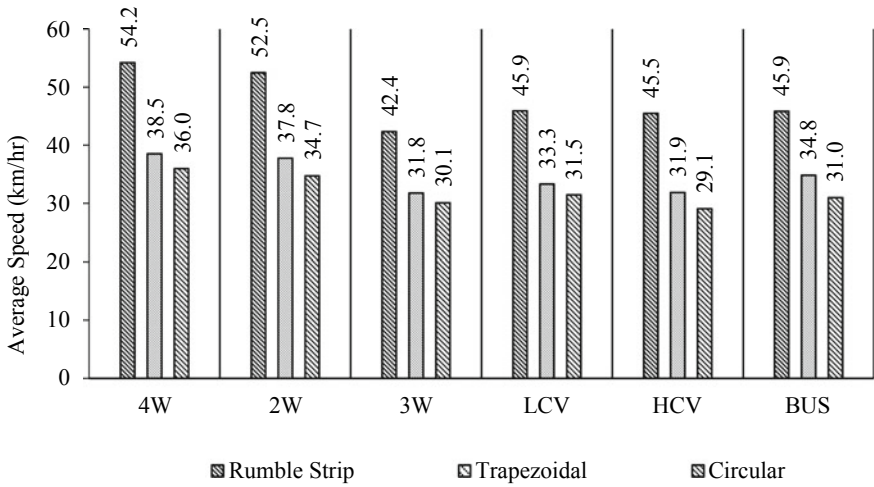


Fig. 6 Average speed before the SCM

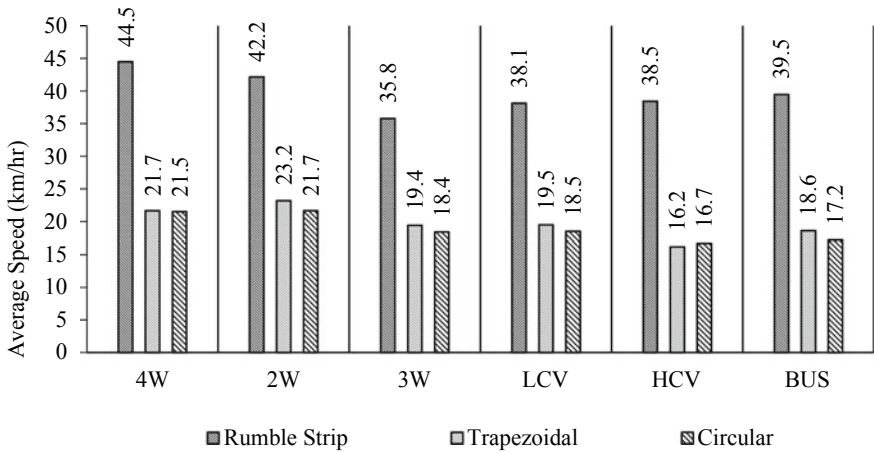


Fig. 7 Average speed at SCM

possible relationship. The p—values of all equations calculated based on ANOVA, was less than 5%, which is the level of significance, and hence the equations are statistically significant. The minimum R2 value for the multilinear equations is 0.89, which reinforced the authenticity of the developed equations.

$$V_{\text{motorbikes}} = - 6.225 - 38.17\log(H) + 1.8131\log(W) - 13.0485\log(L) - 0.58S^3$$

$$R^2 = 0.90006 \tag{1}$$

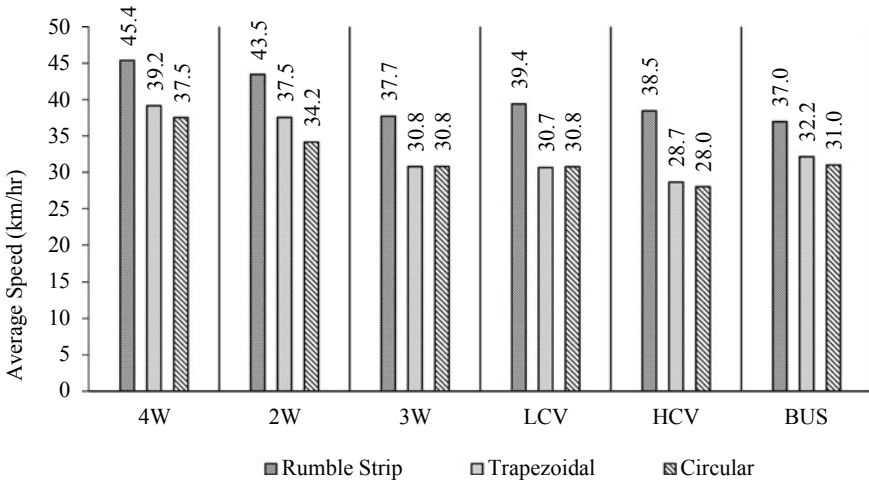


Fig. 8 Average speed after SCM

$$V_{\text{autorickshaw}} = 26.45 - 37.23\log(H) - 1.044\log(W) - 59.56\log(L) - 0.57S^3$$

$$R^2 = 0.9092 \tag{2}$$

$$V_{\text{cars}} = -35.174 - 31.67\log(H) - 1.788\log(W) + 34.64\log(L) - 0.519S^3$$

$$R^2 = 0.9341 \tag{3}$$

$$V_{\text{LCV}} = -11.28 - 35.12\log(H) - 0.72\log(W) - 5.42\log(L) - 0.625S^3$$

$$R^2 = 0.9179 \tag{4}$$

$$V_{\text{HCV}} = -4.52 - 37.073\log(H) - 2.828\log(W) - 20.061\log(L) - 0.593S^3$$

$$R^2 = 0.9433 \tag{5}$$

$$V_{\text{buses}} = -31.1535 - 31.8631\log(H) + 0.4326\log(W) + 23.548\log(L) - 0.5056S^3$$

$$R^2 = 0.8940 \tag{6}$$

where,

V = average speed of vehicle in km/hr.

H = height/thickness of speed calming measure in meter,

W = width of SCM in meter,

L = length of speed hump in meter.

S = type of speed calming measures.

4 Conclusions

The conclusions drawn from the studies are:

- i. The study includes three types of speed calming measures viz., circular humps, trapezoidal humps, and rumble strips on rural highways.
- ii. The circular humps are more effective compared to rumble strips and trapezoidal humps at curve sections. The reduction in the speed at circular humps was found to be 24% more compared to trapezoidal hump and 51.3% more compared to rumble strips.
- iii. The trapezoidal humps are more effective compared to rumble strips at village limits. The trapezoidal humps reduced the vehicle speed 65% more compared to rumble strips.
- iv. Circular humps are effective in reducing the speed of vehicles before, at, and after the SCMs compare to trapezoidal humps and rumble strips.
- v. The highest speed reduction is observed in HCVs.
- vi. The further research is needed in analyzing the effect on the vehicular speed due to road markings and signboards at speed calming measures and effect of damaged speed calming measures on the vehicular speed.
- vii. This analysis is used for effective planning and implementation of speed calming measures on rural roads especially for heterogeneous traffic in Indian conditions.

References

1. Road Accidents in India (2018) Ministry of road transport and highways (MoRTH). Indian Roads Congress New Delhi 2013
2. World Health Organization (2019) World report on road traffic injury prevention, Geneva
3. Liu Y (2013) Highway traffic accident black spot analysis of influencing factors. In: ICTE 2013—proceedings of the 4th international conference on transportation engineering: 2295–2300
4. World Health Organization (2013) Pedestrian safety: a road safety manual for decision-makers and practitioners. Geneva
5. Chadda HS, Cross SE (1984) Speed (road) bumps: issues and opinions. *J Transp Eng* 111(4):0004–0041
6. Mahdy H (2012) Speed calming using vertical deflections in road alignment. In: CICTP 2012: Multimodal transportation systems—convenient, safe, cost-effective, efficient—proceedings of the 12th COTA international conference of transportation professionals, 2085–2094
7. Fwa TF, Tan LS (1992) Geometric characterization of road humps for speed-control design. *J Transp Eng* 118(4):593–598
8. Ardeh HA, Shariatpanahi M, Bahrami MN (2008) Multiobjective shape optimization of speed humps. *Struct Multidisc Optim* 37(2):203–214
9. Shwaly SA, Zakaria MH, Al-Ayaat AH (2018) Development of Ideal hump characteristics for different Vehicle types “case study” urban roads in Kafr-El-Sheikh city (Egypt). *Adv Civ Eng* 2018:12. <https://doi.org/10.1155/2018/3093594>

10. Jateikiene L, Andriejauskas T, Lingyte I, Jasiuniene V (2016) Impact assessment of speed calming measures on road safety. *Transp Res Procedia* 14:4228–4236
11. Chen L, Chen C, Ewing R, McKnight EM, Srinivasan R, Roe M (2013) Safety countermeasures and crash reduction in New York City—experience and lessons learned. *Accid Anal Prev* 50:312–322
12. Antic B, Pesic D, Vujanic M, Lipovac K (2013) The influence of speed bumps heights to the decrease of the vehicle speed—Belgrade experience. *Saf Sci* 57:303–312
13. Abdulmawjoud AA, Jamel MG, Al-Taei AA (2020) Traffic flow parameters development modelling at traffic calming measures located on arterial roads. *Ain Shams Eng J* 10:04–014
14. Kirana KR, Kumara M, Abhinay B (2020) Critical analysis of speed hump and speed bump and geometric design of curved speed hump. *Transp Res Procedia* 48:1211–1226
15. García A, Moreno AT, Romero MA (2011) Development and validation of speed kidney, a new traffic-calming device. *Transp Res Rec* 2223:43–53
16. IRC-99–2018 (2018) Guidelines for traffic calming measures in urban and rural areas. Indian Road Congress 2018

Engineering Properties of Concrete Containing Hazardous Drywalls Waste and GGBS



T. Raghavendra, H. P. Vageesh, M. Lokeshwari, S. Sunil,
and L. Durga Prashanth

Abstract An investigation is planned to know how effects of powdered drywalls and to create a new mix blend proportions for concrete containing crushed and powdered gypsum wallboard and GGBS as partial replacement to cement. Results indicate gypsum wall board in powdered form along with GGBS can serve the criteria of concrete when used as 60% replacement for cement. Reference concrete mixture was compared with sustainable concrete mixtures made by replacing 15, 30, 45, 60 and 75% (by weight) of binder. The concrete bends with lesser cement replacement resulted in better mechanical properties compared to the mixes with higher cement replaced mixes. However, the concrete mixes with higher replacements exhibited higher durability compared to the mixes with lesser replacements. However, all the mixes recorded better later age strength after 28 days. Hence, the usage of above wastes in the manufacturing of concrete is recommended to reduce hazardous H₂S gas emissions.

Keywords Drywalls · H₂S · Sustainable concrete · GGBS · Cement

T. Raghavendra (✉) · H. P. Vageesh · M. Lokeshwari · S. Sunil · L. Durga Prashanth
RV College of Engineering, Visvesvaraya Technological University, Bengaluru, India
e-mail: raghavendrat@rvce.edu.in

H. P. Vageesh
e-mail: vageeshhp@rvce.edu.in

M. Lokeshwari
e-mail: lokeshwarim@rvce.edu.in

S. Sunil
e-mail: sunils@rvce.edu.in

L. Durga Prashanth
e-mail: durgaprashanthl@rvce.edu.in

1 Introduction

In construction industries the most familiar construction material is concrete within India & several abroad countries in creating state of the art infrastructure facilities. However, the best outcome may be expected only by careful selection of its ingredients and proper supervision of the concrete during its fresh and hardened states [1]. Concrete may contain mixture of a binder as cement, water, fine & coarse aggregates with or without admixtures. Concrete is largely adopted in non-structural and structural applications of Civil Engineering [2–4]. The most essential component of concrete is the binder i.e. cement. Usage of cement only in concrete as binding material generates greater heat of hydration. Also cement manufacturing results in CO₂ emission. The large CO₂ emission due to high cement manufacture is very harmful and causing environmental changes. Nowadays many initiatives are introduced by governments to reduce the CO₂ emissions. The productive way of minimizing CO₂ emission due to cement manufacture [5–8] with the help of industrial wastes by replacing cement or use of supplementary cementing materials such as Ground Granulated Blast Furnace Slag (GGBS) [9], Fly Ash (FA) [10, 11], and Silica fume, etc. Gypsum wallboard often called as drywalls or plasterboards [12] are commonly adopted in false ceiling, aesthetic, acoustic and other building products. Gypsum wallboards are made of gypsum, a mineral found in sedimentary rock formation known as calcium sulphate dehydrate [13]. In literature it is reported that discarded Gypsum wallboard sheets dumped at landfills release harmful H₂S gas to the atmosphere under certain anaerobic and temperature conditions [14–16]. Public law suits and environmental protection agencies warrant that these discarded gypsum wallboard sheets or drywalls should be re-used and not dumped at landfills, to ensure that the harmful H₂S gas emission is mitigated. GGBS is a waste generated from the iron and steel industry which is a solid waste discharged in large quantities. GGBS is incorporated in cement making such as Portland Blast Furnace Cement (PBFC) and/ High Slag Blast Furnace Cement (HSBFC) in which few percentages of GGBS will be blended with cement clinkers. Setting times of concrete produced with GGBS cement are relatively slower and depend up on the GGBS contents. However, GGBS incorporated cement concretes long-term strength gain is relatively higher than controlled concrete with OPC [17]. In literature an experiemntal study was carried out on consumption of gypsum wallboard residue in concrete [18]. Sodium sulfate was used as an activator, to the mixture blend containing pulverized gypsum wallboard and ASTM Class C fly ash. Decline in compressive strength values and other properties were reported. The loss in strength was due to the detrimental effects of drywalls in concrete causing expansive cracks within concrete specimens. It was concluded that as much as sixty percent of cement content by weight in concrete blends could be successfully substituted with blends of Class C fly ash and pulverized gypsum wallboard. However, only 10% of the cement content by weight could be replaced by powdered gypsum wallboard. Mere 10% cement content replacement in concrete will not achieve the waste re-utilization objective for discarded gypsum wallboard. In literatures several experimental studies were carried out on utilization

of gypsum wallboard powder in Controlled Low Strength Materials (CLSM) [19–22]. CLSM is used instead of earth backfill, which is a self flowing and self leveling material [9, 23]. In the first literature [20] a blend of gypsum wallboard and Class F fly ash were adopted to replace cement at varying proportions. It was concluded that the CLSM mixes (cement + gypsum wallboard + flyash) attained highest compressive strength values at twenty-eight days age and thereafter reduced strength values were observed at 56 days age. About 36–7% strength loss was reported. The loss in strength was due to the detrimental effects of drywalls in CLSM. In second literature on CLSM [21] a mixture blend of gypsum wallboard and GGBS were used to replace cement at varying proportions. It was concluded that the CLSM mixes (cement + gypsum wallboard + GGBS) could overcome the detrimental effects of sulphates present in drywalls when blended with GGBS and at lesser water contents [19]. However, few CLSM mixes with GGBS and drywalls blend, reported loss in strength and other properties at 56 days age when compared to 28 days age. Hence, it may concluded that the utilization of gypsum wallboard in concrete or CLSM will result in detrimental effects such as reduction in strength and other properties, thus making it not suitable as an admixture in general. However the engineering properties of concrete containing third order binder combination of cement, pulverized gypsum wallboard and GGBS is not investigated and/reported till date. An attempt is made experimentally, to improve and assess the performance and mechanical properties of a sustainable concrete mix in which cement is partially interchanged by blend of GGBS and powdered Gypsum wallboard in varying proportion. Compared to literature this novel sustainable concrete with GGBS and drywalls blend performed better and could overcome the detrimental effects of drywalls in concrete. However, strength loss at early ages was obtained, and also was recovered by strength gain at later ages. Around 60–75% of cement content in concrete can be exchanged by the blends of GGBS and Gypsum wallboard powder and up to 20–25% of cement content by weight can be replaced by powdered drywalls, for improvement of concrete industry in terms of sustainability.

2 Materials and Methods

2.1 Binder Materials

2.1.1 Cement

53 grade Ordinary Portland cement conforming to IS 12269 specifications was used, and its Specific gravity is found to be 3.15.

2.1.2 GGBS

Slag was sourced from Jindal Steel Works, Bellary. Air tight bags were used for storage purpose. The chemical composition of GGBS considered is similar to the typical chemical composition of GGBS adopted in concrete industries and satisfied the minimum requirements as per IS: 12,089. The Silicon dioxide, Aluminium trioxide, Calcium oxide and Magnesium oxide content was 37.21, 13.24, 37.23 and 8.65%, respectively. Specific gravity was 2.91. The above chemical composition and physical property are satisfactory to consider GGBS as a secondary cementitious material.

2.1.3 Gypsum Wallboard

Gypsum wallboards are often called as drywalls or plasterboards that differ from other panel-type building products. These gypsum wallboards are extensively incorporated in novel constructions due to numerous positive reasons and forming a huge quantity of Construction and demolition (C & D) wastes produced in recent times. Figure 1 illustrates the crushing and sieving activity for the extraction of gypsum wallboard powder. Powdered Gypsum wallboard is then sieved using 4.75 mm sieve and collected/stored. The 4.75 mm sieve passing powdered gypsum wallboard is then utilized as admixture and mixed in the sustainable concrete as per the proportions mentioned in Table 1. The powdered gypsum wall boards elemental composition contained 19.52% (by weight) Sulphur. In general, the Sulphur content present within discarded Gypsum wallboard sheets dumped at landfills releases harmful H_2S gas to the atmosphere under certain anaerobic and temperature conditions [14].

Fig. 1 Powdered gypsum wall board



Table 1 Cement replacement (by weight) by Gypsum wallboard powder and GGBS

Mix ID	Cement (%)	Gypsum wallboard powder (%)	GGBS (%)
Controlled concrete	100	0	0
M1	85	5	10
M2	70	10	20
M3	55	15	30
M4	40	20	40
M5	25	25	50

2.2 Aggregates

20 mm sieve passing, crushed stone angular aggregates are used as the coarse aggregates. Specific gravity of the stones was found to be 2.7. River bed sand was used as fine aggregate and is satisfying the requirements of zone-II as-per IS 383. The specific gravity of river bed sand was 2.67. The super plasticizer used was FosrocConplast P509.

2.3 Mix-Proportions

The concrete mix design was performed in accordance with IS 10262-2009 procedure and the summary of mix design calculations is given below:

Cement: 370 kg/m³; Water: 148 kg/m³; Fine aggregate: 925 kg/m³; Coarse aggregates: 1443 kg/m³; Water/cement ratio: 0.40; Super plasticizer: 7.4 L (2% of binder content).

Concrete specimens were prepared in accordance to the mix design calculations. Within controlled concrete cement content by weight was 100%. The cement content was gradually replaced in the sustainable concrete mixes from 15 to 75% by blend of Gypsum wallboard powder and GGBS in the proportions as illustrated in Table 1. A total of six dry concrete mix proportions are considered. Sodium Sulphate (Na₂SO₄) is used as an activator in all the concrete mixes. The amount of activator depends on the binder and for this work the quantity of Na₂SO₄ considered is 1% of binder content, same as that of literature. When the activator (Na₂SO₄) was added in greater quantities, the specimen samples exhibited a white amorphous powder deposition on the specimen (refer Fig. 2).

The (W/C) ratio for the M30 grade concrete considered in the mix design was 0.40 using the super-plasticizer. The slump value considered was 100 mm. When the cement content by weight was replaced with Gypsum wallboard powder and GGBS the workability will vary because both GGBS and Gypsum require more water content. Hence maintaining a fixed W/C ratio was difficult for higher cement

Fig. 2 Concrete cubes with high activator (Na_2SO_4) dosage



Table 2 W/B ratio for concrete mixes

Mix	Controlled concrete	M1	M2	M3	M4	M5
W/B	0.40	0.40	0.42	0.46	0.51	0.59

content replacements as they were less workable and it was very difficult to compact with manual efforts. However, the workability could be maintained by increasing the water-binder (W/B) ratio. Hence in this experimental work the workability was fixed and the W/B ratio is varied considering practical adoptability. The slump values of the mixes were maintained at 75–100 mm and the W/B ratios of the mixes are illustrated in the Table 2.

2.4 Experimental Studies

2.4.1 Fresh Properties

Slump Cone Test

This test was performed to determine the uniformity and workability of the concrete.

2.4.2 Hardened Properties

Compressive Strength

The compression test was carried out as per the code IS 516-1959. Concrete specimens of side dimension 150 mm were cast. After 7, 28, 56 and 90 days of water

curing by ponding, these specimens were tested using CTM and the averaged results for five specimens at each age are described in the results section.

Split-Tensile-Strength

The split-tensile test is made as per the code IS 5816:1999. The cylinder is 300 mm in length and 150 mm in diameter. After 56 and 90 days of curing these concrete cylinders were tested and the averaged results for five specimens at each age are described in the results section.

Flexural Strength

Series of concrete beams (prisms) of standard dimensions (500 × 100 × 100 mm) were cast. After 28 days of curing these concrete beams were tested and the averaged results for five specimens at 28 days age are described in the results section.

2.4.3 Acid Attack Test

ASTM C267 is used to perform acid attack test. Sulphuric acid (1%-concentration) was considered for this accelerated laboratory study to simulate the acidity present in the sewers. Specimens of concrete with side dimension 150 mm were cast. The test specimens were immersed for 56 days and then submerged in 1% Sulphuric acid solution for 30 days. The weight loss was monitored and the averaged results for five specimens at each age are described in the results section. After 30 days of exposure, the samples are taken out and dried in the open air for 24 h. These dried specimens are tested for compression in a CTM and the averaged results for five specimens are described in the results section.

2.4.4 Sulphate Attack Test

A Sodium Sulphate solution (of 5% concentration) was chosen for this laboratory test to simulate the sulphate attack on the structures. Specimens of Concrete of side dimension 150 mm were cast. The test specimens were immersed for 56 days then they are submerged in 5% Na₂SO₄ solution for 30 days. The weight loss was monitored and the averaged results for five specimens at each age are described in the results section.

After 30 days of exposure, the samples are taken out and dried in the open air for 24 h. These dried specimens are tested in a CTM and the averaged results for five specimens are described in the results section.

2.4.5 Water Absorption Test

This test is performed in accordance with BS 1881. Specimens five in number were selected at random for the test. The averaged results for five specimens are described in the results section.

3 Results and Discussion

3.1 Mechanical Properties

3.1.1 Compressive Strength

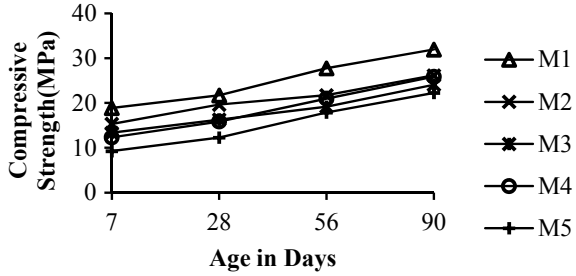
The compressive strength test was conducted on prisms samples of both controlled concrete and sustainable concrete mixes at the age of 7, 28, 56 & 90 days. The averaged results illustrate that as the cement content replacement level increases, early strength gain rate decreases. However, the long-term strength gain rate is higher in cement replaced samples. The 28 days strength obtained for the mixes M1 is 21.70 MPa, M2 is 19.64 MPa, M3 is 16.30 MPa, M4 is 15.87 MPa and M5 is 12.28 MPa. At the later stages the long-term strength improved and the mixes with greater cement replacement resulted in higher rate of strength gain. Table 3, illustrates the compressive strength values for controlled concrete. About 41.49–84.46%, 31.73–56%, 44.83–69.61% and 52.13–74.83% of the compressive strength for controlled concrete were obtained in M5-M1 mixes at 7, 28, 56 and 90 days age, respectively. It may be observed that as reported in literature, the strength reduction is due to the expansive detrimental effects of Sulphate present within powdered gypsum wallboards [18–21]. Controlled concrete of grade M30 was designed for aimed strength of 38.25 MPa at 28 days age and the obtained values are matching in close range. This is due to the absence of powdered gypsum wallboards. Also the values of strength of controlled concrete at later ages are increased marginally due to the absence of GGBS—a mineral admixture possessing pozzolanic property.

Figure 3 illustrates the compressive strength variation for M1 to M5 mixes. At the age of 7 and 28 days it can be seen that the early strength gain is minimizing with the increment in the cement replacement. As the cement is replaced with the mineral admixtures (GGBS) which give rise to the later age strength due to onset of Pozzolanic activity normally after 28 days age, the 28 days strength is lesser for the cement replaced mixes. However, at the age of 56 and 90 days it is witnessed

Table 3 Controlled concrete—compressive strength results

Mix ID	Compressive strength (MPa)			
	7 days	28 days	56 days	90 days
Controlled concrete	22.34	38.70	39.86	42.68

Fig. 3 Sustainable concretes—compressive strength results



that the strength gain is increasing with the increment in the cement replacement. At later ages, Pozzolanic activity of GGBS has contributed to strength gain. The mixes with ID M2 and M4 have gained considerable later age strength higher than the other mixes.

3.1.2 Split Tensile Strength

Figure 4 illustrates the 56 and 90 days age splitting strength values of the mixes, which is found to be reducing with the rise in the partial cement replacement content. However, for M4 mix (20% gypsum powder, 40% GGBS) it is observed that there is slight improvement in tensile strength which obtained a value of 2.59 and 2.63 MPa higher than that for M3 mix value of 2.52 and 2.59 MPa, at 56 and 90 days age, respectively. Table 4, illustrates the split tensile strength values for controlled concrete. About 84.53–93.88% and 88.25–97.15% of the tensile strength

Fig. 4 Sustainable concretes—split tensile strength results

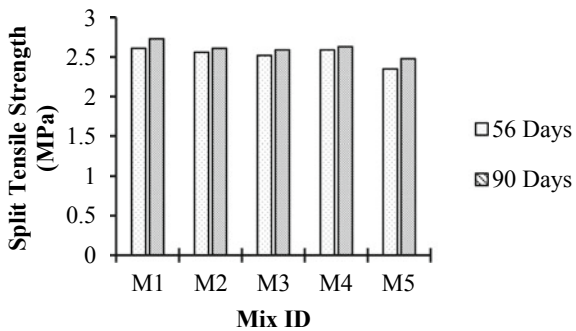


Table 4 Controlled concrete—split tensile strength results

Mix ID	Split tensile strength (MPa)	
	56 days	90 days
Controlled concrete	2.78	2.81

for controlled concrete were obtained in M5-M1 blends at 56 and 90 days age, respectively. The reduction in tensile strength is due to the detrimental effects of Sulphate present in powdered gypsum wallboards [18–21].

3.1.3 Flexural Strength

The flexural strength value for controlled concrete at 28 days age was found to be 5.3 MPa. The flexural strength of the mixes M1-M5 is reducing with the escalation in the cement replacement. The flexural strength values at 28 days age, obtained for the mix M1 is 5.12 MPa, M2 is 4.83 MPa, M3 is 3.96 MPa, M4 is 3.13 MPa and M5 is 2.05 MPa. About 38.6–96.6% of the flexural strength for controlled concrete was obtained in M5-M1 mixes at 28 days age, respectively. The decrement in flexural strength is because of the detrimental effects of Sulphate present in powdered gypsum wallboards [18–21].

3.2 Durability Properties

3.2.1 Strength Loss—Acid Exposure

The compressive strength values of the mixes M1-M5 were reduced when exposed to the Sulphuric acid. The mix M1 obtained strength value of 27.75 MPa before immersion into acid solution, and obtained reduced strength value of 25.77 MPa after immersion. Similarly mix M2 obtained reduced strength value from 21.73 to 19.93 MPa, mix M3 obtained reduced strength value from 19.19 to 14.48 MPa, mix M4 obtained reduced strength value from 20.98 to 19.90 MPa and mix M5 obtained reduced strength value from 17.87 to 17.06 MPa. It may be observed that the increment in cement replacement contents come up with better acid resistance results (in terms of measured strength loss). The compressive strength values of the 56 days cured specimens decreased when it is exposed to 1% sulphuric acid for 30 days.

3.2.2 Weight Loss—Acid Exposure

The weight of the specimen was reduced when exposed to the Sulphuric acid solution for 30 days period. M1 specimens reported weight loss from 7900 to 7895gms, M2 specimens reported weight loss from 7895 to 7891gms, M3 specimens reported weight loss from 7830 to 7826gms, M4 specimens reported weight loss from 7785 to 7780gms and M5 specimens reported weight loss from 7855 to 7850gms. Due to the fact that there was no major weight loss in the samples, the weight change in every 5 days period is not reported in this paper. The above strength and weight loss

values illustrates that the mixes with higher cement replacement (GGBS + Gypsum wallboard) possess better durability than the conventional concrete mixes.

3.2.3 Strength Loss—Sulphate Exposure

The compressive strength values of the sustainable mixes M1-M5 were reduced when exposed to Sodium Sulphate solution. The mix M1 obtained strength value of 27.75 MPa before immersion into Sodium Sulphate solution, and obtained reduced strength value of 24.31 MPa after immersion. Similarly mix M2 obtained reduced strength value from 21.73 to 18.62 MPa, mix M3 obtained reduced strength value from 19.19 to 15.15 MPa, mix M4 obtained reduced strength value from 20.98 to 19.95 MPa and mix M5 obtained reduced strength value from 17.87 to 15.67 MPa. It may be observed that the sulphate resistance (in terms of measured strength loss) increased with the rise in the cement substitute contents. The compressive strength values of the 56 days cured specimen decreased when it is exposed to 1% Sulphuric acid for 30 days.

3.2.4 Weight Loss—Sulphate Exposure

The weight of the specimen was reduced when exposed to the Sodium Sulphate solution for 30 days period. M1 specimens reported weight loss from 7985 to 7990gms, M2 specimens reported weight loss from 7865 to 7868gms, M3 specimens reported weight loss from 7890 to 7900gms, M4 specimens reported weight loss from 7785 to 7787gms and M5 specimens reported weight loss from 7855 to 7860gms. Due to the fact that there was no major weight loss/gain in the samples, the weight change in every 5 days period is not reported in this paper. Slight weight gain in the specimens was observed. This is due to the white crystal deposition on the specimen which is Sodium Sulphate. Figure 5 illustrates the white deposition on specimen.

3.2.5 Water Absorption

Table 5 illustrates the water absorption test results. The cement replacement within concrete had no significant effect on the water concentration values. The water concentration was in the range 5.8 to 6.2%. Results indicate that the density is inversely related to water absorption. The concrete mix specimen with less density obtained higher water absorption and those with higher density obtained lesser water absorption.

Fig. 5 Sulphate exposed specimen with white deposition



Table 5 Water absorption test results

Mix ID	Water absorption (%)	Density (kg/m ³)
Controlled concrete	5.9	2330.4
M1	6.1	2340.7
M2	6.13	2280
M3	5.8	2306.7
M4	6.2	2320
M5	6.18	2327.4

4 Conclusions

Marching toward sustainability goals for concrete industry, sustainable concrete mixes (M1-M5) and controlled concrete mix were cast and tested for their engineering properties. Within the binder content of sustainable mixes cement content was replaced by GGBS + Gypsum wallboard powder contents from 0–75%; and gypsum wallboard powder blend was changed from 0–25% and GGBS blend was changed from 0–75%. With the help of findings of this investigation, the following conclusions are arrived at:

1. About 60–75% of cement content in concrete can be substituted with the blends of GGBS and Gypsum wallboard powder, for specific applications with a margin for strength reduction.
2. As the quantity of cement replacement rises the water demand of the sustainable concrete mixes also raised owing to the finer particle size.

3. Two sustainable concrete mixes (M1 and M4) obtained their long-term strength in close range with that for controlled concrete. Hence, sustainable concrete may be adopted for such suitable applications.
4. The sustainable concrete mixes with higher quantities of GGBS and Gypsum powder resulted in better resistance to acid and Sulphate exposure.
5. Significant weight loss was not observed in sustainable concrete mixes either due to acid or Sulphate exposure.
6. The sustainable concrete mix with 20% Gypsum wallboard powder and 40% GGBS obtained satisfactory results in terms of later age strength. Whereas the sustainable concrete mix with highest replacement (25% Gypsum wallboard powder and 50% GGBS) performed with better durability.
7. This sustainable concrete if used in mass concreting works, huge amounts of discarded gypsum wallboards may be utilized and thus mitigation of H₂S gas emissions will be achieved along with carbon foot print mitigation due to large usage of GGBS and reduction in cement content.
8. LEED or GRIHA—Green rating points may be considered for adoption of this sustainable concrete mix in construction industry.

References

1. Záleská M, Pavlík Z, Čítek D, Jankovský O, Pavlíková M (2019) Eco-friendly concrete with scrap-tyre-rubber-based aggregate—Properties and thermal stability. *Constr Build Mater* 225:709–722
2. Jawad F, Adarsha CY, Raghavendra T, Udayashankar BC, Natarajan K (2019) Structural behavior of concrete beams and columns reinforced with waste plastic incorporated GFRP (WPGFRP) rebars. *J Build Eng* 23:172–184
3. Gurunandan M, Phalgun M, Raghavendra T, Udayashankar BC (2019) Mechanical and damping properties of rubberized concrete containing polyester fibers. *J Mater Civ Eng* 31:04018395
4. Eshwari SK, Chandrashekar GJ, Maaz A, Mohith N, Manjunath TN, Raghavendra T (2017) Experimental studies on effects of steel studs in composite slabs. In: *International conference sustainable infrastructure 2017*. American Society of Civil Engineers, pp 213–224
5. Ramesh CP, Vageesh HP, Raghavendra T, Udayashankar BC, Shashishankar A (2019) Self compacting concrete containing large volumes of class C flyash and processed slag sand for carbon foot print mitigation. *Int J Eng Res Technol* 12:636–641
6. Ramesh CP, Vageesh HP, Raghavendra T, Udayashankar BC, Shashishankar A (2018) Proportioning of CLSM containing class C Fly ash, GGBS, quarry dust and processed slag sand. In: Ameen H, Sorour T (eds) *Sustainable issues environment terotechnology*. Springer, Cham, pp 76–86
7. Ramesh CP, Vageesh HP, Raghavendra T, Udayashankar BC, Shashishankar A, Road M (2019) High volume class C fly ash containing self compacting concrete for sustainable development. *Int J Civ Eng Technol* 10:1740–1752
8. Vageesh HP, Ramesh CP, Raghavendra T, Udayashankar BC, Shashishankar A (2018) Engineering properties of self-compacting concrete containing class C Fly ash and processed slag sand. In: Rodrigues H, Elnashai A (eds) *Advances challenges structure engineering*. Springer, Cham, pp 219–229

9. Raghavendra T, Udayashankar BC (2014) Flow and strength characteristics of CLSM using ground granulated blast furnace slag. *J Mater Civ Eng* 26:04014050
10. Raghavendra T, Sunil M, Udayashankar BC (2016) Controlled low-strength materials using bagasse ash and fly ash. *ACI Mater J* 113:447–457
11. Chandrashekara A, Palankar N, Durga Prashanth L, Mithun BM, Ravi Shankar AU (2019) A study on elastic deformation behavior of steel fiber-reinforced concrete for pavements. *J Inst Eng Ser A* 100:215–224
12. Sormunen P, Kärki T (2019) Compression molded thermoplastic composites entirely made of recycled materials. *Sustainable*. <https://doi.org/10.3390/su11030631>
13. Yamashita M, Tanaka H, Sakai E, Tsuchiya K (2019) Mineralogical study of high SO₃ clinker produced using waste gypsum board in a cement kiln. *Constr Build Mater* 217:507–517
14. Xu Q, Powell J, Jain P, Townsend T (2014) Modeling of H₂S migration through landfill cover materials. *J Hazard Mater* 264:254–260
15. Sun W, Barlaz MA (2015) Measurement of chemical leaching potential of sulfate from landfill disposed sulfate containing wastes. *Waste Manag* 36:191–196
16. Kijjanapanich P, Do AT, Annachhatre AP, Esposito G, Yeh DH, Lens PNL (2014) Biological sulfate removal from construction and demolition debris leachate: effect of bioreactor configuration. *J Hazard Mater* 269:38–44
17. Juenger MCG, Siddique R (2015) Recent advances in understanding the role of supplementary cementitious materials in concrete. *Cem Concr Res* 78:71–80
18. Naik TR, Kumar R, Chun Y, Kraus RN (2010) Utilization of Powdered gypsum-wallboard in concrete. In: *Proceeding international conference sustainable construct material technology*
19. Raghavendra T, Siddanagouda YH, Jawad F, Adarsha CY, Udayashankar BC (2018) Mitigation of H₂S emissions by recycling discarded gypsum wall boards in CLSM. *Glob J Res Eng E Civ Struct Eng* 18:15–27
20. Raghavendra T, Udayashankar BC (2015) Engineering properties of controlled low strength materials using flyash and waste gypsum wall boards. *Constr Build Mater* 101(Part 1):548–557
21. Raghavendra T, Siddanagouda YH, Jawad F, Adarsha CY, Udayashankar BC (2016) Performance of ternary binder blend containing cement, waste gypsum wall boards and blast furnace slag in CLSM. *Procedia Eng* 145:104–111
22. Kaliyavaradhan SK, Ling T-CC, Guo M-ZZ, Mo KH (2019) Waste resources recycling in controlled low-strength material (CLSM): A critical review on plastic properties. *J Environ Manage* 241:383–396
23. Raghavendra T, Udayashankar BC, Lokeshwari M, Vikas M, Reddy NA (2018) Effect of water content on relative flow area and hence predicted flow values of controlled low strength materials. In: Singh UP, Babu GLS (eds) *Urban. Challenges emerging economic resil. sustainable infrastructure american society of civil engineers*, pp 184–195

Mechanical Properties of an Industrial Waste Concrete with Self-compacting Geopolymerization



Endow Mazumder, Nilanjan Tarafder, and L. V. M. Prasad

Abstract The world is moving toward a sustainable state and in search of replacement for one of the most consumable products, that is portland cement, we are slowly shifting toward geopolymerized concrete which is a very potential alternative of convention portland cement. The principal purpose of this research is reporting the outcome of the investigational result of self-compacting geopolymer concrete (SCGPC) which has been prepared at room temperature and eventually curing is done at the same condition. In order to prepare the SCGPC, a combination of furnace slag (FS) and Fly Ash which is of grade F, ranging from 0 to 100% with a gap of 10% of binder substance. Geopolymer polymerization is aided by Sodium Silicate and Hydroxide (Na_2SiO_3 & NaOH) which have an alkaline nature and perform the function of an activating agent. Samples were subjected to experiments by wavering the NaOH intensity from 8–16 M with 2 M intervals for finding out the optimum NaOH concentration for the geopolymer mixes for maximum strength. As per European Federation of the National Association Representing for Concrete also known as E.F.N.A.R.C specifications, the features of fresh SCGPC such as workability were checked by L-box, test for slump flow, V-funnel, J-ring tests. After testing at the ages 7, 14, and 28, the mechanical characteristics of SCGPC were examined and the findings were reviewed.

Keyword Geopolymer · Self Compacting Concrete · Fly Ash · GGBS

1 Introduction

Development in India is taking place at a very high pace in order to meet urban development demand. The construction industry grew very quickly and hence proportionally the demand for cement concrete increased. As manufacturing of cement increases, the natural rock deposit reduces by a significant amount. It's also a matter of concern that to produce 1 ton of Portland cement the factories emit a huge amount

E. Mazumder (✉) · N. Tarafder · L. V. M. Prasad
NIT Silchar, Silchar, India
e-mail: endow.m@hotmail.com

of CO₂ into the atmosphere, which is nearly equals to 1 ton [1, 2]. In the field of construction, efforts were made to reduce the emission of CO₂ with increasing concerns regarding environmental issues attributed to global warming. Hence if we look forward to creating a sustainable environment, to control air pollution, and to limit the usage of valuable natural resources, an alternate binding agent instead of Portland cement should be used [3].

The Slag produced during the production of steel is a waste material [4, 5]. Worldwide a huge quantity of slag is generated on a routine basis and the same is need to be disposed of properly. Also, the ashes produced from the thermal power plants and other factories cannot be dumped in any random ditches as it may show health as well as environmental hazards. The above mentioned waste materials have pozzolanic attributes so they were used from a long time as additional material in concrete to increase the working capacity of concrete [6, 7]. Davidovits first referred the inorganic binders produced by the reaction of Silica, Alumina, and activating liquid (alkaline in nature) as the 'Geopolymers' [8]. Strength gain process of geopolymer as well as the polymerization process depends upon number of factors, such as, alkaline solution type, its concentration, also temperature and condition under which concrete is cured. Presently, NaOH, Na₂SiO₃ are the most commonly used activators [9–12]. The structure and strength developing process of geopolymer during geopolymerization is affected mainly by NaOH solution, concentrated NaOH ensures that solid particles are connected properly in the aqueous also in the final structures of the geopolymer concrete systems [13]. Early studies and usage of modified binder material prepared using alkalinization has been used since beginning of the twentieth century with revolutionary work from German researcher named Kuhl, which concentrated on glass-based slags and the activation is done by alkaline resources [14]. It has been discovered that sodium alumino-silicate (N-A-S-H) gels are the hydrated products of Fly Ash/Metakeoline (MK). C-S H gels formed are the products of hydration from the FS activation process [15, 16]. As an alumino-silicate source material for the majority of research in geo-polymer concrete, Fly Ash is generally used. Geopolymerization process for Fly Ash needs high temperatures, curing at higher temperature enhances mechanical characteristics of the geopolymer concrete but on the other hand the process consumes a lot of energy. [17, 18]. To eliminate higher temperature curing for better compressive strength, Fly Ash is blended with FS from 10–100% in this research. The use of FS speeds up the geopolymerization process as well as the setting time and decreases the time required for handling and compaction [19, 20]. In order to ensure excellent compaction, vibration of standard geopolymer concrete needs to be done properly. There is a better alternative to normal geopolymer concrete, which is self-compacting geopolymer concrete (SCGPC), it can fill every extent of the formwork by its own weight. The benefits of SCGPC include convenient concrete filling in small and limited segments, enriched compaction, better concrete-reinforcement bond-strength, little maintenance, fast rate of erection, enhanced quality of construction also reduced complete construction cost [21, 22]. For developing SCGPC, compaction is not required at all also Portland cement is totally discarded. It is a field of very limited investigations, very few studies have been done on the same. The present analysis aims to explore the

outcome of full Portland cement replacement with FS and thermal plant waste ash (Fly Ash). The following work investigates the behavior and mechanical characteristics of ordinary geopolymer concrete and self-compacting geopolymer concrete during room curing by varying molarity of sodium hydroxide which acts as an activator for geopolymerization process.

2 Material Used and Sample Preparation

2.1 Materials

Waste collected from thermal plant, which is commonly known as Fly Ash and Granulated Blast Furnace Slag (FS) are two of few mineral admixtures referred in IS 456: 2000 which are easily available from thermal power plant and iron–steel industry respectively. Both are powdery fine material, have high specific surface area (SSA) and rich in silica, calcium oxide, alumina, ferric oxide etc. similar to the conventional Portland cement. FS, Fly Ash (chemical compositional property is reported in Table 1) which is used in this experiment were collected from commercial supplier of Chennai region in India, which are used as alumino-silicate material in this investigation. As activating material (Alkaline in nature), sodium hydroxide solution (NaOH) and liquid Sodium Silicate (Na_2SiO_3) was used, both are procured from Chennai-based commercial supplier. Pellets of NaOH (97–98% pure) were dissolved in potable water to make this NaOH solution (8–16 molarity concentration), then kept for 24 h in ambient temperature conditions. After that, NaOH (sodium hydroxide) and Na_2SiO_3 (sodium silicate) were mixed together to prepare a solution. Resulting solution was stored for 24 h at ambient temperature condition, and required additional water was added before the solution was combined with the dry ingredients. (FS, Fly Ash, sand, and stone). Naturally available sand in compliance with zone III as mentioned in IS 383 1970 [23]. For coarse aggregate 20 mm under aggregates were used which are well graded. To attain good workability of the fresh concrete, polycarboxylic ether-based superplasticizer is used which is of make Sika (Viscocrete 3430).

A few prior research on geopolymer concrete curing at ambient temperature were used to produce the mixtures [24, 25]. NaOH/ Na_2SiO_3 ratio in SCGPC is maintained at 1 throughout the research. In order to examine the effects of mixing effect of Fly Ash and FS (at intervals of 10% by weight), mixtures were made. SCGPC were casted with the mix proportions derived to find the strength parameter, also for the

Table 1 Chemical properties of FS and fly ash

Content	SiO_2	Al_2O_3	Fe_2O_3	CaO	MgO	SO_3	Na_2O
FS	33.8	14.96	0.61	38.92	9.23	0.395	0.65
Fly ash	52.75	33.67	5.86	1.84	1.93	0.033	1.31

Table 2 Proportion for preparing SCGPC (kg/m³)

Mix ID	Specimen	Fly Ash	FS	Na ₂ SiO ₃	NaOH	Fine Agg	Coarse Agg	Extra Water	SP (%)
SCGC1	F100G0	485	0	85	85	1065	760	24.50	6
SCGC2	F90G10	436.5	48.5	85	85	1065	760	24.50	6
SCGC3	F80G20	388	97	85	85	1065	760	24.50	6
SCGC4	F70G30	339.5	145.5	85	85	1065	760	24.50	6
SCGC5	F60G40	291	194	85	85	1065	760	24.50	6
SCGC6	F50G50	242.5	242.5	85	85	1065	760	24.50	6
SCGC7	F40G60	194	291	85	85	1065	760	24.50	6
SCGC8	F30G70	145.5	339.5	85	85	1065	760	24.50	6
SCGC9	F20G80	97	388	85	85	1065	760	24.50	6
SCGC10	F10G90	48.5	436.5	85	85	1065	760	24.50	6
SCGC11	F0G100	0	485	85	85	1065	760	24.50	6

comparison of obtained results. As no standard code is available for mix design of SCGPC, the EFNARC specifications [22] were taken in to account for preparing the mix design. Only one technique can explain all of the workability qualities, which are passing-ability, filling ability, and segregation resistance, thus more than one test methods are used to test each design to attain the necessary workability requirements as accordance with EFNARC. After a number of tests, the proportions used to prepare SCGPC were finalized and are shown in Table 2.

For all future mixes, the characteristics of SCGPC were assessed using slump flow tests (H-flow), T₅₀ slump flow tests, V-funnel tests, L-Box tests, and J-ring techniques. In this investigation total dry powder amount was finalized as 485 kg/m³. For all specimens, the additional water to geopolymer solid ratio by weight was held at 24.5%. To achieve the necessary workability in accordance with the EFNARC requirements [22], a dosage of 6% superplasticizer by mass of binding materials was considered. A sum of eleven mixes was casted, and all the mixes were cured under ambient condition of temperature.

2.2 Preparation and Casting of Specimens for Testing

Prior to preparing fresh SCGPC, approximately for 2.5 min dry ingredients like Fly Ash, Sand, and Stone are batched in the machine. A mixture of activator solution, super plasticizer, and the dry mix was moistened with water after it was thoroughly mixed. This is followed by a 3 min thorough mixing of all ingredients. A fresh SCGPC is subjected to a series of tests to assess its workability conditions, including passing ability, filling ability, and segregation resistance, according to EFNARC norms [22].

Table 3 has been prepared for showing the method of testing and their limiting

Table 3 Workability results obtained from different samples

Mix	H-flow	T ₅₀ slump flow (s)	V-funnel (s)	L-box	V-funnel T ₅ min (s)
SCGC1	715	4.3	10	0.9	12.5
SCGC2	714.2	4.2	10	0.9	12.47
SCGC3	712.85	4.2	9.5	0.915	12.38
SCGC4	712.3	4.2	9.5	0.918	12.24
SCGC5	710.55	4.1	9.5	0.923	11.9
SCGC6	708.9	4.1	9.2	0.935	11.66
SCGC7	707.2	4.1	9	0.948	11.45
SCGC8	705.4	4	8.6	0.952	11.4
SCGC9	702.45	3.9	8.4	0.955	11.25
SCGC10	700.2	3.9	8.2	0.96	10.9
SCGC11	698.5	3.8	8.1	0.96	10.8

values which were put forward by EFNARC. SCGPC's flowing performance in terms of concrete spreading diameter was assessed using a slump flow test. The lowest value for slump flow test limits is 650 mm, while the maximum value is 800 mm. Amount of time desirable to achieve a diameter of 50 cm of slump is also noted and Slump-T₅₀ cm is calculated. Slump flow assessment finds out the concrete's capacity to settle by its self-weight against the surface friction with no restraint from external side. SCGPC's segregation resistance is measured by the V-Funnel test when pass through the narrow channel. The cone shaped in opposite direction limits the concrete flow and the duration of time indicates blocking tendency. The time required to empty the V- shaped box of concrete is estimated, as is the viscosity of the concrete. The lowest time restriction is 6 s, while the maximum time limit is 12 s as per EFNARC specifications. The passing ability of SCGPC is determined by L-Box test. The concrete flows through the barrier in the vertical section of the box to the flat portion of the box at the end. A ratio between the heights of SCGPC at the conclusion of a horizontal segment and the height of SCGPC at the start of the horizontal segment was used to determine the passing ability of concrete. Concrete flow is said to be very good if the said ratio is nearly equal to unity. As per EFNARC specifications limits of L-Box ratio are from 0.8 to 1.0. After doing the tests on workability for SCGPC, the fresh SCGPC was poured in to the concrete moulds, cylindrical mould, and prism mould. SCGPC specimens after filling the moulds, moulds are kept without any external vibration. A 24 h period is required for the specimens to cure after they had been casted. After 24 h, the specimens were taken out of the concrete moulds and placed at room temperature for evaluation after 7, 14, and 28 days.

Table 4 Compressive strength of self compacting geopolymer concrete

Mix	Content	Compressive strength (MPa)		
		7 days	14 days	28 days
SCGC1	F100G0	3.97	7.89	12.14
SCGC2	F90G10	12.92	19.08	20.25
SCGC3	F80G20	18.96	25.81	26.72
SCGC4	F70G30	26.31	32.88	36.26
SCGC5	F60G40	30.09	40.11	44.21
SCGC6	F50G50	35.83	48.02	50.69
SCGC7	F40G60	41.23	52.02	55.14
SCGC8	F30G70	46.88	56.32	60.71
SCGC9	F20G80	48.63	59.1	63
SCGC10	F10G90	50.32	62.85	66.87
SCGC11	F0G100	57.33	66.56	69.33

3 Experimental Work and Their Discussions

3.1 Compressive Strength

The SCGPC specimens with minimal or little Fly Ash show great strength at a young age, according to the evaluation. These mixtures reached 85 and 95% of their 28 day strength after 7 and 14 days, respectively. As the concentration of NaOH increases, so does the compressive strength, from 8 to 14 M, after which the strength begins to slope down, SCGPC specimens with 14 M NaOH concentration show maximum strength. Lower NaOH level results in slow polymerization process which also shows lower structural strength (Table 4).

3.2 Flexural Strength

Concrete's resistance to bending is a measure of its flexural strength. It is necessary to indicate the test methods opted in design process for calculating flexural strength. The modulus of rupture, commonly known as flexural strength, of SCGPC specimens was determined, also are shown in Table 5. It is noticed that when self-compacting geopolymer was used the flexural strength increases by about 7.6% that of plain geopolymer concrete for specimen with 100% FS content at 28 days. Compressive strength improves as FS content in the mix grows, while workability diminishes as FS content increases.

Table 5 Flexural strength of self compacting geopolymer concrete

Mix	Content	Flexural strength (MPa)		
		7 days	14 days	28 days
SCGC1	F100G0	0.39	0.69	0.80
SCGC2	F90G10	1.23	1.68	1.81
SCGC3	F80G20	1.83	1.98	2.12
SCGC4	F70G30	2.58	2.29	2.59
SCGC5	F60G40	2.53	2.72	2.83
SCGC6	F50G50	2.81	3.04	3.21
SCGC7	F40G60	3.32	3.45	3.68
SCGC8	F30G70	4.02	4.13	4.41
SCGC9	F20G80	4.81	5.16	5.41
SCGC10	F10G90	5.46	5.92	6.19
SCGC11	F0G100	6.4	6.60	6.85

3.3 Split Tensile Strength

The results of split tensile strength testing performed as per IS 5816: 1999 are shown in Table 6. Testing for split-tensile strength at different ages for different mixtures with varying FS to Fly Ash concentrations is shown in the following table. As a result of the delayed geopolymerization process, SCGC1 had the least amount of split tensile strength of 0.31 MPa at room temperature.

Table 6 Split tensile strength of self compacting geopolymer concrete

Mix	Content	Split tensile strength (MPa)		
		7 days	14 days	28 days
SCGC1	F100G0	0.31	0.44	0.51
SCGC2	F90G10	0.98	1.05	1.09
SCGC3	F80G20	1.26	1.33	1.4
SCGC4	F70G30	1.75	1.81	1.92
SCGC5	F60G40	2.09	2.16	2.21
SCGC6	F50G50	2.38	2.49	2.55
SCGC7	F40G60	2.66	2.82	2.9
SCGC8	F30G70	3.08	3.24	3.38
SCGC9	F20G80	3.34	3.6	3.79
SCGC10	F10G90	3.61	3.94	4.11
SCGC11	F0G100	4.05	4.39	4.57

4 Conclusion

Total 11 number of FS and Fly Ash Geopolymer Concrete samples were tested at the laboratory to determine their properties such as flexural strength, split tensile strength, and compressive strength and have been reported. Listed below are some key results from this study.

- i. As the reaction between CaO and water produces large amount of heat, and the consequent acceleration of the geopolymerization process, hence the mixtures with 100% FS content have very high early compressive strength.
- ii. A geopolymer concrete containing FS-Fly Ash has a high capacity to replace ordinary concrete. By 7 days, the strength of geopolymer concrete based on FS-Fly Ash is roughly 80% of what it is at 28 days. Concrete mixes that use just FS as a binder, on the other hand, are less workable.
- iii. The workability of blended geopolymer concrete increases when Fly Ash is used with FS-based geopolymer, although strength is somewhat reduced. For mixtures with elevated Fly Ash concentration, the strength loss is much more pronounced. Both early and ultimate state of strength has a significant impact by the change.
- iv. At ambient curing temperature, mixing with 100% FA does not produce excellent results. In the presence of alumino silicate precursor, due to slow dissolution of same, ambient curing results in reduced strength, which may produce better outcomes when heat curing is done. Other geopolymer concrete mixtures (combined with FS) outperformed the pure Fly-Ash-based geopolymer concrete.
- v. NaOH at greater concentrations (up-to 14 M in this study) increases the strength of SCGPC mixtures. An increase in NaOH content beyond, reduces the compressive strength suddenly.
- vi. SCGPC mixtures with 100% FS content have the best compressive, flexural, and split tensile strength, but their workability plummets. So, this combination having an equal amount of FS and Fly Ash is recommended for any task since the same offers higher than adequate results for every members, along with aids in the disposal of both the materials in an environmentally friendly manner.

References

1. Statista Inc. (2018) Global cement production from 1990 to 2030. New York, Statista, Inc.
2. Mehta PK (2001) Reducing the environmental impact of concrete. *ACI Concr Int* 23(10):61–66
3. Wang W-C, Chen B-T, Wang H-Y, Chou H-C (2016) A study of the engineering properties of alkali-activated waste glass material (AAWGM). *Constr Build Mater* 112:962–969
4. Lin W.-L. (2009) Study on engineering properties of alkali-activated slag pastes (master's thesis), National Taiwan University of Science and Technology

5. Sáez-de-Guinoa Vilaplana A, Ferreira VJ, López-Sabirón AM, Aranda-Usón A, Lausín-González C, Berganza-Conde C, Ferreira G (2015) Utilization of LFS from a steelwork for laboratory scale production of Portland cement. *Constr Build Mater* 94:837–843
6. Sathawane SH, Vairagade VS, Kene KS (2013) Combine effect of rice husk ash and flyash on concrete by 30% cement replacement. *Procedia Eng* 51:35e44
7. Memon SA, Shaikh MA, Akbar H (2011) Utilization of rice husk ash as viscositymodifying agent in self-compacting concrete. *Construct Build Mater* 25:1044e8
8. Davidovits J (199) Chemistry of geopolymeric systems, terminology. In: Proceedings of geopolymer international conference. Saint-Quentin, France, 1999 Jun 30 and Jul 1–2
9. Lin D.-F. (2014) The curing conditions on the properties of geopolymer produced by the calcined oil contaminated clay. In: 2014 international conference on sustainable development and disaster prevention in civil engineering
10. Wang KT, He Y, Song XL, Cui XM (2015) Effects of the metakaolin-based geopolymer on high-temperature performances of geopolymer/PVC composite materials. *Appl Clay Sci* 114:586–592
11. Duan P, Yan C, Zhou W, Luo W (2016) Fresh properties, mechanical strength and microstructure of fly ash geopolymer paste reinforced with saw dust. *Constr Build Mater* 111:600–610
12. Wang W-C, Wang H-Y, Lo M-H (2015) The fresh and engineering properties of alkali activated slag as a function of fly ash replacement and alkali concentration. *Constr Build Mater* 84:224–229
13. Kürklü G (2016) The effect of high temperature on the design of blast furnaceslag and coarse fly ash-based geopolymer mortar. *Compos B* 92:9–18
14. Provis J (2014) Introduction and scope. In: Provis JL, van Deventer JSJ (eds) Alkali activated materials: state of the art report, RILEM TC 224-AAM. Springer, pp 1–9
15. Singh B, Ishwarya G, Gupta M, Bhattacharyya SK (2015) Geopolymer concrete: a review of some recent developments 85(15):78–90
16. Duxson P, Fernández-Jiménez A, Provis JL, Lukey GC, Palomo A, van Deventer JSJ (2007) Geopolymer technology: the current state of the art. *J Mater Sci* 42:2917–2933
17. Rangan BV, Hardjito D, Wallah SE, Sumajouw DM (2005) Studies on fly ash-based geopolymer concrete. In: Davidovits J (ed) Geopolymer: green chemistry and sustainable development solutions. Geopolymer Institute, Saint-Quentin, France, pp 133–137
18. Chindapasirt P, Chareerat T, Sirivivatnanon V (2007) Workability and strength of coarse high calcium fly ash geopolymer. *Cement Concr Compos* 29:224–229
19. Saha S, Rajasekaran C (2017) Enhancement of the properties of fly ash based geopolymer paste by incorporating ground granulated blast furnace slag. *Construct Build Mater* 146:615e20
20. Hadi MNS, Farhan NA, Sheikh MN (2017) Design of geopolymer concrete with GGBFS at ambient curing condition using Taguchi method. *Construct Build Mater* 140:424e31
21. Boukendakdji O, Kadri EH, Kenai S (2012) Effects of granulated blast furnace slag and superplasticizer type on the fresh properties and compressive strength of self-compacting concrete. *Cement Concr Compos* 34:583e90
22. EFNARC (2002) Specification and guidelines for self-compacting concrete. European Federation of Specialist Construction Chemicals and Concrete Systems, Surrey, UK
23. Nath P, Sarker PK (2012) geopolymer concrete for ambient curing condition. In: Proceedings of Australasian structural engineering conference. Perth, Australia
24. Deb PS, Nath P, Sarker PK (2013) Properties of fly ash and slag blended geopolymer concrete cured at ambient temperature. In: 7th international structural engineering and construction conference. Honolulu, USA
25. Alonso S, Palomo A (2001) Alkaline activation of metakaolin and calcium hydroxide mixtures: influence of temperature, activator concentration and solids ratio. *Mater Lett* 47:55–62

Workers Safety at Indian Construction Sites—A Survey



M. V. Krishna Rao, G. Tarun, and V. Hari Leela

Abstract The construction industry is known as one of the unpredictable and hazardous sectors in which the workers are more susceptible to construction accidents. Despite many efforts put in to enhance construction site safety, construction accounts for quite disproportionate number of occupational injuries and fatalities. Urbanized nations attempt to guarantee stringent lawful enforcement of construction site safety in the industry by implementing various safety management systems. Conversely, occupational safety in the industry is found to be quite poor in a developing country like India due to lack of safety regulations and standards, data on safety at construction sites, safety training, safety awareness, and organized safety management systems. Although much improvement is achieved in construction safety, India is still lagging behind many other countries in this regard. This study focuses on the prevalent safety management practices in the Indian industry and the construction sites in the twin cities of Hyderabad and Secunderabad (TS, India), a hub of Infrastructure development in India, has been chosen as the area of study. The data collection was done through an industry survey by means of questionnaire and interviews with construction workers. The results revealed that the safety level of construction firms in the study area and also other factors are all the reason for non-safety performance of firms. A few recommendations have been made for safer construction, as an outcome of the study.

Keywords Construction industry · Accidents · Worker's safety · Questionnaire survey · Safety management systems

M. V. Krishna Rao (✉) · G. Tarun
Department of Civil Engineering, Chaitanya Bharathi Institute of Technology (A), Hyderabad,
India
e-mail: mvkrishnarao_civil@cbit.ac.in

V. Hari Leela
Faculty of Management Science, Department of M & H, Mahatma Gandhi Institute of Technology
(A), Hyderabad, India
e-mail: vharileela_ms@mgit.ac.in

1 Introduction

The construction industry entails high-risk activities that can result in a variety of human catastrophes, as well as a loss of worker interest, construction disruption, delays, and negative effects on cost, productivity, and reputation of firm [1]. Workers are likely to meet with accidents on construction sites due to two key aspects of the industry: decentralization and mobility. The construction sector has been unable to promote safety management and working conditions that increase safety measures due to denationalization and worker mobility. The reasons for very high accident rate in construction industry could be (i) more relevance of human factors to safety performance unlike other industries, (ii) construction is a complex activity requiring different skilled workers for the completion of a building project, and (iii) most construction workers lack basic education, proper safety and trade skill training pertaining to construction field. Consequently, the construction industry has a poor safety record and the accidents occur due to lack of proper management of workers who lack safety awareness, cut corners to complete the given task and perform unsafe behaviour at work.

In construction sector, the chances of a fatality and risk of major injury are respectively five and two and a half times more as compared to manufacturing industry. Construction in developing countries like India is more labour-intensive in comparison to the developed nations. The construction labour in India is estimated at 7.5% of the global work force which is contributing to 16.4% of fatal occupational accidents, comprising of around 11% of occupational injuries and 20% of deaths globally. Mainly, accidents occur due to unsafe work-site conditions such as missing guardrails, defective tools, hazardous conditions, excessive noise, and lack of sufficient light and they also take place as a result of unsafe behaviour of involvement in smoking at workplace, improper use of equipment, working without safety appliances and protective equipment [1]. The reason for this scenario is failure of management to act in respect of training, maintenance, instruction, and safe systems at workplace. In this scenario, it is an imperative need that all the parties involved in construction works play their individual roles to ensure safe and healthy working environment, failing which the image of construction industry will be damaged. Therefore, construction firms need to improve their safety culture to achieve better safety performance which in turn contributes to minimization of costs to the business, enhanced product quality and worker loyalty towards organization, besides creating a productive, efficient, and a highly profitable company.

2 Review of Literature

A comprehensive literature survey was carried out on worker safety on construction sites and is presented as follows:

Hinze and Raboud [2] highlighted the importance of owners and designers in ensuring a safe building process and also discussed the role of information technology (IT)-based solutions in ensuring site safety. Suazo et al. [3] evaluated the health and safety performance of different construction firms of Pakistan and found that the majority of the fatalities of individuals were due to falling from great heights, electrocution, getting caught between plants, machinery, confined spaces, and struck by an object or machinery. Everett and Frank [4] examined the total costs of accidents and injuries to the construction industry and observed that the total costs of accidents have escalated in the range of 7.9 to 15.0% of the total costs of non-residential new constructions. Anumba and Bishop [5] identified the need for integrating safety considerations with site layout and organization in the early stages of a project and also provided guidelines for integration to improve safety on construction sites. Abdelhamid and Everett [6] presented an accident root causes tracing model (ARCTM), which acknowledges the likely contribution of management and labour to the accident process in construction industry and helps in providing effective measures to prevent the accidents. Sawacha et al. [7] identified the critical factors affecting the successful implementation of construction safety programs in Saudi Arabia. Analytical Hierarchy Process (AHP) was employed to rank different criteria and Pareto principle to construct 7 important success criteria that help in attaining higher levels of safety. Lubega et al. [8], carried out a questionnaire survey, with Malaysian respondents, to ascertain the causes of construction-site accidents and revealed that accidents are caused due to dangerous methods, human error, unsafe equipment, job site circumstances, management, and distinctive nature of the industry. Wilson Jr. and Koehn [9] opined that site safety measures in construction projects differ from one another as each site has its own set of hazards. Larger construction projects are well-organized, whilst small- and medium-sized ones lack sufficient safety programs and supervision as per safety standards. Ho et al. [10] assess the effectiveness of the current site safety plans and contractors' safety performance from the feedback of selected site personnel on the execution of site safety plans. It was concluded that construction businesses consider occupational health and safety as vital requisites for all site activities. Suraji et al. [11] developed a construction industry accident causation model in accordance of which accidents are caused by ineffective construction planning (28.8%), ineffective construction control (16.6%), ineffective construction operation (88.0%), ineffective site condition (6.0%), and ineffective operative action (6.0%). Hughes and Ferret [12] reported that the common on-site accidents are falling from heights, cutting of limbs due to mishandling heavy equipment, objects falling from a height, electric shock from cables, caving in of excavations, and lifting of heavy tools and equipment. Worker fatigue, lack of discipline, carelessness, distractions, top management ignorance, lack of training, and poor communication were also cited as reasons for on-site accidents. Ali et al. [13] conducted a questionnaire survey, with site manager, site safety officer, contractor, and project manager, to determine the causes of accidents on construction sites and devised methods to enhance safety performance. The prime causes of accidents on construction sites were reported to be human element, poor site management, non-utilization of personal protective equipment, and the use of unsafe

equipment. Kumar and Bansal [14] discussed the hazards possible on construction sites, their causes, themes of accident prevention through design (PtD) and safety as a component of long-term sustainability. Authors also highlighted the importance of safety culture, climate and the role of owners and designers in mitigation of site hazards. Guha and Biswas [15] examined the safety status on building construction sites via surveys carried out in Kolkata, India. The safety aspects were compared amongst different construction sites and a cost–benefit analysis based on Monte Carlo’s simulation was adopted for investigating the economic forces that may hinder the proper implementation of safety rules. Selvam and Priyadarshini [16] explored several safety and control measures (SCM) of accidents in construction projects to decrease the occurrence of accidents and subsequent waste generation. Kanchana et al. [17] conducted a detailed review of literature to determine the causes of accidents, preventive measures, and to develop a safe work environment as well.

2.1 Research Significance

A comprehensive review of the literature has revealed that there is a shortage of necessary responsive systems and resources in addressing construction safety. Though safety has a direct relation with productivity and quality, employers undervalue personal safety and resort to contracting out large-scaled and prestigious works. Completion of high-quality work on specified time and within the budgeted cost, together with the safety of workers, requires careful attention. In spite of existing Indian safety codes and contractual obligations, the sites are found to be quite deficient in enforcing the requirements. Much less work is directed in this direction in the Indian context. Hence, this paper addresses the implementation of selected safety practices and safety performance in large, medium, and small construction firms /projects. Data was collected through a questionnaire survey by face-to-face interviews with workers at construction sites in the study area of twin cities of Hyderabad and Secunderabad, Telangana state, India. The responses obtained are analysed and discussed to draw conclusions and make suitable suggestions/recommendations.

3 Methodology

The methodology involved three phases including phase-1: literature review, phase-2: data collection and processing, and phase-3: conclusions. In this study, questionnaire required for the survey, to collect the primary data, was designed based on the necessary base knowledge acquired through literature review. The questionnaire consisting of 58 questions, which were perceived to be important from the safety point of view on the construction site and pertaining to 20 elements/criteria, is designed for primary data collection. The respondents were required to answer questions on a

6-point Likert scale of 1–6 (Unsatisfactory-1; Satisfactory-2; Moderate-3; Good-4; Very Good-5; and Excellent-6).

3.1 Questionnaire Design

This questionnaire is aimed at assessing and analysing the safety awareness levels of workers at work site, and to evaluate the required site-specific training needs provided for improvement in construction worker's ability. The questionnaire contents concentrate on the provision and use of personal protective equipment, communication, and instruction, workers' safety training, safety supervision, accident frequency, safe behaviour and safety enforcement, knowledge on regulations and work standard. A questionnaire with 58 questions, covering 20 criteria was designed to collect the response of construction workers who were selected randomly from 40 different construction firms/companies comprising of 10 large-, 15 medium- and 15 small-scale firms. Various sub-categories of safety criteria (20 in number) used in the questionnaire are as follows:

- i. Job Site Information: These criteria are about job site safety like posting warning posters, providing medical services, etc.
- ii. Dwelling and Sanitation: This category is about House Keeping and Sanitation like provision of adequate lighting, providing drinking water, etc.
- iii. Electrical Installations: this topic is about safety related to electrical installations like type of tag outboard installed, provision of adequate wiring, etc.
- iv. Hand Tools and Power Tools: This basis is about safety related to hand tools and power tools like maintenance of tools.
- v. Fall Protection: This standard is about fall protection safety like provision of guard rails, safety belts, barricades, etc.
- vi. Ladders: These measures concern with safety related to ladders like provision of handrail, securing ladders from slipping, etc.
- vii. Floors and Wall Openings: These criteria are about safety related to floor and wall openings like covering of floor openings, deck openings, etc.
- viii. Scaffolding: These criteria are about safety related to scaffolding like provision of proper site working platform, provision of proper access, etc.
- ix. Trenches Excavation and Shoring: These criteria are about safety related to trenches, excavation, and shoring like provision of excavation barricades, provision of access ladders, etc.
- x. Handling and Storage of Material: This category is about safety related to handling and storage of material like provision of clear passageways, usage of proper lifting methods, etc.
- xi. Welding and Cutting: This category is about safety related to welding and cutting like usage of shields and screens whilst working, usage of goggles, welding helmets, gloves, etc.

- xii. Heavy Equipment: This category is about safety related to heavy equipment like inspection and maintenance of records, operation of equipment by authorized person, etc.
- xiii. Motor Vehicles: This standard is about safety related to motor vehicles like proper maintenance, operation of vehicles by authorized persons, etc.
- xiv. General: These measures are about general safety like provision of assembly point, availability of safety personnel, etc.
- xv. Hoist Cranes and Derricks: These criteria are about safety related to hoist cranes and derricks like inspection of cables and sheaves, etc.
- xvi. Steel Erection: This category is about safety related to steel erection like usage of required PPE's, covering floor openings, etc.
- xvii. Concrete Construction: This standard is about safety related to concrete construction like protection of employees from cement dust, removing nails from the working area, etc.
- xviii. Personal Protective Equipment: This topic is about safety related to personal protective equipment like usage of safety glasses, hard hats, safety belts, dust respirators, etc.
- xix. Women Safety: This criterion is about the safety and treating of the female workers in the construction site.
- xx. Fire Prevention: This criterion is about fire prevention safety, i.e., posting no smoking signs where ever needed.

The final form of the questionnaire was distributed to workers in three different categories of construction companies, viz; Large, Medium, and small companies for data collection. The Large construction companies surveyed deal with the construction of offices, commercial buildings, and metro rail construction. Whilst the medium construction companies deal with private ventures and apartments and small construction companies build mainly housings and residential buildings. The construction companies to be surveyed were randomly selected based on the criterion of projects that were being constructed. The questionnaire was distributed to 200 workers out of which 80 responses i.e., 20, 30, and 30 responses were respectively received from large, medium, and small construction companies/firms/projects with a return rate of 40.0%. Then, the data collected from the respondents were analysed with the use of Statistical Package for the social sciences (SPSS) version 21.0. Finally, the findings of the study were concluded and certain suggestions/recommendations made for the improvement of worker safety on construction project sites.

4 Result Analysis and Discussion

The data collected, on the state of safety in large, medium, and small construction firms/ projects, through questionnaire survey were analysed and discussed in this section. The results obtained, from the analysis of the data collected through a questionnaire survey on the status of safety in large, medium, and small construction firms/

projects, are discussed to draw the conclusions. The safety of the worksite is assessed in this study, by taking into consideration the unsafe conditions existing at the worksite, regardless of whether they are large or medium, or small construction projects. Table 1 presents the safety levels (safety scores), average safety scores, variance, and standard deviation in cases of large, medium, and small projects/firms whilst Table 4 shows the similar results for the cumulative data obtained from merging of data pertaining to all three types of construction firms. Further, Tables 1 and 2 respectively present the results obtained including eigen values, average scores, and ranks of the sub-categories in respect of three construction companies/firms. The alphabets in rating column of Tables 1, 2, 3 and 4 indicate the level of safety performance based on score, viz: E-excellent, VG-very good, G-good, F-fair, and P-poor.

4.1 Evaluation of Worker Safety Status at Large Construction Firms/ Projects

From Table 1, it could be noticed that the average safety score in respect of large construction firms/projects has been higher and of the order 247.25. This could be due to the fact that most of the project sites surveyed were being constructed by established and large firms that apply their own safety codes and practices. Furthermore, the majority of these construction firms had a safety administration section as a critical component of overall structure. Apart from that, the values of variance and standard deviation obtained for the large construction firms have been very low, 190.28 and 13.81 respectively, which could be attributed for the reason that all firms that have been surveyed in this study have the almost same range of safety measures applied in their construction sites. Thus, in case of large construction projects, they showed a consistent level of safety. Table 3 represents the total variance, average safety scores, and rankings of the subcategories of the questionnaire. The highest safety score was obtained in large firms, to the 1st subcategory, i.e., Job Site information, with 4.725 score, and the least score was acquired by the 3rd subcategory, i.e., Electrical Installations, with 4.100 score.

4.2 Evaluation of Worker Safety Status at Medium Construction Firms/ Projects

Table 1 shows that the safety scores, in case of medium construction firms/projects, varied widely with a maximum safety score of 262 (Very good) and a minimum score of 98 (Poor). This scenario may be attributed to non-implementation of the standard safety code and neglect of the set rules and regulations meant for contractors. The average safety score was found to be 187.70. The fluctuation between the highest, average and lowest safety scores indicates that all those medium firms surveyed

Table 1 Safety score and rating of different types of companies

Code of responses	Large companies		Code of responses	Medium companies		Code of responses	Small companies	
	Safety score	Rating		safety score	Rating		safety score	Rating
L 1-1	237	VG	M 1-1	165	P	S 1-1	128	P
L 1-2	236	VG	M 1-2	167	P	S 1-2	142	P
L 2-1	249	VG	M 2-1	175	F	S 2-1	139	P
L 2-2	249	VG	M 2-2	156	P	S 2-2	128	P
L 3-1	254	VG	M 3-1	167	P	S 3-1	131	P
L 3-2	250	VG	M 3-2	167	P	S 3-2	193	F
L 4-1	238	VG	M 4-1	201	G	S 4-1	177	F
L 4-2	251	VG	M 4-2	181	G	S 4-2	178	F
L 5-1	268	VG	M 5-1	158	P	S 5-1	169	P
L 5-2	262	E	M 5-2	192	F	S 5-2	156	P
L 6-1	264	E	M 6-1	203	G	S 6-1	155	P
L 6-2	276	E	M 6-2	220	G	S 6-2	145	P
L 7-1	245	E	M 7-1	185	G	S 7-1	111	P
L 7-2	230	VG	M 7-2	199	F	S 7-2	116	P
L 8-1	223	VG	M 8-1	194	F	S 8-1	118	P
L 8-2	235	G	M 8-2	187	F	S 8-2	116	P
L 9-1	230	VG	M 9-1	184	F	S 9-1	127	P
L 9-2	250	VG	M 9-2	156	F	S 9-2	125	P
L 10-1	241	VG	M 10-1	193	P	S 10-1	138	P
L 10-2	257	VG	M 10-2	184	F	S 10-2	125	P
			M 11-1	216	F	S 11-1	137	P
			M 11-2	179	G	S 11-2	131	P
			M 12-1	262	VG	S 12-1	149	P
			M 12-2	256	F	S 12-2	127	P
			M 13-1	187	P	S 13-1	137	P
			M 13-2	166	F	S 13-2	151	P
			M 14-1	182	VG	S 14-1	146	P
			M 14-2	230	G	S 14-2	157	P
			M 15-1	221	P	S 15-1	137	P
			M 15-2	98	P	S 15-2	135	P
Average score: 247.25 Variance:190.28 Standard deviation: 13.81			Average score:187.70 Variance:1003.87 Standard deviation: 31.68			Average score: 136.63 Variance: 400.64 Standard deviation: 20.01		

Table 2 Total variance explained—large and medium construction companies

Sub category	Initial eigen values			Avg. score	Rank	Sub category	Initial eigen values			Avg. score	Rank
	Total	% of variance	Cumulative %				Total	% of variance	Cumulative %		
Large construction companies											
1	7.015	12.095	12.095	4.725	1	1	13.12	22.622	22.622	3.183	14
2	6.824	11.766	23.860	4.412	7	2	5.079	8.757	31.379	3.233	12
3	5.966	10.286	34.147	4.100	16	3	4.723	8.144	39.523	3.116	15
4	5.270	9.086	43.233	4.366	8	4	3.715	6.406	45.929	3.277	7.5
5	4.991	8.605	51.838	4.233	11	5	3.502	6.039	51.967	3.388	3
6	4.052	6.986	58.823	4.512	3	6	3.293	5.678	57.645	3.300	5
7	3.488	6.013	64.836	4.133	15	7	2.899	4.999	62.645	3.277	7.5
8	3.300	5.690	70.526	4.300	9	8	2.597	4.478	67.122	3.633	1
9	2.772	4.780	75.306	4.566	2	9	2.277	3.926	71.049	3.266	9.5
10	2.425	4.182	79.488	4.175	14	10	1.829	3.154	74.202	2.950	16
11	2.162	3.728	83.216	4.450	5.5	11	1.672	2.883	77.085	3.216	13
12	1.910	3.293	86.508	4.216	12	12	1.530	2.638	79.722	2.244	11
13	1.755	3.026	89.534	4.200	13	13	1.428	2.461	82.184	3.433	2
14	1.651	2.846	92.380	4.450	5.5	14	1.281	2.209	84.393	3.316	4
15	1.153	1.988	94.368	4.500	4	15	1.241	2.139	86.532	3.283	6
16	1.030	1.777	96.144	4.275	10	16	1.141	1.967	88.498	3.266	9.5
Medium construction companies											

Table 3 Total variance explained—small construction companies

Sub category	Initial eigen values		Avg. score	Rank	Sub category	Initial eigen values		Avg. score	Rank
	Total	% of variance				Total	% of variance		
Small construction companies									
1	9.124	15.730	2.425	13	10	2.353	4.057	2.483	11
2	4.907	8.460	2.483	11	11	2.100	3.621	2.383	16
3	4.687	8.080	2.350	17	12	1.903	3.281	2.511	9
4	4.294	7.403	2.522	8	13	1.774	3.059	2.633	2
5	4.004	6.904	2.405	15	14	1.587	2.737	2.550	5
6	3.482	6.003	2.533	6.5	15	1.313	2.264	2.650	1
7	2.742	4.727	2.288	18	16	1.207	2.081	2.483	11
8	2.565	4.423	2.408	14	17	1.156	1.994	2.533	6.5
9	2.384	4.111	2.566	3.5	18	1.031	1.777	2.566	3.5
		15.730				2.353	69.900		
		24.191				2.100	73.521		
		32.271				1.903	76.802		
		39.674				1.774	79.861		
		46.578				1.587	82.598		
		52.582				1.313	84.862		
		57.309				1.207	86.943		
		61.732				1.156	88.937		
		65.843				1.031	90.714		

Table 4 Safety score and rating of all companies

Code of responses	All companies		Code of responses	All companies		Code of responses	Medium companies	
	Safety score	Rating		Safety score	Rating		Safety score	Rating
A 1-1	237	VG	A 14-2	181	P	A 28-1	131	P
A 1-2	236	VG	A 15-1	158	G	A 28-2	193	P
A 2-1	249	VG	A 15-2	192	G	A 29-1	177	F
A 2-2	249	VG	A 16-1	203	P	A 29-2	178	F
A 3-1	254	VG	A 16-2	220	F	A 30-1	169	F
A 3-2	250	VG	A 17-1	185	G	A 30-2	156	P
A 4-1	238	VG	A 17-2	199	G	A 31-1	155	P
A 4-2	251	VG	A 18-1	194	G	A 31-2	145	P
A 5-1	268	VG	A 18-2	187	F	A 32-1	111	P
A 5-2	262	E	A 19-1	184	F	A 32-2	116	P
A 6-1	264	E	A 19-2	156	F	A 33-1	118	P
A 6-2	276	E	A 20-1	193	F	A 33-2	116	P
A 7-1	245	E	A 20-2	184	F	A 34-1	127	P
A 7-2	230	VG	A 21-1	216	P	A 34-2	125	P
A 8-1	223	VG	A 21-2	179	F	A 35-1	138	P
A 8-2	235	G	A 22-1	262	F	A 35-2	125	P
A 9-1	230	VG	A 22-2	256	G	A 36-1	137	P
A 9-2	250	VG	A 23-1	187	VG	A 36-2	131	P
A 10-1	241	VG	A 23-2	166	F	A 37-1	149	P
A 10-2	257	VG	A 24-1	182	P	A 37-2	127	P
A 11-1	165	VG	A 24-2	230	F	A 38-1	137	P
A 11-2	167	VG	A 25-1	221	VG	A 38-2	151	P
A 12-1	175	P	A 25-2	98	G	A 39-1	146	P
A 12-2	156	P	A 26-1	128	P	A 39-2	157	P
A 13-1	167	F	A 26-2	142	P	A 40-1	137	P
A 13-2	167	P	A 27-1	139	P	A 40-2	135	P
A 14-1	201	P	A 27-2	128	P			
Average score: 185.00			Variance: 2282.53			Standard deviation: 47.77		

neither follow excellent safety measures nor do not follow poor safety measures. It was observed that the safety score purely depended on the personal interest of owner or the contractor towards the safety measures that are to be followed. For the same reason, the variance of the medium construction firms is high with a value of 1003.87. In the same way, the standard deviation of the medium firms is found to be double that of larger firms i.e., 31.68. Table 2 shows the total variance, average

safety scores and ranks of the sub categories of safety criteria in the questionnaire. In respect of medium firms, the highest safety score of 3.633 was obtained to the 8th sub category, i.e., Scaffolding and the least score of 3.110 was recorded for 3rd sub category, i.e., Electrical Installations.

4.3 Evaluation of Worker Safety Status at Small Construction Firms/Projects

From Table 1, it is evident that the average safety score obtained by small construction firms is 136.30, which is relatively very much lower than those for large and medium firms. From this result, it is evident that the average safety score in small firms is nearly 50% lesser than the large firms and none of the small firms could achieve a safety score of 200. The variance and standard deviation values in respect of smaller firms have been 400.64 and 20.01 respectively. The standard deviation of smaller firms is lesser than medium firms since the safety scores of small firms are consistent with low safety scores whereas the safety scores of medium firms have been fluctuating between excellent and poor safety scores. Table 3 represents the total variance, average safety scores, and ranks of the subcategories of criteria in the questionnaire. For small firms, the highest safety score of 2.650 was obtained to the 15th subcategory, i.e., Hoist Cranes and Derricks, and the least score of 2.350 was acquired by 3rd subcategory, i.e., Electrical Installations.

4.4 Evaluation of Worker Safety Status at Construction Firms on a Whole

When the data collected from all three types of construction firms/projects is pooled (Table 4), overall data resulted in a safety score of 185. The variance and standard deviation have been 2282.53 and 47.77 respectively. The differences in the safety level scores and safety measures applied by the large, medium and small construction firms cumulatively resulted in a high variance. This is due to the fact that all firms do have same set safety measures in place and hence the varying safety scores. Due to the same reason, standard deviation has turned out to be the highest in this case. The safety level in large firms was observed to be higher than the safety level in medium and small firms. In the evaluation of total data, the highest safety score was obtained to the 8th sub category, i.e., Scaffolding with a score of 3.412 whilst the 3rd sub category, i.e., Electrical Installations acquired the least score of 3.075.

4.5 Comparison of Worker Safety at Various Categories of Construction Project

It is amply evident from the data that the large construction firms have the highest safety scores and average scores as compared to those of medium and small firms/projects and the ones obtained on consideration of the whole data. It also has the least variance and standard deviation since all firms in larger category have taken up almost same kind of safety measures. The medium firms had more variance than small firms as a few of the owners or contractors of medium firms observed good measures whilst others didn't. Thus, the small firms have relatively less variance than medium firms since all the contractors and owners of medium firms did not implement good safety measures. Consequently, safety scores and average safety scores have been consistently low for medium firms than other firms and even when the whole data was considered for analysis. Surprisingly, the 3rd sub category, i.e., Electrical Installations have always been in low priority amongst the safety measures taken up by owners or contractors in three types of construction firms chosen for the study.

5 Conclusions

- The survey conducted on worker safety on construction sites revealed that the safety levels vary with the level of construction firms, i.e., large/medium/small. Large firms are considered to have better safety practices and records compared to the medium and smaller construction firms.
- The results indicated that excepting the reputed construction firms, the others were found not implementing the necessary safety requirements, and hence there is a need to monitor and ensure enforcement of safety practices at medium and small project sites.
- The large construction firms displayed little variation in safety levels, whilst medium firms had no much variance but comparatively less average safety score and lesser scores for each subcategory than larger firms. A wide variation was observed in levels of safety performance in case of small construction firms.
- The results obtained through the analysis of overall data of three types of construction firms showed a lot of variation with three levels of companies/firms individually.
- There is an immediate necessity to keep in place a proper monitoring system at the construction sites and to bring proper awareness amongst the workers on the need for their safety as they are living on a knife-edge.
- Workers perceived organizational commitment and communication as the key factor in ensuring construction safety.

- There is a deficiency of responsive system and resources to support workers in addressing the issues related to construction safety. Hence, a frequent monitoring is obligatory to ensure quality and continuous improvement in safety performance.

References

1. Shamsuddin KA, Ani MNC, Ismail AK, Ibrahim MR (2015) Investigation the safety, health and environment (SHE) protection in construction area. *Int Res J Eng Technol (IRJET)* 6(2):624–636
2. Hinze J, Raboud P (1988) Safety on large building construction projects. *J Constr Eng Manag* 114(2):286–293
3. Suazo GA, Jaselskis EJ (1993) Comparison of construction codes in United States and Honduras. *J Constr Eng Manag* 119(3):560–572
4. Everett JG, Frank PB (1996) Costs of accidents and injuries to the construction industry. *J Construct Eng Manage* 122(2):158–164
5. Anumba C, Bishop G (1997) Importance of safety considerations in site layout and organization. *Can J Civ Eng Manage* 24(2):236
6. Abdelhamid TS, Everrett JG (1998) Identifying root cause of construction accidents. *J Constr Eng Manag* 126(1):52–60
7. Sawacha E, Naoum S, Fong D (1999) Factors affecting safety performance on construction sites. *Int J Project Manage* 17(5):309–315
8. Lubega HA, Kiggundu BM, Tindiwensi D (2000) An investigation into causes of accidents in the construction industry in Uganda. In: 2nd international conference on construction in developing countries, vol 20, no 2, pp 242–259
9. Wilson JM Jr, Koehn E (2000) Safety management: problems encountered and recommended solutions. *J Constr Eng Manag* 126(1):77–79
10. Ho DCP, Ahmed SM, Kwan JC, Ming FYW (2000) Site safety management in Hong Kong. *J Manag Eng* 16(6):34–42
11. Suraji A, Duff AR, Pickitt SJ (2001) Development of casual model of construction accident causation. *J Constr Eng Manag* 127(4):337–344
12. Hughes P, Ferrett E (2005) Introduction to health and safety at work: the handbook for students on NEBOSH and other introductory H and S Courses, 3rd ed. Rutledge Publication
13. Ali AS, Kamaruzzaman SN, Sing GC (2010) A study on causes of accident and prevention of Malaysian construction industry. *J Des + Built* 3:95–104
14. Kumar S, Bansal VK (2013) Construction safety knowledge for Practitioners in the construction industry. *J Front Construct Eng* 2(2):34–42
15. Guha H, Biswas PP (2013) Measuring construction site safety in Kolkata, India. *Int J Sci Eng Res* 4(5):2138–2143
16. Selvam A, Priyadarshini K (2014) Safety management and hazards control measures in construction. *IOSR J Mech Civ Eng* 97–101
17. Kanchana S, Sivaprakash P, Joseph S (2015) Studies on labour safety in construction sites. Hindawi Publish Corporation, *Sci World J* 5:1–6

Sediment Transport Modelling in Stream Flow by HEC-RAS Model—A State-of-the-Art



Bahnisikha Das and T. Senthil Vadivel

Abstract Sediment transport is considered a significant factor having great influence on the river morphology. It is also a major concern of hydraulic engineers during the construction of hydraulic structures including irrigation canals, dams, barrages, weirs or for navigation purposes. Hence, the study of sediment transport is very important to know about sedimentation at the bank of the river, management of the quality of water and construction of hydraulic structures. However, the analysis of sediment is considered the most complicated topic. The development of new computer technologies has empowered the engineers to solve the complex sediment transport equations and hydraulic issues with the help of computer simulations and modelling techniques. There are many models which perform these processes. However, there is a lot of difference between these models because of their input requirements, the types of output that are produced, their complexity, and the way in which they represent various processes. Because of its simplicity and free availability, the Hydrologic Engineering Center's River Analysis System (HEC-RAS) has been greatly used in research areas for modelling of sediment transport. This paper aims to review the performance of the HEC-RAS model which is used to simulate sediment transport mechanism of stream channels.

Keywords Sediment transport · Erosion · Deposition · Modelling · Hydraulic structures · HEC-RAS

1 Introduction

Rivers or streams are considered as the primary resources for supply of water. The river system is dynamic as it undergoes a continuous change. Various human and natural factors influence the river stream due to which it undergoes severe erosion and deposition on its bed or banks. These factors are responsible for the long-run changes in the river geometry, termed as changes in geomorphology. The morphological and

B. Das (✉) · T. Senthil Vadivel
Department of Civil Engineering, School of Engineering and Technology, Adamas University,
Kolkata 700126, India

sedimentation study of river is among the most complicated yet major topics in river engineering. Therefore, the proper knowledge of morphological change in the river like erosion, deposition, meandering and flow properties are the main priorities in a river engineering project.

Sediment transport is a phenomenon by which silt or gravel or even larger boulders are detached from the bed or sides of the channel which are swept downstream by the moving water. Generally, sediment moves in a channel because of two distinct physical transport mechanisms. The first one is the movement of the suspended particle in which they are in suspension due to the turbulence of water flow and second one is the movement of bedload particle in which the sediment particle moves along the bottom of the channel with occasional jumps.

The stream geometry could be altered by the fast movement of sediment particles which may also become dangerous depending on the pattern of movement. The erosion of sediment may destabilize the cross-section of channels which may lead to failure of the hydraulic structures located on the channels whereas the deposition of sediment reduces the channel size which then increases the water surface level, hence providing an additional pressure on the bank and side of the channel. The raised water level may overflow into the floodplain and surrounding areas, thus causing floods in the nearby areas and may also have navigation problems. For many of the water management issues, an approximate determination of sediment transport rates in alluvial river is also considered an important criterion [1]. The physical and chemical environment of shallow lakes can be affected by the presence of sediment particles in large quantities. Suspended sediment can reduce the intensity of light traveling through the water column and hence the growth of phytoplankton is influenced. Moreover, the residues of industries and agriculture discharged into the water bodies are also mixing with the sediment particles which are contaminating the aquatic systems. Hence it is affecting the quality of surface water significantly arising threats to the health of human beings and aquatic life. The transport of sediment in river streams depends on numerous factors including its dimension and type, basin size and its slope, vegetation and land cover near the basin areas, climatic variation, temperature, inundation events.

The studies done previously related to the impacts of sediment transport especially emphasize on its correlation with the flow of water. As an example, relating the sediment discharge to streamflow by rating curve is a familiar method for computing sediment [2]. Single hydrological high discharge can carry a large amount of sediment in a little time, and hence deposit a large amount of sediment [3]. In monsoon period, similar things can be observed as the high fluctuations in water flow leave a considerable change in the sedimentation pattern before and after the monsoon period [4]. Apart from these factors, the sediment transport will also be influenced by the geometry and width of the channel.

The development in the field of computers for modelling the complex mathematical equations has encouraged its implementation for analyzing and predicting the geometrical changes of rivers [5]. It is very important to implement the correct computer model to a certain region and then calibrate it that can accurately simulate the alteration in the bank and bed level of river during inundation. In this regard,

on the basis of certain assumptions, a number of mathematical models have been introduced by many researchers which include: CCHE1D model, CCHE2D model, FLUVIAL, MIKE11, HEC-6, and HEC-RAS model. Out of these models, some became commercial and were used multiple times all around the world in various projects. The key objective of this review is to assess the performance of HEC-RAS model in order to study the mechanism of sediment transport in natural drains. This is performed by reviewing various sediment transport modelling work done by various versions of HEC-RAS model.

2 Literature Review

In the field of water resource engineering, many researches have been done on the process of sediment transport modelling in the past few decades.

In 1984, Chang investigated the meander curvature of rivers by using the energy approach along with the relations for continuity equation, flow resistance, sediment discharge, and stability of riverbank. The result shows that width of the channel remains constant which is in the meandering rivers range [6].

Merritt et al. in 2003 reviewed various existing sedimentation and nutrient transport models, their concept, and the trade-offs which can impact the model's result. The study aimed to produce a resource that can be implemented by various model users in order to guide their on-land or in-stream sediment modelling process. Overall, it was concluded that due insufficient data, over-dependency of the model's result, and the more complex computations for large catchment areas, the application of physics-based and conceptual models are inappropriate for calculating the watershed exports. However, these problems can be resolved by the combination of conceptual and empirical approaches to provide models [7].

Brunner et al. in 2005 introduced the modelling of movable bed sediment transport using HEC-RAS. Various equations and methodologies which include the modelling of sediment transport were discussed. The sediment transport calculations of HEC-RAS were compared with the model, HEC-6 T, for the analysis of sediment transport in equilibrium. The result showed a fair agreement between these models and the measured data. Gibson et al. in 2006 presented the computations of sediment transport with HEC-RAS model. The hydraulic capabilities existing in the model are described to determine the steady flow profile series which is used to develop hydrodynamic parameters needed for transport of sediment [8].

Duan et al. in 2008 evaluated the flow and the sediment transport models for Rillito River. A comparative study was performed between three models (HEC-RAS, IALLUVIAL2, and SRH-1D) to examine the water and bed level of a flood event in the Rillito River that has exceeded 100-year flood. The results so obtained were compared with field survey data. The result showed that both the HEC-RAS model and the IALLUVIAL2 model predicted flood in a similar manner although, IALLUVIAL2 model cannot take into consideration the effect of bridge. Also, both

HEC-RAS model and SRH-1D models showed better performance in the sedimentation effect in the downstream region. The statistical analysis showed that for average bed elevation alteration, the smallest value of mean error and standard deviation was obtained in HEC-RAS model. Hence, HEC-RAS model gives the best performance for predicting the scouring actions occurring near the cross-sections of bridge [9].

Gibson et al. in 2010 performed the sediment processes modelling of catchment and riverine area with HEC-RAS and HEC-HMS. The various methodologies required in these sediment transport models were examined and the hypothesis included to ease the combined modelling of watershed-riverine was focused with both the models. It was concluded that the sediment transport modelling of integrated watershed-riverine systems can be conducted with the data connection between these models through DSS boundary condition editor embedded in HEC-RAS [10].

In 2012, Haghbi and Zaredehdasht evaluated the ability of HEC-RAS 4.0 in forecasting the sedimentation of Karun River, Iran. The HEC-RAS model was run repetitively with various sediment transport equations to select the equation that produces better results. The results obtained from the simulation of river bed are compared with MIKE 11. The analysis of the result indicates significant sedimentation in various parts of Karun River which shows the true representation of the river [5]. In the same year, Hummel et al. [11] compared two different models for simulating the flood flow and the mechanism of sediment transport in Pantano Wash, Arizona. These models are quasi-unsteady flow HEC-RAS model and Finite Volume Method (FVM) based model. The research aims to determine the accuracy among unsteady models and quasi-unsteady models for predicting the transport of sediment. From the result, it was observed that both the model showed a very close result of river bed changes for the study reach. However, the FVM model was better in predicting the flood hydrographs also, among the seven different sediment transport formulas embedded in the HEC-RAS model, Yang's and Engelund-Hansen's equations gave the most similar results when compared with the field measurements [11].

Song et al. in 2015 conducted a study by simulating and then comparing the sedimentation process in the river and floodplain areas on the upper stor catchment of Northern Germany. The HEC-RAS model was linked with the SWAT model (Soil and Water Analysis Tool) to study the complete sedimentation and accumulation processes in the selected reach. The results showed that the upper reaches of the catchment area is dominated by sediment deposition and a very negligible amount of deposition has occurred in the floodplain areas [12]. Shelley et al. in 2015 developed a one-dimensional unsteady flow and sedimentation model using HEC-RAS Version 5.0 Beta. This research has explained all novel developments in the latest version of HEC-RAS model for modelling the sedimentation in the Tuttle Creek Lake [13].

In 2015, Azaran and Bajestan evaluated the ability of HEC-RAS model by considering the geometric changes in cross-section, sediment discharge and river thalweg prediction in order to simulate the scouring and deposition processes in Karun River. The results showed that the aggradations process is dominated in many sections of the river and the degradation process was very rare. The author also suggested stabilizing the bank of the river section that has undergone degradation process [14].

In 2016, Ali and Mohamed conducted a study on the sediment transport modelling by HEC-RAS model in Wadi river, Chemora. The study was done by utilizing the flow data, lithologic data and geometric data. It was observed that if the Van Rijn's velocity computation method is combined with the Yang equation available in HEC-RAS, then the result obtained will be very close to the field conditions of the study area. The study highlighted the spatial and temporal distribution of aggradation and degradation [15].

Fischer et al. in 2016 performed a study by utilizing the HEC-RAS model to recognize the unknown and sensitive parameters of sediment transport. The study was conducted in Brahmaputra River located in southern part of Asia and the climatic conditions of both the present and future period were considered. A significant uncertainty was observed in the estimation of sediment discharge at the downstream section of the river (Bahadurabad gauging station, Bangladesh). However, in spite of this, the simulation result showed the relative changes in the river and it was also observed that there will be 40% increase in sediment discharge in future at the Bahadurabad station. It was also observed that because of the uncertainties in certain parameters, the discharge and geometry of the river will almost become double in future. Hence, getting a correct information will greatly improve the abilities to ascertain and hence to manage the present and future sedimentation problems in the catchment area of Brahmaputra River [16].

Gibson et al. in 2017 presented the new sedimentation features added on the latest version of HEC-RAS 5.0 and 5.1. The latest version included the change in the side slope along with BSTEM Model which stands for Bank Stability and Toe Erosion. It also incorporates many new features to enhance its application in a numerous sectors. The integration of sediment transport with unsteady flow capacity is one of the major developments of model that strengthens sediment analysis function accounting lateral structures, mixed flow regimes, etc. [17].

Rehman et al. in 2018 evaluated the performance of one-dimensional HEC-RAS model in simulating the degradation and flushing characteristics of sediment in various reservoirs. The HEC-RAS model was run by using three different reservoir data which includes the Baira reservoir, Gebidem reservoir and Gmund reservoir located in India, Switzerland, and Austria. The flushing duration as well as the sediment deposition and flushing values obtained in the simulation process are very close to the observed values of all the three reservoirs, which showed a good performance of the model. It was also concluded that the sediment transport function required for modelling sediment deposition depends upon the features of the reservoir and the surrounding hydraulic and climatic conditions [18].

Mohammed et al. in 2018 conducted a study on HEC-RAS (4.1.0) model in order to recognize the sedimentation pattern of a stretch of Euphrates river. The river reach has a combined feature of both straight and meander morphology. The model carried out the flow and sediment transport capacity calculation effectively and has evaluated deposition and erosion at various parts of the river reach. From the rating curve of the sedimentation capacity for all the cross-sections, it was observed that the increasing discharge gives less sediment transport capacity on the straight parts on the studied reach and more sediment transport capacity in the meandering parts [19].

In 2019, Shelley developed 1-D movable boundary hydraulic and sedimentation model for simulating and predicting the sediment deposition on the Missouri river reach by using HEC-RAS model of version 5.0. Various new features which were embedded in the new version was utilized including sediment load specification and gradation through a DSS (Data Storage System) file. The model was calibrated, reproducing significant bed volume changes, elevation of water level, and velocities of river. This model illustrates the effectiveness of the latest version of HEC-RAS model for the analysis of sedimentation process in huge, complicated river channels [20].

Joshi et al. in 2019 conducted study on the application of HEC-RAS on the sediment hydraulics of Maumee River, Ohio. The calibration and validation process of the model was performed by using various sediment transport functions embedded in the HEC-RAS model and with Manning's rugosity coefficient. The result showed the pattern of change in river bed and also the various cross-sections that undergoes erosion or deposition. It was observed that the sediment distribution was not uniform throughout the study reach and there was an overall depletion in river bed elevation. Hence, it was suggested to consider these decreasing trends before the construction of any hydraulic structures. The future sediment scenario can be predicted by building a more robust model by using the cross-sectional sediment load gradation data in the study area [21].

Damte et al. in 2021 utilized the HEC-RAS model to estimate the sedimentation activities for predicting the flood in the Kulfo river located in southern Ethiopia. The impact of flood with 100-year return period were assessed from the geometrical data of 2005 and 2019. Grain size estimation was done from the samples of bed and bank materials. The rating curve was developed by sampling the discharge and suspended sediment concentration thrice a day continuously for three months. The results showed a considerable inundated area in the year 2019 in comparison to the situation in 2005, which signifies a temporal change in the morphology of river during this period. The sediment discharge calculation was performed by Ackers and White method and eventually, the calibration was done. The upstream reach of the study area showed both aggradation and degradation in various cross-sections, whereas the downstream reach was dominated mainly by degradation. The HEC-RAS model was utilized for comparing the flood depth affecting the basin area and the sedimentation process [22].

The relationship between the sedimentation and water quality parameter was analyzed by Monjardin et al. in 2021 in the Naic river, Philippines. The sediment volume of the river and the water quality was predicted in the period January 2020–2021 by utilizing HEC-RAS model. The average weather flow of the river was used for this purpose under the existing geometric characteristics. A strong indirect relationship was obtained between the cumulative sediment volume and dissolved oxygen and a weak direct relationship was obtained between the biological oxygen demand of water and the cumulative sediment volume. The analysis also revealed that the sediment discharge and the precipitation are directly related to each other. From the result, it was also observed that the sediment discharge increases with an increase in the rainfall amount and vice-versa. Apart from these, the output of the

HEC-RAS model is very close to the actual data which signifies the efficiency of the study method [23].

3 Description of Sediment Transport Models

Simulation of sediment transport in a river stream or a reservoir can be achieved by a wide variety of models. These models vary with respect to their data requirement, functions involved, process considered and the complexities. In general, there is no “best” model for all applications. The efficiency of the model depends upon its use and the catchment features that need to be considered. The accuracy and validity of the model as well as the input and output data requirements are the factors affecting the model selection. Various sediment transport models existed till date out of which some are commercial models while others are freely available. Some of the commonly used models are discussed below.

Danish Hydraulic Institute (DHI) MIKE 11 is a software that comprises graphical user interface and the fully integrated windows. This application is having a faster computation speed as compared to the older versions of MIKE and other related software. It is a 1-D user-friendly model used for the simulation of sediment transport, flood flow and water quality parameters in river streams. The salient characteristics of MIKE 11 are that it has various additional functions such as hydrology, water quality model, hydrodynamic model, advection–dispersion, sediment transport, rainfall-runoff model, and flood prediction model.

IALLUVIAL2 is 1-D unsteady movable bed sediment transport and flow model. It includes six friction-factor equations and twenty-two sediment transport formulas. Standard step method is used for calculating the flow by backwater analysis. However, the model cannot perform the simulation of various hydraulic structures such as barrages, weirs, bridges, culverts, etc.

SRH-1D (Sedimentation and River Hydraulics) is a sedimentation and flood flow model used for the river flow simulation of movable or fixed boundaries. The model uses river information based on cross-sections. Many sediment transport formulas are available in the sediment transport functions. It can evaluate sediment load concentrations of a channel with the known values of bed material, sediment inflows, hydrology, and river hydraulics.

HEC-6 (Hydrologic Engineering Center-6) is used for the simulation of sedimentation process in a river which arises because of the change in the frequency and duration of water level and its flow as a result of geometrical changes in the river. This model can be utilized to determine reservoir deposition, scouring during periods of high discharge and sedimentation process in stable channels. However, there are few restrictions in HEC-6 which include the impossibility of sediment transport in distributaries, permission of only one inflow point in between two consecutive cross-sections.

HEC-HMS (Hydrologic Modelling System) was designed for the study procedure used in US Army Corps of Engineers. It calculates sediment yield of watershed

with the help of Modified Universal Soil Loss Equation. It also incorporates various surmises that convert the total load of sediment into a series of times by the sediment grain size class. Various sediment transport methods and their effect on the stream is also included in this system.

4 Overview of Hydrologic Engineering Center's River Analysis System (HEC-RAS)

The Hydrologic Engineering Center's River Analysis System (HEC-RAS) model is a hybrid model which is an improved version of HEC-6 model developed at the Hydrologic Engineering Center. Mr. Gary W. Brunner has designed the software and is also the leader of HEC-RAS team. The model is intended for hydraulic, sedimentation and water analysis of river channels. The system of HEC-RAS incorporates four river channel analysis patterns including the computation of steady and unsteady flow profiles of water surface, sediment transport modelling and analysis of river water quality. Apart from these components, various hydraulic design features are also available in the model that can be applied after the calculation of basic water surface profiles. It uses direct step by step method for calculating the flow profile and a large number of semi theoretical and empirical approaches are used for the computation of sediment transport rate. The dynamic changes in the bed of the channel can be modelled by computing the sediment transport in HEC-RAS model.

HEC-RAS can be downloaded freely from the Hydrologic Engineering Center's website and is supported by the US Army Corps of Engineers. In addition to one-dimensional sediment transport analysis, the latest version of the model can also predict variation in the river cross-sections. Also, the model requires large number of input parameters that are not always available. The previous version was limited to quasi-unsteady sediment transport and longitudinal river bed change. This mainly included a two-dimensional hydrodynamic model and also a huge variety of hydraulic. Apart from that, the two prime developments incorporated the combination of unsteady flow model with the sediment transport model and the addition of erosion capacities and bank failure in the river cross-section. HEC-RAS 6.0 is the latest version released on June 2021 by US Army Corps of Engineers (USACE). Many new features are embedded in its latest version which includes two-dimensional sediment transport computations, addition of many new 1D sediment features, new water quality features, addition of 3D graphics, computational speed improvements for 2D, and many more.

5 Summary of Literature Review

Water bodies such as streams and rivers are considered as the primary source of water for several purposes. Numerous natural and human factors are responsible for the change in river morphology and the sediment transport phenomenon. In spite of many advantages that we get from a natural stream the effect of erosion and deposition in a stream can directly or indirectly lead to many disasters including floods, failure of hydraulic structures, in-stream navigation problems, and many more. Hence it is necessary to carry out the sediment transport modelling to mitigate these problems. From the literature review, it has been observed that various versions of HEC-RAS, which is freely available, have been used widely and successfully for this purpose. New sedimentation features are being continuously added in the newer versions of HEC-RAS. Many novel features including the two-dimensional model, lateral cross-sectional change and many important sediment transport developments are incorporated in HEC-RAS 6.0.

The various new characteristics embedded in HEC-RAS 6.0 adds a great potential of research in the field of sediment hydraulics. In addition to the longitudinal bed changes, the sedimentation occurring in the side slope of a channel cross-section can also be performed in future which will provide a more realistic representation of the actual scenario. Also, while modelling the sediment transport mechanism in a river, sediment transport of all the tributaries of the main channel within the study reach can be included in the future work to get the result much closer to the field data one.

6 Conclusion

The above research study clearly indicates the sediment transport phenomenon by HEC-RAS model and its different provisions, boundary conditions, constraints, and limitations. Based on the above-said observations, the following research areas have been identified by the authors for further investigation.

- 2-D Sediment transport modelling of Ganga River Basin by HEC-RAS 6.0.
- Analysis of the water quality and sediment transport in the Ganga River using HEC-RAS 6.0.

References

1. Bhattacharya B et al (2004) A data mining approach to modelling sediment transport. In: Liong S, Phoon K, Babovic V (eds). Proceedings of the 6th international conference on hydroinformatics. 6th international conference on hydroinformatics. World Scientific Publishing Company, Singapore, pp 1303–1310

2. Horowitz A (2003) An evaluation of sediment rating curves for estimating suspended sediment concentrations for subsequent flux calculations. *Hydrol Process* 17(17):3387–3409
3. Pietron J et al (2015) Model analyses of the contribution of in-channel processes to sediment concentration hysteresis loops. *J Hydrol* 527:576–589
4. Roy N, Sinha R (2014) Effective discharge for suspended sediment transport of the Ganga river and its geomorphic implication. *Geomorphology (Amst)* 227:18–30
5. Haghbi AH, Zaredehdasht E (2012) Evaluation of HEC-RAS ability in erosion and sediment transport forecasting. *World Appl Sci J* 17(11):1490–1491
6. Chang HH (1984) Analysis of River Meanders. *J Hydraul Eng* 110(1):37–50
7. Merritt WS, Letcher RA, Jakeman AJ (2003) A review of erosion and sediment transport models. *Environ Model Softw* 18(8–9):761–799
8. Bruner G, Gibson S (2005) Sediment transport modelling in HEC-RAS. In: Walton R (ed) *Proceedings world water and environmental resources congress 2005*, American Society of Civil Engineers, Anchorage, Alaska
9. Duan JG et al (2008) Evaluation of flow and sediment models for the Rillito river. In: Babcock RW, Walton R (eds) *World environmental and water resources congress 2008*. ASCE Library
10. Gibson SA, Pak JH, Fleming MJ (2010) Modelling watershed and riverine sediment processes with HEC-HMS and HEC-RAS. In: Potter KW (ed) *Watershed management conference 2010*, vol 2. ASCE, Madison, Wisconsin, USA, pp 1340–1349
11. Hummel R, Duan JG, Zhang S (2012) Comparison of unsteady and quasi-unsteady flow models in simulating sediment transport in an ephemeral Arizona stream. *Am J Water Resour* 48(5):987–998
12. Song S, Schmalz B, Fohrer N (2015) Simulation, quantification and comparison of in channel and floodplain sediment processes in a lowland area—a case study of the upper stor catchment in northern Germany. *Ecol Indic* 57:118–127
13. Shelley J, Gibson S (2015) Unsteady flow and sediment modelling in a large reservoir using HEC-RAS 5.0. *Advisory Committee on Water Information*. <https://acwi.gov>
14. Azaran F, Bajestan MS (2015) Simulating the erosion and sedimentation of Karun Alluvial River in the Region of Ahvaz (Southwest of Iran). *Am J Eng Res* 4(7):233–245
15. Ali B, Mohamed M (2016) Sediment transport modelling in Wadi Chemora during flood flow events. *J Water Land Dev* 31:23–31
16. Fischer S, Pietron J et al (2016) Present to future sediment transport of Brahmaputra River: reducing uncertainty in predictions and management Springer. *Reg Environ Change* 17(8):515–526
17. Gibson S, Sanchez A et al (2017) New one-dimensional sediment features in HEC-RAS 5.0 and 5.1. In: Dunn CN, Weeie BV (eds). *World environmental and water resources congress 2017*. Proc., ASCE Library, California, pp 192–206
18. Rehman H, Chaudhry MA et al (2018) Performance evaluation of 1-D numerical model HEC-RAS towards modelling sediment depositions and sediment flushing operations for the reservoirs. *J Environ Monit Assess*. <https://doi.org/10.1007/s10661-018-6755-7>
19. Mohammed HS, Alturfi UAM, Shlash MA (2018) Sediment transport capacity in Euphrates River at Al-Abbasia reach using HEC-RAS model. *Int J Civ Eng Technol* 9(5):919–929
20. Shelley J, Gibson S (2019) Modelling bed degradation of a large, sand-bed river with in channel mining with HEC-RAS 5.0. *Advisory committee on water information*. <https://acwi.gov>
21. Joshi N, Lamichhane GR et al (2019) Application of HEC-RAS to study the sediment transport characteristics of Maumee River in Ohio. In: *World environmental and water resources congress 2019*. ASCE Library, pp 257–267
22. Damte F et al (2021) Computing the sediment and ensuing its erosive activities using HEC-RAS to surmise the flooding in Kulfo River in Southern Ethiopia. *World J Eng*. <https://doi.org/10.1108/WJE-01-2021-0002>
23. Monjardin CEF et al (2021) Sediment Transport and water quality analyses of Naic River, Cavite, Philippines. In: *2021 IEEE conference on technologies for sustainability (SusTech)*. IEEE, Irvine, CA, USA

24. Gibson S, Brunner G et al (2006) Sediment transport computations in HEC-RAS. In: Eighth federal interagency sedimentation conference (8th FISC). Reno, NV, pp 57–64
25. Brunner GW (2010) HEC-RAS, river analysis system hydraulic reference manual. January 2010
26. HEC (2015) HEC-RAS-USDA-ARS bank stability & toe erosion model (BSTEM) user and technical reference manual, CPD-68B, p 73

Application of Waste Tyre Rubber Crumbs in Strengthening of Bituminous Roads



Santanu Haldar, T. Senthil Vadivel, and Sukanta Das

Abstract In the World, India is considered as the second rapid mounting automobile industry and production of waste tyres is just a consequence of this. Tyres become scrap due to continuous frictional force between pavement surface and vehicle tyres. This continuous production and disposal of waste tyres creates several nuisances such as intensifying landfill areas, environmental contamination, and resulting health vulnerability. Hence, solid waste management may be a great option for those scrap tyres that can be used as a modifier in Crumbed Rubber Modified Bitumen (CRMB). Crumbed tyre rubber can be used as partial replacement to the total weight of Bitumen in road construction. Waste crumbed rubber has same properties as bitumen that possesses an improved skid resistance, fatigue cracking interruption, and augmented rut resistance. In this paper, it is seen that CRMB confirms greater softening point, lesser penetration value, and lower ductile value. Also strength properties of CRMB are evaluated by means of Marshall Stability test. The objective of this study was to use waste crumb rubber with neat bitumen that would diminish the costs of construction and as well as possessing improved physical properties in comparison of convention bitumen. At the end of experimental studies, it is observed that 12% addition of crumb rubber has the most suitability for blending with bitumen.

Keywords CRMB · Waste crumbed rubber · Softening point · Penetration value · Ductile value

1 Introduction

Generally, proper communication system in the form of pavement is a sign of a developed society or country. In India, most of the highways are flexible pavement where bitumen plays a vital role as the primary constituting material. The main function of bitumen is to adhere aggregate in their place and provide a better water sealant skid resisting surface for the ongoing vehicles. Globally, nearby 15 million

S. Haldar (✉) · T. Senthil Vadivel · S. Das
Department of Civil Engineering, School of Engineering and Technology, Adamas University,
Kolkata 700126, India

tonnes waste tyres are produced annually and 1 million tonnes out of that are supplied by India [1]. Generally, they are dumped in a place causing landfill occupancy, creating breeding of mosquitoes.

Environmental Protection Agency (EPA), in the year 1990, approximated that in the same year, 78% of the waste tyres, were either accumulated in a place, illicitly deserted, or a land filled [4, 5]. Few of the states burnt those tyres but the problem for this was, after burning it apt to float back on the surface again. Disposal by burning technique also results harmful fumes that go in the atmosphere, originating large amount of hydrocarbons, carbon smoke, residues, causing environmental pollution, and health risk concurrently [2].

So, instead of disposal, solid waste management of the waste tyres may be a great option where reuse of the waste happens in form of partial replacement of bitumen because rubber also possesses same properties as bitumen. Besides of that, in addition of crumbed rubber into conventional bitumen causes hiking in viscosity, lowering the value of penetration, and rising the bitumen softening point [3]. The addition of rubber offers bonus binding strength, escalating flexibility of the bitumen [6]. Moreover, carbon in the rubber inhibits oxidation and protects bitumen from ageing [8].

2 Literature Review

There are several sorts of research had been done by quite a few students, professors, and researchers to examine the behaviour of crumb rubber replacement in typical bitumen to augment the engineering properties of bituminous pavement.

Nabin Rana Magar examines the performance of CRMB for varying its percentages with neat bitumen. Greater percentage of crumb rubber significantly augments penetration and softening point of bitumen. 0.3 to 0.15 mm is recommended as the finest size to be used for crumb rubber amendment for commercial fabrication of CRMB [2].

Nuha S. Mashaan illustrated the convenience of using asphalt mix with crumb rubber modifier. The modifier can use in hot mix asphalt in order to get better counteraction to rutting and fabricate pavement with superior resilience. It is then diminishing distresses reasoned in pavement with hot mix asphalt. Hence, the road user would assure more secure and smooth roads [3].

Senthil Vadivel et al. highlighted on existing traditions associated to the reclaim of waste tyre rubber and discover latest potential use. The progress of new construction material by means of recycled waste tyre is significant to both the construction and rubber industry. Widespread investigation has been carried out to scrutinize the applications of wasted tyre rubber which used as reinforcement in under reinforced beams. 14 beams were cast with 2 numbers of 15×25 mm sized scrap tyre rubber as reinforcement as an alternative of steel in tension zone. Flexural behaviour of different aged tyre reinforced concrete beam was tested in this regard. It was observed that all the test specimens performed in a ductile manner. Based on the experiment

dimensions, flexural stiffness, the ultimate strength, and ductility were measured and compared. The test outcomes also point towards that strength and stiffness of the beam are equivalent to Reinforced Concrete beams [4].

Senthil Vadivel and Thenmozhi aimed on using waste tyre rubber crumbs as a replacement of fine aggregate in concrete combinations. Shredded rubber crumbs with the proportion of 2, 4, 6, 8, and 10% by weight used as an alternative of fine aggregate in casting of total 90 cubes, cylinders, and beam specimens and the experimental outputs compared with total 18 conventional specimens. Properties of fresh and hardened concrete such as tensile strength, compressive strength, workability and flexural strength were recognized and it was concluded that waste tyre rubber of 6% substitution with fine aggregate will offer safest and optimal alternative in concrete combinations [5].

Mashaan et al. presented that addition of crumb rubber with neat bitumen decreases bitumen penetration value and consequent increase in softening point value which also indicates the resulting mix as stiffer and viscous material [6].

Justo et al. stated that the usage of crumb rubber changes the properties of bituminous mixture with his assistance Shankar and Mohd. Imtiyaz. They used the rubber content up to 12 tonnes and proper practical values were obtained from the several applications of CRMB. The temperature was also mentioned there for proper blending of bitumen mix. They have used 60/70 grade bitumen to get optimum binder (bitumen) content [7].

Becker et al. revealed that the mix characteristics are largely influenced by addition of rubber content into bituminous mix. Rubber content in greater extent enhances the mixing property but up to a certain limit of addition should be carried out to get proper one. Crumb rubber replacement effects in penetration, softening point, and ductility [8].

Abedrahman and Carpenter determines the varied percentage of crumb rubber with blending temperature for the preparation of CRMB mix. He mentioned the temperature as 175 °C and 40–45 min as the time of mixing. This research was so much helpful to get sense about the blending temperature where the bitumen can be mixed properly to get proper mixture without any hesitation [9].

Based on the above literature, the current study was intended to:

- Use crumb rubber as a partial substitution of bitumen and make the process of construction economically viable.
- Achieve a greater strength and stiffness of the entire paving mix in order to carry a greater load coming from the moving vehicles.

3 Materials Used

Here in this chapter, selection of materials and their specifications used for this study are discussed below:

Fig. 1 40 mess crumb rubber collected from Kharagpur



3.1 *Crumbed Rubber*

Scrap tyre rubbers are the key constituent of Crumbed Rubber modifier and this scrap tyre is mainly ordinary and synthetic rubbers and it contains carbons. Types of rubber vary with the type of vehicle, for e.g. truck tyres having ordinary rubbers mainly whilst the automobile tyres contain synthetic rubbers [2]. The composition of classic mass of crumb rubber modifier available in present marketplace is generally homogeneous in nature. Standard car tyres have ordinary rubber, synthetic rubber, steel cord, carbon, bead wire, oils, chemicals, waxes, pigments etc.

Crumb rubber fabricating corporations are mainly situated in various states of India like, Hyderabad, Kerala, Tamil Nadu, Gujarat, Maharashtra, Rajasthan, Telangana, Delhi etc. But in West Bengal, it is very hard to find such a corporation like this. “Tri Rubber Republic of India Inc.” assisted during ingathering of crumb rubber by informing about the concern material that is available at Kalaikunda, DewanmaraAyma, Kharagpur, Province—721304. Collection of 40 mess (0.42 mm or 420 micron) crumb rubber (Fig. 1) was done from the reference place.

3.2 *Bitumen*

Bitumen is an extremely viscous, highly sticky, black colour semi solid or liquid product existing in natural deposits. Mainly it is a side-product of the partial distillation of crude petroleum. It is well known for its adhesive and waterproofing properties and using comprehensively for the construction of Flexible Pavements. It is an amalgamated substance which is the mixture of hydrocarbon and integrated elements which comprise sulphur, calcium, iron, and hydrogen.

Table 1 Tests on Bitumen

Sl. No.	Tests	Used apparatus	Reference
1.	Penetration	Standard Penetrometer	IS: 1203-1978
2.	Softening Point	Ring Ball Apparatus	IS: 1205-1978
3.	Ductility	Ductility Test Apparatus	IS: 1208-1978
4.	Flash & Fire Point	Cleveland Flash & Fire Point Apparatus	IS: 1209-1978
5.	Specific Gravity Test	Specific Gravity Bottle	IS:1202-1980

For this study, VG 30 bitumen was collected from Debra—Patashpur Road where construction of 2 lane was happening. Here the grade of bitumen was declared by the supplier, which is later cross checked by experimental procedures.

4 Methods

The testing methodology for this study has embraced with a number of tests to investigate the results on amalgamation, bitumen with crumb rubber substituted hydrocarbon and aggregate-bitumen united material (Table 1).

4.1 Preparation of CRMB

In this part, scrap tyre rubber is integrated into asphalt paving mixes where the aspect temperature was kept at 150–160 °C to make the mix.

5 Tests, Results, and Discussions

Generally, observations were started with measuring properties of aggregates and bitumen. Before preparation of CRMB, physical properties of crumbed rubber like specific gravity and moisture content checked (Table 2). Then change in properties of bitumen with application of crumbed rubber modifier was investigated. During this observation, initially 65 gm bitumen was taken and then partial application of

Table 2 Crumb rubber properties

Sl. No.	Crumb rubber properties	Tested value
1.	Moisture content	0.69%
2.	Specific gravity	1.02

crumb rubber modifier applied for 4, 8, 10, 12, and 14% of crumbed rubber. Changes in the properties were noted for each application.

5.1 Specific Gravity Test of Normal Bitumen

The specific gravity is very much influenced by the chemical formation of binder. It is defined as the ratio of the densities of any material to some other material where one is considered as the standard. For solids and liquids, water is considered as the standard one. Standard temperature is maintained at 27 ± 0.10 °C. The specific gravity confirmation is accomplished by supporting IS: 1202-1980. Test result for VG 30 bitumen was obtained as 1.02 and as per the mentioned IS code the range given as 0.98–1.30. Hence the test result is within satisfactory limit.

5.2 Penetration Test

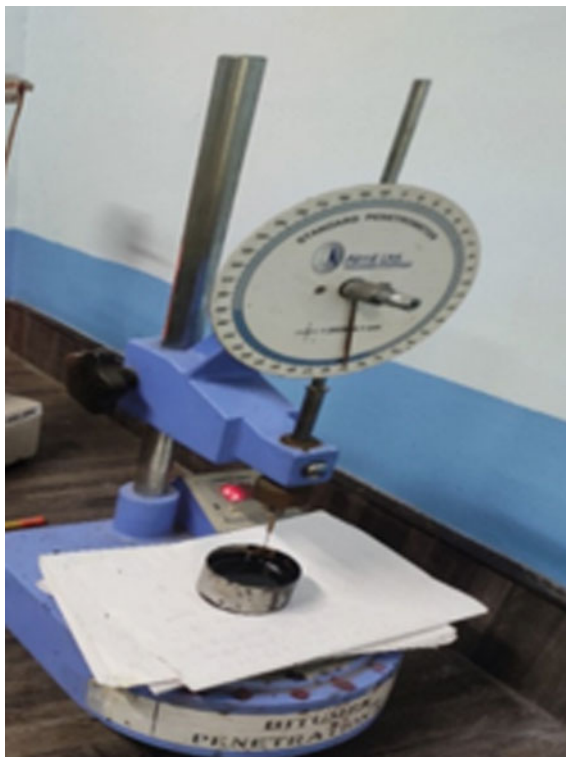
Penetration test is one of a measurement of consistency of bitumen. Grading of bitumen is decided by seeing the penetration of a regular needle vertically beneath the surface of bitumen under specified circumstance of ordinary load, period, and temperature (Fig 2). The penetration test is carried out as per IS: 1203-1978.

It can be concluded from Table 3, penetration value of normal bitumen was 66.67 mm which is reducing continuously with addition of percentage of crumb rubber (Fig. 3).

5.3 Softening Point Test

Bitumen suddenly does not change its state from semi solid to liquid, it progressively becomes softer with rise of temperature and then ultimately start flowing. The objective of this experiment is to determine a lowest temperature at which bitumen conquers a specific extent of softening. Ring and Ball test apparatus is used to find Softening point of Bitumen and CRMB. The experimental method is based as per IS: 1205-1978 (Fig. 4) (Table 4).

For various percentage of CRMB (0, 4, 8, 10, 12, and 14%), softening point is investigated and it is observed in Fig 6 that softening point is increasing continuously with the mounting percentage of crumbed rubber. Generally lower temperature susceptibility is indicated by the higher softening points and it is more acceptable in hot climate regions (Fig. 5).

Fig. 2 Bitumen penetration test**Table 3** Penetration test and results

% of Crumb rubber modifier (%)	Readings during	Trials			Average penetration value in mm	Permissible value as per IS: 1203-1978
		1	2	3		
0	Initial	0	0	0	66.67	60-70
	Final	68	65	67		
4	Initial	0	0	0	54.66	
	Final	50	54	60		
8	Initial	0	0	0	49.33	
	Final	44	48	56		
10	Initial	0	0	0	38.67	
	Final	33	37	47		
12	Initial	0	0	0	19	
	Final	18	19	20		
14	Initial	0	0	0	15	
	Final	16	14	15		

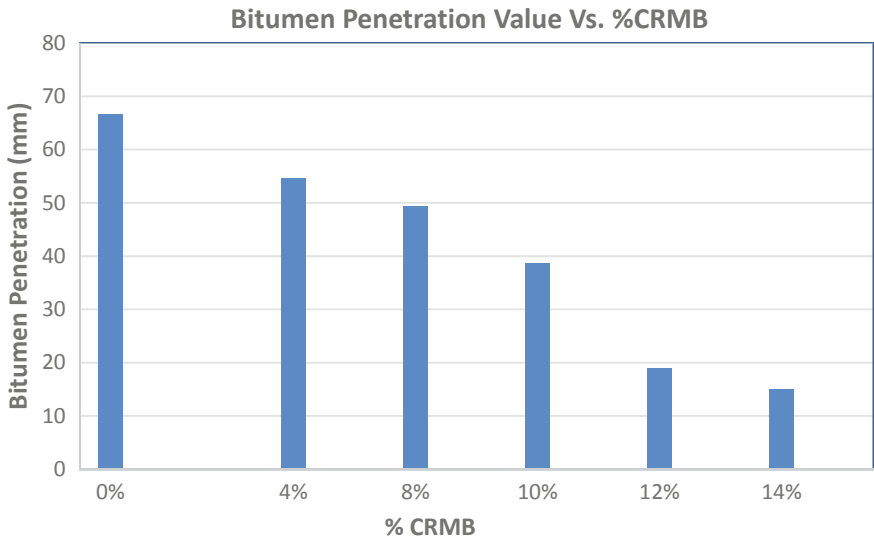


Fig. 3 Relationship between penetration (mm) and % CRMB

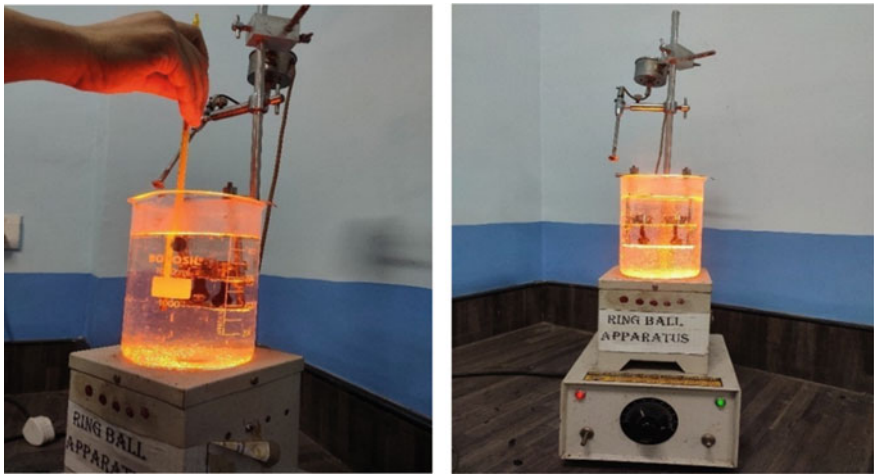


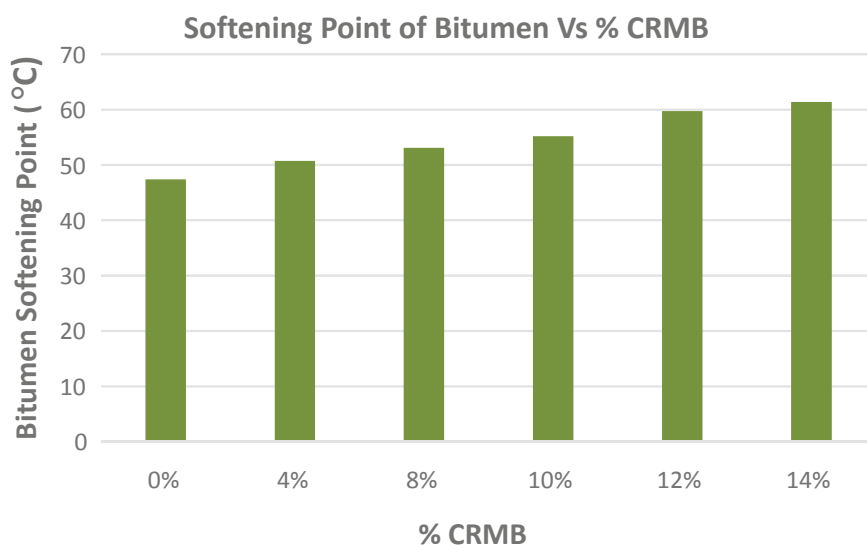
Fig. 4 Ring and ball apparatus for measuring softening point of Bitumen

5.4 Ductility Test

Bituminous material is deliberated ductility through presenting a distance in cm at which the test sample starts lengthen prior to breaking when the standard briquette specimen of the material is dragged away from each other by maintaining a particular

Table 4 Softening point test and results

% of CRMB (%)	Temp. (°C) Reading I	Temp (°C) Reading II	Average Value of Softening Point (°C)	Permissible Limit As per IS:1205-1978
0	47	47.8	47.40	40–55 °C
4	50	51.5	50.75	
8	53	53.2	53.10	
10	55	55.4	55.20	
12	59	60.5	59.75	
14	62	60.8	61.4	

**Fig. 5** relationship between softening point versus % CRMB

steady speed of 50 mm/min at a specified temperature. The ductility test was carried out based on IS: 1208-1978.

Ductility test was carried out for both neat bitumen and for CRMB as well. It was seen that, ductility value is decreasing (Table 5, Fig. 7) with hike in crumb rubber modifier percentage and that indicates subsequent conversion into stiffer material.

Fig. 6 Ductility test



Table 5 Ductility test and results

% of CRMB (%)	Sample Reading in cm			Average Ductility Value in cm	Permissible Limit as per IS:1208-1978
	Reading 1	Reading 2	Reading 3		
0	76	77	75	76	
4	68	72	69	69.67	
8	57	59	58	58.00	
10	52	55	53	53.33	
12	49	52	50	50.33	
14	40	41	43	41.33	

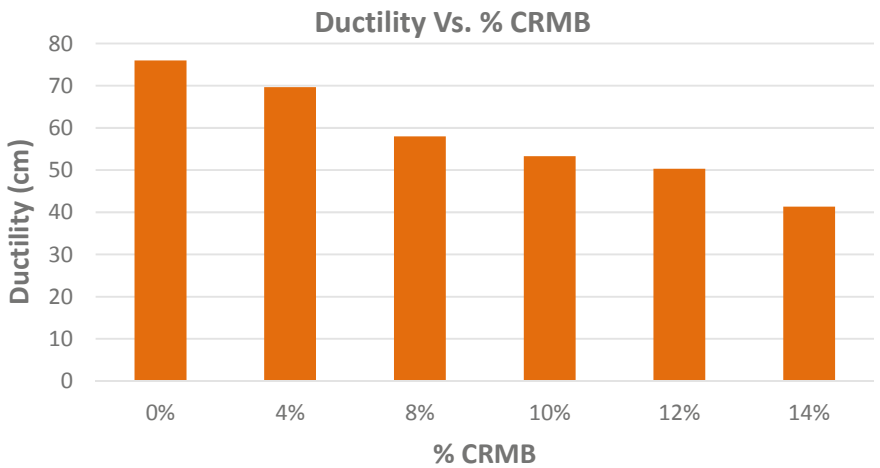


Fig. 7 Relationship between Ductility and % CRMB

Table 6 Flash point and fire point test and results

% of CRMB (%)	Flash point (in °C)	Fire point (in °C)
0	180	220
4	190	210
8	210	235
10	220	250
12	235	265
14	260	280

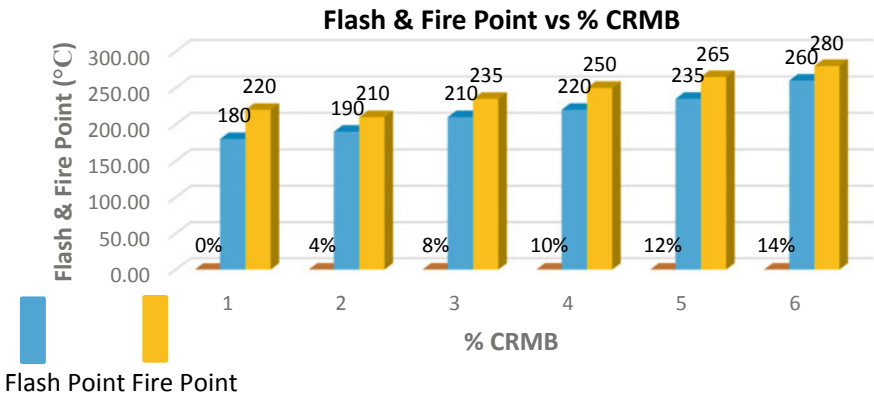


Fig. 8 Relationship between flash point and fire point versus % CRMB

5.5 Flash Point and Fire Point Test

These tests are considered as the safety check carried out on bituminous materials and it is a deciding test of determining the minimum temperature from which bituminous materials can protect from fireplace risks all through its applications.

Flash point is the minimum temperature at which bituminous material tends to get spark on the experimental sample. Fire Point is the least temperature at which the material gets lit and be on fire under mere circumstance of check. The experiment was carried out by following IS1209-1981 (Table 6) (Fig. 8).

With continuous inclusion of crumb rubber modifier, flash point and fire point of the material getting increased. This indicates employing of CRMB gives the preventative process after a little longer time than the normal bitumen.

6 Conclusion

Seeing the experimental results following statements can conclude:

- Neat bitumen becomes harder with successive addition of crumb rubber modifier. Its penetration value decreases, softening point and flash point and fire point increases. It implies crumb rubber modifier provides benefit in form of additional strength to the road.
- From the ductility test result we can conclude that the addition of rubber waste will make the bitumen harder. Addition of crumb rubber up to 12% gives a good result (50.33 cm), because ductility value less than 50 cm is not suitable for the construction of roads [10].
- So, we can conclude that application of crumb rubber is so much effective and useful in the formation of strengthen roads. The durability of the crumb rubber modified bituminous road is also increased than that of bituminous road up to a certain replacement of crumb rubber with bitumen.
- On the other hand, we can use this research further as economically effective as the price of crumb rubber is low with respect to the bitumen or hydrocarbon materials. Hence, if we substitute the required bitumen with the crumb rubber for making a bituminous road, cost optimization also happens there.

References

1. Bhatia A (2017) Play grounds for children from scrap tyres, 5 IIT students came up with this idea to recycle waste. <https://swachhindia.ndtv.com/playgrounds-children-scrap-tyres-5-iit-students-came-idea-recycle-waste-7481/>. Accessed 12 May 2017
2. Magar NR (2014) A study on the performance of crumb rubber modified bitumen by varying the sizes of crumb rubber. *Int J Eng Trends Technol (IJETT)* V14(2):51–56, ISSN:2231-5381. <https://doi.org/10.14445/22315381/IJETT-V14P211>
3. Mashaan NS, Ali AH, Karim MR, Abdelaziz M (2012) An overview of crumb rubber modified asphalt. *Int J Phys Sci* 7(2):166–170. <https://doi.org/10.5897/IJPSX11.007>
4. SenthilVadivel T, Thenmozhi R, Doddurani M (2012) Experimental study on waste tyre rubber reinforced concrete. *J Struct Eng, Struct Eng Res Centre Chennai (India)* 39:291–299
5. SenthilVadivel T, Thenmozhi R (2012) Experimental study on waste tyre rubber replaced concrete—an ecofriendly construction material. *J Appl Sci Res* 8(6):2966–2973
6. Mashaan NS, Ali AH, Karim MR, Abdelaziz M (2011) Effect of blending time and crumb rubber content on compacting-properties of crumb rubber modified asphalt binder. *Int J Phys Sci* 6(9):2189–2193
7. Justo CEG, Veeragavan A (2002) Utilization of waste plastic bags in bituminous mix for improved performance of roads. In: Centre for Transportation Engineering, Bangalore University, Bangalore, India
8. Becker Y, Mendez MP, Rodriguez Y (2001) Polymer modified asphalt. *Vision Tecnologica* 9(1):39–50
9. Abdelrahman MA, Carpenter SH (1999) Mechanism of interaction of asphalt cement with crumb rubber modifier. *Transp Res Record: J Transport Res Board* 1661:106–113
10. Ministry of Road Transport & Highways (MORT & H), Specifications for road and bridge works

Effect of Fly Ash Inclusion on Fresh and Hardened Properties of Concrete: A Review



Subhadip Pramanik, Shashwati Soumya Pradhan, and Umesh Mishra

Abstract Cement is an essential ingredient in concrete and its consumption is directly linked to the development of the country's infrastructure. The production of cement emits a large quantity of CO₂ by consuming a high energy consumption. The utilization of cement as an environmentally hazardous construction material should be curtailed to establish a more sustainable future. Fly ash (FA) is a solid hazardous material produced primarily by thermal power plants that negatively affect the environment by polluting air, soil, groundwater and human health such as lungs, kidneys, breathing problems etc. As a result, FA utilization has to become a growing concern in developing countries. FA can be partially replaced in concrete as a substitute material for cement. This literature review aims to demonstrate the partial substitution of FA for cement for analyzing the workability by slump test and other hardened properties of concrete in terms of compressive, flexural, split tensile strength and modulus of elasticity. This article summarizes numerous studies that evaluate the influence of various waste materials on the properties of FA-based concrete.

Keywords Fly ash · Compressive strength · Flexural strength · Split tensile strength · Modulus of elasticity

1 Introduction

Cement is an essential component of concrete as a binding material with adhesive and cohesive properties [1]. As increases in the demand for concrete, cement production will be increased, and concrete production will be 1.5–3 tons per capita per year [2]. In the world, India is the second position for the production of cement after China [3]. It will generate a major amount of CO₂ during cement production, i.e., producing one ton of cement will yield about one ton of CO₂ [4] and use a high energy level [5]. Almost 7% of the CO₂ gas emission [6] and a total of 5–6% of

S. Pramanik (✉) · S. S. Pradhan · U. Mishra
National Institute of Technology, Agartala, Tripura, India

global SO₂ emission from the cement manufacturing industry [7]. Some agricultural and industrial waste materials such as fly ash (FA) [8], rice husk ash (RHA) [9], wheat straw ash [10], ground granulated blast furnaces slag (GGBS) [11], nano silica (NS) [12] were substituted for cement to enhance the characteristics of concrete and thus cut carbon dioxide emissions.

FA is a complex heterogeneous by-product of coal combustion residue in the thermal power station [13]. FA or pulverized fuel ash can be collected using a suitable process such as an electrostatic precipitator or mechanical dust collector [14]. In conjunction with the rapid growth of thermal power stations, the production of FA will increase [15] and its use becomes more important in society today. According to the central electricity authority thermal civil design division, New Delhi, the total number of thermal power stations is 197, producing about 226.13 million tons of FA each year and maximum FA used in India is 83% in different sectors [16]. ASTM classified FA into two classes as Class C and Class F. For cement production when FA is used, this type of cement is called 'Pozzolana Portland cement' [17]. According to IS 1489-2000, the production of Portland pozzolana cement, a maximum of 35% of FA will be used. The size of FA particles plays an essential part in fly ash-based concrete due to the finer particles improve the strength of concrete, increase the heat of hydration, reduce shrinkage and expansion etc. [18]. Increasing the fineness of FA, the concrete becomes more resistant to chloride penetration and improves the mortar's mechanical properties, such as reducing the water requirement, improving the strength and resistance to sulfate solution [19].

FA in concrete reduces the concrete water sorptivity and chloride in permeation and less the drying shrinkage. From a previous study, it was found that FA-based concrete improves the durability of concrete [6]. As the FA particles are smooth, spherical and finer than cement particles improve the workability with lower water cement (w/c) ratio, leading to higher compressive strength at a later stage [20]. FA substitution in concrete reduces the heat of concrete hydration as a result, it reduces the inside hairline crack [21]. It was concluded that FA in concrete mix retards the setting time, reduces bleeding, improves the surface finishing and pumping characteristics of concrete [22]. The use of FA in concrete will decrease hardened concrete permeability and reduce the cost of concrete [23]. Researchers found that concrete shrinkage will be the same as control concrete in FA inclusion [24]. Some adverse effects can occur by increasing the percentages of fly ash in concrete which decreases the ultimate compressive strength [25]. In presence of water, the pozzolanic reaction occurs between FA and cement in the concrete which required more curing than conventional concrete [14]. Due to their excellent performance and environmental friendliness, the researcher found that FA-based cement is an excellent alternative to OPC [26]. The current article encapsulates a detailed analysis of the partial replacement of FA in cement to achieve more economically and environmentally sustainable construction. Additionally, it has focused on the application of various pozzolanic and non-pozzolanic waste materials on FA-based concrete.

2 Effect of FA on Human and Environment

The maximum quantity of fly ash generated by a thermal power plant creates major disposal problem. This effect on the environment and human health that described below:

2.1 Effect of FA on Humans

For longer inhalation of FA causes severe effect on the human health such as silicosis, fibrosis of lungs, pneumonitis and bronchitis etc. [27]. In the production of FA, it will emit CO, SO, NO, PM and some heavy metal that creates problems on human health such as lung cancer, asthma, cough, headache and chronic obstructive pulmonary disease, etc. [28]. When FA contains excess arsenic, antimony, cadmium and lead, it affects human health. The extra amount of arsenic effects on human health are kidney failure, breathing problems, vomiting, headaches, etc. Effects of antimony are heart problems, skin irritation, lungs problem, hepatitis, anorexia and chest pain etc. Effects of cadmium are stomach cramps, vomiting, diarrhea, liver injury and kidney damage etc. The effects of leads are abdominal pain, nausea, headache, weakness, weight loss, constipation and dispersion of thyroid, etc. [29].

2.2 Effect of FA on Environment

FA disposal in an open field can pollute air, soil and groundwater [30]. FA has a fine particle and is lighter in weight makes it tough to control in the dry state. The flying FA particle corrodes structural elements and affects horticulture [27]. Near the thermal power plant (TPP), the land becomes infertile and transfers into a wasteland. Near the area of TPP, it will decrease flower cultivation and vegetation production and increase the wasteland [31]. The combustion of coal emits CO_x, NO_x and SO_x gas that causes pollution of soil, air and water. FA contains heavy metals such as a high quantity of copper, arsenic and selenium, affecting water and soil quality [28]. Due to the self-hardening properties of FA, it can be used in highway construction as a substitute material for soil to improve the effectiveness and durability of the base course of the road. There is a possibility heavy metals from the FA migrating to the groundwater system can contaminate the drinking water source [32].

3 Fresh Concrete Properties

3.1 Slump

The slump test is a frequently used method for finding out the workability of concrete [33]. When FA is used in concrete, 10–50% with w/c 0.4–0.6 improve the workability of concrete and reduce the demand for water for getting desired slump [34]. When alkali activated FA slag (AAFS) was used to prepare concrete, the result shows that the workability of concrete was less than ordinary concrete due to the presence of silicate, which brings a sticky characteristic [35]. The M15 grade of concrete with a W/C ratio of 0.55 with partial substitution of FA (up to 10%) with RHA (up to 10%) affects concrete slump value. It was concluded that the percentage of increases of FA and RHA, reduces the slump of concrete. The highest slump value was obtained for conventional concrete (42 mm) and the lowest slump value was for mixes of 10% FA with 10% RHA-based concrete (20 mm) [36]. When cement is replaced partially by FA (15–30% by weight) and PPF (0.05–0.2% by volume), then the result indicates that the workability of concrete decreases [37]. The researcher used some amounts of nano particles (0.5–3%) such as nano TiO_2 (NT), nano CaCO_3 (NC) and a combination of NT and NC (NTC) with FA-based concrete. The results identified that slump value only increases with the application of 0.5% of nano particles and reduces as the percentage of nano particles increases [38]. Using M25 grade of concrete revealed that the variations of slump value were achieved as the percentage of FA and GGBS increased and maximum slump obtained at 5% GGBS with 10% FA-based mix [39]. By increasing FA (0–60%) in a fresh concrete mix with w/b ratio of 0.47, the slump value rises, as illustrated in Fig. 1. It also clearly demonstrates that every 10% increase in FA results in an increase of approximately 10–15 mm in slump value [40].

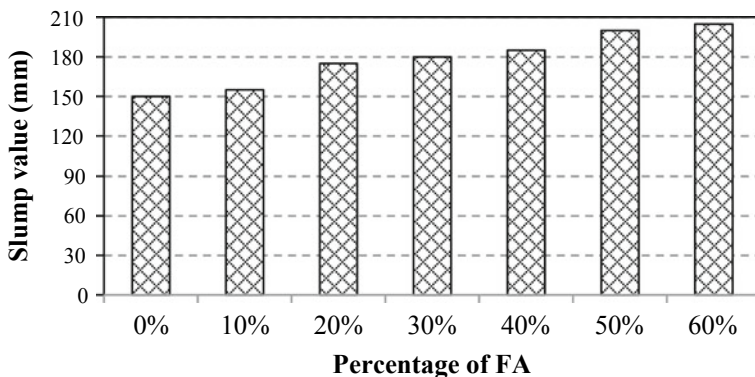
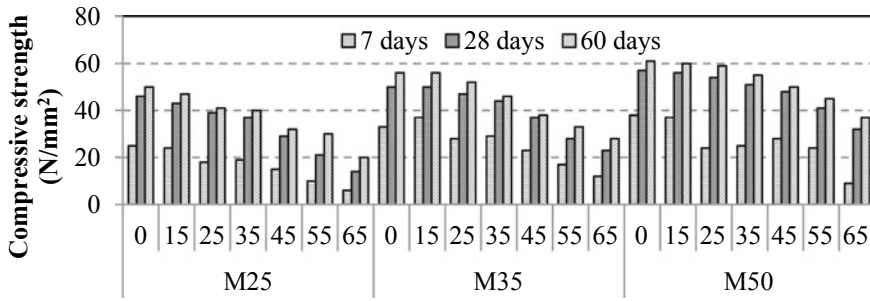


Fig. 1 Slump of concrete with different percentages of FA [40]

4 Hardened Concrete Properties

4.1 Compressive Strength

The most crucial test to evaluate the hardened concrete properties is compressive strength [41]. Many researchers found that compressive strength decreases when a higher quantity of FA is added to the mix. The secondary hydration is slower in the earlier age due to pozzolanic action in FA-based concrete [5]. As concrete mixed with High-loss on ignition (LOI)-based FA, it absorbs more water and necessitates more chemical admixtures, resulting in a strength reduction. For this reason, low LOI-based FA was more preferable to high LOI-based FA [42, 43]. Based on the fineness of class 'F' FA, it is classified into two components as Original Fly Ash (OFA) and Classified Fly Ash (CFA). The medium particle size of OFA and CFA is 19.1 μm and 6.4 μm respectively. Finer particles of FA improve the strength of concrete. The researcher identified that CFA in concrete gives higher compressive strength than OFA [44]. When FA and RHA partially replaced by cement with 0.75% of steel fiber, it will provide maximum compressive strength after curing of 28 days. The unit weight of concrete decreases with its strength by immersing concrete in H_2SO_4 solution for 30 days [45]. In concrete, when ultra-fine fly ash (UFFA) partially replaced cement, the compressive strength increased along with the long-term durability. As UFFA has a greater surface area for hydration, the pozzolanic reaction will be accelerated. Because of the increased heat of hydration, the UFFA gives higher early age strength than class 'F' FA-based concrete [1]. The compressive strength gets affected when FA and small amounts of NS are used to replace cement significantly. NS and FA react with calcium hydroxide then a binder material is formed. FA partially replaced cement by 20%, 30% with NS 1.5%, 3% and 4.5% by weight to prepare M30 grade concrete. The researcher found that substituting up to 3% of NS with 20% of FA increases the strength of concrete, while further inclusion of NS or FA decreases the strength of concrete [3]. The researcher found that in FA-based concrete when the fine aggregate was partially replaced by bottom ash (10–40%), the compressive strength increases [17]. The strength of M25 grade concrete prepared with FA (0–10%), GGBS (0–20%) was determined after 3, 14, 21 and 28 days. After 28 days, maximum strength was obtained when 30% cement was replaced with FA (10%), GGBS (20%) and the strength was greater than the reference mix. The researcher designed for different grades of concrete such as M25, M35, M50 and then cement was replaced by FA at 15–65%. After specified curing period the strength reduces when FA inclusion increases, as represented in Fig. 2. FA-based concrete is more economical than conventional concrete, as reported by the researcher [8].



Percentage of fly ash replacement with different grade of concrete

Fig. 2 Compressive strength of FA-based concrete of different grades [8]

4.2 Flexural Strength

The researcher conducted experiment using RHA (0–15%) and FA (15–30%) to partially replace cement. The maximum flexural strength for the M25 grade of concrete was obtained with a mixture of 22.5% FA and 7.5% RHA, resulting in a 4.57% increase in strength over control concrete after 28 days [46]. In another study, cement was partially replaced by FA (10, 15, 20, 30 and 40%) with a lesser amount of glass fiber (0.25%) to check the flexural strength of concrete. The findings suggest that FA and fiber addition increase the strength except for the 40% replacement of FA. The maximum flexural strength was obtained for the replacement of 20% FA with glass fiber [47]. For M20 grade of concrete, when cement was replaced by FA (20 and 30%) and NS (1.5–4.5%), the result shows that the maximum strength obtained for 20% FA with NS 3% compared to control concrete. Further increase in FA or NS will decrease the strength of concrete [3]. When the low calcium FA (20, 40 and 60%) and Na_2SO_4 (2%) partially replaced cement, it improves the flexural strength. The test results revealed that sulphate activation enhances the early age strength for all levels of FA inclusion. The concrete containing up to 40% fly ash has higher flexural strength than control concrete [48]. The research revealed that replacing cement with FA (15% by weight), nano CaCO_3 (1–4% by weight) and polyvinyl alcohol (PVA) fiber (0.05–0.2% by volume) affects the flexural strength of concrete. The maximum strength will be achieved by substituting 3% replacement of nano CaCO_3 (7.91 MPa) than the control mix strength (6.53 MPa). Additionally when up to 0.15% of PVA fiber is applied, the strength increases slightly [49]. When cement was replaced by FA (10–30%) with Hooked End Steel Fiber 1–3% (HESF) in concrete (M30 grade), the flexural strength increased. The researcher stated that increasing in the percentage of HESF would result in an increase in flexural strength. The maximum strength will be obtained to replace 20% FA with 3% HESF and this strength will be greater than reference mix [50]. The temperature of ordinary concrete rises, the flexural strength

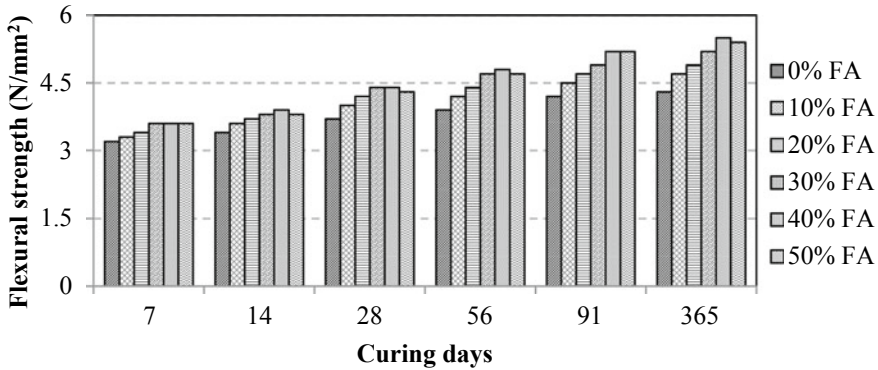


Fig. 3 Flexural strength of FA-based concrete [17]

decreases [51]. The researchers examine the impact of high temperature on the flexural strength when it was partially substituted with FA (10–30% by weight) and heated for 1 h, 2 h, 3 h in an electric oven at for 100 °C, 200 °C, 250 °C respectively. The sample was tested immediately after removal from the oven. When the temperature is raised, the flexural strength decreases with or without the presence of FA in the mixture. But FA-based concrete that contents up to 20% of FA shows improved flexural strength than conventional concrete without FA [52]. Another study used Class ‘F’ FA in concrete as 10–50% for a replacement of fine aggregate and found that the flexural strength increases as curing time and percentage of FA inclusion increase, as shown in Fig. 3 [17].

4.3 Split Tensile Strength

FA can be used in place of cement substitute material or as fine aggregate, depending on the particle size [53]. The cement was replaced partially by FA (40–60%) and the test was done up to 900 °C, obtain decreases the strength. The increase in temperature up to 300 °C increases the strength and further increments decrease the strength [54]. The researcher experimented by using 5–30% FA with 5–20% metakaolin. The results show that the mixture of 30% FA and 15% metakaolin-based concrete gives maximum split tensile strength compared to the reference mix [55]. The higher strength was obtained by mixing 5% FA and 5% RHA, which improved 11.4% and 15.2% strength, respectively compared to control concrete after curing 7 and 28 days. Further increment of FA and RHA content would result in a reduction in strength [36]. The maximum split tensile strength would be generated for the application of 9% GGBS and 40% FA after 28 days of curing for the M25 grade of concrete when cement was partially replaced by FA (20–60%) and GGBS (5–10%)[56]. Maximum strength was observed when 1% of

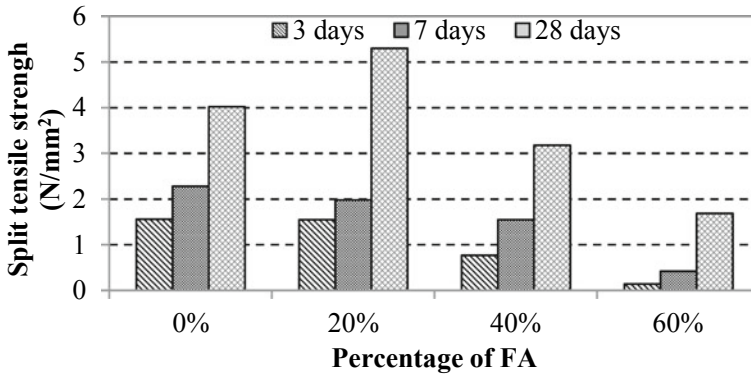


Fig. 4 Split tensile strength of FA based concrete [53]

steel fiber was used in conjunction with 20% FA and also, by using 1% of polypropylene fiber with 20% of FA gives maximum split tensile strength [57]. Figure 4 depicted the split tensile strength of concrete as a function of the increasing FA percentage at various ages of curing [53].

** L35F20: Low-LOI content 20% FA (35 MPa Compressive strength).

**H35F20: High-LOI content 20% FA (35 MPa Compressive strength).

4.4 Modulus of Elasticity

The term modulus of elasticity (E_m) is referred to as the secant modulus [42]. Its value changed when cement was partially replaced by FA and polypropylene fiber reinforced (PPFR) added in the mix. Application of FA is 15–30% and Polypropylene Fiber Reinforced (PPFR) is 0.05–0.2%. In this experiment, E_m of concrete was taken as 40% of maximum concrete stress. The researcher does not explain the effect of the E_m of concrete. But using 0.05% of PPFR slightly improves the E_m value and further increases in the amount of PPFR (1 and 0.2%) reduce its value compared to ordinary concrete [37]. The study found that when FA was added to the concrete at 15–30% by mass and less amount of steel fiber reinforcement as 0.25–1.5% by volume of concrete, the FA had no significant effect on the E_m . It has been observed that using some amount of SF reinforcement in the absence of FA will improve the E_m slightly [58]. The researcher examined the impact of replacing cement with Class 'F' FA (both low-LOI FA and high-LOI FA) as 20–80% on the E_m of concrete. The results show that the E_m increases as the curing period increases from 28 to 365 days in the mix containing 60% FA but increasing FA content to 80% reduces the E_m as depicted in Fig. 5 [42].

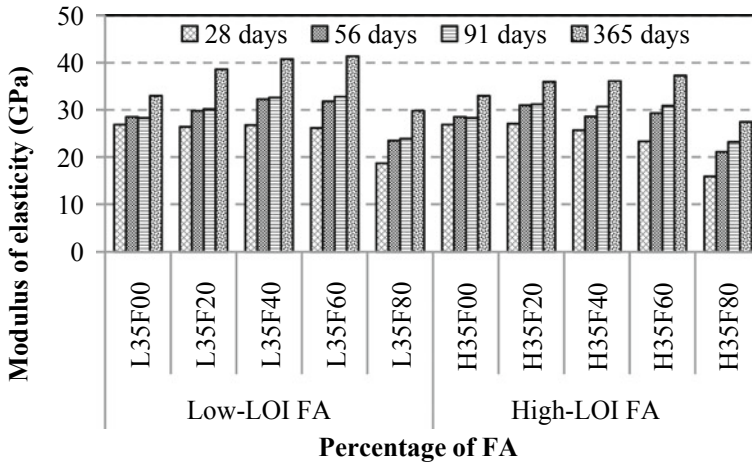


Fig. 5 Modulus of elasticity of FA-based concrete [42]

5 Conclusions

The following conclusion can be reached based on findings from this study:

- FA-based concrete characteristics are influenced by various parameters such as physical properties with the chemical composition of FA, properties of additional additives, percentage of FA inclusion, curing period and exposure condition etc.
- Addition of small amount of FA with a fixed amount of w/c ratio improves the slump without any superplasticizer addition.
- The incorporation of FA, i.e., 20–60% in the mix shows higher hardened concrete strength and can be used advantageously for structural application. However, beyond 60% of FA tends to decrease the strength.
- Additional research is required to evaluate the durability aspect of concrete when FA is partially substituted with cement in concrete for structural component.
- The pozzolanic properties of FA, have the potential to be utilized effectively as a partial cement substitute in concrete by reducing cement consumption and pollution.

References

1. Supit SWM, Shaikh FUA, Sarker PK (2014) Effect of ultrafine fly ash on mechanical properties of high volume fly ash mortar. *Constr Build Mater* 51:278–286. <https://doi.org/10.1016/j.conbuildmat.2013.11.002>
2. Glavind M (2009) Sustainability of cement, concrete and cement replacement materials in construction. Woodhead Publishing Limited
3. Reddy NNP (2020) Experimental investigation on strength of concrete by using fly ash and nano-silica as partial replacement to the cement. *Op Acc J Bio Sci Res* 3(4):1–5. <https://doi.org/10.46718/JBGSR.2020.03.000077>
4. Pradhan SS (2021) Silpozz and steel slag on mechanical properties of concrete. *Lect Notes Civ Eng* 124 LNCE:451–459. https://doi.org/10.1007/978-981-33-4590-4_43
5. Joshi R (2017) Effect on compressive strength of concrete by partial replacement of cement with fly ash. *Int Res J Eng Technol* 4(2):315–318 [Online]. Available: <https://irjet.net/archives/V4/i2/IRJET-V4I2392.pdf>
6. Nath P, Sarker P (2011) Effect of fly ash on the durability properties of high strength concrete. *Procedia Eng* 14:1149–1156. <https://doi.org/10.1016/j.proeng.2011.07.144>
7. Zou F, Hu C, Wang F, Ruan Y, Hu S (2020) Enhancement of early-age strength of the high content fly ash blended cement paste by sodium sulfate and C-S-H seeds towards a greener binder. *J Clean Prod* 244:118566. <https://doi.org/10.1016/j.jclepro.2019.118566>
8. Chakraborty J, Banerjee S (2016) Replacement of cement by fly ash in concrete. *Int J Civ Eng* 3(8):58–60. <https://doi.org/10.14445/23488352/ijce-v3i8p110>
9. Sabat L, Pradhan SS (2020) Experimental evaluation of a composite material using GFRC
10. Bheel N, Haziman M, Ibrahim W, Adesina A, Kennedy C, Ali I (2021) Mechanical performance of concrete incorporating wheat straw ash as partial replacement of cement. *J Build Pathol Rehabil* 7:1–7. <https://doi.org/10.1007/s41024-020-00099-7>
11. Swaroop AHL, Venkateswararao K, Kodandaramarao PP (2013) Durability studies on concrete with fly ash & Ggbs. *Int J Eng Res Appl* 3(4):285–289
12. Yamini G, Siddiraju S (2016) An experimental research on strength properties of concrete by the influence of flyash and nanosilica as a partial replacement of cement. *Int J Civ Eng Technol* 7(3):306–315
13. Vu DH et al (2019) Composition and morphology characteristics of magnetic fractions of coal fly ash wastes processed in high-temperature exposure in thermal power plants. *Appl Sci* 9(9). <https://doi.org/10.3390/app9091964>
14. Patil JV (2017) Partial replacement of cement by fly ash in concrete mix design. *Int Res J Eng Technol* 4(11):1148–1150
15. Alam J, Akhtar MN (2011) Fly ash utilization in different sectors in Indian scenario. *Int J Emerg Trends Eng Dev* 1(1):1–14
16. T. Civil, D. Division, and N. E. W. Delhi, “Report on fly ash generation at coal/lignite based thermal power stations and its utilization in the country for the year 2019–20 central electricity authority no. Nov, 2020
17. Siddique R (2003) Effect of fine aggregate replacement with class F fly ash on the abrasion resistance of concrete. *Cem Concr Res* 33(11):1877–1881. [https://doi.org/10.1016/S0008-8846\(03\)00212-6](https://doi.org/10.1016/S0008-8846(03)00212-6)
18. Hemalatha T, Ramaswamy A (2017) A review on fly ash characteristics – Towards promoting high volume utilization in developing sustainable concrete. *J Clean Prod* 147:546–559. <https://doi.org/10.1016/j.jclepro.2017.01.114>
19. Chindaprasirt P, Chotithanorm C, Cao HT, Sirivivatnanon V (2007) Influence of fly ash fineness on the chloride penetration of concrete. *Constr Build Mater* 21(2):356–361. <https://doi.org/10.1016/j.conbuildmat.2005.08.010>
20. Zala LB (2012) Experimental investigations on partial replacement of cement replacement of cement with fly ash in design, Oct 2012

21. Berryman C, Zhu J, Jensen W, Tadros M (2005) High-percentage replacement of cement with fly ash for reinforced concrete pipe. *Cem Concr Res* 35(6):1088–1091. <https://doi.org/10.1016/j.cemconres.2004.06.040>
22. با. س. س.، “فانون در طب-سنا” p 283, 1386
23. Yazici Ş, Arel HŞ (2012) Effects of fly ash fineness on the mechanical properties of concrete. *Sadhana—Acad Proc Eng Sci* 37(3):389–403. <https://doi.org/10.1007/s12046-012-0083-3>
24. Marthong C, Agrawal TP (2012) Effect of fly ash additive on concrete properties. 2:1986–1991
25. Sumathi A, Mohan KSR, Shankari GS, Sivasankari R (2014) Effect of fly ash on properties of fresh concrete. *Int J Appl Eng Res* 9(1):69–82
26. Xu G, Shi X (2018) Characteristics and applications of fly ash as a sustainable construction material: a state-of-the-art review. *Resour Conserv Recycl* 136(August 2017):95–109. <https://doi.org/10.1016/j.resconrec.2018.04.010>
27. Basu M, Pande M, Bhadoria PBS, Mahapatra SC (2009) Potential fly-ash utilization in agriculture: a global review. *Prog Nat Sci* 19(10):1173–1186. <https://doi.org/10.1016/j.pnsc.2008.12.006>
28. Munawer ME (2018) Human health and environmental impacts of coal combustion and post-combustion wastes. *J Sustain Min* 17(2):87–96. <https://doi.org/10.1016/j.jsm.2017.12.007>
29. Ayanda OS, Fatoki OS, Adekola FA, Ximba BJ (2012) Characterization of fly ash generated from Matla power station in Mpumalanga, South Africa. *E-Journal Chem* 9(4):1788–1795. <https://doi.org/10.1155/2012/451801>
30. Sett R (2017) Flyash : characteristics, problems and possible utilization. *Adv Appl Sci Res* 8(3):32–50 [Online]. Available: <https://pdfs.semanticscholar.org/dd3a/e6b7d5d8c5def2c6a67b76d477a5f875970f.pdf>
31. Dasgupta A, Paul S (2011) Fly ash and its impact on land : a case study of Kolaghat thermal power plant, Purba Medinipur, West Bengal. *Indian J Spat Sci* 2(2):1–11
32. Fan KK, Ouyang P, Wu X, Lu Z (2001) Some aspects of characterisation, utilisation and environmental effects of fly ash. *J Chem Technol Biotechnol* 76(1):9–26. [https://doi.org/10.1002/1097-4660\(200101\)76:1%3e9::AID-JCTB335%3e3.0.CO;2-5](https://doi.org/10.1002/1097-4660(200101)76:1%3e9::AID-JCTB335%3e3.0.CO;2-5)
33. Ravina D (1998) Mechanical properties of structural concrete incorporating a high volume of Class F fly ash as partial fine sand replacement. *Mater Struct Constr* 31(2):84–90. <https://doi.org/10.1007/bf02486469>
34. Mahajan L, Mahadik S, Bhagat SR (2020) Investigation of fly ash concrete by slump cone and compaction factor test. *IOP Conf Ser Mater Sci Eng* 970(1). <https://doi.org/10.1088/1757-899X/970/1/012011>
35. Fang G, Ho WK, Tu W, Zhang M (2018) Workability and mechanical properties of alkali-activated fly ash-slag concrete cured at ambient temperature. *Constr Build Mater* 172:476–487. <https://doi.org/10.1016/j.conbuildmat.2018.04.008>
36. Bheel N, Jokhio MA, Abbasi JA, Lashari HB, Qureshi MI, Qureshi AS (2020) Rice husk ash and fly ash effects on the mechanical properties of concrete. *Eng Technol Appl Sci Res* 10(2):5402–5405. <https://doi.org/10.48084/etasr.3363>
37. Karahan O, Atiş CD (2011) The durability properties of polypropylene fiber reinforced fly ash concrete. *Mater Des* 32(2):1044–1049. <https://doi.org/10.1016/j.matdes.2010.07.011>
38. Kumari K et al (2016) Nanoparticles for enhancing mechanical properties of fly ash concrete. *Mater Today Proc* 3(6):2387–2393. <https://doi.org/10.1016/j.matpr.2016.04.152>
39. Phul AA, Memon MJ, Shah SNR, Sandhu AR (2019) GGBS and fly ash effects on compressive strength by partial replacement of cement concrete. *Civ Eng J* 5(4):913–921. <https://doi.org/10.28991/cej-2019-03091299>
40. Shaikuthali SA, Mannan MA, Dawood ET, Teo DCL, Ahmadi R, Ismail I (2019) Workability and compressive strength properties of normal weight concrete using high dosage of fly ash as cement replacement. *J Build Pathol Rehabil* 4(1). <https://doi.org/10.1007/s41024-019-0065-5>
41. Jatale A (2013) Effects on compressive strength when cement is partially replaced by fly-ash. *IOSR J Mech Civ Eng* 5(4):34–43. <https://doi.org/10.9790/1684-0543443>

42. Huang CH, Lin SK, Chang CS, Chen HJ (2013) Mix proportions and mechanical properties of concrete containing very high-volume of Class F fly ash. *Constr Build Mater* 46:71–78. <https://doi.org/10.1016/j.conbuildmat.2013.04.016>
43. Chen H, Shih N, Wu C (2019) Effects of the loss on ignition of fly ash on the properties of high-volume fly ash concrete
44. Chindapasirt P, Jaturapitakkul C, Sinsiri T (2005) Effect of fly ash fineness on compressive strength and pore size of blended cement paste. *Cem Concr Compos* 27(4):425–428. <https://doi.org/10.1016/j.cemconcomp.2004.07.003>
45. Husk R, Steel U (2012) Effect of partial replacement of cement by fly. 3(6):1–9
46. Sathawane SH, Vairagade VS, Kene KS (2013) Combine effect of rice husk ash and fly ash on concrete by 30% cement replacement. *Procedia Eng* 51:35–44. <https://doi.org/10.1016/j.proeng.2013.01.009>
47. Barbuta M, Bucur R, Serbanoiu AA, Scutarasu S, Burlacu A (2017) Combined effect of fly ash and fibers on properties of cement concrete. *Procedia Eng*. 181:280–284. <https://doi.org/10.1016/j.proeng.2017.02.390>
48. Asad M, Ali B, Ali L, Aslam U, Hussain I, Masood B (2020) Case studies in construction materials effect of sulfate activator on mechanical and durability properties of concrete incorporating low calcium fly ash. 13. <https://doi.org/10.1016/j.cscm.2020.e00407>
49. Zhang P, Zheng Y (2019) Combined influence of nano-CaCO₃ and polyvinyl alcohol fibers on fresh and mechanical performance of concrete incorporating fly ash. Aug, pp 1–11. <https://doi.org/10.1002/suco.201900134>
50. Babu SK et al (2017) Comparative study on compressive and flexural strength of steel fibre reinforced concrete (SFRC) using fly. 8(3):1094–1102
51. MHÃ (2006) The effects of high temperature on compressive and flexural strengths of ordinary and high-performance concrete. 41:155–163. <https://doi.org/10.1016/j.firesaf.2005.12.002>
52. Potha Raju M, Shobha M, Rambabu K (2004) Flexural strength of fly ash concrete under elevated temperatures. *Mag Concr Res* 56(2):83–88. <https://doi.org/10.1680/macr.2004.56.2.83>
53. Pavan S, Rao SK (2014) Effect of fly ash on strength characteristics of roller compacted concrete pavement. *IOSR J Mech Civ Eng* 11(6):04–08. <https://doi.org/10.9790/1684-11620408>
54. Khan MS, Abbas H (2015) Effect of elevated temperature on the behavior of high volume fly ash concrete. *KSCE J Civ Eng* 19(6):1825–1831. <https://doi.org/10.1007/s12205-014-1092-z>
55. Lin MO (2016) Experimental study on split tensile strength of concrete with partial replacement of cement by flyash and, 7(6):73–81
56. Ali SA, Abdullah S (2014) Experimental study on partial replacement of cement by flyash and GGBS. 2(07):304–308
57. Professor A (2014) Effect of steel and polypropylene fibres on strength characteristics of fly ash concrete. *Int J Res Advent Technol* 2(3):2321–9637
58. Atiř CD, Karahan O (2009) Properties of steel fiber reinforced fly ash concrete. *Constr Build Mater* 23(1):392–399. <https://doi.org/10.1016/j.conbuildmat.2007.11.002>

Flexural Performance of Steel Fibre Reinforced Ternary Concrete Slabs



V. B. Reddy Suda

Abstract The paper reports an experimental study on the flexural performance of Conventional slab (CS), Ternary slab (TS) and fibrous ternary slab (TSF). Ground granulated blast furnace slag (GGBS) 30% and Micro silica (MS) 10% were used to cast ternary slabs and crimped steel fiber of four volume fractions i.e. 0.5, 1, 1.5 and 2% with aspect ratio 60, was added to the predetermined optimum ternary mix, obtained from strength studies to cast fibrous ternary slabs (TSF). The weight of supplementary cementing materials (SCMs) and steel fiber on flexural performance such as ultimate load, flexural toughness and energy factors were assessed. The results showed clearly that energy absorption and ductility increased by ternary slabs and further increased by the fibrous ternary slabs over conventional slabs.

Keywords Conventional slab · Ternary slab · MS · GGBS · Crimped steel fiber · Energy absorption · Ductility and energy factor

1 Introduction

The knowledge of ternary concrete (TC) has enormously developed for the reason that of its toughness, superior elastic modulus and predominantly under the sustainable constructions to minimize the emission of CO₂, which otherwise leads to environmental disorders. Industrial by products like Micro silica (MS) and (GGBS) have been used successfully for the past decades as supplementary cementing materials to develop blended concrete to meet the present infrastructure developments without compromising the construction delays. There is sufficient information regarding strength studies of ternary concrete made by MS and GGBS [1]. In the recent and the past, investigators attempted to assess the behavior of conventional slabs, but there is little to understand the effect of GGBS and MS on the strength of RC slabs, furthermore there is an insufficient research on the strength of ternary slabs by fiber. Thus, it is essential to know the performance of slabs. Uday Kumar et al. [2] conducted experimental study on flexural performance of glass fiber reinforced RC slabs with

V. B. R. Suda (✉)

Department of Civil Engineering, CMR Technical Campus, Hyderabad, Telangana, India

plastic rebar's (GFRP) and high strength deformed bars. They reported that load–deflection behavior up to first crack was almost equal in both the slabs and load carrying capacity of both slabs was observed similar at 50 mm deflection. Ramadevi et al. [3] has conducted experimentations on one way slab by using hybrid fiber of both Polypropylene and steel. They reported that the hybrid fiber slab ductility have shown better performance over the conventional slab. Maximum load and deflection also increased by 136.16% and 125% respectively over conventional slab. Finally, accomplished the HFRC slabs have shown better performance over conventional slabs in all respects.

1.1 Research Significance and Objectives

In this investigation, MS and GGBS up to 40% of the total cementitious material were used to cast ternary slabs and crimped steel fiber is incorporated in various volume fractions. The main objective of the study is to determine the flexural strength, load displacement behavior and to estimate the flexural toughness at yield and failure load. Investigational outcome on flexural characteristics like initial crack load, ultimate load capacity, energy absorption and ductility are reported.

2 Experimental Program

The program was designed, to cast conventional slab, ternary slab and fibrous ternary slabs made by adding four volume fractions (0.5, 1, 1.5 and 2%) of the steel fiber into the prearranged ternary mix [4]. All the slab panels are tested at 28 days to assess the flexural performance and the results are compared.

2.1 Material and mixing

Ordinary Portland cement (OPC) of 53 grade, Micro silica and GGBS was used in the study. Chemical and physical properties are given in the Table 1. Physical properties of fine and coarse aggregate have been shown in Table 2. Crimped steel fiber [5] of an aspect ratio 60 having density 7.85 gm/cm³ was used. Sulphonated Naphthalene based Formaldehyde (SNF), is used as chemical admixture to improve the slump. Figure 1 shows the materials used in the mix design was performed as per guideline given in IS: 10262-2009 and mix details are summarized in Table 3. Three groups of concrete mixtures like Conventional concrete was made by OPC, Ternary concrete made by predetermined quantities of MS and GGBS [1] and fibrous ternary mixtures were made by adding steel fiber. Concrete was mixed in a laboratory pan mixer for

Table 1 Oxide compositions of OPC, GGBS and Micro silica [4]

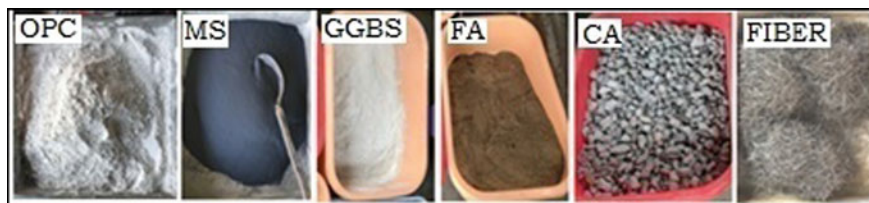
SCMs	Composition (%)								LOI ^a	IM ^b
	CaO	Al ₂ O ₃	FeO ₃	SiO ₂	MgO	Na ₂ O	K ₂ O	SO ₃		
OPC	63.69	4.88	3.82	21.41	1.56	0.47	–	2.36	–	–
GGBS	37.34	14.42	1.11	37.73	8.7	0.39	–	–	1.41	1.59
MS	0.02	1.2	0.74	92.9	1.0	0.42	1.32	0.1	1.8	–

^a Loss on ignition,

^b Insoluble material

Table 2 Physical properties of fine aggregate and coarse aggregate

Aggregate	Particle size (mm)	Specific gravity	Fineness modulus	Bulk density (kg/m ³)
Fine aggregate	<4.75	2.6	3.17	1793
Coarse aggregate	20, Angular	2.9	7.16	1603

**Fig. 1** Binding materials, aggregates and crimped steel fiber [4]**Table 3** Material quantity (kg/m³) and slump values [4]

Mix Id	Cement	MS	GGBS	FA	CA	Water	V _f	Weight	SP	Slump
							(%)	(kg)	(%)	(mm)
CC	324.0	–	–	785	1093	178	–	–	–	111
TC	194.8	32	97.2	785	1093	178	–	–	0.050	113
TCF _{0.5}	194.8	32	97.2	785	1093	178	0.5	39.25	0.304	112
TCF _{1.0}							1.0	78.50	0.460	110
TCF _{1.5}							1.5	117.8	0.610	108
TCF _{2.0}							2.0	157.0	0.688	106

FA Fine aggregate, CA Coarse aggregate, [TC] [OPC60%+MS10%+GGBS30%], V_f fiber volume fraction, [TCF_{0.5}] [OPC60%+MS10%+GGBS30%+Fiber0.5%]

a total of 6 min, by adding up MS and GGBS. All the batches were checked and adjusted to obtain desired slump before casting the slab panels.

2.2 Slab Details

Slabs were designed as per IS: 456-2000. High yield steel deformed bars of 10 mm dia. was used as main steel in both directions at 150 mm spacing. A total six slab specimens ($1200 \times 1200 \times 100$ mm) would be cast with 15 mm clear cover for testing. The specimens were categorized into conventional slab (CS), ternary slab (TS) and fibrous ternary slabs (TSF).

2.3 Casting and Testing of Slabs

Slab specimens were cast by filling the molds with workable mix and then entrapped air was removed by compacting it with wooden bars. Excess concrete is removed, finished smooth and white washed after curing. Loading frame was employed to test all the panels. Two-point loading system with capacity of hydraulic jack as 500 kN was engaged and the deflections were observed on the dial gauge placed at diagonal center. The steady load was applied with increment of 10 kN till the specimen fails and corresponding deflections were recorded. Figure 2 illustrates casting and testing of specimen.

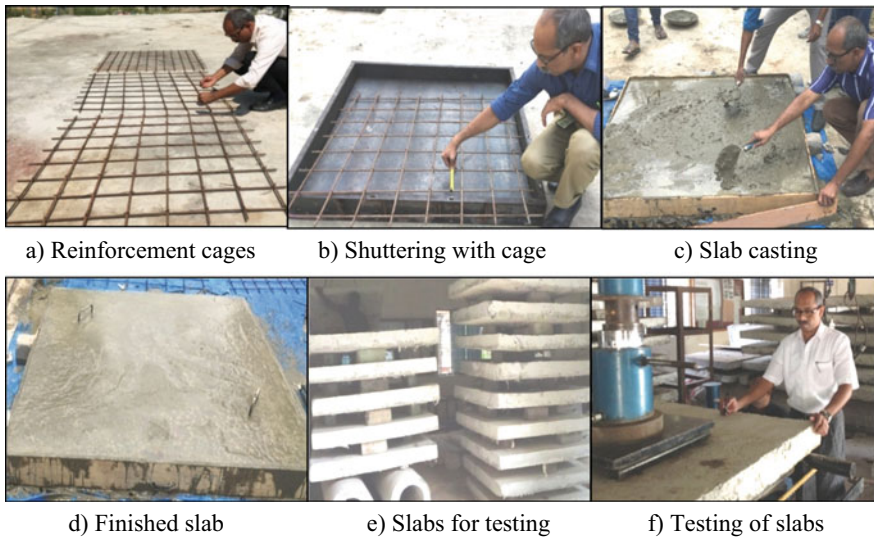


Fig. 2 Reinforcement cages, casting and testing of slabs

Table 4 Compressive strength, flexural loads and deflections

Slab Id	Compressive strength (MPa)	Flexural load (kN) at			Deflection (mm)	
		First crack	Yield	Failure	Yield	Failure
CS	36.50	16.8	41.0	56.0	2.80	4.20
TS	42.95	18.6	48.0	67.0	2.20	4.70
TSF _{0.5}	43.94	25.0	62.0	87.0	2.10	6.50
TSF _{1.0}	44.75	27.5	68.0	95.0	1.90	7.10
TSF _{1.5}	45.36	30.0	76.0	107.0	1.80	7.80
TSF _{2.0}	45.83	33.0	88.0	118.0	1.60	8.70

CS Conventional slab, TS Ternary slab, TSF_{0.5} Ternary slab with steel fiber 0.5%

3 Experimental Results

3.1 Slump of Concrete

The slump in Ternary concrete (TC) had shown an increment over Conventional concrete (CC) and then it was reduced with the increase in fiber volume in Fibrous ternary concrete (TCF) as specified in Table 3 and the quantity of super plasticizer was so adjusted to obtain the workable concrete.

3.2 Compressive Strength

The strength of TC had improved over CC which was 17.67%. Moreover, the strength of TCF improved continuously with steel fiber addition. The mixes TCF_{0.5} and TCF_{2.0} display an increment of 20.38% to 25.56%, respectively over CC and 2.31% to 6.71% over plain TC. The results demonstrate the beneficial advantage with addition of fiber to the TC mixes in Table 4.

3.3 Load Carrying Capacity

3.3.1 First Crack Load

Load carrying capacity at first crack was improved in ternary slab (TS) and fibrous ternary slab (TSF) over conventional slab (CS). It is about 10.7% higher than CS and further increased by TSF about 48.8% to 96.4% CS at 0.5% to 2.0% of fiber respectively over (CS). It means the first crack delays in ternary slabs and marginal delay was observed between TS and TSF and continued as the fiber content increases as presented in Table 4. Same trend was noticed at yield point.

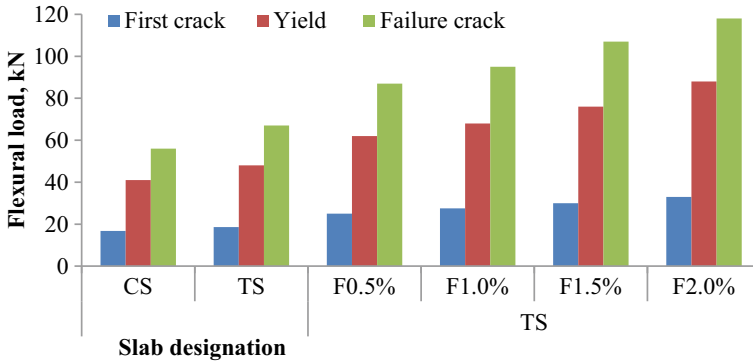


Fig. 3 Flexural load at initial, yield and ultimate

3.3.2 Ultimate Load

As the load increases initial cracks were enlarged and propagated and multiple crack number increased as the fiber content increases. Ultimate load carrying capacity of TS increased by 19.6% compared to CS. Further it is improved by TSF_{0.5} to TSF_{2.0} about 55.4% to 110.7% respectively as the fiber content increased from 0.5% to 2.0%, over CS as given in Fig. 3. Deflection at ultimate load was increased by TS and TSF_{0.5} to TSF_{2.0} over CS. It is about 1.12 times and 1.55–2.07 times respectively.

3.3.3 Load–Displacement Behavior

The load–displacement plots are given in Fig. 4. The deflection at failure load is improved in ternary slabs and further increased continuously as the steel fiber

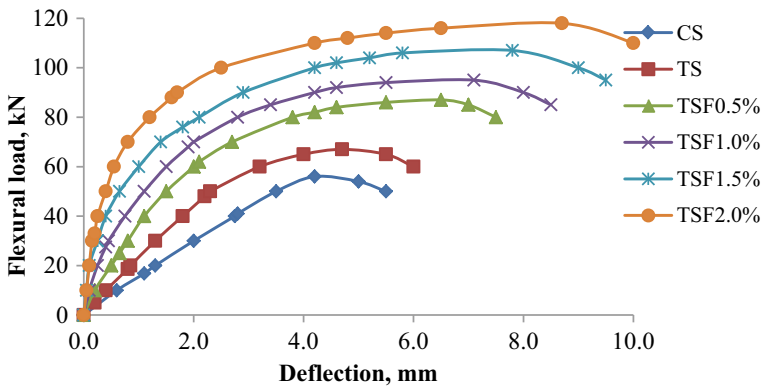


Fig. 4 P-Δ curves

Table 5 Flexural toughness, ultimate deflection, ductility and energy factor

Slab Id	Flexural toughness (kN.mm)		Ultimate deflection (mm)	Ductility factor	Energy factor
	$[E_y]$	$[E_u]$	$[\Delta_u]$	$[\mu] = [\Delta_u/\Delta_y]$	$[\eta] = [E_u/E_y]$
CS	57.4	117.6	4.20	1.50	2.05
TS	58.0	200.35	4.70	2.14	3.45
TSF _{0.5}	62.0	390.0	6.50	3.10	6.29
TSF _{1.0}	69.0	540.0	7.10	3.74	7.83
TSF _{1.5}	82.0	707.62	7.80	4.33	8.63
TSF _{2.0}	90.0	845.0	8.70	5.44	9.39

percentage as specified in Table 4 and the deflections of TS, TSF_{0.5} and TSF_{2.0} increased by 1.12, 1.55 and 2.07 times over CS. It was noticed from the $P-\Delta$ plots that the fibrous ternary slabs show steeper slope in ascending part over CS. The force–displacement plot of TSF had almost flat pattern at ultimate load with respect to CS and thus increasing the ultimate deflection.

3.4 Energy Absorption

3.4.1 Energy at Yield Load

The enclosed area of $P-\Delta$ plots of the Fig. 4 represents yield energy. A small increment of yield energy was observed by the TS over CS, however marginal increment was observed by the TSF. It is the effect of fiber which allows large deformation at failure load Table 5.

3.4.2 Flexural Toughness at Ultimate Load

Flexural toughness at failure load (E_U) is increased marginally by the TS and further enhanced continuously as the fiber content increases as specified in Table 5. E_U of TS, TSF_{0.5} and TSF_{2.0} is about 1.7, 3.32 and 7.19 times higher than CS. Noteworthy improvement in ultimate energy of fibrous ternary slabs is observed and thereafter the rate of growth is linear as revealed in Fig. 5.

3.4.3 Ductility Factor and Energy Factor

Ductility factor is increased linearly; the factor of TS, TSF_{0.5} and TSF_{2.0} is about 1.4, 2.1 and 3.6 times higher than CS. This is for the reason that contribution of fiber

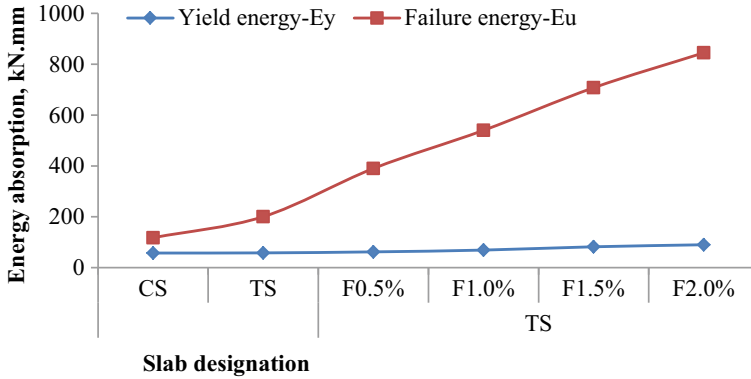


Fig. 5 Energy absorption variation

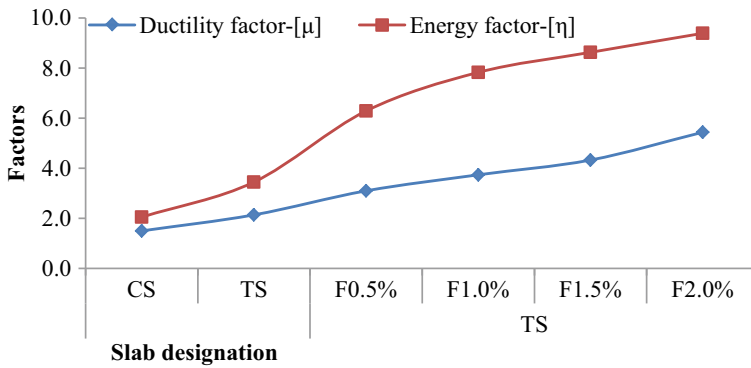


Fig. 6 Ductility and energy factors

which drives to enhance in ultimate deflection (Δ_u) and the rate of growth of Δ_u is more than yield deflection (Δ_y) as specified in the Table 5. It represents the delay in final failure of fibrous slabs.

Energy factor is also improved, but the rate of growth is superior to ductility factor. The factor in TS, TSF_{0.5} and TSF_{2.0} is about 1.69, 3.07 and 4.58 times higher than CS. It appears that the energy factors are highly subjective by fiber content as given in Fig. 6.

3.4.4 Mode of Failure

All the slabs show the yield lines and failed in flexure. Conventional slabs are reached to their ultimate stress earlier than Ternary and Fibrous ternary slabs. Failure cracks in number increased as the fiber quantity increases over CS. Failure mode of slab panels are illustrated in Fig. 7.

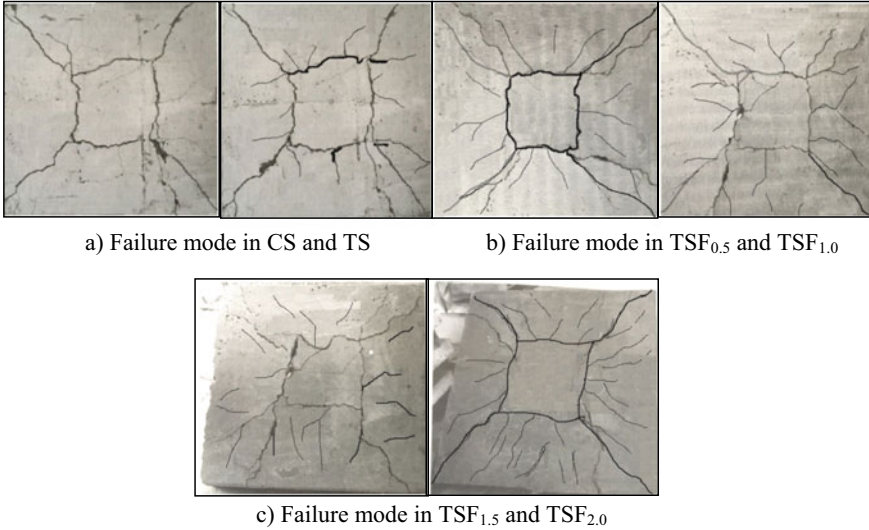


Fig. 7 Failure modes of tested slabs

4 Conclusions

The experimental study is concluded as follows,

- The slump of TC is higher than CC however it is decreased as fiber content increases.
- Compressive strength of TC is higher than CC. Further it is enhanced by the fibrous ternary concrete.
- Load at first crack, yield and failure crack of ternary slabs (TS) are improved over CS, and further improved in fibrous ternary slabs.
- Ultimate strength and deflection of TS and TSF_{2.0} enhanced by 19.6 and 110.7% and about 1.12 and 2.07 times in that order relative to CS.
- Flexural toughness at failure load of TS and TSF_{2.0} had respectively 1.7 and 7.19 times superior than CS.
- Ductility and Energy factor of TS and TSF_{2.0} are improved by 1.4–3.26 times and about 1.69 and 4.58 times correspondingly relative to CS.
- All the specimens were failed after showing the yield lines. Final breakdown occurs in conventional and ternary slabs after developing and propagating numerous cracks particularly in fibrous ternary slabs.

5 Recommendations

The author recommends the inclusion of steel fiber in ternary concrete to enhance the flexural performance.

References

1. Suda VBR, Rao PS (2020) Experimental investigation on optimum usage of Micro silica and GGBS for the strength characteristics of concrete, ELSEVIER Mater Today Proc 27(2):805–811. <https://doi.org/10.1016/j.matpr.2019.12.354>
2. Udhayakumar V, Bharatkumar B, Balasubramanian K, Krishnamoorthy TS, Lakshmanan N (2007) Experimental investigations on flexural behavior of RC slabs reinforced with GFRP rebars. J Inst Eng 88(11):23–27
3. Ms KR, Venkatesh Babu DL (2012) Behavior of hybrid fiber reinforced concrete slabs in frames under static loading. Art Ecol Environ Conserv 18(4):975–979
4. Suda VBR, Rao PS (2020) Experimental studies on steel fiber reinforced short ternary columns under axial loading. Elsevier Mater Today Proc 38(5):2975-2980. <https://doi.org/10.1016/j.matpr.2020.09.319>
5. STEWOLS INDIA (P) LTD, Nagpur Industrial Estate India

Influential Factors and Facilities of Pedestrian Crossings in Heterogeneous Traffic Conditions at Unsignalized Intersections—A Comprehensive Review



Pala Gireesh Kumar and Abhirami Priyanka Pathivada

Abstract Traffic and road safety is the highly influential and predominant aspects under consideration for ages. With every new approach and advancement, the level of safety is witnessing a hike and one such aspect is signalized intersection which is proven to be a befitting approach for a swift and safe crossing and but the increase in population directly affected this concept and exclusively deteriorated the condition especially in case of unsignalized interactions, thereby leaving pedestrians as an impelled category of affected. This paper proceeds with the identification of key areas affecting the working of an unsignalized intersection and thereby, proposing the possible outreaches to overcome the snags. In addition, the factors influencing the pedestrian delays and vehicular delays were also delineated along with a clear briefing. The facilities at the intersections and the several PLOS model proposals were illustrated and the commonly observed delays were put forth. This study elucidates a perspicuous and pellucid way of the pedestrian facilities in heterogeneous traffic conditions at unsignalized intersections.

Keywords Signalized intersections · Unsignalized intersections · Level of Service · Pedestrian delay

1 Introduction

One of the predominant modes for the transportation sector is the roadways and these hold a higher rate of delay when compared to other travel modes. With the roadways enduring the maximum delays, it has become a mandate to entail all possibilities to lower the delay rate along with an escalation in the aspect of safety. Adhering to the aforesaid, the concept of factors affecting the vehicular delay, especially in zones of unsignalized areas comes into the vision [14]. One of the cardinal factors that closely influence the delay graph is the behavioral aspect of the pedestrians. As per the records and revised data, it is clear that the majority of the delay is influenced by the high

P. G. Kumar (✉) · A. P. Pathivada
Department of Civil Engineering, Shri Vishnu Engineering College for Women (Autonomous),
Bhimavaram, West Godavari, Andhra Pradesh, India

pedestrian flow and this is exclusively observed in urban areas where the vehicle flow is higher as well as the pedestrian flow is also high [6]. Focusing on the inhibitory methods adopted by the current transportation sector, it is obvious that the provisions for mitigation of pedestrian accidents and delay of vehicles are lacking in potential effectiveness due to improper amenities provided [9]. It is lucid that the behavior of pedestrians will be regulated depending upon several factors and it is highly advisable for a researcher to concentrate on all the influencing aspects while developing a model. These factors comprise weather, age, and Physical fitness of the pedestrians, and other psychological factors comprehending the potentiality of pedestrians to walk across a crowd, get past huge traffic without involving many danger zones and vehicular delays, and also the credibility of a pedestrian to split from the conflict points and en-route one's own safer and quicker direction [1]. For a more specified and precise detailing of pedestrian behavior, a place is considered, for instance, Bhimavaram, which is the most happening place in East Godavari District, Andhra Pradesh, India. While analyzing the area, we have come across several conflict points as the traffic flow is heavy in Bhimavaram, points of conflict were formulated between vehicles and pedestrians; pedestrians themselves, and vehicle-vehicle conflicts as well. And from the observations made, it was evident that the psychological behavior of the pedestrians, as well as the drivers, closely influences the aspect of smooth traffic flow on roads [14]. Focusing on the aforementioned concerns, this paper deciphers a view over the concept of pedestrians' delay and the traffic accidents determining the behavior of pedestrians and flow characteristics.

2 State of Art

Multiferous studies have been scrutinized in this area with various proposed data. Few studies are as follows,

Arunabhe Benerjee et al. instigated the study over Level of service (LOS) where aspects like delay period, gap acceptance, and flow rate were supremely emphasized for the development of models using the software. In addition, a qualitative survey was carried out with traffic control and the speed of the vehicle as influential parameters [1].

Tao Wang et al. stated that a thorough investigation and observance was mandatory to develop a model for lowering the vehicular delay and this includes the observance of the vehicular and pedestrians demands, pedestrian crossing percentage of crosswalks. Using the aforementioned parameters, the LOS is developed following the demand of the location [2].

Mohamed H. Dridi presented a study on the influence of parameters such as ethnic groups and cultural parameters, age parameter and subject selection, physical fitness (or level of exhaustion), other physical parameters, pedestrian radius parameters, climatic parameters, and psychological parameters [3].

Luca Mantecchini and Filippo Paganalli enthralled the crossing time using the LOS where the time of crossing is given as functionality of lost time of initial start-up. The variation of actual and ideal crossing to the average speed of delay was used as a constraint in computing the LOS of pedestrians of a location [4].

Akash Panchal and Shashikant Dhobale analyzed the reduction of conflict points using high-capacity manual (HCM2010). To create safely walk for pedestrians, PLOS analysis was improved using multilinear regression model [5].

Akash Jain et al. reviewed the influence of psychological constraints of pedestrians such as the behavioral changes with varied situations. Also, the physical customs like the age factor, the gender; mannerisms like the conditions of holding the luggage, if any, were studied. Road safety along with the delay time was given a clear explanation of the working concept of delay time with traffic and conflict points [6].

Anand Kumar Raghuwanshi and Vanadana Tare developed the condition of prediction model for improving the serviceability of mixed lane and for that, they identified the factors which affect the PLOS at mixed lane using High Capacity Manual (HCM) [7].

A. M. Tahsin Emtenan and Showkat Ibna resolute the characteristics of flow rate using a set of sequential steps namely the selection of site and preliminary survey of the traffic flow; schedule for the collection of data; tenure of data collection and finally the application of reduction of data. From the performed study, the parameters like the density of flow (k), rate of flow (q), and walking speed of pedestrians (μ) were determined, and relation is formulated using model parameters that vary depending upon the location of the survey [8].

Gowri A. saithambi et al. elucidated the distinct influence of signals near the intersections. Investigative studies were carried out on pedestrian behavior over the crossing of roads with and without signals. The aspects like gap acceptance and safety of pedestrians were majority focused in the study [10].

J. Sri ram et al. Estimated the pedestrian delay from the existing models, these do not always match with the reality under mixed traffic conditions, so they developed two delay models by considering pedestrian crossing behavior under mixed traffic conditions based on video graphic survey [11].

B. Raghuram Kadali and P. Vedagiri also focused on the concept of evaluation by Level of Service (LOS) under the Highway Capacity Manual where provisions like potential convenience and source of comfortability were set forth. In furtherance to the study of LOS, the accident rate was also inspected along with the pedestrian speed of free flow at the crossroads of signalized intersections [12].

Petrtsch et al. affirmed the perceptions of pedestrians for the LOS development where parameters like the traffic volume and conflict points were identified and a detailed analysis was carried out [13].



Fig. 1 Facilities at signalized intersection

3 Pedestrian Facilities at Signalized and Unsignalized Intersection

3.1 Signalized Intersection

As per the scrupulous and meticulous survey and analysis of the accidents concerning the pedestrians, approximately one-third of the accidental records were proven to take place at a distance of in and around 30 cm from the intersection and exclusively when the drivers take a prompt and remiss turn to their left at the signals and the majority of the pedestrian crashes were noted. And this has aroused the obligation to reform and take up new refinements for promoting the safety rate of pedestrians. The augmented provisional safety measures adopted at signalized intersections are depicted in Fig. 1 and are as follows,

- Cautionary and informative signboards at defined locations
- Installation of signals in crowded and high volume traffic areas
- Markings on the roads with more visibility of clearance
- Application of technology and usage of the PUSH BUTTON at the intersections and signals for safer pedestrian crossings.

3.2 Unsignalized Intersection

An unsignalized intersection is an arm intersection that comprises lanes for each direction of traffic flow. The sidewalks were often seen occupied with street vendors and this creates a ruckus environment that forces the pedestrians to directly walk on the road.



Fig. 2 Pedestrian facilities at unsignalized intersection

Adaptive measures to enhance the level of road safety for pedestrians are depicted in Fig. 2 and are as follows,

- Lawful enforcement of traffic and road safety rules and providing a clearance of sidewalks.
- The road-stream should have enough width so that the pedestrian can't influence the vehicle and thereby, forces the vehicle to decrease its speed and allow pedestrians to cross the road.

4 Categorization of PLOS

The continuous monitoring of traffic concerning the flow rate with time defines the Level of Service (LOS) of a road. Furtherance, the evaluation, and analysis of the existing crosswalks for a sophisticated approach toward pedestrian safety where the functionality and the potentials of the crosswalks were focused is termed as Pedestrian Level of Service (PLOS).

Some specific parameters influencing the PLOS are the pedestrian behavior toward the crossings, the walking speed, capability to detour the possible routes, vehicular and traffic conditions of reverse flow at the locations, etc. LOS was adopted as a major persuasive factor in determining the mode of traffic operations related to pedestrians as per the High Capacity Manual (HCM) of 2010 where the design was categorized into six degrees by the qualitative driver's convenience evaluation and the ratio of flow volume to capacity as shown in Fig. 3. And Table 1 illustrates a clear view of the categories of PLOS considered, Table 2 elucidates the PLOS criteria and Table 3 briefs the PLOS models.).

- A. LOS at A: Free allowance of movement
- B. LOS at B: Movement capable of reverse and crosswalk and is unidirectional with free walking speed

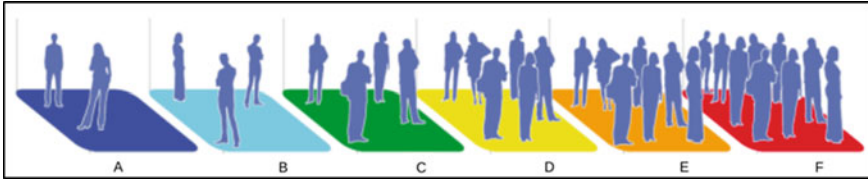


Fig. 3 LOS pedestrian modeling assessment SD-PED-0100

- C. LOS at C: Minuscule limit over walking speed with little hassle in of reverse and crosswalk
- D. LOS at D: Little congestion with regard to movement and the reverse and crosswalk are restricted with variable walking speed
- E. LOS at E: High rejection for reverse and crosswalks with frequent congestions and conflict points
- F. LOS at F: Exclusive complexity and highly restricted walking speed with numerable congestions with remotely vague chances of reverse and crosswalks.

5 Pedestrian Delay Model

One of the major factors causing the delays at unsignalized crosswalks is the arrival pattern of vehicles and pedestrians.

The fabrication of the models for the pedestrian delays is characterized based on three supreme factors namely the diagonal crossing percentage, pedestrian and vehicular demands. And the Adam’s Delay Model was adopted in obtaining the pedestrian’s average delay where it is further utilized in procuring the vehicle headway gap.

$$D = 1/N * e - Nt - 1/N - t$$

where, N = traffic volume.

D = overall pedestrian delay.

t = Minimal gap requirement of pedestrian safe crossing in traffic.

5.1 Types of Delay

Delays being a major snag of the traffic sector, some delays are more commonly observed with time as listed below,

- Delay of Stopped Time
- Delay of Approach

Table 1 Different category of PLOS

Category	Description	Remarks	
		Pedestrian spacing (PS) (units: ft ² /p)	Flow rate (FR) (units: p/min/ft)
A	In the preliminary category, the free-moving pedestrians were considered. The moving speed of the pedestrians is their choice and they choose their path irrespective of the other pedestrian direction of the walk and it is unlikely for the occurrence of conflict points	PS > 60	FR = 5
B	This is a category in which the pedestrian's direction of the path is influenced by the other pedestrians and to avoid the point of conflict, the other pedestrian pathway is also considered. The free-moving speed is somewhat restricted in this category	PS > 40–60	FR > 5–7
C	Here, the pedestrian speed is lowered in comparison to the prior categories, and also the path of the pedestrian is unidirectional. The nominal spacing among the pedestrians allows a smooth walking and crossing other pedestrians	PS > 24–40	FR > 7–10
D	The walking speed is highly restricted and the reverse-direction, crossings are suggested to be avoidable as it causes more conflict points, and thereby, the pedestrians come in close contact with one another	PS > 15–24	FR > 10–15
E	This is a stage where the nominal spacing is highly reduced among the pedestrians and the forward walk becomes slower and frequent variation in the pedestrian walk is required with every step forward. Also, the reverse or crosswalk path is extremely difficult as the pedestrian volume almost reaches the design volume of the crossings	PS > 8–15	FR > 15–23

(continued)

Table 1 (continued)

Category	Description	Remarks	
		Pedestrian spacing (PS) (units: ft ² /p)	Flow rate (FR) (units: p/min/ft)
F	The final categorization is inclusive of an exclusively restricted area of walking speed and the pedestrians need to have a shuffle for every move. It is nearly impossible for the reverse and crosswalk in this zone and the occurrence of conflict points is majorly observed in this category and this category is often known for near-to-stationary movement	PS = 8	Variable

Table 2 Criteria of LOS

LOS	Flow rate (pedestrian/minute/meter)	Density (pedestrian per square meter)
A	<7	<0.08
B	7–23	0.08–0.27
C	23–33	0.27–0.45
D	33–49	0.45–0.69
E	49–82	0.69–1.66
F	>82	>1.66

- Delay of Travel Time
- Delay of Time-in-Queue
- Delay of Control

Depending upon the constraints at the intersections, these delays alter. Figure 4 gives a brief idea and showcases the contrast among the Delay of Stopped Time, Delay of Approach, and the Delay of Travel Time. Figure 5 depicts Delay of Control followed by Fig. 6 showing the Time-in-Queue delay.

- The time interval between the vehicle coming into complete rest and back into movement at an intersection is defined as the Delay of Stopped Time
- The disparity of horizontal slope between departure and extended velocity of approach upon achieving complete acceleration is the Delay of Approach
- The variation of time between the actual time taken and expected travel time at the intersection is termed as the Delay of Travel Time
- The total tenure of the vehicle entering the intersection and joining the queue to leaving the intersection past the departure line is called the Delay of Time-in-Queue

Table 3 Preceding models of PLOS

Authors	Year of study	PLOS constraints	Grade of LOS
Sarkar	1993	<ul style="list-style-type: none"> • Safety and security • Convenience, comfort and continuity • Attractiveness • Coherence of system 	A-F
Khisty	1994	<ul style="list-style-type: none"> • Attractiveness • Level of comfort and convenience • Safety and security • System of coherence and continuity 	A-F
Dixon	1996	<ul style="list-style-type: none"> • Basic provisional facilities • Conflict points • Potentials and amenities provided • LOS of motor vehicles • Complication in maintenance • Provision for multiple modes. 	A-F
Gallin	2001	<ul style="list-style-type: none"> • Width of pathway • Quality of surface • Obstructions, opportunities and facilities at the crossings • Connectivity • Environment at the pathway • Vehicle conflicts and volume of pedestrians Heterogeneous path users • Personal security 	A-F
Nelson & Zaly shah	2010	<ul style="list-style-type: none"> • Provision of amenities and maintenance • Pathway of pedestrians and conflict points • Material of the pavement • Security perception • Level of comfort • Traffic volume 	A-F

- The delay component in relation to the control type adopted at the intersection which is in turn calculated by comparison with the uncontrolled intersection is known as the Delay of Control.

6 Webster's Delay Models

The total uniform delay at the considered triangular area influenced by the departure and arrival functions is given by Webster's Delay Model as in Fig. 7

The total uniform delay is given by,

$$TUD = (R * V) / 2$$

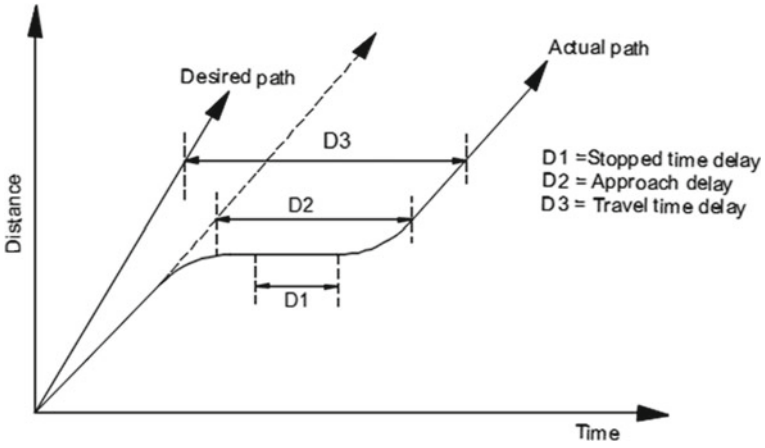


Fig. 4 Common delays and the contrast

Fig. 5 Control delay

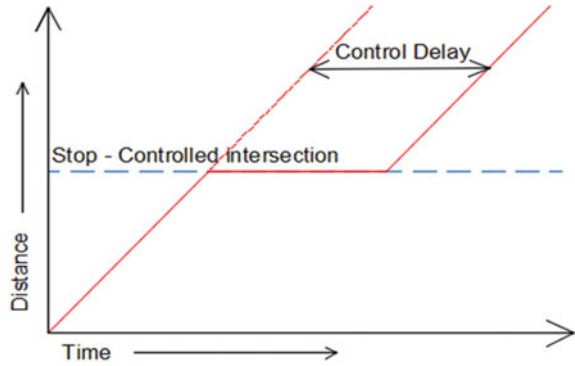


Fig. 6 Time-in-queue delay

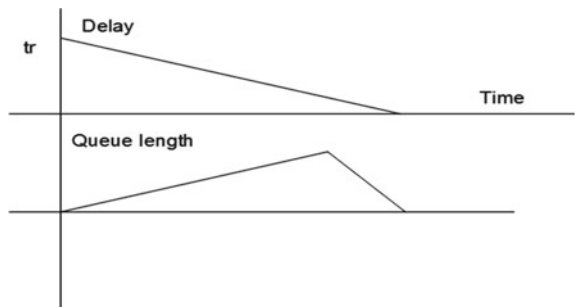
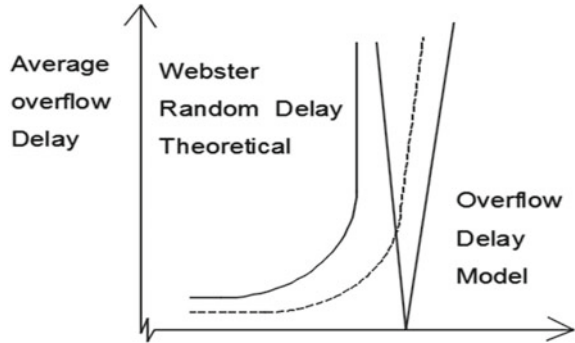


Fig.7 Webster's Delay Models



where TUD = Total Uniform Delay.
 R = Duration of Red.
 V = Number of Vehicles.

7 Factors Affecting Pedestrian Characteristics

There are multifarious factors that influence the delay and safe crossing of pedestrians which are mutually dependent. Considering all the constraints of influence over pedestrian safety, a few of the predominant factors are broadly classified under four heads as listed.

- Physical: Vision, hearing, strength, and general reaction to traffic situations.
- Mental: Knowledge, skill, intelligence, and experience to react to situations and the level of understanding of the traffic regulation. Also, the special instructions to road users depend on intelligence and literacy as well.
- Environmental factors: The behavior of road users to traffic stream characteristics, roadside features, atmospheric conditions, and locality.
- Psychological factors: Emotional factors such as fear, anger, impatience, and general attitude of road users.
- Based on traffic conditions: The reflex of the pedestrians depends on the prevailing conditions of roads, vehicle flow, and spacing, and the possibility for a pedestrian to move between spacing if required in an emergency.

8 Conclusion

After a lot of substantial investigation and research carried out, it was noted that the major delays at the intersections were highly influenced by the prevailing conditions at the crossings. The cloddish and uncoordinated approaches were the supreme influencer that caused a glitch in traffic safety. With every factor considered and

coordinated, the effective approaches of pedestrian facilities and the PLOS were proposed. From the extensive study carried out, the commonly faced delays at the intersections were elucidated and the uniform delay models were also briefed in the run. It was observed that the unsignalized intersections were the hub of extended delays and unsafe crossings while the signalized intersections were proven to be in a better orientation under sophisticated planning and maintenance. From the absolute investigation, it was evident that the rate of pedestrian safety was closely dependent on various factors in accordance with the traffic volume at a particular intersection as well as the pedestrian's way of approach.

References

1. Benerjee A, Maurya AK, Lammel G (2018) *Am J Civ Eng* 5(5):282–292. <https://doi.org/10.17815/CD.2018.17>
2. Wang T, Zhao J, Li C (2019). *Math Probl Eng*. <https://doi.org/10.1155/2019/1016261>
3. Dridi MH (2015) *Int J Soc Sci Res* 3(4). <https://doi.org/10.11114/ijsss.v3i4.870>
4. Mantecchini L, Paganalli F (2015) *Contemp Eng Sci* 8(21). <https://doi.org/10.12988/CES.2015.57202>
5. Panchal A, Dhobale S (2019) *Int J Res* 7. <https://doi.org/10.22214/ijraset.2019.8114>
6. Jain A, Gupta A, Rastogi R (2014) *J Traffic Transp Eng* 4(1):103–116. [https://doi.org/10.7708/ijtte.2014.4\(1\).08](https://doi.org/10.7708/ijtte.2014.4(1).08)
7. Raghuvanshi AK, Tare V (2016) *RJET* 7. <https://doi.org/10.5958/2321-581X.2016.00003.9>
8. Emtenan AMT, Shahid SI (2017) *Am J Civ Eng* 5(5):282–292. <https://doi.org/10.11648/j.ajce.20170505.13>
9. Vanumu LD, Ramachandra Rao K, Thivari G (2017) *Eur Transp Res Rev* 9(4). <https://doi.org/10.1007/s12544-017-0264-6>
10. Saithambi GA, Kuttan MO, Chandra S (2016) *Transp Dev Econ* 2, 14. <https://doi.org/10.1007/s40890-016-0018-5>
11. Sri Ram J, Ashok Yadav V, Hemantha Raja K (2019) *Int J Recent Technol Eng* 7(6C2). F10010476C219/19©BEIESP
12. Raghuram Kadali B, Vedagiri P (2016) *Transp Res Rec* 2581(1):37–47. 10.3141/2F2581-05
13. Petritsch TA, Landis BW, McLeod PS, Huang HF, Challa S, Skaggs CL, Guttenplan M, Vattikuti V (2006) *Transp Res Rec* 1982(1):84–89. <https://doi.org/10.3141/1982-12>
14. Ridel D, Rehder E, Iauer M, Stiller C, Wolf D In: *IEEE ITSC 2018*, pp. 3105–3112. <https://doi.org/10.1109/ITSC.2018.8569415>

Study on Characteristics of Geopolymer Concrete



Ward Nasser Al Banna and Kiran Kumar Poloju

Abstract Cement is used in enormous quantities for concrete applications in construction projects across the world which contributes to CO₂ emissions. Geopolymer concrete (GPC) is a cutting-edge construction material used as a substitute for ordinary Portland concrete (OPC) as it reduces cement usage and preserves the environment through the utilization of by-product materials. This study aims to find out how the molarity of sodium hydroxide affects the durability and strength of geopolymer concrete, as well as the appropriate GGBS/fly ash proportion in GPC. The paper has concentrated on characteristics of workability, compressive strength, and durability properties such as drying shrinkage and sorptivity. Curing procedures, Na₂SiO₃/NaOH ratio, and alkaline/binder ratio were all taken into account in the study. The findings state that increased molarity up to 14_M and 100% of GGBS in fly ash achieves the best strength and durability performance of GPC. A 1.5 Na₂SiO₃/NaOH ratio and curing at elevated temperatures have also been proven to improve the strength and durability of GPC. The study found that the geopolymer concrete is exceedingly durable and is highly recommended as a construction material.

Keywords Geopolymer concrete · Molarity · Alkaline activator · Sodium silicate · Sodium hydroxide · Strength characteristics

1 Introduction

In recent times, concrete is one of the important materials in the construction field all around the world due to the availability of its materials, low cost, resilience, and longevity. In ordinary Portland concrete (OPC), the main constituent to bind the aggregates together is cement, which is used in a very tremendous quantity for

W. N. Al Banna (✉) · K. K. Poloju
Department of Civil Engineering, Middle East College, Seeb, Oman

K. K. Poloju
e-mail: kpoloju@mec.edu.om

concrete applications that are around 1.6 billion tons yearly. The cement manufacturing process in this amount is a massive cause of greenhouse gases emission which is responsible for 7% of total carbon dioxide emissions into the atmosphere each year across the world, and this is a crucial matter taken into consideration since these released gases are causing an atmospheric pollution. Therefore, many studies focus nowadays on finding a suitable alternative for cement in concrete applications to reduce the environmental degradation caused by cement manufacturing process. Provided that by-products from different industries are disposed off as waste materials to exposed lands, which as a result contributes to an environmental pollution [1]. Geopolymer concrete (GPC) is a cutting-edge construction material used as a substitute for (OPC) due to its environmental benefits as it is made by utilizing by-products. The term “geopolymer” was invented in 1978 by Davidovits which represents mineral polymers linking with a covalent bond. Geopolymer is formed by activating a pozzolanic material that is rich in aluminum (Al) and silicon (Si) with an alkaline solution and binds the aggregates in GPC at an elevated temperature, this chemical reaction is known as the geopolymerization process. Mainly produced by mixing Ground Granulated Blast Furnace Slag (GGBS) and Fly Ash with aggregates and an alkaline activator. Alkaline activator is controlled by Sodium Silicate to Sodium Hydroxide (SS/SH) ratio [2]. According to [3], the alkaline activator solution can be prepared using either sodium hydroxide (NaOH) or potassium hydroxide (KOH), it was proved in their study higher alkalinity level is provided by the KOH, whereas higher potency for monomer liberation was by the NaOH solution. However, a mixture of both sodium silicate and sodium hydroxide is the alkaline solution often used. A study conducted by Poluju [4] on alkaline solution impact on compressive strength of geopolymer mortar, they have used combined and single solutions, the combined solution used were combination of Na_2SiO_3 and NaOH, while the single solution was a Na_2SiO_3 solution. They have also examined the strength with varying replacement of fly ash with GGBS up till 100%, their findings observed a higher strength with a single solution and mixtures of 100% of GGBS. Molarity in GPC reflects the molar concentration of sodium hydroxide given by its number of moles per liter of solution. As it increases, the viscosity of solution increases which improves strength properties, [5] executed a study on GPC in terms of workability and compressive strength with varying molarities from 8 to 12 M and fly ash replacement with GGBS by 30–70%. The results demonstrated that the increase of GGBS content and molarity decrease workability and increases the strength. Another experimental study was conducted by Babu [6] on the concentration of NaOH on GPC strength properties with molarities of [6 M, 8 M, 10 M] and 2 SS/SH ratio. The results indicated maximum strength by 10 M. Ganesan [7] have studied the influence of alkaline activator/binders ratio on the compressive strength of geopolymer concrete up to 56 days of ambient curing. The mixture was prepared with 1:2:5 ratio of sodium hydroxide/sodium silicate solutions. The solution to binder ratios tested ranged from 0.30 to 5. It has been indicated that the strength continued to increase until 56 days of curing, and decreased with increasing the ratio, the alkaline solution/binder ratio of 0.30 had attained the higher strength. A durability comparison study was carried out by Luhar [8] on sorptivity and water absorption of

m25 grade of GPC and OPC. Their findings have shown that geopolymer concrete is more durable than conventional concrete as both the sorptivity and water absorption were less in geopolymer concrete. Dave [9] have carried out a study on GGBS based GPC with two more binders which are fly ash and silica fume, hence, the mixtures will be tested containing overall of three binders. They were prepared with 14 M with a SS/SH Sodium ratio of 3. Five mixtures were prepared, first mixture was prepared with GGBS only, three mixtures incorporated silica fume with GGBS and last two mixtures were prepared using fly ash, silica fume, and GGBS. It has been indicated from the findings that the GGBS based GPC mixture resulted in the highest sorptivity, following the mixtures with silica fume and GGBS. While the lowest sorptivity value was observed by the mixture with the three binders; fly ash, silica fume, and GGBS. Therefore, the study comes to a conclusion that fly ash and GGBS combination for GPC mixture reduces sorptivity which is an indication of a denser structure with less pore spaces, the combination of these binders reduces the pore structure by increasing the packing density. Heat curing is a very significant factor affecting geopolymer concrete performance, [10] have carried out a research on the curing method impact on the compressive strength of GPC, the samples were prepared using 10 M, with a 1.75 SS/SH ratio and a 0.4 activator/fly ash ratio. The results were compared by curing under ambient and hot temperature at 75 °C, it has been found that heat curing samples had attained higher strength, the sample was also compared with OPC where it was also shown that heat curing can contribute to a strength higher than the OPC. Additionally, SEM analysis was also done to observe the shape of the particles of fly ash, sodium silicates, and sodium hydroxide. The results have observed a rounded and circular shape for the fly ash particles and comparing the silicon particles between fly ash and Na_2SiO_3 solution, finer particles were observed by the Na_2SiO_3 solution. Furthermore, hydrargillite-like layer structure was noticed by the particles of sodium (Na) in NaOH. Geopolymer mortar strength was examined by Shinde [11] in terms of alkaline/binder ratio which varied between 0.2 and 0.8 and $\text{Na}_2\text{SiO}_3/\text{NaOH}$ ratios varying from 1 to 3, with heat curing of temperatures from 40 to 100 °C. Highest strength was attained by the alkaline/binder ratio of 0.5 and 1.5 $\text{Na}_2\text{SiO}_3/\text{NaOH}$ ratio, higher ratios decreased the strength. Whereas the temperature of heat curing at 80 °C is the optimum temperature for heat curing as further increase of temperature leads to decrease in strength. Activation impact has been studied by Zhang [12] in terms of crystalline phases formation using sodium hydroxide alone comparing it with the addition of sodium silicate. The study was carried out using XRD, SEM, and other testing methods. They reported that the crystallite formation is significantly reduced by the presence of sodium silicate, while the use of sodium hydroxide alone can increase crystalline zeolite formation. Rovnanik [13] have analyzed curing temperatures (10–80 °C) and methods' effect on GPC strength and microstructure properties. The results have inferred that the gain of strength is faster with elevated temperatures, however, the samples have observed deterioration after 28 curing days. While the ambient cured samples had low strength gain but on the other side, they have exhibited better properties after 28 curing days. Performance of geopolymer concrete is also affected by the type of fly ash which are classified into Class C and Class F, higher calcium

presence in class C may affect the geopolymerization process and interfere with the microstructure, therefore, low calcium fly ash is more preferable [14]. A study was conducted by Bakharev [15] on the durability of geopolymer concrete after exposing the samples to 5% of acetic and sulphuric acid solutions and compared with OPC. The study deduces that geopolymer concrete has higher resistance to acids than OPC. Another comparison study between GPC and OPC was reported by Mali [16] on abrasion resistance and water absorption of GPC samples, it has been inferred that GPC has much higher resistance to abrasion wear and absorption of water compared to OPC which makes it excellent in durability properties. The aim of this research paper is to examine properties of GPC in terms of its workability, compressive strength, and durability according to the literatures. Parameters considered in this study will include molarity of NaOH, curing methods, GGBS/fly ash proportions, and SS/SH ratio.

2 Methodology

Instead of hydrating cement, geopolymer concrete is developed by chemically activating industrial by-products which contain aluminosilicates by an alkaline solution. Geopolymer concrete can be made by mixing GGBS, fly ash, coarse and fine aggregate, and alkaline activator. GGBS is a by-product of steel industry and fly ash is a thermal industry by-product, both are rich in silica and alumina and used as fine powder form. Conventional standard sizes of coarse and fine aggregates are used in GPC similarly as used in OPC. An incorporation of both solutions (H_2SO_4 & Na_2SiO_2) is mixed for alkaline solution. This solution when reacted with silica and alumina of the materials, a binder material will be formed [17].

To develop geopolymer concrete using these materials, alkaline solution is first prepared according to the molarity of sodium hydroxide. Molarities commonly used range between 6 and 18 M. To prepare an alkaline solution with 10 M of NaOH, the molarity (10 M) is multiplied by the molecular weight of NaOH (40 g/mol) which gives 400 g of NaOH pellets. This weight is taken into a liter of jar with adding water and mixing them together, NaOH solution is then weighed. To prepare the amount of sodium silicate according to $\text{Na}_2\text{SiO}_3/\text{NaOH}$ ratio, if 1.5 ratio is selected, then 1.5 is multiplied by NaOH solution weight and is added to the mixture. Due to the heat generated as a result of NaOH dissolution in water, mixture is left for a day before use. After 24 h of alkaline solution preparation, required quantity of binders are mixed with the aggregates according to mix proportion and activated with the alkaline solution. From the available literature, specimens are cured under ambient and heat temperatures to undergo geopolymerization. This study will be carried out as a research study by collecting data from previous studies. Varying molarities and SS/SH ratios will be examined from different studies on workability, compressive strength, and durability properties of geopolymer concrete.

3 Results and Discussion

3.1 Results

3.2 Discussion

GGBS and strength ratio effect on workable and strength is represented by Figs. 1 and 2, strength ratios (1.5 and 2.5), GGBS of 10 and 20% content were examined. The results infer that increased content of GGBS and reduced ratio of SS/SH to 1.5 has increased the workability and strength. Workability, strength, and sorptivity results of GPC are presented in Table 1 with varied molarities (8, 10, 12) and fly ash substitution with GGBS. It is demonstrated from results that the increased substitution of fly ash with GGBS till 100% has increased the strength, reduced the workability and sorptivity. Moreover, higher molarity (12 M) has increased strength, decreased

Fig. 1 GGBS & SS/SH ratio impact on compressive strength [18]

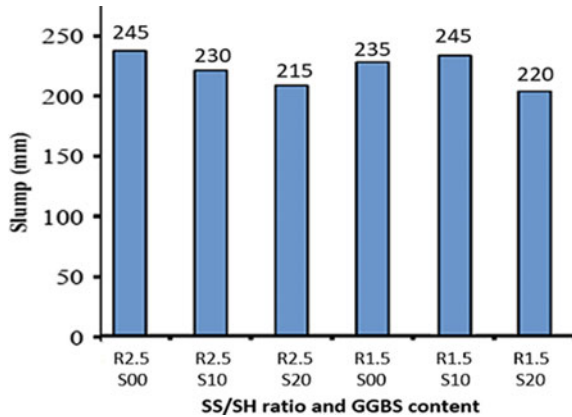


Fig. 2 GGBS & SS/SH ratio impact on workability [18]

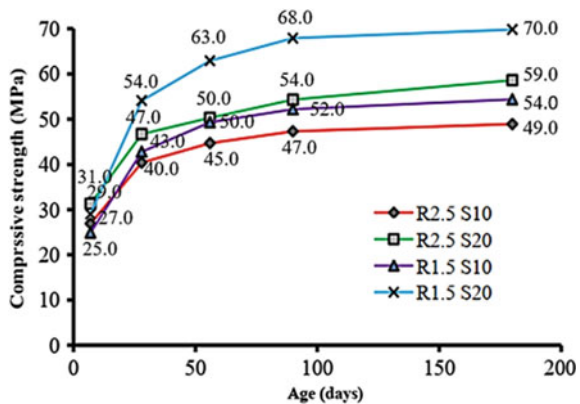


Table 1 GGBS and molarity effect on workability, strength and sorptivity [1]

Molarity (M)	% Replacement of fly ash by GGBS	Slump values (mm)	Compressive Strength (MPa)		Sorptivity mm/mm ^{0.5}
			14 days	28 days	
8	100	34	36.6	44.5	1.06
	90	35	35.6	42.9	1.13
	60	36	33.9	40.8	1.29
	30	38	35.5	37.2	1.40
	0	40	29.2	35.6	1.52
10	100	50	41.4	46.8	1.01
	90	51	40.5	45.4	1.09
	60	53	38.4	43.2	1.15
	30	56	36.1	42.5	1.35
	0	58	35.5	40.6	1.43
12	100	67	43.5	53.2	0.90
	90	68	42.8	40.5	0.95
	60	71	41.03	47.5	1.04
	30	73	39.4	45.09	1.20
	0	75	35.4	43.5	1.31

workability, and sorptivity. Compressive strength with 12 M has increased from 43.5 to 53.2 MPa with increment of GGBS content from 0 to 100%, while the sorptivity reduced from 1.31 to 0.90 mm/mm^{0.5}. Whereas for increasing molarity from 8 to 12, the strength has increased from 44.5 to 53.2 MPa, and sorptivity reduced from 1.06 to 0.90 mm/mm^{0.5}. Figures 4 and 6 show the molarities (8–14 M) impact on strength and ultrasonic pulse velocity (UPV) of GPC, increasing molarity from 8 to 14 has increased the strength for all grades and UPV results. Comparing strength of GPC mixtures with OPC, GPC with molarities 12 and 14 can achieve higher strength than OPC. Figures 3 and 5 show the curing impact on their strength and UPV, the strength increased and UPV also increased when samples were oven-cured than ambient cured. Also, UPV was tested with varying fly ash/GGBS proportion, sample having 25% of GGBS has the highest velocity than samples with higher GGBS content or no replacement at all. Sorptivity results are presented in Figs. 7 and 8 for two examined phases, first phase in Fig. 7 shows results for varying fly ash/GGBS proportions either fly ash-based, GGBS-based or equal proportions. Second phase in Fig. 8 is varied molarities (M6–M14). The results illustrate that GGBS reduces sorptivity, as the fly ash-based GPC had the highest sorptivity (0.3 mm/mm^{0.5}) while GGBS based GPC had the lowest sorptivity (0.23 mm/mm^{0.5}). 6 M mixture had the highest sorptivity (0.36 mm/mm^{0.5}) than the 14 M mixture which had the least sorptivity (0.11 mm/mm^{0.5}), hence, increasing molarity reduces sorptivity. Drying shrinkage in Fig. 9 examines GPC with GGBS content (0, 10%, 20%) and compared with OPC. Increased GGBS content in GPC reduced shrinkage more than OPC sample.

Figure 10 observes shrinkage results with dry and steam curing, it is inferred that steam curing leads to less shrinkage than dry curing. Results in Figs. 11 and 12 show shrinkage values in two phases, phase 1 examined GGBS content (10–20%) effect and phase 2 examined impact of 2.5 and 1.5 SS/SH ratios. Least shrinkage was noted by GGBS of 20% and 1.5 SS/SH ratio. Figures 13 and 14 show resistance of GPC and OPC to abrasion and acid attack, it is illustrated that GPC has higher abrasion resistance and acid attack resistance.

All results prove that increasing molarity and GGBS content with reducing SS/SH ratio and oven curing improves GPC strength and durability. High molarity indicates an increase in NaOH concentration, hence, silicate and aluminate monomers are greatly dissolved. As a result, strength and durability of GPC are improved because leaching of these compounds induces stronger geopolymerization. On the other side, due to cohesiveness of increased NaOH concentration, workability is reduced [1]. Increasing SS/SH ratio increases the viscosity of mixture, which restricts the flowability. This decreases the workability, additionally, strength and durability are affected too because SS/SH ratio increment decreases NaOH solution and hydroxide ions. Thus, gel is decreased and GPC microstructure is adversely affected [18]. Decreased workability with adding GGBS is due to its shape which has larger surface area than

Fig. 3 Effect of curing on compressive strength [19]

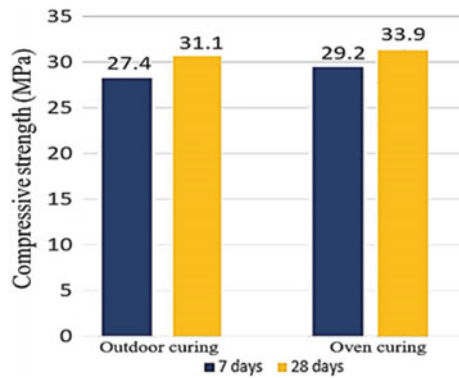
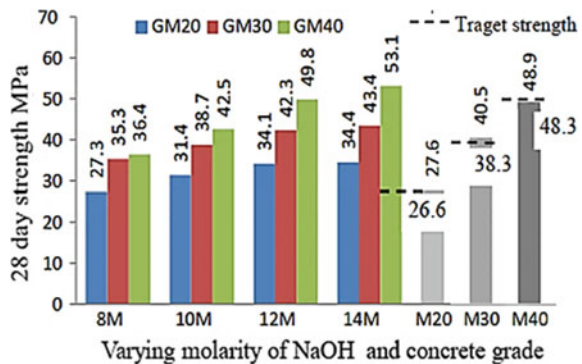


Fig. 4 Effect of molarity on compressive strength [20]



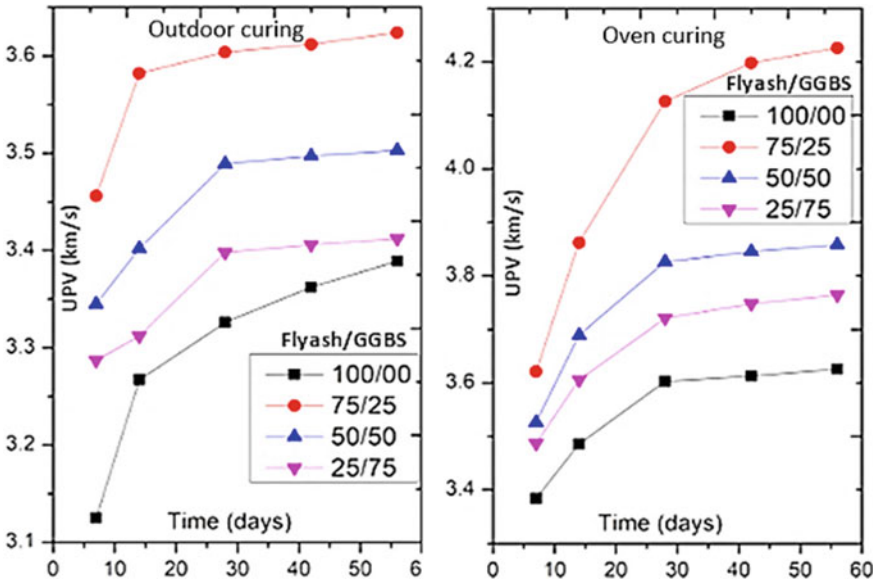


Fig. 5 Effect of curing on UPV [21]

Fig. 6 Effect of molarity on UPV [22]

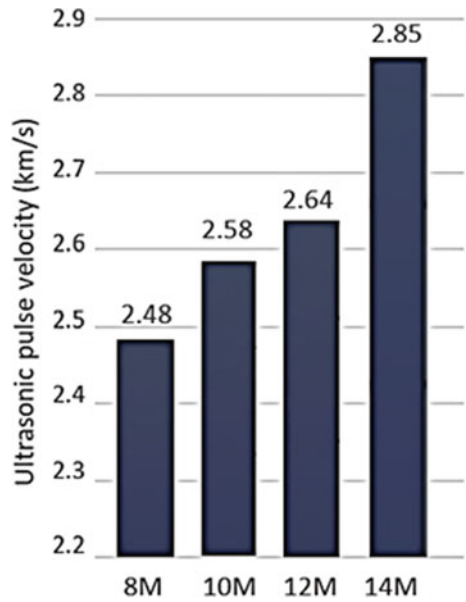


Fig. 7 Effect of GGBS on sorptivity [23]

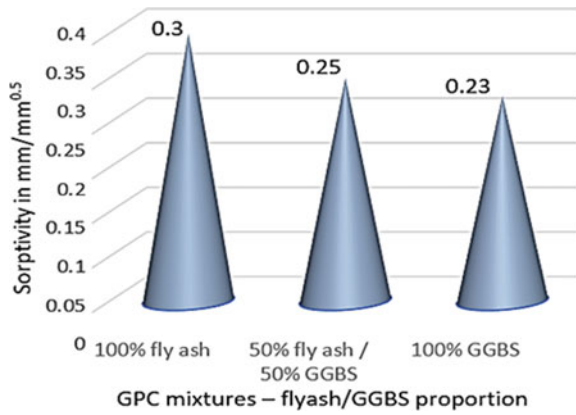


Fig. 8 Molarity effect on sorptivity [23]

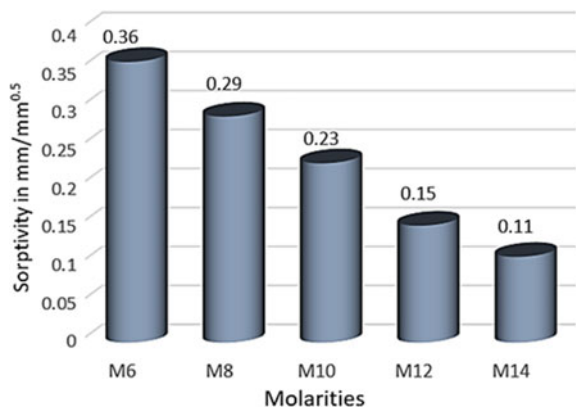


Fig. 9 Impact of GGBS on drying shrinkage [24]

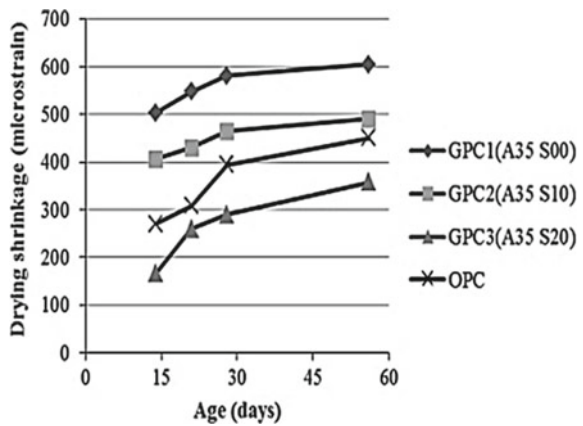


Fig. 10 Impact of curing on drying shrinkage [25]

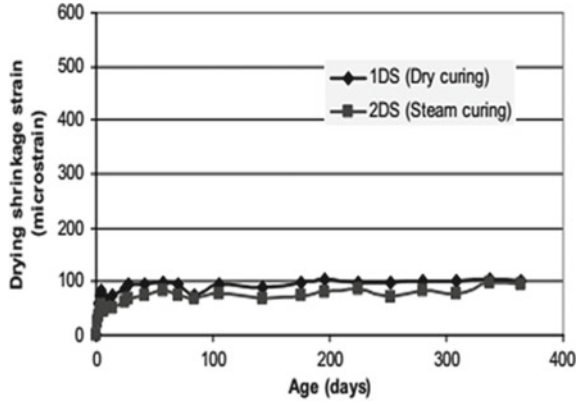


Fig. 11 Impact of GGBS on drying shrinkage [26]

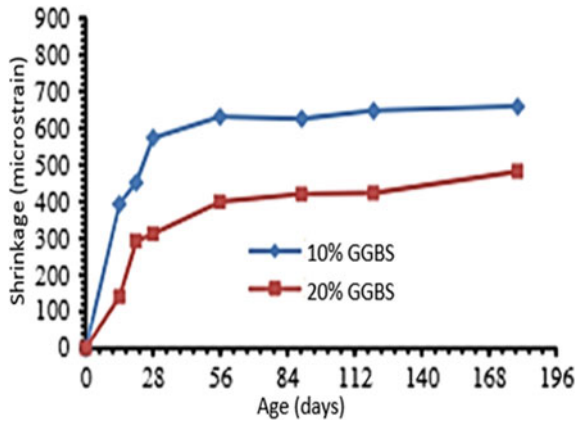


Fig. 12 SS/SH ratio impact on drying shrinkage [26]

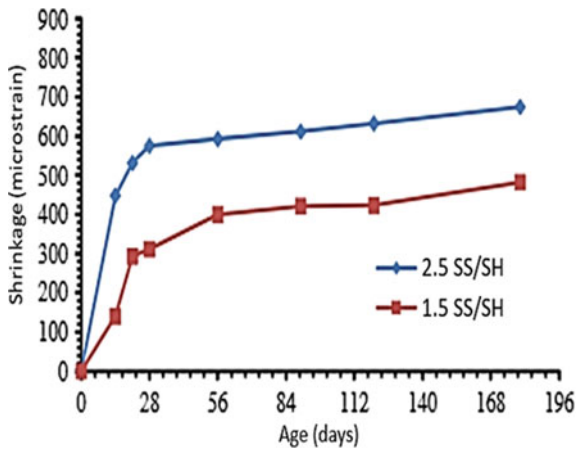


Fig. 13 Abrasion resistance [26]

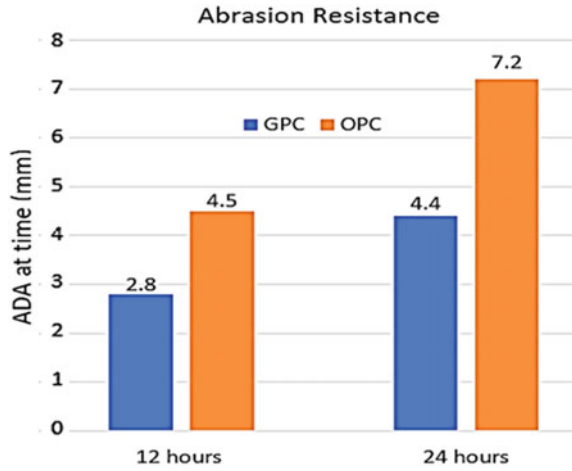
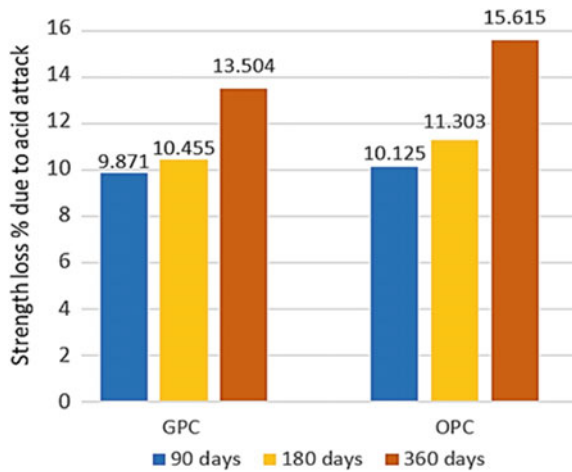


Fig. 14 Strength loss due to acid attack [27]



fly ash. This leads to more water demand, thus workability is reduced. The shape of GGBS also improves the bonding property which increases strength and durability. In addition, GGBS is higher in calcium oxide than fly ash, hence when used in GPC the chemical reaction is improved. A denser and less porous microstructure is formed [23]. Curing at elevated temperatures causes water content in GPC sample to be given out as the water is vaporized. As a result, pores in GPC contain less moisture, shrinkage is negligible at this point, and strength and durability are improved [25]. Generally, all samples had low shrinkage since they were below 1000 micro strain, this falls within the acceptable range in accordance with the Australian standard AS1379-2007 [26].

4 Conclusion

Geopolymer concrete strength and durability properties were examined according to previous literature. The study has found that the GPC is exceedingly durable and is highly recommended as a construction material as it assists to reduce cement usage and preserves the environment through the utilization of by-product materials. The findings of this study can be concluded as followed:

- Workability can be improved by increasing molarity of NaOH up to 12 M, reducing strength ratio to 1.5 and GGBS percentage in fly ash.
- Compressive strength is increased by increasing NaOH molarity up to 14 M, reducing strength ratio to 1.5, increasing GGBS content, and using oven curing.
- UPV can be increased by heat curing and increasing molarity of NaOH to 14 M.
- Sorptivity can be reduced by increased molarity up to 14 M and 100% GGBS content.
- Drying shrinkage can be minimized by increasing GGBS content to 20%, decreasing strength ratio to 1.5, and using steam curing.
- GPC has better durability and resistance to abrasion and acid attack than OPC.

References

1. Gowda N, Shivananda K (2019) Studies on geopolymer concrete with GGBS as partial replacement to fly ash. *Int Res J Eng Technol* 6(12):806–812. <https://1library.net/document/q7wrnvnz-studies-geopolymerconcrete-ggbs-partial-replacement-fly-ash.html>
2. Sharma A, Ahmad J (2017) Experimental study of factors influencing compressive strength of geopolymer concrete. *Int Res J Eng Technol* 4(5):1306–1313. <https://www.academia.edu/33549768>
3. Bhattacharyya K, Gupta M, Ishwarya G, Singh B (2015) Geopolymer concrete: a review of some recent developments. *Constr Build Mater* 85:78–90. <https://doi.org/10.1016/j.conbuildmat.2015.03.036>
4. Poluju K, Srinivasu K, Rao M (2020) Study on mechanical characterization of geopolymer cement mortar with single solution and combined solution. *J Xi'an Univ Archit Technol* 12(8):481–487. https://www.researchgate.net/publication/343627471_Study_on_Mechanical_Characterization_of_Geopolymer_Cement_Mortar_with_Single_Solution_and_Combined_Solution
5. Arun R, Nagaraja S, Mahalingasharma S (2018) Combined effect of flyash & GGBS on workability and mechanical properties of self compacting geopolymer concrete. *Int J Pure Appl Math* 119(15):1369–1380. <https://www.acadpubl.eu/hub/2018-119-15/4/743.pdf>
6. Babu N, Rahul B, Kumar Y (2017) Experimental study on strength and durability properties of GPC with GGBS. *Int J Civil Eng Technol* 8(4):39–50. https://iaeme.com/Home/issue/IJC_IET?Volume=8&Issue=4
7. Ganesan N, Babu C, Meyyapan P (2019) Influence of alkaline activator ratio on compressive strength of GGBS based geopolymer concrete. *Mater Sci Eng* 561:1–6. <https://iopscience.iop.org/article/https://doi.org/10.1088/1757-899X/561/1/012083>
8. Luhar S, Khandelwal U (2015) A study on water absorption and sorptivity of geopolymer concrete. *SSRG Int J Civil Eng* 2(8):1–9. <https://doi.org/10.14445/23488352/IJCE-V2I8P101>

9. Dave S, Bhogayata A, Arora K (2019) Durability study of geopolymer concrete cured at ambient temperature. *Constr Build Mater* 1:1–8. <https://ukierconcretecongress.com/Home/files/Proceedings/pdf/UCC-2019-131.pdf>
10. Hassan A, Arif M, Shariq M (2019) Effect of curing condition on the mechanical properties of flyash-based geopolymer concrete. *SN Appl Sci* 1:1–9. <https://doi.org/10.1007/s42452-019-1774-8>
11. Shinde B, Kadam K (2015) Properties of fly ash based geopolymer mortar. *Int J Eng Res Technol* 4(7):971–974. <https://www.ijert.org/research/properties-of-fly-ash-based-geopolymer-mortar-IJERTV4IS070750.pdf>
12. Zhang B, Makenzie K, Brown I (2009) Crystalline phase formation in metakaolinite geopolymers activated with NaOH and sodium silicate. *J Mater Sci* 44:4668–4676. <https://doi.org/10.1007/s10853-009-3715-1>
13. Rovnanik P (2010) Effect of curing temperature on the development of hard structure of metakaolin-based geopolymer. *Constr Build Mater* 24(7):1176–1183. <https://doi.org/10.1016/j.conbuildmat.2009.12.023>
14. Lloyd N, Rangan B (2010) Geopolymer concrete with fly ash. In: *Second international conference on sustainable construction materials and technologies*, vol 3, pp 139–143. <https://www.researchgate.net/publication/228825101>
15. Bakharev T (2005) Resistance of geopolymer materials to acid attack. *Cem Concr Res* 35(4):658–670. <https://doi.org/10.1016/j.cemconres.2004.06.005>
16. Mali B, Abraham A (2005) Study on geopolymer concrete used for paving blocks. *Int J Innov Res Adv Eng* 3(9):62–66. <https://doi.org/10.6084/m9.figshare.4052382>
17. Kulkarni S (2018) Study on geopolymer concrete. *Int Res J Eng Technol* 12(5):784–788. <https://www.irjet.net/archives/V5/i12/IRJET-V5I12146.pdf>
18. Deb P, Nath P, Sarker P (2014) The effects of ground granulated blast-furnace slag blending with fly ash and activator content on the workability and strength properties of geopolymer concrete cured at ambient temperature. *Mater Design* 62:32–39. <https://doi.org/10.1016/j.matdes.2014.05.001>
19. Goriparthi M, Rao G (2017) Effect of fly ash and GGBS combination on mechanical and durability properties of GPC. *Adv Concr Constr* 5(4):313–330. <https://doi.org/10.12989/acc.2017.5.4.313>
20. Mohankumar G, Manickavasagam R (2017) Study on the development of class C fly ash-based GPC by ambient curing. *Int J Appl Eng Res* 12(7):1227–1231. https://www.ripublication.com/ijaer17/ijaerv12n7_19.pdf
21. Verma M, Dev N (2021) Effect of ground granulated blast furnace slag and fly ash ratio and the curing conditions on the mechanical properties of geopolymer concrete. *Struct Concr* 1–15. <https://doi.org/10.1002/suco.202000536>
22. Budh D, Warhade N (2014) Effect of molarity on compressive strength of geopolymer mortar. *Int J Civil Eng Res* 5(1):83–86. https://www.ripublication.com/ijcer_spl/ijcerv5n1spl_13.pdf
23. Sudhan M, Brahmini A (2016) A study on performance of geopolymer concrete. *Int J Sci Eng Technol Res* 5(21):4223–4230. <http://ijsetr.com/uploads/421563IJSETR10436-767.pdf>
24. Deb P, Nath P, Sarker P (2013) Properties of fly ash and slag blended geopolymer concrete cured at ambient temperature. *New Develop Struct Eng Constr* 5(7):1–6. https://doi.org/10.3850/978-981-07-5354-2_M-55-433
25. Edward S (2009) Drying shrinkage of heat-cured fly ash-based geopolymer concrete. *Mod Appl Sci* 3(12):14–21. <https://doi.org/10.5539/mas.v3n12p14>
26. Deb P, Nath P, Sarker P (2015) Drying shrinkage of slag blended fly ash geopolymer concrete cured at room temperature. *Procedia Eng* 125(4):594–600. <https://doi.org/10.1016/j.proeng.2015.11.066>
27. Ramujee K, Potharaju M (2014) Permeability and abrasion resistance of geopolymer concrete. *Indian Concr J* 88(12):34–43. <https://www.researchgate.net/publication/288388226>

A Machine Learning Perspective for Remote Sensing



Nagendra Panini Challa, Parupally Sridhar, and J. S. Shyam Mohan

Abstract Machine Learning (ML) deals with different sets of algorithms ranging from data collection to classification for producing effective outcomes with good accuracy. ML is a subset of Artificial Intelligence (AI) which is utilized as an effective approach to solve wide number of problems related to remote sensing and many more. The growing availability of datasets in remote sensing with different domain-specific properties helps us to classify them for different real-time applications. These datasets provide us a promised pathway for future research of remote sensing using different new-age computing techniques. This paper showcases different ML techniques which are applied to various datasets for solving different remote sensing problems with various demonstrated capabilities for ML modelling.

Keywords Machine learning · Artificial intelligence · Datasets · Algorithms · Remote sensing · Algorithmic analysis

1 Introduction

Machine Learning (ML) is a constructive strategy that combines various heuristic approaches for classification of different non-structural systems. These systems combine different variables for wide range of applications that are dependent on various training datasets for achieving good accuracy after classification [1]. ML deals with different subsets of problems which are collected from multiple observations from the real-time world. These instances provide multivariate solutions which are based on wider classification techniques. Remote Sensing (RS) has been very

N. P. Challa (✉) · P. Sridhar
Shri Vishnu Engineering College for Women (A), Bhimavaram, India
e-mail: cnpanini@svecw.edu.in

P. Sridhar
e-mail: parupallysridhar@svecw.edu.in

J. S. Shyam Mohan
Sri Chandrasekharendra Saraswati Viswa Mahavidyalaya, Kanchipuram, India

successful in classification of various images right from pre-processing to classification in ML [2]. There is change in techniques from neural networks to efficient SVM classifiers like Regression, Decision Trees, and Support Vector Machines (SVM). These techniques suit better for remote sensing due to their effectiveness toward handling high dimensionality datasets [3]. Some of the algorithms like Random Forest (RF) are very popular as they are compatible toward different classification parameters and are highly accurate.

Many RS datasets utilize various image analysis algorithms to identify land, land-covers, scenes, and various physical objects [4]. All these input data are transformed into different accuracy-based solutions which rely on various parameters or attributes. All these features are learned to form a high-level feature database that enhances the output effectively according to the user perspective [5]. There are different new-age computing methods like Deep Learning (DL) and machine learning which help easy classification of input to build an effective solution [6]. In deep learning, there are multivariate hidden layers that are focused on data dissemination to all the layers in the system. Due to the advancements in computing algorithms, all the techniques are abstracted into a single word library which does all the functionalities required from the input provided [7, 8]. As a part of these advancements, all the high dimensionality datasets are transformed into effective solutions by considering different classification experiments. One such technique in ML-like maximum likelihood classifier is most commonly used in RS due to its parametric way of approach. The author has identified that the accuracy is highest among different ML methods due to its wide availability of abstracted software packages [9]. Many datasets are answered with wide ML techniques which are identified as better solutions to address the complexities in the data attributes and to provide an effective solution [10]. This paper is organized with second section for literature survey on machine learning methods with remote sensing, third section for ML applications with remote sensing, next section with conclusion and future directions.

2 Literature Survey

In early 90s different ML methods are utilized for different RS datasets as they are ignored because of the computation complexity and non-availability of pre-defined algorithm libraries [11]. Many researchers addressed various issues in computation with RS datasets which are listed as below (Table 1).

RS datasets are more responsive when computer vision algorithms are applied to them. The ML approaches are accepted by different remote sensing communities than DL as they are hard to train the collected datasets. Many algorithms such as backpropagation in SVM classifiers are more efficient to obtain the accurate output [12].

Deep Learning provides less accuracy when compared with new-age computing techniques like machine learning and artificial intelligence. This is due to the lack

Table 1 Literature survey

Paper title/topic	Findings	Summary/solutions
(1) Deep Learning for image analysis	Neural Network comprises units with certain parameters	Transform input data to outputs while learning progressively high-level attributes
(2) Multivariate deep neural network for traffic sign identification	Deep Neural Network for traffic sign classification	Outperforming various ML algorithms in wide application areas
(3) Deep learning in remote sensing	Deep learning application with a comprehensive review	DL subsequently received much greater attention in different sub-fields of computer vision

of understanding of the domain-specific properties of the datasets which lacks interpretation for major algorithms. Many algorithms are designed for achieving better accuracy which involves in high prediction rate. Due to this, the decision-making aspect of the system is affected which affects the overall system performance mainly with medicine and banking sector. Nowadays various data-driven methods are implemented to handle RS applications such as flash floods susceptibility, soil erosion, landslide detection, and others. These natural hazard detection involves various advanced machine learning techniques like decision trees, regression, neuro-fuzzy systems, artificial neural networks (ANN), and support vector machines (SVM). Some of the RS applications utilize multi-layer perception neural networks for achieving high accuracy as the data is probably multivariate in nature. These techniques are used for landslide assessment and soil erosion detection [13]. The data is always complex in nature as the real-time detection of these unexpected hazards is an unsolvable challenge. Different advanced techniques involving artificial intelligence are much needed to detect natural hazards.

3 ML Datasets for Remote Sensing

ML algorithms are applied to various datasets related to RS which are enhanced with R and python programming language in variety of research papers. The observations in many articles are carried out using Scikit-learn for python, R Statistical tool, and Weka tool which provides all possible accurate outcomes related to RS [14]. A comparison of various available datasets for RS are listed below (Table 2).

Table 2 Repositories of datasets for remote sensing

Paper/dataset title	Problems identified/information	Solution/summary
Remote sensing image classification	To classify images using neural network classifier	Dataset consisting of different traffic conditions is constructed and individual classes are identified as outcomes
Statlog dataset	Original Landsat data for this database was generated	Data purchased from NASA by the Australian Center for Remote Sensing
SpaceNet	High-resolution satellite imagery and labeled training data	Largest Open Data repository available for training your (remote sensing) machine learning algorithms
Landsat data	Created by taking average values from image ranges from each individual year	Used for classification in different tropical ecosystems

3.1 Indian Pines Dataset

This dataset is made available by Purdue University which consists of images of 20 m pixels collected from Indiana, USA [15]. This dataset images have agricultural data which are categorized into seven classes namely corn, grass, hay, oats, soybeans, trees, and wheat. The classification done by one of the researchers has resulted in a single class (soybeans class in this case) outcome as the training data is not adequate to train the model. Hence random sampling is implemented here to treat this imbalanced dataset and the results are below (Table 3).

Table 3 Number of samples for Indian pines dataset

Class	Number of pixels		
	Training	Validation	Total
Corn	14	40	54
Grass	626	1876	2502
Hay	131	392	523
Oats	5	15	20
Soyabeans	1012	3038	4050
Trees	324	970	1294
Wheat	53	159	212
Total	2287	6857	9144

Table 4 Number of samples for GEOBIA dataset

Class	Number of pixels		
	Training	Validation	Total
Building	14	45	59
Car	25	97	122
Concrete	15	21	36
Grass	23	93	116
Pool	29	83	112
Shadow	15	14	29
Soil	16	45	61
Tree	17	89	106
Total	154	487	641

3.2 GEOBIA Dataset

This dataset is collected by University of California which consists of landcover dataset from a beach in USA [16]. This collection uses image-based analysis which is classified into nine classes namely trees, grass, soil, and others. All these object features are trained comparatively less with analysis of presently available datasets. This dataset is mapped with different raw data of locations facilitating efficient classification of classes (Table 4).

4 ML Algorithms for Remote Sensing

The knowledge mentioned in any dataset does not require information about the relationship between attribute selection pairs within the dataset [17]. The ML algorithms are categorized into three different areas such as

- i. Using ML as an accelerator tool than utilizing traditional methods
- ii. Retrieving empirical analysis from available data
- iii. Identification classification problems in dataset.

Machine Learning includes wide variety of algorithms as mentioned in Sect. 2 which are effective toward various earth science applications. Generally, ANN and SVM are widely used for RS and Geoscience applications. Many researchers focus on extensive use of neuro-computing using fuzzy logic approach for geoscience applications. Some research works are combined with various ML-based hybrid methods like neural-genetic, fuzzy-genetic, and many more. These approaches are successful in solving different problems related to geological, geophysical, and reservoir engineering. Some applications related to genetic programming (GP) are successful toward RS domain which facilitates automatic selection of computer programs naturally to build effective individual solutions. These GP approaches are utilized to

classify behaviors of different physical objects like rocks. These approaches are focused on estimating various rock properties which identify the rock strength from a computational perspective.

Various GP approaches are based on gene and multi-expression programming interfaces which are developed using different experimental datasets which produce good accuracy in terms of tensile strength as they are related to hard physical rock masses [18]. This form of analysis forms a strong base for constructing high-rise buildings that aim to be reliable and durable in a long way. This analysis is hence a potential tool for predicting granite rock strength [19]. The differentiation between rocks for easy identification of their usability is implemented by using 40 k dataset attributes which have produced good accuracy by analyzing their characteristics. Various rocks are classified from GP methods like basalt, ignimbrite with different colors, and many more. Various ML techniques are successful for easy perception of RS images whose outcomes are based on different parameters such as rainfall, water quality detection, landslide detection, soil moisture analysis, and many more [20]. RS is widely used in agricultural sector for widely analyzing crop yield and crop growth through various physical devices called as sensors. These devices are helpful in identifying similarities between various data attributes which are computed from cloud-based methods.

5 Conclusion

There are different computational impacts of ML on remote sensing datasets that are capable of producing interesting analyses about the real-time environment. There are different ML algorithms such as regression, decision trees, neural networks, SVM, and many more efficient techniques which are ideal for RS datasets. This paper focuses on ML perspective on RS which addresses various methods, impacts, and identifications of various RS datasets. Various researchers are committed to producing effective results utilizing these computational advancements in real world. In future various works on RS datasets with AI-based approaches can be implemented for advanced analysis of real-time data scenarios.

References

1. Turner MG, O'Neill RV, Gardner RH, Milne BT (1989) Effects of changing spatial scale on the analysis of landscape pattern. *Landsc Ecol* 3:153–162
2. Vanderhoof MK, Alexander LC, Todd MJ (2016) Temporal and spatial patterns of wetland extent influence variability of surface water connectivity in the Prairie Pothole Region, United States. *Landsc Ecol* 31:805–824
3. Zhou W, Pickett STA, Cadenasso ML (2017) Shifting concepts of urban spatial heterogeneity and their implications for sustainability. *Landsc Ecol* 32:15–30

4. Bertrand C, Burel F, Baudry J (2016) Spatial and temporal heterogeneity of the crop mosaic influences carabid beetles in agricultural landscapes. *Landsc Ecol* 31:451–466
5. Street GM, Fieberg J, Rodgers AR, Carstensen M, Moen R, Moore SA et al (2016) Habitat functional response mitigates reduced foraging opportunity: implications for animal fitness and space use. *Landsc Ecol* 31:1939–1953
6. Azam C, Le Viol I, Julien J-F, Bas Y, Kerbirou C (2016) Disentangling the relative effect of light pollution, impervious surfaces and intensive agriculture on bat activity with a national-scale monitoring program. *Landsc Ecol* 31:2471–2483
7. McGarigal K, Wan HY, Zeller KA, Timm BC, Cushman SA (2016) Multi-scale habitat selection modeling: a review and outlook. *Landsc Ecol* 31:1161–1175
8. Baudron F, Schultner J, Duriaux J-Y, Gergel SE, Sunderland T (2019) Agriculturally productive yet biodiverse: human benefits and conservation values along a forest-agriculture gradient in Southern Ethiopia. *Landsc Ecol* 34:341–356
9. Wan HY, Cushman SA, Ganey JL (2019) Improving habitat and connectivity model predictions with multi-scale resource selection functions from two geographic areas. *Landsc Ecol* 34:503–519
10. Cushman SA (2016) Calculating the configurational entropy of a landscape mosaic. *Landsc Ecol* 31:481–489
11. Seidl R, Donato DC, Raffa KF, Turner MG (2016) Spatial variability in tree regeneration after wildfire delays and dampens future bark beetle outbreaks. *Proc Natl Acad Sci USA* 113:13075–13080
12. Herold M, Scepan J, Clarke KC (2002) The use of remote sensing and landscape metrics to describe structures and changes in urban land uses. *Environ Plan A* 34:1443–1458
13. Shean DE, Alexandrov O, Moratto ZM, Smith BE, Joughin IR, Porter C et al (2016) An automated, open-source pipeline for mass production of digital elevation models (DEMs) from very-high-resolution commercial stereo satellite imagery. *ISPRS J Photogramm Rem Sens* 116:101–117
14. Vermote E, Justice C, Claverie M, Franch B (2016) Preliminary analysis of the performance of the Landsat 8/OLI land surface reflectance product. *Rem Sens Environ* 185:46–56
15. Immitzer M, Vuolo F, Atzberger C (2016) First experience with Sentinel-2 data for crop and tree species classifications in Central Europe. *Rem Sens* 8:166
16. Dwyer J, Roy D, Sauer B, Jenkerson C, Zhang H, Lyburner L (2018) Analysis ready data: enabling analysis of the Landsat archive. *Rem Sens* 10(9):1363
17. Egorov AV, Roy DP, Zhang HK, Hansen MC, Kommareddy A (2018) Demonstration of percent tree cover mapping using Landsat analysis ready data (ARD) and sensitivity with respect to Landsat ARD processing level. *Rem Sens* 10:209
18. Hermosilla T, Wulder MA, White JC, Coops NC, Hobart GW, Campbell LB (2016) Mass data processing of time series Landsat imagery: pixels to data products for forest monitoring. *Int J Digit Earth* 9:1035–1054
19. Gao F, Hilker T, Zhu X, Anderson M, Masek J, Wang P et al (2015) Fusing Landsat and MODIS data for vegetation monitoring. *IEEE Geosci Rem Sens Mag* 3:47–60
20. Zhao Y, Huang B, Song H (2018) A robust adaptive spatial and temporal image fusion model for complex land surface changes. *Rem Sens Environ* 208:42–62

A Review on Structural Stabilization and Strengthening Through Retrofitting



Pala Gireesh Kumar and Sahitya Yeegalapati

Abstract Reinforced Cement Concrete Structural members experience several problems like structural damages through cracks, over loadings, constructional and design faults, rusting effects, intensive earthquake damages, etc., which are needed to be tackled. Stabilization and strengthening of structural components are very important which can address the above-mentioned problems in concrete structures known as retrofitting. A number of structures till date are severely affected due to frequent earthquakes, disasters etc. With the elucidation on retrofitting, the paper deals with numerous techniques in use and those carried out on retrofitting of structures. State-of-the-art developments and the important approaches relevant to this field of retrofitting of structures were discussed. It has been observed that retrofitting is to be used upon many of the structures like bridges, schools, hospitals, pipelines to decline the rate of failure as they tend to incur huge loss to the society and the observations made from the studies are, health of the structures are to be monitored and assessed about every ten years. It has become evidential that the structures which have undergone retrofitting has proven to have controlled the level of damage and often aided in retrieving the lost strength thereby, averting any further distresses. The current study reveals the necessity of retrofitting and discussed various retrofitting methods like Epoxy Injection, Section enlargement and Grouting, Fiber Reinforced Polymer (FRP) composites, External Post-tensioning and plate bonding and Near Surface Mounted FRP bars or Strips were also reported in this paper. However, further investigations can be carried out on effective utilization of retrofitting technique to the existing structures which can increase the chances of surviving future earthquakes.

Keywords Retrofitting · Structural stabilization · Techniques · Earthquake · Strength · Rehabilitation

P. Gireesh Kumar (✉)

Department of Civil Engineering, Shri Vishnu Engineering College for Women (A), Bhimavaram, W.G District, Andhra Pradesh 534202, India

S. Yeegalapati

Department of Civil Engineering, Shri Vishnu Engineering College for Women (Autonomous), Vishnupur, Bhimavaram, Andhra Pradesh, India

1 Introduction

It has become noticeable that most of the structures built in the past have undergone severe damage due to the earthquakes and resulting in distress. And due to the intensive effect caused, a survey has become mandatory after the earthquake to identify the level of distress the structure suffered [1]. As there are a multiferous variety of structures to be dealt with a unique rule of retrofitting, it isn't easy to have controlled customs for the process, rather the process is purely dependent on the strength aspects of the structure. The health of the structure gets deteriorated over period of time which is very similar to human beings, and the capacity of the structure also gets reduced considerably [2] because of the damages caused to the concrete structure as portrayed in Fig. 1. And it draws to the part of the decision-making whether to have the structures which are already distressed and work on restoration or retrofitting else, completely obliterating the structure. Retrofitting refers to the operation of diminishing the distress that might affect an actual structure caused due to natural disasters like earthquakes etc., by incorporating supplementary characteristics to the structures [3]. It deals with the process of reckoning strength to the structures with the design codes of earthquake-prone areas in line. Unlike the conventional approaches, this has to deal with recovering the strength of damaged structures or taking prior action to structures from experiencing severe conditions such as soil failure or ground movement owing to earthquake or seismic actions that might occur or has already happened due to catastrophes [4]. In most cases, a structure stands out to be of absolute value in society, and thus, it is unwelcoming to demolish such buildings. Therefore, retrofitting has become a handy option in strength recovery for such structures which also deals with the enhancement of the actual lifetime of construction [5].

Of all the natural cataclysms, an earthquake is one of the most critical events which eventually destroy the structure. And as a result, the structure falls short of strength and loses its resistance to loads [4]. Loss of strength due to such activities often results in roof deterioration, beam and column failure, cracks in the walls, and a flawed foundation [6]. This makes the structure uncertain of the safety and often collapses in most unfavorable scenarios. In addition to the enhanced strength attribute, retrofitting also inclines the level of safety during such activities and it has been practically proven that a retrofitted structure has more damage-control in comparison to a normal structure with a high rate of structural resistance [7].

This paper gives sound knowledge on the necessity of retrofitting undertaken in order to regain structure strength and stability during seismic activity. The various repairs and retrofitting techniques and methods were elaborately discussed and presented in this paper as stated in Fig. 2. However, there is an ample scope that exists to carry out further investigations on effective utilization of retrofitting technique to the existing structures which can increase the chances of surviving future earthquakes.

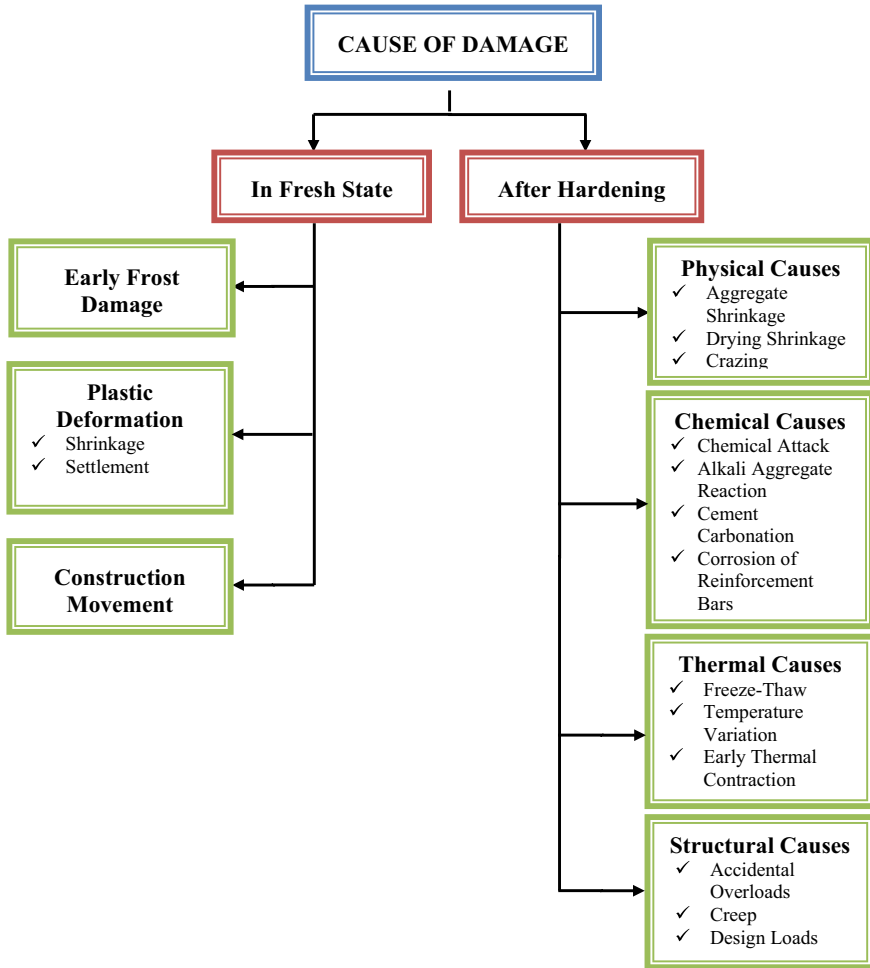


Fig. 1 Causes of damage (in fresh and hardening stage)

2 Principles of Structural Strengthening and Retrofitting Design

As aforesaid, retrofitting deals with strength recovery with the enhancement of structures survivability and durability. It is based on certain policies as stated below.

- Structural system versus Members Strengthening.

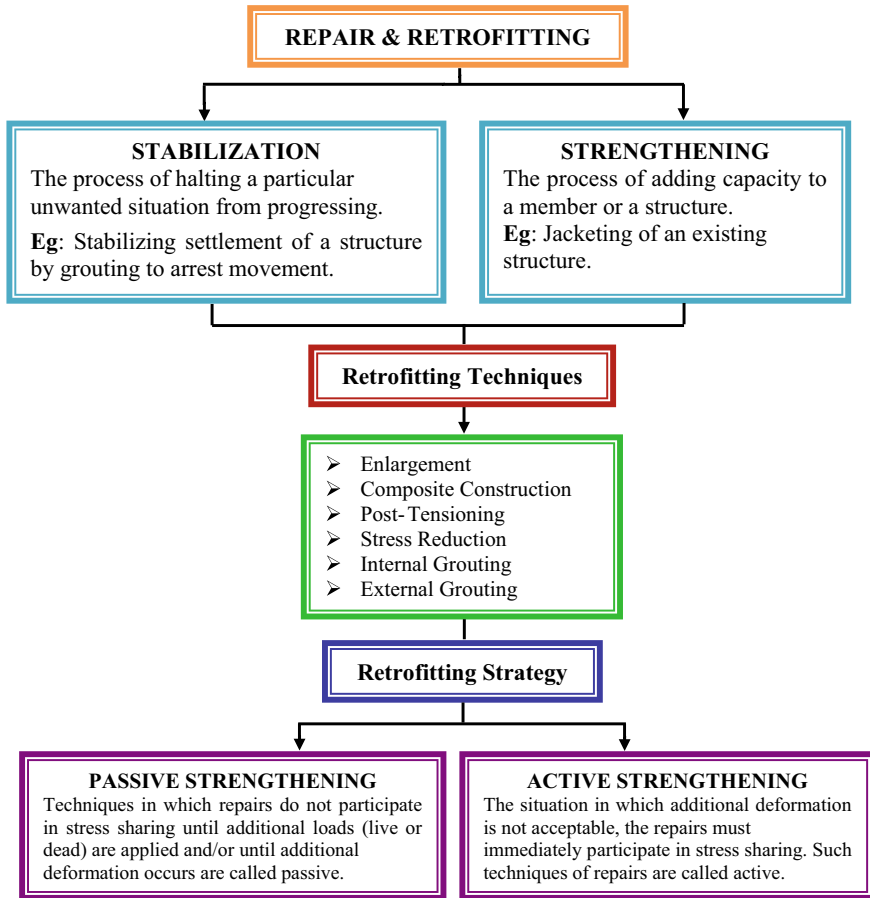


Fig. 2 Repair and retrofitting techniques, strategies

It is observed that retrofitting for strengthening is focused on members which are distressed. But it is recommended for a check of the entire structural system to avoid failure of the structure.

- Global versus Local Strengthening.

The latter is a case where the individual units are retrofitted without disturbing the entire structural unit. This is recommended only when no adverse effect on the structure as a complete unit.

- Permanent versus Temporary Strengthening.

Temporary strengthening goes with short course retrofitting where the repaired units function for a certain amount of time. Permanent strengthening enhances the overall life span of a structure.

- Strengthening with explicit deliberations for resistance to earthquakes.
- Usage of contemporary seismic techniques.

3 Literature Reviews

Zengyan and Hiroyuki, states that, collapses of adobe structures due to earthquakes and leads to tremendous losses of human life and property. A numerical method has been developed for predicating the earthquake responses of adobe structures. Nonlinear finite element method is utilized and the discontinuity of the interfaces between adobe bricks is also considered applied to estimate the earthquake responses of an adobe house. Finally, a retrofitting technique with wooden frame is proposed and its efficiency is verified [8].

Jack P. Moehle, proffered that a high rate of structures in the United States falls out of codal provisions of seismic requirements. This, in turn, makes them exposed to earthquakes resulting in a higher scale of destruction. To defend and shield the structures from such losses, National Science Foundation has proposed a program of coordinated research in 1990 that deals with the repair and retrofitting of structures. The submitted reports by NSF, it has suggested that the maximum number of failures have occurred in columns. The failures comprised numerous causes like soft-storey development, reinforcement buckling in the longitudinal section of the columns, distress of shear in columns, etc. It is reported that the breakdown of more than one storey caused column failures in several cases. Eventually, this disturbed the limit state of the structure and the way it is designed to withstand the load [9].

Matthys and Noland, study stated that three-fourth of the structures are masonry and an earthquake of intermediate to intense level is capable of causing a huge loss of lives and end up creating massive destruction. Improper reinforcement of structures is recorded as one of the causes for such devastating failures and retrofitting is suggested as a snag for preventing such losses. Also, surface treatment involved shot creting, reinforced plastering, and ferro cementing. The surface processing has helped in escalating the exterior properties of masonry structures and thereby, furnishing a pleasing appearance to the structure [10].

Motavalli et al., explained about his focused study on the influential aspects on which a structure's life span is altered. The concept of ductility, shear, and flexural strength, durability, and stiffness are reported with the reasoning of how retrofitting helps in improving each aspect. The codal provisions where seismic retrofitting is required are stated as the structures fall off the line of codes and, often end up failing. His study also dealt with the effect of environmental conditions and effects on structures and revised loading patterns with design and damage control [11].

Canales et al., declared that structures are characterized by having heavy live loads, large storey heights and long spans. Through elastic structural analysis, seismic response of the building is computed. For a better resistance, foundation must be modified to be able to transmit the loads generated by the new lateral force resisting system into the supporting soil. Based on many practical analysis and test results,

it is found that the seismic behavior of telephone building has been improved with adequate retrofitting techniques like strengthening of masonry walls, concrete walls, braced steel frames, strengthening of foundation [12].

Muhammad Ammad Hassan et al., carried out an experiment on strength intensification using strips of steel in the walls of masonry structures. Focusing on compressive and shear strength of masonry structures, all the results of uncracked state to fully cracked state were noted. From the results and conclusions obtained, it is evident that the inclusion of steel strips in the walls of masonry structures has proven to withstand loads and sudden movements due to earthquakes. Especially in the case of retrofitting and rehabilitation, this technique equipped a good life span with recovered strength to deteriorated structures [13].

Carpinteri et al., explained that fibre reinforced sheets are becoming extensively used as structural repair method when concrete deteriorates. In this subject area the repair process must successively accommodate with new materials in previously constructed one. To improve their loading carrying capacity a set of FRC has been retrofitted with FRP sheets. Many tests have been resulted up to failure under three point bending. During the test process the acoustic emission technique has been used for damage evaluation [14].

4 Retrofitting Techniques

From the performed studies from diverse papers, it has become obvious that earthquakes are of primary concern as they cause severe damage to the structures. Eventually, resulting in loss of strength and collapsing even before the design lifetime. Despite knowing the major concern, the majority of the structures are not designed under seismic loading provisions which are leading to structural distress and failures. In the recent times, the earthquakes have once again proven to deteriorate the structures and thereby proving that structures needs to be retrofitted to avoid such devastating effects. Diversified techniques have come into the practice with added improvements that sustain the design life and strength of masonry structures. The predominant approaches are FRP composites using FRP plates and sheets, Adobe Structure Modelling, Identification of failures using techniques, and Braced Steel Frame inclusions.

4.1 FRP Composites

This is one of the advantageous techniques which are handy to install and considered to be the preferred application of strength restoration. FRP composites economic capacity is one of the assets that devise it to be a good substitute to machinery and is also favored in the place where mechanical techniques using machines cannot be accessed for retrofitting. Figure 3 indicates different forms of FRP composites

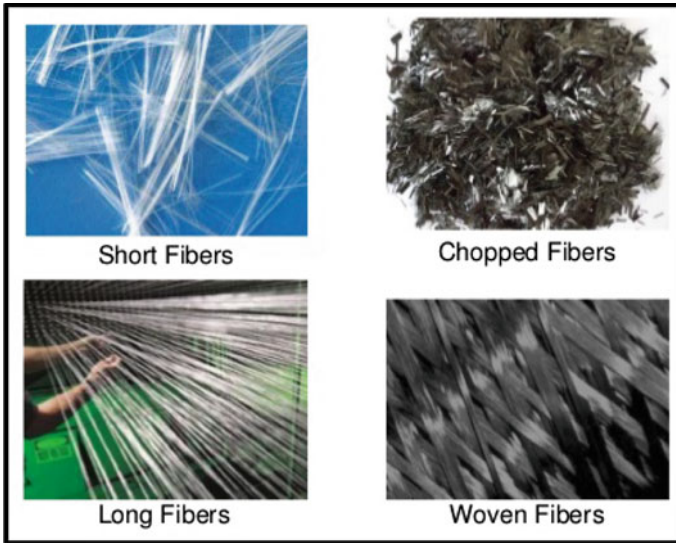


Fig. 3 Types of FRP composites

available [15].

4.1.1 Flexural Strengthening of RC Structures Using FRP Plates and Sheets

Epoxy is used in strengthening using FRP composites. The structural units like columns, beams, and plates are affixed by employing FRP composites which work in strengthening agents with epoxy serving as an additive for attaching the units to the zone of tension. The fibers of the FRP composites are laid in parallel to tensile stresses. The FRP composites used in the process can be either sheets or strips depending upon the necessity for flexural strengthening of structures. Figure 4

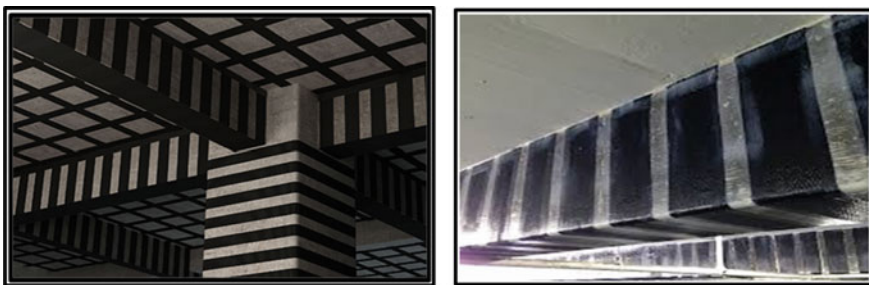


Fig. 4 Usage of FRP sheets and plates in RC structure for shear strengthening

showcases a RC girder with prefabricated CFRP strips in Poland.

The method for shear strengthening involves affixing FRP composites to the web on either side. The fibers of FRP composites are placed opposite to the stress. The fiber can either be placed perpendicularly or at an acute angle of 45°. CRFP plates of L-shape should be in this technique and, this method has been practically implemented in the design of Duttweiler Bridge, Switzerland. Also, CRFP strips of L-shaped are affixed for flexural strengthening.

4.1.2 Advantages

- Handy and no skilled labor is required for installation purposes.
- FRPs are a cheaper source of retrofitting where the installation cost is minimal in comparison to other techniques available.
- Despite the fact of manufacturing materials posing a high rate, the post-installation comprising of fabricating the structure, application of fibers, protection against exterior deteriorating forces, and cost of maintenance makes it more favored technique
- These are a source of retrofitting for minor works as well. Though FRP composites cannot alter a complete replacement of conventional type, they prove to be an ideal source for medium-level projects. With proper design guidelines and provisions, they can also be used for complicated structures.

4.2 Modeling of Adobe Structures

With the establishment of a theoretical correlation between discontinuity principle and method of finite element analysis, a 3-D nonlinear analytic method is developed for analyzing the earthquake responses of adobe structures [16]. In this study, for predicating the earthquake responses of adobe structures, a numerical method has been developed, where nonlinear finite element method is utilized and the discontinuity of the interfaces between adobe bricks is considered. Then, the methodology is applied to estimate the earthquake responses of an adobe house. Finally, a retrofitting technique with wooden frame is proposed and its efficiency is verified [17].

4.2.1 Separation of Walls

Separation at the junctures of the longitudinal walls and the gable walls occurs when earthquake shaken in the right-left direction. Separation started from the tops of the junctures and with the extension of the shaking time and the increment of shaking intensity, the separation extended vertically downward until the collapse of the house [5]. Although the physical connection at the junctures of the walls is considered in the model, this type of failure is still dominant.

Fig. 5 Opening corner crack

4.2.2 Opening Corner Crack

Serious opening corner cracks as shown in Fig. 5 occurred independently on the shaking direction. But with the variation of shaking direction, the mechanism of such failure changed. The trembles in the longitudinal direction of the house result in opening corner cracks based on the level of concentration of shear stress in that range. On the other side, when earthquake shake in the direction perpendicular to the longitudinal walls, such cracks occurred due to the tensile stress concentration [18]. This kind of tensile crack is inferred to be a subsequent result of the failure mode “out of plane bending”.

4.2.3 Retrofitting Measures

For improving the dynamic material properties of adobes, some reinforcement materials such as gypsum and straw, etc., are used and for improving the structural stability, some measures such as concrete and wooden frames, columns, etc., are being considered. It is thought that a retrofitting technique should raise the earthquake resistibility effectively with least cost increment [3].

It is clear that the retrofitting techniques proposed in the study can improve the earthquake resistance of adobe houses remarkably. Other additional measures such as adding corner wooden columns, etc., may strengthen the adobe house, and their effects are under investigation at present. But taking account of the balance of effectiveness and its cost and applicability, the measures proposed in the paper are considered to be reasonable (Table 1).

4.3 Failure Techniques

Earthquakes have adverse effects on structures and, as referenced earlier, column failures imply the serious condition for structural failure. It is often that buildings collapse

Table 1 Analytic result when the maximum earthquake acceleration was 300 cm/s² [8]

Retrofitting measure	Shaking direction	
	Right-left	Back-forth
Method 1	The top of the gable walls fallen down	Concentrated shear damage at the bottom of the walls occurred, but no collapse
Method 2	Crack in the opening corner area occurred, but no collapse	Horizontal cracks occurred in the upper part of the longitudinal walls, but no collapse



Fig. 6 Column failure and building collapse

due to column failure caused by seismic movements when no proper reinforcement is designed as in Fig. 6.

4.3.1 Two General Approaches

The former method involves the structural modification in the global level where non-structural and structural units are replaced when they are on a lower level than their actual capacities. This approach entails the incorporation of braces of steel, isolating base, structural walls, etc. Also, the scheme of energy distribution (passive) is rare as the requisite capacities are high than the existing ones and, active control also falls under rare mode of implementation [19].

The second approach is to focus locally on intensifying the capacity of deformation of structural units which possess low capacity than their actual design. This leads to a gap so that the units don't reach the level of deterioration. This approach customs the inclusion of concrete, jackets of fiber-reinforced polymer composites (FRPC), steel, etc.

Global modification is one of the common approaches local modifications followed in the United States. Despite the approaches and designed provisions, there are a lot of complications in framing specific models for the required flexibility

of foundations. Therefore, the criterion for conservative acceptance comprises the combined application of both local and global modifications [20].

4.4 Failure of URM Buildings

Failure of a structure results in massive loss of lives and property. One of the strongest reasons for the occurrence of failure is the inappropriate reinforcement used in the design of structures. As three-fourth of the world's structures are of masonry type, earthquakes can bring down structures to the ground and, this is quite common in the case of unreinforced masonry (URM) structures. Table 2 portrays the summary of retrofitting methods.

Based on various survey and investigations it is proved that there are various methods and techniques to retrofit the URM structures. Some of the methods are as follows:

- (a) Injection
- (b) External Reinforcement
- (c) Center Core
- (d) Post-tension
- (e) Reinforced Plaster
- (f) Ferrocement
- (g) Confinement
- (h) Shotcrete

4.5 Braced Steel Frames

Braced steel frames plays a predominant role in strengthening schemes with many advantages toward the concrete structures. In braced steel frame system of strengthening, an additional braced steel frames added to the existing structure as in Fig. 7. This frames work as a vertical Trusses and can be placed in interior as well as exterior of the building. For the installation of steel bracings, existing beams must be avoided and the columns must run continuously [21].

In order to have the needed strength and the guaranteed good ductility avoiding elastic instability of its members an elastic design must be adopted for braced frames. The stiffness of the structure can also be considerably increased [6]. To control lateral displacement and to insure load transfer from the existing structure to the frames and adequate stiffness is mandatory.

Major considerations on use of Braced Steel Frame,

- The location of frames in plan must be as symmetrical as possible.
- Desirable torsions are to be eliminated with symmetry.
- The number of frames depends on the magnitude of the load applied.

Table 2 Summary of retrofitting methods [2]

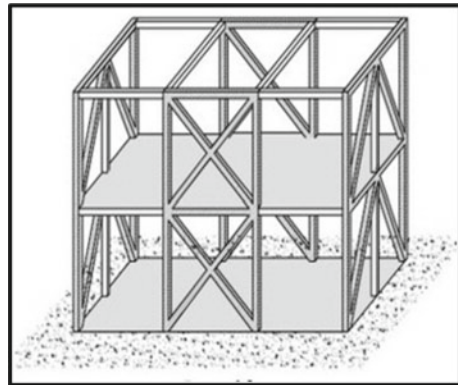
Method of approach	Productivity	Precedence	Drawbacks
Injection	Initial Stiffness Restoration	<ul style="list-style-type: none"> No considerable change in mass of the structural unit with no effect on the functionality of structure Also, there is no shrinkage of spacing and impact on arch 	<ul style="list-style-type: none"> The additive, Epoxy, often invents strength and stiffness zones variations The rate of epoxy is significantly high Also, there is no evident note of any escalation with the usage of grout (cement-based) in Fr
External Reinforcement	N.A	<ul style="list-style-type: none"> Considerable higher increment in F_{ur} Holds back disintegration and improves ductility and E.D 	<ul style="list-style-type: none"> Occurrence of Corrosion, Higher rate of mass (heavy) Performance level violations Arch requirement and proper finishing, occupancy disturbances
Center Core	F_{ur} Escalation	<ul style="list-style-type: none"> No shrinkage in space No decline in impact of arch and on functionality of building 	<ul style="list-style-type: none"> Zones formation with differential strength and strength
Post-tension	F_{ur} Escalation	<ul style="list-style-type: none"> No addition if mass and effect on functionality of building 	<ul style="list-style-type: none"> Losses are high Systems of anchorage Potential of corrosion
Reinforced Plaster	Enhancement in stability	<ul style="list-style-type: none"> Addition of very less mass and technology 	<ul style="list-style-type: none"> Decline in space, Decline in the impact of arch and required arch Requirement of proper finishing
Ferro cement	Enhancement in stability	<ul style="list-style-type: none"> Addition of very less mass and lower cost and technology 	<ul style="list-style-type: none"> Decline in Space, Decline in the impact of arch and required arch Requirement of proper finishing limitation in efficiency and E.D
Confinement	Holds back disintegration	<ul style="list-style-type: none"> Holds back disintegration with improvement in ductility and E.D 	<ul style="list-style-type: none"> Introduction of limited effect is hard on F_{ur} of arch requirement Requirement of proper finishing Occupancy disturbances

(continued)

Table 2 (continued)

Method of approach	Productivity	Precedence	Drawbacks
Shotcrete	Enhancement in stability	<ul style="list-style-type: none"> • Considerable higher High increment in F_{ur} significant rise in E.D 	<ul style="list-style-type: none"> • Decline in Space • Higher rate of mass (heavy) • Performance level violations, • Occupancy disturbances, need for impact of arch and required arch • Requirement of proper finishing

Fig. 7 Braced steel frames model



- Load concentration can be generated in foundations.
- Number of configuration of frames must be adjusted to reduce load concentration.

4.5.1 Types of Braced Frame Connections

- The beam of the frame is welded with a plate made of steel. Also, plates and anchor bolts are used to connect the actual structure’s beam to the strengthening beams. The required friction strength is generated by using rods on the contacting surfaces.
- The shear is transmitted by bearings using steel angle placed in boxes made in the beam. Other important connections are to those to the foundation.

5 Conclusion

With the elongated studies and intense research in the field of structural retrofitting, multifarious techniques have been surfaced into existence for the strengthening of structures. These proposals not only advanced the measures to control damage and deterioration of structures but also enhanced the technology to withstand harsh environmental conditions and devastating impacts of seismic loads. In addition to the new flanged techniques, the revision of load requirements and codal provisions has also been a comforting step in the field of structures dealing with retrofitting. With the growing dependence on high-strength structures, a lot of scope in the study of retrofitting is ameliorated and this led to experimentations with multifarious possibilities of dealing with distresses and stabilization of structural units. Furthering, the necessity for seismic retrofitting has been added to cardinal objectives where theoretical and practical examination along with numerical evaluation and analysis is set forth. Finally, this paper elucidated the call for retrofitting as raising demand for ensuring structural safety and potential approaches dealt with the technique of retrofit.

References

1. Masoud M, Christoph C Swiss Federal Laboratories for Materials Testing and Research Ueberlandstrasse 129, 8600 Dübendorf, Switzerland
2. ElGawady M, Lestuzzi P, Badoux M (2004) A review of retrofitting of URM walls using composites. In: 4th international conference on advanced composite materials in bridges and structures, Calgary, Canada
3. Corazao M, Durrani A (1989) Repair and strengthening of beam-to-column connections subjected to earthquake loading. NCEER Report No. NCEER-89-13
4. Vera R, Albiter A, Miranda S (2000) Seismic capacity evaluation and retrofitting of adobe constructions. Paper No.1981, 12th WCEE, Auckland, New Zealand
5. Perret S, Khayat K, Gagnon E, Rhazi J (2002) Repair of 130-year old masonry bridge using high performance cement grout. *J Bridge Eng ASCE* 7:31–38
6. Aboutaha R, Aboutaha M, Engelhardt J, Jirsa M. Kreger (1999) Rehabilitation of shear critical concrete columns by use of rectangular steel jackets. *ACI Struct J*
7. ElGawady MA, Lestuzzi P Applied computing and mechanics laboratory (IS-IMAC). Swiss Federal Institute of Technology EPFL Lausanne, CH-1015, Switzerland
8. Zengyan CAO, Hiroyuki W (2004) 13th world conference on earthquake engineering Vancouver, B.C., Canada, Paper No. 2594
9. Pan A, Moehle JP (1989) Lateral displacement ductility of reinforced concrete flat plates. *Struct J* 86(3):250–258
10. Matthys H, Noland L (1989) Evaluation, strengthening and retrofitting of masonry buildings. TMS, Colorado
11. Motavalli M, Czaderski C (2007) FRP composites for retrofitting of existing civil structures in Europe: state-of-the-art review. In: International conference of composites and polycon. American Composites Manufacturers Association Tampa, FL, USA
12. Canales ND, de la Vega RB (1992) Retrofitting techniques used in telephone buildings in Mexico. In: Proceeding of the tenth world conference on earthquake engineering, vol 9, pp 5143–5147

13. Hassan MA et al (2020) Improving structural performance of timber wall panels by inexpensive FRP retrofitting techniques. *J Build Eng* 27:101004
14. Carpinteri A, Lacidogna G, Manuello A (2007) An experimental study on retrofitted fiber-reinforced concrete beams using acoustic emission, vol 2. In: Proceedings of the 6th international conference on fracture mechanics of concrete structures, FraMCoS, Catania, Italy
15. Meier U (2004) External strengthening and rehabilitation: where from—where to? , vol 1(2). IIFC FRP International, The Official Newsletter of the International Institute for FRP in Construction, pp 2–5
16. Laursen P, Davidson B, Ingham J (2002) Seismic analysis of prestressed concrete masonry shear walls. In: 12th ECEE, London, England, Paper reference 247
17. Islam MS, Watanabe H (2001) Low cost earthquake resistant reinforcement for adobe houses. ERES, Malaga, Spain, pp 755–764
18. Webster FA, Tolles EL (2000) Earthquake damage to historic and older adobe buildings during the 1994 Northridge, California earthquake. Paper No. 0628, 12th WCEE, Auckland, New Zealand
19. Willie LA, Dean RG (1975) Seismic failures and subsequent performance after repair. In: Proceedings, ASCE national structural engineering convention, New Orleans, April 1975
20. Borri A, Corradi M et al (2002) New materials for strengthening and seismic upgrading interventions. International Workshop Ariadne 10, Arcchip, Prague, Czech Republic
21. Goel S, Lee H (1990) Seismic strengthening of RC structures by ductile steel bracing system, vol 3. 4USNCEE, Palm Springs, CA
22. ElGawady M (In-press) Seismic in-plane behaviour of URM walls upgraded with composites. Thesis dissertation, IS-IMAC, EPFL, Switzerland

Performance Analysis of Jute Fiber Reinforced Concrete Composite



Bidhan Ghosh and T. Senthil Vadivel

Abstract Fibers in concrete are deemed best to increase the lifetime of concrete by avoiding propagation of cracks and doing it with natural fibers is priority in present day. In the current study, Olitorius and Capsularis Jute fibers were used in concrete to find out the manners of Jute Fiber Reinforced Concrete (FRC) which will be the green approach for concrete industry. The current study has proven rise in tensile strength up to 2% of fiber addition and flexural strength up to 1.25% fiber fraction in both jute fibers. Even though the compressive strength decreased while increasing jute fiber fraction but up to 0.75% fiber fraction of Capsularis was found linear increase among other fiber fractions. In Olitorius jute the compressive strength was linearly decreasing from 0.25 fraction itself. Henceforth the optimal percentage of fiber fraction usage in concrete can be 0.75% Capsularis and 0.25% Olitorius.

Keywords Fiber Extraction · Olitorius fiber · Capsularis fiber · Fiber reinforced concrete · Mechanical properties

1 Introduction

Concrete Technologists are continuously executing the research to progress the behavior of concrete. Nowadays, Jute fibers are also another tough waste material to dispose of as all jutes are not being utilized for making packaging bags or other products as end products cost is higher than polymer or polyethylene-based products. The reason for hike in cost of jute is due to long journey of extracting the fibers from the stem which needs to harvest also. Henceforth finding out feasible use of this waste material is really an important task. The current study was motivated to utilize the Jute Fibers available in the eastern part of India namely Olitorius and Capsularis in Concrete and to determine its physical and mechanical properties.

B. Ghosh · T. Senthil Vadivel (✉)

Department of Civil Engineering, School of Engineering and Technology, Adamas University, Kolkata 700126, India

1.1 Literature Review

Limited literature is available in this jute fiber reinforced concrete and those studies are discussed here in this chapter. Mansur et al. [2] did the study on jute fibers. Experiment revealed that jute fibers are appropriate for a low-cost construction material. Razmi et al. [3] investigated that there is remarkable development in compressive, tensile, flexural, and toughness behavior. Ramakrishna et al. [4] revealed that different natural fibers like coir, sisal, jute, hibiscus cannebinus in concrete reveal enhancement in ductility, Impact and fracture toughness and also reduction of shrinkage. Zakaria et al. [5] were inveterate from the test result that the aspect ratio has a vital role. Warke et al. [7] found out jute fiber reinforced concrete is better in performance than plain concrete. For instance, Senthil Vadivel and Doddurani [1] studied the optimal use of waste PET Bottle scraps as fibers in concrete and got satisfactory results with 3% of fiber. Kim et al. [6] noticed high Strength values for jute fiber concrete compared to normal concrete. Tiwari et al. [8] did the comparison of strength for different mixtures of concrete. Zhang et al. [9] identified more increase in Compressive strength than Tensile strength in their study. Sahu and Tudu [10] reported that Modulus of rupture is high for Jute fiber concrete based on their research. Romualdi and Batson [12] revealed in their study that Tensile strength is more for smaller spacing of fibers. Shaikh et al. [11] studied Steel fiber concrete and Jute fiber concrete. They found that Concrete characteristics compressive potency of Steel fiber is more than Jute fiber. Based on the observation, the current study focuses to recognize the optimum utilization.

2 Experimental Study

2.1 Raw Materials

2.1.1 Cement

In the study Portland, Pozzolanic-based Cement (PPC) was adopted.

2.1.2 Fine Aggregate

Fresh sand was taken from local river. The relative density of such aggregate was set up at 2.53. All sieve analysis test results were found within the permissible results as guided by IS 383-1970.

2.1.3 Coarse Aggregate

Fresh angular aggregate was taken from local shop. The relative density of such aggregate was set up at 2.75. All sieve analysis test results were found within the permissible results as guided by IS 383-1970.

2.1.4 Water

Water free of deleterious concrete and steel was adopted.

2.1.5 Jute

Two types of Jute namely Olitorius and Capsularis were taken from research institute (CRIJAF, Kolkata-700120).

3 Methods

3.1 Characteristics Compression Strength

The characteristics compression test is done to calculate the characteristics compression strength of concrete after 7, 14, and 28 days of curing as per Indian standard IS:516-1959. Mold size of 150 mm × 150 mm × 150 mm cube is used for finding out the strength (Fig. 1).

Fig. 1 Test on compression strength

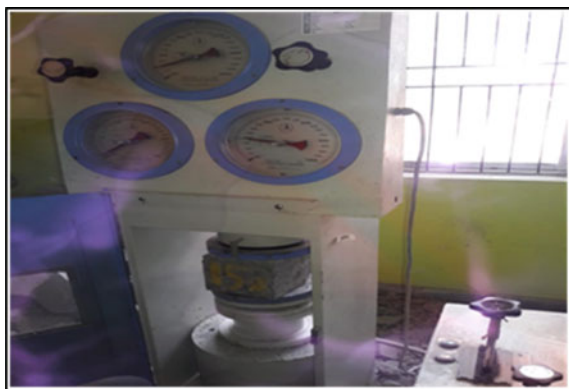


Fig. 2 Test on tension strength



3.2 Tension Test

Cylindrical specimen was considered for determining the tension strength. The length of the specimens for testing is 300 mm with diameter of 150 mm. Generally, the mold is filled in five layers providing tamping bar stroke of 30 for each layer using 16 mm tamping rod. But in this research vibration table is used for compaction (Fig. 2).

3.3 Bending Strength

Bending (flexure) strength is the characteristic of concrete which shows the capacity to resist deformation under a certain bending moment. The sample is bent using a two-point flexural test technique until the specimen is cracked. The two-point load is placed at a distance of one-third of span. Mold size of 100 mm × 100 mm × 500 mm prism is used for finding out the strength (Fig. 3).

Fig. 3 Test on bending strength



4 Results and Discussion

Two types of jutes namely Olitorius and Capsularis are taken and tested from CRIJAF, Kolkata-700120. The properties of Jute are shown in Tables 1, 2, 3 and 4.

Portland Pozzolanic-based Cement (PPC) was used in the study. Its physical and chemical properties are shown in Tables 5 and 6.

Naturally, available sand is utilized in this project. All the tests were conducted as per IS 383 Indian standard code. The physical parameter of such aggregate is shown in Table 7.

Adequately cleaned dry stones are used as a coarse aggregate for all the mix in this project. All the tests were conducted as per IS 383 Indian standard code. The physical parameter of such aggregate is shown in Table 8.

The mix design was done as per IS 10262. The target strength was M40 with standard deviation of 5. Adopted w-c ratio is taken as 0.45 with target slump of 100 mm. Per cubic meter of concrete, the weight-mass of Cement, Sand, Aggregate (Coarse), and Water mandate as 438 kg, 659.8 kg, 1136 kg, and 197 L, respectively. Two natural bast fibers namely Olitorius and Capsularis are taken as Jute reinforcement. Three different types of lengths of each fiber are chosen as 10, 15, and 20 mm maintaining minimum aspect ratio of 5.55 and maximum aspect ratio of 11.76. Total 08 Jute fractions were incorporated in cement concrete as 0.25, 0.5, 0.75, 1, 1.25,

Table 1 Physical properties of fibers

Physical components	Capsularis jute	Olitorius jute
Average thickness (mm)	1.8	1.7
Bulk density g/cc	0.7455	0.728
Moisture content (%)	13.2	13.6

Table 2 Fineness of fibers

Fineness of fiber		
S. No	Fiber wt (g)	Fineness
<i>Fiber: Olitorius</i>		
1	3.0039	2.4
2	3.0017	2.4
3	3.0002	2.4
4	3.0043	2.4
5	3.0028	2.2
<i>Fiber: Capsularis</i>		
1	3.0028	0.9
2	3.0029	0.9
3	3.0038	1
4	3.0032	0.9
5	3.0017	0.9

Table 3 Tensile strength of fibers

Fiber strength			
S. No	Fiber length	Fiber wt (mg)	Tensile strength (N/mm ²)
<i>Fiber: Olitorius</i>			
1	12.5	298	18.2
2	12.5	294	14.6
3	12.5	301	13.4
4	12.5	295	21.6
5	12.5	303	10.8
<i>Fiber: Capsularis</i>			
1	12.5	305	10.9
2	12.5	314	5.1
3	12.5	320	10.4
4	12.5	308	4.8
5	12.5	310	7.9

Table 4 Chemical properties of jute fiber

Chemical components	Capsularis jute	Olitorious jute
α -Cellulose	62.43–62.43	62.15–63.66
β -Cellulose	–	–
Hemicellulose	18.94–19.69	19.02–20.95
Lignin	9.93 to 17.10	10.70–14.86

Table 5 Properties of Portland Pozzolana (PPC)

S. No	Characteristics	Experimental value	As per IS:1489 (Part-I) 1991
1	Normal consistency	33 min	34 min
2	Specific gravity	3.13	3.15
3	Setting time (Initial)	140 min	30 min, Minimum
4	Setting time (Final)	525 min	600 min, Maximum
5	Soundness of cement	6 mm	10 mm
6	Compression strength (i) At 7 days (ii) At 28 days	28 N/mm ² 44 N/mm ²	22 N/mm ² , Minimum 33 N/mm ² , Minimum

Table 6 Chemical properties of Portland Pozzolana cement

S. No	Characteristics	Value	As per IS:1489 (Part-I) 1991
1	% Magnesia	1.1	6 max
2	% Sulfur	2.3	3 max
3	% Loss on ignition	2	5 max
4	% Chloride	0.022	0.1

Table 7 Physical parameter of sand

S. No	Characteristics	Experimental result
1	Relative density	2.5
2	Modulus of fine	2.48 (Zone IV)
3	Water absorption	2%

Table 8 Physical parameter of aggregate (Coarse)

S. No	Characteristics	Experimental result
1	Relative density	2.75
2	Modulus of fine	7.89 (Maximum Aggregate size = 20 mm)
3	Water absorption	0.5%

1.5, 1.75 and 2%. All strength tests were conducted with dry condition of concrete surface after 7 days, 14 days, and 28 days of casting of specimens. The results of all strength tests at 7 days, 14 days, and 28 days are shown in Figs. 4, 5, 6, 7, 8, 9, 10, 11, 12, 13, 14, 15, 16, 17, 18, 19, 20, and 21.

Fig. 4 Capsularis (L = 10 mm)

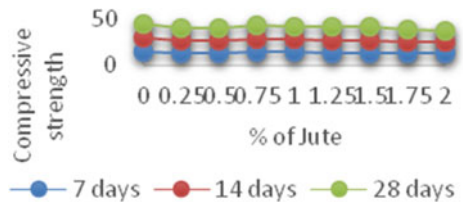


Fig. 5 Capsularis (L = 15 mm)

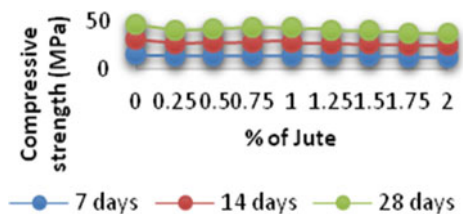


Fig. 6 Capsularis (L = 20 mm)

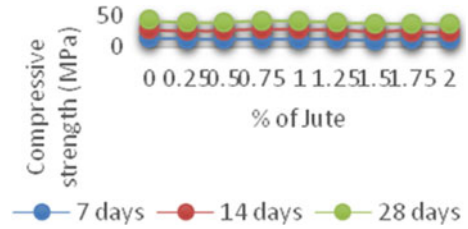


Fig. 7 Olitorius (L = 10 mm)

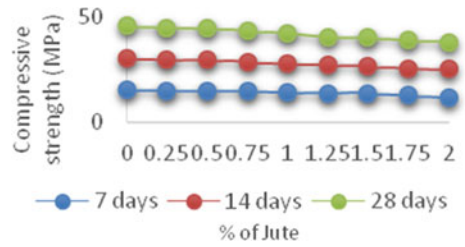


Fig. 8 Olitorius (L = 15 mm)

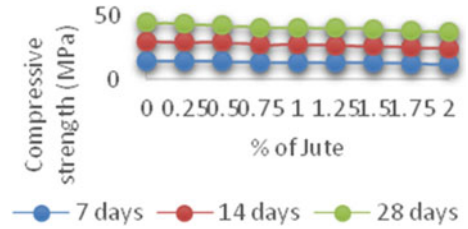


Fig. 9 Olitorius (L = 20 mm)

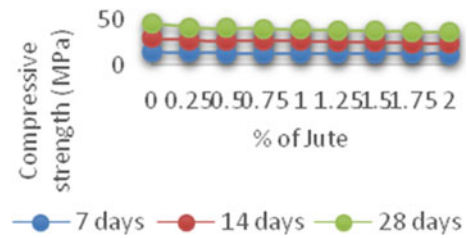


Fig. 10 Capsularis (L = 10 mm)

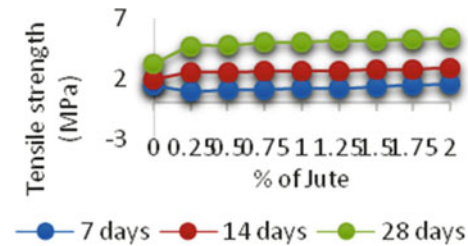


Fig. 11 Capsularis (L = 15 mm)

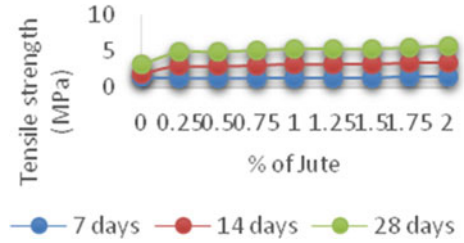


Fig. 12 Capsularis (L = 20 mm)

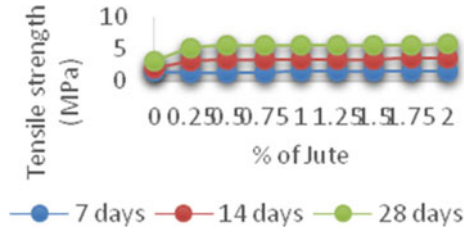


Fig. 13 Olitorius (L = 10 mm)

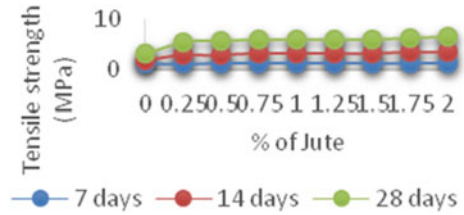


Fig. 14 Olitorius (L = 15 mm)

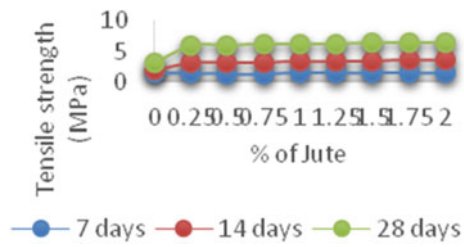


Fig. 15 Olitorius (L = 20 mm)

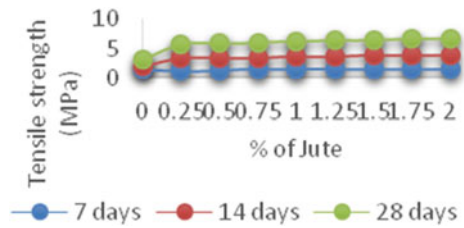


Fig. 16 Capsularis (L = 10 mm)

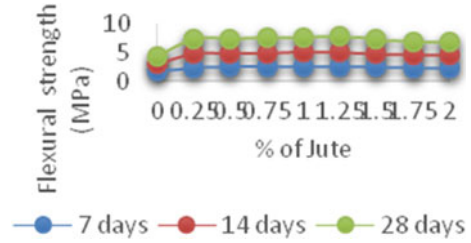


Fig. 17 Capsularis (L = 15 mm)

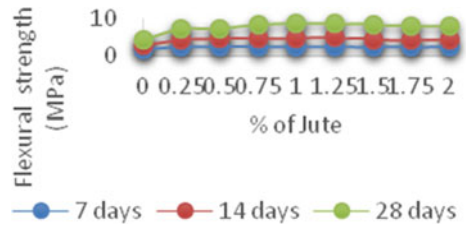


Fig. 18 Capsularis (L = 20 mm)

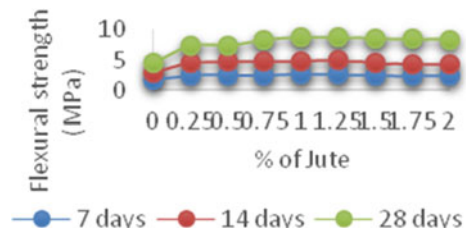


Fig. 19 Olitorius (L = 10 mm)

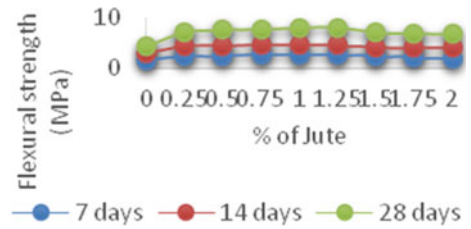


Fig. 20 Olitorius (L = 15 mm)

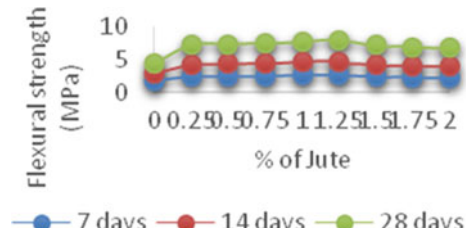
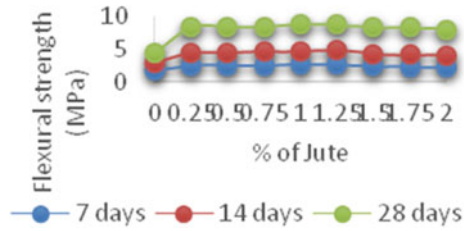


Fig. 21 Olitorius (L = 20 mm)



The present study clearly proves that Compressive strength of FRC decreases while increasing the jute fiber (Olitorius) fraction in concrete but compressive strength increases up to 0.75% fiber fraction while incorporating Capsularis jute. The maximum strength reduction was identified in both Olitorius and Capsularis of 20 mm length fiber at 2% fiber fraction. As predicted the tension strength and bending strength of FRC increase while increasing fiber fraction. In tensile strength, it shows complete increase in strength up to 2% fraction in all the lengths and types of fibers used in the study. But in the flexural strength after 1.25% fraction, the strength started decreasing but it was very less in percentage.

5 Conclusion

- i. Compressive strength decreases while increasing the jute fiber (Olitorius) fractions but compressive strength increases up to 0.75% fiber fraction while using Capsularis jute.
- ii. Tensile strength rises while increasing the jute fiber fractions up to 2.0%.
- iii. Flexural strength rises while increasing the jute fiber fractions up to 1.25%.
- iv. The length of fiber played a vital role in the FRC. The compressive strength decreases whereas rising the length of the fiber but flexural strength and tensile strength rises while rising length of fiber.
- v. Comparing Capsularis and Olitorius, the olitorius performance was better than capsularis.
- vi. The optimal percentage of olitorius was 0.25% of length 10 mm and capsularis was 1.25% of length 10 mm.

References

1. Vadivel TS, Doddurani M (2013) An experimental study on mechanical properties of waste plastic fiber reinforced concrete. *Int J Emerg Trends Eng Dev* 2(3). Available in online http://www.rpublication.com/ijeted/ijeted_index.htm
2. Mansur MA (1981) Jute fibre reinforced composite building materials. In: *Proceedings of 2nd Australian conference on engineering materials*, University of New South Wales, pp 585–596

3. Razmi A, Mirsayar M (2017) On the mixed mode I/II fracture properties of jute fiber-reinforced concrete. *Constr Build Mater* 148:512–520. <https://doi.org/10.1016/j.conbuildmat.2017.05.03>
4. Ramakrishna G, Thirumalai, Sundararajan (2005) Impact strength of a few natural fibre reinforced cement mortar slabs: a comparative study. *Cem Concr Compos* 27:547–553. <https://doi.org/10.1016/j.cemconcomp.2004.09.006>
5. Zakaria M, Ahmed M, Hoque M, Islam S (2016) Scope of using jute fiber for the reinforcement of concrete material. *Text Clothing Sustain* 2. <https://doi.org/10.1186/s40689-016-0022-5>
6. Kim J, Park C, Choi Y, Lee H, Song G (2012) An investigation of mechanical properties of jute fiber-reinforced concrete. In: *High performance fiber reinforced cement composites 6 (HPRCC-6)*-Springer book series, pp 75–82. https://doi.org/10.1007/978-94-007-2436-5_10
7. Warke P, Dewangan S (2016) Evaluating the performance of jute fiber in concrete. *Int J Trend Res Dev* 3(3). ISSN 2394-9333
8. Tiwari S, Sahu AK, Pathak RP (2009) Mechanical properties and durability study of jute fiber reinforced concrete. *IOP Conf Ser Mater Sci Eng* 961:012009. IOP Publishing. <https://doi.org/10.1088/1757-899X/961/1/012009>
9. Zhang T, Yin Y, Gong Y, Wang L (2019) Mechanical properties of jute fiber-reinforced high-strength concrete. *Struct Concr J fib*. Available in online <https://doi.org/10.1002/suco.201900012>
10. Sahu P, Tudu C (2020) Effect of jute fibre orientation and percentage on strength of jute fibre reinforced concrete. *Int J Eng Adv Technol (IJEAT)* 9(3). ISSN 2249-8958
11. Shaikh MA, Razzaq A, Selvarani G, Mujahid F (2021) Comparative study between fibre reinforced concrete (Glass, Jute, Steel Fibre) with traditional concrete. *Int J Eng Res Technol*. ISSN (Online) 2278-0181
12. Romualdi JP, Batson GB (1963) Mechanics of crack arrest in concrete. *J Eng Mech Div* 89:147–168

Numerical Investigation on the Flexural Behaviour of CFRP Strengthened Steel Pipes



A. Cyril Thomas, Mubashir Qayoom, S. Manoranjith, K. Madhan Kumar, and N. Praveen Kumar

Abstract Pipe is the main component of a liquid and gas transport system. Steel is widely used in the pipe manufacturing process. But encounters the common problem of corrosion. Traditional steel structure strengthening processes like welding and bolting are executed under hot-conditions. Heat generated during these processes affects the inherent properties of the steel pipes resulting in catastrophic failures. The main intention of this study is to propose an effective cold-condition strengthening method for steel pipes. A detailed numerical study was executed to understand the behaviour of CFRP strengthened steel pipes using the commercial Finite Element (FE) tool ABAQUS. In total, 100 FE models were developed with two different pipe diameters, thicknesses, and lengths, six stages of corrosion, and three types of strengthening techniques. To understand flexural behaviour, the FE models were analysed under a four-point loading system. From the numerical test results, it was observed that the load carrying capacity of the Type 3 strengthened steel pipes increased by 80 to 90% (Avg.). On the other hand, the load carrying capacity of Type 1 and Type 2 strengthened steel pipes increased by 60 to 70%. Thus the proposed strengthening technique improved the flexural behaviour of the steel pipes under cold-conditions without changing or modifying their original properties.

Keywords Steel pipes · Corrosion · Structural strengthening · CFRP · Numerical study · FE analysis

1 Introduction

Installation of steel pipes has increased drastically due to an increased demand for water and petroleum products. Improper maintenance leads to damage in steel pipes. Generally, petrochemical pipelines are damaged due to high operational temperatures. A high temperature level reduces the overall performance of the steel pipes.

A. Cyril Thomas (✉)

School of Civil Engineering, SASTRA Deemed to be University, Thanjavur 613401, India

M. Qayoom · S. Manoranjith · K. M. Kumar · N. P. Kumar

Department of Civil Engineering, National Engineering College, Kovilpatti 628503, India

Fig. 1 Typical view of CFRP strengthening of steel pipes [1]



Fractures in steel pipes are the most common failures that occur in petroleum industry. Similarly, corrosion is one of the most important failures in water supply pipelines. Frequently used conventional repair and rehabilitation techniques include corrosion-resistant coating, addition or removal of the additional surface from the periphery of the damaged pipe, and replacement of the damaged pipes. Utilization of fibre composites in the strengthening of steel structures increased in the past decades. The present study also explains the advantages of using Carbon Fibre Reinforced Polymer (CFRP) to strengthen steel pipes (Fig. 1).

2 Background

Steel pipes are the most common component in a water supply system. They are also used in the Oil and Gas (OG) industries to transport oil and gas. In general, metal pipelines are the most common, effective, and safest way to transport natural resources over long distances. Around the globe, about 1.7 million km of pipelines are used to move gas and petroleum products such as crude oil [2]. The West–East Gas Pipeline is the world’s longest pipeline located in China. The total length of this pipeline is 8707 km. Metal pipelines get corroded due to temperature variations (50°–130 °C), internal pressure variations, chemical erosion, etc.. [3]. Corrosion damages metal pipes both internally and externally. It leads to leakage or ruptures in the pipeline. It also causes huge fire accidents. Koch (2017) stated that corrosion was one of the most important terms in global economic development. It is estimated that the current cost of corrosion is US\$2.5 trillion globally which is equal to 3.4% of the global GDP [4]. Popoola et al. (2013) listed the major types of corrosion in metal pipes, they are Sweet corrosion, Sour corrosion, Oxygen corrosion, Galvanic corrosion, Crevice corrosion, Erosion corrosion, Microbiologically induced corrosion, and Stress corrosion cracking [5].

The presence of moisture in the environment leads to the formation of rust on the surface of steel pipes whilst rust formation leads to corrosion. Numerous research works were carried out on corrosion formation in steel pipes. Popoola et al. (2013)

investigated various types of corrosion in steel pipes and listed the various causes. They also found the difficulties associated with corrosion during oil and gas production and its mitigation [4]. Hou et al. (2016) experimentally investigated the effects of corrosion on the mechanical properties of buried metal pipes. They observed that an acidic environment caused corrosion in steel and cast iron pipes extensively used in oil and gas industries. Increase in corrosion reduced the tensile strength and fracture toughness of the metal considerably [6].

Due to the availability of a limited number of steel pipe strengthening techniques, corroded steel pipes are replaced by new ones. Most steel pipe strengthening techniques are executed by welding. Generally, welding generates a huge amount of heat which changes the inherent property of the steel pipes [7, 8]. In recent years, utilization of fibre composite materials to strengthening steel pipes was considered one of the best methods. This paper presents the advantages of fibre composite material utilization in the strengthening of steel pipes. A detailed numerical investigation was carried out on 100 finite element (FE) models developed with two different pipe diameters, thicknesses, and lengths, six stages of corrosion, and three types of strengthening techniques. The obtained test results are discussed.

3 Numerical Study

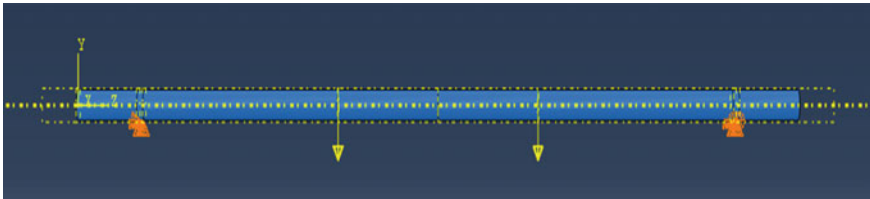
FE Analysis (FEA) is one of the best methods to solve complex engineering problems within a stipulated time. It also reduces experimental costs and minimizes manpower. In this study, a numerical investigation was carried using the commercial FE software ABAQUS. The complete set of parameters considered for this study are mentioned in Table 1. Commercial FE tool ABAQUS has the ability to perform non-linear analysis with the incorporation of material non-linearities. For performing non-linear analysis, un-damaged pipes and damaged material properties were considered from the Yang et al. (2020) experimental work. The yield stress of the pipe was 490 MPa,

Table 1 Parameters considered for the study

Test condition	Four point loading
Diameter of the pipe	30 and 40 mm
Thickness of the pipe	3 and 4 mm
Length of the pipe	1200 and 2200 mm
Corrosion rate	10.45, 30.65, 40.89, 51.86, 60.19, and 71.02%
Categories	Steel pipes with and without damage, Steel pipes with CFRP strengthening (Single and multiple layer)
Strengthening type	<i>Type1 (Single Layer—0° Fibre orientation), Type2 (Single Layer—90° Fibre orientation) Type3 (Two Layers—0°/90° Fibre orientation)</i>
Boundary condition	Simply supported condition

Table 2 Material properties of the corroded steel pipes [9]

Corrosion rate (%)	Ultimate strain (mm/mm)	Ultimate stress (N/mm ²)	Yield strain (mm/mm)	Yield stress (N/mm ²)
0	431.06	0.00148	301.62	10.45
10.45	431.06	0.00148	301.62	10.45
30.65	408.65	0.00134	279.18	30.65
40.89	429.98	0.00148	302.08	40.89
51.86	325.47	0.00113	235.32	51.86
60.19	236.94	0.000907	189.36	60.19
71.02	217.17	0.000673	140.35	71.02

**Fig. 2** Typical view of the steel pipe with loading and boundary condition

yield strain 0.0023 mm/mm, and modulus of elasticity 210 GPa [9]. The considered material properties are mentioned in Table 2. Steel pipes were modelled with four noded doubly curved shell elements with reduced integration and denoted as S4R in ABAQUS [10]. CFRP composite matrix was modelled as lamina [11]. Multiple layers were modelled using the “composite layup” feature and the interaction between the steel substrate and CFRP matrix was considered a perfect bonding (Fig. 2).

“Tie-constraint” was used to ensure perfect bonding. To induce failure in the CFRP matrix, “Hashin damage” model properties were included in the strengthened pipe models [11]. From the mesh convergence study, a mesh size of 23.36 mm was considered for both the steel pipe and the CFRP matrix (Fig. 3). The developed FE model was validated with established experimental test results. Material properties of the CFRP matrix are mentioned in Table 3.

Validation of the FE model is one of the most important steps in a numerical study. In this study, two series of experimental tests were conducted to validate the FE model. Two sets of steel pipes (of 30 mm diameter with 3 mm thickness and 40 mm diameter with 4 mm thickness) having a length of 1.2 m were tested under a 3-point loading system. Based on the obtained results, the FE models were validated. Failures from both the experimental and numerical tests are mentioned in Fig. 3. The labels of the numerical models were finalized based on geometrical, corrosion, and types of strengthening methods. For example, undamaged steel pipes with 30 mm diameter and 3 mm thickness were named 30D3TU. Here, “30D” represents pipes

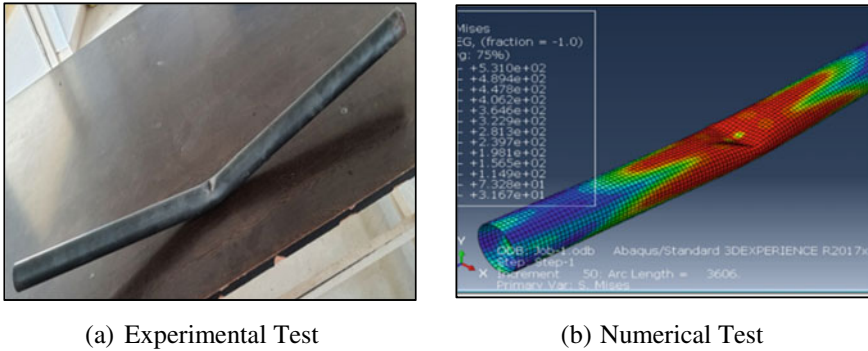


Fig. 3 Comparison of failure modes in both experimental and numerical tests

Table 3 Material properties of CFRP [11]

Details of the parameter	Values	
Longitudinal/transverse tensile strength	2700 MPa	45 MPa
Longitudinal/Transverse compressive strength	2700 MPa	200 MPa
Longitudinal/Transverse shear strength	80 MPa	80 MPa
Elastic modulus in x direction, E_{11}	130,000 MPa	
Elastic modulus in y direction, E_{22}	13,500 MPa	
Shear modulus, $G_{12} = G_{13}$	5700 MPa	
Shear modulus, G_{23}	3500 MPa	
Poisson's number, γ_{12}	0.2	

diameter, “3 T” represents pipe thickness, and “U” the undamaged pipe. Likewise, labels of the damaged pipes were denoted 30D3TCR11.

Here, “CR” represents corroded and “11” the corrosion rate (10.45%). All damaged pipes were defined similarly. The strengthened pipes were denoted 30D3TS0ORCR11 where, “S” represents the strengthened pipes and “0OR” the 0° fibre orientation.

- 30D3TU—Undamaged pipe 30 mm dia. 3 mm thick.
- 30D4TU—Undamaged pipe 30 mm dia. 4 mm thick.
- 30D3TDCR11—Damaged pipe 40 mm dia. 3 mm thick. 10.45% corrosion.
- 30D3TS0ORCR11—Strengthened pipe 30 mm dia. 0° orientation 10.45% corrosion.
- 30D3TS90ORCR11—Strengthened pipe 30 mm dia.90° orientation 10.45% corrosion.
- 30D3TS090ORCR11—Strengthened pipe 30 mm dia.0° and 90° orientation 10.45% corrosion.

The above-mentioned notations were followed for the rest of the pipes. The developed FE model of the steel pipe is mentioned in Fig. 3. A detailed discussion on the obtained test results is mentioned in the following section.

4 Results and Discussion

4.1 Behaviour of the 30D3T Steel Pipe

The ultimate load carrying capacity of steel pipes depends on the percentage of corrosion it has. The ultimate load carrying capacity of the steel pipe 30D3T was 66.09 kN. The percentage of corrosion in the steel pipes extremely affected their flexural behaviour. At each corrosion stage, the load carrying capacities of the steel pipes decreased by 68 to 94% respectively. In each strengthening process, the CFRP matrix enhanced the load carrying capacities of the steel pipes. Maximum load carrying capacity was attained during the *Type 1* strengthening process for pipe 30D3TU with 60.19% corrosion. The proposed *Type 1* strengthening process increased the load carrying capacity from 55 to 58%.

In *Type 2* strengthening, load carrying capacities of corroded steel pipes were enhanced from 58 to 63%. Maximum load increment noted in the steel pipe 30D3TU with 60.19% corrosion was 6.92 kN which was 67.32% higher than the load carrying capacity of the damaged pipe. Compared to *Type 1* and *Type 2* strengthening, *Type 3* strengthening achieved maximum load increment.

It enhanced load carrying capacity by 87.78% in the 71.02% corroded steel pipe. By providing two CFRP matrix layers, load carrying capacities of the corroded steel pipes were enhanced from 80 to 90%. Failure in the strengthened pipes occurred due to the rupture of the CFRP matrix layers. The proposed CFRP strengthening method delayed local buckling in the pipes. Failure in the CFRP strengthened pipes was due to delamination of CFRP and rupture of CFRP failure modes (Fig. 4). A typical view

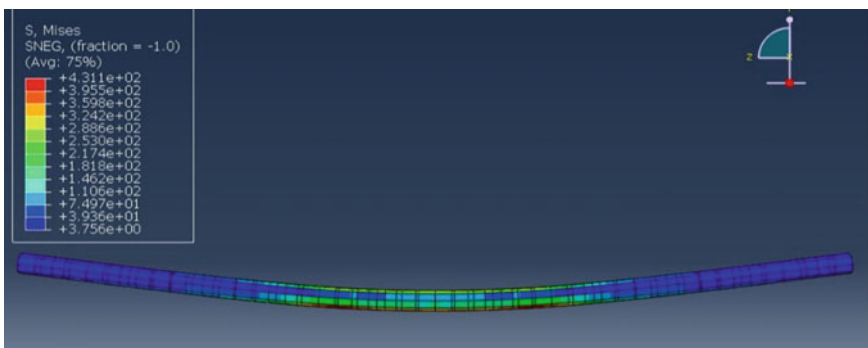


Fig. 4 Typical view of the developed CFRP strengthened steel pipe

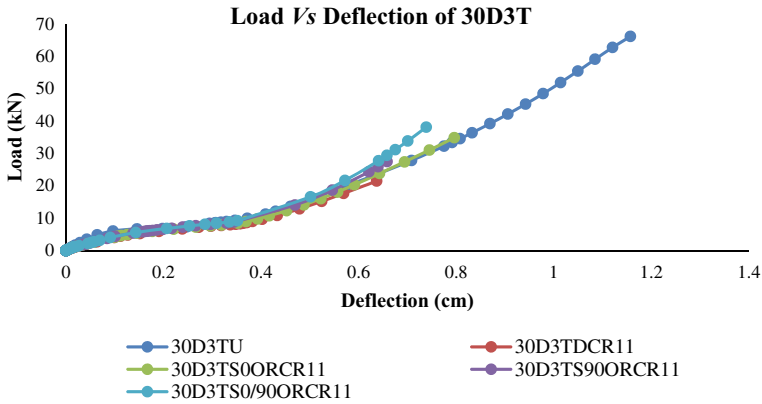


Fig. 5 Load versus deflection behaviour of steel pipe 30D3T

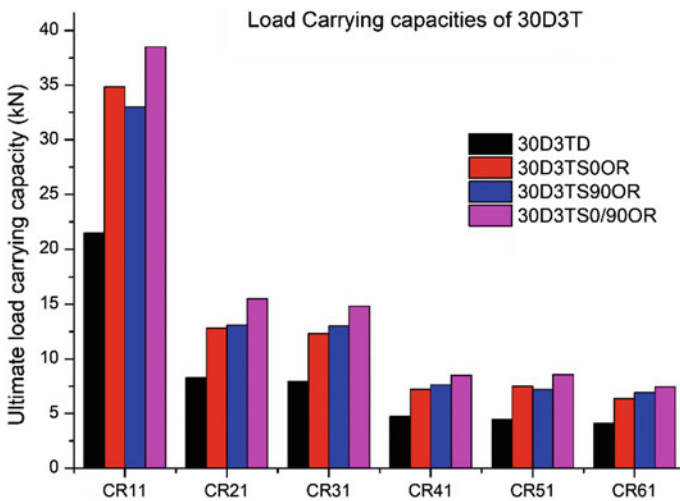


Fig. 6 Load carrying capacities of the steel pipe 30D3T with and without CFRP

of load deflection behaviour of CFRP strengthened steel pipe 30D3T is mentioned in Fig. 5. The obtained load carrying capacities of the CFRP strengthened steel pipe 30D3TU are mentioned in Fig. 6.

4.2 Behaviour of the 30D4T Steel Pipe

The ultimate load carrying capacity of the 30D4T steel pipe was 90kN. The rate of corrosion is directly proportional to the load carrying capacity of a steel pipe.

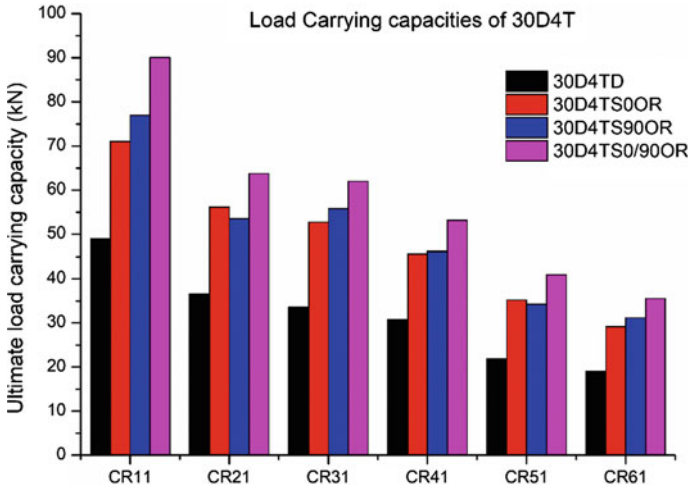


Fig. 7 Load carrying capacities of the steel pipe 30D4T with and without CFRP

From the numerical results, it was observed that the load carrying capacity values of the corroded pipes (6 stages of corrosion) reduced from 48.92 to 19.06 kN which was 45.86 to 94% lesser than the load carrying capacities of the undamaged pipes. Average increment in *Type 1* strengthening was 45.86 to 60.69% respectively.

Maximum increment in load carrying capacity was noted in the steel pipe with 60.19% corrosion. Compared to the strength of the damaged pipes, *Type 2* strengthening increased its load carrying capacity by 46.32 to 63.64%. Steel pipes with 71.02% corrosion attained maximum load carrying capacity which was 19.06 kN. After the strengthening process (*Type 2*), its load carrying capacity increased by 63.64% (31.19 kN). Similarly, the ultimate load carrying capacities of corroded steel pipes increased by 72.61 to 86.77%. The obtained load carrying capacities of strengthened 30D4T steel pipes are mentioned in Figs. 6 and 7.

4.3 Behaviour of the 40D3T Steel Pipe

The ultimate load carrying capacity of 40D3T steel pipes was 52.72kN. The percentage of corrosion in the steel pipes affects the flexural behaviour of the steel pipes greatly. From the numerical results, it was observed that load carrying capacity values decreased by 64 to 88% and the proposed strengthening process increased load carrying capacity values by 45to 90%. Load carrying capacities of the corroded steel pipes varied from 48.98 to 60.37%. Maximum load increment in *Type 1* strengthening was noted in the 60.19% corroded steel pipe. It was observed that *Type 2* strengthening enhanced the load carrying capacity of a 10.45% corroded pipe by 67.37%. The load carrying capacities of other corroded pipes varied from 45.39 to

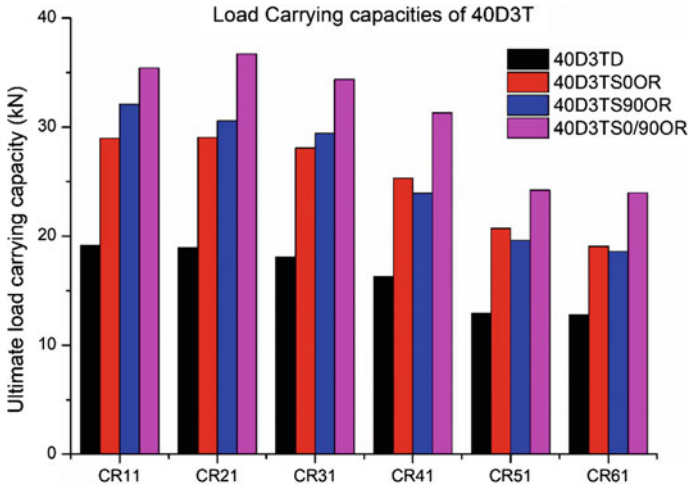


Fig. 8 Load carrying capacities of the steel pipe 40D3T with and without CFRP

61.14%. Maximum increment was noted in the *Type 3* strengthening process alone. A maximum increment of (91.65%) was noted in the 40.89% corroded steel pipe. After the strengthening process, load carrying capacity values of the corroded steel pipes varied from 85.10 to 93.46%. The load carrying capacity of the 30.65% corroded steel pipe increased by 18.97 to 36.70 kN. The obtained load carrying capacities of the 40D3T steel pipes before and after strengthening are mentioned in Figs. 7 and 8.

4.4 Behaviour of the 40D4T Steel Pipe

The ultimate load carrying capacity of a 40D4T steel pipe was 85.87kN. From the numerical results, it was observed that load carrying capacity values decreased by 47 to 83% respectively. The proposed strengthening process increased load carrying capacity values by 47 to 92%. Maximum strength increment was in the 71.02% corroded steel pipe that underwent *Type 3* strengthening. The load carrying capacity values increased by 59.39 and 52% in *Type 1* and *Type 2* strengthening processes respectively. Load carrying capacities of the corroded steel pipes increased by 87.67% (Avg.) in *Type 3* strengthening. Delamination of CFRP and Rupture of CFRP failures were the major failure modes in the strengthened steel pipes (Fig. 9).

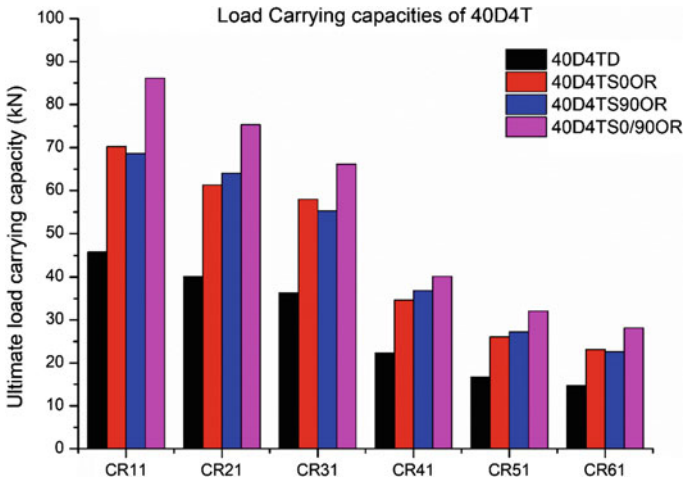


Fig. 9 Load carrying capacities of the steel pipe 40D4T with and without CFRP

5 Conclusion

Three types of strengthening methods were considered to improve the flexural behaviour of steel pipes. From the numerical investigations, the following conclusions were drawn:

- When the percentage of corrosion increased, flexural behaviour of the steel pipe decreased. This reveals that the flexural strength of pipes is inversely proportional to the percentage of corrosion.
- In each strengthening process, the flexural behaviour of the steel pipes increased. It was observed in all the 6 stages of corrosion. *Type 1* and *Type 2* strengthening enhanced the flexural behaviour of steel pipes by 50 to 65% (Avg.). Maximum percentage increment was observed in *Type 3* strengthening process alone. This process improved flexural behaviour of the damaged steel pipes by 80 to 90% (Avg.).
- Delamination of CFRP and fracture of CFRP were observed as major failure modes in the strengthened steel pipes. Thus, the CFRP strengthening process enhanced the flexural behaviour of the damaged steel pipes without changing or modifying its original properties under cold conditions.

References

1. Process pipe repair and strengthening, Structural Technologies (2021). <https://perma.cc/5BKZ-JB6W> Accessed 20 August 2021

2. Mohitpour M, Golshan H, Murray A (eds) (2003) Pipeline design and construction: a practical approach, 3rd edn. ASME Press, Newyork, USA
3. Sirimanna CS, Manalo AC, Karunasena W, Banerjee S, McGarva L (eds) (2015) Fibre-reinforced polymer (FRP) repair systems for corroded steel pipelines. Rehabilitation of pipelines using fibre-reinforced polymer (FRP) composites, Wood Head Publishing, Sawston, UK, pp 267–285
4. Koch G (ed) (2017) Cost of corrosion trends in oil and gas corrosion research and technologies. Wood Head Publishing, Sawston, UK, pp 3–30
5. Popoola LT, Grema AS, Latinwo GK et al (2013) Corrosion problems during oil and gas production and its mitigation. *Int JI Ind Chem* 4:35. <https://doi.org/10.1186/2228-5547-4-35>
6. Hou Y, Lei D, Li S, Yang W et al (2016) Experimental investigation on corrosion effect on mechanical properties of buried metal pipes. *Int JI Corrosion*. <https://doi.org/10.1155/2016/5808372>
7. Cyril Thomas A, Baskar K (2018) Strengthening of thin-webbed castellated beams using CFRP. *Int JI Comp Mtds Eng Sci Mech* 19(6):396–404. <https://doi.org/10.1080/15502287.2018.1534153>
8. Cyril Thomas A, K Baskar (2021) Behaviour of thin-webbed castellated beams strengthened using CFRP. *Structures* 30:338–351. <https://doi.org/10.1016/j.istruc.2020.12.083>
9. Yang Y, Liu F, Xi F (2020) Tensile fracture behavior of corroded pipeline: part 1—experimental characterization. *Adv In Mat Sci Eng* <https://doi.org/10.1155/2020/4058452>
10. ABAQUS CAE Manual
11. Muthyala SK, Sandeep Kumar GAVS, Cyril Thomas A (2021) Behavior of reinforced concrete beams bonded with side bonded FRP. *Mat Tdy: Procd* 43(2):2404–2410. <https://doi.org/10.1016/j.matpr.2021.02.140>

Traffic Crowd Assessment and Placing of Traffic Signal at Unsignalized Intersection—A State of Art



Pala Gireesh Kumar, Satya Ranjan Samal,
and Abhirami Priyanka Pathivada

Abstract A steep rise in population eventually results in higher usage of transportation facilities which in turn causes congestion of traffic. Traffic crowd on urban road networks has increased rapidly. Due to no traffic signal at intersections, heavy traffic leads to blockage and long queues of vehicles form at intersections, leading people to lose valuable time. Traffic crowd assessment can be done using methods like Speed, Travel and Delay time, Crowd indices, and Level of Service. One of the techniques to investigate the cause of traffic congestion due to the heavy volume of vehicles is microscopic traffic modeling. In continuation to the study, the contemporary effects of the increased volume of traffic can also be examined with the use of “Simulation of Urban Mobility (SUMO)”. This concedes the freight-transport modeling of pedestrians and vehicles of transportation (public & private). New traffic strategies can be executed via simulation for analysis before they are used in real-world. This paper brings out the collective information about recent works carried out on traffic simulation using SUMO software and gives detailed information about problems that occurs at unsignalized intersection and different methodologies to assess traffic crowd.

Keywords Traffic crowd · Assessment · Intersections · SUMO

1 Introduction

India is the most populous country after China. Continuous increment in populace demands transportation with basic amenities, which has a direct impact on the volume of traffic on the roads. The demand for a better road network is increasing at the same rate. People daily fight with traffic, crowd and sometimes this chaos results

P. G. Kumar (✉) · A. P. Pathivada
Department of Civil Engineering, Shri Vishnu Engineering College for Women (Autonomous),
Bhimavaram, India

S. R. Samal
School of Civil Engineering, KIIT Deemed to be University, Bhubaneswar, India
e-mail: satya.samalfce@kiit.ac.in

in unnecessary problems in their lives. The development of better road networks is a big concern in populated countries like India. Indian traffic is the mixed flow of both urban and rural roads. More than 50% of vehicle collisions take place at road intersections. Traffic signals were introduced at intersections to decrease problems related to traffic crowd, accidents, over the speed of vehicles, etc. Traffic signals were found commonly in metropolitan cities, whereas rarely found in small urban towns. The population in small towns is increasing at the same rate as the population in the metropolis. So, placing traffic signals in small towns is as necessary as in metropolises. New elements are tested using simulations before being applied in the actual world. SUMO is one such software facilitating traffic system modeling of pedestrians, public transit, automobiles, etc.

Traffic Jam is sometimes referred to as traffic crowd which is defined as the state of traffic when it either stops completely or slows down below its normal speed. The differential gap accounted for between the supply and demand of vehicles results in traffic crowding [1]. Incorrect structures for stop signs, a paucity of workers, a narrow breadth of the road, and overtaking of motorists increase road crowd [2]. So, assessment of traffic crowd is important.

The purpose of this article is to help you have a better grasp of the importance of placing Traffic signals at unsignalized intersections using SUMO software based on the findings of earlier studies conducted in India. Different methods to assess traffic crowd are also reported and presented.

2 Literature Review

Bieker et al. proposed adopting SUMO to replicate a real-world scenario by providing traffic networking, traffic requirements, and depictions of traffic infrastructure and suggested an improvement of open issues in the city of Bologna [3].

Lopez et al. and the team want to explain how the research and software tools increase nowadays by taking SUMO software as an example. To explain the tools in SUMO, Bologna city in Italy was taken as a study area. To simulate SUMO the scenario of Bologna city is created in SUMO software. For simulation, the data like roads, number of lanes, pedestrians, traffic signals, Bus stops, etc. are needed. They have explained how to create a network file in SUMO using NETEDIT. And how to create needed data in SUMO and how to run the Simulation is addressed. Finally, they concluded that how SUMO software helps researchers to do research and the features available in the SUMO software [4]

Akhtar et al. focused on how the increase in usage of vehicles affects traffic volume and causes crowd. So, they decided to implement a system for smart traffic management with a Deep-Neuro-Fuzzy model. Dijkstra is the algorithm used to calculate road segments from the model. First, they set up a simulation in SUMO software and later formulated the road weights. They have used IoT-based sensors to collect the input. They tested the Graphical User Interface and calculated the traffic flow and finally found the algorithms in different tests. So finally, they successfully

installed the ITMS with the help of SUMO software and concluded that Deep-Neuro-Fuzzy can improve the route situations [5].

Arroyo et al. aim to control traffic in the Medellín city. For this project, Nicolas Arroyo and the team use different software like SUMO, Python, and C++ . In these multiple scenarios are tested to know the behavior and synchronization of partitions are done. They have adopted a new Synchronization method that works as per the master–slave scheme. They clearly explained the “dead-end” node. And how this dead-end causes effects. To manage the dead ends in C++ TraCI-API, an algorithm was developed. From the results of the simulation, the performance and precision tests are conducted. By observing the results, the team observed that the method is acceptable in the case of precision but not acceptable in terms of partitioning because it will increase the errors. And they need to do some future work for completion and suggest some ideas to control the urban traffic [6].

Krajzewica et al. explain the road traffic Simulation using open-source simulation software like SUMO. The main motto behind the project is to acquaint the software and to extend the use of the software. They have just explained how to use the software and have not provided any results of the simulation. They have explained the main principles and features of the software. And how to create the scenario of simulation of car /car drivers in the software. The creation of the network file and how to run the simulation are explained. From this project, they have explained that SUMO software is capable to create any microscopic traffic simulation [7].

Daniel et al. focused on an algorithm based on agent simulation for sign management systems of traffic within SUMO which has the potential to improve traffic flow. This agent-based algorithm makes use of the traffic jam length as input in front of a traffic light. A considerable amount of region was tested with OIS system close to an institute in Berlin. The algorithm along with the description of the simulation was discussed. Concludes that the agent-based traffic light logics will give benefits at some conditions only and no improvement could be attained until the flows are small and are balanced in all directions of a traffic light [8].

Erdagi et al. did a research to notice an optimum penetration rate of CACC in highways amid cities. They have generated two imaginary networks with various levels of complications and performed simulations on microscopic simulation software Eclipse SUMO. The networks that were considered had a different number of intersection legs, but the same number of intersections. Two Scenarios were created in which the first intersection was fixed time signalized and the second was adaptive signalized. For inspecting traffic improvements Total Time Spent (TTS) was taken as the comparison parameter. The simulation was carried out at different penetration rates varying from 0 to 100% on both scenarios. The simulation shows that rise in the penetration of CACC rate has given a positive impact on the environment with a 20% reduction in total emissions in most cases [9].

Zaky et al. demonstrated the usage of SUMO to simulate within two intersections namely Dioponegoro-Soetomo and Diponegoro-Musi in Surabaya. The parameters that were used for simulation through SUMO are the gap between vehicles, acceleration, vehicle speed, deceleration, and size of each type of vehicle. At both intersections, SCATS sensors were positioned to obtain the data of the actual flow of

arrival for each consecutive 15 min span of every day of October 2015. The data that was acquired by the sensors was given as input to SUMO. The configuration was performed in SUMO and connected with MATLAB. The simulation result symbolized the condition concerned with the real-time. The investigative simulation resulted in the identification of arms overflowing at numerous intersections. This in turn made the flow data arrival far to precise in comparison to the real-world [10]

Akyol et al. investigated the performance of two traffic lights at Ferry and City Center intersections in the Kadikoy area of Istanbul city. They collected the data during morning and evening peak hours manually. They opted Non-Interacting and Stripping models to simulate the behavior of pedestrians. They compared the conditions at Fixed time and Adaptive Traffic Control Systems concerning pedestrians, traffic flows of road vehicles along with field data. They carried out a simulation 10 times using the Eclipse SUMO micro simulator which is connected to the Traci. From the results of the simulation, they decided that there is a reduction in the lag time for both the pedestrians and vehicles was accomplished with the utilization of adaptive signal controllers [11].

Griggs et al. built a simulation platform in order to build a large-scale smart transportation system, hardware must be included in the loop. The platform consists of thousands of simulated vehicles and real vehicles which run in real-time. This platform allows the legit drivers to attain a feeling of existence in a large-scale vehicle to vehicle [12].

Afrin et al. concentrate on traffic crowd, the problems that arise due to crowd, and how it affects the sustainability of transportation. Identified the mitigation measures to reduce the crowd based on different measures of traffic crowd. By applying those measures on weekly and daily data of traffic. This paper clearly explains how to conduct and apply the crowd measures at a particular location and how to evaluate the data and analyze the data. Daily and weekly analyses are done, and the analysis identifies the gains and downsides of the crowd measures. By using the measures, they conclude the Level of crowd like whether the locations are congested or not if congested what is the level of crowd. From the data, they have approached some mitigation measures and they explained that the crowd cannot be resolved completely but up to some extent. And finally, the team concluded with, how to approach the crowd measures and how to attain sustainability in the transportation system [13].

Kumar et al. investigated the available models on Level of Service (LOS) for both roads in the city and in the countryside. They thoroughly explained about diverse parameters that can be used for defining the LOS. They provided the LOS criteria for suburban and urban arterial roads as six categories using the parameters they have discussed. Based on their study on the concept of LOS they concluded that the Volume to Capacity Ratio is discovered to be the most simple and easiest approach than the rest of the methods available. They also looked into LOS depending on median travel speed and Percentage Speed Reduction (PSR) and provided their findings [14].

Hossain and the team have conducted a study at Pabna Town which is the secondary Town in Bangladesh, to measure the traffic crowd and find out which is the most congested-prone route in the town. For this study, they have conducted a

Traffic volume study and spot speed study and approached different computer packages. They have observed that there is a traffic conflict at the intersections. The traffic system in Pabna town is two-way traffic. And they have conducted traffic flow characteristics for Ataikula road and AH road. They calculated the density and capacity of each road and determine the LOS. And the crowd is more in the peak hours and finally, they suggested that the one-way traffic flow is the correct solution to control the traffic crowd [15].

Satya Ranjan Samal et al. team explains how the crowd makes an impact on the day-to-day life of a traveler and the overall economy. They want to improve the existed infrastructure to reduce the crowd with low investment. For that, the team considers the urban highway system to conduct the study. They employed a visual graphic study to use the number plate matching approach to collect the required data. They have considered a time slot of 8° clock to 10° clock in the morning as the peak hour of the day for the investigation. After that, they have included the impacts of crowd and finally suggested the Mitigation measures [1].

Pirdavani et al. have developed a micro-level behavioral technique for assessing crash potential for varied traffic variables at signalized and unsignalized crossings and therefore the ability of a micro simulator to evaluate safety effects has been shown in the city of Belgium. The evaluation of safety situations at signalized and unsignalized intersections is done by two different safety indicators a micro simulator called S-Paramics is used in their investigation for changing speed limits. Finally, they used PET as a security indicator, which allowed them to make useful comparisons between safety conditions at unsignalized intersections in different scenarios with varying traffic volumes and speed limits. The authors believe that safety indicators can help with a safety evaluation, particularly at unsignalized intersections where the majority of collisions are traverse collisions [2].

3 Traffic Crowd at Unsignalized Intersection

Traffic crowd is defined as the state of traffic when it either stops completely or slows down below its normal speed. Generally, traffic crowd is categorized into two types:—Recurring crowd and nonrecurring crowd. Recurring Crowd occurs in Blockages, insufficient infrastructure, Variation in traffic flow, and inadequate traffic controllers. Nonrecurring crowds cause unforeseen circumstances such as traffic crashes, road closures, meteorological conditions, etc.

Due to no traffic signal at intersections, heavy traffic causes gridlock and long lines of vehicles to form at junctions, causing individuals to waste valuable time, particularly during rush hours. Additionally, traffic crowd has a significant influence on the state's economy. Intersections are traffic capacity bottlenecks that pose specific safety problems due to dangerous driving actions and maneuvers that cause traffic disputes such as traffic jams and traffic accidents. So, placing traffic signals at intersections is one of the best solutions for controlling the traffic flow and conflicts at intersections. When a properly timed traffic signal is placed at an intersection it will handle



Fig. 1 Traffic crowd at intersection

the capacity of traffic more efficiently, eventually, the traffic follows the orderly movement. Traffic crowd at intersection is shown in below Fig. 1 (Sciencemarg.org).

Many problems occur at an unsignalized intersection. Problems could be related to an individual intersection or occur along a section of road with successive intersections. The following shows problems experienced at unsignalized intersections that are presented in the *Unsignalized Intersection Improvement Guide* (UIIG was set up to help professionals at agencies with design selection, operation, implementation, and other treatments aimed at improving safeness, mobility, and availability at unsignalized crossings). Unsuitable traffic control, insufficient visibility of the intersection or devices that control traffic, insufficient intersection sight distance, insufficient guidance for motorists, over intersection conflicts within the intersection, conflicts between vehicles and non-motorists, weak operational performance, misapprehension of gaps in traffic, and speed.

Traffic crowd assessment can be done using methods like Speed, Travel and Delay time, Crowd indices, and Level of Service.

3.1 Speed

Speed of the Vehicles plays an important role in finding different traffic parameters like crowding, Level of Service, and many more. Speed Reduction Index and Speed Performance Index are two such speed parameters that are used to find out traffic crowd.

3.1.1 Index of Speed Reduction

Speed reduction index implies the proportion between change in the relative speed between crowded and free-flowing traffic [14]. If the SRI value exceeds 4 to 5 then crowd occurs. If the SRI value is lower than 4 it shows a non-crowded flow.

$$SRI = \left(1 - \frac{V_{ac}}{V_{ff}}\right) \times 100 \tag{1}$$

where,

- SRI = index of speed reduction
- V_{ac} = speed of travel,
- V_{ff} = speed of free-flow

3.1.2 Index of Speed Performance

The speed performance index signifies the term for ratio of the speed of a vehicle and the maximum permissible speed [14]. SPI ranges from 0 to 100. Refer Table 1.

$$SPI = \left(\frac{V_{avg}}{V_{max}}\right) \times 100 \tag{2}$$

where,

- SPI = Index of Speed Performance
- V_{avg} = average speed of the travel,
- V_{max} = permissible speed at maximum level

Table 1 Index of speed performance in regard to the state of traffic [14]

Index of speed performance	Level of traffic state	Traffic state elucidation
(0, 25)	Heafy crowd	Poor road traffic, relatively low speed
(25, 50)	Mild crowd	Substantially lower speed and a fragile situation of traffic on road
(50, 75)	Considerably smooth	Enhanced road for flow of traffic, Speed is of higher median
(75, 100)	Extremely smooth	Speed is of higher median, Fair traffic conditions

3.2 Rate of Travel

Rate of Travel implies motion of a certain road portion rate denoted by the fraction of the traveling time of the portion to the length of the segment [14].

The inverse of speed also gives Rate of Travel.

$$T_{tr} = \frac{Tt}{Ls} \quad (3)$$

where,

T_{tr} = Rate of travel

Tt = Time of travel,

Ls = Length of the segment

3.3 Rate of Delay

The delay rate describes the amount of time lost by cars traveling in a crowded area for a specific route segment [14]. The disparity between factual and permissible travel rates can be calculated as follows

$$Dr = Trac - Trap \quad (4)$$

where,

Dr = Rate of delay

$Trac$ = Rate of actual travel

$Trap$ = Rate of acceptable travel

3.3.1 Ratio of Delay

The delay rate to the actual travel rate ratio is used to compute the delay ratio. It is used to compare the degree of traffic crowd on various roads [14].

$$D = \frac{Dr}{Trac} \quad (5)$$

where,

D = Ratio of delay

Dr = Rate of delay

$Trac$ = Rate of actual travel

3.4 Road Segment’s Level of Service

Level of Service (LOS) has become popular in the field of transportation because of its simplicity. Highway Capacity Manual adopts LOS method. Diverse traffic factors, such as, speed of the vehicle, flow rate of maxima, ratio of volume to capacity (V/C), and road density, can be used to calculate the LOS. The V/C intervals can be used to calculate a roadway’s LOS.

V denotes the Average volume of the road segment. The maximal count of automobiles passing through a spot of a lane within a span of an hour is called capacity (C). The following is the theoretical capacity formula:

$$\text{Theoretical Capacity}(C) = 1760 * \frac{v}{i}$$

where

v = vehicle’s constant speed (miles/hr)

i = intra vehicular lead (yards)

Approximately, the intra vehicular lead is assumed to be around 15 feet. Traffic state based upon V/C ratio is given in the below table (Refer Table 2).

4 SUMO Tool

SUMO is a free and publicly accessible software that stands for “SIMULATION OF URBAN MOBILITY”, designed by the German Aerospace Center and Community users. Since 2001 it is available as free simulation software and allows users for modeling intermodal traffic systems including transportation, automobiles, and pedestrians. SUMO includes many supporting tools which is automated for the creation, execution, and evaluation of simulations, like importing network, visualization, calculation of routes, and emission.

Table 2 V/C Ratio based LOS [15]

S. No	LOS	Traffic state and condition	V/C ratio
1	A	Free-flow	Less than 0.125
2	B	Speed unaffected in case of stable flow	Between 0.125 and 0.276
3	C	Speed affected in case of stable flow	Between 0.276 and 0.479
4	D	Stable flow with dense population	Between 0.479 and 0.715
5	E	Volume of traffic at a lower speed (maximal or to the nearest level)	Between 0.715 and 1.000
6	F	Flow breakdown	Greater than 1.000

4.1 SUMO Applications

- Examine the operation of traffic signals, along with the examination of current algorithms and the assessment of weekly timescales.
- The event of recent approaches, the assessment of eco-aware routing supported pollutant emission, and studies on network-wide implications of independent route choice have all been investigated.
- At the time of the Pope's visit to Cologne in 2005, SUMO was accustomed to providing traffic forecasts for city officials.
- SUMO aids in assessing the performance of GSM-based traffic inspection by simulating in-vehicle transmission behavior.
- The V2X body uses SUMO extensively for both giving practical vehicle remains and analyzing usage in an online loop with a web simulator.
- Simulation of the traffic effects of independent platoons and vehicles.
- Simulation and attestation of independents driving function in collaboration with other simulators.
- Simulation of the traffic of both railway and parking.
- Calculation of several emissions of pollutants and noise.
- Traffic safety measures and risk assessments can also be done using Sumo.

5 Conclusions

In this populated country traffic crowd is one of the major issues we all are experiencing. As the facilities keep on increasing in urban areas day by day population is also increasing. So that the available traffic facilities are not enough in today's world. As a result, there is increase in traffic crowd. The conclusions are given according to the present study. How Traffic crowd is assessed by using the measures like Speed Reduction Index(SRI), Speed Performance Index (SPI), Rate of delay and travel, Ratio of delay, and Level of Service (LOS) are explained in detail. The problems that occur at unsignalized intersections are discussed and presented. Keen insight into SUMO- Traffic simulation software and various applications were covered as a result of the literature review. SUMO is one of the best software to conduct the traffic analysis. From the different approaches available, the handiest for determining traffic crowd is noted to be the ratio of volume to capacity. Traffic Crowd levels based on the Speed performance index (SPI) were summarized (Refer Table 1). Crowd based upon the V/C ratio is discussed and presented (Refer Table 2).

References

1. Samal SR, Gireesh Kumar P, Cyril Santhosh J, Santhakumar M (2020) Analysis of traffic congestion impacts of urban road network under indian condition. In: IOP conference series

- materials science and engineering, December 2020. <https://doi.org/10.1088/1757-899X/1006/1/012002>
2. Pirdavani A, Brijs T, Bellemans T, Wets G (2011) A simulation-based traffic safety evaluation of signalized and unsignalized intersections. <http://hdl.handle.net/1942/11428>
 3. Bieker L, Krajzewicz D, Morra AP, Michelacci C, Fabio (2015) Traffic simulation for all: a real-world traffic scenario from the city of Bologna. *Lecture Notes in Control and Inform Sci* 13:47–60. https://doi.org/10.1007/978-3-319-15024-6_4
 4. Alvarez P, Behrisch LM, Bieker-Walz L, Erdmann J, Flotterod Y-P, Hilbrich R, Lucken L, Rummel J, Wagner P, Wiebner E (2018) Microscopic Traffic Simulation using SUMO. In: 21st international conference on intelligent transportation systems (ITSC) Maui, Hawaii, USA
 5. Akhter S, Ahsan MN, Quaderi SJS, Al Forhad MA, Sumit SH, Rahman MR (2020) A SUMO based simulation framework for intelligent traffic management system. *J Traffic Logistics Eng* 8(1)
 6. Arroyo N, Acosta A, Espinosa J, Espinosa J (2018) A new strategy for synchronizing traffic flow on adistributed simulation using SUMO. In: EPiC series in engineering 2018, SUMO 2018-Simulating Autonomous and Intermodal Transport Systems, vol 2. pp 152–161
 7. Krajzewicz D, Rossel C (2003) An example of microscopic car models validation using the open-source traffic simulation SUMO. In: 14th European simulation symposium
 8. Krajzewicz D, Brockfeld E, Mikat J, Ringel J, Rossel C, Tuchscheerer W, Wagner P, Wosler R (2005) Simulation of modern traffic lights control systems using the open-source traffic simulation SUMO. In: 3rd industrial simulation conference 2005
 9. Erdagı IG, Silgu MA, Celikoglu HB (2019) Emission effects of cooperative adaptive cruise control: a simulation case using SUMO. In: EPiC series in computing, vol 62. SUMO User Conference 2019, pp 92–100
 10. Zaky M, Airulla DG, Joelianto E, Sutarto HY (2017) Urban traffic simulation using SUMO open-source tools. *Internetwork Indonesia J* 9(1)
 11. Akyol G, Silgu MA, Celikoglu HB (2019) Pedestrian-friendly traffic signal control using eclipse SUMO. In: EPiC series in computing, vol 62. SUMO User Conference 2019, pp 101–106
 12. Wynita M, Ordonez-Hurtado RH, Crisostomi E, Haeusler F, Massow K, Shorten RN (2015) A large-scale SUMO-based emulation platform. *IEEE Trans Intell Transport Syst* <https://doi.org/10.1109/TITS.2015.2426056>
 13. Afrin T, Yodo N (2020) A survey of road traffic congestion measures towards a sustainable and resilient transportation system. *Sustainability* 12:4660. <https://doi.org/10.3390/su12114660>
 14. Kumar PG et al (2019) Level of service of urban and rural roads—a review. In: IOP Conference series: material science engineering, vol 1006. pp 012018
 15. Hossain MT, Hasan MK (2019) Assessment of traffic congestion by traffic flow analysis in Pabna Town. *American J Traffic Transp Eng*. <https://doi.org/10.11648/j.ajtte.20190403.11>

Stabilization of Marine Clay Using Palm Bunch Ash



Bernard Oruabena, Okoh Elechi, Ebiteisintei Nelson, Okiridu Ugochukwu, and George Deinbofa

Abstract Stabilization of poorly subgrade soil is required to upgrade it to withstand construction loads by reducing compressibility, permeability and increasing the strength of the soil shear and load-bearing capacity. This paper presents the effects of Palm Bunch Ash (PBA) on soil properties such as liquid limits, plastic limits, plasticity index, compaction characteristics, unconfined compressive strength, Atterberg's limits, California bearing ratio (CBR), and Maximum dry density (MDD) in marine clay mangrove soil stabilization. In this work, a marine clay mangrove soil has been checked for its effect on strength characteristics by gradually adding palm bunch ash while observing the strength and load-bearing capacity of the soil. The expansive soil collected from Nembe, Bayelsa State, Southern Nigeria's was gradually stabilized by up to 30% PBA at an increment of 5%. Several additions were considered and the trend in properties shows a linear increase in OMC, CBR, and MDD, with increased addition of PBA. The addition of 10% of PBA resulted in an OMC increase from 1.65 to 1.70KN / m² and 20% addition of PBA gave a UCS of 393.20kN / m² in 28 days. A 5% addition of PBA resulted in a 200.23kN / m² UCS. The level of reliability dropped as the PBA addition peaked at 53.3%. This result shows that UCS improved and stabilization is achieved when PBA is added to the expansive marine clay soil for the soaked and unsoaked conditions. The addition of palm bunch ash to marine clay soil improved the bearing capacity and the maximum dry density of the soil.

Keywords Palm Bunch ash · Portland cement · Stabilization · Marine clay soil · Load-bearing capacity · Subgrade

B. Oruabena (✉) · O. Ugochukwu · G. Deinbofa
Department of Civil Engineering, Federal Polytechnic Ekowe, Ekowe, Nigeria

O. Elechi · E. Nelson
Department of Chemical Engineering, Federal Polytechnic Ekowe, Ekowe, Nigeria

1 Introduction and Background

Weak soils need to be stabilized to strengthen their load-bearing capacity and to withstand the load placed on their foundation, making the soil structure a critical factor in road construction. Soil is the basis and raw materials required for the construction process [1, 2]. There is a need to stabilize the soil when it lacks essential properties required for the intended construction by improving soil strength and increasing its resistance to softening by water through eliminating voids in the soil grains [3]. The sub-soils of most construction sites in Yenagoa, Southern Nigeria consists of sedimentary deposits that form alternate layers of clay and sand, a soft marine clay soil having natural moisture content higher than its liquid limit [4] This soil is characterized by high compressibility causing high settlement and instability, low bearing capacity, low strength, low permeability, and high moisture content above 80% and poor drainage which make it shrinks or swell based on the water content. The swell and shrink factor make the soil inadequate for load-bearing structures [5–7]. There are therefore reasons to stabilized marine clay soils to improve on the geotechnical properties of these soils and extend their load-bearing capacity. Marine clay soil stabilization may involve the replacement of the existing soil with another quality soil with good properties or addition of stabilizing agents to improve the strength and ensure complete resilience to softening by water [8–10]. Numerous researchers including [11, 12] have found Portland Limestone Cement (PLC) to be an effective agent and the material of choice in stabilizing the fine-grain soils to provide base course material for roads. But cement as a stabilization material is expensive, and the need to replace it with a less costly alternative is imperative. In an engineering study of properties and classification of the superficial marine clay soils and modalities for reducing the cement contents required to stabilize it [13–15] has found empty palm fruit bunch ash to be useful in partial replacement of cement. But the degree to which PBA will replace cement in marine clay soil stabilization has not been fully treated. Observation shows that stabilization of marine clay soil with cement provides the best performance, but alternative methods are tested daily due to high cement costs [5]. [16–19], have shown through experiments that solid waste derivatives, because of their high pozzolanic quality possesses the properties that can replace cement in parts or whole and improve the engineering properties of extensive soft clay soils. The solid waste derivatives can be compressed into suitable binders, fillers, and modifiers for soil stabilization. This study has been carried out to relates PBA as supplementary cementing materials in civil engineering works and the effect on soil properties through the elucidation of the volume change properties (swelling and shrinkage) including bulk density, moisture content, plasticity, shear strength, and bearing capacity influencing the critical behavior of marine clay soils as foundation materials that suffer moisture attacks through capillary action, suction, rise and fall of the water table and lateral percolation that can be minimized through the addition of PBA in a stabilization procedure. Other soil properties such as the California Bearing Ratio (CBR), a strength characteristic attribute of soils used to assess their suitability through punching and penetration to withstand shear deformations, and has a direct

relationship to compacted soil density is variously evaluated. MDD is directly linked to CBR bearing ratios calculated under penetrations of 2.50 and 5.00 mm. According to Onyelowe et al. [20], when ash material or derivatives are applied to an expansive soil, it improves the density properties as determined by the California bearing ratio under axial loads.

2 Materials and Method

2.1 Materials

2.1.1 Marine Clay

The marine clay soil was collected from Nembe axis in Nembe L G A of Bayelsa State, at a depth of 1.5 m. The marine clay soil was dried and sieved after manually removing the unwanted materials that were also collected during excavation. The soil index properties, including the moisture content, density, optimum moisture content of the soil, were determined as per BS1377 (1990) standard.

2.1.2 Palm Bunch

The empty fruit bunch waste of the palm oil industry was collected from Bayelsa palms limited waste dump site. The sourced empty fruit bunch was dried under the sun for four weeks and burned with a locally constructed muffler without fuel. The ash was then pulverized on a dry shear surface and sieved through 0.75 μm to obtain a uniform smooth particle size and stored in an airtight container for later use. The physicochemical properties of the used materials are listed in Table 1.

2.1.3 Water

The water utilized for the tests was collected from the Federal Polytechnic Ekowe, Civil Engineering Technology Department. The water was also presumed free from any destructive pollutants and of good portable standard.

Table 1 Physicochemical properties of soil and treatment agents

S/No	Properties	Portland cement (42.5R)	Palm bunch ash	Marine clay soil
1	Specific gravity	3.02	1.54	2.44
2	pH	12	10.8	11
3	SiO ₂ (%)	18.92	52.55	62.96
4	Fe ₂ O ₃ (%)	3.04	7.85	3.57
5	Al ₂ O ₃ (%)	6.11	10.86	17.18
6	CaO (%)	65.02	13.70	0.16
7	MgO (%)	1.33	2.75	1.05
8	SO ₃ (%)	1.98	3.63	0.76
9	K ₂ O (%)	1.12	4.10	2.09
10	P ₂ O ₃ (%)	0.19	–	–
11	TiO ₂ (%)	0.29	0.50	–

2.2 Methodology

2.2.1 Index Properties

Standard procedures recommended in the respective I.S. Codes were used for all the laboratory tests and methods including: [21–26]. A detailed explanation of the materials used was also undertaken and reported.

2.2.2 California Bearing Ratio (CBR) Tests

The marine clay soil obtained was dried, homogenized and sieved, and mixed with the PBA to prepare different CBR specimens. The CBR values, at different percentages (5, 10, 15, and 20%) of PBA was done for the soaked and unsoaked conditions.

2.2.3 Compaction Properties

Optimum moisture content and maximum dry density of the expansive marine clay soil with various percentages PBA addition were determined according to the standard heavy compaction test. The MDD and OMC values were determined for each test.

3 Results and Discussion

3.1 Classification Characteristics

The properties of the marine clay soil, Cement, and Palm Bunch Ash used as stabilizing agents are presented in Table 1. Chemical analyses were performed to classify the materials and determine their reactivities. The specific gravity of cement taken from literature was 3.02, the determined marine clay soil pH was 2.44 while PBA had the least pH value of 1.54. The result showed that SiO₂, Al₂O₃ and Fe₂O₃ account for over 50% of the marine clay soil contents. The PBA has a CaO to SiO₂ mass ratio of 0.25, with low calcium oxide content of 13.7% below the recommended value for pozzolanas. According to BS EN 197-1 (2000), the ratio of CaO/SiO₂ must be ≥ 2 and must have calcium oxide content of between 60 and 68% for cementitious binders thereby making PBA not be seen as cementitious materials (Tables 2 and 3).

The results of the marine clay soil treatment with different percentages of PBA and the analysis produced the following third and second-order polynomial equations for OMC, MDD, soaked and unsoaked CBR, and UCS when fitted with quadratic model and the significant coefficients. The coefficient estimate represents the expected change in dry density per unit change in moisture contents (Fig. 1), MDD per unit change in % PBA addition (Fig. 2), and OMC per unit change PBA (Fig. 3). The

Table 2 Evaluated properties of marine clay soil

Properties	Marine clay soil	Marine clay soil + PBA	Marine clay soil + portland cement
Liquid limit (%)	49.83	28.85	41.74
Plastic limit (%)	28.20	23.40	31.88
Plasticity index	29.32	5.45	9.86
MDD (g/cm ³)	1.70	1.66	1.68
OMC (%)	26.7	16.7	15.35
CBR (%)—unsoaked	8.26	15.08	56.62
CBR (%)—soaked (24 h)	2.5	10.47	117.49

Table 3 Variation of MDD, OMC with PBA (%) addition

S/No	Marine clay soil	% PBA addition	Maximum dry density (g/cm ³)	Optimum moisture content (%)
1	100.0	0.0	1.62	14.6
2	100.0	5.0	1.68	14.0
3	100.0	10.0	1.67	16.6
4	100.0	15.0	1.70	14.4
5	100.0	20.0	1.66	16.7

Fig. 1 Variation of % moisture content with dry density

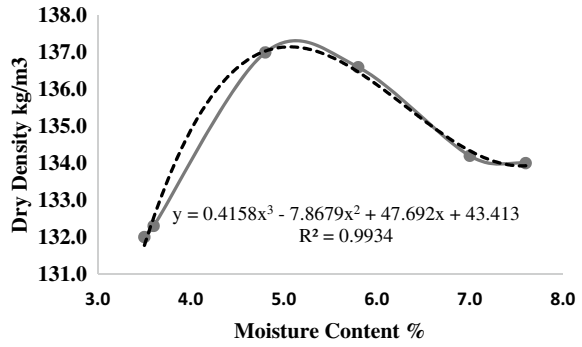


Fig. 2 Variation of MDD with PBA (%) addition

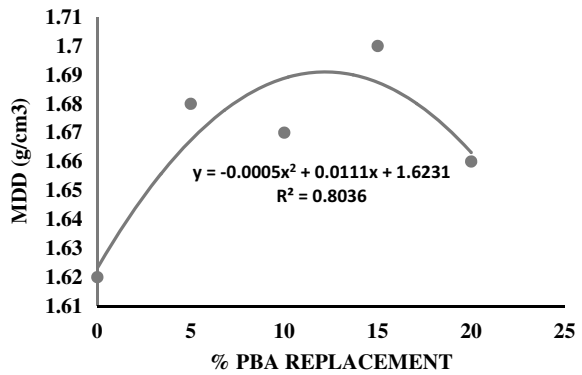
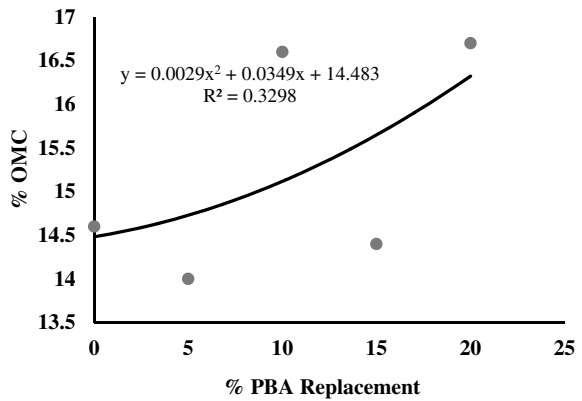
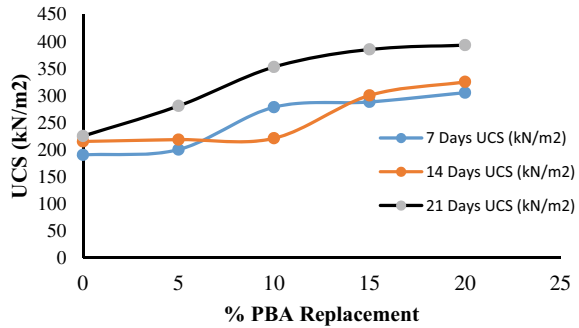


Fig. 3 Variation of OMC with PBA addition



MDD or OMC of the marine clay soil treated with PBA were both affected in a significant way by the addition of PBA.

Fig. 4 The UCS plot for 7, 14, and 21 days curing periods



3.2 Unconfined Compressive Strength (UCS)

To determine the quantity of PBA needed to stabilize an expansive soil to improve the strength characteristic and enable the use as base material in road construction, the soil UCS is evaluated. For the marine clay soil treated with PBA, it is observed from Fig. 4 that increasing the PBA content of the soil from 5 to 10% increased the 7-day UCS by about 50%, an average of 10 kN/m², while it was just around 1.5% for 14 days UCS and 26% for the 21 days UCS. The result is seen to have a linear increase in UCS with increasing PBA content. Which also increases with curing time. The increase in strength on addition of PBA was because of the cementitious properties of PBA that solidify the soil matrix.

3.3 Soaked and Unsoaked CBR

To determine the suitability of the soil to withstand shear deformation using the CBR characteristic strength of punching and penetration. We observed a significant improvement in the densification of the soil treated with PBA as seen in the soaked and unsoaked CBR values shown in Figs. 5 and 6. The CBR values increased linearly

Fig. 5 Soaked CBR for PBA treated marine clay soil

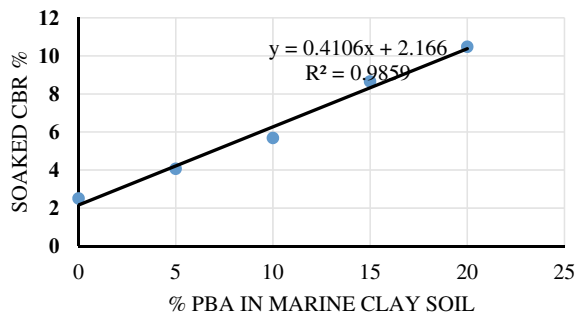
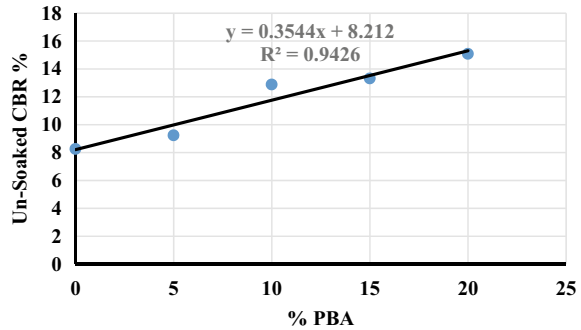


Fig. 6 Unsoaked CBR for PBA treated marine clay soil



with the addition of PBA approaching optimum at about 20% PBA addition. The linear correlation with the addition of PBA is attested by the high R-square values of 99% and 94% for the soaked and unsoaked CBR, respectively. The result shows that the soil's ability to withstand shear deformation was substantially improved when stabilized with PBA. The stabilized soil could be used as a sub-base material in road construction.

4 Conclusion

Cement stabilization of marine clay soil is an established practice to strengthen the soil for road base courses. Application of cement on such weak soils effectively produces strong and durable road base. But, despite the numerous benefits of cement treatment, its application in soil stabilization is grossly expensive and the need for supplementation with pollozonic materials becomes the desirable.

It was shown that PBA as supplementary cementing materials improved the engineering properties of the expansive soft clay soil. This was seen in the significant improvement in the density, shear strength, and soaked and unsoaked CBR, when about 20% PBA was used to stabilize the marine clay soil. The rate of improvement in soil stability varies linearly with the quantity of PBA added upto 20% to achieve a value comparable to that of cement.

20% PBA addition to soil gave the best stabilizing effect on the marine clay. The observed enhancements were for soaked CBR values > 20% after 24 h and > 10% after 96 h. Thus, this study revealed that the marine clay could be optimized for subgrade application using PBA as a stabilizing agent.

References

1. Onyelowe K (2016) Effect of temperature changes on the unconfined compressive strength of OPC stabilized engineering soil using palm bunch ash as admixture. Civil and Environ Eng

- Res J 1–9
2. Otunyo A, Chukuigwe C (2018) Investigation of the impact of palm bunch ash on the Stabilization of poor lateritic soil. *Niger J Technol* 37(3):600–604
 3. Youdeowei P, Nwankwoala H, Ayibanimiworio G (2020) Soil stabilization and improvement of marine clays using cement and lime in a marshland. *Eng Heritage J (GWK)* 4(1):08–14
 4. Rao D, Raju Gx (2011) Laboratory studies on the properties of stabilized marine clay from Kakinada Sea Coast, India. *Inter J Eng Sci Tech* 3(1):421–428
 5. Mohammed A-B, Marto A (2017) A review on the geotechnical and engineering characteristics of marine clay and the modern methods of improvements. *Malaysian J Fundamental Appl Sci* 13(4):825–831
 6. Pakir F, Marto A, Yunus M, Latifi N, Tan C (2014) Effect of sodium silicate as liquid based stabilizer on shear strength of marine clay. *Jurnal Teknologi* 76(2):45–50
 7. Otoko R, Fubara-Manuel I, Chinweike S, Oyebo J (2016) Soft soil stabilization using palm oil fibre ash. *J Multidisciplinary Eng Sci Technol* 3(5):4954–4958
 8. Mukesh A, Patel H (2012) A review on effect of stabilizing agent for stabilization of weak soils. *Civil Environ Res* 2(6):1–7
 9. Otoko G, Blessing O (2014) Cement and lime stabilization of a Nigerian deltaic marine clay (chikoko). *European Inter J Sci Tech* 3(4)
 10. Lucia Bulíková L, Kresta F, Rochovanský M (2017) Potential use of fly ash to soil treatment in the Morava region. In: *IOP Conference series: materials science engineering*, vol 236. Ludvica Podeste
 11. Onyelowo KC (2012) Soil stabilization techniques and Procedures in the developing countries—Nigeria. *Global J Eng Tech* 5(1):65–69
 12. Dumessa G, Verma R (2018) Compacted behaviour of cement stabilized lateritic soil and its economic benefit over selected borrow material in road constr.: a case study in Wolayita Sodo. *World J Eng Res Tech* 4(2):1–34
 13. Akpokodje E (1986) A method for reducing the cement content of two stabilized Niger delta soils. *Quarterly J Eng Geol Hydrol* 19:359–363
 14. Ahmad M, Omar RC, Malek M, Md-Noor N, Thiruselvam S (2014) Compressive strength of palm oil fuel ash concrete. *Onn Malaysia*
 15. Karim H, Samueel Z, Ahmed S (2015) Geotechnical properties of soft clay soil stabilized by reed ashes. Baghdad, Iraq
 16. Sukmak P, Horpibulsuk S, Shen S (2013) Factors influencing strength development in clay–fly ash geopolymer. *Constr Build Mater* 47:1125–1136
 17. Onyelowo K, Ubachukwu O (2015) Stabilization of olokoro-umuahia lateritic soil using Palm Bunch Ash (PBA) as admixture. *Umudike. J Eng Technol* 1:67–77
 18. Oluremi J, Ijimdiya S, Eberemu A (2018) Reliability evaluation of hydraulic conductivity characteristics of waste wood ash treated lateritic soil. *Geotech Geol Eng Int J*
 19. Onyelowo K, Duc Bui V, Ubachukwu O (2019) Recycling and reuse of solid wastes; a hub for ecofriendly, eco-efficient and sustainable soil, concrete, wastewater and pavement reengineering. *Int J Low-Carbon Technol* 14:440–451
 20. Onyelowo K, Bui Van D, Ubachuku O, Ezeugwu C (2019) Recycling and reuse of solid wastes. *Int J Low-Carbon Technol* 14:440–451
 21. BS1377–1 (1990) Method of test for soil for civil engineering purposes. *General Requirements and Sample Preparation*
 22. NGS (1997) Nigerian general specifications for roads and bridges
 23. ASTM D6913–04 (2009) Standard test methods for particle size distribution (Gradation of soils using sieve analysis). Retrieved from www.astm.org
 24. ASTM D2487–11 (2015) Standard practice for classification of soils for engineering purposes (Unified Soil Classification System). Retrieved from www.astm.org
 25. ASTM D2488–09a (2015) Standard practice for description and identification of soils (Visual Manual Procedure). Retrieved from www.astm.org
 26. BS5930 (2015) Code of practice for site investigation. www.bsigroup.com